

A Thesis Submitted for the Degree of PhD at the University of Warwick

Permanent WRAP URL:

<http://wrap.warwick.ac.uk/148985>

Copyright and reuse:

This thesis is made available online and is protected by original copyright.

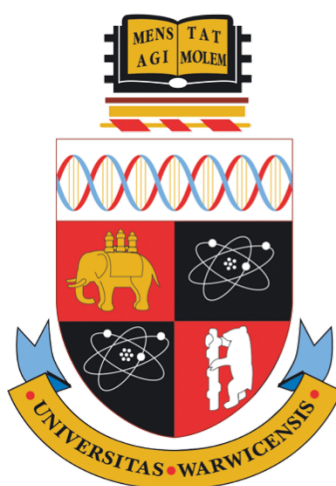
Please scroll down to view the document itself.

Please refer to the repository record for this item for information to help you to cite it.

Our policy information is available from the repository home page.

For more information, please contact the WRAP Team at: wrap@warwick.ac.uk

Structures and Ligand Interactions of Penicillin Binding Proteins in Gram-negative Bacteria



Carmina Micelli

This thesis is submitted for the degree of Doctor of Philosophy

University of Warwick
School of Life Sciences

September 2019

Contents

Contents	ii
List of figures	vii
List of tables	xii
Acknowledgements	xv
Declaration	xvi
Abstract	xvii
Abbreviations	xix
CHAPTER 1. Introduction	1
1.1 Antibiotic resistance	2
1.1.1 What is antibiotic resistance and why is it a problem?	2
1.1.2 Causes of antibiotic resistance and drivers of transmission	4
1.1.3 Strategies to tackle antibiotic resistance	6
1.1.3.1 Therapeutic strategies to combat antibiotic resistance	8
1.2 The bacterial cell wall as a source of antibacterial targets	10
1.2.1 The bacterial cell wall	10
1.2.1.1 Structure and composition of peptidoglycan	11
1.2.1.2 Peptidoglycan biosynthesis in Gram-negative bacteria	16
1.3 Penicillin binding proteins: a validated target for antibacterial therapy	17
1.3.1 The high-molecular weight PBPs	17
1.3.2 PG synthase machineries	19
1.3.2.1 The elongasome	20
1.3.2.2 Regulation of the PBP function	22
1.3.3 The reactions catalysed by PBPs	23
1.3.3.1 Transglycosylation	23
1.3.3.2 Transpeptidation and carboxypeptidation	24
1.3.4 Inhibition of the transpeptidase reaction	28
1.3.4.1 Mode of action of β -lactam compounds	28
1.3.4.2 Non- β -lactam compounds	30
1.4 Resistance mechanisms to β-lactam antibiotics	31
1.4.1 β -lactamases	34
1.4.2 Low-affinity PBPs	36
1.4.3 Outer membrane porins	36
1.4.4 Efflux pumps	37
1.5 Thesis aims	38
CHAPTER 2. Materials and methods	39
2.1 Growth and maintenance of <i>E. coli</i> strains	40
2.1.1 Bacterial cloning and expression strains	40
2.1.2 Growth media	40
2.1.3 Transformation of bacterial strains	41
2.2 DNA manipulation and cloning	41
2.2.1 Polymerase chain reaction (PCR)	41

2.2.2 Agarose gel electrophoresis	41
2.2.3 DNA purification	42
2.2.4 Plasmid purification	42
2.2.5 DNA quantification	42
2.2.6 Restriction enzyme digestion of DNA	42
2.2.7 Ligation of DNA fragments with complementary ends	42
2.2.8 Site-directed mutagenesis	43
2.3 Protein expression, purification and analysis	43
2.3.1 Expression of recombinant plasmids	43
2.3.2 Cell harvesting and cell lysis	44
2.3.3 Immobilized metal ion affinity chromatography (IMAC)	44
2.3.4 Glutathione affinity chromatography	45
2.3.5 Size exclusion chromatography	45
2.3.6 Protein electrophoresis	45
2.3.7 Protein quantification	46
2.4 Protein structure determination by X-ray crystallography	46
2.4.1 Screening of crystallisation conditions	46
2.4.2 Optimisation of crystallisation conditions	47
2.4.3 Crystal seeding	47
2.4.4 Crystal harvesting, soaking and cryo-cooling	47
2.4.5 Collection of X-ray diffraction data	48
2.4.6 Processing of X-ray diffraction data	48
2.4.6.1 Diffraction image processing with iMosflm	48
2.4.6.2 Data reduction: Pointless, Aimless, Ctruncate	49
2.4.6.3 Cell content analysis- the Matthews coefficient	49
2.4.6.4 Maximum likelihood molecular replacement	50
2.4.6.5 Model building and refinement	50
2.4.6.6 Model validation	51
2.4.7 Collection of X-ray fluorescence data	51
2.5 Fluorescent and spectrophotometric assays	51
2.5.1 Bocillin-FL binding assay	51
2.5.2 Differential scanning fluorimetry	52
2.5.3 Spectrophotometric assay with nitrocefin	52
2.5.4 Ellman's assay	54
2.6 Mass spectrometry	54
2.6.1 Mass spectrometry of test compounds	54
2.6.2 Mass spectrometry of intact proteins	55
2.6.3 Mass spectrometry of protein-molecule covalent adducts	55
2.7 ¹H-NMR spectroscopy	56
2.8 Minimal inhibitory concentration tests	56
CHAPTER 3. Discovery of a novel zinc-binding site in the structure of <i>A. baumannii</i> PBP2	57
3.1 Introduction to chapter 3	58
3.2 Plasmid construction, expression and purification of <i>A. baumannii</i> PBP2	59
3.3 Crystallisation of <i>A. baumannii</i> PBP2	59
3.3.1 Screening of coarse crystallisation conditions	59
3.3.2 Optimisation of crystal hits	61
3.4 Structure determination of <i>A. baumannii</i> PBP2	62
3.4.1 Data collection	62
3.4.2 Data integration with iMosflm	62

3.4.3 Data reduction	64
3.4.4 Cell content analysis	67
3.4.5 Molecular replacement	67
3.4.6 Model building and refinement	67
3.4.7 Identification of a metal-coordination site	69
3.4.8 Metal B factor and occupancy	73
3.4.9 Model validation	74
3.5 Description of <i>A. baumannii</i> PBP2 structure	74
3.5.1 Overall three-dimensional architecture	74
3.5.1.1 The N-terminal domain	75
3.5.1.1.1 Role of the pedestal domain in the interaction with MreC	78
3.5.1.2 The C-terminal domain	80
3.5.2 Active site structure	85
3.5.3 A novel zinc-binding site	86
3.5.3.1 Zinc-binding site structure	86
3.5.3.2 A new class B subtype: the Zn-containing PBPs	89
3.5.3.3 Biological significance of the S-X-N/D motif conserved interaction	91
3.6 <i>In-vivo</i> activity of wild-type and Zn-binding site mutants of <i>A. baumannii</i> PBP2	92
3.6.1 Plasmid construction	92
3.6.2 <i>In-vivo</i> experiments	93
3.6.2.1 Cell morphology assays	93
3.6.2.2 Antibiotic resistance assays	96
3.7 <i>In-vitro</i> characterisation of wild-type and Zn-binding site mutants of <i>A. baumannii</i> PBP2	98
3.7.1 Generation of <i>A. baumannii</i> PBP2 D350A, D365A, H371A and C384A mutants	98
3.7.2 Differential scanning fluorimetry assays	99
3.7.3 Spectrophotometric assays with DTNB	101
3.7.4 Spectrophotometric assays with nitrocefin	105
3.8 Conservation of the zinc-binding site in PBPs of Gram-positive and Gram-negative bacteria	114
3.8.1 Protein BLAST search of D-X ₁₄ -D-X ₅ -H-X ₁₂ -C motif and its cysteine variants	114
3.8.2 A potential zinc-binding site in SpoVD	116
3.9 Crystallisation trials of <i>B. subtilis</i> SpoVD	118
3.9.1 Expression and purification of SpoVD _{WT} and SpoVD _{C332D}	118
3.9.2 Crystallisation of SpoVD _{WT}	122
3.10 Discussion and future work	123
CHAPTER 4. Characterisation of <i>A. baumannii</i> PBP2 in complex with β-lactam and non-β-lactam compounds	130
4.1 Introduction to chapter 4	131
4.2 Interactions of <i>A. baumannii</i> PBP2 with β-lactams	132
4.2.1 Interactions of <i>A. baumannii</i> PBP2 with mecillinam	132
4.2.1.1 <i>In-vivo</i> and <i>in-vitro</i> activities of mecillinam from the literature	132
4.2.1.2 Mass spectrometry of <i>A. baumannii</i> PBP2 with mecillinam	136
4.2.1.3 Structure of <i>A. baumannii</i> PBP2 bound to mecillinam	137
4.2.1.3.1 Crystallisation, data collection and structure determination	137
4.2.1.3.2 Binding mode of mecillinam in complex with PBP2	139
4.2.2 Interactions of <i>A. baumannii</i> PBP2 with meropenem	144
4.2.2.1 <i>In-vivo</i> and <i>in-vitro</i> activities of meropenem from the literature	144
4.2.2.2 Structure of <i>A. baumannii</i> PBP2 bound to meropenem	147
4.2.2.2.1 Crystallisation, data collection and structure determination	147
4.2.2.2.2 Binding mode of meropenem in complex with PBP2	147

4.3 Interactions of <i>A. baumannii</i> PBP2 with DBOs	153
4.3.1 Interactions of <i>A. baumannii</i> PBP2 with avibactam	153
4.3.1.1 <i>In-vivo</i> and <i>in-vitro</i> activities of avibactam from the literature	153
4.3.1.2 Mass spectrometry of <i>A. baumannii</i> PBP2 with avibactam	156
4.3.1.3 Structure of <i>A. baumannii</i> PBP2 bound to avibactam	157
4.3.1.3.1 Crystallisation, data collection and structure determination	157
4.3.1.3.2 Structure of the PBP2- avibactam complex	159
4.3.2 Interactions of <i>A. baumannii</i> PBP2 with zidebactam	163
4.3.2.1 <i>In-vivo</i> and <i>in-vitro</i> activities of zidebactam from the literature	163
4.3.2.2 Mass spectrometry of <i>A. baumannii</i> PBP2 with zidebactam	166
4.3.2.3 Structure of <i>A. baumannii</i> PBP2 bound to zidebactam	167
4.3.2.3.1 Crystallisation, data collection and structure determination	167
4.3.2.3.2 Structure of the PBP2- zidebactam complex	169
4.4 Distinctive features in the active site of <i>A. baumannii</i> PBP2	174
4.4.1 Active site comparison with PBP1a and PBP3	174
4.4.2 Dissecting the role of Asp385	179
4.4.2.1 Generation of PBP2 D385N mutant	179
4.4.2.2 Mass spectrometry of D385N PBP2 with mecillinam	181
4.4.2.2 Differential scanning fluorimetry assays of PBP2 with β -lactams and DBOs	183
4.4.2.3 <i>In-vivo</i> studies of PBP2 D385N mutant	185
4.5 Discussion and future work	187
CHAPTER 5. Exploring the interaction of ampicillin-derived molecules with PBPs in Gram-negative bacteria	194
5.1 Introduction to chapter 5	195
5.2 Formation of ampicillin oligomers: the reaction	196
5.3 Cloning, expression and purification of PBPs	198
5.3.1 <i>P. aeruginosa</i> PBP1a and its mutant S461A	198
5.3.2 <i>A. baumannii</i> PBP1a	199
5.3.3 <i>A. baumannii</i> PBP3	199
5.3.4 <i>E. coli</i> DacB	199
5.4 Mass spectrometry of ampicillin in a time course experiment with PBPs	200
5.5 Structural studies of <i>P. aeruginosa</i> PBP1a	214
5.5.1 Controlled proteolysis of <i>P. aeruginosa</i> PBP1a	214
5.5.2 MS of the room temperature tryptic cleaved PBP1a	217
5.5.3 Crystallisation of <i>P. aeruginosa</i> PBP1a	222
5.5.4 Structural studies of <i>P. aeruginosa</i> PBP1a	225
5.5.4.1 Crystal harvesting, data collection and structure determination	225
5.5.4.2 Overall structure of PBP1a	225
5.5.4.2.1 The transpeptidase domain	230
5.5.4.2.2 Additional domains	231
5.5.4.3 Structure of PBP1a bound to ampicillin	232
5.6 Structural studies of <i>P. aeruginosa</i> PBP3 with ampicillin polymers	233
5.6.1 X-ray structure of <i>P. aeruginosa</i> PBP3 bound to ampicillin dimer	233
5.7 MIC testing of ampicillin oligomers	238
5.8 NMR studies of ampicillin oligomers	239
5.9 Discussion and future work	243
CHAPTER 6. Discussion	250
6.1 Discussion	251

Bibliography	259
Appendices	287

List of figures

Figure 1.1	Antibiotic discovery timeline	3
Figure 1.2	Schematic of the cell wall structure in Gram-positive and Gram-negative bacteria	11
Figure 1.3	Chemical structure of peptidoglycan in Gram-negative bacteria	14
Figure 1.4	Schematic diagram of peptidoglycan biosynthesis in Gram-negative bacteria	15
Figure 1.5	PBP classification in <i>E. coli</i>	18
Figure 1.6	Representation of the elongasome and the divisome complex	21
Figure 1.7	Schematic of the transglycosylase reaction	24
Figure 1.8	D,D-transpeptidation and D,D-carboxypeptidation catalysed by HMW-PBPs in Gram-negative bacteria	27
Figure 1.9	Structural similarity between the D-ala-D-ala termini of the PG stem pentapeptide and the β -lactam antibiotics	29
Figure 1.10	Schematic of the reaction of β -lactam antibiotics, lactvicins and boronic acids with PBPs and β -lactamases	32
Figure 2.1	Reaction of nitrocefin with PBPs and serine β -lactamases	53
Figure 2.2	Reaction of a cysteine sulfhydryl group with DTNB	54
Figure 3.1	Purification of <i>A. baumannii</i> PBP2	60
Figure 3.2	Intact protein mass spectrometry of <i>A. baumannii</i> PBP2	60
Figure 3.3	Crystallisation of <i>A. baumannii</i> PBP2	61
Figure 3.4	Crystal of <i>A. baumannii</i> PBP2 mounted in a loop	62
Figure 3.5	Indexing and cell refinement	63
Figure 3.6	Aimless graphs	64
Figure 3.7	Models generated by molecular replacement, model building and refinement	68
Figure 3.8	Metal coordination site	71
Figure 3.9	X-ray fluorescence emission spectrum (MCA) from a PBP2 crystal	71
Figure 3.10	Calculated anomalous scattering at the Ni, Cu and Zn K edge	71
Figure 3.11	Edge scans for metals of interest in a PBP2 crystal	72
Figure 3.12	Models and electron density maps based on the data collected below (left) and above (right) the zinc absorption edge	72
Figure 3.13	Domain organisation in the structure of <i>A. baumannii</i> PBP2	75
Figure 3.14	Structure of <i>A. baumannii</i> PBP2	76
Figure 3.15	The pedestal domain in structures of <i>H. pylori</i> and <i>A. baumannii</i> PBP2	79
Figure 3.16	Sequence alignments of PBP2 and MreC from different bacteria.	82
Figure 3.17	Close-up view of the PBP2 TP active site	85
Figure 3.18	Close-up view of the zinc coordination site in chain A of <i>A. baumannii</i> PBP2	87

Figure 3.19	Snapshot of the interaction between the X residue of the S-X-N/D motif and the β -hairpin region in class B PBPs	90
Figure 3.20	Phase-contrast microscopy of <i>A. baumannii</i> ATCC 17978 bacteria grown to -mid-exponential phase in antibiotic-free LB medium	94
Figure 3.21	Detection of PBP2 by Western blotting	95
Figure 3.22	CFE with bacteria grown on increasing concentrations of sulbactam on solid medium	97
Figure 3.23	Coomassie staining of the SDS-PAGE gel and Bocillin-FL binding assay of the four PBP2 mutants, along with the marker	99
Figure 3.24	Thermal shift assay of PBP2	100
Figure 3.25	Spectrophotometric assays with DTNB	102
Figure 3.26	MS of PBP2 _{WT} reacted with DTNB	103
Figure 3.27	MS of PBP2 _{EDTA} reacted with DTNB	104
Figure 3.28	Spectrophotometric assays with nitrocefin	106
Figure 3.29	MS of PBP2 _{WT}	109
Figure 3.30	MS of PBP2 _{WT} reacted with nitrocefin for 5 min	110
Figure 3.31	MS of PBP2 \blacklozenge	111
Figure 3.32	MS of PBP2 \blacklozenge reacted with nitrocefin for 2 min	112
Figure 3.33	MS of PBP2 \blacklozenge reacted with nitrocefin for 30 min	113
Figure 3.34	Alignment of the PBP homologues retrieved by a BLAST search bearing the D-X ₁₄ -D-X ₅ -H-X ₁₂ -C motif	114
Figure 3.35	Alignment of the PBP homologues retrieved by a BLAST search bearing the C-X ₁₄ -D-X ₅ -H-X ₁₂ -C motif	115
Figure 3.36	Alignment of the PBP homologues retrieved by a BLAST search bearing the C-X ₁₄ -C-X ₅ -H-X ₁₂ -C motif	115
Figure 3.37	Section of the sequence alignment between <i>A. baumannii</i> PBP2 and <i>B. subtilis</i> SpoVD wild-type and mutant C332D	116
Figure 3.38	Section of the sequence alignment between <i>A. baumannii</i> PBP2 and <i>C. perfringens</i> SpoVD wild-type	117
Figure 3.39	Purification of SpoVD _{WT}	120
Figure 3.40	Coomassie staining of the SDS-PAGE gel (left) and Bocillin-FL binding assay (right) of SpoVD _{WT}	120
Figure 3.41	Intact protein MS of <i>B. subtilis</i> GST-SpoVD _{WT}	121
Figure 3.42	Intact protein MS of <i>B. subtilis</i> GST-SpoVD _{C332D}	121
Figure 3.43	SpoVD crystal hits	123
Figure 4.1	Chemical structure of mecillinam	135
Figure 4.2	Effect of mecillinam <i>in-vivo</i>	135
Figure 4.3	Intact protein MS of <i>A. baumannii</i> PBP2 with mecillinam	136
Figure 4.4	Crystal of <i>A. baumannii</i> PBP2 soaked with mecillinam	137
Figure 4.5	Graphs from the statistics	138
Figure 4.6	Schematic of the reaction of <i>A. baumannii</i> PBP2 with mecillinam	141
Figure 4.7	Electron density of mecillinam in the acylated structure of <i>A. baumannii</i> PBP2	141
Figure 4.8	Mecillinam bound to the active site of <i>A. baumannii</i> PBP2	141

Figure 4.9	Active site of PBP2 unbound and in complex with mecillinam	143
Figure 4.10	Superimposition of acylated structures of PBP2 and PBP1a from <i>A. baumannii</i>	143
Figure 4.11	Chemical structure of meropenem	146
Figure 4.12	<i>In-vivo</i> effect of meropenem	146
Figure 4.13	Crystal of <i>A. baumannii</i> PBP2 soaked with meropenem	147
Figure 4.14	Graphs from the statistics	148
Figure 4.15	Schematic of the reaction of <i>A. baumannii</i> PBP2 with meropenem	150
Figure 4.16	Electron density of meropenem in the acylated structure of <i>A. baumannii</i> PBP2	151
Figure 4.17	Meropenem bound to the active site of <i>A. baumannii</i> PBP2	151
Figure 4.18	Active site of PBP2 unbound and in complex with meropenem	152
Figure 4.19	Superimposition of acylated structures of <i>A. baumannii</i> PBP2 and <i>P. aeruginosa</i> PBP3 bound to meropenem	152
Figure 4.20	Chemical structure of avibactam	155
Figure 4.21	Effect of avibactam <i>in-vivo</i>	155
Figure 4.22	Intact protein MS of <i>A. baumannii</i> PBP2 with avibactam	156
Figure 4.23	Crystal of <i>A. baumannii</i> PBP2 soaked with avibactam	157
Figure 4.24	Graphs from the statistics	158
Figure 4.25	Schematic of the reaction of <i>A. baumannii</i> PBP2 with avibactam	161
Figure 4.26	Electron density of avibactam in the acylated structure of <i>A. baumannii</i> PBP2	161
Figure 4.27	Avibactam bound to the active site of <i>A. baumannii</i> PBP2	161
Figure 4.28	Comparison of avibactam bound-PBP2 with the native structure	162
Figure 4.29	Binding mode of avibactam in <i>E. coli</i> and <i>A. baumannii</i> PBP2	162
Figure 4.30	Chemical structure of zidebactam	165
Figure 4.31	Microscopy-based live-dead staining of <i>A. baumannii</i> MDR ST2 expressing OXA-23	165
Figure 4.32	Intact protein MS of <i>A. baumannii</i> PBP2 with zidebactam	166
Figure 4.33	Crystal of <i>A. baumannii</i> PBP2 soaked with zidebactam	167
Figure 4.34	Graphs from the statistics	168
Figure 4.35	Schematic of the reaction of <i>A. baumannii</i> PBP2 with zidebactam	170
Figure 4.36	Electron density of zidebactam in the acylated structure of <i>A. baumannii</i> PBP2	170
Figure 4.37	Zidebactam bound to the active site of <i>A. baumannii</i> PBP2	170
Figure 4.38	Comparison of zidebactam bound-PBP2 with the native structure	172
Figure 4.39	Superimposition of <i>A. baumannii</i> PBP2 structures bound to DBOs	172
Figure 4.40	<i>A. baumannii</i> PBP2 in complex with β -lactam and DBO molecules	173
Figure 4.41	Differences in the TP binding site of PBP1a, PBP2 and PBP3	177

Figure 4.42	Purified mutant (D385N) of <i>A. baumannii</i> PBP2	180
Figure 4.43	Intact protein MS of <i>A. baumannii</i> PBP2 D385N mutant with mecillinam	182
Figure 4.44	Intact protein MS of <i>A. baumannii</i> PBP2 wild-type with mecillinam	182
Figure 4.45	Differential scanning fluorimetry assays	184
Figure 4.46	Phase-contrast microscopy of <i>A. baumannii</i> ATCC 17978 bacteria grown to mid-exponential phase in antibiotic-free LB medium	187
Figure 4.47	CFE with bacteria grown on increasing concentrations of sulbactam on solid medium	187
Figure 5.1	Dimerization of ampicillin by aminolysis	196
Figure 5.2	Chemical structures of ampicillin and its oligomers derived from aminolysis	197
Figure 5.3	Molecular ions of ampicillin and ampicillin polymers detected in the aged solutions	201
Figure 5.4	MS of <i>P. aeruginosa</i> PBP1a reacted with a 10-fold molar excess of ampS1	209
Figure 5.5	MS of <i>P. aeruginosa</i> PBP1a reacted with a 10-fold molar excess of either ampS2 or ampS3	210
Figure 5.6	MS of <i>P. aeruginosa</i> PBP1a and PBP3	211
Figure 5.7	MS of <i>A. baumannii</i> PBP1a/PBP2/PBP3 and <i>E. coli</i> DacB with aged ampicillin solution	212
Figure 5.8	MS of <i>P. aeruginosa</i> PBP1a reacted with a 10-fold molar excess of a solution containing equimolar concentrations of penicillin G and ampicillin	213
Figure 5.9	Published structure of <i>P. aeruginosa</i> PBP1a ^{400N}	215
Figure 5.10	Purification of <i>P. aeruginosa</i> PBP1a after controlled proteolysis	216
Figure 5.11	MS of <i>P. aeruginosa</i> PBP1a proteolyzed at room temperature	219
Figure 5.12	MS of <i>P. aeruginosa</i> PBP1a proteolyzed at room temperature and reacted with a 10-fold molar excess of a solution of aged ampicillin	220
Figure 5.13	MS of <i>P. aeruginosa</i> PBP1a proteolyzed at room temperature and reacted with a 10-fold molar excess of fresh ceftazidime	221
Figure 5.14	Schematic of the reaction of <i>P. aeruginosa</i> PBP1a with ceftazidime	222
Figure 5.15	Crystals of <i>P. aeruginosa</i> PBP1a	224
Figure 5.16	Domain organisation in the structure of <i>P. aeruginosa</i> PBP1a	226
Figure 5.17	Structure of <i>P. aeruginosa</i> PBP1a solved in this work	228
Figure 5.18	Cleavage sites of <i>P. aeruginosa</i> PBP1a treated with trypsin for 2 h at room temperature	229
Figure 5.19	Taurine in the active site of <i>P. aeruginosa</i> PBP1a structure	231
Figure 5.20	Schematic of the reaction of <i>P. aeruginosa</i> PBP1a with ampicillin	233
Figure 5.21	Ampicillin bound to <i>P. aeruginosa</i> PBP1a	233

Figure 5.22	Schematic of the reaction of <i>P. aeruginosa</i> PBP3 with ampicillin dimer	236
Figure 5.23	<i>P. aeruginosa</i> PBP3 in complex with ampicillin dimer	237
Figure 5.24	Reaction of ampicillin and its oligomers with β -lactamases	241
Figure 5.25	Structure of ampicillin and ampicillin polymers before and after hydrolysis by β -lactamases	242
Figure 5.26	Hydrolysis of ampicillin and ampicillin oligomers by AmpC in a time course experiment	243
Figure S1	Amino acid sequence of <i>A. baumannii</i> PBP1a Δ 51-764 encoded by pMIC15	290
Figure S2	Amino acid sequence of <i>A. baumannii</i> PBP2 Δ 53-672 encoded by pMIC10	291
Figure S3	Amino acid sequence of <i>A. baumannii</i> PBP3 Δ 64-610 encoded by pMIC16	292
Figure S4	Amino acid sequence of <i>P. aeruginosa</i> PBP1a Δ 36-822 encoded by pMIC13	293
Figure S5	Amino acid sequence of <i>P. aeruginosa</i> PBP3 Δ 50-579 encoded by pDB1	294
Figure S6	Amino acid sequence of <i>E. coli</i> <i>DacB</i> Δ 21-477 encoded by pMIC17	295
Figure S7	Amino acid sequence of GST-SpoVD Δ 33-645 encoded by pLYM020	296
Figure S8	Sequence alignment of HMW-PBPs from selected ESKAPE pathogens	300
Figure S9	ESI-MS of variously concentrated ampicillin solutions in a time course experiment for 14 days	301
Figure S10	ESI-MS spectra of penicillin G and in combination with ampicillin, zoomed in selected m/z range	302
Figure S11	Superimposition of combined spectra (black) and theoretical spectra (light blue) for the experiment illustrated in figure 5.4	303
Figure S12	Superimposition of combined spectra (black) and theoretical spectra (light blue) for the experiment illustrated in figure 5.5	304
Figure S13	Superimposition of combined spectra (black) and theoretical spectra (light blue) for the experiment illustrated in figure 5.6	305
Figure S14	Superimposition of combined spectra (black) and theoretical spectra (light blue) for the experiment illustrated in figure 5.7	306
Figure S15	Superimposition of combined spectra (black) and theoretical spectra (light blue) for the experiment illustrated in figure 5.8	306
Figure S16	$^1\text{H-NMR}$ spectra of ampicillin reacted with AmpC in a time course experiment	307
Figure S17	$^1\text{H-NMR}$ spectra of ampicillin dimer reacted with AmpC in a time course experiment	307
Figure S18	$^1\text{H-NMR}$ spectra of ampicillin trimer reacted with AmpC in a time course experiment	308

List of tables

Table 1.1	WHO priority pathogens list for which new antibiotics are urgently needed	4
Table 1.2	Bacterial targets recognised by clinically used antibiotics	8
Table 1.3	Representative structures of β -lactam and non- β -lactam compounds targeting PG transpeptidation	33
Table 2.1	Cell strains used in this study	40
Table 2.2	PCR programme	41
Table 3.1	Symmetry elements scored by Pointless	65
Table 3.2	Scores for all possible Laue groups which are sub-groups of lattice group	65
Table 3.3	Summary table for the point group I 2 2 2	65
Table 3.4	Summary of the results from Aimless	66
Table 3.5	Summary of the results from Matthews coefficient analysis	67
Table 3.6	Refinement statistics of the dataset for PBP2	69
Table 3.7	Theoretical values of the excitation and emission energies for the heavy atoms investigated in crystals of PBP2	71
Table 3.8	B-factor and occupancy of the atoms in the zinc-coordination site	73
Table 3.9	Ligands and distances in the Zn-binding site of <i>A. baumannii</i> PBP2	87
Table 3.10	Thermal shift assay of PBP2	100
Table 3.11	Summary of the results from the DTNB assay	102
Table 3.12	MS of PBP2 _{WT} and PBP2 _{EDTA} reacted with 100-fold molar excess of DTNB	102
Table 3.13	Hydrolysis rate of nitrocefin by PBP2 wild-type and mutants	105
Table 3.14	MS of PBP2 \blacklozenge and PBP2 _{WT} before and after reaction with a 20-fold molar excess of nitrocefin	108
Table 3.15	Intact MS of GST-SpoVD _{WT} and GST-SpoVD _{C332D}	121
Table 4.1	Antimicrobial activity of mecillinam	135
Table 4.2	PBP sensitivity to mecillinam acylation in various Gram-negative pathogens	135
Table 4.3	MS of PBP2 _{WT} before and after reaction with 10-fold molar excess of mecillinam	136
Table 4.4	Statistics of the PBP2: mecillinam dataset	138
Table 4.5	Statistics of the PBP2: mecillinam dataset	139
Table 4.6	Antimicrobial activity of meropenem	146
Table 4.7	PBP sensitivity to meropenem acylation in various Gram-negative pathogens	146
Table 4.8	Statistics of the PBP2: meropenem dataset	148
Table 4.9	Statistics of the PBP2: meropenem dataset	149
Table 4.10	List of polar interactions observed in the active site of <i>A. baumannii</i> PBP2 in complex with meropenem	150
Table 4.11	Antimicrobial activity of avibactam	155

Table 4.12	PBP sensitivity to avibactam acylation in various Gram-negative pathogens	155
Table 4.13	MS of PBP2 _{WT} before and after reaction with 10-fold molar excess of avibactam	156
Table 4.14	Statistics of the PBP2: avibactam dataset	158
Table 4.15	Statistics of the PBP2: avibactam dataset	159
Table 4.16	List of polar interactions observed in the binding site of <i>A. baumannii</i> PBP2 in complex with avibactam	160
Table 4.17	PBP sensitivity to zidebactam acylation in various Gram-negative pathogens	165
Table 4.18	Antimicrobial activity of zidebactam	165
Table 4.19	MS of PBP2 _{WT} before and after reaction with 10-fold molar excess of zidebactam	166
Table 4.20	Statistics of the PBP2: zidebactam dataset	168
Table 4.21	Statistics of the PBP2: zidebactam dataset	169
Table 4.22	List of polar interactions observed in the binding site of <i>A. baumannii</i> PBP2 in complex with zidebactam	171
Table 4.23	MS of PBP2 _{WT} before and after reaction with 10-fold molar excess of mecillinam	181
Table 4.24	Differential scanning fluorimetry assays	183
Table 5.1	List of molecular ions identified in the ESI-MS spectra of a 20 % (w/v) ampicillin solution stored at room temperature for two weeks	202
Table 5.2	List of molecular ions identified in the ESI-MS spectra of a 50 % (w/v) ampicillin solution stored at room temperature for two weeks	203
Table 5.3	List of molecular ions identified in the ESI-MS spectra of a 50% (w/v) ampicillin solution stored at -20°C for two weeks	204
Table 5.4	List of peaks identified in the ESI-MS spectra of <i>P. aeruginosa</i> PBP1a reacted with a 10-fold molar excess of an aged ampicillin solution	207
Table 5.5	List of peaks identified in the ESI-MS spectra shown in figure 5.6a-b and 5.7	208
Table 5.6	List of peaks identified in the ESI-MS spectra of <i>P. aeruginosa</i> PBP1a shown in figure 5.8	213
Table 5.7	Sequence and mass of the six polypeptides separated by SDS-PAGE and identified in the MS spectra of <i>P. aeruginosa</i> PBP1a digested at room temperature with trypsin	217
Table 5.8	MS of tryptic digested <i>P. aeruginosa</i> PBP1a reacted with either aged ampicillin or fresh ceftazidime	218
Table 5.9	Data collection and refinement statistics for <i>P. aeruginosa</i> PBP1a structures	227
Table 5.10	Comparison between the polypeptides of the tryptic digested <i>P. aeruginosa</i> PBP1a protein observed in solution by MS, and in the X-ray structure	229
Table 5.11	Data collection and refinement statistics for <i>P. aeruginosa</i> PBP3 bound to ampicillin dimer	235

Table 5.12	Antimicrobial activity of ampicillin and ampicillin polymers against a panel of Gram-positive and Gram-negative bacteria	239
Table S1	List of oligonucleotides used in this thesis	288
Table S2	List of plasmids generated in this thesis	289

Acknowledgements

I would first like to thank Prof David Roper for his supervision, trust and support over my three years of research at Warwick University. Also my co-supervisor Prof Chris Dowson and advisory panel members Prof Richard Napier and Dr Christophe Corre for their help and guidance.

I would like to acknowledge my examiners Prof Alex Cameron (University of Warwick) and Prof Ivo Boneca (Institut Pasteur) for making my PhD viva an enjoyable experience.

Special thanks to Dr Adrian Lloyd for all his help with biochemistry and mass spectrometry, his academic advice, wisdom and moral support. I would also like to thank Dr Allister Crow for both his guidance and very patiently teaching me X-ray crystallography.

Thanks also to my collaborators Dr Edward Geisinger from Northeastern University and Dr Chris Lohans from Oxford University for their contributions to the project.

I would also like to thank Julie Todd, Anita Catherwood and John Moat for all of their help in the lab, as well as my past group members Dr Avinash Punekar and Dr Dom Bellini, my group colleagues and everyone else from the C10 lab and beyond.

Finally, I would like to thank my family and friends in Italy and the UK, for all of their love and support over the years.

Declaration

This thesis is submitted to the University of Warwick in support of my application for the degree of Doctor of Philosophy. It has been composed by myself and has not been submitted in any previous application for any degree. The work presented (including data generated and data analysis) was carried out by myself and any deviation from this is acknowledged in the text.

Abstract

Antibiotic resistance has become one of the major threats to global health, because of the increasing emergence of multi-drug resistant bacteria and the lack of new effective antibiotics to counteract them. Therefore, new antibiotics need to be developed, and bacterial cell wall biosynthesis has long been recognised as an excellent target for antibacterial discovery. Transpeptidation is the last reaction in the synthesis of peptidoglycan and is catalysed by penicillin binding proteins, the enzymes targeted by β -lactam antibiotics.

In this project, a novel crystal structure of PBP2 has been determined from *Acinetobacter baumannii*, a Gram-negative pathogen commonly causing nosocomial infections, to aid the structure-based design of new PBP-targeting molecules. Structures of PBP2 in complex with β -lactam antibiotics and diazabicyclooctane compounds have been also generated, highlighting particular protein-ligand interactions that could inform the optimisation of PBP inhibitors from existing and novel chemical classes. Moreover, the structure of *A. baumannii* PBP2 has disclosed distinctive features in the transpeptidase domain of this enzyme, including a new zinc-binding site proximal to the catalytic pocket, that is essential for the cell wall elongation in this pathogen.

β -lactam molecules generated by the polymerisation of ampicillin in solution have been also investigated, with particular emphasis on the interactions with PBPs and β -lactamases. The covalent binding of ampicillin and its polymers to various PBPs from Gram-negative bacteria have been confirmed by mass spectrometry, and structural studies of *Pseudomonas aeruginosa* PBP1a and PBP3 have been undertaken to elucidate the binding mode of these particular molecules. Ampicillin and ampicillin polymers are hydrolysed by the β -lactamase AmpC at different rates, and they also show differences in antimicrobial activity.

This study provides the structural basis for the inhibition of important HMW-PBPs by β -lactam and non- β -lactam compounds, and it could be useful for the development of potent PBP inhibitors.

Abbreviations

°	degrees
∞	infinite
µg	micro grams
µl	micro litres
µm	micro meters
°C	degrees Celsius
A ₂₈₀	absorbance at 280 nm
aa	amino acid
Abs	absorbance
AMR	antimicrobial resistance
aPBP	class A PBP
APS	ammonium persulfate
asu	asymmetric unit
ATP	adenosine triphosphate
BL	β-lactamase
BLAST	Basic local alignment search tool
BLI	β-lactamase inhibitor
bPBP	class B PBP
C55-P	undecaprenyl phosphate
CDC	Centers for Disease Control and Prevention
cm	centimetres
CP/CPase	carboxypeptidation/carboxypeptidase
CV	column volume
Da	Dalton
DBO	diazabicyclooctane
DLS	Diamond light source
DNA	deoxyribonucleic acid
DNase I	deoxyribonuclease I enzyme
DSF	differential scanning fluorimetry
DTNB	5,5'-dithio- <i>bis</i> -(2-nitrobenzoic acid)
EDTA	ethylenediaminetetraacetic acid
ESBL	extended-spectrum β-lactamase
FDA	Food and Drug Administration
FT	flow-through
GlcNAc	<i>N</i> -acetylglucosamine
GST	glutathione S-transferase
h	hour
HEPES	4-(2-hydroxyethyl)-1-piperazineethanesulfonic acid
HGT	horizontal gene transfer
HMW	high-molecular weight
HP	high performance
HPLC	high-performance liquid chromatography
IC ₅₀	inhibitory concentration
IF	insoluble fraction

IMAC	immobilized metal ion affinity chromatography
IPTG	isopropyl- β -D-thiogalactopyranoside
kb	kilo bases
keV	kilo electron volts
kg	kilo grams
kDa	kilo Daltons
kV	kilo volts
L	litres
LB	Luria-Bertani broth
LC/MS	liquid chromatography/mass spectrometry
Lipid I	undecaprenyl-pyrophosphoryl- <i>N</i> -acetylmuramyl-L-alanyl- γ -D-glutamyl-L-lysyl/meso-DAP-D-alanyl-D-alanine
Lipid II	undecaprenyl-pyrophosphoryl- <i>N</i> -acetylmuramyl (<i>N</i> -acetylglucosaminy)-L-alanyl- γ -D-glutamyl-L-lysyl/meso-DAP-D-alanyl-D-alanine
LMW	low-molecular weight
LPS	lipopolysaccharide
M	marker
M	molar
<i>m/z</i>	mass to charge ratio
mAU	milli-absorbance unit
MBL	metallo β -lactamase
MDR	multi-drug resistant
<i>meso</i> -DAP	<i>meso</i> -diaminopimelic acid
MGT	monofunctional glycosyltransferase
MIC	minimal inhibitory concentration
min	minute
mm	millimetres
ml	millilitres
MR	molecular replacement
MRSA	methicillin-resistant <i>Staphylococcus aureus</i>
MS	mass spectrometry
MurNAc	<i>N</i> -acetylmuramic acid
MW	molecular weight
NADPH	nicotinamide adenine dinucleotide phosphate
NCS	non-crystallographic symmetry
nm	nano meters
nl	nano litres
NMR	nuclear magnetic resonance
O/N	overnight
OM	outer membrane
OD	optical density
P	phosphate
PBP	penicillin binding protein
PCR	polymerase chain reaction
PDB	Protein Data Bank
PEP	phosphoenolpyruvate

PG	peptidoglycan
rmsd	root mean square deviation
rpm	revolutions per minute
s	seconds
SAR	structure-activity relationship
SBL	serine β -lactamase
SDS-PAGE	sodium dodecyl sulphate - polyacrylamide gel electrophoresis
SEC	size exclusion chromatography
SEDS	shape-elongation-division-sporulation
SF	soluble fraction
TAE	TRIS-acetate-EDTA
TEMED	<i>N,N,N',N'</i> -tetramethylethylenediamine
TG/ TGase	transglycosylation/ transglycosylase
TM	transmembrane
T_m	melting temperature
TNB	2-nitro-5-thiobenzoic acid
TP/ TPase	transpeptidation/ transpeptidase
TRIS	Tris(hydroxymethyl)aminomethane
UDP	uridine diphosphate
UV/Vis	ultraviolet-visible spectroscopy
V	volume
v/v	volume to volume ratio
w/v	weight to volume ratio
v/w	volume to weight ratio
WHO	World Health Organisation
WT	wild-type

List of the 20 standard amino acids and their abbreviations and the genetic code

Amino acid	3-letter	1-letter	Codon
Alanine	Ala	A	GCU GCC GCA GCG
Arginine	Arg	R	CGU CGC CGA CGG AGA AGG
Asparagine	Asn	N	AAU AAC
Aspartic acid	Asp	D	GAU GAC
Cysteine	Cys	C	UGU UGC
Glutamic acid	Glu	E	GAA GAG
Glutamine	Gln	Q	CAA CAG
Glycine	Gly	G	GGU GGC GGA GGG
Histidine	His	H	CAU CAC
Isoleucine	Ile	I	AUU AUC AUA
Leucine	Leu	L	UUA UUG CUU CUC CUA CUG
Lysine	Lys	K	AAA AAG
Methionine	Met	M	AUG
Phenylalanine	Phe	F	UUU UUC
Proline	Pro	P	CCU CCC CCA CCG
Serine	Ser	S	UCU UCC UCA UCG AGU AGC
Threonine	Thr	T	ACU ACC ACA ACG
Tryptophan	Trp	W	UGG
Tyrosine	Tyr	Y	UAU UAC
Valine	Val	V	GUU GUC GUA GUG
stop	-	-	* UAA UAG UGA

CHAPTER 1

Introduction

1.1 Antibiotic resistance

1.1.1 What is antibiotic resistance and why is it a problem?

Antimicrobial resistance (AMR), and more specifically resistance to antibiotics, refers to the condition where antibacterials become ineffective, due to the ability of bacteria to develop mechanisms that help circumvent the toxic action of these agents. Antibiotic resistance is a natural selection process that occurs over time when antibiotics are used, due to genetic changes that allow bacteria to survive in the presence of the drug and spread the resistance mechanism to the progeny or other bacteria (Davies and Davies, 2010). As a result of this process, bacteria can acquire resistance to multiple antibiotic classes (classified as multidrug-resistant (MDR)/ extensively drug-resistant/ pandrug-resistant bacteria depending on susceptibility testing) (Magiorakos *et al.*, 2012), leading to infections that are harder to treat and can be life-threatening. Drug-resistant infections are typically more difficult to treat than drug-susceptible infections, as they limit the number of usable therapeutic options and, depending on the bacterial resistance profile, may require the use of “last resort” antibiotics, these agents being generally more toxic and also more expensive (Lim *et al.*, 2010). Bacterial isolates resistant to the last resort antibiotic colistin have already been reported (McGann *et al.*, 2016). Drug-resistant infections are associated with higher morbidity and mortality, longer stays in hospitals, and higher healthcare costs (Mauldin *et al.*, 2010; Cosgrove, 2006).

Antibiotic resistance is a major threat to the public’s health and a matter of extreme urgency that needs to be addressed globally. Currently, at least 50,000 people die every year of drug-resistant infections across Europe and the US alone, and by 2050 antimicrobial resistance is expected to be the first cause of death worldwide, leading to 10 million people dying every year if no global action is taken soon (O’Neil, 2014; WHO, 2014). Bacterial resistance has been reported for nearly all classes of antibiotics developed so far (Ventola, 2015), and without new effective medicines, cancer treatments, caesarean sections and other medical procedures will be at risk (Prestinaci *et al.*, 2015). Because of this, a return to the pre-antibiotic age has been envisioned where bacterial infections will no longer be curable (Appelbaum, 2012).

The “golden age” of antibiotics (1940s-1960s) had been a very profitable time in the area of antibiotic discovery and development, for the generation of many and novel antibiotic classes still currently in use (Singh, 2014) (figure 1.1). Access to these powerful life-saving medicines meant a great reduction in mortality rates due to bacterial infections, but also improper use of the antibiotics that determined the rapid emergence of resistance to the novel classes. The last novel antibiotic agent being discovered was in 1987, and thereafter a discovery void has followed where only re-elaborated versions of existing chemical classes have been FDA approved, so far (Silver, 2011). In this period of time, Big Pharma have abandoned research in this area, even though the need for new antibacterials was recognised, due to scientific challenges, commercial and regulatory reasons (Payne *et al.*, 2015).

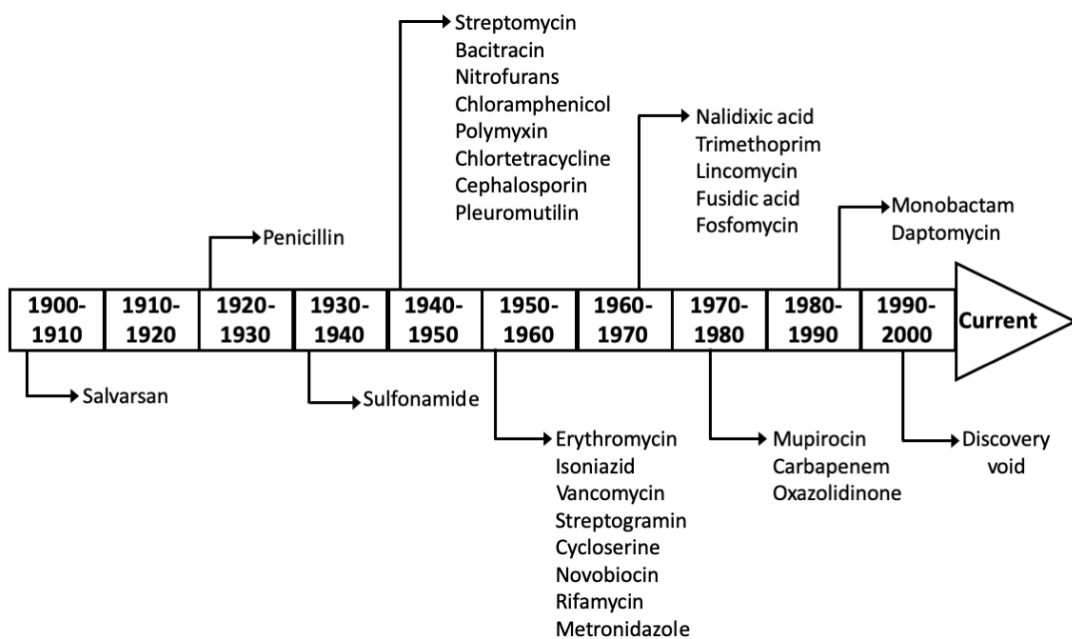


Figure 1.1. Antibiotic discovery timeline. Image adapted from Silver (Silver, 2011).

The AMR problem is now being tackled by many public health agencies around the world, and in 2016, WHO was commissioned to create a list of antibiotic-resistant bacteria to help prioritize the research and development of new effective antibiotics (table 1.1) (Tacconelli *et al.*, 2018).

Priority: critical
<i>Acinetobacter baumannii</i> , carbapenem resistant <i>Pseudomonas aeruginosa</i> , carbapenem resistant <i>Enterobacteriaceae</i> , carbapenem resistant, 3 rd generation cephalosporin resistant
Priority: high
<i>Enterococcus faecium</i> , vancomycin resistant <i>Staphylococcus aureus</i> , methicillin resistant, vancomycin resistant <i>Helicobacter pylori</i> , clarithromycin resistant <i>Campylobacter spp.</i> , fluoroquinolone resistant <i>Salmonella spp.</i> , fluoroquinolone resistant <i>Neisseria gonorrhoeae</i> , 3 rd generation cephalosporin resistant, fluoroquinolone resistant
Priority: medium
<i>Streptococcus pneumoniae</i> , penicillin non-susceptible <i>Haemophilus influenzae</i> , ampicillin resistant <i>Shigella spp.</i> , fluoroquinolone resistant

Table 1.1. WHO priority pathogens list for which new antibiotics are urgently needed. Table adapted from (Tacconelli et al., 2018)

1.1.2 Causes of antibiotic resistance and drivers of transmission

Aetiology of antibiotic resistance is multifaceted, and different socioeconomic and political factors contribute to the rise in the prevalence of antibiotic resistance, in developed and developing countries (Ventola, 2015). Overuse of antibiotics is the main cause of resistance development, as first warned by Sir Alexander Fleming in the Nobel Prize acceptance speech in 1945, when penicillin was made available for general use. Indeed, the connection between the consumption of antibiotics and the emergence and spread of antibiotic resistance has since been documented by a number of epidemiological studies (Mackenzie et al., 2007; Hsueh et al., 2005; Meyer et al., 2010). Antibiotics are overprescribed worldwide, and inadequate regulations regarding their use have substantially contributed to the antibiotic resistance crisis. In many developing countries there is a lack of regulation on the retail of antibiotics, which are easily accessible without a prescription, and cheap, thus promoting overuse (Morgan et al., 2011; Michael et al., 2014; Auta et al., 2019). Clinical misdiagnosis and antibiotic misuse is another factor contributing to the evolution of resistance. Several studies have revealed that proper diagnostic methods are often not utilised when treating infections and therefore antibiotics are prescribed when not necessary, for instance in cases of viral infections (Caliendo et al., 2013; Bhavnani

et al., 2007). Patient misconduct including self-medication and sharing of medications prescribed to other individuals, is also a significant problem in both industrialised and low-income countries (Grigoryan *et al.*, 2006; Ocan *et al.*, 2015). Excessive use of antibiotics in food-producing animals has also been associated to the presence of antibiotic-resistance bacteria in humans (Tang *et al.*, 2017; Hoelzer *et al.*, 2017). The global consumption of antibiotics in animal husbandry is estimated to be 65,000 tons, which accounts for approximately two-thirds of all antibiotics produced each year worldwide, intended for growth promotion and infection prevention (Gelband *et al.*, 2015). The practice of using antibiotics for growth promotion has been banned in Europe since 2006 (Castanon, 2007), and in the USA since 2017 (Brussow, 2017), while this is still ongoing in many developing countries (Manyi-Loh *et al.*, 2018). Transmission of resistant bacteria from farm animals to humans may occur directly, through consumption of meat products, and indirectly, through the feco-oral route (Founou *et al.*, 2016). A large fraction of antibiotics given to livestock is released in the environment in the biologically active form, through urine and stool. These, together with the use of antibiotics and metals in agriculture, increase the proportion of resistant versus susceptible microorganisms in the environment (Kirchhelle, 2018; Singer *et al.*, 2016).

Bacterial resistance to antibiotics can occur by gene mutations or can be acquired via horizontal gene transfer. Plasmid-mediated transmission is the most prevalent mechanism of horizontal gene transfer (Davies and Davies, 2010). Understanding the drivers of antibiotic resistance transmission is key to be able to control/reduce the spread of drug-resistant bacterial infections. Drivers of transmission include poor sanitation and hygiene habits, particularly concerning the low-income countries; hospitalisation and cross-transmission between patients; low efficacy of waste water treatment plants in removing antimicrobial resistance genes and antibiotics disposed in the environment, thus representing breeding ground for bacteria to acquire resistance; intercontinental travel and migration that allow bacterial plasmids to be transported rapidly between countries (Holmes *et al.*, 2016; Kristiansson *et al.*, 2011; Friedrich, 2019; Wuijts *et al.*, 2017; van der Bij and Pitout, 2012).

1.1.3 Strategies to tackle antibiotic resistance

The problem of antibiotic resistance cannot be eradicated, but its progression may be decelerated. In order to realise strategic measures to control the dissemination of antibiotic resistance, it is important to understand the magnitude of the problem worldwide. A comprehensive analysis of resistance development across the globe is currently limited by the lack of surveillance in most of the developing countries (WHO, 2014). In order to narrow the gaps in surveillance, the WHO has launched the Global AMR surveillance system in 2015 (WHO, 2018). Additional global agencies taking action against the menace of antibiotic resistance include Food and Agriculture Organisation, CDC, and Office International des Epizooties. Other programs dealing with the global threat of antibiotic resistance include the Global Health Security Agenda, Antimicrobial Resistance Action Package (Aslam *et al.*, 2018). Several countries have realised national plans to control the spread of resistance that include AMR surveillance, improving AMR education for patients and healthcare professionals, restricting the availability of antimicrobials and developing strategies for AMR containment and disease control (UK GOV, 2019; ECDC, 2016).

Both economic reasons and regulatory barriers have made research on antibiotics a less attractive field for investment by pharma companies. The present net value, a prediction of the economic return, is low for antibiotics (about US\$ 100 million) compared to musculoskeletal drugs (+ US\$ 1 billion) (Sharma and Towse, 2010). This is due to the fact that, as antibiotics are typically administered as a curative medicine to treat acute infections, they are generally prescribed over much shorter timescales than the non-curative medicines that are often used in the treatment of chronic disease. Moreover, antibiotics are generally priced low (US\$ 1000-3000 maximum per course) compared to antitumoral drugs (US\$ >10000), due to the public perception that they are largely available and easy to use (Bartlett *et al.*, 2013).

Also, new antibiotics would be prescribed only as drugs of last resort, when older agents of comparable efficacy do not work, which would further reduce return on investment. Furthermore, new incentive strategies are being proposed to encourage pharma companies to develop new antibiotics, such as a new payment model being explored by the UK's National Institute for Health and Care Excellence in which the

monetary value paid for antimicrobials corresponds to their clinical value rather than the quantity of each antimicrobial purchased (UK GOV, 2019).

Another element contributing to the slow development of antibiotics is represented by the regulatory approval, more difficult to obtain due to changes in standards for antibiotic clinical trials. Differently from other medicines where comparison with a placebo is used to evaluate the effectiveness of a new drug, a new antibiotic must demonstrate noninferiority compared to existing drugs, which implies recruitment of a large sample population and consequently high costs (Ventola, 2015). To help accelerate approval of new antibiotics, the 21st Century Cures Act has introduced the Limited Population Antibacterial Drug regulatory pathway, that allows smaller and less expensive clinical trials, provided that indication of the new antibiotic is focused on a limited and specific population of high-risk patients (Spellberg *et al.*, 2012; Mullard, 2018; US FDA, 2018).

To decelerate the progression of antibiotic resistance, prescription of antibiotics should be kept low and reserved to patients that really need it. To reduce the unnecessary use of antibiotics in clinical practice, implementation of rapid diagnostic technology in primary and secondary care would guide medical professionals to better informed prescriptions that do not rely only on the patient symptoms (O'Neil, 2014). Infection prevention is another important measure to limit antibiotic consumption, hence the emergence of drug-resistant bacteria. Investments to improve the quality of water and sanitation infrastructures in low and middle-income countries, would significantly reduce the number of infections contracted, and promote urbanisation and economic growth (O'Neil, 2014).

Prevention measure are also needed in health-care settings such as hospitals and nursing homes, that represent high-risk environments for the spread of bacterial infections. It has been estimated that 7-10 % of hospitalised patients contract some form of healthcare-associated infection and simple measures like handwashing between contact with patients, has been shown to be very effective (WHO, 2016; O'Neil, 2014). Public awareness and understanding of antibiotic resistance are a crucial part of tackling AMR, behaviour change campaigns can be cost effective and lead to lasting changes. Since 2015, WHO has introduced a World Antibiotic

Awareness Week aiming at educating the general public on the correct use of antibiotics (WHO, 2015; Edgar *et al.*, 2008).

1.1.3.1 Therapeutic strategies to combat antibiotic resistance

Although efforts to reduce the use of antibiotics worldwide is hoped to curb the spread of antimicrobial resistance, the development of new resistance mechanisms is unlikely to be prevented as it is a product of natural selection (Davies and Davies, 2010). For this reason, research into new therapeutics is of primary importance if clinicians are to be able to treat MDR bacterial infections that, today may be relatively limited, but in the near future may pose a serious threat to the world's population health.

To counteract the rising bacterial resistance, several drug discovery approaches are currently being explored (Lakemeyer *et al.*, 2018; Monserrat-Martinez *et al.*, 2019; Brötz-Oesterhelt and Sass, 2010). One such approach, is the development of molecules with the same mechanism of action of clinically used antibiotics, which target essential bacterial structures or processes such as the bacterial cell wall, cell membrane, DNA synthesis and protein synthesis (table 1.2) (Kohanski *et al.*, 2010).

Target	Antibiotic
Cell wall biosynthesis	β -lactams, cycloserine, fosfomycin, glycopeptides, lipoglycopeptides
Protein synthesis	Aminoglycosides, tetracyclines (subunit 30S) Oxazolidinones, macrolides, thiopeptides, chloramphenicol, fusidic acid, clindamycin (subunit 50S)
DNA/ RNA synthesis	Rifamycins, ansamycins, actinomycins, tiacumycins (RNA polymerase) Fluoroquinolones, aminocoumarins (DNA gyrase)
Folic acid metabolism	Sulfonamides, trimethoprim
Membrane structure	Lipopeptides, polymyxins

Table 1.2. Bacterial targets recognised by clinically used antibiotics. Table adapted from Gonzalez-Bello (2017).

In this respect, chemical modification of existing antibiotics may be pursued with the aim of improving the compound efficacy as exemplified by the four generations of cephalosporins, or the compound pharmacokinetics by synthesis of prodrugs, for instance (Monserrat-Martinez *et al.*, 2019). Furthermore, the discovery of new

chemotypes aided by target-based high throughput screening technologies is intended to generate molecules that are potentially immune to the bacterial resistance mechanisms against available classes of antibiotics, that include enzymatic modification of the antibacterial drug to disable it, target mutation to reduce antibiotic binding and changes in membrane permeability to reduce intracellular accumulation of antibiotic (Munita and Arias, 2016).

Another approach for the discovery of new antibiotics is based on the identification of novel target sites in bacteria, which can lead to the development of drugs with a new mechanism of action (Lakemeyer *et al.*, 2018). Target identification and validation is currently a bottleneck in the drug discovery programs of new antibacterials (and many other therapeutic agents), due to challenges in the discovery of targets that meet certain criteria. A good antibacterial target must perform an essential function in the bacterial cell, it has to be druggable, and ubiquitous among several bacterial species, and it should not have human homologues (Montserrat-Martinez *et al.*, 2019). Phenotypic screening of library compounds may lead to the discovery of molecule hits with some antimicrobial activity, but unknown or alleged mechanism of action. Various methods can then be used to aid the identification of these potentially novel molecular targets such as generation of laboratory bacterial strains that are resistant to the active molecule followed by genome sequencing, or conjugation of the active compound with molecular probes and subsequent analysis of the bacterial proteins being modified by the tagged molecules (Lakemeyer *et al.*, 2018).

Although these two approaches have so far been successful in providing many of the currently available antibiotics, they inadvertently create a selective pressure towards the development of new drug resistance as they are aimed at targeting essential cellular functions. To mitigate the insurgence of such bacterial resistance, alternative strategies targeting non-essential bacterial processes are being investigated, as these are believed to relieve the evolutionary pressure for adaptation (Lakemeyer *et al.*, 2018; Monserrat-Martinez *et al.*, 2019). These approaches are aimed at disarming the pathogen of virulence factors, so that it can be more easily cleared by

the host immune system. Therapeutic strategies being currently pursued include the use of small molecules, antimicrobial peptides or antibacterial monoclonal antibodies for the inactivation of quorum-sensing signals, inhibition of secretion systems and toxin neutralisation, and enhancement of the host cell immune response. Alternative therapies based on phages and phage products are also being evaluated (Lakemeyer *et al.*, 2018; Monserrat-Martinez *et al.*, 2019).

1.2 The bacterial cell wall as a source of antibacterial targets

1.2.1 The bacterial cell wall

The bacterial cell wall is a complex multi-layered structure that encases the entire bacterium, is essential to cell survival and growth, and is a major target of antibiotics (Vollmer *et al.*, 2008). Peptidoglycan (also known as murein) (PG) is a major component of the cell wall, and one of the largest macromolecules in the cell ($>10^9$ Da) (Vollmer and Höltje, 2004). Typically bacteria are classified as either Gram-positive or Gram-negative on the basis of a staining technique that distinguishes between the two different cell-envelope architectures (Coico, 2005). Gram-positive bacteria have a thick multi-layered peptidoglycan (PG) sacculus (approximately 10-40 nm) outside the cytoplasmic membrane, where long anionic polymers called wall teichoic acids are covalently attached to the PG, and lipoteichoic acids anchored to the cell membrane (Silhavy *et al.*, 2010; Egan *et al.*, 2017). In contrast, Gram-negative bacteria have a thin peptidoglycan layer (approximately 3-6 nm) in the periplasm, and an external envelope called outer membrane (Vollmer and Seligman, 2010) (figure 1.2). The outer membrane differs from the cytoplasmic membrane in having phospholipids in the inner leaflet only, and glycolipids such as lipopolysaccharide (LPS) in the outer leaflet. The outer membrane also contains two types of proteins, the lipoproteins and the β -barrel proteins (Silhavy *et al.*, 2010). A few bacteria are exceptional in that they lack a cell wall peptidoglycan, these are the *Mycoplasma* species and the L-forms (Baron, 1996; Errington, 2013).

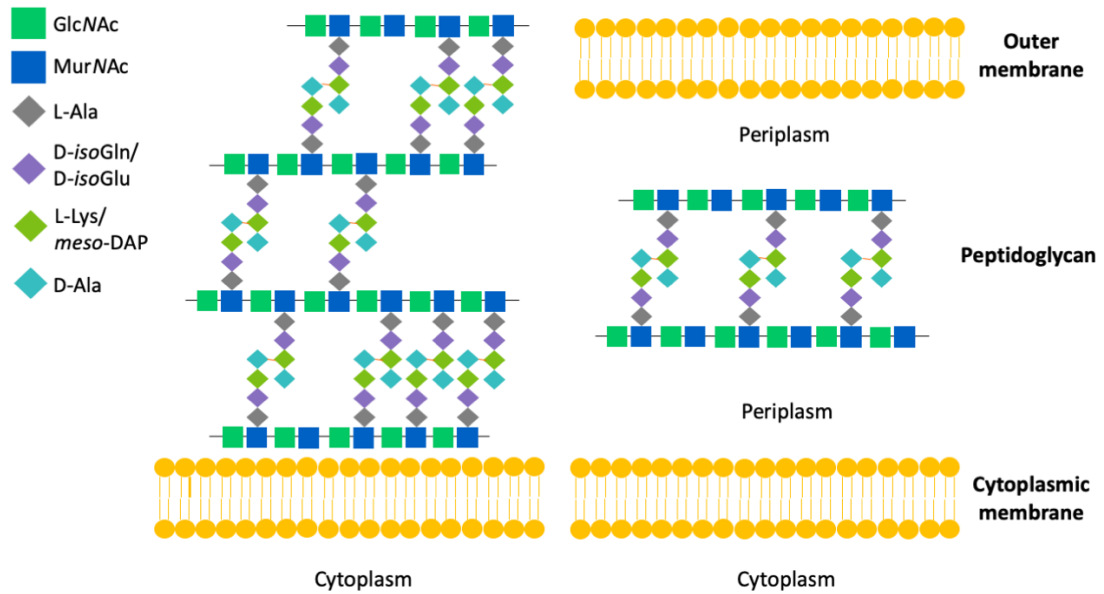


Figure 1.2. Schematic of the cell wall structure in Gram-positive (left) and Gram-negative (right) bacteria. Variability exists between Gram-positive and Gram-negative bacteria in terms of peptidoglycan composition, and the most common amino acid variations are labelled. Additional polymers present in the bacterial cell wall and surface proteins are omitted.

1.2.1.1 Structure and composition of peptidoglycan

Peptidoglycan (PG) is an essential component of the cell wall of nearly all bacteria, with key roles in numerous functions including maintenance of cell shape and protection from lysis due to internal turgor (Vollmer *et al.*, 2008). It is a complex, three-dimensional mesh-like sacculus surrounding the entire cell, consisting of glycan strands held together by short peptides.

The glycan strands are made of alternating *N*-acetylglucosamine (GlcNAc) and *N*-acetylmuramic acid (MurNAc) residues linked by β -1,4 glycosidic bonds (figure 1.2, 1.3b). The glycan strands may present secondary modifications such as *N*-deacetylation, *O*-acetylation and *N*-glycosylation, in some bacteria (Vollmer, 2008). The average length and length distribution of the glycan strands is highly variable among bacteria and can even change according to strain and growth conditions. For instance, in *E. coli* and most Gram-negative species the average chain length is 20-40 disaccharide units, whereas in *B. subtilis* glycan strands up to 5000 disaccharides have been isolated, and in *S. aureus* much shorter glycan strands \sim 6 disaccharide units are predominant (Vollmer and Seligman, 2010; Hayhurst *et al.*, 2008).

The MurNAc sugars are connected to pentapeptides, containing L- and D- amino acids, and their composition can largely vary across bacterial species (Vollmer *et al.*, 2008). The PG peptide sequence in most Gram-negative bacteria is L-Ala₍₁₎- γ -D-Glu₍₂₎-*meso*-DAP₍₃₎-D-Ala₍₄₎-D-Ala₍₅₎ (*meso*-DAP, *meso*-diaminopimelic acid) (figure 1.3a), whereas in most Gram-positive species the amino acid at position 3 is replaced by L-Lys. Additional modifications to the pentapeptide are possible, and these are introduced by enzymes different from the Mur ligases. Examples include amidation of the α -carboxyl group of D-Glu₍₂₎ (yielding γ -D-Gln) and addition of different interpeptide bridges to the ϵ -amine group of L-Lys₍₃₎ (e.g., *S. aureus* has a pentaglycine bridge) in Gram-positive bacteria (Münch and Sahl, 2015). In Gram-negative bacteria, the α -carboxyl group of *meso*-DAP₍₃₎ can be covalently bound to the Braun lipoprotein, thus firmly connecting the peptidoglycan to the outer membrane (Dramsı *et al.*, 2008).

To form peptidoglycan, the glycan strands are linked to one another by formation of peptide bonds between the stem peptides. The mode of cross-linkage and the degree of cross-linkage, in addition to the murein composition, constitutes another variable affecting the final PG structure and architecture. The 4-3 cross-linkage is very common among bacteria, and its formation is due to the enzymatic activity of D,D-transpeptidases such as Penicillin binding proteins (PBPs). In the 4-3 cross-linkage, the carboxyl group of D-Ala₍₄₎ (acyl donor) from one strand and the amino group of the residue side chain at position 3 (*meso*-DAP₍₃₎ in Gram-negative and L-Lys₍₃₎ or L-Lys₍₃₎-peptide branch in Gram-positive bacteria) (acyl acceptor) from a second strand, form an amide bond (figure 1.3a). Another type of connection includes the 3-3 cross-linkage, formed by L,D-transpeptidases. In the 3-3 cross-linkage, the peptide bond extends from the α -carboxyl group of the amino acid at position 3 (acyl donor) of one strand, to the amine at the extremity of the side chain of the residue at position 3 (acyl acceptor) of another strand. This type of cross-linkage is common in *Mycobacteria* (Lavollay *et al.*, 2008), and is also present, although at lower abundance in other bacteria. An increase in 3-3 cross-link formation has been reported for bacteria at the stationary phase of growth, and

bacteria tolerant to β -lactam antibiotics (Pisabarro *et al.*, 1985; Hugonnet *et al.*, 2016a).

The degree of cross-linkage is variable among bacteria species, and even within the same species in different growth states. In *E. coli*, this is approximately 20 % whereas in *S. aureus* is over 93 % (Vollmer *et al.*, 2008).

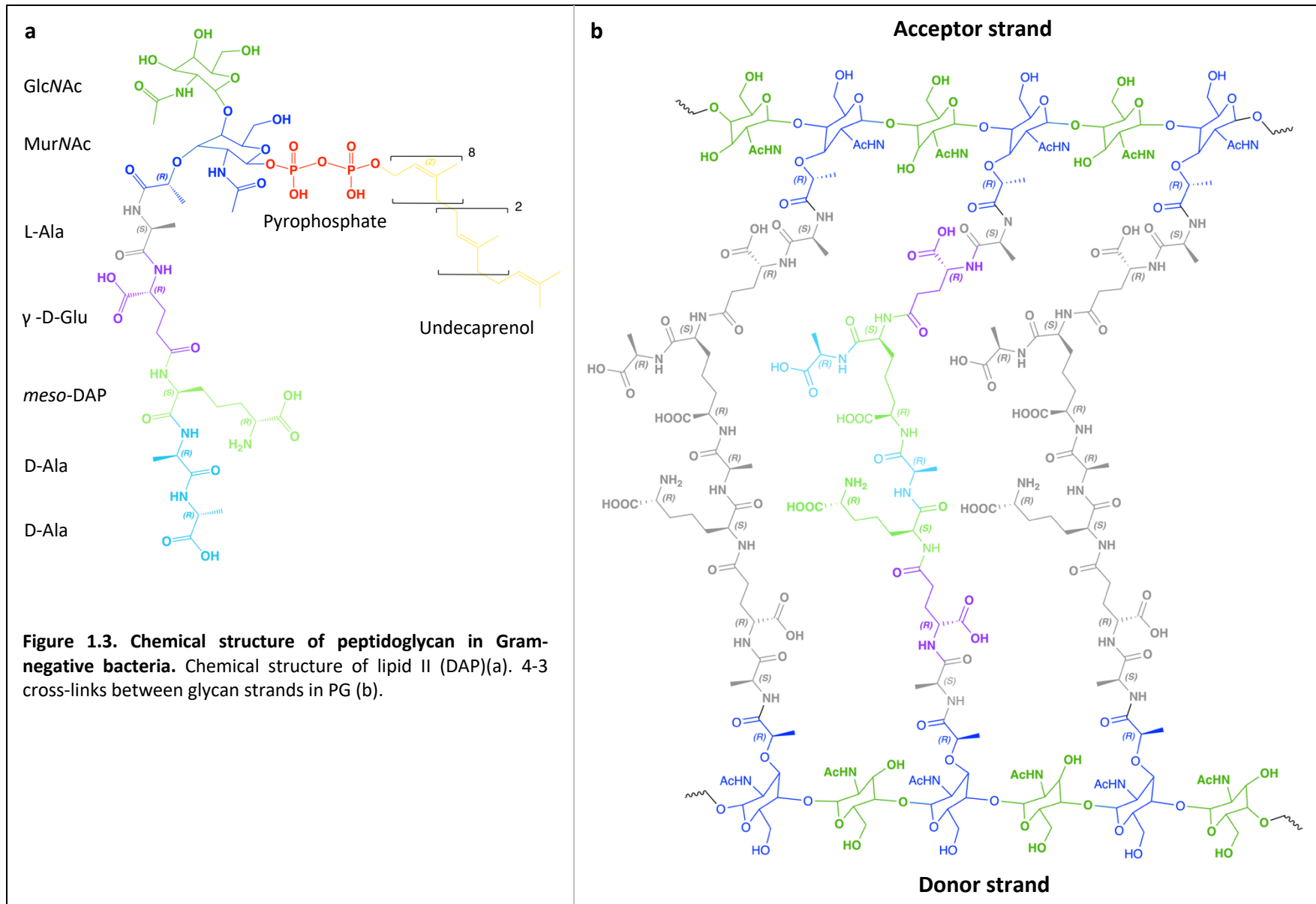


Figure 1.3. Chemical structure of peptidoglycan in Gram-negative bacteria. Chemical structure of lipid II (DAP)(a). 4-3 cross-links between glycan strands in PG (b).

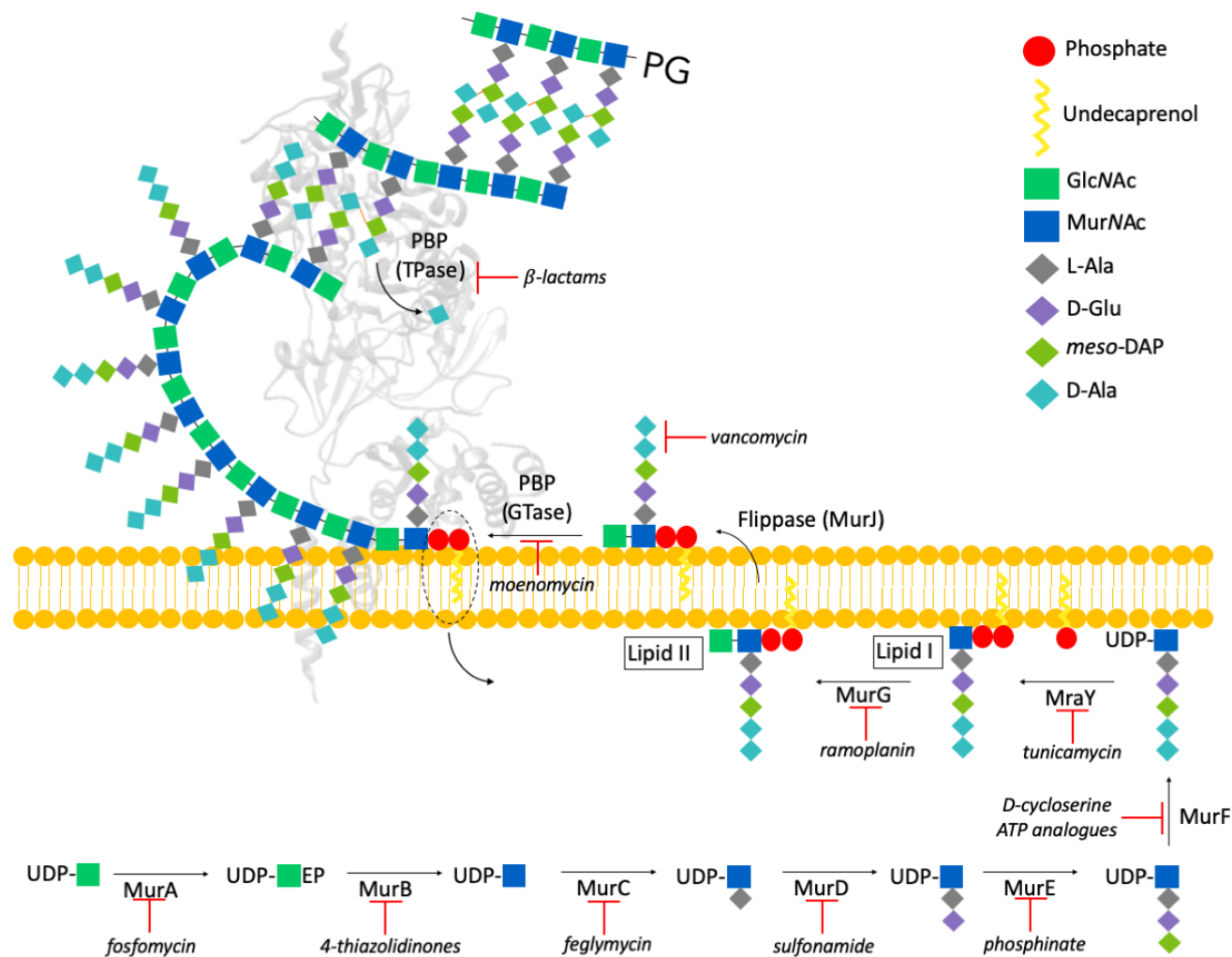


Figure 1.4. Schematic diagram of peptidoglycan biosynthesis in Gram-negative bacteria. Uridine diphosphate N-acetylglucosamine (UDP-GlcNAc), the product of the GlmSMU enzymes (not shown), enters the PG pathway when it is recognised as substrate by MurA. This enzyme catalyses the transfer of enolpyruvyl moiety from phosphoenolpyruvate (PEP) to UDP-GlcNAc with the release of inorganic phosphate. The resulting product undergoes a NADPH-dependent conversion to UDP-MurNAc, by the enzyme MurB. The MurNAc sugar is then connected to a pentapeptide stem, by the stepwise addition of amino acids in reactions catalysed by the Mur ligases (C, D, E, F) and requiring ATP. The first residue, L-alanine, is added by MurC followed by the addition of D-glutamic acid by MurD. The third amino acid is *meso*-DAP in most Gram-negative bacteria, and its incorporation into the peptide stem is catalysed by MurE. The final dipeptide D-ala-D-ala, that is pre-formed in the cell by an alanine racemase and a D-ala-D-ala ligase (not shown), is added to the peptide by MurF (Barreteau *et al.*, 2008). The phospho-MurNAc pentapeptide moiety is transferred onto an undecaprenyl phosphate carrier (C_{55} -P) by the translocase MraY

to produce undecaprenyl-pyrophosphoryl-MurNAc-pentapeptide (lipid I). Lipid I is used by MurG to generate the PG building block, namely undecaprenyl-pyrophosphoryl-MurNAc-pentapeptide-GlcNAc (lipid II), by transfer of the GlcNAc moiety from UDP-GlcNAc. The flippase MurJ translocates Lipid II across the cytoplasmic membrane so as it can be polymerised and cross-linked by PBPs to make peptidoglycan. The enzymes catalysing the reactions in the PG biosynthesis pathway are excellent candidates for antibiotic development, representative inhibitors are shown. Image adapted from Lovering *et al.* (2012).

1.2.1.2 Peptidoglycan biosynthesis in Gram-negative bacteria

The biosynthetic pathway of PG is a complicated process involving at least 15 enzyme reactions and taking place across three compartments, namely the cytoplasm, the cytoplasmic membrane and the extra-cytoplasmic space where PG resides. The PG synthesis begins in the cytoplasm, where the PG precursors UDP-GlcNAc and UDP-MurNAc-pentapeptide are synthesized in sequential steps by the GlmSMU and MurABCDEF enzyme systems, respectively, from fructose-6P (Barreteau *et al.*, 2008) (figure 1.4). At the inner leaflet of the inner membrane, the MurNAc-pentapeptide moiety is assembled with undecaprenyl phosphate lipid carrier (C-55 polyisoprenyl lipid) to form lipid I, by the integral membrane protein MraY. Then, the GlcNAc moiety is added to lipid I in a reaction catalysed by MurG, and the substrate for the synthesis of the PG polymer is generated, called lipid II (figure 1.4) (Bouhss *et al.*, 2007). Additionally, further modification such as the insertion of the pentaglycine bridge in *S. aureus* PG synthesis or the amidation of the C-1 carboxyl of the D-glutamyl residue in many Gram-positive organisms, occurs at this point (Bouhss *et al.*, 2007).

Lipid II is transported across the membrane by a flippase enzyme, whose identity has been much debated in the last decade (Ruiz, 2015; Mohammadi *et al.*, 2011; Ruiz, 2008; Inoue *et al.*, 2008). Although it was shown that FtsW can bind lipid II and work as a transporter *in-vitro* (Mohammadi *et al.*, 2011; Mohammadi *et al.*, 2014), it is now being accepted that, based on *in-vivo* and *in-vitro* studies, MurJ is the primary lipid II flippase in *E. coli* (Inoue *et al.*, 2008; Sham *et al.*, 2014; Rubino *et al.*, 2018; Qiao *et al.*, 2017; Bolla *et al.*, 2018; Liu *et al.*, 2018).

Lipid II is polymerized in the periplasm by glycosyltransferase enzymes, and the new glycan chains are inserted into the sacculus by the activity of transpeptidases (Lovering *et al.*, 2012; Egan *et al.*, 2015; Sauvage *et al.*, 2008) (figure 1.4).

The enzymes of the bacterial cell wall biosynthesis pathway are essential and most of them do not have counterparts in mammalian cells, which make them an excellent target in antibiotic development (Walsh, 2003; Kohanski *et al.*, 2010). The emergence of antibiotic resistance against clinically used drugs targeting the final

steps of PG synthesis (for instance β -lactam antibiotics targeting PBPs and vancomycin binding to lipid II), has prompted efforts to better characterise the other enzymes of the pathway for the discovery new antibacterial agents.

1.3 Penicillin binding proteins: a validated target for antibacterial therapy

1.3.1 The high-molecular weight PBPs

Penicillin binding proteins (PBPs) are a large enzyme family, located outside the cytoplasmic membrane where they catalyse important reactions for the final synthesis of peptidoglycan. PBPs have been the most successful and extensively targeted enzymes of the bacterial cell wall, since they are located in the periplasm and therefore, are more easily accessible to antibacterial agents. Moreover, they do not have mammalian homologs, hence the risk of unwanted side effects of drugs targeting these proteins is greatly reduced in human (Sauvage and Terrak, 2016; Zervosen *et al.*, 2012b).

Bacteria express a unique (species-specific) set of PBPs, and these enzymes have been classified according to their activity and sequence similarity (Sauvage *et al.*, 2008; Goffin and Ghuysen, 1998) (figure 1.5).

The high-molecular weight (HMW) PBPs are bitopic proteins, they are anchored to the cytoplasmic membrane via a single transmembrane helix, and perform the polymerisation of lipid II (transglycosylation, TG) and the peptide bond formation between glycan chain stem peptides (D,D-transpeptidation, TP). The low-molecular weight PBPs are required for PG maturation and recycling, and cell separation (Sauvage *et al.*, 2008); their activities modulate the degree of cross-linking in PG, and are dispensable in laboratory conditions (Denome *et al.*, 1999). The LMW-PBPs are associated either with the membrane or the PG, and are specialised in the catalysis of reactions such as D,D- carboxypeptidation and D,D-endopeptidation, causing the cleavage of the D-Ala₍₄₎-D-Ala₍₅₎ peptide bond of pentapeptide stems and the cleavage of the D-Ala₍₄₎-meso-DAP₍₃₎ peptide bond in cross-linked PG, respectively (Sauvage *et al.*, 2008).

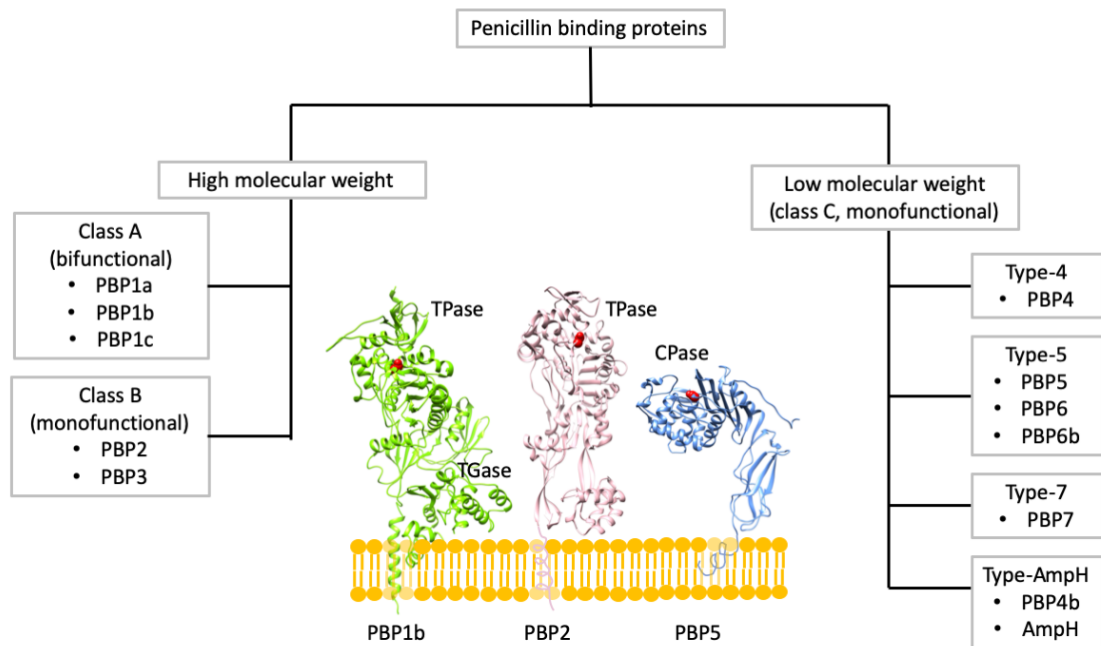


Figure 1.5. PBP classification in *E. coli*. Representative structures for each class are displayed, namely *E. coli* PBP1b (5FGZ.pdb), PBP2 (6G9P.pdb) and PBP5 (1NZO.pdb). The catalytic serine is coloured red.

The HMW-PBPs include the class A and class B PBPs. Class A PBPs (aPBPs) are bifunctional enzymes and include PBP1a, PBP1b and PBP1c in *E. coli* (figure 1.5). They possess two interconnected functional domains, a N-terminal glycosyltransferase domain that polymerises lipid II, and a C-terminal transpeptidase domain responsible for the formation of cross-links between glycan strands (figure 1.5). PBP1a and PBP1b perform partially redundant functions, since they are individually dispensable but deletion/inactivation of both proteins is lethal (Yousif *et al.*, 1985). Because PBP1a and PBP1b catalyse both TG and TP reactions, hence they are self-sufficient in making PG, they have been considered for long time as the principal enzymes for the PG synthesis in bacterial cell wall elongation (rod-shaped bacteria) and division.

The role of PBP1c in PG synthesis remains elusive, as this protein is thought not to be a functional transpeptidase *in-vivo* (Schiffer and Höltje, 1999). Instead, PBP1c could play a part in the periplasmic defence system together with bacterial α_2 -macroglobulins (protease inhibitors). Where the former would aid the repair of damaged PG by using its transglycosylase activity, the α_2 -macroglobulins protect bacteria from host proteases and proteases produced by other bacteria (Budd *et al.*, 2004; Schiffer and Höltje, 1999; Neves *et al.*, 2012).

Class B PBPs (bPBPs) are essential monofunctional enzymes and comprise PBP2 and PBP3 in *E. coli*. These proteins consist of a C-terminal transpeptidase domain, like aPBPs, and a N-terminal noncatalytic domain preceded by a transmembrane helix and a cytoplasmic tail, with roles in protein-protein interactions and regulation (figure 1.5) (Contreras-Martel *et al.*, 2017; Berg *et al.*, 2014). Since PBP2 and PBP3 lack a TG domain, they rely on the transglycosylase activity of other enzymes to produce the glycan strands, and this function has been recently attributed to the SEDS family (shape, elongation, division and sporulation) of proteins (Meeske *et al.*, 2016; Cho *et al.*, 2016). SEDS enzymes are integral membrane proteins known to interact with bPBPs (Fraipont *et al.*, 2011; Fay *et al.*, 2010; Taguchi *et al.*, 2019). RodA-PBP2 and FtsW-PBP3 are considered the key enzymes for PG synthesis in the cell wall elongation and division respectively (Emami *et al.*, 2017; Sjodt *et al.*, 2018; Rohs *et al.*, 2018, Taguchi *et al.*, 2019). Sporulating bacteria, such as *Bacillus subtilis*, possess an additional SEDS-bPBP complex represented by SpoVE-SpoVD that is active in spore formation. Interestingly, the SEDS proteins represent a new class of enzymes, since they exhibit a unique overall fold. Furthermore, they are insensitive to moenomycin, a phosphoglycolipid antibiotic that prevents lipid II polymerisation in aPBPs and monofunctional glycosyltransferases (MGTs), thus pointing out to a completely new mechanism for the catalysis of transglycosylation. The first structure of a SEDS enzyme, namely *Thermus thermophilus* RodA, has been recently determined (Sjodt *et al.*, 2018) representing a first step towards the understanding of the functioning of this new class of enzymes. Importantly, the SEDS proteins are considered a novel antibiotic target for the development of new antibacterial agents (Emami *et al.*, 2017).

1.3.2 PG synthase machineries

Currently, little is known about the fundamental mechanisms that allow bacteria to enlarge the cell wall and divide, while concurrently preserving the integrity of the cell wall itself to avoid osmotic rupture, and coordinate these processes with central metabolism (Typas *et al.*, 2012). It is now understood that cell wall elongation and division depend upon formation of large dynamic multiprotein complexes spanning

the cytoplasm, the cytoplasmic membrane, the periplasm and, in Gram-negative bacteria, also the outer membrane (Trip and Scheffers, 2015), as well as containing cytoskeletal elements and scaffolding structures with a central role in the temporal and spatial orchestration of PG morphogenesis for bacterial cell growth. Progress has been made to elucidate the composition and spatiotemporal construction of these complexes, through genetic, subcellular protein localization, biochemical and structural studies (Di Lallo *et al.*, 2003; Alexeeva *et al.*, 2010; Typas *et al.*, 2012; Egan *et al.*, 2015), although much still needs to be determined.

Cell wall division is essential in all bacteria, and relies on a large complex including more than 20 proteins, called the divisome (Errington *et al.*, 2003; Trip and Scheffers, 2015). The tubulin-like protein FtsZ polymerises on the inner side of the cytoplasmic membrane, and accumulates at the division site where they form a ring-like structure called the Z-ring. The Z-ring recruits a number of other division proteins, including the PG synthases PBP1b and FtW-PBP3 (figure 1.6) (Hugonnet *et al.*, 2016).

1.3.2.1 The elongasome

Cell wall elongation is an essential process in rod-shaped bacteria that is mediated by the elongasome, a multi-protein complex which synthesises and inserts new PG in the lateral cell wall (Typas *et al.*, 2012). The transpeptidase activity of PBP2 is essential in this complex, in fact either deletion of the PBP2 gene or enzyme inhibition by the PBP2 specific β -lactam mecillinam, induce a spherical morphology (Spratt, 1975; Legaree *et al.*, 2007). RodA and MreB are also essential proteins in cell wall elongation, and together with PBP2 constitute the core of the elongasome system (Rohs *et al.*, 2018). The actin-like protein MreB forms filaments throughout the cell cylinder, on the cytoplasmic side of the membrane, and coordinates PG synthesis through interaction with transmembrane proteins, such as MreC/MreD and RodZ (Typas *et al.*, 2012) (figure 1.6).

PBP2 interactions with the PG polymerase RodA likely map onto the N-terminal transmembrane helix (Sjodt *et al.*, 2018), while the pedestal domain is a docking site

1.3.2.2 Regulation of the PBP function

D,D-transpeptidases catalyse the final reaction in PG synthesis and are engaged in multiprotein complexes, where their activity is spatiotemporally controlled by regulatory mechanisms that remain unclear. So far, only a few mechanisms regulating the enzymatic activities of PBPs have been elucidated, and these include protein-protein interactions and post-translational modifications (Egan *et al.*, 2017).

The outer membrane lipoprotein cofactors LpoA and LpoB are essential for the *in-vivo* function of PBP1a and PBP1b, respectively, in *E. coli* and other Gram-negative bacteria (Typas *et al.*, 2010; Paradis-Bleau *et al.*, 2010). LpoA and LpoB interact with noncatalytic docking domains of PBP1a (OB domain) and PBP1b (UB2H domain), respectively, thus stimulating the enzyme TG and TP rates in *in-vitro* assays. PBP1b mutants that bypass LpoB requirement for *in-vivo* activity have also been isolated (Markovski *et al.*, 2016), and these mutants presumably adopt an activated conformation that does not require interaction with LpoB. In *P.aeruginosa*, the lipoprotein LpoP substitutes for the lack of LpoB, using a similar activation mechanism (Greene *et al.*, 2018). In *S. pneumoniae*, MacP is an activator of PBP2a (aPBP) and interaction is likely to occur at the TM domain or N-terminal cytoplasmic tail of the latter enzyme (Fenton *et al.*, 2018). Protein-protein interactions play also a crucial role in the localisation or spatial regulation of proteins of the PG synthases multi-protein complexes (Egan *et al.*, 2015).

The post-translational control of PBP function by phosphorylation and disulphide bond cleavage is uncommon, but there are a few cases reported in literature. The *in-vivo* activity of PonA1 (aPBP) in *Mycobacteria*, is modulated by phosphorylation of the cytoplasmic tail, although it is not clear how this modification affects the TG and/or TP activity of the protein (Kieser *et al.*, 2015). Another protein from the same organism is PBPA (bPBP), this is phosphorylated in the TP domain *in-vivo* and this modification seems to regulate the cellular localisation of the protein, although it is unclear whether or not it can also have an effect on the TP activity (Fedarovich *et al.*, 2010; Dasgupta *et al.*, 2006). Structures of *N. gonorrhoeae* PBP2 have revealed a

phosphorylation site in the TP domain, however, at the moment there are no *in-vivo* data supporting the biological relevance of this modification (Powell *et al.*, 2009). Some PBPs display disulphide bonds in their TP domain, and the *in-vivo* function is modulated by Cys oxidation and reduction, as is the case of *B. subtilis* SpoVD (bPBP) (Bukowska-Faniband and Hederstedt, 2017), and the same could also be true for *Mycobacterium tuberculosis* PBPA (bPBP) which presents a disulphide bond close to the catalytic site.

1.3.3 The reactions catalysed by PBPs

In bifunctional PBPs, TG and TP catalytic reactions are functionally coupled in that the N-terminal domain polymerises glycan chains from lipid II, and these are concurrently delivered to the C-terminal domain where cross-linking reactions take place. In fact, bifunctional PBPs inactivated in the TG domain are not able to cross-link pre-oligomerised glycan chains (Egan *et al.*, 2015). Conversely, monofunctional transpeptidases are able to cross-link glycan chains either produced by the SEDS proteins or other lipid II polymerases (Taguchi *et al.*, 2019) and regardless of the glycan chain provenience, the mechanisms of transpeptidation are conserved.

1.3.3.1 Transglycosylation

Class A PBPs and monofunctional glycosyltransferases possess a catalytic domain that polymerises lipid II, and this reaction is initiated by the binding of two lipid II molecules to the TG domain, one binding to the donor site and the other binding to the acceptor site. After the 4-OH of the acceptor lipid II GlcNAC is deprotonated by a conserved glutamate of the catalytic site, it performs a S_N2 -like nucleophilic attack on the C1 of the donor lipid II MurNAC, resulting in the formation of a $\beta 1-4$ glycosyl bond between donor and acceptor molecules (figure 1.7). The product of this reaction is called lipid IV and the negatively charged C_{55} -PP from the donor molecule is concurrently released. Lipid IV is then relocated from the acceptor to the donor site, so as to allow a new lipid II molecule to bind to the acceptor site and react with lipid IV/the growing glycan chain at the donor site (King *et al.*, 2017b; Barrett *et al.*, 2007; Lovering *et al.*, 2007).

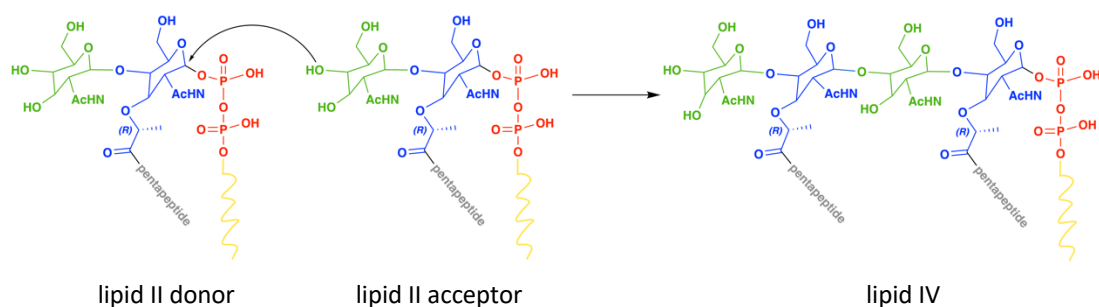


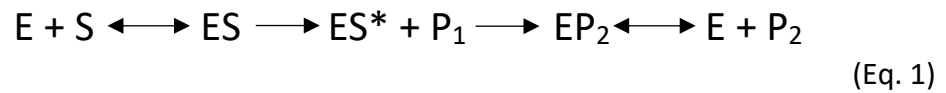
Figure 1.7. Schematic of the transglycosylase reaction

1.3.3.2 Transpeptidation and carboxypeptidation

HMW-PBPs possess a C-terminal domain where the final reaction of PG synthesis is catalysed, namely the peptide cross-linking of the lipid II polymers to the sacculus. The TP active site is located at the bottom of an elongated cleft, formed by an all- α subdomain and an α/β subdomain. The active site carries three strictly conserved motifs: Ser-X-X-Lys encompassing the catalytic serine, Ser-X-Asn/Asp and Lys-Thr/Ser-Gly-Thr, in addition to a conserved Gly located at the rear of the active site. These motifs play a role in the catalysis of the reaction and/or recognition and positioning of the substrate into the active site (Sauvage *et al.*, 2008). Although a full mechanistic understanding of the PBP catalysed reactions has not been achieved yet, a two-step model for D,D-transpeptidation and D,D-carboxypeptidation is generally accepted. A detailed description of the reaction mechanisms has been aided by structural studies of PBPs and β -lactamases with PG-mimetic peptidic substrates, β -lactam antibiotics and substrate-like peptide boronic acids (Nicola *et al.*, 2005; Sauvage *et al.*, 2007; McDonough *et al.*, 2002; Nicola *et al.*, 2010; Lee *et al.*, 2001; Macheboeuf *et al.*, 2008; Silvaggi *et al.*, 2003). Moreover, mutagenesis and kinetic studies of the LMW-PBPs specialised in D,D-carboxypeptidation (Nicholas *et al.*, 2003) and computational modelling of PBPs with substrates in different stages of the transpeptidase reaction (Shi *et al.*, 2011), have expanded knowledge on PBP catalysis.

In the acylation step, the donor glycan chain pentapeptide (L-Ala₍₁₎-γ-D-Glu₍₂₎-*meso*-DAP₍₃₎-D-Ala₍₄₎-D-Ala₍₅₎) (S) is accommodated into the binding cleft of a PBP enzyme (E), leading to the rapid formation of a noncovalent Henri-Michaelis complex (ES) (Eq. 1). The nucleophilic serine attacks the substrate on the carbonyl carbon atom of the penultimate D-Ala₍₄₎, resulting in a tetrahedral intermediate followed by a covalent acyl-enzyme complex (ES*) and release of the C-terminal D-Ala₍₅₎ (P₁) (Eq. 1) (Macheboeuf *et al.*, 2008). The activation of the catalytic serine as a nucleophile is mostly likely performed by the nearby Lys (S-X-X-K motif) that, deprotonated, can act as a general base and accept a proton (Gordon *et al.*, 2000; Lim and Strynadka, 2002; Nicola *et al.*, 2005; Macheboeuf *et al.*, 2006; Sauvage *et al.*, 2007). The collapse of the tetrahedral intermediate to generate the acyl-enzyme complex is caused by protonation of the C-terminal D-ala nitrogen atom. Different pathways for the leaving group protonation have been put forward, including a direct proton transfer from the protonated Lys of the S-X-X-K motif or the Lys from K-T/S-G-T motif, or even an indirect proton transfer from either lysine mediated by Ser of the S-X-N/D motif or an active site water molecule (Shi *et al.*, 2011).

In the deacylation step, the free amino group of *meso*-DAP₍₃₎ of an acceptor glycan chain peptide (L-Ala₍₁₎-γ-D-Glu₍₂₎-*meso*-DAP₍₃₎-D-Ala₍₄₎) (P₂), attacks the acyl-enzyme on the carbonyl carbon atom of the ester bond, although the exact activation mechanism by which the amino group acts as a nucleophile has yet to be established. The proton withdrawal from this group could be carried out by the Lys of the S-X-X-K motif, or the Ser of the S-X-N/D motif together with the Lys of the K-T/S-G-T motif, and this proton would be later back-donated to the active site serine (Goffin and Ghuysen, 1998; Nicola *et al.*, 2010; Sauvage *et al.*, 2008). This leads to formation of a tetrahedral intermediate complex followed by peptide bond formation between the donor D-Ala₍₄₎ and the acceptor *meso*-DAP₍₃₎ in a noncovalent complex between the enzyme and the PG product (EP₂) (4-3 cross-links), which culminates in the release of free enzyme (E) and the cross-linked PG (P₂) (Ghuysen, 1991, Goffin and Ghuysen, 1998) (Eq. 1) (figure 1.8).



In the absence of an acceptor peptide, a D,D-carboxypeptidase reaction takes place instead. The deacylation step is carried out by a nucleophilic water molecule, activated by a yet unclear mechanism, and resulting in the trimming of the donor peptide (from L-Ala₍₁₎-γ-D-Glu₍₂₎-*meso*-DAP₍₃₎-D-Ala₍₄₎-D-Ala₍₅₎ to L-Ala₍₁₎-γ-D-Glu₍₂₎-*meso*-DAP₍₃₎-D-Ala₍₄₎) (P₂) and release of free enzyme (E), that would otherwise be stalled in the acyl-enzyme (ES*) complex with consequent enzyme inhibition (figure 1.8) (Eq. 1) (McDonough *et al.*, 2002).

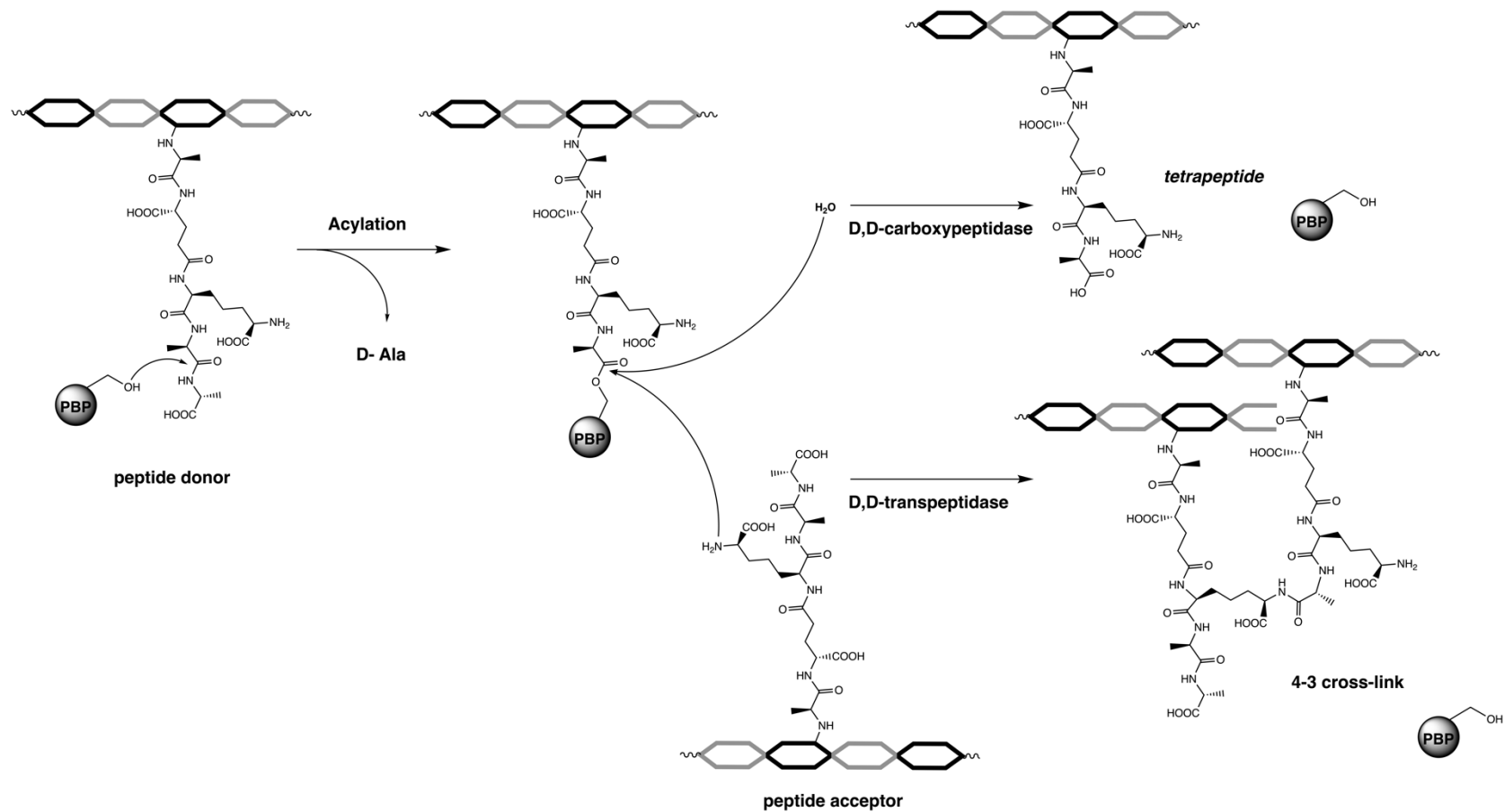


Figure 1.8. D,D-transpeptidation and D,D-carboxypeptidation catalysed by HMW-PBPs in Gram-negative bacteria.

1.3.4 Inhibition of the transpeptidase reaction

1.3.4.1 Mode of action of β -lactam compounds

β -lactam antibiotics are among the most used drugs to treat bacterial infections worldwide, since penicillin became commercially available in the 1940s (Kong *et al.*, 2010; Bush and Bradford, 2016). After the discovery of penicillin, semi-synthetic and synthetic derivatives of the beta-lactam core have been developed to either extend the spectrum of action of the molecule, or confer resistance to beta-lactamase hydrolysis, or both. The beta-lactam family of antibiotics includes several classes such as penicillins, cephalosporins, carbapenems and monobactams (Bush and Bradford, 2016) (table 1.3), which present different antimicrobial activities against both Gram-positive and Gram-negative bacteria.

β -lactam antibiotics possess chemical features that are critical for PBP inhibition. All β -lactam antibiotics contain a four-membered β -lactam ring that irreversibly binds to the TP active site of PBPs, thus preventing the formation of new PG cross-links and leading to weakening of the bacterial cell wall and ultimately cell lysis. The vast majority of β -lactam antibiotics are bicyclic molecules, where the β -lactam ring is fused to a second ring (thiazolidine ring in penicillins; pyrrolidine ring in carbapenems; dihydrothiazine ring in cephalosporins). The increased strain of the β -lactam ring reduces amide resonance and therefore increases the reactivity of the β -lactam ring towards nucleophiles compared to normal amides (Page, 1984). However, the bicyclic ring structure is not an absolute requirement for PBP inhibition, in fact, monocyclic β -lactams such as aztreonam can also bind to these proteins.

Beside the β -lactam ring, clinically used β -lactam antibiotics also possess a negatively charged group attached to the ring structure that is within 3.6 Å of the β -lactam carbonyl carbon, such as a carboxylic group in penicillins, cephalosporins and carbapenems and a sulfonic acid in monobactams, that mimics the C-terminal D-ala carboxylate of the PG stem peptide (Konaklieva, 2014). The presence of this ionizable group is an important recognition element in the TP site of PBPs, although a few studies have reported PBP inhibition by β -lactams bearing a neutral group such as an

amide and methyl ester (Dave *et al.*, 2013) and inhibition by β -lactone-based molecules (Sharifzadeh *et al.*, 2017).

The β -lactam core is connected to different R side chains and these are responsible for the different kinetics of PBP inactivation, antimicrobial activities and levels of resistance to β -lactamase hydrolysis (Zervosen *et al.*, 2012a).

The mode of action of β -lactam antibiotics has been first described by Tipper and Strominger (1965), who noticed the structural similarity between penicillin and the terminal dipeptide of the acetylmuramyl-pentapeptide substrate (figure 1.9). The fast acylation of PBPs by β -lactam antibiotics is therefore ascribed to these molecules acting as substrate analogues, but also as transition state analogue inhibitors, as they mimic the conformation in which the D-ala-D-ala forms a tetrahedral intermediate with the catalytic serine (Tipper and Strominger, 1965; Lee, 1971; Shi *et al.*, 2011). On the other hand, the slow deacylation of PBPs by these drugs which is cause of enzyme inactivation, is due to the formation of an inert complex following acylation of the catalytic serine, reason why β -lactam antibiotics are also considered as mechanism-based inhibitors (Nicola *et al.*, 2010; Silvaggi *et al.*, 2005).

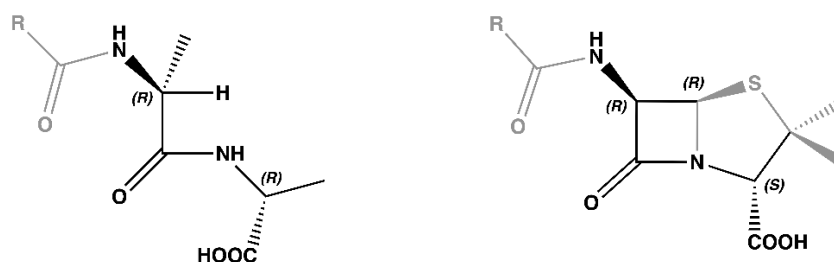


Figure 1.9. Structural similarity between the D-ala-D-ala termini of the PG stem pentapeptide and the β -lactam antibiotics.

The binding of β -lactam antibiotics to PBPs proceeds in a similar way as for the PG pentapeptide substrate. The catalytic serine performs a nucleophilic attack on the carbonyl carbon of the β -lactam ring, resulting in a tetrahedral intermediate, followed by formation of an acyl-enzyme complex (figure 1.10). In contrast to the PG substrate, deacylation of this acyl-enzyme complex by a hydrolytic water molecule or the terminal amino group of an incoming acceptor peptide, is precluded by the

steric hindrance of the pendant leaving group (the thiazolidine ring in penicillins), resulting in PBP inactivation (Nicola *et al.*, 2010; Silvaggi *et al.*, 2005; Page, 1984).

The antimicrobial activity of β -lactam antibiotics is ascribed to inhibition of the essential HMW-PBPs (aPBPs and bPBPs), whereas the LMW-PBPs are typically non-essential and represent a minor target. Since β -lactam antibiotics form a long-lived acyl-enzyme complex with PBPs, typically in the order of several hours (Bush, 2018) and the bacterial doubling time is approximately 30min, the mechanism of action of β -lactam antibiotics is considered irreversible. The lethal activity of this class of drugs arises from a blockage in the formation of new PG cross-links, resulting in an imbalance between the activities of PG synthases (HMW-PBPs) and PG hydrolases (LMW-PBPs), which leads to cell wall damage and ultimately cell lysis. Moreover, binding of β -lactam antibiotics to the TP active site of HMW-PBPs has been shown to induce a futile cycle of PG synthesis and turnover, that causes depletion of the PG precursors (i.e., lipid II) and disrupts PG synthesis in the elongasome and divisome systems, thus contributing to the bactericidal activity of this class of drugs (Cho *et al.*, 2014).

1.3.4.2 Non- β -lactam compounds

Besides β -lactams, there are other classes of molecules that can inhibit PBPs by covalently binding to the enzyme's catalytic Ser. One such type of molecules are lacticins, natural antibiotics consisting of a functionalised L-cycloserinyl ring linked to a γ -lactone ring (Nozaki *et al.*, 1987) (table 1.3). Acylation of PBPs occurs through the nucleophilic attack of the enzyme catalytic Ser-O γ on the L-cycloserine carbonyl carbon of lacticins, resulting in the opening of both L-cycloserine and γ -lactone rings (figure 1.10). Lacticins cause irreversible inhibition of PBPs and form with these enzymes stable covalent adducts that, similarly to β -lactam antibiotics, prevent deacylation by steric hindrance of the pendant leaving group (γ -lactone skeleton) (Macheboeuf *et al.*, 2007). Lacticins are active against Gram-negative and Gram-positive bacteria including penicillin-resistant strains of *S. pneumoniae*, and these molecules are sensitive to β -lactamase inactivation (Macheboeuf *et al.*, 2007).

The diazabicyclooctane (DBO) class constitutes another type of molecules that can covalently bind to the catalytic Ser of PBPs and inhibit transpeptidation, showing particular high binding affinity and specificity for PBP2 of rod-shaped Gram-negative bacteria (Papp-Wallace *et al.*, 2018). DBOs were initially studied as β -lactamase inhibitors, which culminated in the development of avibactam, the first DBO-based SBL inhibitor (Ehmann *et al.*, 2012). Structures and mechanism of action of DBOs will be described in chapter 4 of this thesis (4.3) (table 1.3)

Boronic acids are transition state analogues in which the boron atom can covalently bind to the catalytic Ser-O γ of β -lactamases and PBPs, thus forming a reversible tetrahedral complex that mimics the anionic tetrahedral intermediate generated during β -lactam acylation and hydrolysis (figure 1.10) (table 1.3). Boronic acids have been primarily studied as β -lactamase inhibitors, leading to the recent clinical introduction of vaborbactam, the first boronic acid used as inhibitor of SBLs (Dhillon, 2018). Due to the active site similarity between SBLs and PBPs, it is not surprising that boronic acids can also bind to and inhibit PBPs such as *E. coli* PBP5, *S. pneumoniae* PBP1b and *Actinomadura* R39 transpeptidase. Antimicrobial activity in Gram-positive bacteria, including MRSA, has also been shown (Contreras-Martel *et al.*, 2011, Nicola *et al.*, 2005, Woon *et al.*, 2011). Therefore, boronic acids seem to be promising PBP inhibitors which opens avenues for the development of this class of molecules as potential novel antibiotics.

1.4 Resistance mechanisms to β -lactam antibiotics

The widespread use of β -lactam antibiotics has led to the global emergence of bacterial resistance, where bacteria have evolved various mechanisms to protect themselves from the killing activity of these drugs. Bacteria use three main mechanisms to escape the action of β -lactam antibiotics and these are (i) antibiotic inactivation by β -lactamases, (ii) PBP modification to reduce β -lactam binding, and (iii) reduced uptake and increased efflux of β -lactams (King *et al.*, 2017a).

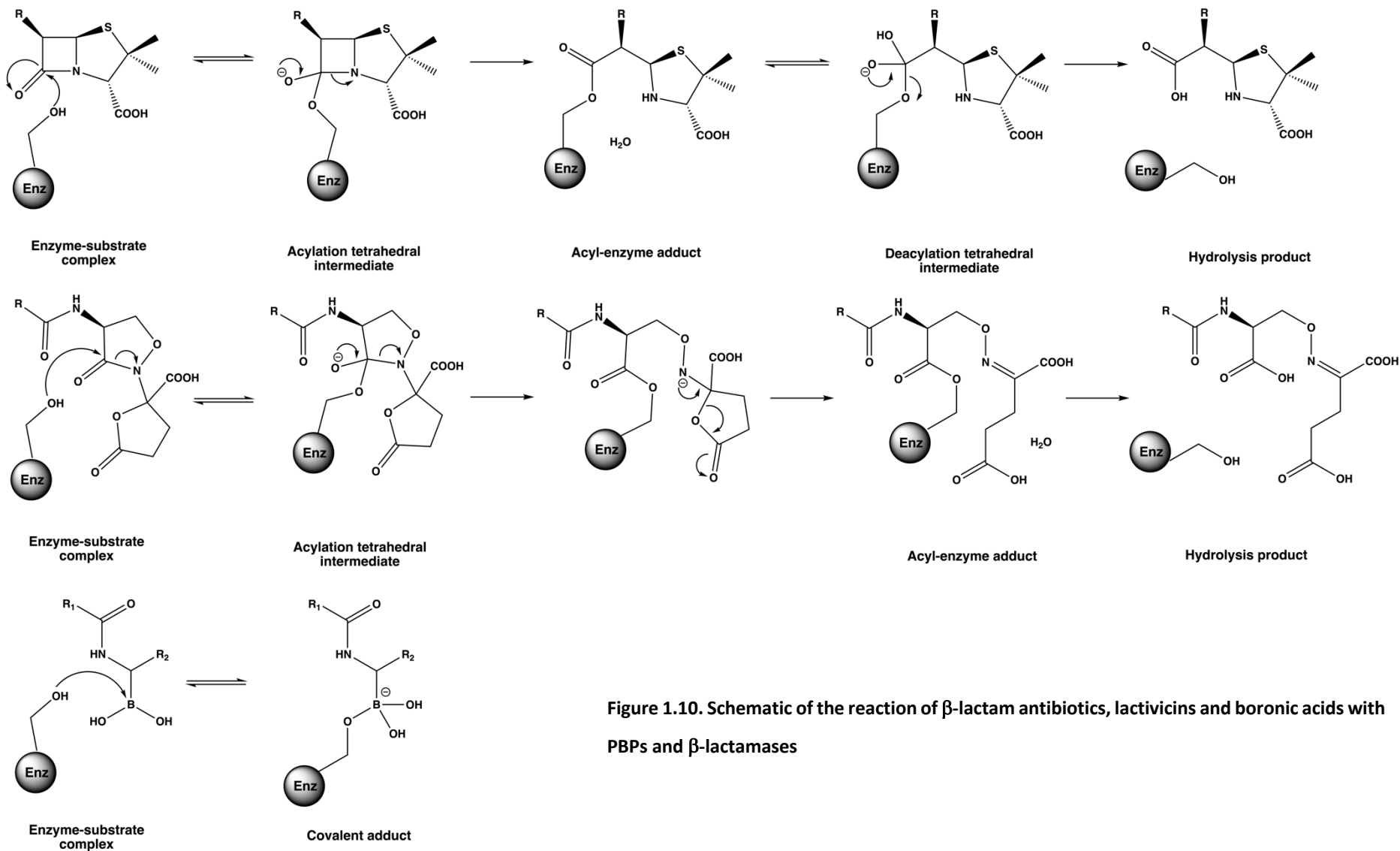
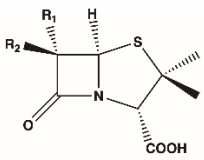
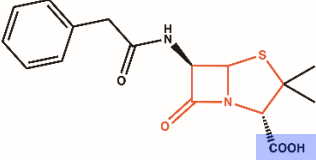
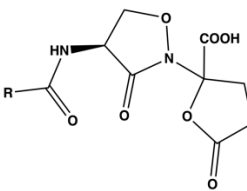
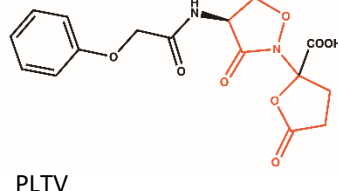
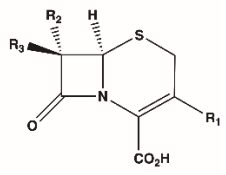
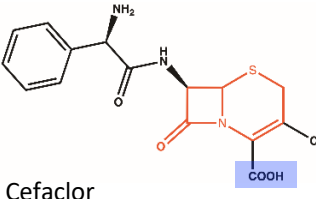
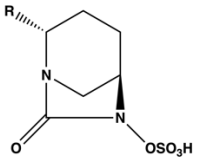
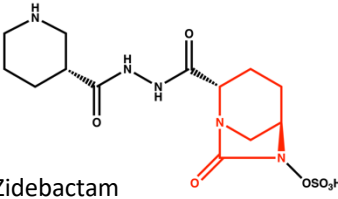
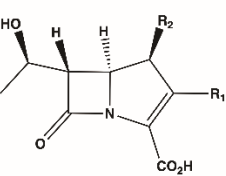
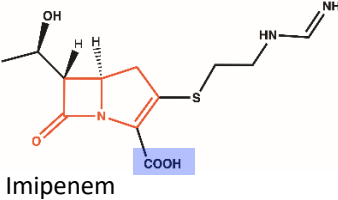
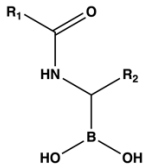
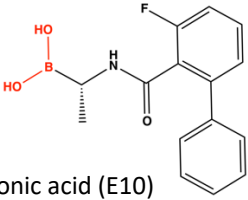
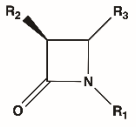
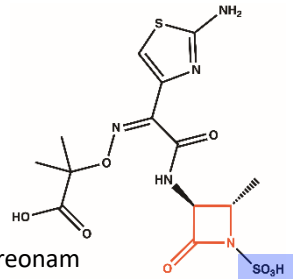


Figure 1.10. Schematic of the reaction of β -lactam antibiotics, lacticins and boronic acids with PBPs and β -lactamases

β-lactams	Non-β-lactams	
<p>Penicillins</p>   <p>Penicillin G</p>	<p>Lactvicins</p>   <p>PLTV</p>	
<p>Cephalosporins</p>   <p>Cefaclor</p>	<p>Diazabicyclooctanes</p>   <p>Zidebactam</p>	
<p>Carbapenems</p>   <p>Imipenem</p>	<p>Boronates</p>   <p>Boronic acid (E10)</p>	
<p>Monobactams</p>   <p>Aztreonam</p>	<p>Table 1.3. Representative structures of β-lactam and non-β-lactam compounds targeting PG transpeptidation. The active moiety of the molecules is highlighted in red, whereas the ionisable group of β-lactams that is important for enzyme recognition is highlighted in purple.</p>	

1.4.1 β -lactamases

β -lactamases are, by far, the major resistant determinant in Gram-negative bacteria, and these enzymes were discovered in the early 1940s just before the commercialisation of penicillin (Abraham and Chain, 1940), although many studies have shown that the origins of β -lactamases date back millions of years ago, and currently more than 2000 unique β -lactamases have been identified (Bush, 2018). Most of the β -lactamase genes are located on transmissible plasmids which are cause of increased spread of these resistance genes among bacteria, reason why it is not uncommon to find bacterial strains carrying multiple β -lactamases specific for a β -lactam subset (Bush, 2013b).

β -lactamases are specialised enzymes for the hydrolysis of the β -lactam ring in β -lactam antibiotics and produce inactivated drugs that can no longer inhibit PBPs. β -lactamases are typically grouped into four Ambler classes A-D based on amino acid sequence similarity (Ambler, 1980). Class A, C and D β -lactamases contain an active site serine, therefore called serine β -lactamases (SBLs), and they have evolved from PBPs with which they share highly conserved catalytic motifs (S-X-X-K, S/Y-X-N, KT/S-G-X) (Massova and Mobashery, 1998; Bush, 2013a). On the other hand, class B β -lactamases contain one or two functional zinc ions in their active sites, therefore called metallo β -lactamases (MBLs) and these are mechanistically and structurally distinct from PBPs and SBLs (Mojica *et al.*, 2016).

The catalytic mechanism of SBLs is similar to that of PBPs as it proceeds through the formation of an acyl-enzyme complex with the β -lactam (figure 1.10). However, β -lactamases use water molecules to quickly deacylate the enzyme-antibiotic covalent adducts, such that they can reach diffusion-limited reaction rates (Bulychev and Mobashery, 1999), resulting in β -lactam turnover and consequent antibiotic resistance (figure 1.10) (Drawz and Bonomo, 2010).

In contrast to SBLs, a different hydrolytic mechanism is used by class B enzymes to inactivate β -lactam antibiotics, consisting in the cleavage of the scissile amide bond

of the β -lactam by a nucleophilic hydroxide group from a water molecule, that is coordinated by zinc (Drawz and Bonomo, 2010).

Since the introduction of β -lactams into clinical practice as medicines to treat bacterial infections, new β -lactamases have emerged with evolved substrate specificities to counteract the selective pressure of newly developed β -lactam antibiotics. Clinically relevant β -lactamases that represent a great concern for the continued efficacy of β -lactams include the extended-spectrum β -lactamases (ESBLs) and the carbapenemases (Poole, 2004b). Examples include class A β -lactamases (TEM, SHV, and CTX-M) which show high hydrolytic efficiency towards extended spectrum cephalosporins, and KPC β -lactamases that are commonly found in carbapenem resistant bacteria, and can efficiently hydrolyse other β -lactam classes such as penicillins, cephalosporins and monobactams. Class C enzymes such as AmpC confer bacterial resistance to penicillins, whereas the class D β -lactamases are more heterogeneous with respect to substrate specificity, and can be active against penicillins and cephalosporins (OXA-type ESBLs), or carbapenems (OXA-type carbapenems). The class B enzymes (NDM, VIM and IMP) can inactivate almost all β -lactams but not the monobactams (Poole, 2004b; Bonomo, 2017; King *et al.*, 2017a).

The emergence of β -lactamase-mediated resistance stimulated the pharma industry to develop β -lactam antibiotics that are more stable to the β -lactamase activity, and β -lactamase inhibitors to be used in combination therapies with the no longer effective β -lactams. Currently available β -lactamase inhibitors include β -lactams (clavulanic acid, sulbactam and tazobactam) diazabicyclooctanes (avibactam), and boronic acids (vaborbactam) used in combination with β -lactam antibiotics, such as Augmentin (Amoxicillin and clavulanate), Avycaz (ceftazidime and avibactam) and vabomere (meropen and vaborbactam) (Drawz and Bonomo, 2010; Zhanel *et al.*, 2013; Dhillon, 2018).

1.4.2 Low-affinity PBPs

Bacterial resistance against β -lactam antibiotics can be caused by alteration of the PBPs, such that acylation and consequent inhibition by β -lactams is reduced, and this mechanism of resistance is highly frequent in Gram-positive bacteria. Low-affinity PBPs can be either acquired from other bacterial species, as is the case of *S. aureus* PBP2a, or derived from recombination or mutation events, as is the case of *S. pneumoniae* PBP2x and PBP2b and *N. gonorrhoeae* PBP2 (Grebe and Hakenbeck, 1996; Takahata *et al.*, 2006). This mechanism of resistance is becoming more common in Gram-negative bacteria too, including *E. coli*, *P. aeruginosa* and *H. influenzae* (Dabernat *et al.*, 2002; Clark *et al.*, 2019; Alm *et al.*, 2015).

PBP2a is the enzyme responsible for the broad spectrum β -lactam resistance in methicillin-resistant *S. aureus* (MRSA), as it provides transpeptidase activity even at clinically relevant β -lactam concentrations due to its low affinity for these drugs. PBP2a is resistant to inhibition by available β -lactam antibiotics and its encoding gene *mecA* is carried on a large mobile genetic element that could have been acquired from coagulase-negative staphylococcus species by horizontal gene transfer (Shore and Coleman, 2013). PBP2a function is controlled by an allosteric mechanism; When the targeting of the PBP2a allosteric site by molecules such as quinazolinones is combined with the targeting of the TP active site by β -lactam antibiotics, it produces a bactericidal synergy. This indicates that the allosteric site of PBP2a could be a potential target for the development of new effective drugs against MRSA (Janardhanan *et al.*, 2019).

1.4.3 Outer membrane porins

Another well-known mechanism of resistance to antibiotics, including β -lactams, in Gram-negative bacteria consists in the modification of the outer membrane permeability. The OM is a selective permeability barrier that controls the influx of molecules inside the bacteria, therefore allowing the entry of nutrient molecules while excluding environmental toxic compounds. Transport of β -lactams through this barrier is mediated by porins, such as the *E. coli* OmpF and OmpC, that are OM

β -barrel proteins forming aqueous channels through which hydrophilic molecules approximately < 700 Da can diffuse (Nikaido and Vaara, 1985; Jaffe *et al.*, 1982). β -lactam antibiotics in their zwitterionic form (such as ampicillin and imipenem) typically diffuse at higher rates compared to anionic β -lactams (such as carbenicillin and piperacillin) due to the simultaneous interaction with positively and negatively charged residues within the porins (Yoshimura and Nikaido, 1985). Antibiotic resistant bacteria can impair the porin-mediated diffusion of β -lactams by loss of porins or reduced expression thereof, and mutations that alter the porin structure and function (Nikaido, 2003). *P. aeruginosa* is an opportunistic pathogen recognised as a major cause of nosocomial infections and the leading cause of morbidity and mortality in cystic fibrosis patients. Its intrinsic resistance to a wide range of antibiotics is contributed by the lack of high-permeability porins combined with an efficient drug efflux system (Nikaido, 2003; Poole, 2001).

To overcome the problem of low OM permeability in Gram-negative bacteria, strategies based on the use of siderophores as a means of drug delivery have been explored since the 1980s. Siderophores are small iron chelating molecules secreted by bacteria to acquire this essential nutrient from the environment, and include hydroxamates, catecholates and carboxylates (Neilands, 1995). The bacterial iron uptake system can therefore be exploited for the transport of siderophore-conjugated β -lactams across the OM (Möllmann *et al.*, 2009). A number of these antibiotic conjugates have been investigated so far, leading to the development of BAL30072, a monobactam conjugated to a dihydroxypyridone siderophore, active against MDR Gram-negative bacteria and currently in clinical development (Page *et al.*, 2010).

1.4.4 Efflux pumps

Gram-negative bacteria possess active transport systems for the export of noxious compounds including antimicrobials, thus representing another mechanism by which bacteria can escape the bactericidal activity of antibiotics such as β -lactams (Poole, 2004a). These extrusion systems consist in multidrug efflux pumps located in the inner membrane, that use either ATP hydrolysis (ABC transporter) or

electrochemical gradients (RND/MFS/MATE/SMR transporters) as the driving force for efflux, and their activity can lower antibiotic concentration to sub-toxic levels (Du *et al.*, 2018). Upregulation of the efflux systems is observed in MDR bacteria such as *A. baumannii*, that is an opportunistic pathogen and a common cause of healthcare-associated infections worldwide, for which limited effective therapeutic treatments are available (Vila *et al.*, 2007). The overproduction of efflux pumps together with a reduced expression of porins, make the OM a nearly impenetrable barrier, as increasingly found in clinically relevant drug resistance (Poole, 2004a).

Currently, there are no efflux pump inhibitors for clinical use, although there is extensive research in this area and several compounds with promising inhibitory activity against efflux pumps are being investigated (King *et al.*, 2016).

1.5 Thesis aims

Molecular modelling and crystallographic studies of PBPs are playing an important role in the elucidation of the molecular basis of antibiotic resistance caused by mutations of these protein targets, as well as supporting the rational design of new inhibitors with desired selectivity towards biologically relevant mutants or specific PBP isoforms. Despite the conservation of sequence motifs, the catalytic site of PBPs from different classes presents some structural diversity, that would possibly reflect differences in the catalytic activities and contexts in which PBPs operate within the cell wall. Elucidation of such structural differences would help rationalise the protein functions and targeting by different classes of molecules, that could inform the development of the next generation of PBP inhibitors.

The objectives of this thesis are to generate structural information on novel and pre-existing structures of HMW-PBPs from *A. baumannii* and *P. aeruginosa*, alone and in complex with clinically relevant molecules, by using X-ray crystallography. Additional biochemical and biophysical characterisation of such proteins in the presence of various ligands, and *in-vivo* studies, will also provide complementary information to the structural data and detailed structure-function understanding of selective HMW-PBPs.

CHAPTER 2

Materials and methods

All reagents for media and buffer preparation were purchased at the highest available purity from Fisher Scientific, Sigma-Aldrich, and Melford, unless otherwise stated.

2.1 Growth and maintenance of *E. coli* strains

2.1.1 Bacterial cloning and expression strains

Bacterial cloning and expression strains used in this project are listed in table 2.1.

<i>E. coli</i> strain	Genotype	Reference
Top 10	F ⁻ <i>mcrA</i> Δ(<i>mrr-hsdRMS-mcrBC</i>) ϕ80 <i>lacZ</i> ΔM15 Δ <i>lacX74 recA1 araD139</i> Δ(<i>ara-leu</i>)7697 <i>galU galK</i> λ ⁻ <i>rpsL(Str^R) endA1 nupG</i>	(Grant <i>et al.</i> , 1990)
BL21(DE3)	F ⁻ <i>ompT hsdS_B (r_B⁻, m_B⁻) gal dcm</i> (DE3)	(Studier and Moffatt, 1986)
C41(DE3)	F ⁻ <i>ompT hsdS_B (r_B⁻, m_B⁻) gal dcm</i> (DE3)	(Miroux and Walker, 1996)

Table 2.1. Cell strains used in this study

2.1.2 Growth media

- Luria-Bertani (LB) media: 1 % (w/v) tryptone, 1 % (w/v) NaCl, 0.5 % (w/v) yeast extract.
- LB agar plate: 1 % (w/v) tryptone, 1 % (w/v) NaCl, 0.5 % (w/v) yeast extract, 1.5 % (w/v) agar
- ZY media: 1 % (w/v) N-Z amine (peptone from casein), 0.5 % (w/v) yeast extract
- Autoinduction media (Studier, 2005): 1x NPS (20x NPS stock solution: 0.5 M (NH₄)₂SO₄, 1 M KH₂PO₄, 1 M Na₂HPO₄), 1x 5052 (50x 5052 stock solution: 25 % (w/v) glycerol, 2.5 % (w/v) glucose, 10 % (w/v) α lactose, 10 mM MgSO₄, 92 % (v/v) ZY media.

2.1.3 Transformation of bacterial strains

Transformations were performed with competent *E. coli* cells obtained through the rubidium chloride method (Corporation *et al.*, 1996). Competence was induced by heat-shock treatment at 42 °C for 45 s. Transformed bacteria were plated on LB agar plates, with the appropriate antibiotic for selection of bacteria containing the plasmid.

2.2 DNA manipulation and cloning

2.2.1 Polymerase chain reaction (PCR)

PCR amplification of selected nucleotide sequences from either genomic DNA or gBlocks® gene fragments (Integrated DNA Technologies, IDT) was performed using Phusion® High-Fidelity DNA polymerase (New England BioLabs, NEB) according to the manufacturer's instructions. PCR amplification was carried out in the SureCycler 8800 Thermal Cycler (Agilent Technologies) under the conditions illustrated in table 2.2. Primers were designed and purchased from IDT.

Step	Temperature	Duration
Initial denaturation	98 °C	5 min
x 35 cycles	98 °C	30 s
	50-60 °C	30 s
	72 °C	2 min
Final Extension	72 °C	5 min
Hold	4 °C	∞

Table 2.2. PCR programme

2.2.2 Agarose gel electrophoresis

Gels were made with 0.8 % (w/v) agarose (Clever Scientific) dissolved in 1x Tris acetate EDTA (50x TAE stock solution: 2 M Tris, 1 M acetic acid, 50 mM EDTA).

GelRed 10000x in water (Biotium) was used for DNA staining, and 1 kb DNA ladder (NEB) was used as molecular weight standard. DNA samples were loaded with 1x gel loading dye (purple, NEB) and the electrophoresis was run in 1x TAE buffer at 120 V for 1 hour. DNA fragments were visualized by illumination of the gel under ultraviolet light in a G:Box bioimaging system (Syngene).

2.2.3 DNA purification

Purification of DNA sequences was performed either with the QIAquick PCR purification kit or the QIAquick gel extraction kit (Quiagen), following the manufacturer's instructions.

2.2.4 Plasmid purification

Plasmid purification was performed with the QIAprep spin miniprep kit (Quiagen) following the manufacturer's guidelines.

2.2.5 DNA quantification

DNA concentration was measured using a Nanophotometer N60 UV/Vis spectrophotometer (Geneflow) at 260 nm.

2.2.6 Restriction enzyme digestion of DNA

DNA fragments amplified by PCR and provided with the appropriate restriction sites to the 5' and 3' end, and plasmid vectors were cleaved with the appropriate restriction endonucleases (NEB), to give DNA with complementary "sticky" ends. Restriction digestion of DNA was carried out as per the manufacturer's instructions, at 37 °C overnight. DNA concentration was measured using a Nanophotometer N60 UV/Vis spectrophotometer (Geneflow) at 260 nm.

2.2.7 Ligation of DNA fragments with complementary ends

DNA fragments and plasmid vectors resulting from restriction digestion were ligated in frame by using the T4 DNA ligase (New England BioLabs) according to the manufacturer's instructions, at room temperature for 1 h. The ligation

reaction was used to transform *E. coli* Top10 competent cells, and colonies were screened for the presence of the DNA insert by either colony PCR (Azevedo *et al.*, 2017) or restriction digestion of the isolated plasmid.

Insertion of the cloned gene, reading frame, and correct sequence were checked by sequencing (GATC Biotech, Germany), prior to any expression test.

2.2.8 Site-directed mutagenesis

Mutations in the genes of interest were introduced by using the Q5 site-directed mutagenesis kit (New England BioLabs) and following the manufacturer's instructions. Design of mutagenic primers was supported by the use of NEBaseChanger (<http://nebasechanger.neb.com/>).

2.3 Protein expression, purification and analysis

2.3.1 Expression of recombinant plasmids

Competent cells of the chosen expression strain were transformed with the recombinant plasmid. Transformed cells were first grown at 37 °C on LB agar plates supplemented with antibiotic (working concentrations: kanamycin 50 µg/mL, ampicillin 100 µg/mL, chloramphenicol 25 µg/mL), used as selection marker by the specific vector.

A single colony was inoculated into 75 mL of fresh LB medium supplemented with the appropriate selective antibiotic. After overnight growth at 37 °C with shaking (180 rpm, shaker incubator Innova®44), 7 mL of the starter culture were transferred to a baffled flask containing 1 L of fresh medium and selective antibiotic.

IPTG induction- The larger culture was grown in LB medium at 37 °C with shaking (180 rpm) to a density of OD₆₀₀ 0.6 and cooled down at 4 °C for 1 h, at which point expression of recombinant protein was induced by addition of IPTG to 1 mM. The culture was incubated at 25 °C with shaking (180 rpm) overnight.

Autoinduction- The larger culture was grown in autoinduction media and the same procedure described for IPTG induction was followed, except addition of IPTG was omitted.

2.3.2 Cell harvesting and cell lysis

Bacterial cells from 1 litre cultures, were harvested by centrifugation at 4000 rpm in a JLA-8.1000 rotor for 20 min at 4 °C. Cell pellets were stored at -20 °C until use.

Frozen pellets were thawed on ice prior to lysis. Cells were resuspended in 7 volumes (v/w) of binding buffer, whose composition is given for each purified protein in the appropriate experimental chapter of this thesis, supplemented with 20 µg/mL DNase I from bovine pancreas (Sigma). The resuspended cells were sonicated on ice, 10 times at 70 % amplitude for 30 s separated by 1 min cooling interval on ice, using a Bandelin sonopuls sonicator.

Cell lysate was clarified by centrifugation at 4 °C for 45 min in a JA-25.50 rotor at 20000 rpm. The supernatant was filtered with a 0.2 µm syringe filter (Sartorius), and loaded onto the appropriate affinity chromatography column.

2.3.3 Immobilized metal ion affinity chromatography (IMAC)

A HisTrap HP 5 mL column (GE Healthcare) was pre-equilibrated with 6 CV of binding buffer. The column was connected to an ÄKTA pure chromatography system (GE Healthcare) and washed with binding buffer until the A_{280} reached values close to zero. Recombinant proteins were eluted with elution buffer, containing the desired concentration of imidazole, using one of the following methods.

Method 1 - linear gradient (0 % v/v -100 % v/v elution buffer) for 22 column volumes (CV).

Method 2 - linear gradient (0 % v/v -10 % v/v elution buffer) for the first 3 CV, step (10 % v/v elution buffer) for 4 CV, linear gradient (10 % v/v -100 % v/v elution buffer) for 6 CV, and a final step (100 % v/v elution buffer) for 5 CV.

Column washing and protein elution were carried out at 2 mL/min flow rate, at room temperature.

2.3.4 Glutathione affinity chromatography

A GSTrap HP 5 mL column (GE Healthcare) was pre-equilibrated with 6 CV of binding buffer. After loading the supernatant, the column was washed with binding buffer to remove unbound protein. Recombinant proteins were eluted with 100 % (v/v) elution buffer, which contains glutathione, using an AKTA system.

Column washing and protein elution were carried out at 1 mL/min flow rate, at room temperature.

2.3.5 Size exclusion chromatography

Where necessary, size exclusion chromatography was employed to increase purity of the recombinant protein resulting from affinity chromatography techniques. Fractions containing protein were pooled and concentrated to 5 mL using an Amicon® centrifugal filter unit (Merck Millipore) at 3300 rpm and 4 °C. Protein was loaded onto a HiLoad Superdex 200 16/600 gel filtration column (GE Healthcare) pre-equilibrated in running buffer, whose composition is given for each purified protein in chapters 3-5. Recombinant proteins were eluted with 1 CV of running buffer at 1 mL/min flow rate and selected fractions were pooled and concentrated as required by the final use of the protein.

2.3.6 Protein electrophoresis

Protein samples were analysed by sodium dodecyl sulphate polyacrylamide gel electrophoresis (SDS PAGE). Runs were performed at 5 V/cm in the stacking gel, and 15 V/cm in the resolving gel. Gels were stained with Instant Blue (expedon)

and imaged with a Gel Doc XR+ (Bio-Rad). Reagents for gel preparation, loading buffer and running buffer are detailed below:

- *stacking gel*: 0.125 M Tris-HCl pH 6.8, 0.1 % (w/v) SDS, 13.4 % (v/v) acrylamide/*bis*-acrylamide (30 % /0.8 % w/v), 0.1 % (w/v) ammonium persulfate (APS), 0.1 % (v/v) *N,N,N',N'*-Tetramethylethylenediamine (TEMED).
- *10%/12% acrylamide separating gel*: 0.39 M Tris-HCl pH 8.8, 0.1 % (w/v) SDS, 34%/40 % (v/v) acrylamide /*bis*-acrylamide (30 % /0.8 % w/v), 0.1 % (w/v) APS, 0.1 % (v/v) TEMED.
- *running buffer*: 0.025 M Tris, 0.2 M glycine, 0.05 % (w/v) SDS.
- *loading buffer*: 55 mM Tris pH 6.8, 1.6 % (w/v) SDS, 8.3 % (v/v) glycerol, 0.002 % (w/v) Bromophenol Blue, 5 % (v/v) β -mercaptoethanol.
- *molecular weight marker*: colour prestained protein standard 11-245 kDa (NEB).

2.3.7 Protein quantification

Quantification of pure proteins was carried out by measuring the absorbance at 280 nm, using a Nanophotometer N60 UV/Vis spectrophotometer (Geneflow), given known protein molecular weight and molar extinction coefficient.

A Bio-Rad protein assay (Bio-Rad) was used when the composition of a protein sample was unknown, following the manufacturer's instructions.

2.4 Protein structure determination by X-ray crystallography

2.4.1 Screening of crystallisation conditions

The initial screening of crystallisation conditions for proteins described in chapter 3 and 5, was carried out by using the sitting drop vapour diffusion technique and commercially available crystallisation screens. Protein was concentrated to at least 10 mg/mL, and drops consisting of half protein stock solution and half mother liquor, were set up in 96-well crystallisation plates with a 2-drop chamber (Hampton Research), by using a Mosquito LCP crystallisation robot (TTP Labtech). Drop size was either 200 nL, 400 nL or 600 nL, and the mother liquor volume in the reservoir

chamber was 50 μ L. Crystallisation plates were sealed with qPCR sealing film, and stored at either room temperature, 18 °C or 4 °C.

2.4.2 Optimisation of crystallisation conditions

From the initial screening matrix, those crystallisation conditions yielding protein crystal hits were optimised by creating a new matrix of conditions where components present in the coarse condition (concentration and type of precipitant, pH, ion concentration) were incrementally and systematically varied. Refinement of conditions also involved addition or variation of additives, temperature change, modification of sample volume or methodology.

2.4.3 Crystal seeding

A seed stock was made from crystals of interest by using a seed bead kit (Hampton Research). The drop containing crystals was diluted in its reservoir solution (50 μ L) and then transferred into a seed bead tube kept on ice. Crystals were pulverised by vortexing, and serially diluted in crystallisation solution at ratio of 1:10. Seed solutions were flash-cooled in liquid nitrogen and stored at -80 °C.

Seeding experiments were carried out in 96-well plates, with drops consisting of 300 nL protein solution, 200 nL mother liquor and 100 nL of diluted seed solution (typically diluted by 10^{-2} , 10^{-3}).

2.4.4 Crystal harvesting, soaking and cryo-cooling

Crystals of interest were harvested from the drop by using cryogenic loops of compatible size (0.05 -1 mm typically) connected to a metal pin and a magnetic base (Litholoop from Molecular Dimensions; Mounted CryoLoop from Hampton Research). The crystallisation plate well containing crystals was open, and 1-2 μ L of mother liquor was immediately added to the drop, in order to avoid excessive evaporation. Crystals were then briefly soaked in a 1-2 μ L drop of cryoprotectant solution, that is the crystallisation condition supplemented with a cryoprotectant, or soaked for longer time in a cryoprotectant solution containing ligands of interest,

and finally vitrified in liquid nitrogen and placed into a unipuck. Unipucks were stored in liquid nitrogen until the synchrotron visit.

2.4.5 Collection of X-ray diffraction data

Diffraction data acquisition for all proteins crystallised in this thesis, was carried out at Diamond Light Source synchrotron (Harwell Science & Innovation Campus, Oxfordshire, UK) (DLS), at beamlines I03, I04, and I04-1. Diffraction images were collected either *in-situ* or remotely.

Unipucks containing crystals were transported to the synchrotron in a dry shipping dewar, inside a shelved shipping cane. Unipucks were loaded into the BART sample changer, samples were registered in the ISPyB (information system for protein crystallography beamlines) and data collection was started.

For each sample, the crystal was automatically or manually centred, and two images at 90° apart were taken to evaluate its diffraction quality. Where diffraction was good, one or more datasets per crystal were collected by changing exposure time, starting position or crystal centring.

2.4.6 Processing of X-ray diffraction data

2.4.6.1 Diffraction image processing with iMosflm

X-ray diffraction datasets collected at the synchrotron beamlines were downloaded from the Diamond file system, and processed with iMosflm (Battye *et al.*, 2011). After the backstop shadow and the resolution limits were set, images were then ready to be processed by iMosflm as follows:

Indexing- two images ~ 90° apart in φ were automatically selected by iMosflm and indexed. Spots found in the selected images, that were above a certain threshold $I/\sigma(I)$, were used to determine the Bravais lattice symmetry, and a list of solutions sorted on increasing penalty score was given as output. Typically, the highest symmetry solution with low penalty (< 20) and small $\sigma(xy)$ (error in predicted spot positions) was chosen in first instance. Mosaicity, a measure of crystal imperfections, was also estimated for a given solution.

Cell refinement- based on the symmetry chosen and the mosaicity, a series of images were automatically selected by iMosflm to refine crystal parameters, detector parameters, and mosaic spread.

Integration- Detector and crystal parameters were refined for each image of the dataset, while the unit cell dimensions were fixed during integration. Results were written in an output file (1.mtz), containing reflection indices with their intensities and standard deviations, for use in other programs of the ccp4 program suite (Winn *et al.*, 2011).

2.4.6.2 Data reduction: Pointless, Aimless, Ctruncate

The unmerged intensities contained in the output file of iMosflm (1.mtz) were processed with the data reduction module of ccp4 (Winn *et al.*, 2011) as follows:

Pointless- the Laue group symmetry was determined from the symmetry of the diffraction pattern (positions of the reflections in the reciprocal space lattice). For protein crystals, 11 Laue groups are possible (Evans, 2006).

Aimless- symmetry-related reflections were scaled and merged. This analysis provides measures of data quality, and assists in determining the effective resolution of the data set (Evans and Murshudov, 2013).

Ctruncate- measured intensities were converted to structure factors (2.mtz) (French and Wilson, 1978).

2.4.6.3 Cell content analysis- the Matthews coefficient

The Matthews coefficient was used to determine the most likely number of protein copies in the asymmetric unit (asu), to be used later on for molecular replacement (Kantardjieff and Rupp, 2003). In order to determine the asu composition, different numbers of macromolecules were fitted in the unit cell, and a likely solvent content for the possible cell compositions was calculated. Typically, the most likely number of macromolecules in the asu was the one giving ~50 % of solvent content. This analysis requires the scaled and merged data (2.mtz) and the amino acid sequence of the protein (.seq).

2.4.6.4 Maximum likelihood molecular replacement

Molecular replacement was used to solve the structure of all proteins crystallised in chapter 3 and 5, as protein homologs were available for use in PDB. Molecular replacement is based on the principle that, if a similar structure can be correctly oriented and positioned in the unit cell of the structure to be solved, it can be used as a starting point for phase calculation and refinement. It has been reported that, about two thirds of the structures deposited in PDB have been solved using MR (Long *et al.*, 2008).

Molecular replacement was carried out using Phaser (McCoy *et al.*, 2007), given the scaled and merged data (2.mtz), the search model (1.pdb) and sequence identity (%) with the target protein, the amino acid sequence of the target protein (.seq), and the number of macromolecules in the asu as indicated by the Matthews coefficient calculations. As a result of this analysis, the search model was fitted into the density map of the dataset (2.pdb).

2.4.6.5 Model building and refinement

Parrot- density modification was performed with the software Parrot (Cowtan, 2010), providing the MR model (2.pdb), the target protein sequence (.seq) and the scaled and merged data (2.mtz). Non-crystallographic symmetry (NCS) averaging was also included in the calculation, when more than one monomer was present in the asymmetric unit. This analysis lead to an improvement of the initial phases (3.mtz).

Buccaneer- an initial model of the target protein consistent with the electron density map, was generated with Buccaneer, an automated protein model building program (Cowtan, 2006). The analysis required the MR model (2.pdb), the target sequence (.seq) and the structure factor amplitudes and phase probability distributions (3.mtz). The result of the analysis was an atomic model of the target protein (3.pdb).

Coot & Refmac5- the initial protein model (3.pdb) was visually inspected in Coot (Emsley *et al.*, 2010), and manually built where necessary. The model was subjected to various cycles of building and refinement with Refmac5 (Murshudov *et al.*, 2011), and terminated when the R_{work} and R_{free} values could not be improved further. The

output of this analysis consisted in the final model of the protein target, and the final electron density map.

Figures of protein structures were generated either in PyMOL (The PyMOL Molecular Graphics System, Schrödinger, LLC) or Chimera (Pettersen *et al.*, 2004).

2.4.6.6 Model validation

Validation of the model was carried out using Rampage (Lovell *et al.*, 2003) and Procheck (Laskowski *et al.*, 1993). Before deposition in the Protein Data Bank (PDB), the model will also be validated using the wwPDB Validation Service (<https://validate.wwpdb.org>) (Smart *et al.*, 2018).

2.4.7 Collection of X-ray fluorescence data

X-ray fluorescence data were collected on protein crystals in order to identify the type of metal ion present in the structure discussed in chapter 3. Fluorescence data were collected on either a broad energy range (keV) to have an indication of the elements present in the crystal, or in edge scan mode, to look for specific elements. Data were collected at the DLS synchrotron.

2.5 Fluorescent and spectrophotometric assays

2.5.1 Bocillin-FL binding assay

Bocillin-FL (Thermo Fisher Scientific) is a fluorescent penicillin that can covalently bind to PBPs, thus allowing the fluorescent labelling of these proteins (Zhao *et al.*, 1999). Bocillin-FL was used to stain purified PBPs in SDS-PAGE gels, as a means of confirming the expression of the protein of interest, and the correct folding of the transpeptidase site. Prior to separation of the protein sample by SDS-PAGE (2.3.6), the sample was incubated with 10-fold molar excess of Bocillin-FL at 37 °C for 30 min and the reaction stopped by addition of loading buffer. Gels were imaged on a Typhoon FLA 7000 (GE Healthcare Life Sciences), with excitation at 488 nm and emission at 530 nm.

2.5.2 Differential scanning fluorimetry

Differential scanning fluorimetry is an established technique to assess changes in thermal stability of a protein upon interaction with a test molecule (Huynh and Partch, 2015). The protein thermal stability is measured by calculating the melting temperature (T_m), that corresponds to the maximum point of inflection of a thermal unfolding curve. Favourable interactions between protein and test molecule would generally result in increased thermal stability (increase of T_m); conversely, unfavourable interactions would cause protein destabilisation (decrease of T_m).

The DSF assay was used to measure the thermal stability of PBP2 wild-type and mutants, and after interaction with test molecules (chapter 3 and 4).

The reaction consisted of protein (10 μ M) or protein buffer (control), SYPRO Orange dye (10x) (Invitrogen), made up to 50 μ L volume with buffer (50 mM HEPES pH 7.5 and 400 mM NaCl). Molecules of interest were tested at the concentration stated in chapter 3 and 4. Fluorescence was measured in an optical 96-well plate (Bio-rad), sealed and heated in a real-time thermocycler (Agilent Technologies Stratagene Mx3005P) from 25 $^{\circ}$ C to 95 $^{\circ}$ C at a rate of 1 $^{\circ}$ C/min. Excitation and emission wavelengths were set to 492 and 610 nm, respectively. The assays were carried out in triplicate, and data analysis to retrieve the T_m for each sample was performed in GraphPad Prism, according to Huynh & Partch (2015).

2.5.3 Spectrophotometric assay with nitrocefin

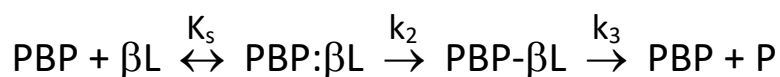
Nitrocefin (1) is a chromogenic cephalosporin that can react with the catalytic serine of PBPs and β -lactamases, resulting in a colour change from yellow to red following the opening of the β -lactam ring (figure 2.1) (O'Callaghan *et al.*, 1972). Nitrocefin can be used to study the activities of PBPs and β -lactamases and the reaction is monitored at 486 nm ($\epsilon = 20,500 \text{ M}^{-1} \text{ cm}^{-1}$).

The reaction is denoted by equation 1 (Eq.1), where PBP: β L is the non-covalent enzyme- β -lactam complex, PBP- β L is the acyl-enzyme complex, and P is the hydrolysed β -lactam antibiotic. The initial rate of formation of the covalent complex is described by the second-order acylation rate constant k_2/K_s , where $K_s = k_{-1} + k_2/k_1$, under subsaturating concentrations of the β -lactam. Reaction with PBPs mostly

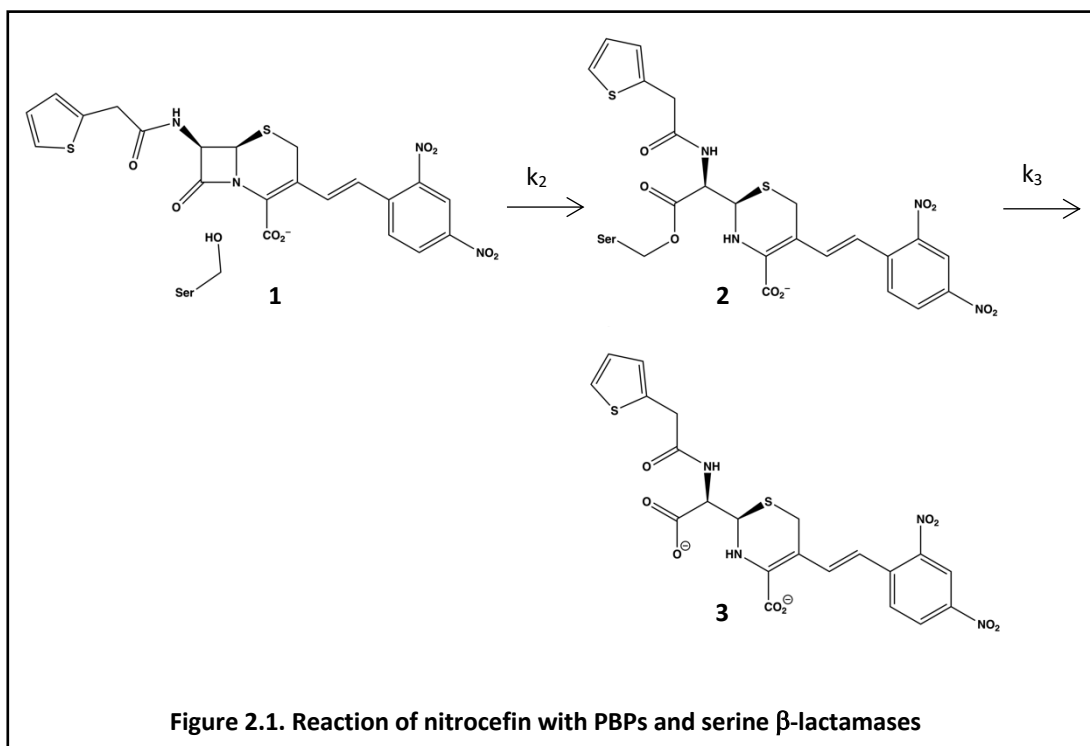
results in species (2), as the deacylation rate k_3 is typically very slow, whereas β -lactamases hydrolyse β -lactams quickly generating species (3) (figure 2.1).

This assay was used to measure the hydrolysis turnover of nitrocefin by PBP2_{WT} and mutants (chapter 3). The initial linear rate of the graph ($\Delta\text{Abs}/\text{min}$) of nitrocefin reacted with PBP2, was representative of the deacetylation rate given that, the acylation reaction was almost immediate upon addition of nitrocefin, causing an absorbance increase consistent with protein concentration.

The reaction consisted of protein (10 μM) and nitrocefin (200 μM), up to a volume of 100 μL in buffer (50mM HEPES pH 7.5 and 400mM NaCl). The assay was performed in 50 μL quartz cuvettes, using a Cary 100 Bio UV-Vis spectrophotometer at 30 $^\circ\text{C}$. Following addition of nitrocefin, the acetylation of PBP2 was immediate and the deacetylation rate was calculated from taking the initial linear rate ($\Delta\text{Abs}/\text{min}$).



(Eq.1)

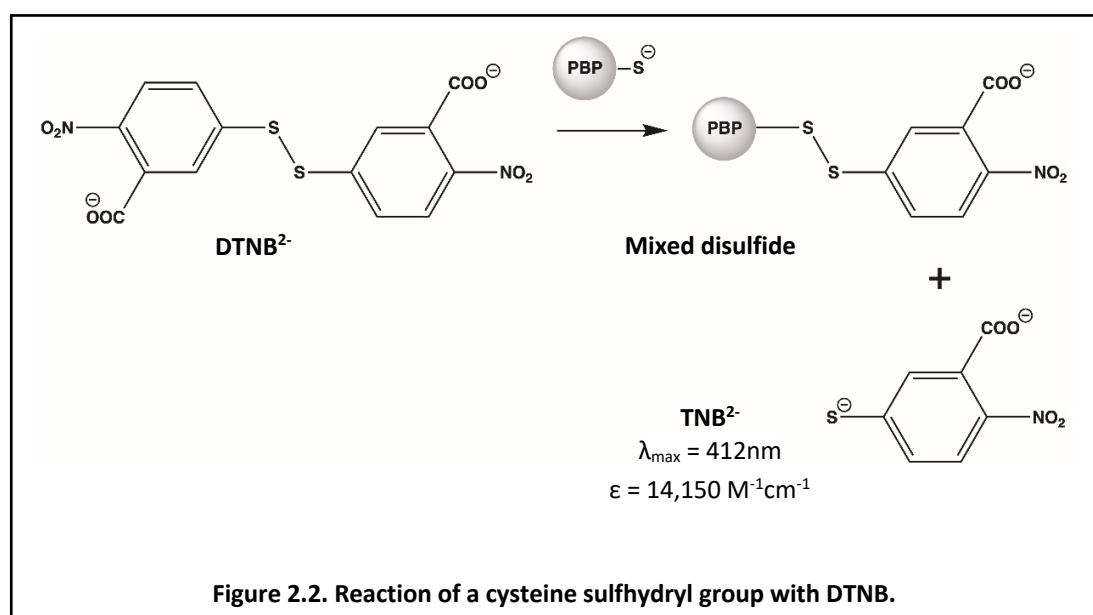


2.5.4 Ellman's assay

Ellman's assay was used to probe the state of the only cysteine (Cys384) of *A. baumannii* PBP2, that is involved in the coordination of zinc (chapter 3).

When the Ellman's reagent (5,5'-dithio-bis-(2-nitrobenzoic acid)) (DTNB) reacts with a free cysteine sulfhydryl group of a protein, it leads to the formation of a Cys-thionitrobenzoate (TNB) adduct and stoichiometric amount of TNB (2-nitro-5-thiobenzoic acid) that can be monitored at 412 nm (figure 2.2).

The spectrophotometric assay was carried out in a quartz cuvette at 30 °C, and absorption at 412 nm was monitored using a Cary 100 Bio UV-Vis spectrophotometer. The assay mixture consisted of protein (11 μM) or protein buffer, DTNB (1.1 mM), and assay buffer (50mM HEPES pH 7.5 and 400mM NaCl) in 200 μL final volume. Absorbance was measured for 2 min prior to the addition of DTNB. The final absorbance value was calculated as $Abs_{\text{sample}} - Abs_{\text{control}}$.



2.6 Mass spectrometry

2.6.1 Mass spectrometry of test compounds

A solution of test compound was mixed with an equal volume of 99.9 % (v/v) acetonitrile and 0.1 % (v/v) formic acid, to 5 mM final concentration. Approximately 5 μL of sample was introduced indirectly via a gold tipped capillary into the nano-

spray source of a Synapt G2SI Q-TOF mass spectrometer (Waters) calibrated between 250-5000 m/z with NaI. Spectra were acquired in the positive mode with a capillary voltage of 2500 kV, combined and the accurate mass generated.

2.6.2 Mass spectrometry of intact proteins

Purified proteins were analysed by MS as follows: 200 µL of protein (11 µM) were loaded onto a PD10 desalting column (GE Healthcare) equilibrated in 10 mM ammonium acetate, and eluted with 3CV of 10 mM ammonium acetate at room temperature. Protein was collected in 1 mL fractions, and the fraction containing the highest concentration of protein was used for mass spectrometry analysis. Protein samples were mixed with an equal volume of 99.9 % (v/v) acetonitrile and 0.1 % (v/v) formic acid, and introduced in the mass spectrometer as in 2.6.1. Combined spectra were deconvoluted with the Maximum Entropy 1 algorithm from the MASSLYNX software suite (Waters Corp) to derive the protein mass.

2.6.3 Mass spectrometry of protein-molecule covalent adducts

Formation of drug-enzyme adducts was tested by incubating the protein with a molecule of interest, the reaction conditions are stated for each specific PBP in chapter 4 and 5. Reactions were stopped by addition of an equal volume of denaturing buffer (30 % v/v methanol, 0.1 % v/v formic acid). Samples were loaded onto a PD10 desalting column (GE Healthcare) equilibrated with 3 CV of ice-cold denaturing buffer, and the protein was eluted with 3 CV of the same buffer and collected in 1 mL fractions. The fraction with the highest protein concentration was analysed in the mass spectrometer as described in 2.6.1 and 2.6.2, and the mass of the protein adducts was derived.

For each protein MS experiment performed in this work, the combined spectra was deconvoluted in a selected mass range that will be specified case by case in each chapter. The agreement between the combined and theoretical spectra confirmed by an excellent superimposition, was indicative of a deconvoluted solution that could explain the recorded spectra in its entirety.

2.7 ¹H-NMR spectroscopy

NMR analysis were carried out using a Bruker AVIIIHD 600 MHz spectrometer equipped with a Prodigy N2 broadband cryoprobe. The spectrometer was operated using TOPSPIN 3 software. The reaction consisted in test compound (188 μM) and enzyme (5 μM), in 50 mM sodium phosphate pH 7.5, and 10 % (v/v) D₂O. The water signal was suppressed using excitation sculpting with perfect echo. NMR spectra were processed using MestReNova.

2.8 Minimal inhibitory concentration tests

The antimicrobial activity of compounds described in chapter 5 was evaluated against a panel of Gram-positive and Gram-negative strains. Antimicrobial susceptibility testing by broth microdilution was done according to the Clinical and Laboratory Standards Institute guidelines, using cation adjusted Mueller-Hinton broth, in a final volume of 100 μL.

CHAPTER 3

Discovery of a novel zinc-binding site in the structure of *A. baumannii* PBP2

3.1 Introduction to chapter 3

Class B penicillin binding proteins (PBPs) are monofunctional transpeptidases, and the dynamics that regulate the interactions with other proteins of the divisome/elongasome complex are not completely understood. Part of the reason is the lack of structural information concerning these proteins, either alone or with interacting partners, that could offer a glimpse into the way they function *in-vivo*.

Although, Penicillin binding protein 2 is the main transpeptidase enzyme of the elongasome complex in rod-shaped bacteria, this protein remains poorly characterised in terms of structures and enzymatic activities both *in-vitro* and *in-vivo*. While there is a wealth of structural data for its counterpart in the divisome complex (i.e., PBP3) in *P. aeruginosa*, X-ray structures of PBP2 from prominent ESKAPE pathogens are limited. In fact, at the time the work presented in this chapter was started, the structure of *Helicobacter pylori* PBP2 was the only one available (Contreras-Martel *et al.*, 2017). Meanwhile, during the writing of this thesis, a structure of *E. coli* PBP2 was published (Levy *et al.*, 2019).

While the structural interactions between *E. coli* PBP2 and the glycosyltransferase RodA are currently being investigated by a number of groups around the world, the interactions between PBP2 and small molecules (which requires a resolution that only X-ray crystallography can currently achieve) remains to be explored. With this purpose in mind, crystallisation and structure determination of PBP2 from the ESKAPE pathogen *A. baumannii*, was pursued.

The work presented in this chapter received support from Dr Allister Crow (University of Warwick, UK), who contributed to the data acquisition and modelling of the structure of *A. baumannii* PBP2. The *in-vivo* experiments in *A. baumannii* ATCC 17978 were performed by Dr Edward Geisinger (Northeastern University, Massachusetts, USA).

3.2 Plasmid construction, expression and purification of *A. baumannii* PBP2

The nucleotide sequence of the *mrdA* (PBP2) gene encoding amino acid residues 53-672 was amplified from the genomic DNA of *A. baumannii* ATCC 19606 using 0098-F and 0098-R primers (table S1). The amplicon was ligated into a pET-47b vector between the plasmid's KpnI and EcoRI restriction sites, resulting in the pMIC10 vector encoding this region of *A. baumannii* PBP2 with an N-terminal His₆-tag which could be removed using 3C protease if required (table S2, figure S2).

pMIC10 was transformed in competent *E. coli* C41 (DE3) cells and the protein expressed by autoinduction (2.3.1).

Cell pellets were resuspended in buffer A (50 mM HEPES pH 7.5, 400 mM NaCl), supplemented with 20 mM imidazole, 2.5 % (w/v) CHAPS and DNase I, and lysed by sonication (2.3.2). PBP2 was purified in buffer A using nickel affinity chromatography, and the protein was eluted using a step gradient of imidazole from 20-500 mM (figure 3.1a). Fractions containing PBP2 were pooled and concentrated to 5 mL. PBP2 was further purified by size exclusion chromatography in buffer A (2.3.3 and 2.3.5) (figure 3.1b) and its purity and ability to bind β -lactams were checked by SDS-PAGE and Bocillin-FL staining assay, respectively (2.3.6 and 2.5.1)(figure 3.1c). Furthermore, PBP2 was analysed by intact protein mass spectrometry to confirm its mass (expected MW= 70544.87 Da) (figure 3.2) (2.6.2). The final yield of purified *A. baumannii* PBP2 was approximately 20 mg from 1 L of cell culture medium.

3.3 Crystallisation of *A. baumannii* PBP2

3.3.1 Screening of coarse crystallisation conditions

The commercially available screens Wizard Classic 1 and 2, Wizard Classic 3 and 4, PACT premier™, Midas™, Morpheus® (Molecular Dimensions), and Crystal Screen HT (Hampton Research) were trialled for the crystallisation of *A. baumannii* PBP2.

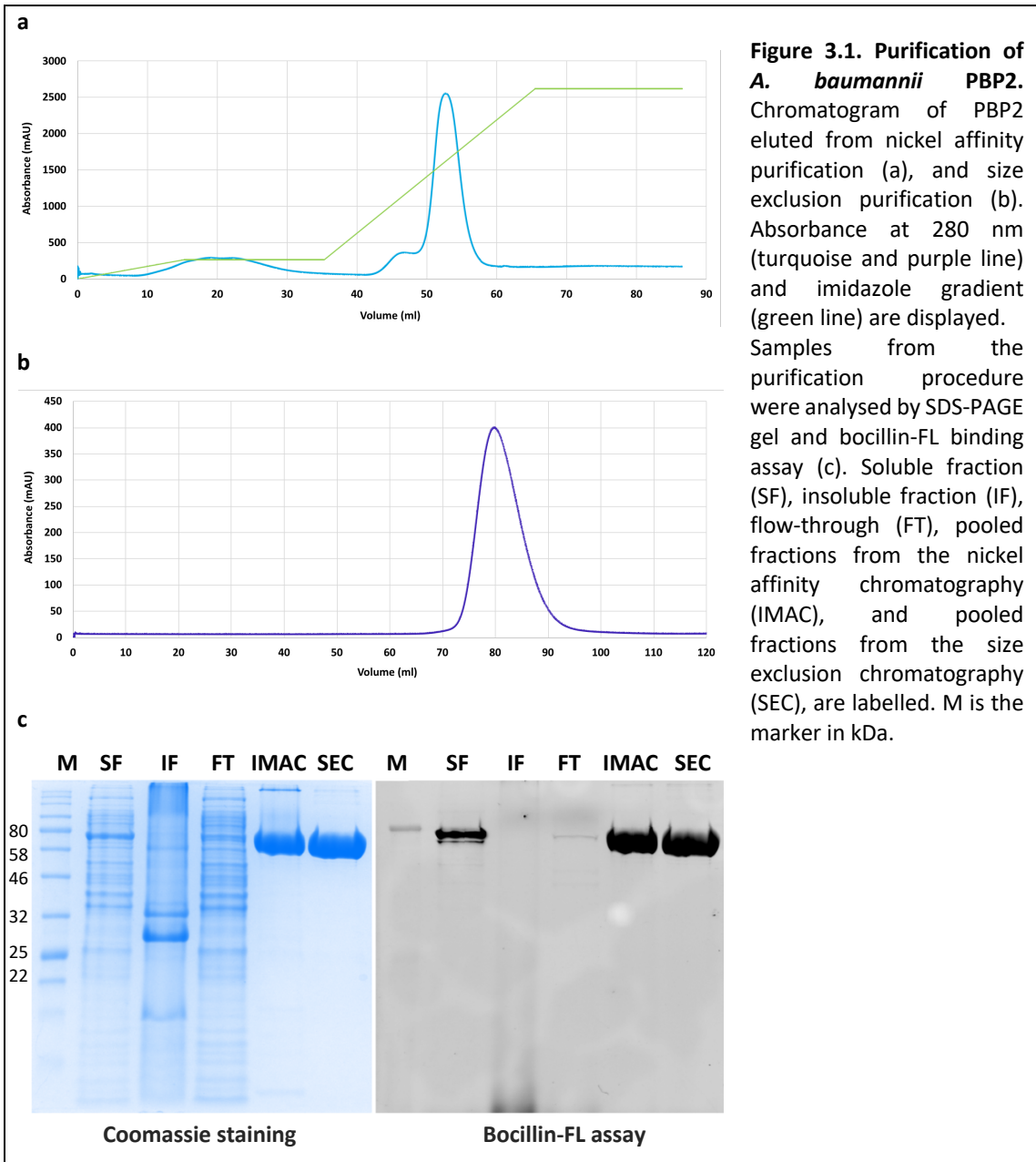


Figure 3.1. Purification of *A. baumannii* PBP2.

Chromatogram of PBP2 eluted from nickel affinity purification (a), and size exclusion purification (b). Absorbance at 280 nm (turquoise and purple line) and imidazole gradient (green line) are displayed.

Samples from the purification procedure were analysed by SDS-PAGE gel and bocillin-FL binding assay (c). Soluble fraction (SF), insoluble fraction (IF), flow-through (FT), pooled fractions from the nickel affinity chromatography (IMAC), and pooled fractions from the size exclusion chromatography (SEC), are labelled. M is the marker in kDa.

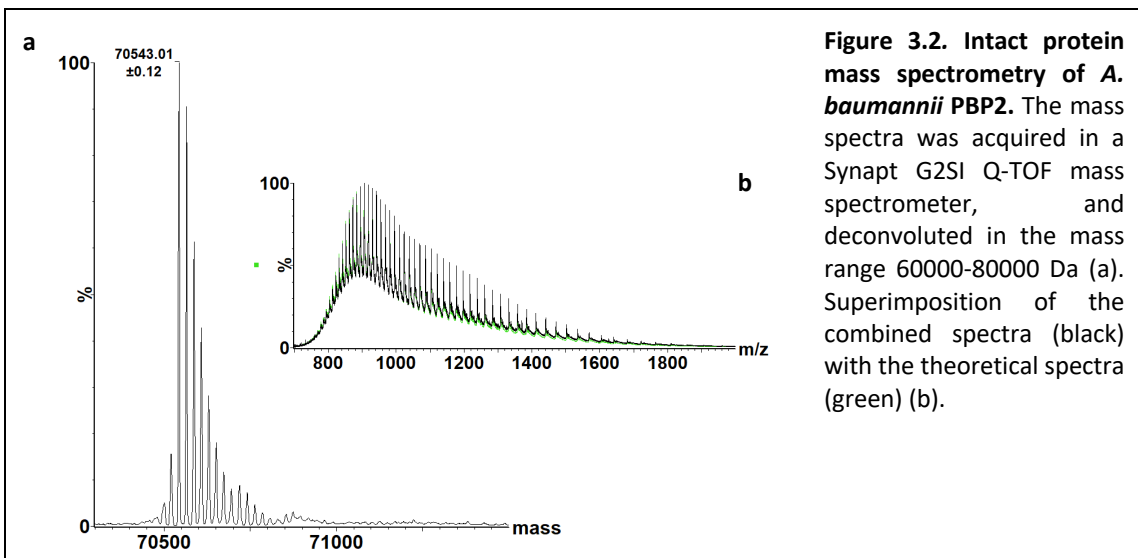
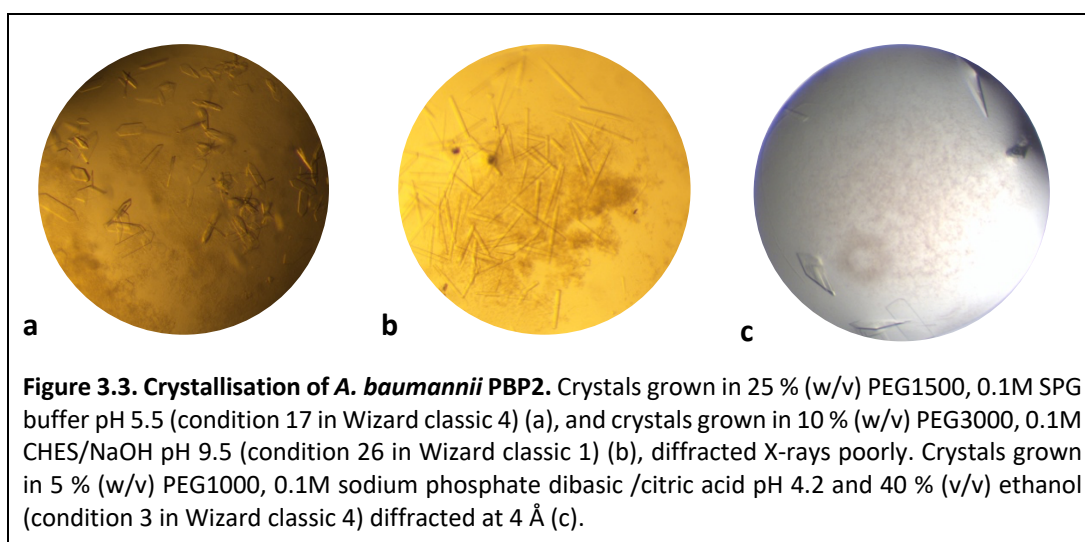


Figure 3.2. Intact protein mass spectrometry of *A. baumannii* PBP2.

The mass spectra was acquired in a Synapt G2SI Q-TOF mass spectrometer, and deconvoluted in the mass range 60000-80000 Da (a). Superimposition of the combined spectra (black) with the theoretical spectra (green) (b).

PBP2(Δ 53-672) in 50 mM HEPES pH 7.5 and 400 mM NaCl, was concentrated to 10.5 mg/mL and 15.9 mg/mL (2.3.7) using a 50 kDa cut-off Amicon centrifugal concentrator. 96-well sitting-drop crystallisation plates (100 nL stock protein solution + 100 nL mother liquor) were set up with the two concentrations of PBP2 and stored at 18 °C (2.4.1).

After 3 days, crystals were noted in all the crystallisation plates and in varied conditions. Crystals from representative conditions were harvested after 3 weeks, at which point they had reached their full size, cryoprotected in 20 % (v/v) ethylene glycol (2.4.4) and tested at the I04 beamline of the DLS synchrotron (UK) (figure 3.3a-b). X-ray diffraction images confirmed the crystals to be protein, however, the quality of diffraction was poor ($> 5 \text{ \AA}$) for all the crystals tested, except one for which diffraction was more promising (4 \AA) (figure 3.3c).



3.3.2 Optimisation of crystal hits

Crystals that yielded modest diffraction at 4 \AA were grown in a precipitant solution consisting of 5 % (w/v) PEG1000, 0.1 M sodium phosphate dibasic /citric acid pH 4.2 and 40 % (v/v) ethanol. This condition was taken forward to the optimisation stage (2.4.2), which led to the generation of PBP2 crystals diffracting at 2.6 \AA (figure 3.4).

PBP2 diffracting crystals were grown using the sitting drop vapour diffusion method at 18 °C. The drop consisted of 100 nL of 10.2 mg/mL protein combined with an equal volume of precipitant (5 % w/v PEG1000, 0.1 M sodium phosphate dibasic /citric acid

pH 4.2 and 16 % v/v ethanol). Crystals were soaked for a few seconds in a cryoprotectant solution (mother liquor + 25 % v/v glycerol), then mounted on a loop and flash-cooled in liquid nitrogen (2.4.4).

3.4 Structure determination of *A. baumannii* PBP2

3.4.1 Data collection

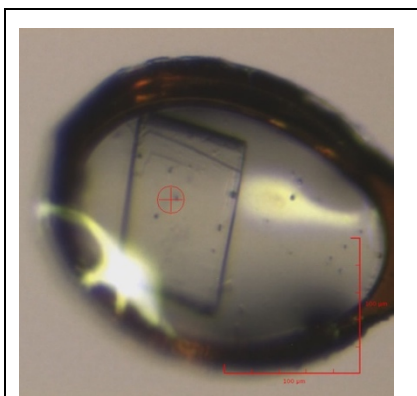


Figure 3.4. Crystal of *A. baumannii* PBP2 mounted in a loop. From this protein crystal a structure at 2.6 Å was solved.

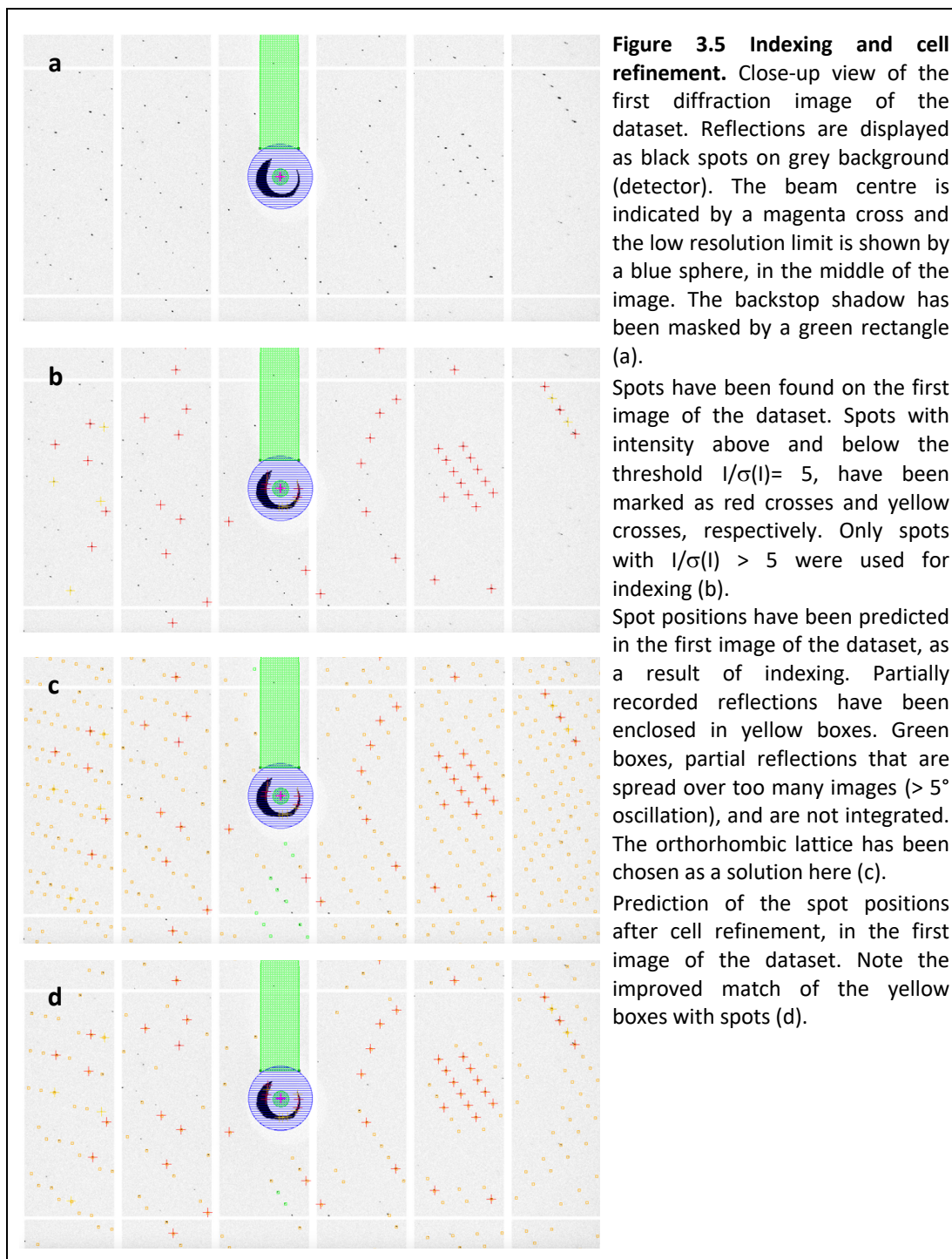
Data collection was performed at the I03 beamline (2.4.5) in remote access, using a wavelength of 0.9763 Å with a Pilatus3 6M detector. A complete dataset was acquired by collecting 1440 images with an oscillation step of 0.25° and 0.08 s exposure time. Data collection was carried out with beam size 20x20 μm and transmission of 75.12 %. The crystal to detector distance was set up for collecting data up to 2.5 Å resolution.

3.4.2 Data integration with iMosflm

The dataset of *A. baumannii* PBP2 was processed with iMosflm (2.4.6.1). To index the reciprocal lattice, the low and high resolution limits were set to 40.2 Å and 2.47 Å, respectively; autoindexing on two images (1 and 360) was carried out, after spot finding (intensity threshold of 5) (figure 3.5A-C). The preferred solution was a body-centred orthorhombic lattice ($a \neq b \neq c$, $\alpha = \beta = \gamma = 90^\circ$) over a side-centred monoclinic lattice ($a \neq b \neq c$, $\alpha = \gamma = 90^\circ$, $\beta \neq 90^\circ$) and a primitive triclinic system ($a \neq b \neq c$, $\alpha \neq \beta \neq \gamma \neq 90^\circ$). The space group I 2 2 2 was chosen as it was the highest symmetry point group with a low penalty score. Moreover, values of $\sigma(xy)$ (error in spot positions) and visual inspection of the predicted spots gave confidence that I 2 2 2 or I 2₁ 2₁ 2₁ could have been the correct solution, although the true Laue group had to be determined in Pointless (2.4.6.2).

Cell refinement was carried out on two segments of images (1-4 and 361-364), that were automatically selected by iMosflm based on the chosen space group, mosaic

spread and oscillation angle. Detector parameters and crystal parameters refined reasonably smoothly. The unit cell dimensions were refined to a standard deviation < 0.1 ($a=121.60$, $b=151.40$, $c=177.57$, $\alpha=\beta=\gamma=90^\circ$) with a mosaicity of 0.43. After cell refinement, spots were predicted for each image of the dataset, with most of the spots being enclosed in yellow prediction boxes (figure 3.5d).



The entire dataset was integrated, while keeping the unit cell parameters fixed. The output file from integration contained the reflection indices with intensities and standard deviations among the parameters.

3.4.3 Data reduction

The integrated data were used in the data reduction module of ccp4 (2.4.6.2). Pointless determined the true Laue symmetry from unmerged intensities (table 3.1-3.3). The best solution was point group $I\ 2\ 2\ 2$, however, at this stage it was still not possible to know the true space group, as $I\ 2\ 2\ 2$ and $I\ 2_12_12_1$ are enantiomorphous and so, indistinguishable by looking at the systematic absences. Also, the data did not appear to be twinned, according to the L-test statistics.

Aimless scaled and merged the intensities in the $I\ 2\ 2\ 2$ space group, and the results have been summarised in table 3.4 The scale factor profile illustrated in figure 3.6a was typical of a plate-like crystal, which diffracted well in 2 dimensions, but not in the third one.

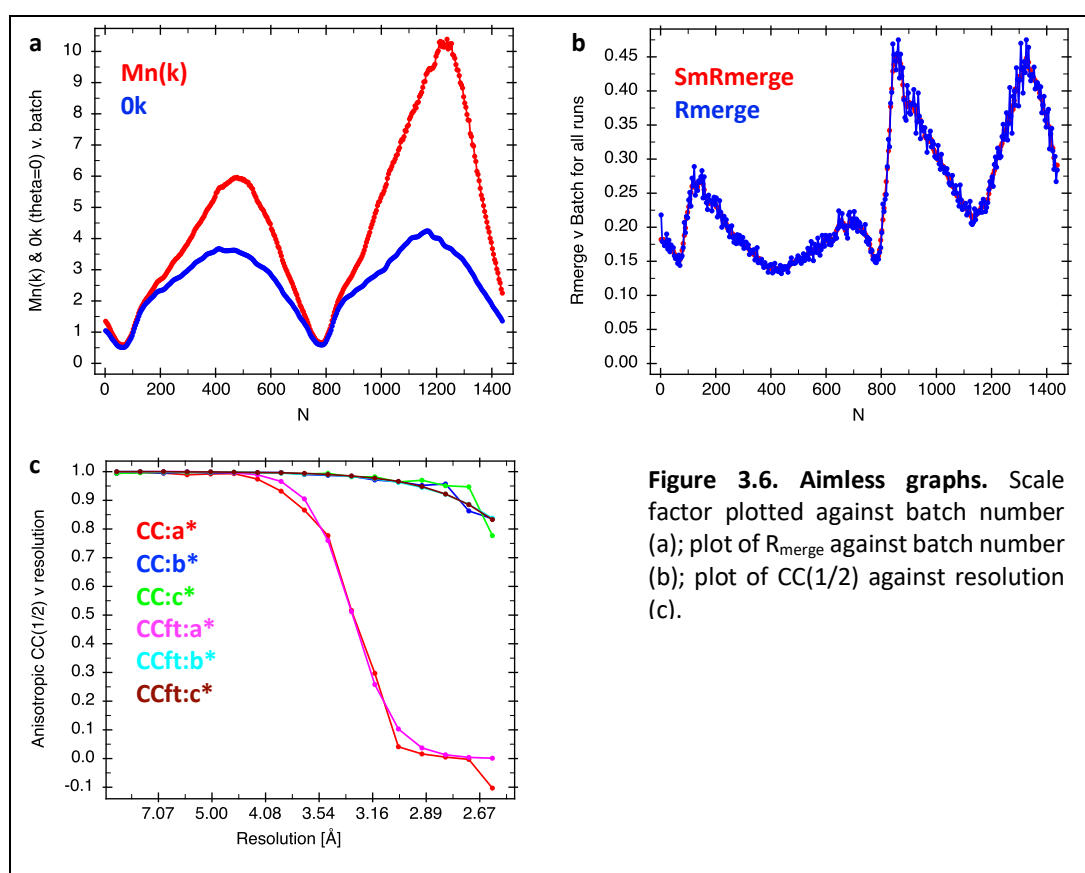


Figure 3.6. Aimless graphs. Scale factor plotted against batch number (a); plot of R_{merge} against batch number (b); plot of $CC(1/2)$ against resolution (c).

Nelmt	Lklhd	Z-cc	CC	N	Rmeas		Symmetry & operator
1	0.909	8.59	0.86	296640	0.279		identity
2	0.921	8.25	0.83	378260	0.315	***	2-fold l (0 0 1) {-h,-k,l}
3	0.922	8.19	0.82	377105	0.335	***	2-fold k (0 1 0) {-h,k,-l}
4	0.917	8.41	0.84	378033	0.326	***	2-fold h (1 0 0) {h,-k,-l}

Table 3.1 Symmetry elements scored by Pointless. Lklhd, likelihood; Z-cc, Z-scores for correlation coefficients; CC, correlation coefficients; Rmeas, R-factors for symmetry elements.

Best point group:	I 2 2 2
Reindex operator:	[h,k,l]
Laue group probability:	0.977
Systematic absence probability:	1.000
Total probability:	0.977
Space group confidence:	0.000
Laue group confidence	0.973

Table 3.3 Summary table for the point group I 2 2 2.

Laue Group		Lklhd	NetZc	Zc+	Zc-	CC	CC-	Rmeas	R-	Delta	ReindexOperator
= 1 m m m	***	0.977	8.30	8.30	0.00	0.83	0.00	0.31	0.00	0.0	[h,k,l]
2 1 2/m 1		0.008	0.03	8.32	8.30	0.83	0.83	0.31	0.32	0.0	[-h,-k,l]
3 1 2/m 1		0.007	0.11	8.41	8.30	0.84	0.83	0.30	0.33	0.0	[h,-l,k]
4 1 2/m 1		0.007	0.23	8.42	8.19	0.84	0.82	0.30	0.33	0.0	[k,-h,l]
5 P -1		0.001	0.34	8.59	8.25	0.86	0.83	0.28	0.33	0.0	[-h,-1/2h+1/2k+1/2l,-1/2h+1/2k-1/2l]

Table 3.2 Scores for all possible Laue groups which are sub-groups of lattice group.

The correlation coefficient $CC(1/2)$ dropped substantially below 1 as function of the resolution, along the a- direction, consistent with the plate-like crystal (figure 3.6c). The dataset also contained some bad patches, as suggested by the high R_{merge} of images after 750 in figure 3.6b.

A real resolution for this dataset was 2.6 Å, as indicated by the $Mn(I)/sd(Mn(I))$ being 2, the $CC(1/2)$ being well above 0.5, and R_{pim} being well below 2. Completeness of the dataset was near to 100 %, and multiplicity was moderately high (table 3.4). Finally, Ctruncate converted the intensities (I) to structure factor amplitudes (F), the statistics of which suggested absence of twinning.

	Overall	Inner Shell	Outer Shell
Low resolution limit	25.77	25.77	2.69
High resolution limit	2.60	10.40	2.60
Rmerge (within I+/I-)	0.232	0.060	1.540
Rmerge (all I+ and I-)	0.239	0.061	1.599
Rmeas (within I+/I-)	0.253	0.065	1.685
Rmeas (all I+ & I-)	0.250	0.064	1.671
Rpim (within I+/I-)	0.101	0.025	0.678
Rpim (all I+ & I-)	0.072	0.019	0.482
Rmerge in top intensity bin	0.074	-	-
Total number of observations	604001	9518	54815
Total number unique	50557	822	4635
Mean((I)/sd(I))	8.8	25.2	2.0
Mn(I) half-set correlation CC(1/2)	0.996	0.998	0.793
Completeness	99.9	93.6	100.0
Multiplicity	11.9	11.6	11.8
Mean (Chi^2)	0.97	0.63	1.00
Anomalous completeness	99.9	95.2	100.0
Anomalous multiplicity	6.1	6.6	6.0
DelAnom correlation between half-sets	-0.055	-0.123	0.015
Mid-Slope of Anom Normal Probability	0.901	-	-

Table 3.4 Summary of the results from Aimless

3.4.4 Cell content analysis

The scaled and merged data were used to calculate the Matthews coefficient (2.4.6.3). The statistics indicated that the most likely number of copies of PBP2 in the asymmetric unit was 2, for which the solvent content was ~50 % (table 3.5).

Nmol/asym	Matthews Coeff	% solvent	P (2.59)	P (tot)
1	5.78	78.74	0.01	0.01
2	2.89	57.48	0.64	0.63
3	1.93	36.22	0.35	0.36
4	1.45	14.96	0.00	0.00

Table 3.5 Summary of the results from Matthews coefficient analysis

3.4.5 Molecular replacement

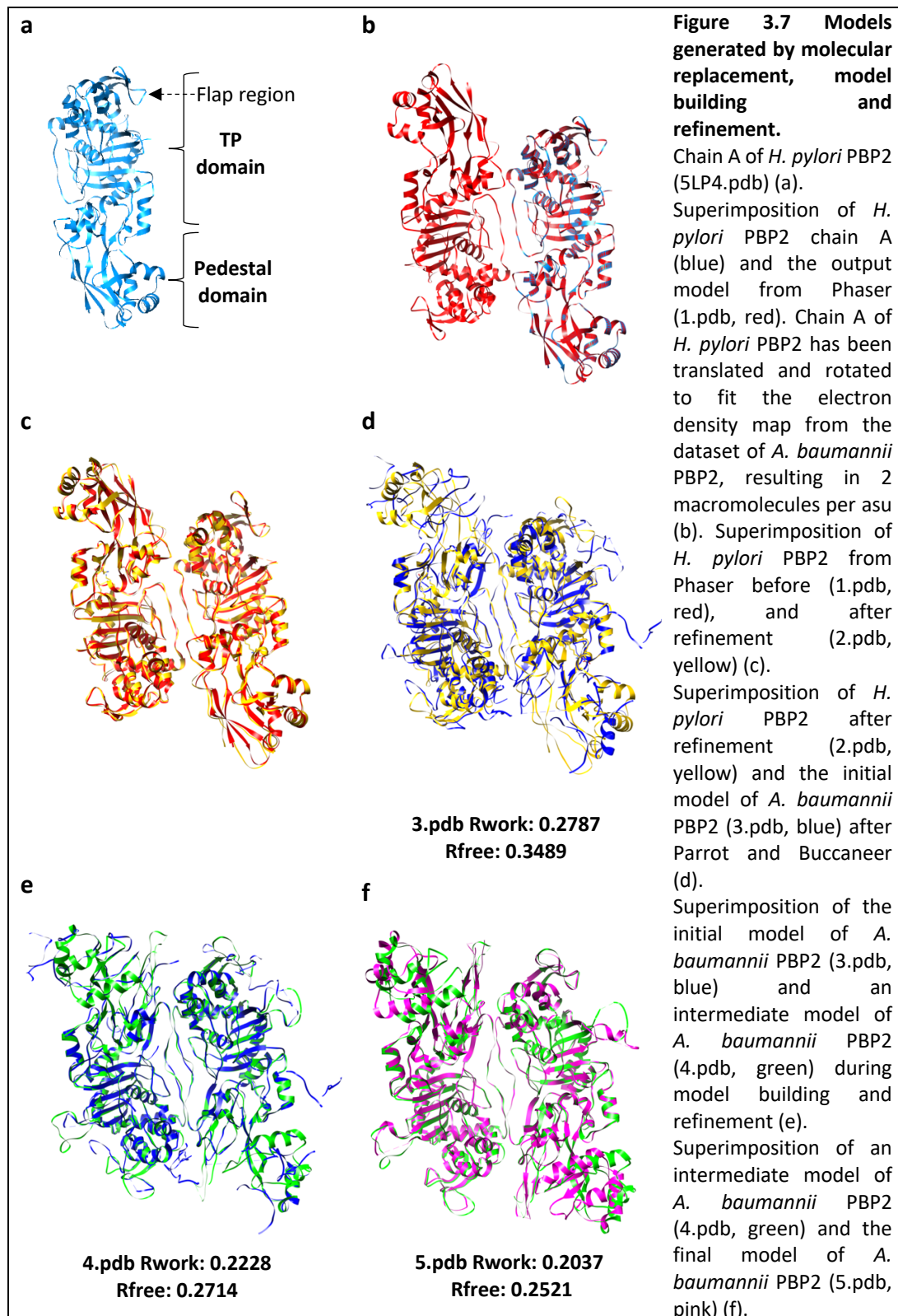
Since a structure of a PBP2 homolog from the bacteria *Helicobacter pylori* was available (5LP4.pdb), and the sequence identity between the two homologs (28 %) was sufficiently good, the structure of PBP2 from *A. baumannii* could be solved by molecular replacement (2.4.6.4). As a search model, chain A of *H. pylori* PBP2 structure was used, after removal of water and ions (figure 3.7a). Space groups I 2 2 2 and I 2₁2₁2₁ were both tested.

Phaser successfully found a solution, with 2 macromolecules of *H. pylori* PBP2 in the asymmetric unit (NCS) and in space group I 2 2 2. Confidence in this solution was given by the TFZ > 8 (= 16.3) and the high LLG score (= 236). The output file (1.pdb) was a model of *H. pylori* PBP2 fitting an electron density map calculated from the *A. baumannii* PBP2 dataset (figure 3.7b).

3.4.6 Model building and refinement

The model from Phaser was refined with Refmac5 (2.4.6.5) (2.pdb, figure 3.7c). Density modification and phase improvement were carried out with Parrot (2.4.6.5), then Buccaneer (2.4.6.5) attempted an automatic building of a model of *A. baumannii* PBP2 into the electron density map. The output model from Buccaneer (3.pdb) was well built at the transpeptidase domain (TP) core, due to the high conservation of amino acids between *H. pylori* and *A. baumannii* PBP2 (figure 3.16a).

Instead, extensive manual building was required at the pedestal domain (N-terminal domain), and the upper part of the catalytic site, due to the low sequence similarity and low quality of the electron density (figure 3.7d).



The newly generated PBP2 model underwent many cycles of manual building with Coot and refinement with Refmac5, using local NCS restraints (2.4.6.5). The evolution of the PBP2 model can be followed in figure 3.7d-f. The final model was refined to $R_{\text{work}} = 0.2037$ and $R_{\text{free}} = 0.2521$ (table 3.6).

No. atoms		B-factors (\AA^2)	
Protein	8350	Protein	69
Ligand	2	Ligand	72
Water	65	Water	50
R.m.s deviations		Ramachandran plot	
Bond lengths (\AA)	0.0076	Favoured (%)	94.4
Bond angles ($^\circ$)	1.5385	Allowed (%)	5.1
		Outliers (%)	0.5

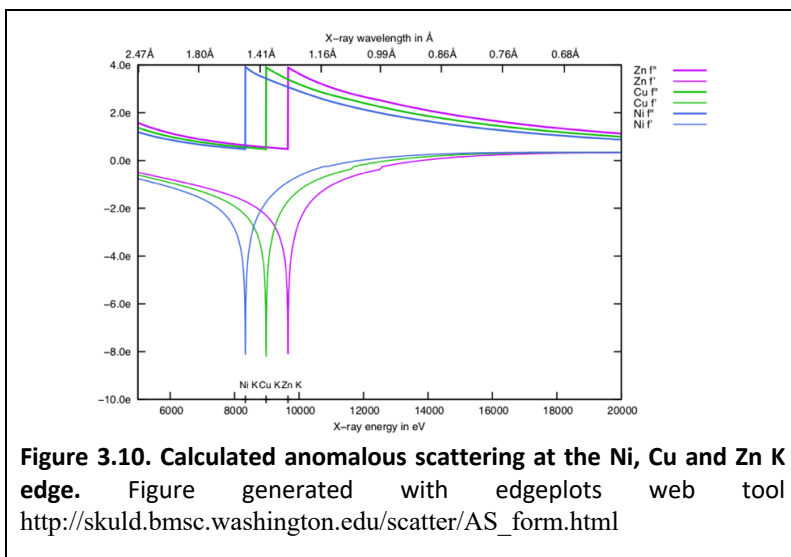
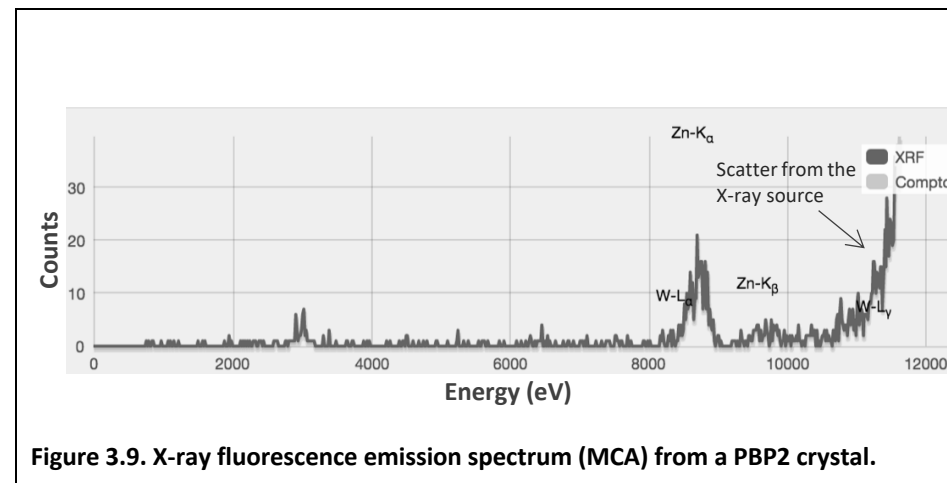
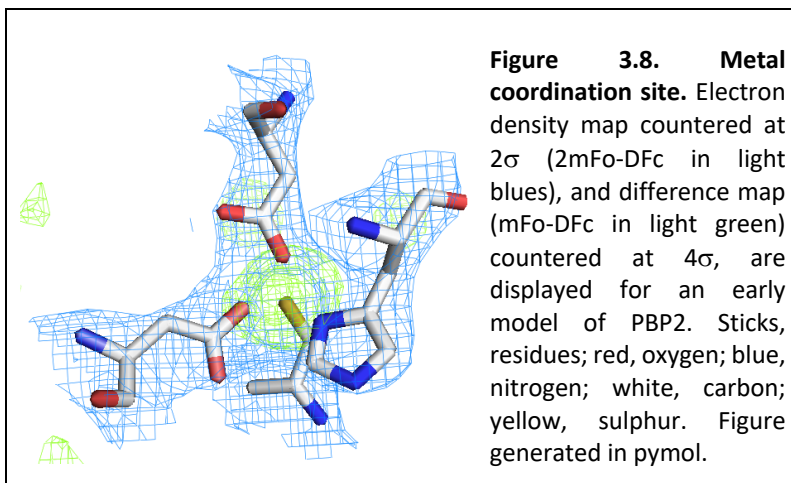
Table 3.6. Refinement statistics of the dataset for PBP2. Data refinement with Refmac5 and validation with Procheck and Rampage.

3.4.7 Identification of a metal-coordination site

During the course of model building and refinement, an extra region of electron density consistent with a metal coordination site was surprisingly found in a flap region that lies above the active site cleft (figure 3.7a, 3.8). In order to identify the heavy metal, an X-ray fluorescence experiment was carried out on PBP2 crystals at the i04 beamline (2.4.7). An X-ray fluorescence spectrum (MCA) was first collected, using an incident X-ray beam at 12657.90 eV, to identify the heavy elements present in the sample. The experiment was carried out at 32 % transmission and 1 s exposure time. The MCA spectrum clearly showed K_{α} and K_{β} peaks for zinc, that were automatically labelled by the AutoPyMCA software (table 3.7) (figure 3.9).

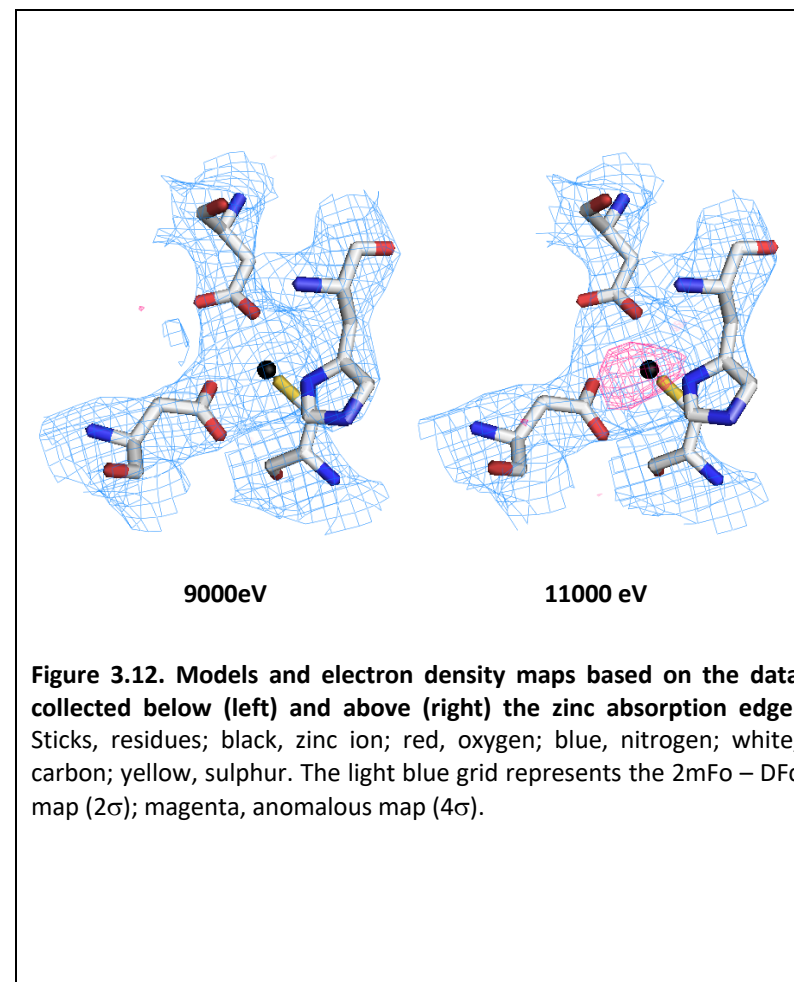
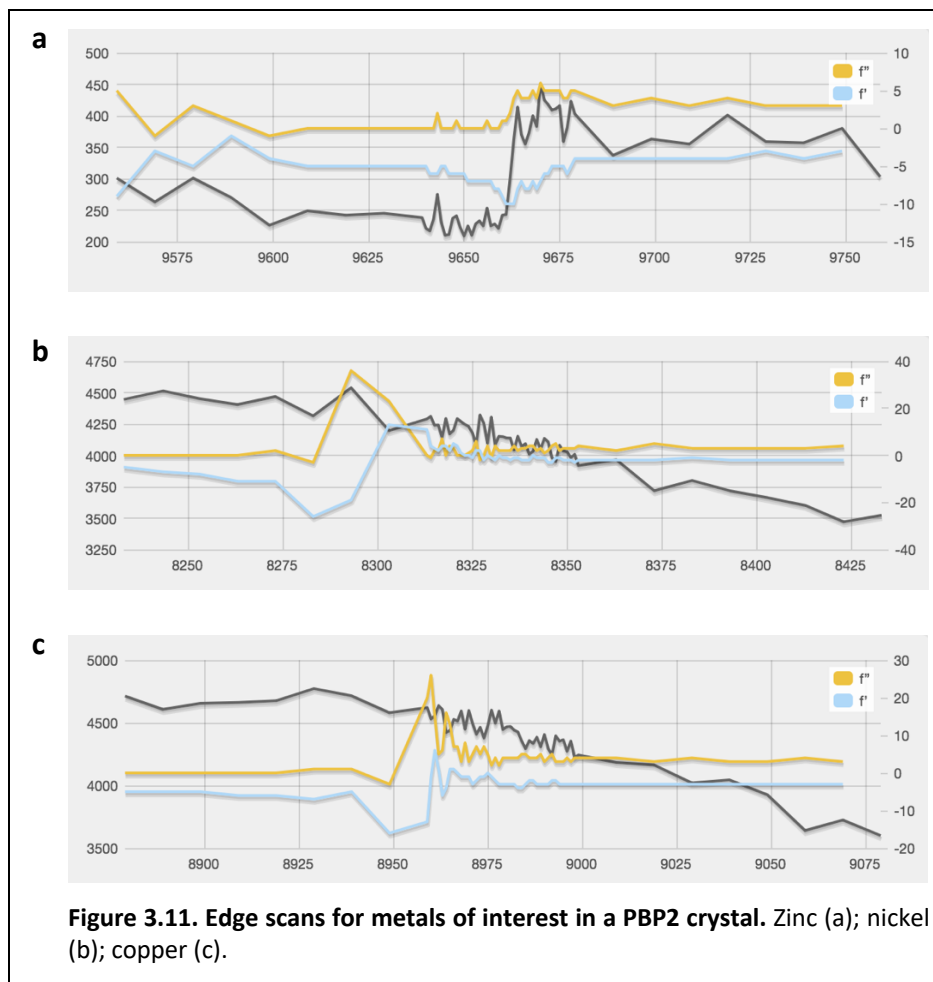
To further investigate the presence of zinc, edge scans were collected for this, and other alternative heavy metals, on the same crystal. For instance, nickel could have been possibly stripped from the metal affinity chromatography resin during IMAC purification of PBP2, and copper is of similar atomic weight to Zinc (Cu= 63.55 Da, Zn= 65.38 Da) and frequently encountered in metalloenzymes. Anomalous scattering coefficients f' and f'' for elements of interest, were used to select the wavelength at which collect the edge scans (figure 3.10). All the edge scans were acquired in the range +/- 100 eV of the theoretical excitation energy of the element under

examination (table 3.7) (figure 3.11a-c), at 4 % transmission and 1 s exposure time. The edge scan for zinc, suggested the presence of this metal based on the increase in fluorescence, with scattering factors f' and f'' resembling those plotted in figure 3.10. Conversely, the presence of either nickel or copper was not indicated by their respective edge scans.



Z	Element	Excitation		Emission $K\alpha_1$	Emission $K\beta_3$
		Edge	Energy (eV)	Energy (eV)	Energy (eV)
28	Ni- Nickel	K	8332.8	7478.2	8264.7
29	Cu- Copper	K	8978.9	8047.8	8905.3
30	Zn- Zinc	K	9658.6	8638.9	9572.0

Table 3.7. Theoretical values of the excitation and emission energies for the heavy atoms investigated in crystals of PBP2.



To definitely prove that zinc was the metal responsible for the anomalous scattering close to the active site, diffraction data were collected at energies above (11000 eV) and below (9000 eV) the zinc absorption K edge, on the same crystal. Anomalous electron density maps were calculated for these datasets. The anomalous signal was present in the data collected above the zinc absorption edge, while it was absent in the data collected below the zinc absorption edge (figure 3.12), thus unambiguously determining the presence of a zinc-binding site.

3.4.8 Metal B factor and occupancy

Isotropic refinement of temperature factors was applied to the zinc coordination site. Generally, the *B*-factor of the zinc ion was close to the *B*-factor of the zinc-coordinating atoms (table 3.8) within the same chain. Because the solution in which PBP2 crystallised, had not been supplemented with zinc, the occupancy of the metal could have required some adjustment. The occupancy for the zinc ion in chain A and B was gradually increased from 0.2 to 1, and the B-factors for the zinc and its coordinating residues were measured (table 3.8). Considering the difference between the average B-factor of the atoms making the coordination sphere, and the B-factor of the zinc atom, occupancy for zinc was close to 1 in both chain A and chain B. It was noted that, temperature factors were much higher in chain B than in chain A, even after adjusting the metal occupancy.

Occupancy		0.2	0.4	0.6	0.8	0.9	1
Atom	Chain	B-factor	B-factor	B-factor	B factor	B-factor	B-factor
Asp350- O ^{δ2}	A	27	32	34	39	43	45
	B	98	100	111	124	125	134
Asp365- O ^{δ2}	A	28	44	48	50	52	53
	B	57	62	62	64	68	68
His371- N ^{δ1}	A	36	38	40	43	45	45
	B	71	76	81	86	89	92
Cys384- S ^γ	A	45	45	44	47	48	50
	B	93	95	101	107	107	111
Average B-factor	A	34	40	42	45	47	48
	B	80	83	89	95	97	101
Zinc	A	21	23	30	40	47	52
	B	66	66	76	90	97	105

Table 3.8. B-factor and occupancy of the atoms in the zinc-coordination site. At occupancy of 0.9, the average B-factor of the zinc-coordinating residues and the metal are equivalent.

A better quality of the electron density map, and the additional stability provided by the packing interactions with the zinc-binding site in chain A, could possibly account for the B-factor differences in the zinc-coordination site of the two NCS protomers.

3.4.9 Model validation

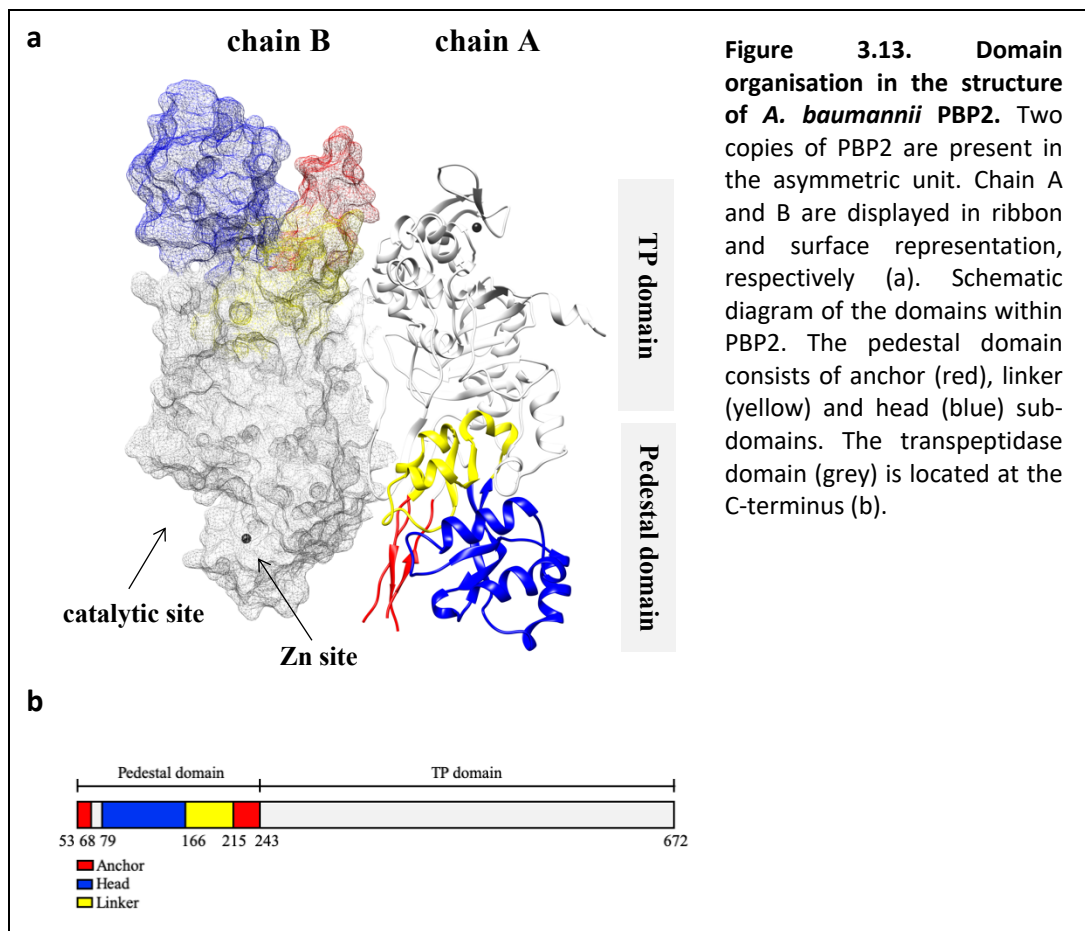
Given the resolution and the density map (2mFo-DFc) generated from the dataset, it was possible to build a near complete model of PBP2. Where electron density was missing or very poor, the protein chain was truncated. Water and other molecules present in the protein sample or crystallisation condition were also built as part of model where appropriate, according to the difference map (mFo-DFc) and refined. Validation was performed with Rampage and Procheck (2.4.5.6).

3.5 Description of *A. baumannii* PBP2 structure

3.5.1 Overall three-dimensional architecture

A. baumannii PBP2 crystallised with two protein monomers within the asymmetric unit (asu), termed chain A and chain B, and these are arranged head-to-tail. Both chains contained high structural similarity (root mean square deviation (rmsd) of 0.339 Å between C α). Electron density map quality appeared to be better for chain A than for chain B throughout the entire protein, hence description of the structure will be limited to chain A only, unless otherwise stated.

The structure of *A. baumannii* PBP2 retains the typical bimodular fold of class B HMW-PBPs. It consists of an elongated N-terminal module, also referred to in literature as the pedestal domain, and a C-terminal module bearing the catalytic site and termed transpeptidase domain. This domain organization can also be appreciated in other available X-ray structures of class B PBPs (for instance *P. aeruginosa* PBP3 and *E. coli* PBP2). Note that the structure is devoid of the transmembrane helix that precedes the pedestal domain, since a truncated version of PBP2 was crystallised (figure 3.13a).



3.5.1.1 The N-terminal domain

The N-terminal module can be further divided into three subdomains, named anchor, head and linker domains (figure 3.13b).

The anchor domain (residues 53-68 and 215-243) is partially built in *A. baumannii* PBP2, due to very poor electron density for residues 53-59 and 224-234 (figure 3.14). Note that PBP2 has been crystallised with a 21 residues long extension at the N-terminus, corresponding to the His₆-tag and additional amino acids of the cloning vector, upstream of the restriction enzyme site used. Electron density for these additional amino acids was also not detectable. The anchor domain is inclusive of two anti-parallel β strands (β 1 and β 7) alongside a loop and makes few contacts to

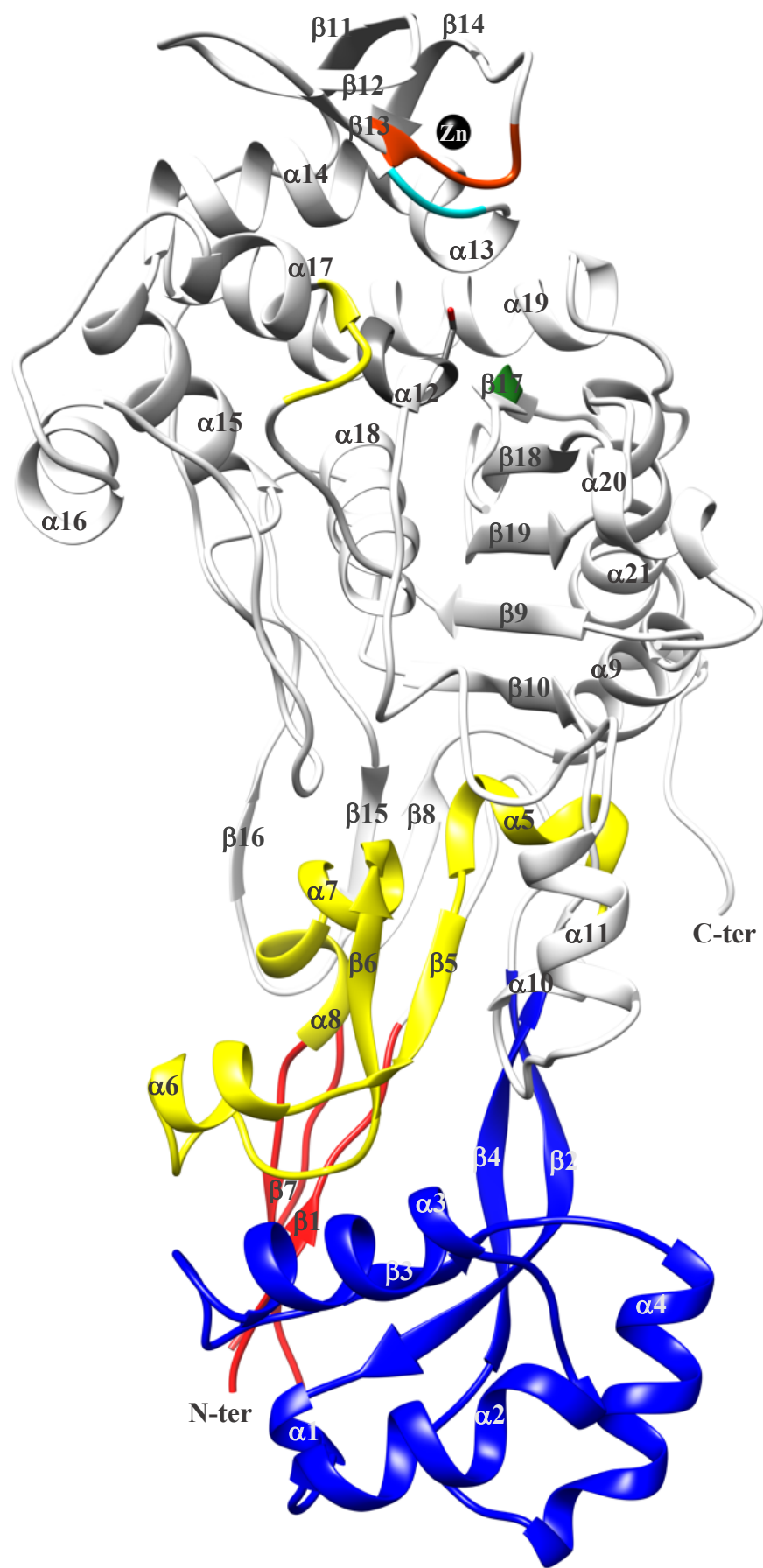


Figure 3.14. Structure of *A. baumannii* PBP2. The pedestal domain is colour coded according to figure 3.13b. The conserved motifs are also labelled in the TP domain according to the scheme colour in figure 3.16d. Secondary structure elements are labelled in chain A.

the remainder of the protein. The overall folding of the anchor domain is β -strand rich and it is quite conserved among class B PBPs of Gram-negative bacteria, whereas in Gram-positive bacteria, additional structural elements may be present, that could be required for the interaction with species specific proteins (for instance in *E. faecium* PBP5- 6MKJ.pdb). However, the anchor domain is not always completely built in these structures, suggesting some degree of flexibility associated with this region. The anchor domain is followed by the 'head', a predominantly globular and α helical domain.

The head domain (residues 79-166), includes four α helices (α 1- α 4) and one short β strand (β 3). The latter forms, together with two long twisted β strands (β 2 and β 4), an anti-parallel three β -stranded sheet, that connects the head to the linker domain (figure 3.14). Similarly to the anchor domain, the head domain in Gram-positive bacteria may display extra structural elements (for instance in methicillin resistant *Staphylococcus aureus*- 3VSK.pdb). Notably, the non-catalytic head domain occupies a similar position to the transglycosylase domain of class A PBPs, a fact that could imply a possible role in maintaining the TP domain at approximately the same distance from the membrane as in class A PBPs (Contreras-Martel *et al.*, 2009).

The linker domain (residues 166-215), is composed of four α helices (α 5- α 8) and two anti-parallel β strands (β 5 and β 6) and is in close contact with the basal region of the transpeptidase domain (figure 3.14). The sequence enclosed by α 5 and α 7 is notably shorter in PBPs associated with the divisome (i.e. PBP3), compared to PBPs pertaining to the elongasome (i.e. PBP2) in Gram-negative bacteria. Structures of *E. coli*, *A. baumannii* and *P. aeruginosa* PBP3 display a short loop, whereas *E. coli* and *H. pylori* PBP2 resemble the *A. baumannii* PBP2 structure in this region. There is also variability in the length of this sequence among class B PBPs in Gram-positive bacteria.

The three sub-domains of the pedestal module are engaged in a very well conserved interaction that takes place between residues Arg68, Arg164 and Glu207, belonging

to anchor, head and linker domains, respectively. These three residues are conserved in Gram-positive and Gram-negative species (Goffin and Ghuysen, 1998) and superimpose and align well in the structures and sequences, respectively, of all class B PBPs solved to date (figure 3.16a). The Arg-Arg-Glu constellation may play a role in the stabilization of the pedestal domain as suggested by Contreras-Martel and coworkers (Contreras-Martel *et al.*, 2009).

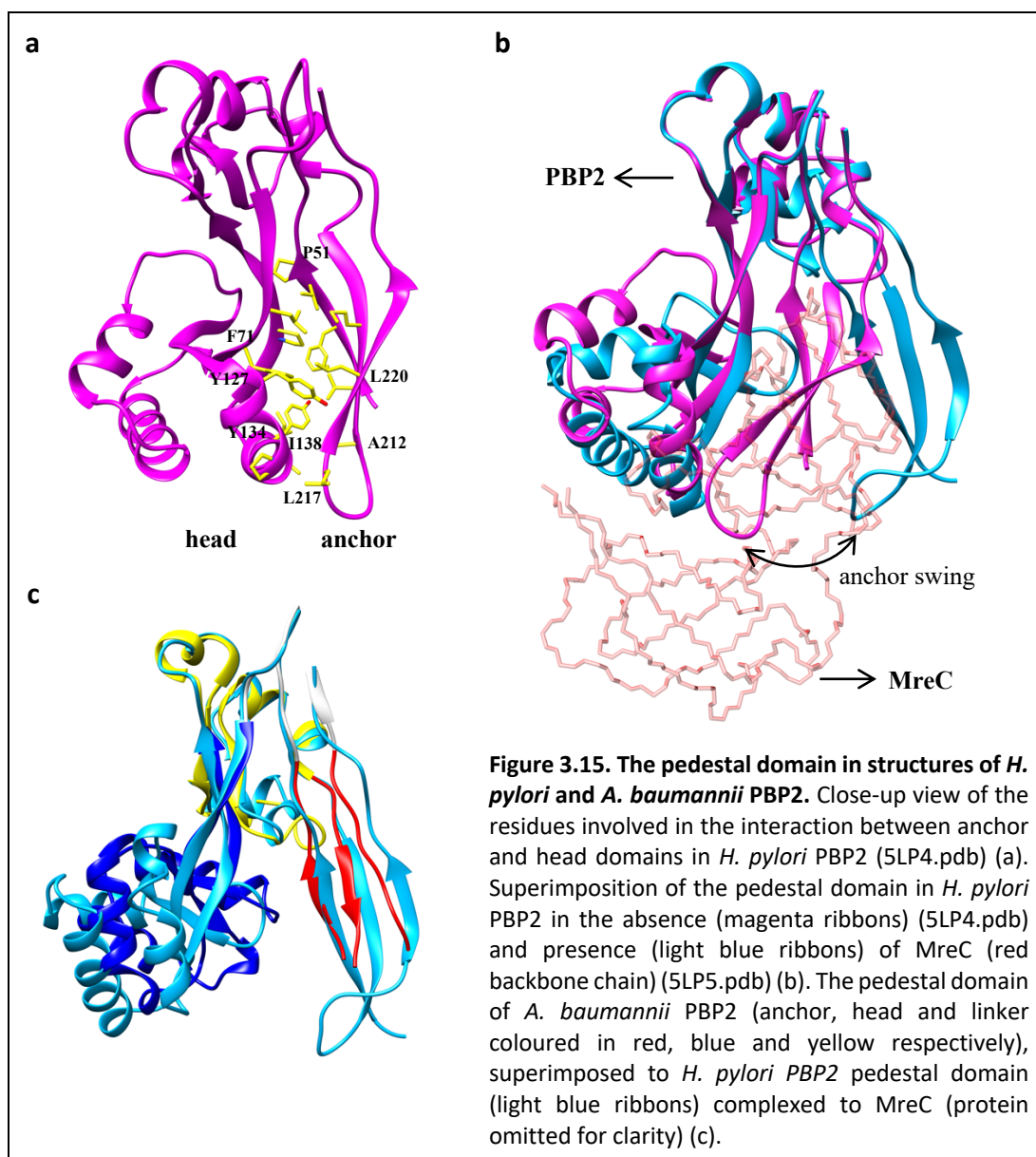
3.5.1.1.1 Role of the pedestal domain in the interaction with MreC

The pedestal domain of bPBPs is characterised by high flexibility with respect to the relative position of anchor and head domains. This is supported by structures of *E. faecium* PBP5 (6MKJ.pdb and 6MKA.pdb) in which the pedestal domain was captured in closed (anchor and head domains make contacts) and open (anchor and head domains move apart) conformations, possibly serving as a binding platform for interaction with other proteins of the divisome machinery.

Another example of pedestal domain flexibility can be found in the X-ray structures of *H. pylori* PBP2 and in complex with the scaffold protein MreC (Contreras-Martel *et al.*, 2017). In the structure of *H. pylori* PBP2 (5LP4.pdb) the pedestal domain is well resolved and adopts a closed conformation, where intimate interactions between anchor and head domains occur at the interdomain interface and are mostly of hydrophobic nature (figure 3.15a). Residues located at this hydrophobic interface include Pro51, Phe71, Tyr127, Tyr134, Ile138, Ala212, Leu217 and Leu 220, and are highly conserved in the sequence of *A. baumannii* PBP2 (figure 3.16a). It can be inferred from sequence alignments (figure 3.16c) and structural data that, similar apolar contacts between head and anchor domains are possible for homologue PBP2 proteins and other HMW-PBPs of Gram-positive and Gram-negative bacteria (Contreras-Martel *et al.*, 2017).

PBP2 is recruited to the elongasome complex by MreC, a bitopic membrane protein that together with MreB and MreD, serves a cytoskeletal function for the assembly of the elongasome machinery, and is essential for cell shape determination in

elongated bacteria, like *E. coli*, *Caulobacter crescentus*, *Bacillus subtilis* and *H. pylori* (Kruse *et al.*, 2005; Leaver and Errington, 2005; Dye *et al.*, 2005; El Ghachi *et al.*, 2011). The X-ray structure of *H. pylori* PBP2: MreC complex (1:2) offers a snapshot of the way these two proteins interact within the multiprotein elongasome complex, in addition to the mechanism by which MreC can self-associate to form coiled structures *in-vivo* (Vats *et al.*, 2009). Particularly, the C-terminal β -domain of *H. pylori* MreC docks between the head and anchor domains of *H. pylori* PBP2, disrupting the interdomain interface and pushing the anchor ~ 18 Å away from the head domain (distance between the C α of K45 in PBP2 and PBP2: MreC structures) (figure 3.15b)



The newly formed PBP2: MreC interface is mostly hydrophobic, where the head residues interacting with the anchor region of *H. pylori* PBP2 (i.e., L69, F71, Y127, Y134, I138) are also employed to establish new interactions with *H. pylori* MreC (F169, Val184, F182, Y222) (figure 3.16a). *H. pylori* MreC residues F169, F182 and Y222 stabilise the binding to PBP2 (Contreras-Martel *et al.*, 2017), and similar PBP2: MreC hydrophobic contacts could also occur in *A. baumannii* (corresponding MreC residues are I195, Y209 and G249) based on a sequence alignment (figure 3.16b).

It is of note that, the X-ray structure of *A. baumannii* PBP2 shows the pedestal domain in open conformation, although the anchor domain is not completely resolved. This conformation closely resembles that of *H. pylori* PBP2 when bound to MreC (figure 3.15c), indicating that *A. baumannii* PBP2 similarly to its homologue in *H. pylori*, could possibly adopt a competent conformation for the interaction with its cognate MreC. The open conformation of crystallised *A. baumannii* PBP2 is stabilised by packing effects, where anchor-anchor and head-head contacts between neighbouring molecules take place.

3.5.1.2 The C-terminal domain

The C-terminal module of bPBPs harbours the active site where transpeptidation occurs and is mostly α helical in nature ($\alpha 9$ - $\alpha 21$). The TP domain of *A. baumannii* PBP2 exhibits a central anti-parallel five stranded β sheet ($\beta 9$, $\beta 10$, $\beta 17$ - $\beta 19$) packed between two α helices on one side ($\alpha 9$ and $\alpha 21$), and one α helix on the opposite side ($\alpha 18$). The active site lies at the interface between the aforementioned five stranded β sheet and the α helical cluster ($\alpha 12$ - $\alpha 19$). Additional short anti-parallel β strands are located at the bottom ($\beta 8$, $\beta 15$ and $\beta 16$) and the top ($\beta 11$ - $\beta 14$) regions of the TP domain (figure 3.14). It is of note that, the 55 residue long termination of the polypeptide chain was untraceable on the electron density map, implying high local flexibility. Primary sequence alignment of bPBPs in Gram-negative bacteria indicates that there is variability in length and amino acid composition of this segment (figure S8). Moreover, the loop connecting strands $\beta 17$ and $\beta 18$ close to the active site, is partially built due to poor electron density for residues 548-552.

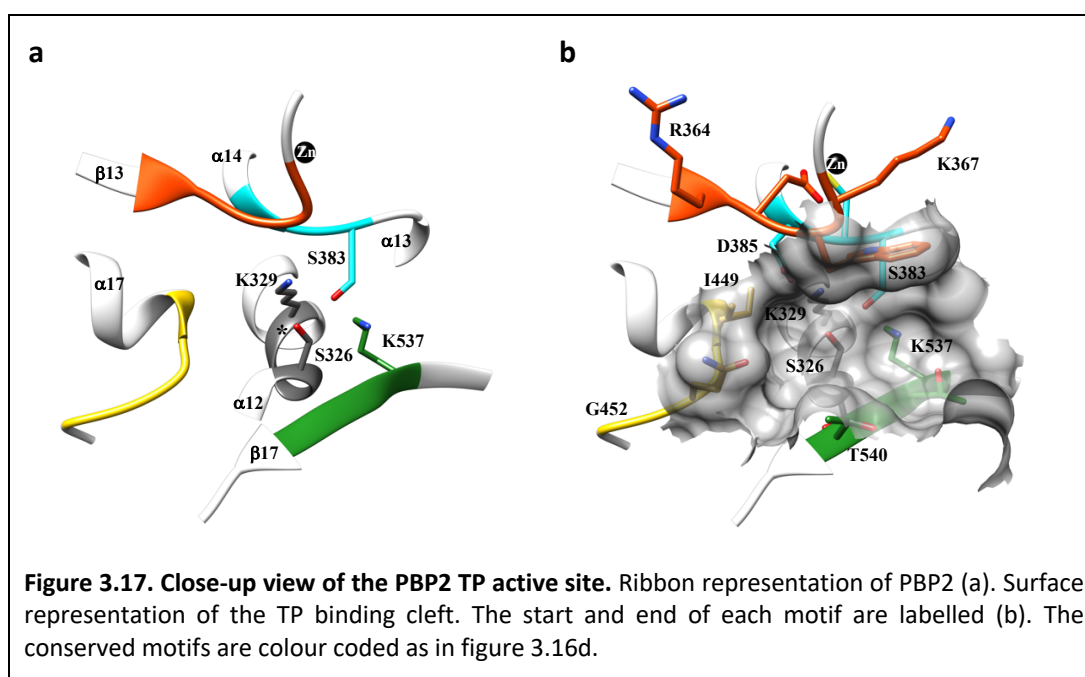
Notably, the corresponding loop in other class B PBP structures is also often incomplete even when β -lactam molecules are bound (for instance in *P. aeruginosa* PBP3 apo form- 3PBN.pdb and in complex with aztreonam- 3PBS.pdb, *S. pneumoniae* PBP2b apo form- 2WAE.pdb). Perhaps the natural substrate stabilises this region of the protein. Given its adjacent position to the entrance of the active site, such flexibility could be needed for the displacement of the PG chain from the glycosyltransferase enzyme (RodA/FtsW) to the respective PBP for its cross-linking to the murein sacculus. Similarly, a disordered loop is present in the TG domain of bifunctional PBPs (class A PBPs) and is thought to guide the elongating glycan chain from the donor site to the acceptor site (Sauvage *et al.*, 2014). The aforementioned loop could also be stabilised by interaction with proteins of the elongasome complex; interestingly, it is replaced by a short hairpin in class A PBPs. Despite many efforts in mapping the interaction surfaces within the elongasome/divisome complex, current knowledge of the dynamics of protein recruitment and complex formation are scarce. This is due to the transient nature of such interactions, which makes them difficult to study *in-vitro*. Unlike the pedestal domain, important conformational changes have not been seen within the TP domain of PBP structures, so far. The TP domain overall fold is pretty well conserved in HMW-PBPs of Gram-positive and Gram-negative bacteria. Subtle variations in the residues lining the active site may be found within and between subgroups. Diversely, the C-terminal end of the TP module can largely deviate, particularly between subgroups, as suggested by structure- and sequence- based alignments (Figure S8).

<i>Hp_PBP2</i>	-----MKNLRYKLLLFVFIGFWGLLALNLFILSVKNQEYYEKLAEARNMTKKE FLVPT RGNITDRNDEFLATNEL LVFGV FLPSGLKQK----D-LLEKIEIIQ	92
<i>Cj_PBP2</i>	-----MRMLVVGFILLFFIFLLSRVYYSIKSNVYYEELAKQNAIKTE FLPPV RGQITDRNGTLLAIND LGFS ISIKPYLSIKKSNKGILDKELSEL	94
<i>Hi_PBP2</i>	MNLKKFFNTPTEPFDRDKAERNLFAARRTLVAFILGILLTGVLFNTNIYQLQIVNFDTYQTRSNGNRIKLL PLPPT RGLIYDRYGKLLAENL TFGLY IVPEKTEN-----LDRTLDEL	114
<i>Kp_PBP2</i>	-----MKLQNSFRDYTAESSLFVRRALVAFILGILLTGVLIANLYNVQIVRFDDYQTRSNENRIKLV PIPPS RGIYDRNGTPLALN RTIYQ LEMMPEKVDN-----VQQTLDALR	106
<i>Ec_PBP2</i>	-----MKLQNSFRDYTAESALFVRRALVAFILGILLTGVLIANLYNLQIVRFTDYQTRSNENRIKLV PIAPS RGIYDRNGIPLALN RTIYQ IEMMPEKVDN-----VQQTLDALR	106
<i>St_PBP2</i>	-----MKRQNSFRDYTAESALFVRRALVAFILGILLTGVLIANLYNLQILRFDTYQTRSNENRIKLV PIAPS RGIYDRNGIPLALN RTIYQ IEMMPEKVDN-----VQQTLDALR	106
<i>Pa_PBP2</i>	-----MPQPIHLKDHEKDARLVRRRVIVGAVAVVLLTLVLVARMYHLQVTOYQYEHSTLSENNRVHVQ PIPP TRGIYDRNGVVIADNR PSF SLTITRERTED-----LQKTLDTLV	106
<i>Ab_PBP2</i>	-----MKQHFLPKDIQQEKRIYRGRIFFAVGLVIICLLVLSARYAYLQIFHYDEFSTASDKNRIRLQ PLPPA RGIYDRNGVLLADNY PVF TATLSKADVEN-----VDTVIEQLQ	106
	* . . : . * . : : . . : * : : * * * * . : * * : : . : : :	
<i>Hp_PBP2</i>	KFFPNFSKETLLNNYQKENSLYNHNLIKVVGFIP-YATM QPLYA -KLIQ TQGI FAL PLDK RYYPNNALASHVLGYVGVASLQDLKDDEE-NQYS----QIVGKTGI E KEYNKLLQGKVG	204
<i>Cj_PBP2</i>	NLFPDLNASKLAEIYKRNDSYNQDFIKVVDVIP-YDEI ISHYS -ELN LNKT IK IDPV VKKRKYPFGLASHIIGYVGKANLQDVQENEI-AKLS----NYTGKSGI E RYNDILQGEKG	206
<i>Hi_PBP2</i>	YIV-GLTDNDI-ENFKKERRRGTR-YTPI LLKPNL T EEQI S RFA VNGYQYPSLE V RPYFKRHLYGETMAHILGYVGKMNKDVRLKREDFANYAGTNDIGKLG E RYYEDILQGTG	231
<i>Kp_PBP2</i>	DVV-DLTDDDI-AGFKKERARSHR-FTSIPVKVNL SEVQ V ARFA VNQYRFP GV EV KGY KRRYPYNSALTHVIGYVSKINDKDVRLDKEGKLANYASTHDIGKLG E RYYEDVLHGQTG	223
<i>Ec_PBP2</i>	SVV-DLTDDDI-AAFKKERARSHR-FTSIPVKTNL TEVQ V ARFA VNQYRFP GV EV KGY KRRYPYGSALTHVIGYVSKINDKDVRLNNDGKLANYAATHDIGKLG E RYYEDVLHGQTG	223
<i>St_PBP2</i>	SVV-DLNDDDI-AAFKKERARSHR-FTSIPVKTNL TEVQ V ARFA VNQYRFP GV EV KGY KRRYPYGSALTHVIGYVSKINDKDVRLDRENKLANYAATHDIGKLG E RYYEDILHGQTG	223
<i>Pa_PBP2</i>	EIL-GLTEDDR-AIFEKRMKQGRPFEPVIMFEL NEEQI A RIA VNQ FRL PGVD VATQ FVRHYPLKEHFAHSVGYVGRINEQELKNLDP----INYSGTHHIGK TGI ERFYESELHGTVG	220
<i>Ab_PBP2</i>	PIL-ELTQEDV-DRFKSRIKTARK-TERVAIKLNL TETNI A KF SEVKYK FP GV RIETQ MTRYYPHGDLFAHVIGYVGRINDKELKSIDK----DLYAGTNLIGK IGV EKSYEDLLHGTPG	219
	. . : . . : : : : : * * : * : * * . : : . . : : * * * : * . * * *	
<i>Hp_PBP2</i>	YK IMR VNALNQELAT LEV VLPSTN	228
<i>Cj_PBP2</i>	TRVYK VNAL NQ EV EQLSY-TPAMS	229
<i>Hi_PBP2</i>	FEEVE INNR GK VI RTLRSPAVAG	255
<i>Kp_PBP2</i>	YEEVE VNNR GR VI RQLKEVPPQAG	247
<i>Ec_PBP2</i>	YEEVE VNNR GR VI RQLKEVPPQAG	247
<i>St_PBP2</i>	YEEVE VNNR GR VI RQLKEVPPQAG	247
<i>Pa_PBP2</i>	YEEVE TNA GR VL RLKRTDPIPG	244
<i>Ab_PBP2</i>	YESVE ADA HSN ILR H LGR KDPTRG	243
	. . : . . : *	

Figure 3.16c. Sequence alignment of PBP2 pedestal domain from Gram-negative bacteria of the WHO priority pathogens list. The triad Arg/Arg/Glu is highlighted in pink, whereas residues interacting at the head-anchor domain interface of *H. pylori* PBP2, and their corresponding residues in other bacteria, are shown in bold.

3.5.2 Active site structure

The catalytic site of *A. baumannii* PBP2 is located in a deep solvent accessible cleft of the TP domain; it encompasses broadly conserved residues in PBPs and serine β -lactamases, that participate in the transpeptidase reaction and binding of β -lactam antibiotics. These key residues are carried by three conserved motifs. The S*-X-X-K motif (Ser326- Thr327- Ile328- Lys 329) bears the catalytic Ser326 and is located at the N-terminus of α 12 (figure 3.14 and 3.17a-b), thus occupying a central position in the active site. The S-X-N/D motif (Ser383- Cys384- Asp385) is positioned on a short loop between α 13 and α 14 above the catalytic serine, and forms part of the first wall of the substrate binding cleft. The K-T/S-G-T motif (Lys537- Thr538- Gly539- Thr540) is located at the C-terminus of β 17, opposite side of the S-X-N/D motif, and forms the second wall of the binding pocket (figure 3.14 and 3.17a-b). Additional residues participate in the construction of PBP2 active site and are carried by two motifs conserved in subgroup B2. The R-D/N-W-K/N motif (Arg364- Asp365- Trp366- Lys367) is located on a long loop connecting β 13 and β 14 that protrudes above the active site, thus completing the first wall with the S-X-N/D motif. The I-G-Q-G motif (Ile449- Gly450- Gln451- Gly452) is situated in the rear of the binding site, at the C-terminus of α 17 and the loop connecting α 17 to α 18 (figure 3.14 and 3.17a-b), .



Strikingly, the third residue of the S-X-N/D motif is asparagine in all but class B2 PBPs, where it is replaced by aspartic acid. To date, the biological significance of this amino acid substitution is unclear, although it would be expected to affect the interaction with terminal residues of the pentapeptide substrate (L-ala- γ -D-Glu-*meso*DAP-D-ala-D-ala). In fact, the Asn N^{δ2} hydrogen bonds to the backbone carbonyl oxygen of the third residue of the substrate, in co-structures of *Streptomyces sp.* strain R61 D,D-peptidase and *Bacillus subtilis* PBP4a with PG mimetic peptides (McDonough *et al.*, 2002; Sauvage *et al.*, 2007). Hence, Asn is believed to be required for the proper positioning of the terminal pentapeptide residues within the binding cleft.

To be noted that, an extra electron density is observed in the TP active site of *A. baumannii* PBP2, both chains, and it is consistent with the non-covalent binding of a molecule. This molecule could possibly be glycerol, present in the cryoprotectant solution, or Hepes present in the protein buffer, and either way it could not be confidently modelled, therefore it will not be discussed.

3.5.3 A novel zinc- binding site

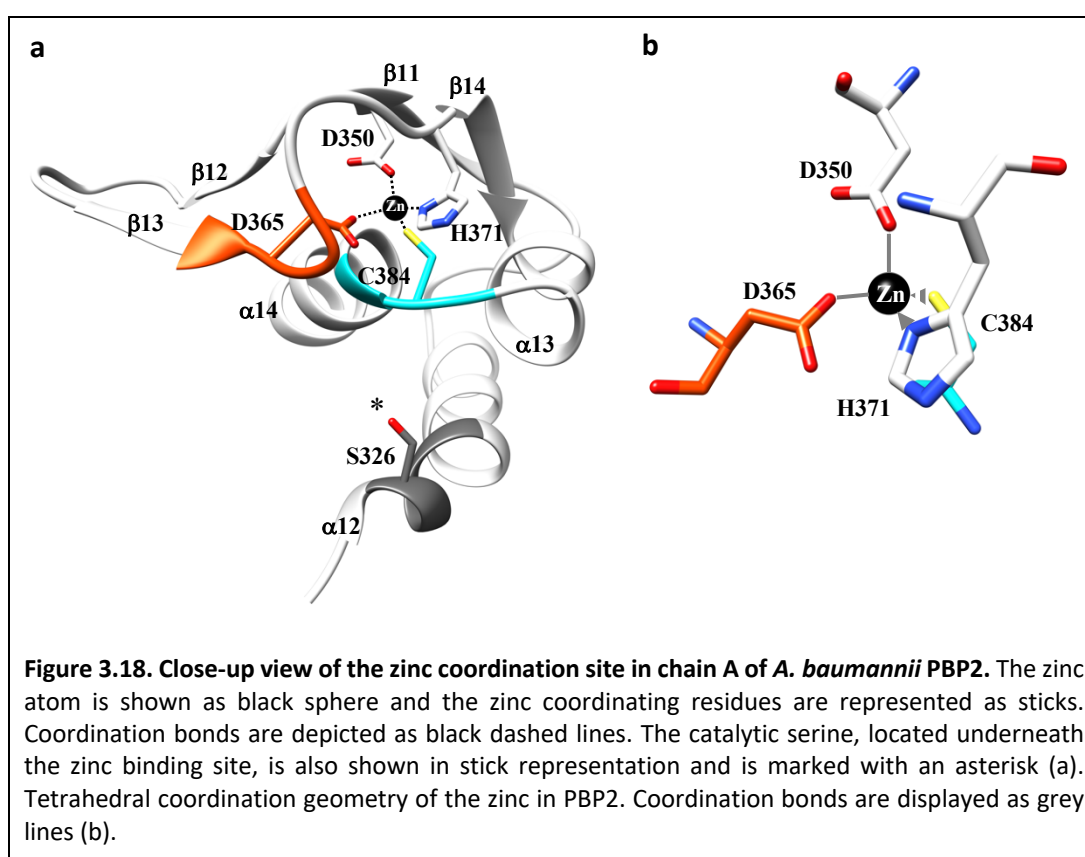
A. baumannii PBP2 harboured an authentic zinc-coordination site in the TP domain, as observed in section 3.4.7. As this structural feature is unprecedented among PBPs, it was taken forward for further investigation as described below.

3.5.3.1 Zinc-binding site structure

The zinc-binding site is enclosed on one side, by a β -hairpin loop (β 11- β 14) that extends over the top of the TP domain. A short loop connecting α 13 and α 14, and the N-terminus of α 14, complete the remainder of the site (figure 3.14). As a result, the zinc atom is shielded from solvent and sits atop the catalytic serine, from which is only 10.2 Å away (distance Zn- Ser326 O^γ). The zinc binding site encompasses four residues. Asp350 is located at the C-terminus of β 11, Asp365 and His371 are positioned on a loop connecting β 13 and β 14, Cys384 is placed on a short loop connecting α 13 and α 14, representing the middle residue of the conserved S-X-N/D motif in PBPs. The coordination geometry is tetrahedral (table 3.9, figure 3.18).

Coordinating residue	Coordinating atom	Measured distance (Å)	Reference distance (Å) (\pm SD)
Asp350	O ^{δ2} - Zn	1.96	2.17 \pm 0.23
Asp365	O ^{δ2} - Zn	2.12	2.17 \pm 0.23
His371	N ^{δ1} - Zn	2.00	2.18 \pm 0.17
Cys384	S ^γ - Zn	2.37	2.36 \pm 0.20

Table 3.9. Ligands and distances in the Zn-binding site of *A. baumannii* PBP2. Note the agreement between calculated zinc- ligand bond lengths in PBP2, and the average values from analogous zinc coordinating ligands in structures at 2.5 Å resolution, deposited in PDB (Laitaoja *et al.*, 2013).



The region spanning $\alpha 12$ to $\alpha 14$ (inclusive) is structurally conserved in all HMW-PBP structures solved so far (figure 3.14 and 3.18). Particularly, the $\beta 11$ - $\beta 14$ hairpin extension loop appears to be conformationally more flexible than the helical component. In a few cases, lack of sufficient electron density precluded modelling of the β -hairpin region in *M. tuberculosis* PBPA, *S. pneumoniae* PBP2x and *E. coli* PBP5 (Fedarovich *et al.*, 2010; Dessen *et al.*, 2001; Nicholas *et al.*, 2003; Nicola *et al.*, 2005b). Notably, a residue within this loop makes a contact with the X residue of the

S-X-N/D motif. This contact is highly conserved and seems to be crucial for the function of class B PBPs (Tomberg *et al.*, 2012; Liu *et al.*, 2010; Bukowska-Faniband and Hederstedt, 2017).

Due to the absence of a metal binding site in published PBP structures, the MetalS³ web tool (<http://metalweb.cerm.unifi.it/tools/metals3/>) (Valasatava *et al.*, 2014) was used to search structurally similar zinc coordination sites in known protein structures. Surprisingly, the search failed to identify any closely resembling zinc-binding site.

It is widely observed that zinc atoms in protein structures are found to fulfil either a catalytic function, serving as a Lewis acid in enzymatic reactions, or a structural role, maintaining protein stability and folding (Laitaoja *et al.*, 2013). Despite its vicinity to the catalytic serine, it is unlikely that the zinc atom could participate in the catalysis of PBP2; instead, a structural role could be more plausible. This was suggested by the fact that, the zinc ion is coordinated by four amino acid side chains, compared to a catalytic zinc where at least one water molecule is typically required in the coordination sphere of the catalytic metal, where it can be ionised, polarised, or displaced by the substrate/inhibitor (McCall *et al.*, 2000). Moreover, the amino acids that coordinate the zinc in the PBP2 structure are mostly located on flexible regions such as loops, as commonly featured by structural sites. Whereas, catalytic zinc coordinating residues are frequently positioned in rigid secondary structure elements (McCall *et al.*, 2000).

Inspection of all protein structures deposited in PDB that claim a zinc-binding site, has remarkably showed that a substantial number of these (1/3) contain artefacts. Spurious zinc ions are mostly found on protein surfaces, where they mainly aid crystallographic packing interactions (Laitaoja *et al.*, 2013). This seems not to be the case for the zinc binding site found in PBP2. In fact, in PBP2, the zinc ion is not solvent exposed, and does not participate in intermolecular interactions within the crystal. Also, zinc was not an additive in the solutions prepared for the purification and crystallisation of PBP2. Additionally, the zinc binding site appears to be consistently occupied by the metal (occupancy close to 1), which leads to exclude a fortuitous

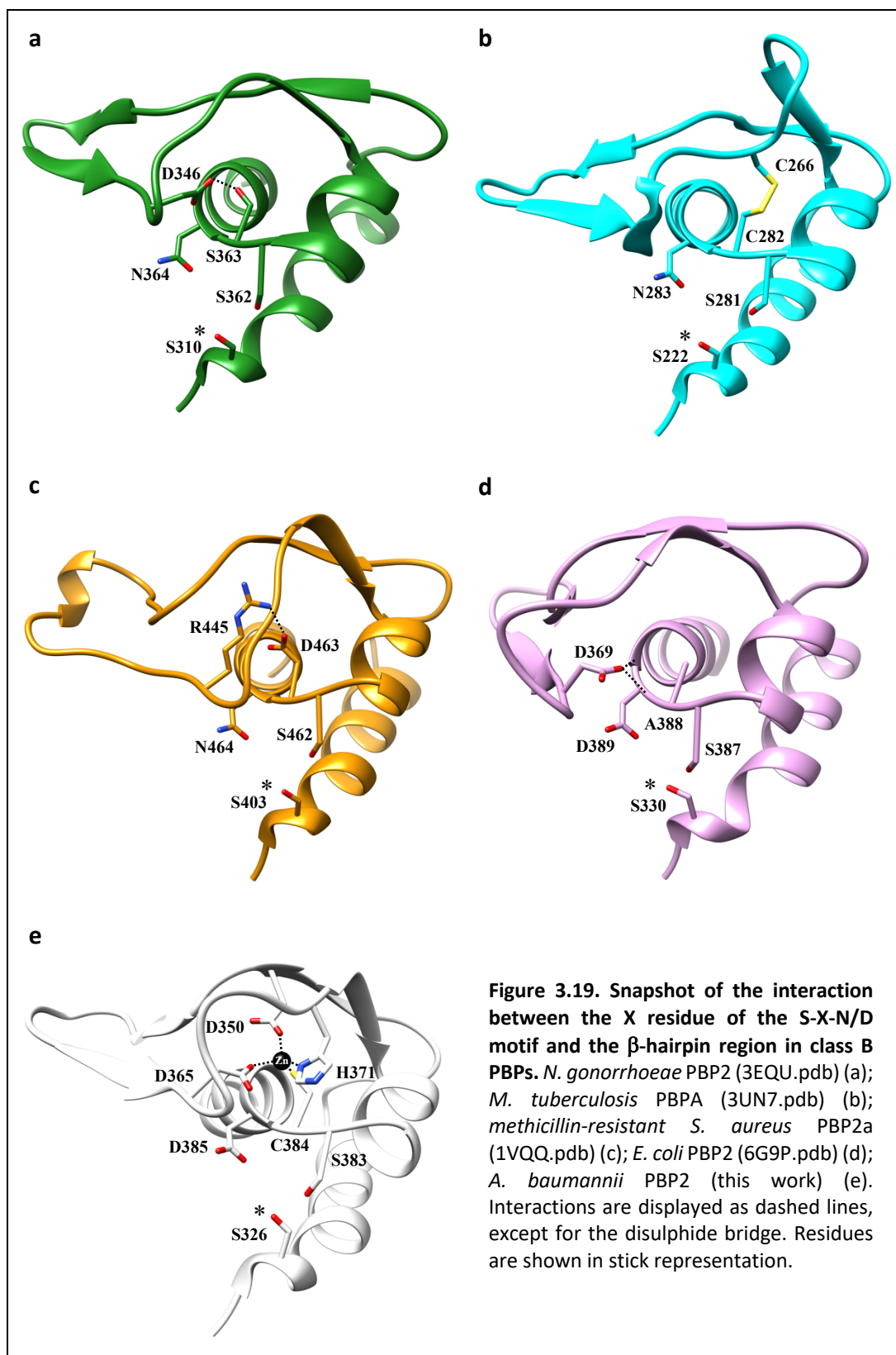
acquisition of trace zinc from the chemicals used. Thus, the most likely source of zinc detected in PBP2 crystals might have been *E. coli*, in which PBP2 was expressed and the zinc possibly acquired.

3.5.3.2 A new class B subtype: the Zn-containing PBPs

As previously discussed, all PBPs contain three conserved sequence motifs that form the catalytic center of the active site: the SXXK tetrad, which contains the serine nucleophile that reacts with bacterial cell-wall muramyl peptides and β -lactam antibiotics, the SXN/D triad, and the KT/SGT tetrad. However detailed visual and bioinformatic analysis of PBP structures, allowed Tomberg and coworkers (Tomberg *et al.*, 2012) to divide the class B PBPs into three distinct subgroups, depending on the nature of the conserved interaction in respect of the SXN/D triad. Representative members of these subgroups are illustrated in figure 3.19a-c. Three subtypes were described with variations in the middle position of the S-X-N/D motif, namely SSN-, SCN-, and SDN- containing PBPs. The middle Ser in SSN-containing PBPs commonly hydrogen bonds to the side chain γ -oxygen of a conserved Asp within the loop (for instance in structures of *N. gonorrhoeae* PBP2, *P. aeruginosa* PBP3, *S. pneumoniae* PBP2x) (figure 3.19a). The Cys of SCN-containing PBPs, forms a disulphide bond with a second Cys located either at the Asp position (in SSN- containing PBPs) or even further away (for instance in the structure of *M. tuberculosis* PBPA) (Figure 3.19b). Finally, the Asp in SDN-containing PBPs, may contact the side chain of Arg/Thr residues, located in a close or equivalent position to the Asp (in SSN- containing PBPs) (for instance in the structure of MRSA *S. aureus* PBP2a) (Figure 3.19c).

PBPs bearing a residue different from S/C/D in the middle position of the SXN/D triad, may use the backbone chain of this motif to contact the loop, as observed in X-ray structures *H. pylori* PBP2 (X= Val) and *E. coli* PBP2 (X= Ala) (Figure 3.19d).

Importantly, the new structure of *A. baumannii* PBP2 presented in this thesis unveils another, unexpected, way by which the conserved hairpin loop can make contacts with the X residue of the S-X-N/D motif. This consists of a metal coordination site, assigned to zinc in this thesis work (Figure 3.19e).



3.5.3.3 Biological significance of the S-X-N/D motif conserved interaction

A few *in-vitro* and *in-vivo* studies have tried to shed light whether or not the conserved interaction between the equivalent of β 11- β 14 hairpin loop and the S-X-N/D motif, plays a part in the catalytic activity of PBPs, and their ability to covalently bind β -lactam antibiotics.

N. gonorrhoeae PBP2, an essential PBP of the divisome complex in this pathogen, was studied *in-vitro* by mutagenesis (Tomberg *et al.*, 2012) based upon an X-ray crystal structure for *N. gonorrhoeae* PBP2 which identified S310 as the active site serine within the SXXK motif (Powell *et al.*, 2009b) (figure 3.19a). Single mutations to the residues involved in the conserved interaction between the loop region and the SXN/D motif (D346A and S363A corresponding to Asp365 and Cys384, respectively in *A. baumannii* PBP2) could not support cell growth, consistent with loss of TPase activity. Moreover, a decreased acylation rate of penicillin G was reported for the same mutants, in comparison to the wild-type (Tomberg *et al.*, 2012).

Additional evidence for the functional role of this conserved interaction concerned *B. subtilis* SpoVD, a PBP essential for the synthesis of endospore cortex peptidoglycan. In fact, SpoVD deficient mutants were completely unable to produce heat-resistant spores (Liu *et al.*, 2010). SpoVD carries two cysteine residues, Cys332 and Cys351 (corresponding to Asp365 and Cys384 in *A. baumannii* PBP2), that can potentially form a disulphide bridge, similarly to Cys266 and Cys282 in *M. tuberculosis* PBPA (figure 3.19b). Liu and coworkers found that, mutations of SpoVD at either Cys332 (C332G/S/N/E/T/A) or Cys351 (C351S), caused severe impairment to the capability of *B. subtilis* to form heat-resistant spores, suggesting a defective SpoVD TPase activity. The ability to bind bocillin was retained instead, at least for C351S. The authors attributed a structural and functional role at the interaction taking place within the Cys-Cys pair and, interestingly, this role could not be equally fulfilled by an Asp-Ser pair, frequently encountered in PBPs, without complete loss of activity (Liu *et al.*, 2010).

All of these observations point to a functional role of the loop region above the active site serine which may be structurally organised by a variety of different mechanisms.

Our finding that the *A. baumannii* protein has a separate and previously unidentified metal dependent mechanism in constraining the flexibility of this loop region adds further weight to this observation.

The exact mechanism underlying the loss of function of class B PBPs, following disruption of the conserved interaction between the β -hairpin region and the S-X-N/D motif, has not been elucidated yet. However, structures of wild-type and catalytically inactive (G105D) *E.coli* PBP5 (LMW-PBP), offer a glimpse in this regard (Nicholas *et al.*, 2003). The structural data point to the disordering of the β -hairpin region as the major determinant in the loss of enzymatic activity. Although the β -hairpin region does not participate directly in catalysis, it has been postulated that it could have a modulatory effect on the function of the S-X-N/D motif, that on the contrary, has a role in deacetylation (Nicholas *et al.*, 2003).

3.6 *In-vivo* activity of wild-type and Zn-binding site mutants of *A. baumannii* PBP2

Data gathered on different PBPs from various bacteria (Tomberg *et al.*, 2012; Bukowska-Faniband and Hederstedt, 2017), encouraged further investigation of the role played by the zinc-binding site, in mediating the crucial interaction between the β -hairpin region and the S-X-N/D motif, in *A. baumannii* PBP2. For this purpose, *in-vivo* experiments were performed in collaboration with Dr Edward Geisinger (Northeastern University, Boston, USA). Plasmids used in these studies were generated at the University of Warwick (3.6.1) and tested in *A. baumannii* ATCC 17978 by Dr Edward Geisinger (3.6.2).

3.6.1 Plasmid construction

The nucleotide sequence encompassing the full-length PBP2 encoding gene and an upstream predicted native promoter, was PCR amplified from genomic DNA of *A. baumannii* ATCC 17978, provided by Dr Edward Geisinger, using Eddie-F and Eddie-R primers (table S1). The fragment was cloned into pEGE305 (Geisinger *et al.*, 2018), provided by Dr Edward Geisinger, by using EcoRI and PstI restriction enzyme sites,

resulting in plasmid pEGE306. The same fragment was also cloned into pUC19 with the same restriction enzymes, resulting in plasmid pMIC01, to be used as template for the insertion of the mutations. The insert was checked by DNA sequencing, using M13-F and M13-R primers (table S1).

Alanine-scanning mutagenesis of PBP2 at the zinc-coordinating residues Asp350, Asp365, His371 and Cys384, yielded the pUC19 derived plasmids pMIC02, pMIC03, pMIC04 and pMIC05, respectively. Mutations were introduced in pMIC01 by site directed mutagenesis, using primers 0100-F and 0100-R, 0101-F and 0101-R, 0102-F and 0102-R, 0103-F and 0103-R (table S1). Successful mutagenesis was verified by DNA sequencing using the 0099-primer (table S1).

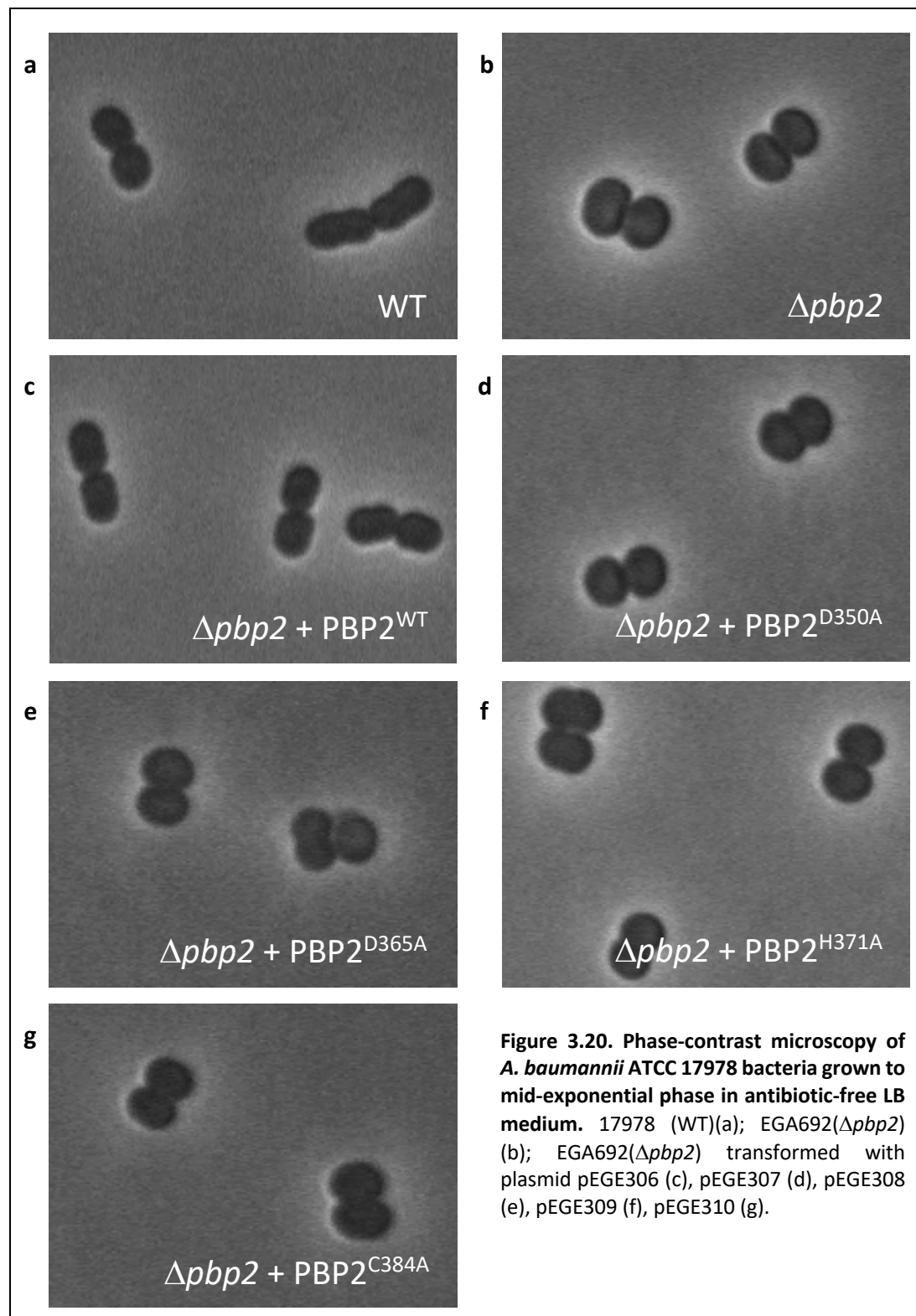
To transfer the mutated PBP2 inserts into pEGE305 plasmid, pMIC02, pMIC03, pMIC04 and pMIC05 were used as template in a PCR reaction with Eddie-F and Eddie-R primers. The amplified DNA was cut with EcoRI and PstI restriction enzymes and ligated into pEGE305, resulting in pEGE307, pEGE308. pEGE309 and pEGE310, respectively. All inserts in pEGE305-based plasmids were checked by DNA sequencing, using pEGE305-F and pEGE305-R primers (table S1).

3.6.2 *In-vivo* experiments

3.6.2.1 Cell morphology assays

The *in-vivo* experiments were performed on *A. baumannii* ATCC 17978, both the wild-type strain (for simplicity called 17978 (WT)) and the PBP2 deleted strain (referred as EGA692(Δ *pbp2*)) (Geisinger *et al.*, 2018). Under conditions of exponential growth in antibiotic-free LB medium, strain 17978 (WT) grew as short rods while EGA692(Δ *pbp2*) propagated as spheres, due to a block in the cell wall elongation resulting from PBP2 deletion (Geisinger *et al.*, 2018) (figure 3.20a-b). The cellular morphology (rod/sphere) could therefore be indicative of the functional state (on/off) of the elongosome *in-vivo*, and could be used as a way of testing any functional detrimental effect caused by mutations of PBP2, for instance in the zinc-binding site. When EGA692(Δ *pbp2*) was complemented with pEGE306 carrying a wild-type copy of the PBP2 gene, the rod-shape morphology was restored (figure 3.20c) suggesting that the protein was correctly expressed from the plasmid gene

and was functional *in-vivo*. Conversely, none of the PBP2 zinc-binding site mutants encoded by pEGE307-310, could complement EGA692($\Delta pbp2$) to revert the spherical phenotype (figure 3.20d-g).



To confirm expression of wild-type or mutant PBP2 proteins in EGA692($\Delta pbp2$) cells transformed with the appropriate plasmids, a Western blot was carried out on cell lysates. A rabbit anti-PBP2 antiserum was generated by immunizing a rabbit with purified recombinant *A. baumannii* PBP2 ($\Delta 53-672$) (3.2), according to standard protocols (Pocono Rabbit Farm and Laboratory), and this was provided by Prof Ralph Isberg (Tufts University School of Medicine, Boston, USA). Rabbit anti-PBP2 antiserum (1:12000 dilution) was used with a secondary HRP-conjugated goat anti-rabbit antibody (1:5000 dilution, Invitrogen), for detection of PBP2. Activity of the coupled antiserum-antibody system was first tested on various amounts of purified *A. baumannii* PBP2 ($\Delta 53-672$) (figure 3.21a).

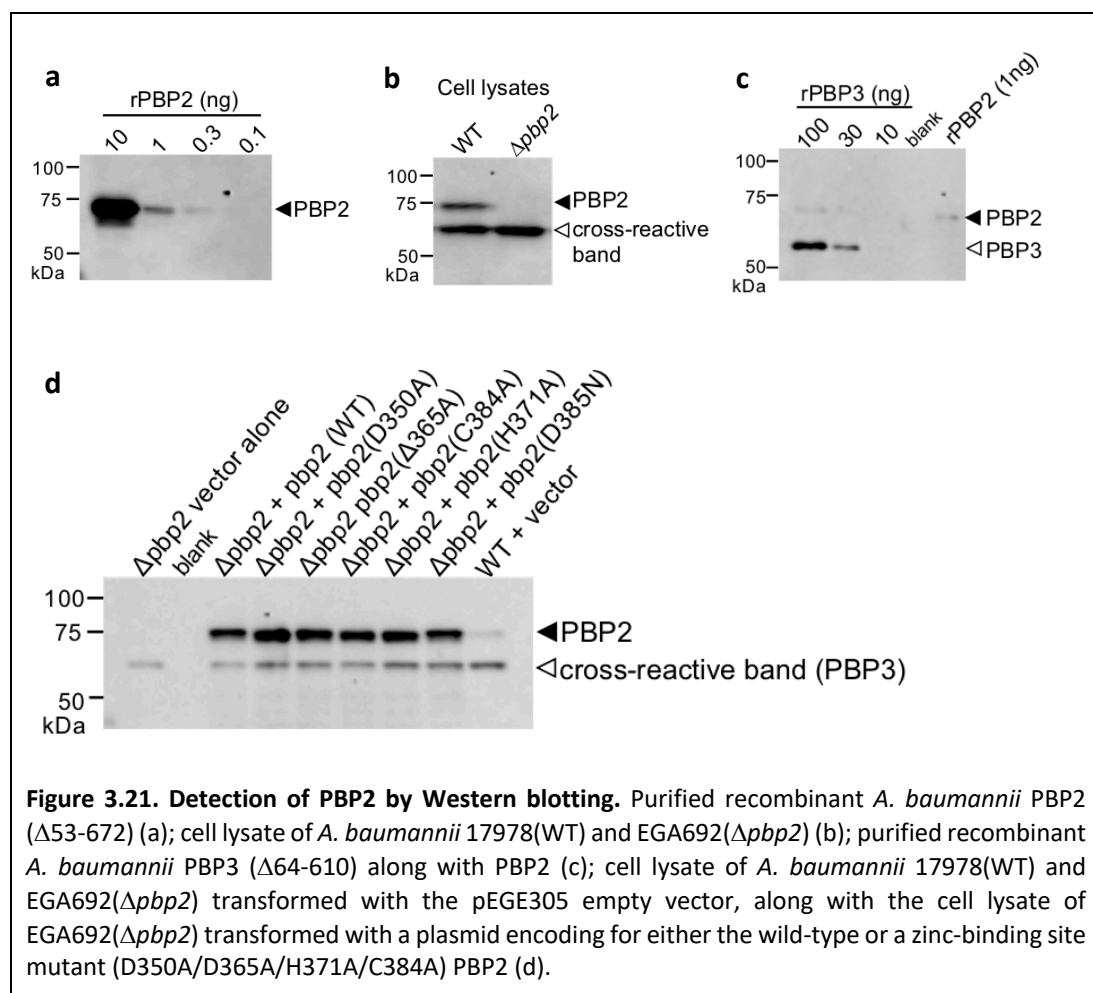


Figure 3.21. Detection of PBP2 by Western blotting. Purified recombinant *A. baumannii* PBP2 ($\Delta 53-672$) (a); cell lysate of *A. baumannii* 17978(WT) and EGA692($\Delta pbp2$) (b); purified recombinant *A. baumannii* PBP3 ($\Delta 64-610$) along with PBP2 (c); cell lysate of *A. baumannii* 17978(WT) and EGA692($\Delta pbp2$) transformed with the pEGE305 empty vector, along with the cell lysate of EGA692($\Delta pbp2$) transformed with a plasmid encoding for either the wild-type or a zinc-binding site mutant (D350A/D365A/H371A/C384A) PBP2 (d).

The purified PBP2 was detectable by the rabbit anti-PBP2 antiserum, as indicated by a chemiluminescent signal appearing at approximately the molecular weight of PBP2 ($\Delta 53-672$, MW= 70.5 kDa), and the detection limit was of 0.3 ng of protein.

Thereafter, a Western blot was carried out on the cell lysate of 17978(WT) and EGA692($\Delta pbp2$) (figure 3.21b). As expected, the 17978(WT) cell lysate produced a chemiluminescent signal consistent with the full-length PBP2 (MW= 74.5 kDa), whereas this signal was absent in the EGA692($\Delta pbp2$) cell lysate. Unexpectedly, a secondary chemiluminescent signal was observed in both cell lysates, corresponding to a protein of approximately 60 kDa (figure 3.21b). Due to cross-reactivity, this protein could have been the full-length PBP3 (MW= 67.7 kDa) which shows high sequence similarity with PBP2, particularly in the TP domain, and this was later confirmed by Western blot of purified recombinant *A. baumannii* PBP3 ($\Delta 64-610$, MW= 62.5 kDa) with rabbit anti-PBP2 antiserum (figure 3.21c).

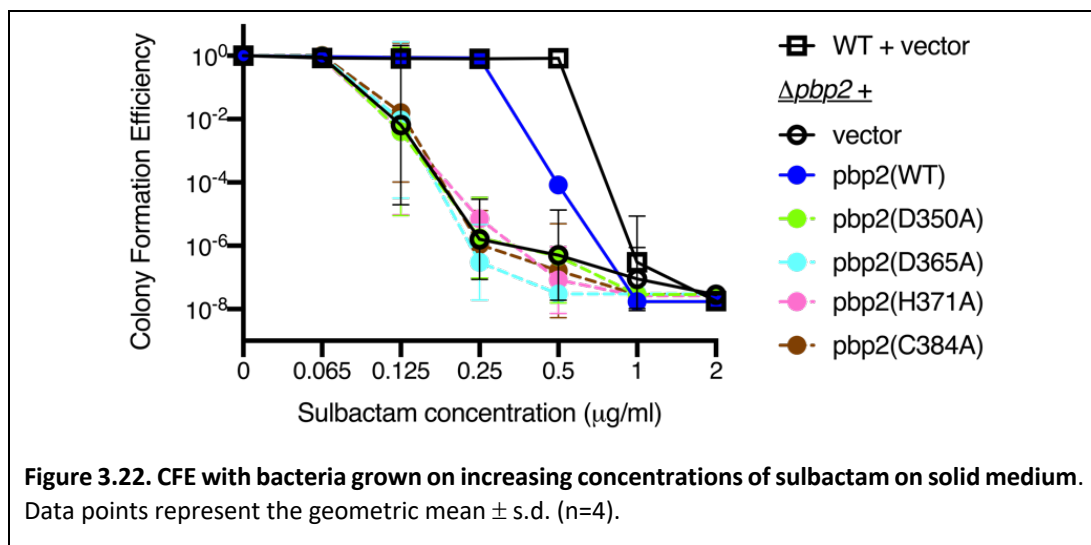
Since the coupled antiserum-antibody system could detect the native PBP2 in the bacteria cell lysate, Western blot analysis were extended to the cell lysate of EGA692($\Delta pbp2$) transformed with pEGE306-pEGE310 (3.21d). Both the wild-type and the zinc-binding site mutants of PBP2 were expressed from the plasmid in EGA692($\Delta pbp2$), as indicated by a chemiluminescent signal at ~75 kDa. As anticipated, EGA692($\Delta pbp2$) transformed with pEGE305 empty vector was negative for the PBP2 signal. Consistent with the results observed in figure 3.21b, a cross-reactive band was present in all the cell lysates tested and corresponding to the full-length PBP3. Although the PBP2 ORF was cloned along with the endogenous promoter, PBP2 expression levels were much higher when the protein was expressed from plasmid (pEGE306-pEGE310) compared to 17978(WT) transformed with pEGE305 empty vector. Notably, the protein expression level was not affected by the zinc-binding site mutations.

The analysis included also an additional PBP2 mutant (D385N), and this protein will be discussed in chapter 4.

3.6.2.2 Antibiotic resistance assays

The strains investigated in 3.6.2.1 were also studied with respect to sulbactam resistance by colony formation efficiency (CFE) assay (figure 3.22). Sulbactam is a β -lactamase inhibitor with intrinsic antibacterial activity against *A. baumannii* and

other Gram-negative bacteria, arising from inhibition of PBP1a and PBP3, but not PBP2 (Penwell *et al.*, 2015). Briefly, bacteria were grown to early post-exponential phase, serially diluted in PBS, and spotted onto solid LB agar medium without antibiotic or containing 2-fold serial dilutions of sulbactam. The CFU resulting after overnight incubation at 37 °C were counted. Colony formation efficiency was defined as (# CFU on the antibiotic test plate x dilution factor)/(# CFU on the antibiotic-free plate x dilution factor) (Geisinger and Isberg, 2015 ;Geisinger *et al.*, 2018).



The antibiotic resistance assays showed that, in the absence of PBP2 (i.e., EGA692($\Delta pbp2$)) *A. baumannii* became hypersensitive to sulbactam as suggested by the drop in MIC from 0.5-1 $\mu\text{g}/\text{mL}$ (17978(WT)) to 0.125-0.250 $\mu\text{g}/\text{mL}$ (EGA692($\Delta pbp2$)). EGA692($\Delta pbp2$) hypersensitivity to sulbactam could be explained by the fact that, in this strain PG synthesis relies completely on the activity of the main transpeptidase PBP3. Hence, in a $\Delta pbp2$ background any molecule targeting PBP3 would have an improved antibacterial effect. Note that, in this experiment both strains contained a pEGE305 empty vector, to take into account any contribution given by the vector itself.

When EGA692($\Delta pbp2$) was complemented with a wild-type PBP2 gene, the sulbactam resistance profile of the bacteria closely resembled that of 17978(WT), although a slight drop in MIC was present (0.5 $\mu\text{g}/\text{mL}$). Conversely, each of the strains

EGA692(Δ *pbp2*) expressing a Zn-binding site PBP2 mutant mirrored the EGA692(Δ *pbp2*) resistance profile, that is sulbactam hypersensitivity.

Taken together, the *in-vivo* assays showed that, expression of PBP2 mutated in the Zn-coordination site (D350A/D365A/H371A/C384A) cannot support PG elongation *in-vivo*, thus phenocopying the PBP2 deficient strain EGA692(Δ *pbp2*) with respect to cell morphology and sulbactam resistance.

3.7 *In-vitro* characterisation of wild-type and Zn-binding site mutants of *A. baumannii* PBP2

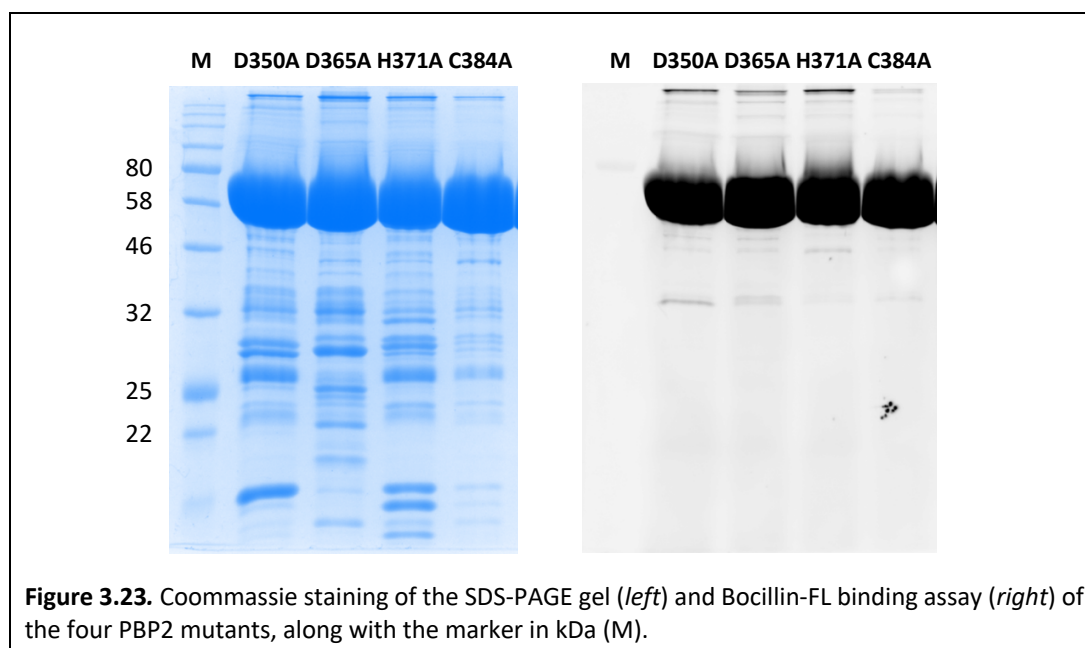
3.7.1 Generation of *A. baumannii* PBP2 D350A, D365A, H371A and C384A mutants

A mutagenesis approach was employed to determine whether disruption of the zinc-coordination site would solely affect protein stability, or would also have repercussions for the reactivity of the protein towards β -lactam molecules. To do so, each of the PBP2 residues coordinating the zinc ion, i.e., Asp350, Asp365, His371 and Cys384, was mutated to alanine.

The pUC19-derived plasmids pMIC02 (D350A), pMIC03 (D365A) and pMIC04 (H371A) which contain a mutated copy of the full-length PBP2 encoding gene from *A. baumannii* ATCC 17978, were used as template in a PCR reaction with 0098-F and 0098-R primers (table S1-S2). The generated amplicons, encoding for a truncated version of PBP2 (aa 53-672) were cloned into pET-47b, resulting in pMIC06 (D350A), pMIC07 (D365A), and pMIC08 (H371A) (table S2). Plasmid pMIC09 (C384A) was generated from pMIC10 by site directed mutagenesis, using 0105-F and 0105-R primers (table S1-S2). Presence of the insert with the desired mutation was confirmed by DNA sequencing, using T7-F, T7-R and 0099-primers (table S1).

The pET-47b derived plasmids pMIC06-09 were transformed into *E. coli* C41 (DE3) competent cells. Expression and purification of the four zinc-binding site mutants (figure S2) was achieved by following the protocol established for the wild-type PBP2 (3.2), although the protein yields were quite low (~1 mg per litre of bacteria culture).

Purity of the four PBP2 mutant preparations was > 90 %, and the mutations did not seem to prevent the binding of bocillin (figure 3.23).



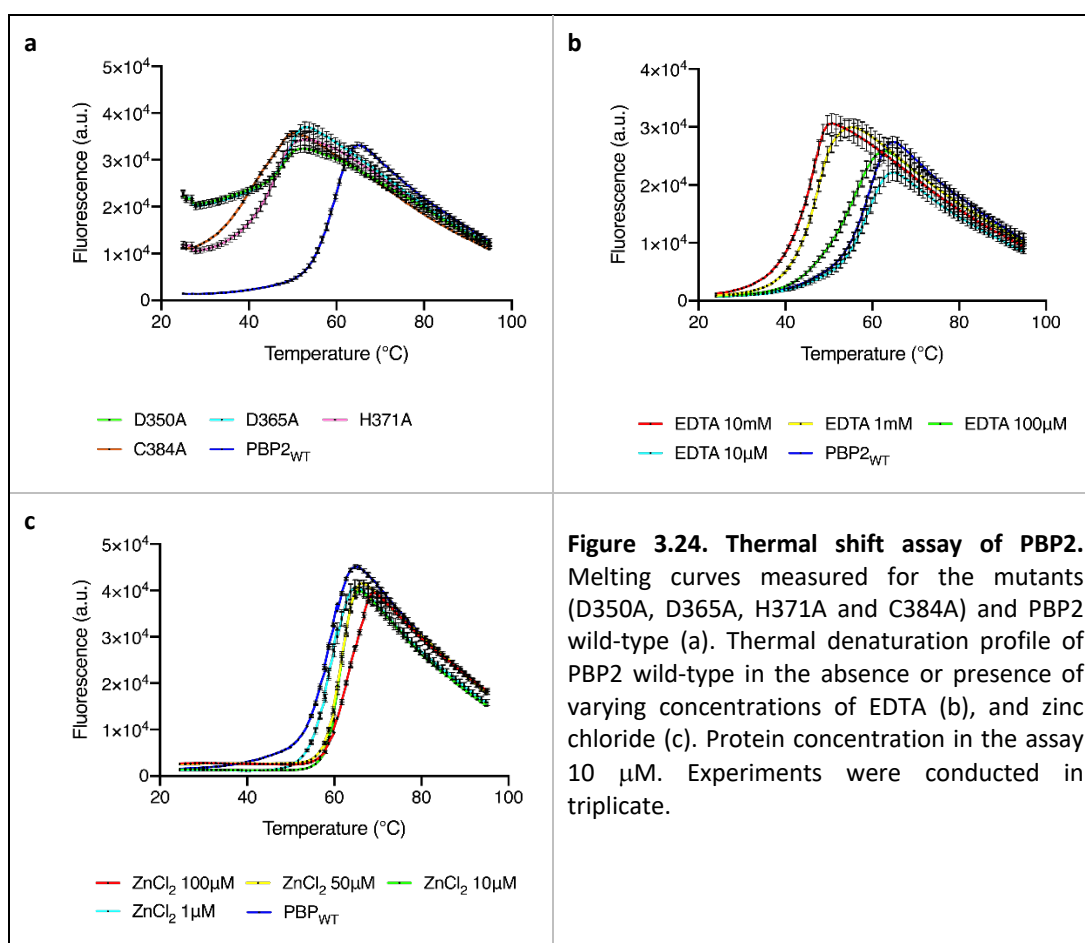
3.7.2 Differential scanning fluorimetry assays

The impact of the mutations (i.e., D350A, D365A, H371A and C384A) on the thermostability of PBP2, was tested by differential scanning fluorimetry (2.5.2). The melting temperatures (T_m) of wild-type and mutated PBP2 were measured (figure 3.24a, table 3.10). All four zinc-binding site mutants appeared to be less stable compared to the PBP2_{WT}, as indicated by large negative ΔT_m (difference between the T_m of PBP2_{WT} and the T_m of the tested protein), suggesting that the zinc-binding site could be possibly disrupted by the introduction of the mutations. A similar effect on the thermostability of the protein was also expected when PBP2 was treated with EDTA, a chelating agent that can sequester metals from proteins, including zinc. Therefore, a differential scanning fluorimetry assay was carried out on PBP2_{WT}, pre-incubated for one h with varying concentrations of EDTA (figure 3.24b). EDTA had a destabilising effect on PBP2, and this effect was concentration dependent. The negative ΔT_m in presence of ≥ 100 -fold excess of EDTA, closely resembled the results obtained with the PBP2 mutants (table 3.10). Conversely, addition of 10-fold excess of zinc chloride led to a little increase in protein thermostability (figure 3.24c, table

3.10); higher concentrations of zinc chloride were not tested due to the property of zinc of causing protein precipitation.

PBP2	ΔT_m ($^{\circ}\text{C}$) \pm SD	PBP2 _{WT}	ΔT_m ($^{\circ}\text{C}$) \pm SD	PBP2 _{WT}	ΔT_m ($^{\circ}\text{C}$) \pm SD
D350A	-12.00 ± 0.14	+ EDTA (10 mM)	-14.96 ± 0.13	+ ZnCl ₂ (100 μM)	$+4.89 \pm 0.20$
D365A	-8.07 ± 0.44	+ EDTA (1 mM)	-14.00 ± 0.08	+ ZnCl ₂ (50 μM)	$+2.70 \pm 0.22$
H371A	-14.78 ± 0.14	+ EDTA (100 μM)	-5.76 ± 0.18	+ ZnCl ₂ (10 μM)	$+2.59 \pm 0.20$
C384A	-17.90 ± 0.20	+ EDTA (10 μM)	-1.15 ± 0.10	+ ZnCl ₂ (1 μM)	$+0.30 \pm 0.21$

Table 3.10. Thermal shift assay of PBP2. The melting temperature was calculated from the thermal denaturation curves of PBP2 mutants (D350A, D365A, H371A and C384A, and PBP2 wild-type in the absence or presence of varying concentrations of either EDTA or zinc chloride. ΔT_m is the difference between the T_m of the protein reference (i.e., PBP2 wild-type) and the T_m of the protein being analysed (PBP2 mutant or PBP2_{WT} treated with EDTA/ZnCl₂). Protein concentration in the assay 10 μM . Experiments were conducted in triplicate.



3.7.3 Spectrophotometric assays with DTNB

A. baumannii PBP2(Δ 53-672) carries one cysteine only at position 384, and this residue is engaged in a zinc-binding site as revealed by the X-ray crystallographic structure of PBP2. The redox state of Cys384 under different conditions, could be monitored by the Ellman's assay (2.5.4).

Reaction of PBP2_{WT} with DTNB caused a negligible increase in absorbance (table 3.11) (figure 3.25a); this result was expected since Cys384 coordinates the zinc ion, therefore the thiol would not be available for the reaction with DTNB. When PBP2_{WT} was pre-incubated with 10000-fold excess EDTA for one h (PBP2_{EDTA}), addition of DTNB caused an increase in absorbance (table 3.11) (figure 3.25b), consistent with the production of TNB²⁻ due to reaction of DTNB with the free thiol of Cys384. This result suggested that, EDTA could chelate the zinc ion in PBP2. An analogous result was obtained when PBP2_{WT} was pre-incubated with 8M urea for ten min (PBP2_{UREA}) (table 3.11) (figure 3.25c). Since urea is a denaturing agent, it was expected that treatment with urea would cause PBP2 unfolding and disruption of the zinc-coordination site, thus rendering Cys384 available for the reaction with DTNB.

The reaction of PBP2_{WT} and PBP2_{EDTA} with DTNB was also verified by intact protein MS (2.6.2). As expected, PBP2_{WT} was unmodified by DTNB, whereas only the adduct of PBP2_{EDTA} with the thionitrobenzoate (+ 196 Da) could be detected (table 3.12, figure 3.26 and 3.27). MS spectra were deconvoluted in a large mass range (from 60000-160000 Da) in order to check for the presence of dimers. The MS spectra of PBP2_{WT} reacted with DTNB indicated that the protein is mostly monomeric and some dimer could form, although the intensity of the dimeric peak was considerably lower than the monomeric peak. The dimer could not be modified by DTNB, suggesting that the cysteines may interact by disulphide bond. The MS spectra of PBP2_{EDTA} reacted with DTNB showed a mostly monomeric protein. Surprisingly, the dimeric peak presented a double TNB modification, indicative of reduced cysteines. It was not clear how the dimer could have formed without a disulphide bond and resist to the denaturing conditions of the MS, pointing out to a possible artefact produced by the charge-deconvolution algorithm (Bern *et al.*, 2018).

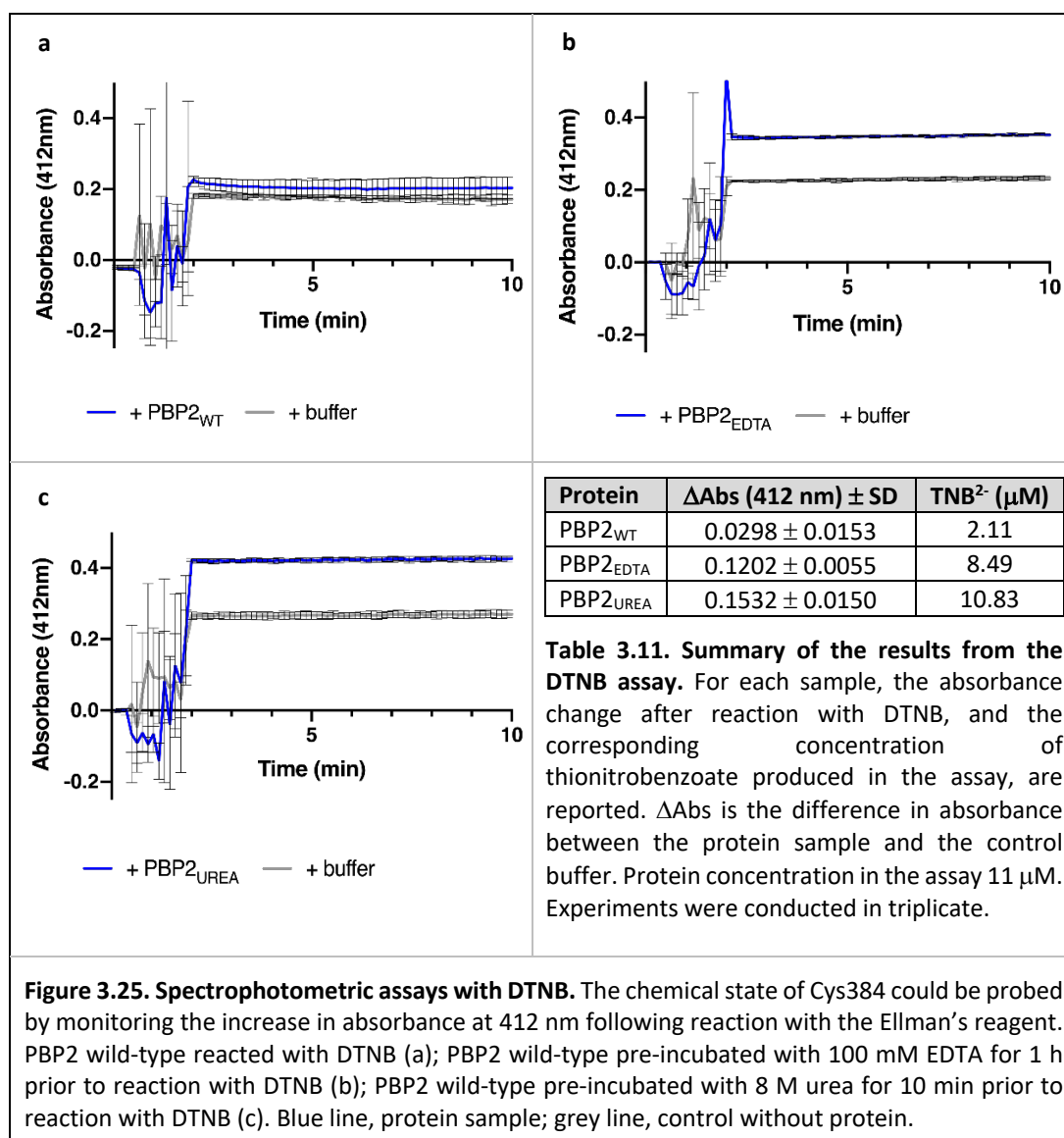


Figure 3.25. Spectrophotometric assays with DTNB. The chemical state of Cys384 could be probed by monitoring the increase in absorbance at 412 nm following reaction with the Ellman's reagent. PBP2 wild-type reacted with DTNB (a); PBP2 wild-type pre-incubated with 100 mM EDTA for 1 h prior to reaction with DTNB (b); PBP2 wild-type pre-incubated with 8 M urea for 10 min prior to reaction with DTNB (c). Blue line, protein sample; grey line, control without protein.

PBP2 _{WT} (reference)	PBP2 _{WT} + DTNB		PBP2 _{EDTA} + DTNB	
Calculated mass (\pm error) (Da)	Calculated mass (\pm error) (Da)	$\Delta\text{mass (Da)}$	Calculated mass (\pm error) (Da)	$\Delta\text{mass (Da)}$
70543.41 (\pm 0.14) (monomer)	70543.23 (\pm 0.05)	-	70740.10 (\pm 0.05)	+ 196.69
141086.63 (\pm 2.23) (dimer)	141086.48 (\pm 1.20)	-	141084.89 (\pm 2.63) 141480.22 (\pm 1.02)	- + 393.59

Table 3.12. MS of PBP2_{WT} and PBP2_{EDTA} reacted with 100-fold molar excess of DTNB. Δmass is the difference in observed mass between the protein reacted with DTNB and the reference (PBP2_{WT}).

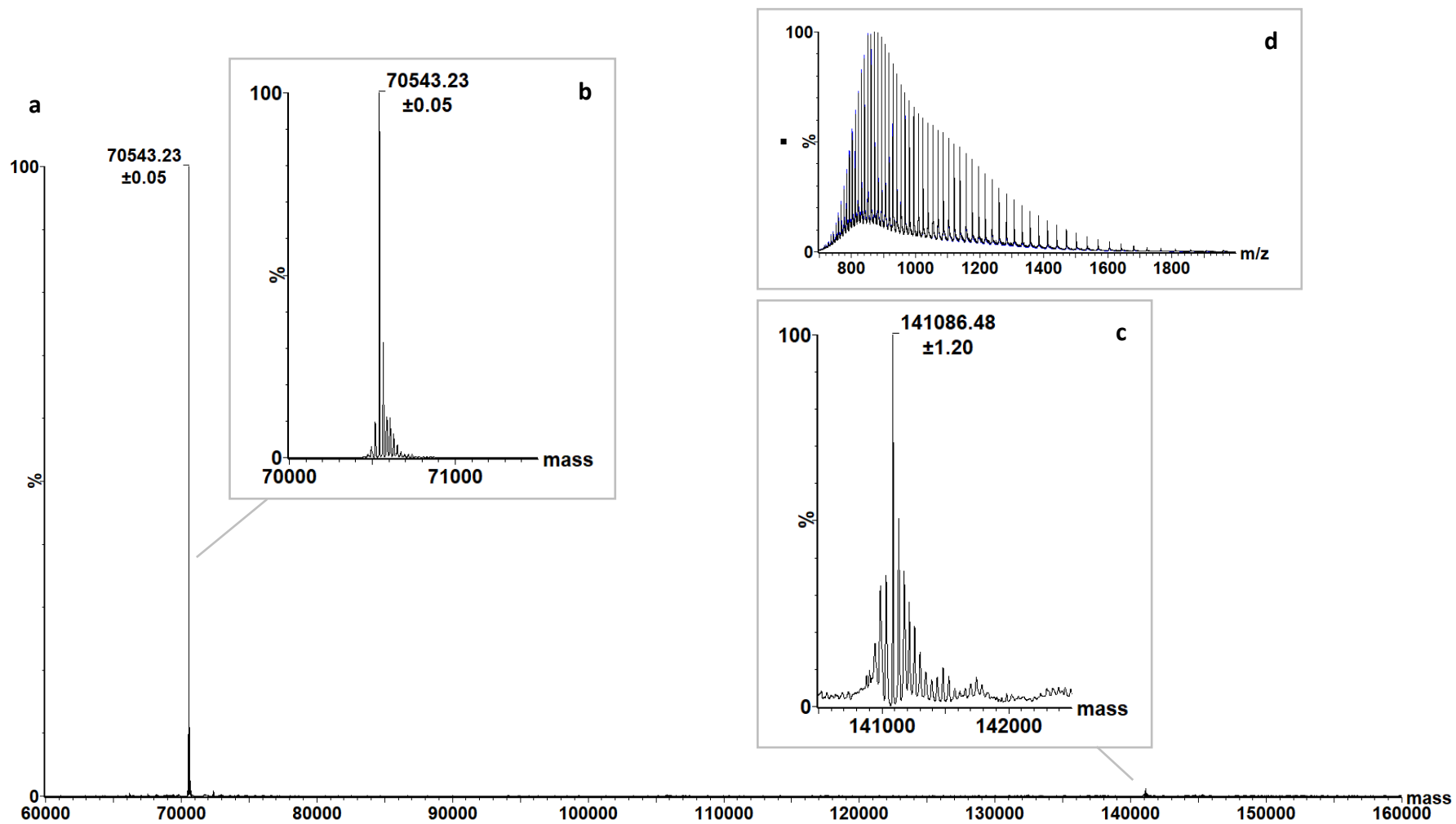


Figure 3.26. MS of PBP₂_{WT} reacted with DTNB. Spectra deconvoluted in the mass range 60000-160000 Da (a); close-up view of the monomeric peak (b) and dimeric peak (c); The combined spectra (black) superimposes well to the theoretical spectra (blue) (d).

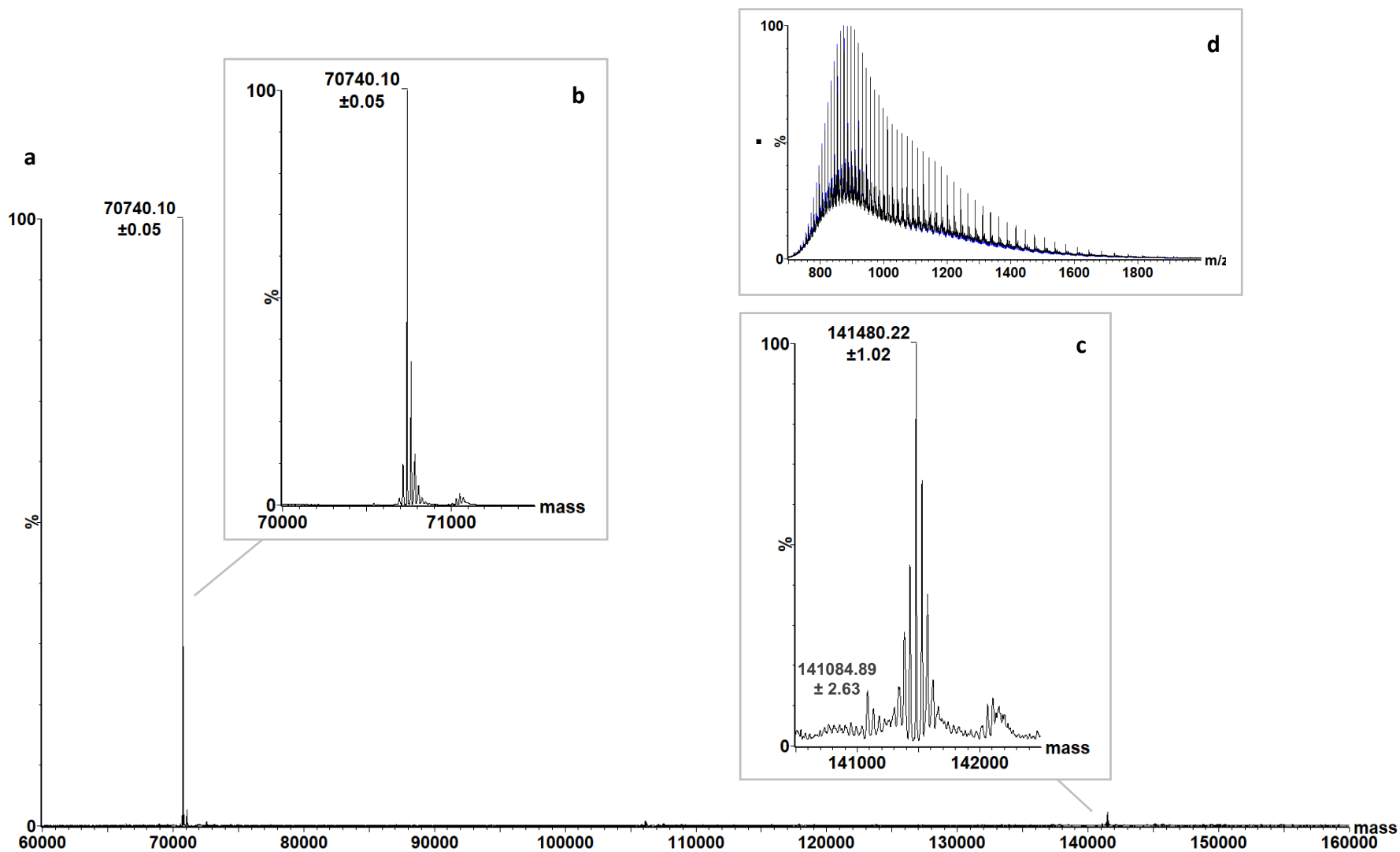


Figure 3.27. MS of PBP2_{EDTA} reacted with DTNB. Spectra deconvoluted in the mass range 60000-160000 Da (a); close-up view of the monomeric peak (b) and dimeric peak (c); The combined spectra (black) superimposes well to the theoretical spectra (blue) (d).

3.7.4 Spectrophotometric assays with nitrocefin

To test whether the mutations in the zinc-binding site could affect the reaction of PBP2 with β -lactam antibiotics, nitrocefin was chosen as a probe molecule in a spectrophotometric assay, due to its chromogenic properties that allow easy monitoring of its binding and turnover by PBPs and β -lactamases (2.5.3).

The rate of deacetylation was measured for *A. baumannii* PBP2_{WT} and mutants (i.e., D350A, D365A, H371A and C384A). The turnover of nitrocefin expresses the μmol of hydrolysed nitrocefin generated per second per μmol of enzyme. PBPs are efficient transpeptidase enzymes and can show β -lactamase activity to some extent; the rate of β -lactam hydrolysis is variable among PBPs and can be different for different β -lactams (Calvez *et al.*, 2017; Edoo *et al.*, 2017).

A. baumannii PBP2_{WT} exhibited poor β -lactamase activity against 200 μM nitrocefin ($0.0008 \pm 0.0001 \text{ s}^{-1}$), and this is clear if compared to a β -lactamase, for instance BlaC ($k_{\text{cat}} 38 \pm 2 \text{ s}^{-1}$) (Chow *et al.*, 2013) or another PBP, such as *P. aeruginosa* PBP3 ($k_{\text{cat}} 0.128 \pm 0.26 \text{ s}^{-1}$) (unpublished data from Dr Adrian Lloyd, University of Warwick)(table 3.13, figure 3.28e). Neither the mutation of the zinc-coordinating residues to alanine, nor the reaction of PBP2 wild-type with 100 μM zinc chloride (PBP2_{ZINC}) appeared to significantly change the hydrolysis rate of nitrocefin (table 3.13, figure 3.28a-d, f).

Protein	Turnover at 200 μM NCF (s^{-1}) \pm SD
D350A	0.0015 ± 0.0003
D365A	0.0007 ± 0.0001
H371A	0.0014 ± 0.0001
C384A	0.0012 ± 0.0002
PBP2 _{WT}	0.0008 ± 0.0001
PBP2 _{EDTA}	0.0027 ± 0.0003
PBP2 _{ZINC}	0.0021 ± 0.0002
PBP2 \blacklozenge	0.0119 ± 0.0011

Table 3.13. Hydrolysis rate of nitrocefin by PBP2 wild-type and mutants. D350A/D365A/H371A/C384A, PBP2 zinc-binding site mutants; PBP2_{WT}, PBP2 wild-type; PBP2_{ZINC}, PBP2 wild-type reacted with 100 μM ZnCl₂; PBP2_{EDTA}, PBP2 wild-type reacted with 100 mM EDTA; PBP2 \blacklozenge , PBP2 wild-type reacted with 100 mM EDTA O/N and dialysed in buffer without EDTA 2 O/N. In the assay, the protein concentration was 10 μM and the NCF concentration was 200 μM . Experiments were conducted in triplicate, values are arithmetic mean \pm standard deviation.

Interestingly, a preparation of PBP2 wild-type treated with EDTA (PBP2 \blacklozenge) exhibited a 15-times higher hydrolysis rate of nitrocefin (0.0119 ± 0.0011) compared to PBP2_{WT} (figure 3.28h).

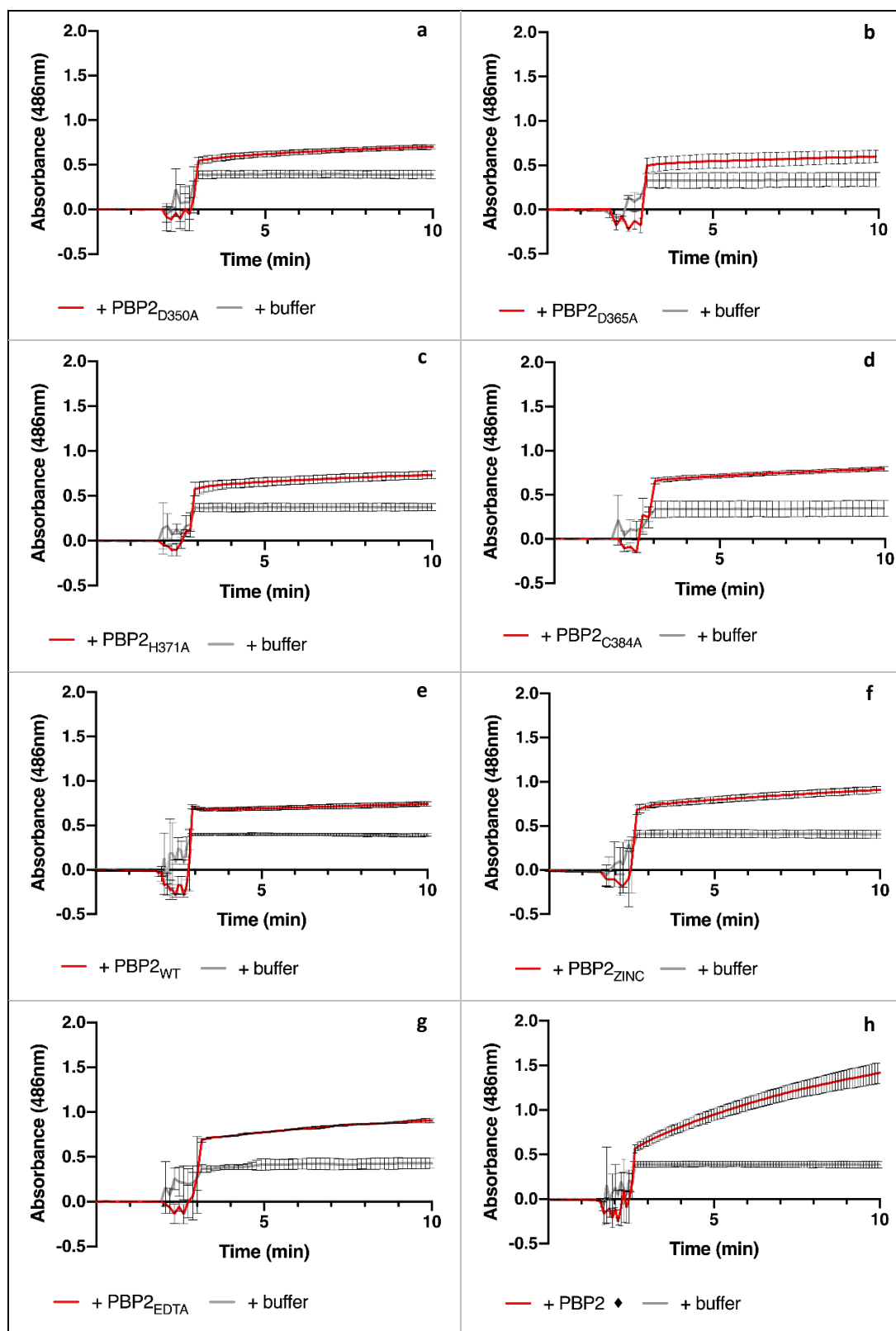


Figure 3.28. Spectrophotometric assays with nitrocefin. The hydrolysis rate of nitrocefin was calculated by monitoring the rate of increase in absorbance at 486 nm for D350A/D365A/H371A/C384A mutants (a-d); PBP2 wild-type (PBP2_{WT})(e); PBP2 wild-type reacted with 100 μ M ZnCl₂ (PBP2_{ZINC}) (f), and 100 mM EDTA (PBP2_{EDTA}) (g); PBP2 wild-type reacted with 100 mM EDTA O/N and dialysed in buffer without EDTA 2 O/N (PBP2_♦)(h). Experiments were conducted in triplicate. Red line, protein sample; grey line, control without protein.

In this preparation, PBP2 wild-type was incubated with 100 mM EDTA O/N to strip the zinc ion, and dialysed in buffer (50 mM HEPES pH 7.5 and 400 mM NaCl) for a double overnight (O/N), to remove the EDTA-Zn complex. During dialysis, protein underwent heavy precipitation, and the protein that remained in solution showed enhanced β -lactamase activity.

Intriguingly, the same result could not be reproduced by PBP2 wild-type pre-incubated with 100 mM EDTA for one h (PBP2_{EDTA}) and tested in the nitrocefin assay (figure 3.28g). Since, incubation with 100 mM EDTA for one h was sufficient to chelate most of the zinc ion, as suggested by the DTNB assays (3.7.3), disruption of the zinc-binding site only could not explain the difference in β -lactamase activity between PBP2 \blacklozenge and PBP2_{EDTA}.

To further investigate the cause of the enhanced β -lactamase activity, PBP2 \blacklozenge was analysed by intact protein MS. One possible cause for this enhanced activity was that following zinc stripping, the resulting free thiol could have undergone oxidation, and this modification could have been easily detected by MS. Thus, a MS spectra was acquired for PBP2 \blacklozenge (figure 3.31) and compared to the spectra of PBP2_{WT} (figure 3.29). Protein mass was the same in PBP2 \blacklozenge (70543.35 ± 0.14 Da) and PBP2_{WT} (70543.01 ± 0.12 Da), therefore the Cys384 was not oxidised in PBP2 \blacklozenge (table 3.14). Another possibility was the formation of dimers, as a result of disulphide bonds between free cysteines (C384). Spectra were deconvoluted on a much larger mass range (from 60000 to 160000 Da). PBP2 \blacklozenge could indeed form dimers, but the peak corresponding to the dimer (141086.02 ± 1.29 Da) was much less intense than the monomeric peak (70543.35 ± 0.14 Da), and no difference was found with PBP2_{WT} (table 3.14).

Because no difference in mass was found between PBP2 \blacklozenge and PBP2_{WT}, perhaps the reaction of the protein with nitrocefin and MS analysis of the acyl-enzyme complex would have helped explain the enhanced activity of PBP2 \blacklozenge . Therefore, this protein and PBP2_{WT} were reacted with a 20-fold molar excess of nitrocefin, and the MS spectra were acquired (figure 3.30 and 3.32). Both monomeric and dimeric protein

were able to covalently bind nitrocefin (table 3.14). Even in this instance, MS analysis did not report obvious mass differences between PBP2 \blacklozenge and PBP2_{WT} with respect to the acyl-enzyme complexes with nitrocefin. Interestingly, when PBP2 \blacklozenge was incubated with nitrocefin for longer time (i.e., 30 min), the MS spectra showed two prominent peaks corresponding to the acylated and free- form of the protein (71059.57 ± 0.13 Da and 70543.20 ± 0.26 Da) (figure 3.33). This was a clear sign of nitrocefin turnover, since 2 min of incubation with nitrocefin were sufficient to acylate most of the protein (figure 3.32), while a longer incubation time (i.e., 30 min) allowed \sim half of the acylated protein to revert to the free-form due to nitrocefin hydrolysis, thus confirming the β -lactamase activity observed in the NCF spectrophotometric assay.

The MS investigation carried out on PBP2 \blacklozenge was not able to clarify its augmented β -lactamase activity compared to PBP2_{WT}. Possibly, a rearrangement of residues within the catalytic site following zinc stripping, could make the binding pocket more water accessible, causing an increased hydrolysis of nitrocefin. If this is the case, X-ray crystallography of PBP2 \blacklozenge may be able to elucidate such conformational changes, and help us understand the mechanisms that regulate the binding and hydrolysis of β -lactams to *A. baumannii* PBP2.

PBP2 \blacklozenge mass Da \pm error	PBP2 \blacklozenge + NCF (2min incubation) mass Da \pm error	Δ mass Da	PBP2 \blacklozenge + NCF (30min incubation) mass Da \pm error	Δ mass Da
70543.35 (\pm 0.14) <i>monomer</i>	70542.17 (\pm 2.49) 71059.59 (\pm 0.52)	- +516.24	70543.20 (\pm 0.26) 71059.57 (\pm 0.13)	- +516.22
141086.02 (\pm 1.29) <i>dimer</i>	141082.06 \pm 6.68 Da 142118.67 \pm 3.50 Da	- +1032.65	141087.06 \pm 3.03 Da 142119.39 \pm 1.64 Da	- +1033.37
PBP2 _{WT} mass Da \pm error	PBP2 _{WT} + NCF (5min incubation) mass Da \pm error	Δ mass Da	Table 3.14. MS of PBP2\blacklozenge and PBP2_{WT} before and after reaction with a 20-fold molar excess of nitrocefin. Observed masses for the monomer and dimer, and respective adducts with nitrocefin (NCF) are indicated. Δ mass is the difference in	
70543.41 (\pm 0.14) <i>monomer</i>	70543.09 (\pm 0.23) 71060.00 (\pm 0.04)	- +516.59		
141086.63 (\pm 2.23) <i>dimer</i>	141085.89 \pm 1.96 Da 142119.91 \pm 0.57 Da	- +1033.28		

observed mass of the protein unbound and acylated by nitrocefin. PBP2 \blacklozenge was incubated with nitrocefin at two different times, in independent experiments.

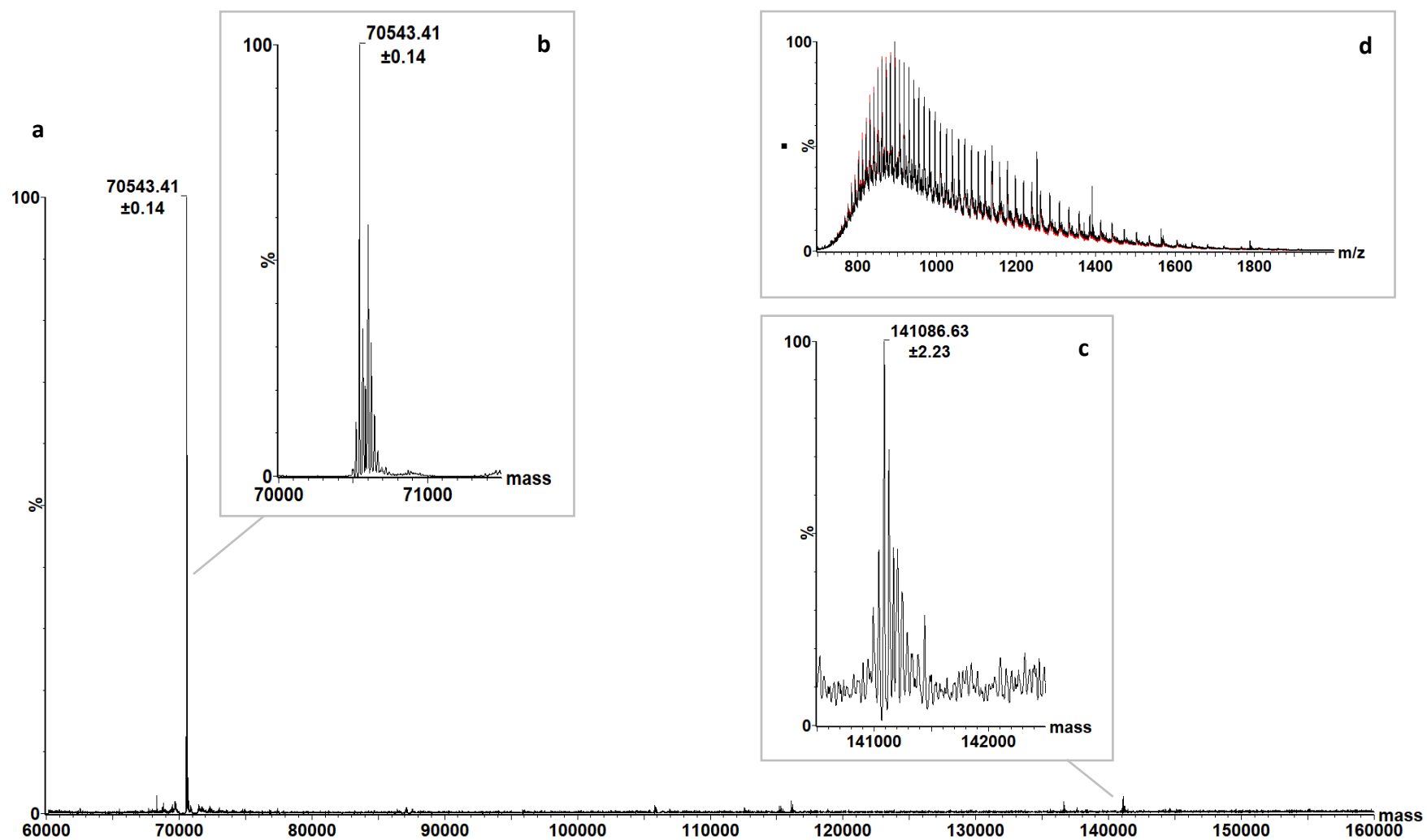


Figure 3.29. MS of PBP2_{WT}. Spectra deconvoluted in the mass range 60000-160000 Da (a); close-up view of the monomeric peak (b) and dimeric peak (c); The combined spectra (black) superimposes well to the theoretical spectra (red) (d).

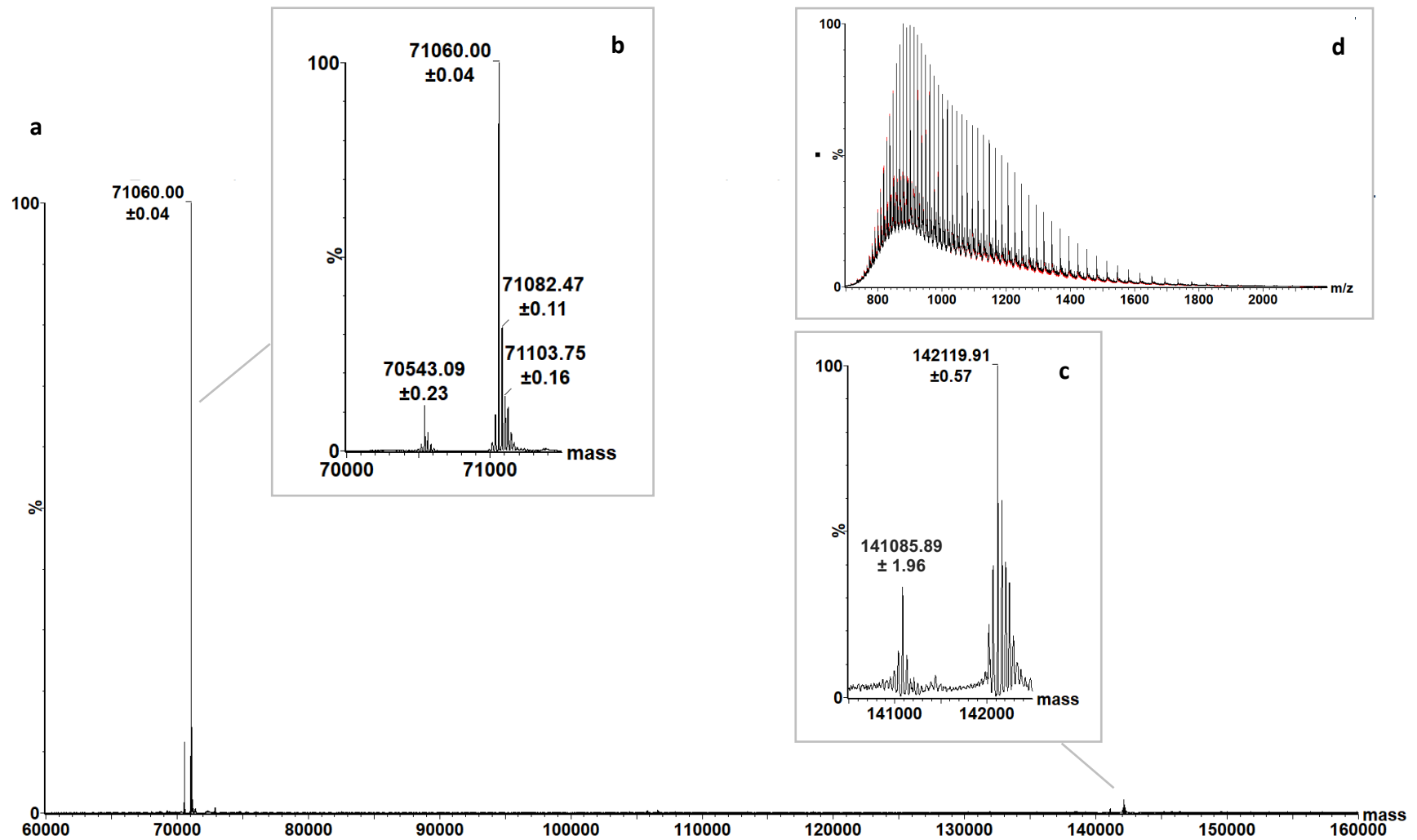


Figure 3.30. MS of PBP2_{WT} reacted with nitrocefin for 5 min. Spectra deconvoluted in the mass range 60000-160000 Da (a); close-up view of the monomeric peak (b) and dimeric peak (c); The combined spectra (black) superimposes well to the theoretical spectra (red) (d).

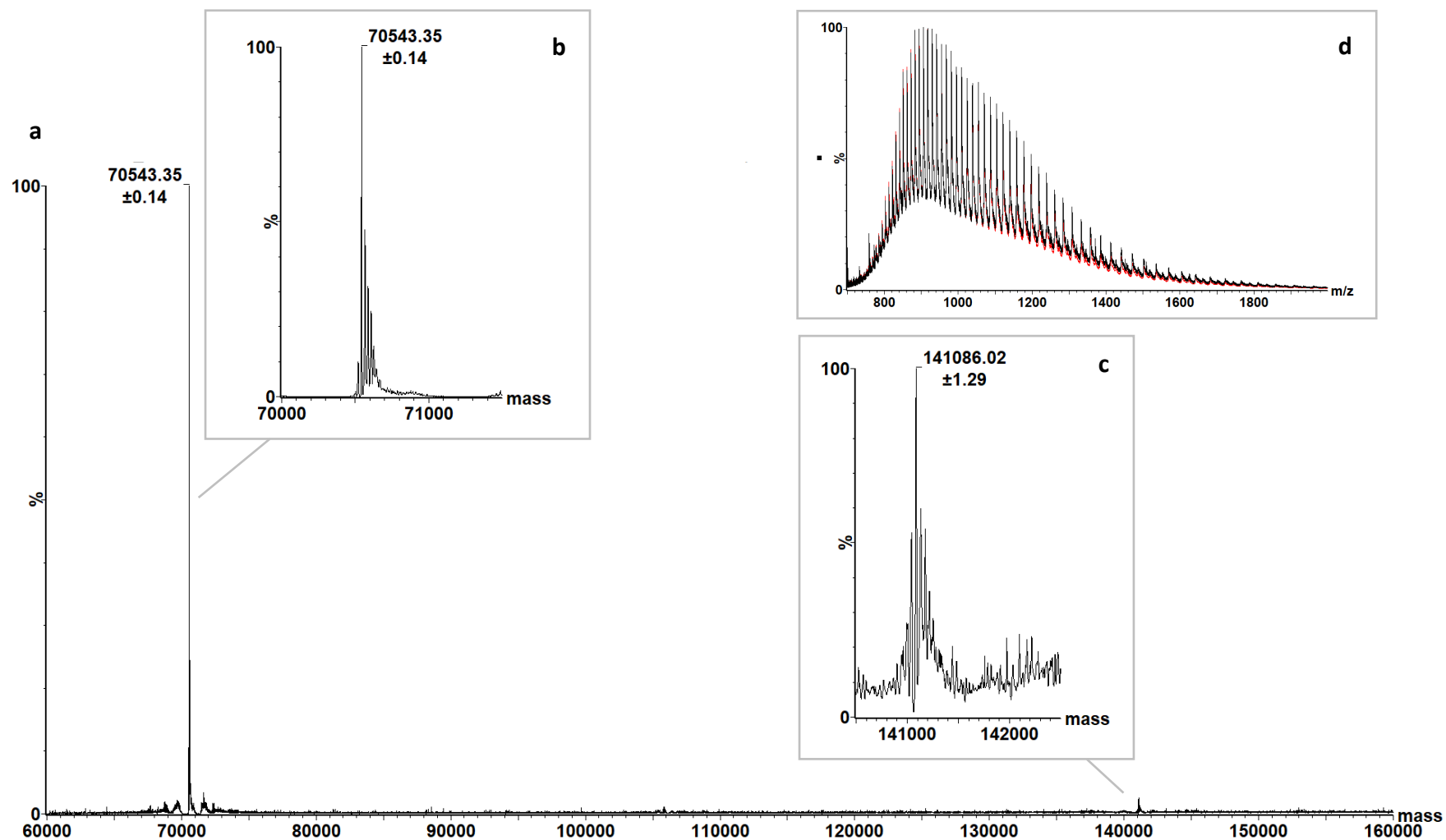


Figure 3.31. MS of PBP2♦. Spectra deconvoluted in the mass range 60000-160000 Da (a); close-up view of the monomeric peak (b) and dimeric peak (c); The combined spectra (black) superimposes well to the theoretical spectra (red) (d).

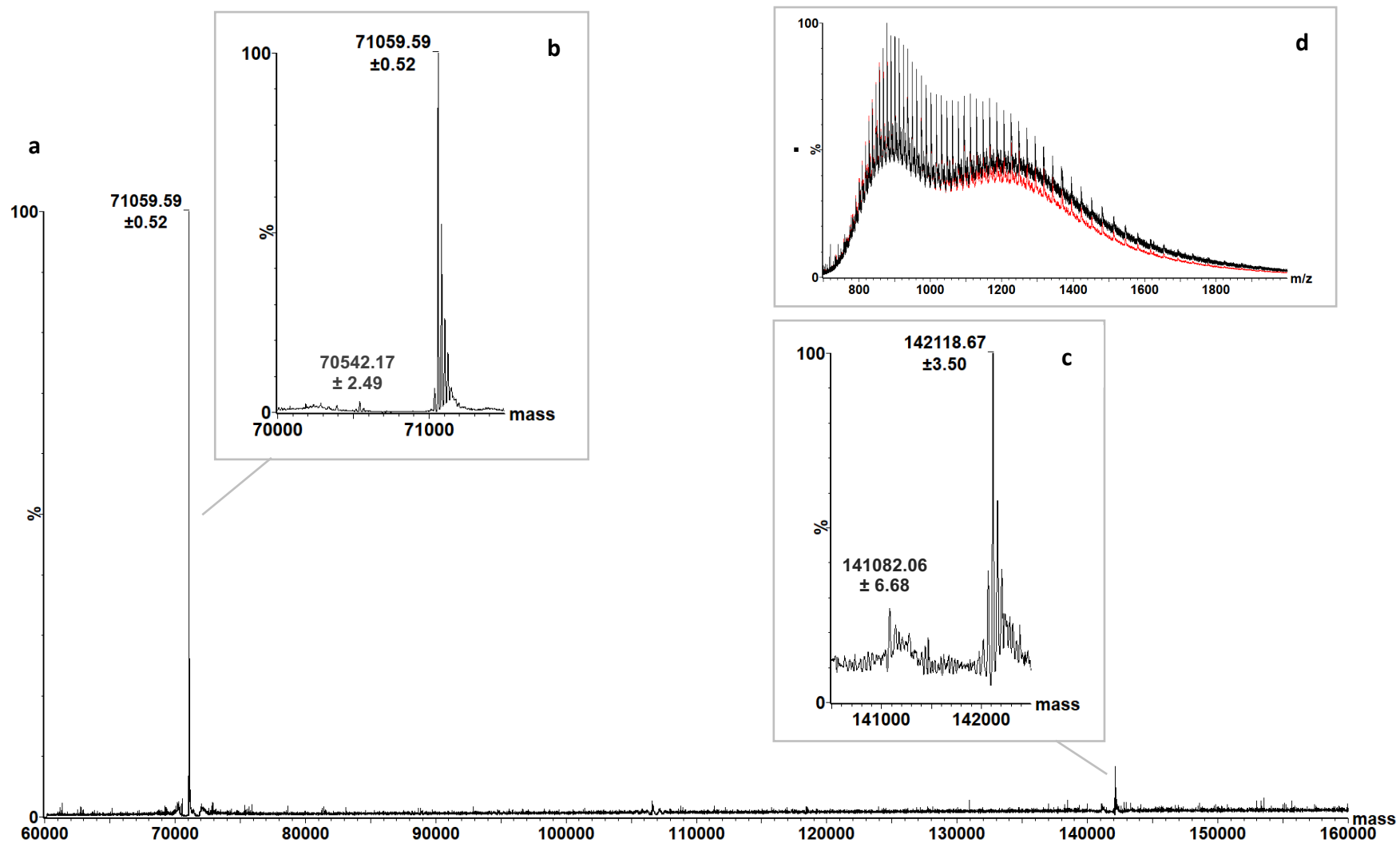


Figure 3.32. MS of PBP2♦ reacted with nitrocefim for 2 min. Spectra deconvoluted in the mass range 60000-160000 Da (a); close-up view of the monomeric peak (b) and dimeric peak (c); The combined spectra (black) superimposes well to the theoretical spectra (red) (d).

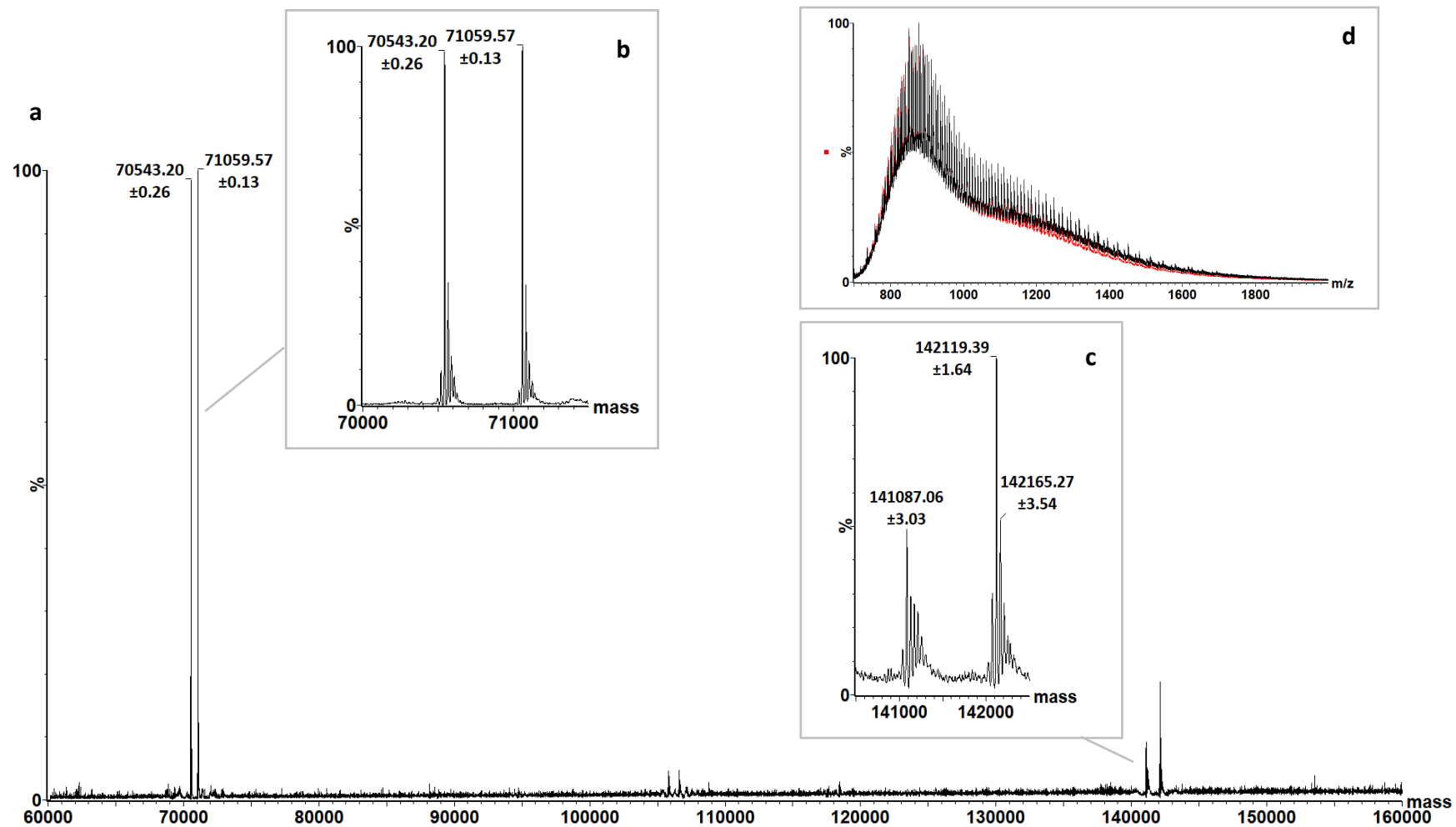


Figure 3.33. MS of PBP2♦ reacted with nitrocefin for 30 min. Spectra deconvoluted in the mass range 60000-160000 Da (a); close-up view of the monomeric peak (b) and dimeric peak (c); The combined spectra (black) superimposes well to the theoretical spectra (red) (d).

3.8 Conservation of the zinc-binding site in PBPs of Gram-positive and Gram-negative bacteria

3.8.1 Protein BLAST search of D-X₁₄-D-X₅-H-X₁₂-C motif and its cysteine variants

With the aim of identifying PBP homologs likely to bear a zinc-coordination site, sequence Ala345-Gly396 of *A. baumannii* PBP2, encompassing the D-X₁₄-D-X₅-H-X₁₂-C motif, was used as query in a protein BLAST search. Besides species belonging to the genus *Acinetobacter*, a metal coordination site was also predicted in PBPs from species belonging to other genera (figure 3.34)

<i>Acinetobacter</i>	AISD	PGYFHLPGD	SHKFRD	WKKTG	HG	I	V	N	M	H	K	A	I	M	S	C	D	T	F	Y	I	L	A	N	Q	M	G	
<i>Serratia</i>	AIND	PGYFHLPGD	SHKFRD	WKKTG	HG	I	V	D	L	N	K	A	I	Q	E	S	C	D	T	F	Y	I	L	S	N	Q	M	G
<i>Agitococcus</i>	-IRD	PGYFHLPGD	SHLFRD	WKKTG	HG	I	V	N	L	H	R	A	V	E	I	S	C	D	T	F	Y	Q	L	S	S	R	M	G
<i>Sulfuriferula</i>	-IVD	PGYFSLPGD	SSHRFRD	WKPSG	HG	M	V	N	M	H	N	A	I	V	Q	S	C	D	T	F	Y	R	L	A	N	N	M	G
<i>Prolinoborus</i>	-ISD	PGYFSLPGD	SHRFRD	HKKSG	HG	A	V	N	M	H	K	A	Q	V	V	S	C	D	T	F	Y	V	M	S	Y	R	M	G
<i>Nitrosomonas</i>	AIND	PGYFSLPGD	SSHRFRD	WRPSG	HG	R	V	N	L	H	K	S	L	V	I	S	C	D	T	Y	Y	T	L	A	N	D	L	G
<i>Alkanindiges</i>	-IYD	PGYFHLPGD	SHRFRD	WKKSG	HG	T	V	D	L	N	K	A	I	T	W	S	C	D	T	F	F	V	L	A	Y	R	M	G
<i>Nitrosospira</i>	AIDD	PGYFSLPGD	STHRFRD	WKAGG	HG	V	V	D	L	H	K	S	L	V	V	S	C	D	T	Y	Y	A	L	A	N	D	L	G
<i>Legionella</i>	-IYD	PGWYRLPGV	SHKYRD	WKRTG	HG	I	I	N	L	T	R	A	I	T	V	S	C	D	T	F	Y	Q	L	G	N	K	M	G
<i>Perlucidibaca</i>	-ISD	PGYFMLPGV	NHRFRD	WKKQG	HG	I	V	D	L	Y	R	A	E	I	S	C	D	T	F	Y	Q	M	S	D	R	M	G	
<i>Nitrosovibrio</i>	SIND	SGYFSLPGD	STHRFRD	WKAGG	HG	V	V	D	L	H	K	S	L	V	V	S	C	D	T	Y	Y	G	L	A	N	D	L	G
	*	*	*	::	***	.	*	::**	:	***	:::	::	****	::*	::	*												*

Figure 3.34. Alignment of the PBP homologues retrieved by a BLAST search bearing the D-X₁₄-D-X₅-H-X₁₂-C motif. The zinc chelating residues in *A. baumannii* PBP2 are coloured red, and are present in PBPs from diverse bacteria genera as follows: *Serratia* (sp. *S1B*), *Agitococcus* (sp. *lubricus*), *Sulfuriferula* (sp. *AH1*), *Prolinoborus* (sp. *fasciculus*), *Nitrosomonas* (sp. *Nm34*, sp. *communis*, sp. *Nm58*, sp. *Nm132*, sp. *Nm33*, sp. *nitrosa*, sp. *mobilis*), *Alkanindiges* (sp. *H1*, sp. *illinoisensis*), *Nitrosospira* (sp. *Nsp1*, sp. *Nsp2*, sp. *Nsp13*, sp. *Nsp14*, sp. *Nsp18*, sp. *Nsp22*, sp. *Nsp44*, sp. *NI5*, sp. *NpAV*, sp. *multiformis*, sp. *lacus*, sp. *56-18*, sp. *briensis*), *Legionella* (sp. *adelaidensis*, sp. *jamestowniensis*, sp. *jordanis*, sp. *brunensis*, sp. *lansingensis*, sp. *donaldsonii*, sp. *feeleei*, sp. *hackeliae*, sp. *quinlivanii*, sp. *birminghamensis*), *Perlucidibaca* (sp. *HR-E*, sp. *aquatica*, sp. *piscinae*), *Nitrosovibrio* (sp. *tenuis*), and order: *Burkholderiales* and *Gallionellales*.

To increase the number of PBP2 homologs predicted to exhibit a zinc-coordination site, amino acid variation among the zinc-coordinating ligands should be taken into account, while preserving the coordination of the metal. For instance, cysteine is one of the most frequent residues encountered in zinc-binding sites, and variants of the D-X₁₄-D-X₅-H-X₁₂-C motif with a higher content of cysteines could be possible. In order to determine those PBP2 homologs bearing more than one Cys in the predicted

zinc-binding site, a BLAST search was performed with the sequence of PBP2 bearing appropriate mutations. PBP2 homologs were found that exhibit either the C-X₁₄-D-X₅-H-X₁₂-C motif (2Cys-1Asp-1His) (figure 3.35) or the C-X₁₄-C-X₅-H-X₁₂-C motif (3Cys-1His) (figure 3.36).

```

Acinetobacter  AISDPGYFHLPGDShkFRDwkkTGHGIVNMHKAIIMSCDTYFYILANQMG
S.l.           PVVCPGWFTLPGSSHQFRDwkkTGHGIVNLHDAVVQSCDVYFYKLAVAME
C.m.           PVTCPGWFTLPGDRHLFRDwkkTGHGVVTLHEAIVQSCDVYFYRFAAAVG
P.b.           RIMCPGYQQLPKQTHKYRDWkKNGHGLMNLHNSIVQSCDVYFYILAHQLK
C.b.           TVFCPGYYQLPGDShKYRDWKRWGHGLVNLNSAIVQSCDVYFYGLAHALG
Endosymb.     KNYCPGYQQLPGKEHKYRDWkkTGHGVTDMHKAIVQSCDVYYYELARTLG
               **:: ** . * :*****: ***: ::::: ***.*:* :* :

```

Figure 3.35. Alignment of the PBP homologues retrieved by a BLAST search bearing the C-X₁₄-D-X₅-H-X₁₂-C motif. *S.l.*, *Sulfuricaulis limicola*; *C.m.*, *Candidatus Muproteobacteria* bacterium RBG_16_65_34 and RIFCSPHIGHO2_01_60_12; *P.b.*, *Piscirickettsiaceae* bacterium; *C.b.*, *Chromatiales* bacterium 21-64-14; Endosymb., endosymbiont of *Riftia pachyptila*/ *Tevnia jerichonan*/ *Ridgeia piscesae*. PBP2 zinc-coordinating residues in *A. baumannii* are coloured red.

```

Acinetobacter  AISDPGYFHLPGDShkFRDwkkTGHGIVNMHKAIIMSCDTYFYILANQMG
C.m.           TVFCPGWYSLPGDTHRFRcWkkDGHGAVNLHDAVVQSCDVYFYQLAVALG
Thiocapsa     VTHCPGSFSLPGHSHRFRcWRRGGHGSLNLEQALVQSCDVYFYDLANRMG
AllochroMatium TTYCPGYFSLPGQKHRFRcWRRGGHGTVDLQESIVESCDVYFYWLANQMG
T.d.          NTFCPGYFSLPGQSHKFRcWRRGGHGSTNLQQAIVQSCDVYFYALANHMG
I.p.          TIHCPGYFTLPGQSHRFRcWRRGGHGSLNLEEAIQVSCDVYFYSLANHMG
T.p.          ITFCPGHFSLPGQSHRFRcWKRtGHGSTNLEKAIVESCDVYFYDLASRMG
T.v.          TTYCSGSFSLPGQSHRFRcWRKGGHGTVNLERAIIVESCDVYFYSLANQMG
               * : ***.*:*:* *:: *** ::. .:: ***.*** ** :*

```

Figure 3.36. Alignment of the PBP homologues retrieved by a BLAST search bearing the C-X₁₄-C-X₅-H-X₁₂-C motif. *C.m.*, *Candidatus Muproteobacteria* bacterium RBG_16_64_1; *Thiocapsa*, *Thiocapsa* sp. KS1 and *Thiocapsa rosea*; *AllochroMatium*, *AllochroMatium warmingii* and *AllochroMatium vinosum*; *T.d.*, *Thiorhodococcus drewsii*; *I.p.*, *Imhoffiella purpurea*; *T.p.*, *Thiobaca trueperi*; *T.v.*, *Thiocystis violascens*. PBP2 zinc-coordinating residues in *A. baumannii* are coloured red.

The number of PBPs bearing a zinc-binding site could be more than the ones highlighted in these BLAST searches, due to the bias of the *A. baumannii* PBP2 sequence, but certainly this analysis shows that cysteine (and possibly other known zinc coordinating residues) variations can exist.

3.8.2 A potential zinc-binding site in SpoVD

A zinc-coordination site could be present in *B. subtilis* SpoVD wild-type and its mutant C332D. SpoVD (Stage V sporulation protein D) is a class B PBP with a Cys-Cys pair mediating the conserved interaction between the β -hairpin loop and the S-X-N/D motif. It has been reported that the redox state of Cys332 and Cys351 is controlled *in-vivo* by BdbD and StoA, and it is essential that SpoVD is maintained in a reduced state for it to be active as a transpeptidase. Cys332 and Cys351 are then predicted to interact by hydrogen bonding (Liu *et al.*, 2010; Bukowska-Faniband and Hederstedt, 2017). Interestingly, the only permissive mutation at Cys332 that could reproduce wild-type SpoVD levels of activity, was to aspartate. However, the authors could not explain why aspartate but not glutamate or other amino acids capable of hydrogen bonding to Cys351, could substitute Cys332 without causing significant loss of activity. Intriguingly, the discovery of a zinc-binding site in *A. baumannii* PBP2 could provide a plausible explanation to the SpoVD data.

Sequence alignment of *A. baumannii* PBP2 with SpoVD_{WT} and SpoVD_{C332D} strikingly reveals the restoration of the zinc-ligation set (2Asp, 1His, 1Cys) when Cys332 was replaced by Asp in the functional mutant of SpoVD (figure 3.37). Although an X-ray structure of SpoVD is not currently available, it is likely that the four zinc-coordinating residues in PBP2, occupy comparable positions in SpoVD_{C332D}, due to the good conservation of the nearby amino acids. In other words, the existence of a zinc-binding site could be speculated in SpoVD_{C332D}, that can fully substitute for the Cys332-Cys351 interaction, while maintaining the D,D-transpeptidase fully active *in-vivo*.

```

Bs_SpoVDWT      LKRDQFYDKG--HAEVDGARLRCWKRGGHGLQTYLEVQNSCNPGFVEL
Bs_SpoVDC332D  LKRDQFYDKG--HAEVDGARLRDWKRGGHGLQTYLEVQNSCNPGFVEL
Ab_PBP2        WAT-AISDPGYFHLPGDSHKFRDWKKTGHGIVNMHKAIIMSCDTYFYIL
                : * * * * * . : : * ** : *** : . : : ** : * *

```

Figure 3.37. Section of the sequence alignment between *A. baumannii* PBP2 and *B. subtilis* SpoVD wild-type and mutant C332D. PBP2 zinc-coordinating residues are coloured red.

It is intriguing that, an Asp-Ser interaction (C332D C351S SpoVD- double mutant), commonly found in class B PBPs (for instance in *N. gonorrhoeae* PBP2) (figure 3.19a), could not replace the Cys-Cys interaction, without complete loss of transpeptidase activity *in-vivo* (Bukowska-Faniband and Hederstedt, 2017). Somehow, an Asp-Ser interaction within the SpoVD motif (D-X₁₂-D-X₅-H-X₁₂-S) did not exhibit the same functional properties of a Cys-Cys interaction (D-X₁₂-C-X₅-H-X₁₂-C), whereas an Asp-Cys interaction (D-X₁₂-D-X₅-H-X₁₂-C) could replicate the functional properties of the SpoVD Cys-Cys interaction.

It is known that, the disulphide bridge Cys332-Cys351 introduced by Bdbd is reduced by StoA *in-vivo* (Bukowska-Faniband and Hederstedt, 2017). The resulting free-cysteines could hydrogen bond as suggested by the authors of the study, but another exciting alternative is that, they could participate in a zinc-binding site in concert with Asp219 and His238 in SpoVD_{WT}. The postulated zinc-binding site would be maintained by the mutant SpoVD_{C332D}, so that that no difference in transpeptidase activity could be detected *in-vivo* (Bukowska-Faniband and Hederstedt, 2017). Although it is an interesting hypothesis, the presence of a zinc-binding site in SpoVD_{C332D} and possibly in SpoVD_{WT} does not have any experimental evidence, and remains a conjecture for now.

The D-X₁₂-C-X₅-H-X₁₂-C motif of SpoVD is conserved among species of the *Bacillus* genus. SpoVD orthologues are also found in other sporulating bacteria, for instance *Clostridium*. Interestingly, in *Clostridium* species, the D-X₁₂-C-X₅-H-X₁₂-C motif changes to C-X₁₂-C-X₅-H-X₁₂-C, resulting in 3Cys and 1His residues occupying the same positions of the zinc-coordinating residues in *A. baumannii* PBP2 (figure 3.38). *Clostridium perfringens* SpoVD_{WT} resembles the PBP2 homologs 3Cys-1His (figure 3.36), and this supports the fact that many other PBPs bearing a potential zinc-binding site may have not been determined yet.

<i>Cp</i> _SpoVD _{WT}	KDETYTCSGG--LQKGDRFIKCWKRGGHGTQTFEEIIQNSCNVGF MNL
<i>Ab</i> _PBP2	WATAISDPGYFHLPGDSHKFRDWKKTG HGIVNMHKAI IMSCDTYFYIL
	: : * * . . : : ** : *** . . : : * ** : . * *

Figure 3.38. Section of the sequence alignment between *A. baumannii* PBP2 and *C. perfringens* SpoVD wild-type. PBP2 zinc-coordinating residues are coloured red.

3.9 Crystallisation trials of *B. subtilis* SpoVD

In section 3.8.2, a zinc-binding site was anticipated in the structure of SpoVD_{C332D} on the basis of sequence similarity to *A. baumannii* PBP2. In principle, a zinc-binding site could also form in SpoVD_{WT} when C332 and C351 are in their reduced form. To explore this possibility, SpoVD_{WT} and SpoVD_{C332D} were expressed and purified, and crystallisation of SpoVD_{WT} was initially attempted.

3.9.1 Expression and purification of SpoVD_{WT} and SpoVD_{C332D}

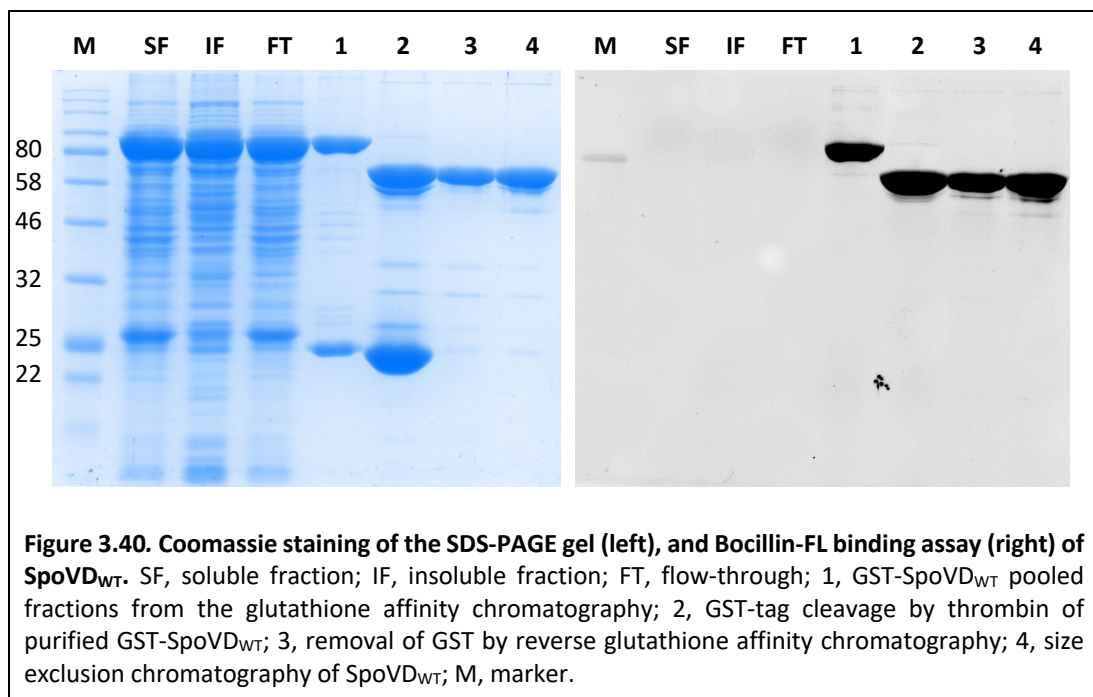
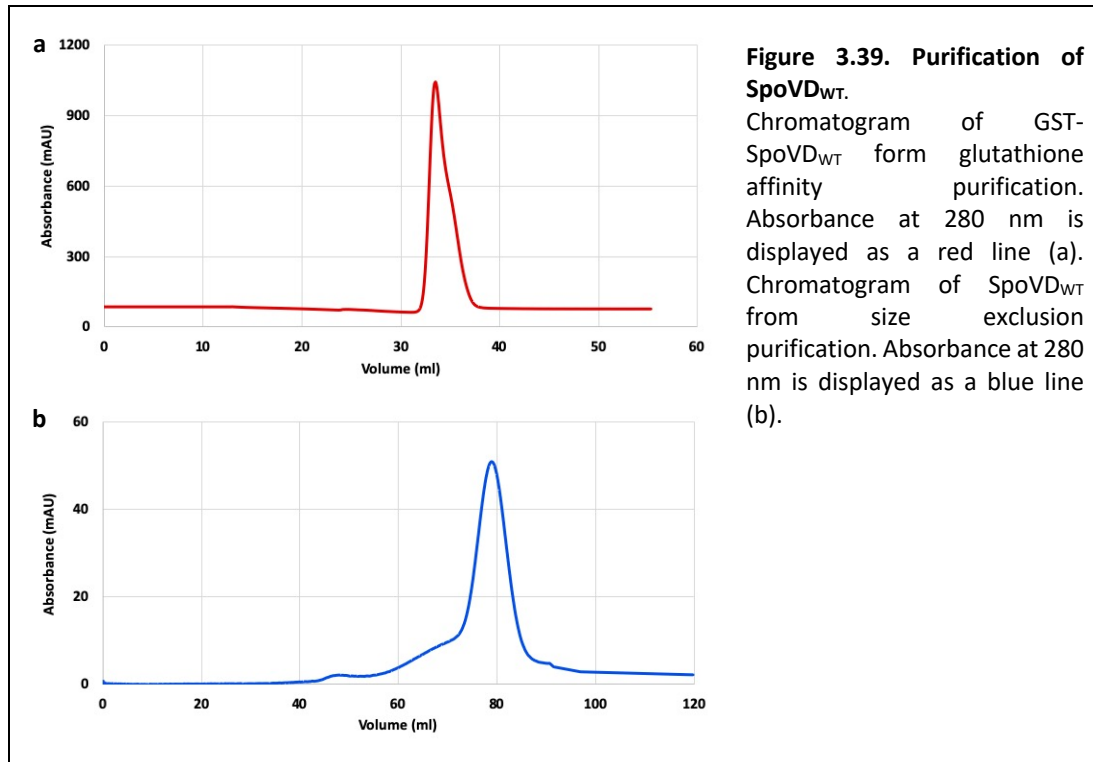
A truncated version of SpoVD (residues 33-645), devoid of the transmembrane helix, was produced as a fusion protein with a N-terminal thrombin-cleavable GST tag from pGEX-2T/4T vectors (figure S7). Plasmids pLYM020 and pLYM034, encoding GST-SpoVD_{WT} and GST-SpoVD_{C332D}, respectively, were a kind gift of Prof Lars Hederstedt (Lund University, Sweden) (Liu *et al.*, 2010; Bukowska-Faniband and Hederstedt, 2017). Plasmids were transformed into *E. coli* C41 (DE3) competent cells, and bacteria grown in auto-induction media in the presence of ampicillin, to achieve protein expression (2.3.1). Pellets were resuspended in PBS supplemented with 10 mM DTT, 2.5 % (w/v) CHAPS and DNase I, and bacteria were disrupted by sonication (2.3.2). GST-SpoVD_{WT/C332D} was purified by glutathione affinity chromatography (2.3.4) (figure 3.39a), where the column was washed with binding buffer (PBS pH 7.3, 5 mM DTT), prior to elution of the protein with elution buffer (50 mM Tris-HCl pH 8, 10 mM reduced glutathione, 5 mM DTT) (figure 3.39).

For the crystallisation of SpoVD_{WT}, the GST tag was cleaved off by thrombin, at 4 °C overnight (1 unit of thrombin per 0.25 mg of purified protein). The protein preparation was dialysed in binding buffer to remove glutathione. To separate SpoVD_{WT} from the cleaved GST, a reverse glutathione affinity chromatography was performed (figure 3.40). SpoVD_{WT} was further purified by size exclusion chromatography (figure 3.39b and 3.40) (2.3.5), in 25 mM Tris-HCl pH 8 and 400 mM NaCl buffer.

Purified GST-SpoVD_{WT} and GST-SpoVD_{C332D} were both able to bind bocillin (figure 3.40, data not shown for GST-SpoVD_{C332D}). Interestingly, the binding of bocillin could only be detected after the two proteins had been purified by glutathione affinity chromatography. Labelling of GST-SpoVD_{WT} was not possible when the protein was either in the soluble fraction (SF) or insoluble fraction (IF) following sonication, or the flow through (FT) following loading onto the GST-trap column (figure 3.40). GST-SpoVD_{C332D} could not be labelled in the cell lysate either, in PBS buffer (data not shown). The binding of bocillin to the purified SpoVD proteins indicates that the catalytic Ser is free, thus a possible covalent adduct formed by the protein with another molecule, such as ampicillin used in bacterial growth, could be excluded. Moreover, in the cell lysate there is virtually nothing that could impede the binding of bocillin to the catalytic Ser of the SpoVD proteins, and this was suggested by the successful bocillin staining of *A. baumannii* PBP2 in the soluble fraction (figure 3.1c). It is unclear whether the presence of reduced glutathione, used to strip the SpoVD proteins from the column resin, has played a role on the bocillin staining of the proteins, or whether the fluorescence of bocillin has been somehow quenched or even the molecule hydrolysed by the β -lactamase expressed from the pGEX-2T vector, that would still be present in the soluble- (SF), insoluble- (IF) and flow-through fractions (FT).

The exact mass of GST-SpoVD_{WT} and GST-SpoVD_{C332D} was obtained by intact protein mass spectrometry (2.6.2). The presence of the mutation in GST-SpoVD_{C332D} (table 3.15) (figure 3.41-3.42) was confirmed by a difference in mass of +11.98 Da (expected Δ mass of + 11.90 Da) compared to the wild-type protein. Both GST-SpoVD_{WT} and GST-SpoVD_{C332D} were 2 Da lighter compared to their expected MW (GST-SpoVD_{WT}: 93676.21 Da and GST-SpoVD_{C332D}: 93688.16 Da, calculated considering all Cys reduced), indicative of the presence of a disulphide bond, presumably in the GST-tag given that SpoVD_{C332D} cannot form an intramolecular disulphide bond. Additional peaks were observed at higher mass, consistent with the covalent binding of one or more glutathione molecules (MW= 307.32 Da) to the protein. It is possible that these covalent adducts were formed via disulphide bridges between the glutathione thiol group and Cys residues of either the GST-tag or the

SpoVD protein, although the protein purification was carried out in the presence of DTT.

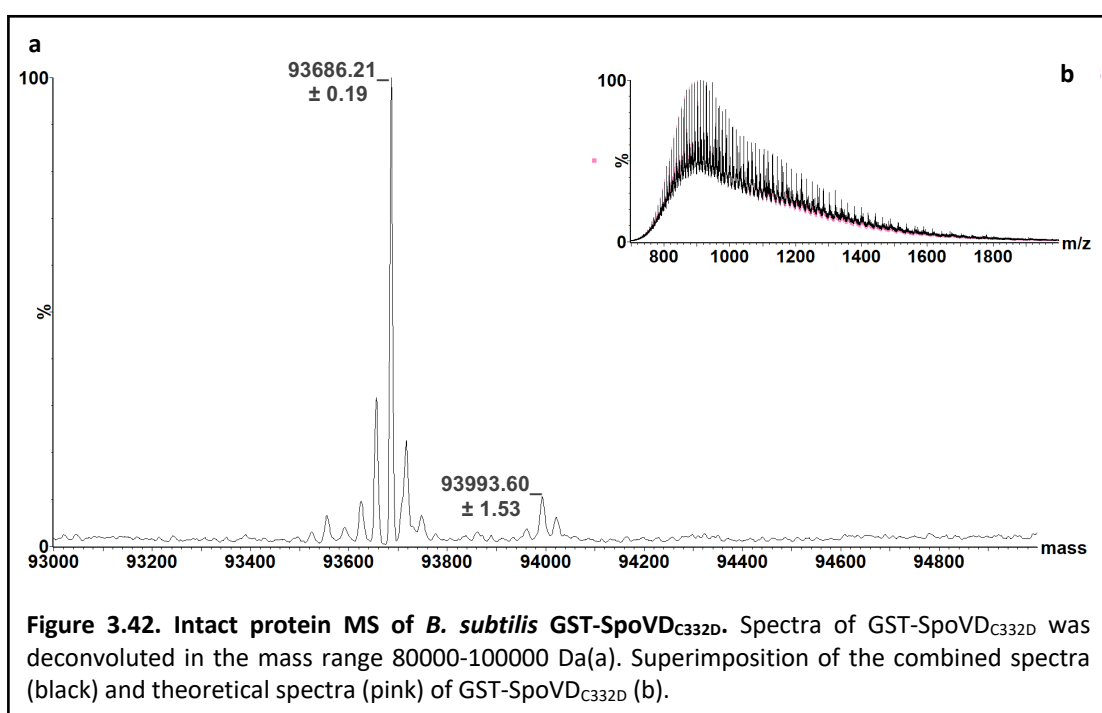
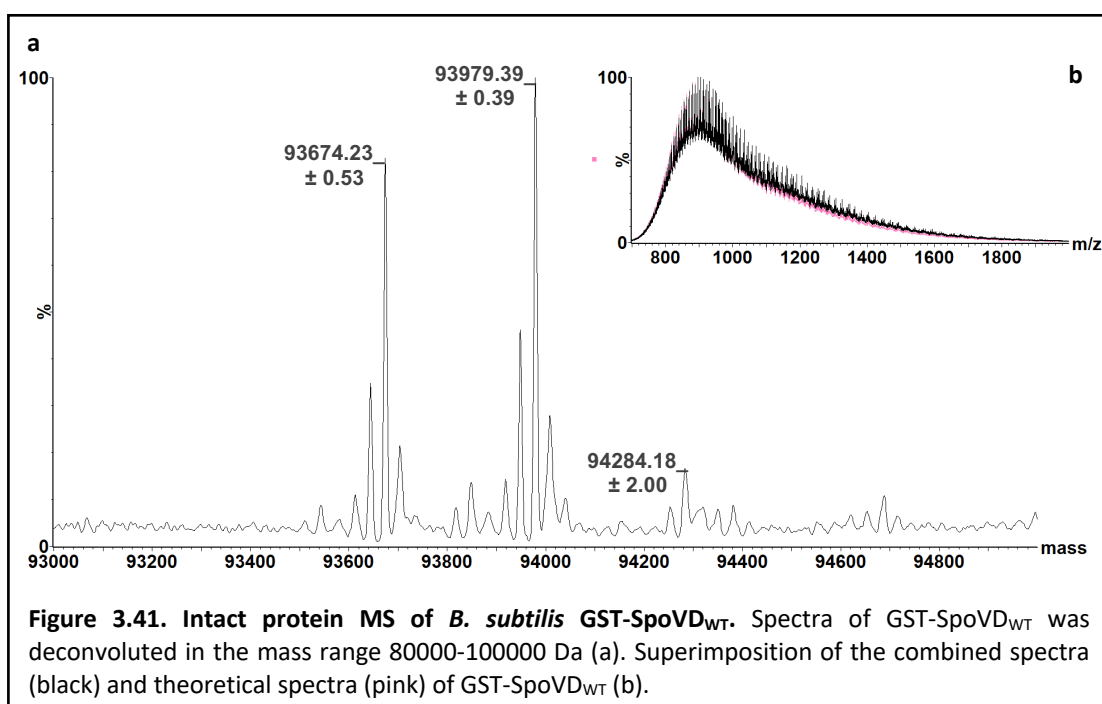


A MS analysis of GST-cleaved SpoVD_{WT} and SpoVD_{C332D} would help clarify whether the site of modification is located in SpoVD or the fusion tag. Moreover, the GST-

cleaved SpoVD_{WT} was used in crystallisation trials, thus would be important to know if any protein modification was present.

Protein	Calculated mass (Da) (\pm error)	Δ mass (Da)
GST-SpoVD _{WT}	93674.23 (\pm 0.53) reference	-
	93979.39 (\pm 0.39)	+ 305.16
	94284.18 (\pm 2.00)	+ 609.95
GST-SpoVD _{C332D}	93686.21 (\pm 0.19) reference	-
	93993.60 (\pm 1.53)	+ 307.39

Table 3.15. Intact MS of GST-SpoVD_{WT} and GST-SpoVD_{C332D}. Δ mass is the difference between the calculated mass and the expected mass for a given protein.

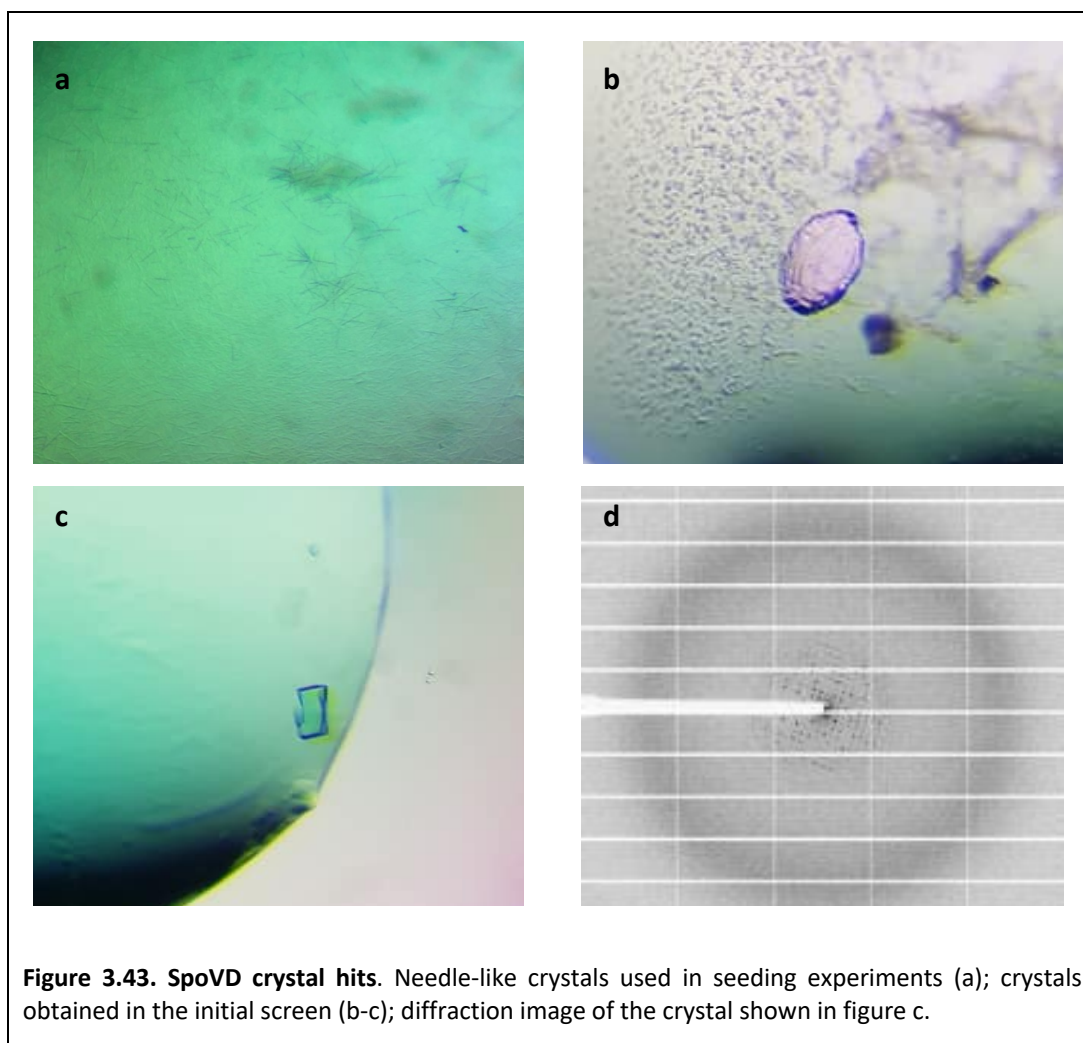


3.9.2 Crystallisation of SpoVD_{WT}

Crystallisation of SpoVD_{WT} Δ33-645 was attempted. Commercial sparse-matrix crystallisation kits, such as Wizard Classic 1 and 2, Wizard Classic 3 and 4 (Molecular Dimensions), and Crystal Screen HT (Hampton Research) were screened for initial crystallisation conditions. 96-well crystallisation plates were set up at 18 °C, and crystallisation drops consisted of 100 nL protein solution (13.3 mg/mL) and 100 nL mother liquor solution.

Needle-like crystals were obtained from Wizard Classic 4 condition No. 33 (800 mM Potassium phosphate dibasic, 100 mM HEPES/ Sodium hydroxide pH 7.5, 800 mM Sodium phosphate monobasic) (figure 3.43a) after 3 weeks. Because of their small size, crystal looping was not possible, thus a seed stock was made instead. Wizard Classic 1 and 2, Wizard Classic 3 and 4, and Crystal screen HT were trialled in seeding experiments (2.4.3); two trays were set up at 18 °C, with protein concentrated to 11.5 mg/mL and 18.8 mg/mL. In the seeding experiment, a few conditions gave crystal hits that could be looped, but only crystals grown in Crystal screen HT condition No. 39 (0.1 M HEPES sodium pH 7.5, 2 % v/v PEG400 and 2 M ammonium sulphate), turned to be protein when tested at the synchrotron.

Additional crystal hits emerged from the initial trays, in Wizard Classic 3 condition No. 10 (20 % w/v PEG3350, 200 mM Sodium thiocyanate) (figure 3.43b), and condition No. 31 (14 % v/v 2-Propanol, 70 mM Sodium acetate/ Hydrochloric acid pH 4.6, 140 mM Calcium chloride, 30 % v/v Glycerol) (figure 3.43c). Crystals shown in figure 3.43b diffracted poorly, as it was expected by their morphology. The crystal shown in figure 3.43c gave the best diffraction among all, at 7 Å resolution (figure 3.43d). Optimisation of the conditions that produced the crystal hits shown in figure 3.43b-c is underway.



3.10 Discussion and future work

A. baumannii is currently one of the most threatening Gram-negative pathogens, due to the increasing rate of multi-drug resistance to all known antibacterial classes, including the latest carbapenems (Perez *et al.*, 2007). For this reason, the WHO has classified carbapenem-resistant *A. baumannii* as high-priority pathogen for which new antibiotics are urgently required (Tacconelli *et al.*, 2018). Discovery of any drugs, including antibiotics, needs a validated target for which knowledge of its structure and the reaction kinetics (if an enzyme) is preferable. Penicillin binding proteins (PBPs), are the enzymes catalysing the last step in the synthesis of peptidoglycan, and are well validated targets for the discovery of new antimicrobials. Penicillin binding protein 2 (PBP2) is one such enzyme, so far poorly characterised in its structures and kinetics across Gram-negative pathogens, particularly those cited in

the WHO priority pathogen list. In the last decade, significant pharmaceutical investment has been made for the design of highly selective PBP2 inhibitors, some of which are in clinical development, and will be thoroughly examined in chapter 5.

With the aim of providing structural information on PBP2 from the clinically relevant pathogen *A. baumannii*, so as to rationalise the interactions with selective binders and informing the design of new PBP inhibitors, the first crystallographic structure of *A. baumannii* PBP2 has been determined in this study. The *A. baumannii* PBP2 structure strongly resembles the counterpart PBP2 structure in Gram-negative *H. pylori* and *E. coli*, with remarkable similarity at the level of the transpeptidase site. Interestingly, the novel structure of *A. baumannii* PBP2 unveils an unprecedented zinc-binding site, through which the conserved β -hairpin loop makes contacts with the X residue of the S-X-N/D motif. Evidence for the zinc-coordination site comes from anomalous scattering and X-ray fluorescence experiments. Direct participation of the zinc in the catalytic activity of PBP2, likewise class B metallo β -lactamases, is unlikely, due to the presence of catalytic residues that are typical of serine hydrolases such as PBPs and serine β -lactamases (Sauvage *et al.*, 2008). Instead, a structural role for this zinc-binding site is more plausible and consistent with its location and coordination sphere in *A. baumannii* PBP2. Particularly, the zinc-coordination site may play a role in the stabilisation of the β -hairpin region, whose ordering state may in turn affect the transpeptidase activity of the protein. The notion that the catalytic activity of PBPs might be hampered by a more flexible and disordered β -hairpin loop, comes from studies performed on *E. coli* PBP5 (Nicholas *et al.*, 2003; Nicola *et al.*, 2005a).

Adoption of a zinc-binding site in the upper part of the transpeptidase domain, would constitute another way of controlling the flexibility of the β -hairpin loop, in addition to the other types of interactions already described in literature for PBPs (3.5.3.2). However, it is unclear why, from an evolutionary point of view, *A. baumannii* and possibly other bacteria have maintained a metal-coordination site in PBP2 and its homologues, preferring it to the more common hydrogen bonding interaction Ser-

Asp (5.3.2.2). In some PBPs, the β -hairpin region is restrained by a pair of Cys residues, which can form a disulphide bridge. In *B. subtilis* SpoVD there is a precise mechanism controlling the redox state of these two Cys (Liu *et al.*, 2010; Bukowska-Faniband and Hederstedt, 2017), which translates into activation and inactivation of SpoVD when the Cys residues are reduced and oxidised, respectively. This implies that, the choice of the physical nature of the interaction tethering the β -hairpin loop to the S-X-N/D motif is not casual, but could reflect a regulatory mechanism coordinating the functional activity of PBPs with precise bacterial growth stages or life cycle stages (for instance SpoVD is active only during sporulation), or with local intracellular environmental changes or adaptation to different external changes. It is intriguing to think that, the *in-vivo* transpeptidase activity of *A. baumannii* PBP2 could be affected by variations of the intracellular concentration of zinc. Interestingly, as reported by Lonergan *et al.* (2019) there is a link between zinc uptake and cell wall homeostasis in *A. baumannii*. ZrIA, a novel zinc-binding D,D-carboxypeptidase enzyme, seems to play a crucial role in this respect. ZrIA becomes overexpressed when *A. baumannii* is grown in zinc-starved conditions, presumably to locally modify the PG architecture and allow the assemblage of cell wall spanning-zinc importer systems. Moreover, Lonergan *et al.* (2019) found that, the wild-type strain of *A. baumannii* grown in zinc limiting conditions has a rounded morphology, consistent with a connection between the activity of the elongasome complex and the availability of zinc. PBP2 is the major D,D-transpeptidase enzyme in the cell wall elongation of *A. baumannii*, and the structural requirement for zinc could be an explanation for the observed morphology response to zinc starvation.

Although the coordination of the zinc by PBP2 is supported by crystallographic data in this work, further complementary analysis will be required to confirm the presence and identity of the metal in PBP2 wild-type. The same metal-binding site is expected to be no longer available when each of the zinc coordinating residues is mutated to alanine (D350A/D365A/H371A/C384A). One such analysis is ICP-MS (inductively coupled plasma- mass spectrometry) that can provide a quantitative measure of the metal content in proteins, from which the stoichiometry of the metal-protein complex can be determined. A thermodynamic analysis of the metal binding

to PBP2 could also be performed by ITC (isothermal titration calorimetry), in order to confirm the binding stoichiometry observed in the crystal structure (1:1), to measure the metal binding affinity, and determine the metal selectivity. Because the zinc detected in the X-ray structure of *A. baumannii* PBP2 is likely to come from the bacterial expression strain, which may contain a variety of metal ions, high metal binding affinity and high specificity for zinc would be expected from this experiment.

The zinc-binding site confers stability to PBP2. In fact, either chelation of the zinc by EDTA or alanine mutagenesis of the zinc-coordinating residues cause a profound decrease of the melting temperature of the protein when analysed in thermal shift assays. This result is in line with other data reported for PBPs, where mutagenesis of the residues involved in the conserved interaction between the β -hairpin region and the S-X-N/D motif, render the proteins more susceptible to degradation in trypsin sensitivity assays (Tomberg *et al.*, 2012; Bukowska-Faniband and Hederstedt, 2017).

The introduction of mutations in the zinc-coordination site, does not preclude interaction with bocillin, indicating that the tether of the β -hairpin loop to the S-X-N/D motif is not absolutely required for the acylation of this and possibly other β -lactams. Similar results have been reported for other HMW-PBPs, such as *B. subtilis* SpoVD and *N. gonorrhoeae* PBP2 (Tomberg *et al.*, 2012, Bukowska-Faniband and Hederstedt, 2017), where mutagenesis of the residues participating in the conserved interaction, that takes the form of a zinc-binding site in *A. baumannii* PBP2 (3.5.3.2), does not impede β -lactam binding but it can cause a reduction of the acylation rates. In this work, the impact of the mutations D350A/D365A/H371A/C384A on the efficiency of acylation by β -lactam molecules has not been explored yet. Methods reported in literature for the measurement of the acylation rate constants of PBPs by covalent inhibitors include a stop-time radioactive assay with [¹⁴C] penicillin G (Stefanova *et al.*, 2003), change in intrinsic tryptophan fluorescence (Fedarovich *et al.*, 2012), a stop-time in-gel fluorescence assay with bocillin (Calvez *et al.*, 2017), a continuous colorimetric assay with nitrocefin (Roychoudhury *et al.*, 1996; Calvez *et al.*, 2017), and continuous fluorescence anisotropy-based assays with either bocillin

or 5-TAMRA-ampicillin (Shapiro *et al.*, 2013; Shapiro *et al.*, 2014; Shapiro *et al.*, 2019). The latter assay may not be optimal for the analysis of the acylation kinetics in *A. baumannii* PBP2, as reported by the authors, due to the very small anisotropy increase upon reaction with the fluorescent probes.

Amino acid variations in the β -hairpin loop as a means of reducing the acylation efficiency by β -lactam antibiotics, have emerged as a mechanism of resistance in a number of resistant clinical strains. One such example is PBP2x (bPBP), the primary determinant of β -lactam resistance in *S. pneumoniae*, that can accumulate tens of mutations in the TP domain. Two mutations (I371T/R384G), reported in *S. pneumoniae* 5204, map in the β -hairpin loop and appear to destabilise this region in proteolytic susceptibility assays, although they do not affect directly the conserved interaction with the S-X-N/D motif (Carapito *et al.*, 2006). It is known that increased flexibility of this region is associated with TP catalysis defects, possibly the presence of additional amino acid substitutions may confer functional compensation to maintain the transpeptidase activity *in-vivo*, while conferring increased resistance to β -lactams (Carapito *et al.*, 2006).

Another example of sequence variation in the β -hairpin loop related to β -lactam resistance, comes from penicillin-resistant strains of *N. gonorrhoeae*. PBP2 (bPBP) is the primary target of penicillin in this pathogen, and in resistant strains, it generally contains the insertion of an aspartic acid (D346a) in the β -hairpin loop, along with 4-8 substitutions near the C-terminal end of the protein (Powell *et al.*, 2009a). Curiously, this insertion is adjacent to Asp346, the residue forming the conserved interaction with Ser362 from the S-X-N/D motif. A crystal structure of the protein mutant shows that the insertion does not cause disordering of the β -hairpin region, consistently with the trypsin susceptibility assay results (Tomberg *et al.*, 2012), and the Ser-Asp interaction is preserved (Fedarovich *et al.*, 2014). This mechanism of resistance seems to be tailored for the insertion of aspartate only, in fact other amino acids in the same position are not tolerated *in-vivo*, and the mechanistic basis that allow retention of TP activity while lowering β -lactam acylation are not clear yet (Tomberg *et al.*, 2012).

In this thesis, a zinc-binding site has been anticipated in *B. subtilis* SpoVD_{C332D}, on the basis of sequence similarity and conservation of the residues coordinating the metal in *A. baumannii* PBP2. After the disulphide bond between Cys332 and Cys351 of SpoVD_{WT} is reduced by StoA in living *B. subtilis*, a potential zinc-binding site could form, that differs from *A. baumannii* PBP2 in having a Cys in place of Asp365. To explore the presence of zinc in SpoVD_{WT/C332D}, the two proteins have been expressed in fusion with a GST-tag as previously reported (Liu *et al.*, 2010), with the intent of performing ICP-MS analysis. However, protein purification by glutathione-affinity chromatography involved the use of DTT, and this reducing agent was later found to be a strong chelator of metal ions (Krężel *et al.*, 2001). Due to a possible interference of DTT with the ICP-MS analysis, the purification of the SpoVD proteins will require a different protocol, for instance expression with an N-terminal His6-tag and purification by nickel-affinity chromatography, similarly to *A. baumannii* PBP2. Protein purification by glutathione-affinity chromatography was also hampered by covalent modification of GST-SpoVD_{WT/C332D} by glutathione as determined by MS. The site of modification was not determined, but a possible S-glutathionylation of SpoVD_{WT/C332D} was certainly not desired, given the intention that the proteins devoid of GST-tag were to be crystallised. Crystallisation trials have been initially performed on SpoVD_{WT} only, and these have generated a few crystal hits that could be improved in optimisation experiments. However, the protocol used for the purification of SpoVD has been shown to be not suitable for the study of metals in this protein, possibly altering the native state of the Cys residues which would make any type of analysis inconclusive.

Another important finding of this work, is the disruptive effect of the PBP2 zinc-binding site mutations (D350A/D365A/H371A/C384A) on the cell wall elongation of *A. baumannii*, as indicated by the loss of rod-shaped morphology. The Δ *pbp2* strain as well as this strain harbouring the complementation plasmid with PBP2 mutated in the Zn-site, grew as spheres and were viable, indicating that PBP2 is not essential for growth in laboratory conditions (Geisinger *et al.*, 2018). A similar phenotype was reported for a Δ *pbp2* strain of *P. aeruginosa* (Legaree *et al.*, 2007). The Zn-binding site mutations would be expected to impair the transpeptidase activity of PBP2

through increased flexibility of the β -hairpin loop, as reported for other PBPs, possibly causing a displacement of the conserved S-X-N/D motif and impaired interaction with the PG substrate. Furthermore, the β -hairpin loop is surface exposed and the mutations could be detrimental for potential protein-protein interactions occurring at this site, thus contributing to the malfunctioning of the elongasome machinery.

The impact of the zinc-binding site mutations on the catalytic activity of PBP2 has not been explored yet, and it could be elucidated by *in-vitro* assays that use the substrate lipid II. In this respect, Rohs *et al.* (2018) have generated a *E. coli* RodA-PBP2 fusion protein, functional both *in-vitro* and *in-vivo*, and used this protein in a gel-based assay to separate the glycan chains produced by RodA, in order to study the effect of selected point mutations on the TG activity. An analogous experiment could be attempted with PBP2 (wild-type and mutants) and RodA from *A. baumannii*. In this assay the transpeptidase activity of PBP2 would be evidenced by a band at the top of the polyacrylamide gel, corresponding to cross-linked glycan chains that can hardly migrate into the gel due to their size. If a mixture of native lipid II and fluorescently-labelled lipid II (for example a lipid II where a dansyl group is attached to *meso*-Dap) is used, fluorescence could be incorporated in the cross-linked chains and the bands could be visualised under UV transillumination (Calvez *et al.*, 2017). While this method is qualitative and does not provide information on the degree of cross-linking, additional *in-vitro* assays could be used for the quantification of the TP and CP activities, that are either based on HPLC (Egan *et al.*, 2015) or spectrophotometric analysis (Catherwood *et al.*, 2020).

X-ray crystallography of the PBP2 mutants could also provide useful insight into the impact of the mutations on the structure of PBP2, particularly the residues of the catalytic pocket, that could help explain the possible loss of enzymatic activity.

CHAPTER 4

Characterisation of *A. baumannii* PBP2 in complex with β -lactam and non β -lactam compounds

4.1 Introduction to chapter 4

The reactivity of a range of β -lactam antibiotics, tested against PBPs in *E. coli*, *K. pneumoniae*, *A. baumannii*, and *P. aeruginosa*, have been published (Asli *et al.*, 2016; Penwell *et al.*, 2015; Moya *et al.*, 2017a; Moya *et al.*, 2017b; King *et al.*, 2016; Sutaria *et al.*, 2018; Kocaoglu and Carlson, 2015; Papp-Wallace *et al.*, 2012). Strikingly, mecillinam binds exclusively to PBP2, representing the only β -lactam selectively targeting this protein, reported so far. However, a thorough comparative analysis of the binding of mecillinam to PBP2 has not been carried out yet, hence the chemical basis of this selectivity remains obscure.

A new generation of β -lactamase inhibitors is represented by the diazabicyclooctane class, of which avibactam is the flagship drug approved by the FDA in combination with ceftazidime, for the treatment of patients with limited therapeutic options (Shirley, 2018). Several DBO-based molecules are being developed by the pharmaceutical industry, that show improved PBP2 inhibition compared to avibactam, and in some cases, even better spectrum of activity against β -lactamases. Examples include FPI-1465, FPI-1523, FPI-1602 synthesized by Fedora Pharmaceuticals (Maiti *et al.*, 2014); OP0595 discovered by Meiji Seika Pharma Co. Ltd (Morinaka *et al.*, 2015); WCK5107 (zidebactam), WCK5153, and WCK4234 discovered by Wockhardt Ltd. (Moya *et al.*, 2017b; Moya *et al.*, 2017a; Moya *et al.*, 2019; Papp-Wallace *et al.*, 2018); EXT2514 developed by Entasis Therapeutics (Durand-Réville *et al.*, 2017), and CPD4 generated by Mirabilis (Levy *et al.*, 2019). It is worthy of note that, the aforementioned avibactam derivatives also show antibacterial activity due to inhibition of PBP2, hence acting as dual inhibitors of serine- β -lactamases and PBPs (King *et al.*, 2016). Due to difficulties in crystallising PBP2, (King *et al.*, 2016) determined the structure of *E. coli* PBP1b in complex with FPI-1465 (5FGZ.pdb). During the time of writing this thesis, structures of *E. coli* PBP2 in complex with avibactam and CPD4 have been disclosed (Levy *et al.*, 2019).

The work described in this chapter aims at elucidating the binding mode of molecules of interest with *A. baumannii* PBP2, with particular emphasis on those interactions

that could explain the selective targeting of this protein and could inform the rational design of new PBP2 selective inhibitors. Particular attention is given to Asp385, with respect to its role in the interaction with selective antibiotics and the *in-vivo* activity of PBP2.

The *in-vivo* experiments in *A. baumannii* ATCC 17978 were performed by Dr Edward Geisinger as in section 3.6.2 (Northeastern University, USA).

4.2 Interactions of *A. baumannii* PBP2 with β -lactams

4.2.1 Interactions of *A. baumannii* PBP2 with mecillinam

4.2.1.1 *In-vivo* and *in-vitro* activities of mecillinam from the literature

Discovery of mecillinam (also known as amdinocillin) dates back to 1972, when Leo Pharmaceutical Laboratories (Ballerup, Denmark) reported a new group of penicillins, called β -amidinopenicillanic acids (Lund and Tybring, 1972; Matsushashi *et al.*, 1974). Mecillinam (previously called FL1060) was the most active molecule within this new class of antibiotics and showed fundamental differences with other penicillins. To start with, mecillinam exhibits a 6-amidino group joining the β -lactam ring to the side chain, rather than the 6-acylamino group typical of penicillins (figure 4.1).

With regard to antimicrobial activity, mecillinam has a narrow spectrum being highly active against most Gram-negative bacteria and Enterobacteriaceae in particular, while it shows poor activity against Gram-positive cocci (table 4.1) (Fass, 1980; Advic, 2017). Notably, *P. aeruginosa* and *A. baumannii* are both mecillinam resistant. Moreover, it has been reported that rod-shaped bacteria treated with mecillinam become large spherical cells that eventually lyse (Lund and Tybring, 1972; Spratt, 1975; Legaree *et al.*, 2007) (figure 4.2).

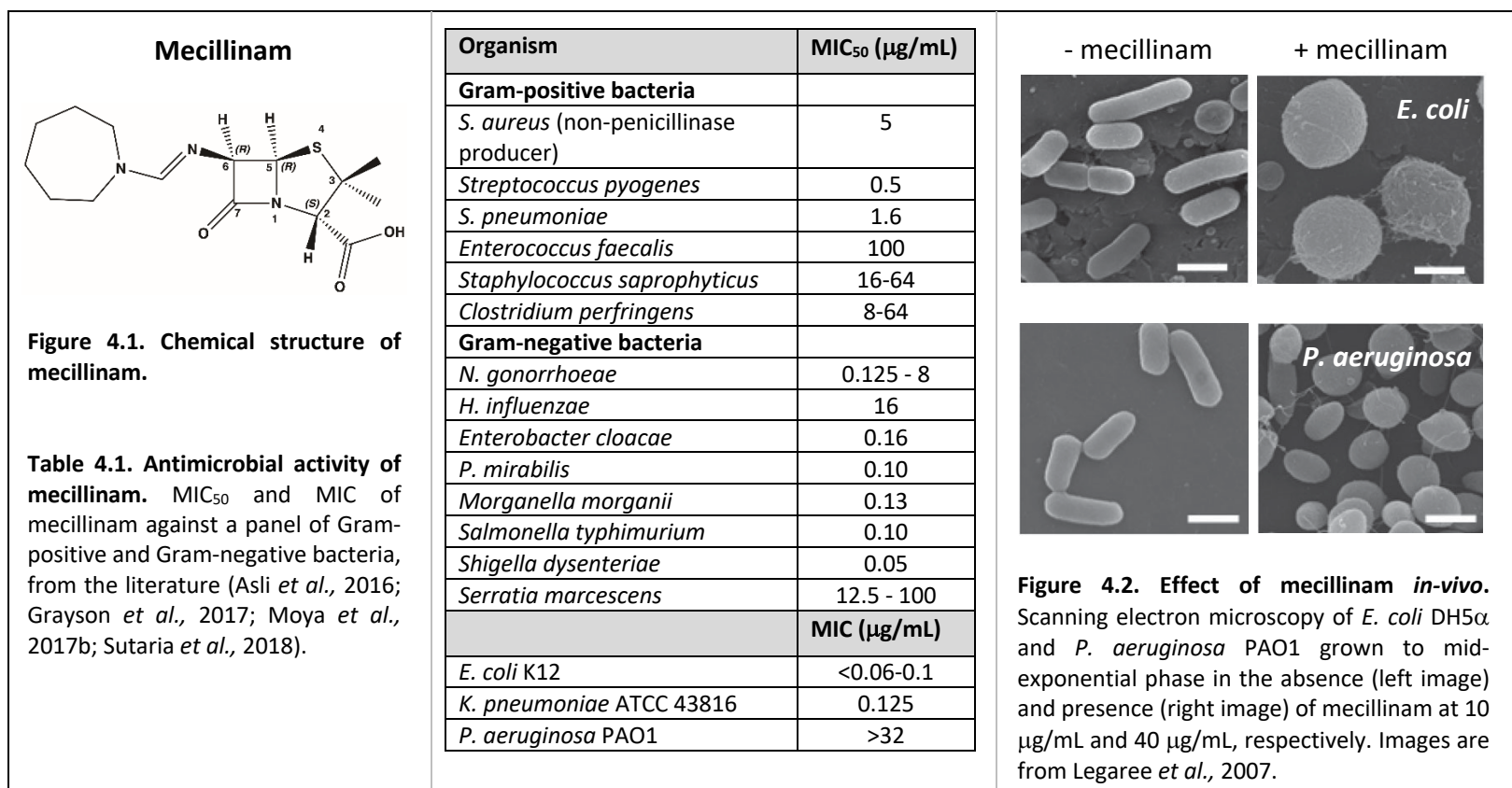
With respect to PBP binding affinity, mecillinam specifically inactivates PBP2 only (Spratt, 1977), unlike the majority of β -lactams targeting PBP1a, PBP1b, or PBP3 from Gram-negative organisms (Asli *et al.*, 2016; Bulitta *et al.*, 2018; Moya *et al.*, 2017b;

Sutaria *et al.*, 2018) (table 4.2). Because of this specificity, combinations of mecillinam with a β -lactam antibiotic are synergistic, due to the multiple targeting of PBP2 and PBP1a/PBP1b/PBP3, thus reducing the risk of resistance development (Hickman *et al.*, 2014; Skarp *et al.*, 2019; Satta *et al.*, 1995).

Pivmecillinam (pivaloyloxymethyl ester of mecillinam), is the orally active prodrug of mecillinam, where the latter released by the action of non-specific esterases, after absorption (LEO Pharma Inc., 2018). Pivmecillinam has been used successfully as first-line antibiotic in the Scandinavian countries, for the treatment of acute uncomplicated urinary tract infections (uUTIs), since the early 1980s (Hooton, 2000; Nicolle, 2000; Nicolle, 2001; Graninger, 2003; Gupta *et al.*, 2011). In fact, mecillinam is especially effective against *E. coli*, the primary uropathogen accounting for 75-85% of acute uncomplicated UTI cases. Less frequently, other species have been isolated including *Staphylococcus saprophyticus* (5-10 % of all uUTI cases), *K. pneumoniae*, *Proteus mirabilis* and group B streptococci (5 % or less of all uUTI cases) (Nicolle, 2001). Surprisingly, in spite of more than 40 years of use, the resistance rate to mecillinam has remained low in Nordic countries (5-6 %) (NORM/NORM-VET, 2016; Borck Høg *et al.*, 2017), and this could be possibly due to the large fitness-cost associated with mutations conferring resistance to this antibiotic (Wachi *et al.*, 1987; Thulin *et al.*, 2015).

ESBL-producing Enterobacteriaceae are frequently susceptible to mecillinam (Titelman *et al.*, 2011; Tärnberg *et al.*, 2011), due to its higher stability to β -lactamase hydrolysis compared with other penicillins (Sougakoff and Jarlier, 2000). Because of this and other favourable properties, including low occurrence of resistant bacteria, high absorption rate in the gastrointestinal tract, minimal effect on the host microflora, and good tolerance, mecillinam is being reconsidered for further clinical evaluation to assess its applicability on treatment of infections caused by emerging multi-drug resistant Gram-negative bacteria (Dewar *et al.*, 2013). Due to its excellent clinical efficacy, pivmecillinam is currently recommended as first-line antibiotic for UTI treatment by the Infectious Diseases Society of America and the European Society for Microbiology and Infectious Diseases (Gupta *et al.*, 2011).

Given the clinical relevance of mecillinam and the lack of structural information of PBPs with this antibiotic, the structure of *A. baumannii* PBP2 has been used as a model protein to explore the interactions with this molecule by X-ray crystallography, so as to rationalise the selective PBP2 binding properties.



PBP	IC ₅₀ (µg/mL)			
	<i>E. coli</i> K12	<i>P. aeruginosa</i> PAO1	<i>K. pneumoniae</i> ATCC 43816	<i>A. baumannii</i> ATCC 19606
1a	>13	>4	>256	256
1b	>13	>4	>256	256
2	0.02	0.19 ± 0.02	<0.0075	<0.06
3	>13	>4	128	64

Table 4.2. PBP sensitivity to mecillinam acylation in various Gram-negative pathogens. IC₅₀ are from gel based bocillin-FL competition assays, using either purified PBPs or cell membranes, published by Asli *et al.* (2016), Bulitta *et al.* (2018), Moya *et al.* (2017b) and Sutaria *et al.* (2018). IC₅₀ defines the concentration of compound that reduces by 50% the binding of bocillin-FL to individual PBPs.

4.2.1.2 Mass spectrometry of *A. baumannii* PBP2 with mecillinam

To confirm binding of mecillinam to *A. baumannii* PBP2, adduct formation between the protein and the drug was confirmed by mass spectrometry. Mecillinam (exact mass: 325.15 Da) was solubilized in LC/MS grade water and incubated at 10-fold molar excess with *A. baumannii* PBP2 (11 μ M) in 50 mM HEPES pH 7.5 and 400 mM NaCl, at 37 °C for 5 min. The ESI-MS spectra of PBP2 were collected (2.6.1 and 2.6.2), and deconvoluted in the mass range 60000-80000 Da. The major peak at 70868.76 Da accounts for the entire mass of PBP2: mecillinam adduct. The less intense peak at 70789.82 Da could correspond to the protein acylated by a fragment of mecillinam, possibly due to degradation (Baltzer *et al.*, 1979). The peak at 70543.04 Da corresponds to the native protein (expected MW: 70544.87 Da)(table 4.3, figure 4.3).

Protein	Compound	Calculated mass (Da) (\pm error)	Δ mass (Da)
PBP2 _{WT}	none	70543.01 (\pm 0.12)	reference
PBP2 _{WT}	mecillinam	70543.04 (\pm 0.64)	-
		70789.82 (\pm 0.43)	+ 246.81
		70868.76 (\pm 0.18)	+ 325.75

Table 4.3. MS of PBP2_{WT} before and after reaction with 10-fold molar excess of mecillinam. Δ mass is the difference between the observed mass of the protein unbound (reference) and acylated by mecillinam.

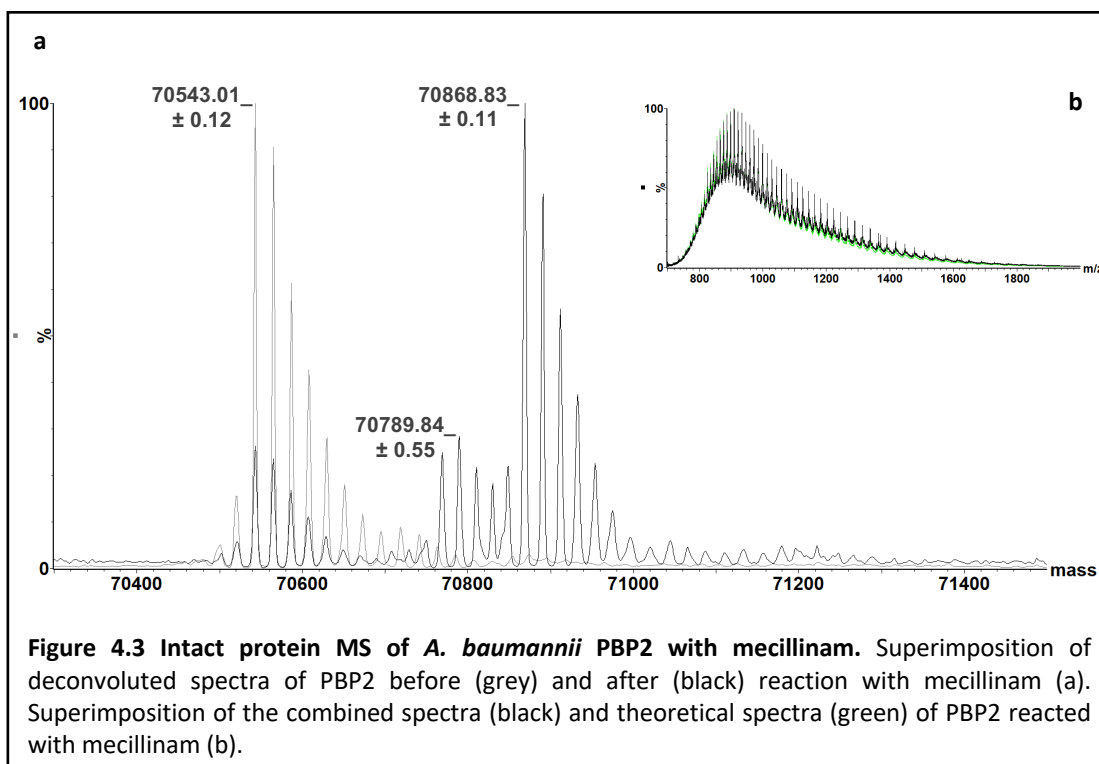


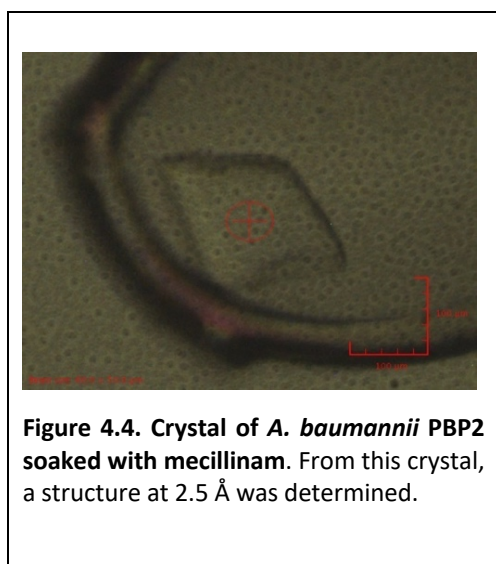
Figure 4.3 Intact protein MS of *A. baumannii* PBP2 with mecillinam. Superimposition of deconvoluted spectra of PBP2 before (grey) and after (black) reaction with mecillinam (a). Superimposition of the combined spectra (black) and theoretical spectra (green) of PBP2 reacted with mecillinam (b).

4.2.1.3 Structure of *A. baumannii* PBP2 bound to mecillinam

4.2.1.3.1 Crystallisation, data collection and structure determination

Crystallisation plates of PBP2 were set up using the sitting drop vapour diffusion method at 18 °C. Drops consisted of 300 nL protein concentrated to 18.7 mg/mL, combined with 200 nL of precipitant and 100 nL of seeds, prepared by a 10-fold dilution of a stock of PBP2 crystals grown in a similar condition as the 2.6 Å diffracting crystal in 3.3.2. Diffracting PBP2 crystals grew in 5 % (w/v) PEG1000, 100 mM sodium phosphate dibasic/citric acid pH 4.2, 15 % (v/v) ethanol and 2 mM zinc chloride. Zinc chloride was found to promote crystal growth, possibly due to the presence of a zinc-coordination site in PBP2 (3.5.3).

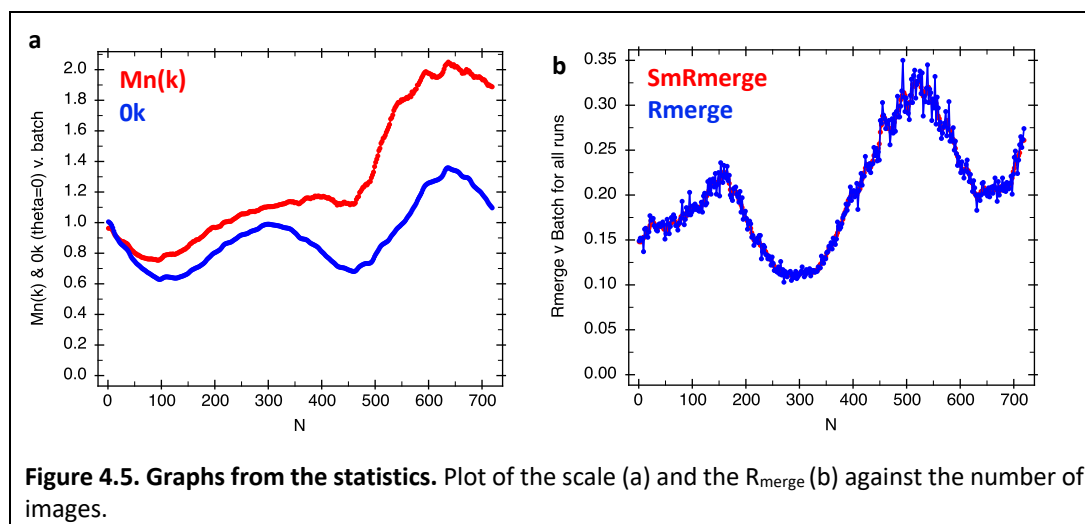
A structure of PBP2 in complex with mecillinam was obtained by soaking experiments. Crystals were soaked for 7 min in cryoprotectant solution (mother liquor + 25 % v/v glycerol) supplemented with mecillinam at 10 mM final concentration. Crystals were harvested and flash vitrified in liquid nitrogen (figure 4.4).



Data collection was performed at the I04-1 beamline (DLS, Didcot, United Kingdom) in remote access, using a wavelength of 0.9159 Å and a Pilatus 6M-F detector. A complete dataset was obtained by collecting 720 images with an oscillation step of 0.5° and 0.5 s exposure time. Beam size was 60x50 μm and transmission was 100%. The crystal to detector distance was set up for collecting data up to 2.5 Å resolution.

Even though the dataset was mistakenly collected at high exposure time and high transmission, the scale and R_{merge} plots (figure 4.5) indicate that the quality of the data has not been severely compromised by radiation damage. The dataset was integrated with iMosflm (2.4.6.1), merged and scaled with Aimless (2.4.6.2) (table

4.4), and the structure of PBP2 bound to mecillinam was determined by refining the PBP2 structure (chapter 3) against the new experimental data, where local NCS restraints were used. (2.4.6.5).



	Overall	Inner Shell	Outer Shell
Low resolution limit	47.29	47.29	2.57
High resolution limit	2.50	10.61	2.50
Rmerge (within I+/I-)	0.195	0.058	1.833
Rmerge (all I+ and I-)	0.201	0.059	1.897
Rmeas (within I+/I-)	0.212	0.062	2.002
Rmeas (all I+ & I-)	0.210	0.062	1.981
Rpim (within I+/I-)	0.082	0.024	0.801
Rpim (all I+ & I-)	0.059	0.018	0.567
Rmerge in top intensity bin	0.055	-	-
Total number of observations	713508	9691	56244
Total number unique	56616	824	4647
Mean($I/sd(I)$)	11.0	32.1	1.9
Mn(I) half-set correlation CC(1/2)	0.997	0.998	0.765
Completeness	100.0	98.9	100.0
Multiplicity	12.6	11.8	12.1
Mean (χ^2)	0.99	0.94	1.01
Anomalous completeness	100.0	99.5	100.0
Anomalous multiplicity	6.5	6.8	6.1
DelAnom correlation between half-sets	-0.053	-0.097	-0.028
Mid-Slope of Anom Normal Probability	0.935	-	-

Table 4.4. Statistics of the PBP2: mecillinam dataset. Output data from Aimless.

An extra electron density was noted in the active site of PBP2, extending from the catalytic serine (Ser326), in both molecules of the asu, indicative of the presence of the ligand following PBP2 acylation (figure 4.6). The molecular structure of mecillinam was downloaded (entry DH4) from the PDB and manually fitted into the electron density, in Coot (2.4.6.5). A description of its covalent bond to Ser326 was generated with JLigand (Lebedev *et al.*, 2012). The co-structure has been refined with Refmac5 and is currently under a cyclic process of refinement and validation prior to deposition (2.4.6.5 and 2.4.6.6).

The binding mode of mecillinam and other molecules examined in this chapter will be discussed in reference to both PBP2 polypeptide chains of the asu. However, crystal packing interactions occurring between the binding pocket of chain A, and the flap region (aa. 351-369) of a symmetry-related neighbouring molecule, result in partial closure of the binding cleft. Hence, the binding mode of a molecule in the active site of chain B, that is free from crystal contacts and completely exposed to the solvent, will be regarded as a more reliable representation of the binding event occurring in solution.

4.2.1.3.2 Binding mode of mecillinam in complex with PBP2

The structure of acylated PBP2 with mecillinam was solved at 2.5 Å resolution, in space group I 2 2 2 with unit cell parameters of $a = 121.19 \text{ \AA}$ $b = 151.30 \text{ \AA}$ $c = 177.37 \text{ \AA}$ and $\alpha = \beta = \gamma = 90^\circ$ and refined to $R_{\text{work}} 0.2084$ and $R_{\text{free}} 0.2515$ (table 4.4 and 4.5).

No. atoms		B-factors (Å ²)	
Protein	8330	Protein	67
Ligand	46	Ligand	106
Water	62	Water	53
R.m.s deviations		Ramachandran plot	
Bond lengths (Å)	0.0079	Favoured (%)	94.5
Bond angles (°)	1.5019	Allowed (%)	5.1
		Outliers (%)	0.5

Table 4.5. Statistics of the PBP2: mecillinam dataset. Data refinement with Refmac5 and validation with Procheck and Rampage.

In both PBP2 chains of the *asu*, there was clear electron density in the omit map ($F_o - F_c$) (3σ) corresponding to a C7-S326 O- γ ester linkage. After refinement, electron density ($2F_o - F_c$) (1σ) was well resolved for most of the mecillinam ligand (figure 4.7).

In chain A, the carbonyl of the ligand ester linkage is directed into the oxyanion hole and forms hydrogen bonds with the amide nitrogens of Ser326, corresponding to the catalytic residue of the S*-X-X-K motif, and Thr540, corresponding to the fourth residue of the K-T/S-G-T motif of PBP2 (2.8 and 3.4 Å, respectively). In chain B, the carbonyl of the acyl linkage is only within hydrogen-bonding distance of Ser326 (2.7 Å) and not of Thr540 (3.8 Å) amide nitrogens (figure 4.8).

Electron density for the overall ligand is well resolved in chain B, except for the seven-membered hexamethyleneimine ring (figure 4.7). The weak electron density and the higher B-factors of the hexamethyleneimine ring compared to the rest of the antibiotic, suggest that this moiety is flexible, probably due to the absence of strong interactions with residues of the binding cleft.

The hexamethyleneimine ring of mecillinam is connected to C6 by an amidine link. At physiological pH, the amidino group is protonated on the imino nitrogen and the amidinium ion is stabilised by resonance. In both PBP2 polypeptides of the *asu*, the mecillinam amidino group is close to the Asp385 carboxylate (from the S-X-N/D motif) and within distance to form a salt-bridge (N- O δ^1 and N-O δ^2 at 3.6 and 3.7 Å, respectively, in chain A; N- O δ^1 and N-O δ^2 at 3.9 and 3.9 Å, respectively, in chain B) (figure 4.8).

The mecillinam β -lactam ring is fused to a five-membered thiazolidine ring, which fits well into the electron density map in both PBP2 chains of the *asu*. The nitrogen of the mecillinam thiazolidine ring is close to the hydroxyl of Ser383 (from the S-X-N/D motif) but not within hydrogen-bonding distance (4.2 and 3.8 Å in chain A and B, respectively). PBP2 residues from the K-T/S-G-T motif orient the mecillinam thiazolidine ring via a number of interactions.

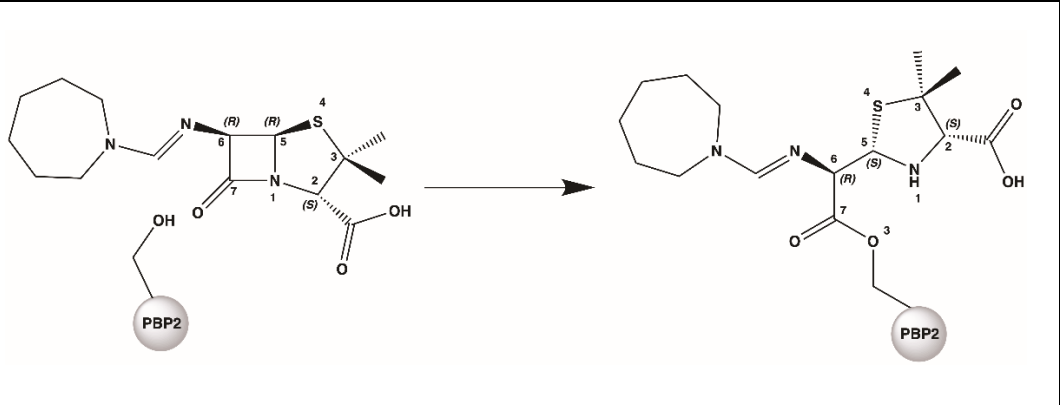


Figure 4.6. Schematic of the reaction of *A. baumannii* PBP2 with mecillinam. Following acylation, Ser326 is linked to C7 by an ester bond.

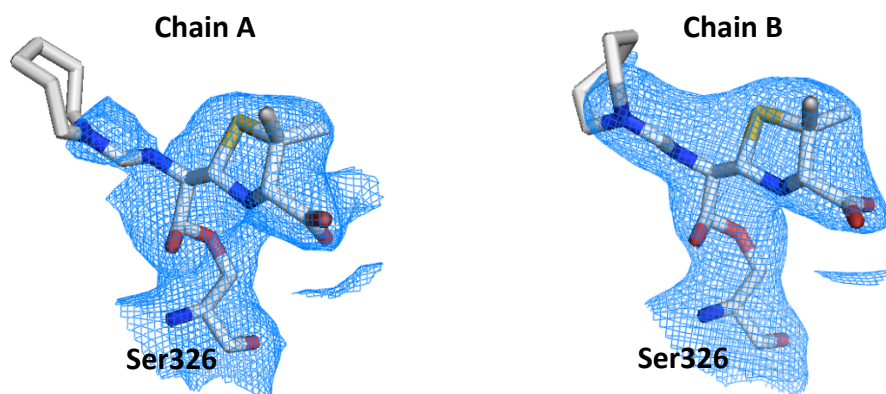


Figure 4.7. Electron density of mecillinam in the acylated structure of *A. baumannii* PBP2. The 2Fo-Fc map is contoured at 1σ around mecillinam covalently bound to Ser326 in chain A (left) and chain B (right).

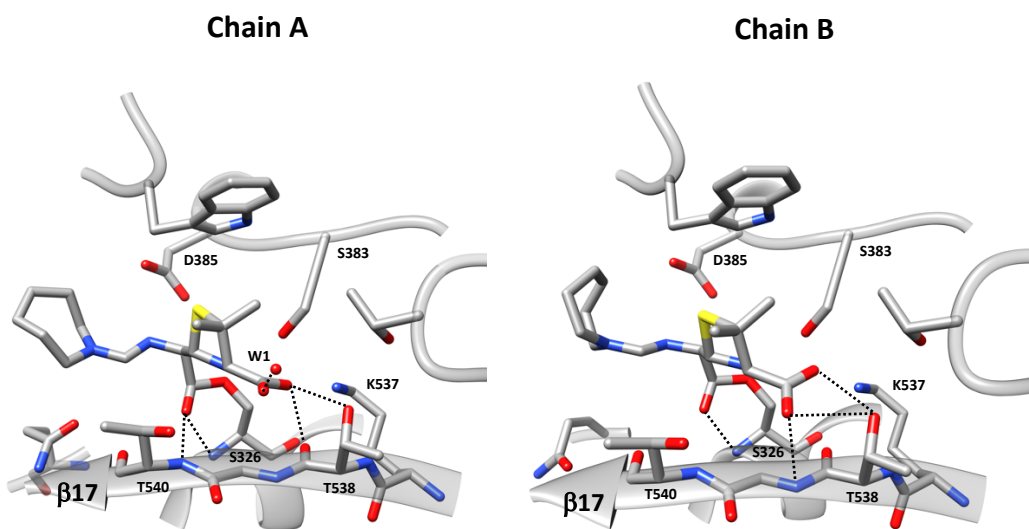


Figure 4.8. Mecillinam bound to the active site of *A. baumannii* PBP2. Hydrogen bonds between mecillinam and the active site residues of chain A (left) and chain B (right), are depicted as dashed lines.

In both chain A and B, the mecillinam carboxylate group is anchored by hydrogen bonds to Thr538-OH (2.6 and 2.8 Å in chain A and B, respectively). Also, this group makes interactions with the side chain of Lys537, the backbone carbonyl oxygen of Thr538, the backbone nitrogen of Gly539, and the hydroxyl of Thr540. Electron density consistent with a water molecule is present in PBP2 chain A, bridging the mecillinam carboxylate to the backbone nitrogen of Gly591 (figure 4.8).

Superimposition of the PBP2 structures with and without antibiotic indicates that, upon binding of mecillinam there are no major structural rearrangement occurring in both the pedestal domain and the transpeptidase domain of the protein. In fact, the rmsd between all C α atoms of PBP2 and PBP2: mecillinam structures is 0.366 Å in chain A, and 0.277 Å in chain B. Specifically, the rmsd between all the atoms of the residues making the binding pocket (residues 537-542, 521-527, 324-330, 446-452, 379-388, 364-372 and 587-592) between the two structures is 0.524 Å in chain A and 0.613 Å in chain B. Minor movements include the shift of the backbone of β 17 towards the exit of the cleft (rmsd between C α of Lys537-Thr540 is 0.25 Å in chain A, and 0.37 Å in chain B), rotation of the Lys537 side chain towards the carboxylate of mecillinam, and rotation of the Gln451 away from the benzyl group of the mecillinam side chain (figure 4.9).

Currently, there are no available structures of other PBPs in complex with mecillinam, thus the binding mode of mecillinam in PBP2 could not be compared to any. However, there are HMW-PBP structures bound to various penicillins, which could be used for comparison to highlight differences in the type of interactions occurring in the PBP2: mecillinam active site, that could help explain the selective targeting of this antibiotic. The structure of *A. baumannii* PBP1a bound to penicillin G has been chosen for this comparative analysis, since mecillinam and penicillin G differ only in the chemistry of the side chain at C6, and the TP motifs are conserved between PBP1a and PBP2. Mecillinam and penicillin G have in common a β -lactam ring fused to the thiazolidine ring, and acylate the catalytic serine by the same mechanism (figure 4.6). The resulting ester linkage formed by penicillin G with the

catalytic Ser of PBP1a is directed into the oxyanion hole and the thiazolidine ring occupies a similar position in both PBP1a and PBP2 (figure 4.10), with the carboxylate group establishing conserved hydrogen bonds with the K-T/S-G-T motif.

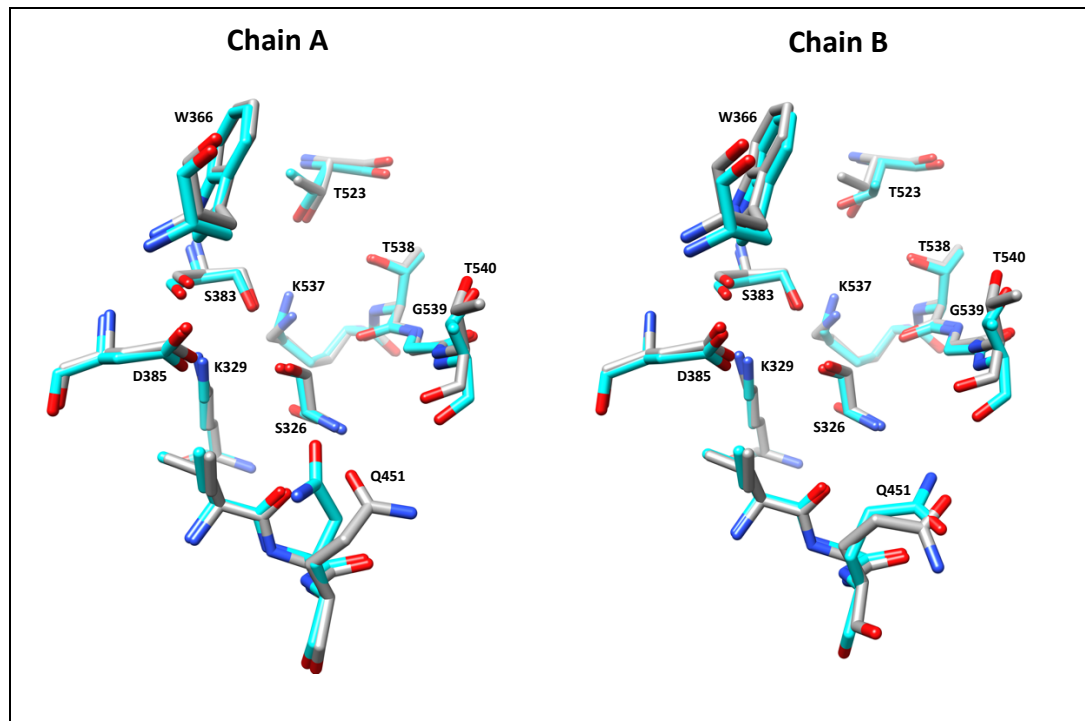


Figure 4.9. Active site of PBP2 unbound and in complex with mecillinam. PBP2: mecillinam structure (grey) superimposed to the PBP2 structure (cyan), in chain A (left) and chain B (right). The ligand has been omitted for clarity.

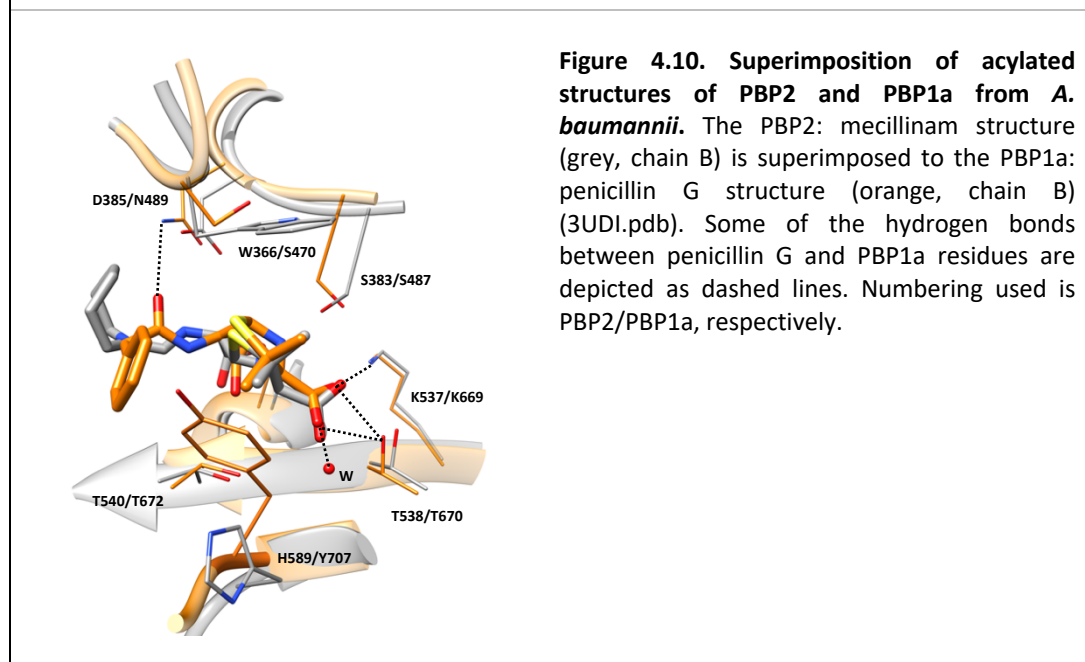


Figure 4.10. Superimposition of acylated structures of PBP2 and PBP1a from *A. baumannii*. The PBP2: mecillinam structure (grey, chain B) is superimposed to the PBP1a: penicillin G structure (orange, chain B) (3UDI.pdb). Some of the hydrogen bonds between penicillin G and PBP1a residues are depicted as dashed lines. Numbering used is PBP2/PBP1a, respectively.

However, the *gem*-dimethyl groups of penicillin G and mecillinam interact differently with PBP1a and PBP2, respectively, due to amino acid sequence variations. A van der Waals interaction occurs between the *gem*-dimethyl of penicillin G and the phenyl ring of Tyr707 in PBP1a, whereas in PBP2, the same type of interaction involves the *gem*-dimethyl of mecillinam with the indole ring of Trp366.

Distinctive interactions are displayed by the antibiotic side chain with residues at the entrance of the binding pocket. The penicillin G side chain consists of a benzyl group joined to C6 by an amide linkage. The amide bond, reminiscent of the peptide bond between the meso-Dap and the fourth D-Ala of the PG substrate, makes a hydrogen bond with the Thr672 backbone carbonyl and the Asn489 side chain of PBP1a, whereas in PBP2, this interaction is not present and the asparagine is replaced by aspartate (Asp385). Because the only difference between mecillinam and other penicillins, including penicillin G, resides in the chemistry of the side chain, the selective targeting of PBP2 must arise from particular interactions of the mecillinam side chain with residues of PBP2. The salt-bridge interaction with Asp385 would be a good candidate.

4.2.2 Interactions of *A. baumannii* PBP2 with meropenem

4.2.2.1 *In-vivo* and *in-vitro* activities of meropenem from the literature

Meropenem (previously SM-7338) is a β -lactam antibiotic developed in the late 1980s by Sumitomo Pharmaceuticals, and is a member of the carbapenem class (Sunagawa *et al.*, 1990; Papp-Wallace *et al.*, 2011). Like other carbapenems, meropenem shows broad spectrum of activity against Gram-positive and Gram-negative bacteria (Edwards *et al.*, 1989) (table 4.6) and is clinically used for the treatment of complicated skin infection, serious intra-abdominal infections and bacterial meningitis (Mohr, 2008). Meropenem is stable to hydrolysis by most β -lactamases, including penicillinases and cephalosporinases, but not carbapenemases. In 2017, meropenem was approved by the FDA in combination with vaborbactam for the treatment of cUTIs (Dhillon, 2018). Vaborbactam is a cyclic boronic acid-BLI, that can restore the activity of meropenem against carbapenemase

producing Enterobacteriaceae, most notably the *Klebsiella pneumoniae* carbapenemase (KPC) enzyme (Dhillon, 2018).

Analogous to other carbapenems, meropenem possesses a β -lactam ring fused to a pyrroline ring that differs from the thiazolidine ring typical of penicillins, in having a double bond between C2 and C3 (figure 4.11). The substitution of sulphur to carbon at position 1 is believed to underpin the exceptional potency and spectrum of activity, as well as, stability to β -lactamases. Also, the hydroxyethyl R₂ side chain contributes to the β -lactamase resistance profile of this class of antibiotics (Moellering Jr *et al.*, 1989; Papp-Wallace *et al.*, 2011). Moreover, meropenem displays a 1- β -methyl group at C1 that confers resistance to hydrolysis by the renal dehydropeptidase I (DHP-I) (Edwards *et al.*, 1989; Papp-Wallace *et al.*, 2011). Therefore, coadministration with a DHP-I inhibitor (i.e., cilastatin) is not required, which is the case for imipenem. The R₁ side chain consists of a sulphur atom bridging the pyrroline to the carbamoyl pyrrolidine group, and contributes to the broader antimicrobial spectrum of meropenem (Papp-Wallace *et al.*, 2011) (figure 4.11).

Carbapenems are known to have high affinity for multiple PBPs in Gram-negative bacteria, and PBP2 is the primary target (table 4.7). For instance, meropenem shows the greatest binding affinity for PBP-2 and -3 in *P. aeruginosa* and PBP2 in *E. coli* (Davies *et al.*, 2008). Bacteria exposure to meropenem causes morphological transition from rod-shape to spherical-shape cells due to inhibition of PBP2 (Monahan *et al.*, 2014; Penwell *et al.*, 2015), and depending on the specific binding affinity profile in the organism, even filamentation due to inhibition of PBP3 (Curtis *et al.*, 1979; Hayes and Orr, 1983) (figure 4.12).

To rationalise the potency of meropenem towards PBP2, X-ray crystallography has been used to elucidate the molecular interactions of this drug with *A. baumannii* PBP2 and compare its binding mode with that of other HMW-PBP structures in complex with the same ligand.

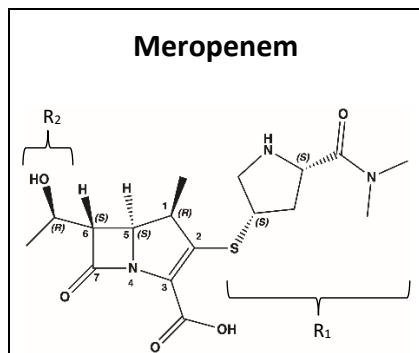


Figure 4.11. Chemical structure of meropenem.

Table 4.6. Antimicrobial activity of meropenem. MIC₅₀ and MIC of meropenem against Gram-positive and Gram-negative bacteria, from the literature (Bhagwat *et al.*, 2019; Edwards *et al.*, 1989; Moya 2017b; Sutaria *et al.*, 2018).

Organism	MIC ₅₀ (µg/mL)
Gram-positive bacteria	
<i>S. aureus</i> MRSA	0.06
<i>S. pneumoniae</i>	≤0.008
<i>E. faecalis</i>	4
<i>Clostridium difficile</i>	1
Gram-negative bacteria	
<i>N. gonorrhoeae</i>	≤0.008
<i>H. influenzae</i>	0.06
<i>S. marcescens</i>	0.06
<i>P. mirabilis</i>	0.03
<i>M. morgani</i>	0.03
Organism	MIC (µg/mL)
Gram-negative bacteria	
<i>A. baumannii</i> ATCC 19606	2
<i>P. aeruginosa</i> PAO1	0.5
<i>K. pneumoniae</i> ATCC 43816	0.06
<i>E. coli</i> MC4100	0.03

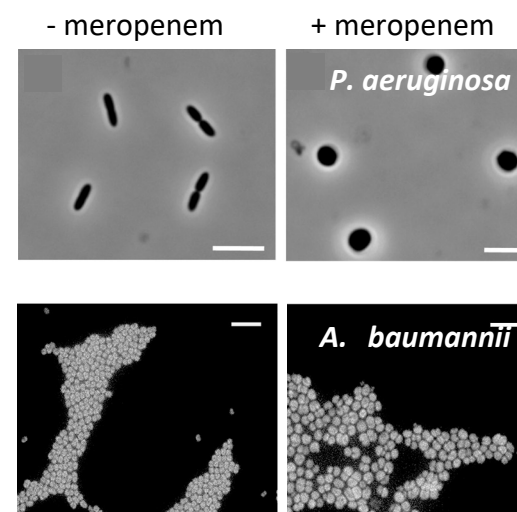


Figure 4.12. In-vivo effect of meropenem. Phase-contrast microscopy of *P. aeruginosa* PA14 before (left) and after incubation with meropenem (5xMIC) for 24 h. Images are from Monahan *et al.*, 2014. Fluorescence microscopy of *A. baumannii* ARC2058 before (left) and after incubation with meropenem (0.5xMIC) for 3 h. Images from Penwell *et al.*, 2015.

PBP	IC ₅₀ (µg/mL)			
	<i>E. coli</i> MC4100	<i>P. aeruginosa</i> PAO1	<i>K. pneumoniae</i> ATCC 43816	<i>A. baumannii</i> ATCC 19606
1a	1.7	0.5	2	0.12 ± 0.08
1b	1.3	0.5	2	1.67 ± 0.55
2	0.008	0.05	<0.0075	0.02 ± 0.01
3	0.06	0.08	0.12	0.67 ± 0.22

Table 4.7. PBP sensitivity to meropenem acylation in various Gram-negative pathogens. IC₅₀ are from gel based bocillin-FL competition assays using bacterial cell membranes, published by Davies *et al.* (2008), Moya *et al.* (2017a) and Sutaria *et al.* (2018). IC₅₀ defines the concentration of compound that reduces by 50% the binding of bocillin-FL to individual PBPs.

4.2.2.2 Structure of *A. baumannii* PBP2 bound to meropenem

4.2.2.2.1 Crystallisation, data collection and structure determination

Crystallisation trays were set up as in 4.2.1.3.1, and diffracting crystals grew in 6 % (w/v) PEG1000, 100 mM sodium phosphate dibasic/citric acid pH 4.2, 18 % (v/v) ethanol and 2 mM zinc chloride. Crystals were soaked for 5 min in cryoprotectant solution (mother liquor + 25 % v/v glycerol) supplemented with meropenem at 1 mM final concentration. Crystals were harvested and flash vitrified in liquid nitrogen (figure 4.13). Diffraction data were collected as in 4.2.1.3.1.



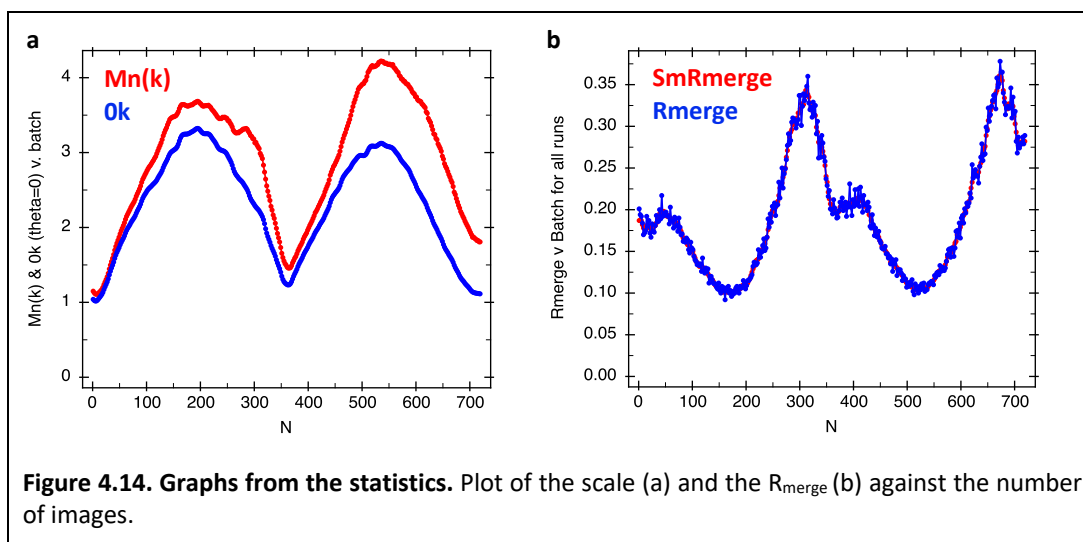
Figure 4.13. Crystal of *A. baumannii* PBP2 soaked with meropenem. This crystal allowed to determine the structure of PBP2: meropenem at 2.5 Å.

Similar to 4.2.1.3.1, the dataset was collected at high exposure time and transmission. The scale and R_{merge} plots (figure 4.14) indicate that, although there may be some radiation damage, the quality of the data was not severely compromised. After data integration with iMosflm (2.4.6.1), data were scaled and merged with Aimless (2.4.6.2) (table 4.8).

A structure of PBP2 acylated by meropenem was solved, by refining the PBP2 structure (chapter 3) against the new experimental data, and using local NCS restraints. The co-structure has been refined with Refmac5 (2.4.6.5) and is currently under a cyclic process of refinement and validation prior to deposition (2.4.6.6).

4.2.2.2.2 Binding mode of meropenem in complex with PBP2

The acylated complex of PBP2 with meropenem was determined at 2.5 Å, in space group I 2 2 2, with unit cell parameters of $a = 123.51$ Å $b = 151.24$ Å $c = 177.19$ Å and $\alpha = \beta = \gamma = 90^\circ$, and refined to $R_{\text{work}} 0.2103$ and $R_{\text{free}} 0.2558$ (table 4.8 and 4.9).



	Overall	Inner Shell	Outer Shell
Low resolution limit	40.10	40.10	2.57
High resolution limit	2.50	10.90	2.50
Rmerge (within I+/I-)	0.172	0.049	1.505
Rmerge (all I+ and I-)	0.179	0.050	1.568
Rmeas (within I+/I-)	0.188	0.053	1.654
Rmeas (all I+ & I-)	0.186	0.052	1.642
Rpim (within I+/I-)	0.074	0.021	0.680
Rpim (all I+ & I-)	0.053	0.016	0.483
Rmerge in top intensity bin	0.048	-	-
Total number of observations	697085	8766	50882
Total number unique	57580	754	4449
Mean(I)/sd(I)	12.5	39.2	1.8
Mn(I) half-set correlation CC(1/2)	0.998	0.999	0.780
Completeness	100.0	97.8	100.0
Multiplicity	12.1	11.6	11.4
Mean (Chi ²)	0.99	1.13	0.90
Anomalous completeness	100.0	98.6	100.0
Anomalous multiplicity	6.2	6.8	5.8
DelAnom correlation between half-sets	- 0.045	- 0.093	- 0.010
Mid-Slope of Anom Normal Probability	0.942	-	-

Table 4.8. Statistics of the PBP2: meropenem dataset. Output data from Aimless.

No. atoms		B-factors (\AA^2)	
Protein	8381	Protein	66
Ligand	54	Ligand	109
Water	42	Water	51
R.m.s deviations		Ramachandran plot	
Bond lengths (\AA)	0.0072	Favoured (%)	94.2
Bond angles ($^\circ$)	1.4711	Allowed (%)	5.0
		Outliers (%)	0.8

Table 4.9. Statistics of the PBP2: meropenem dataset. Data refinement with Refmac5 and validation with Procheck and Rampage.

In both PBP2 chains of the asu, the electron density corresponding to the acyl-linkage between meropenem-C7 and Ser326-O γ is well defined, indicating the formation of a covalent adduct following acylation (figure 4.15 and 4.16). Electron density for the 5-membered ring and the R₂ side chain is also well resolved, except for the R₁ side chain (4.16). Overall, electron density for the antibiotic is better in chain B than in chain A.

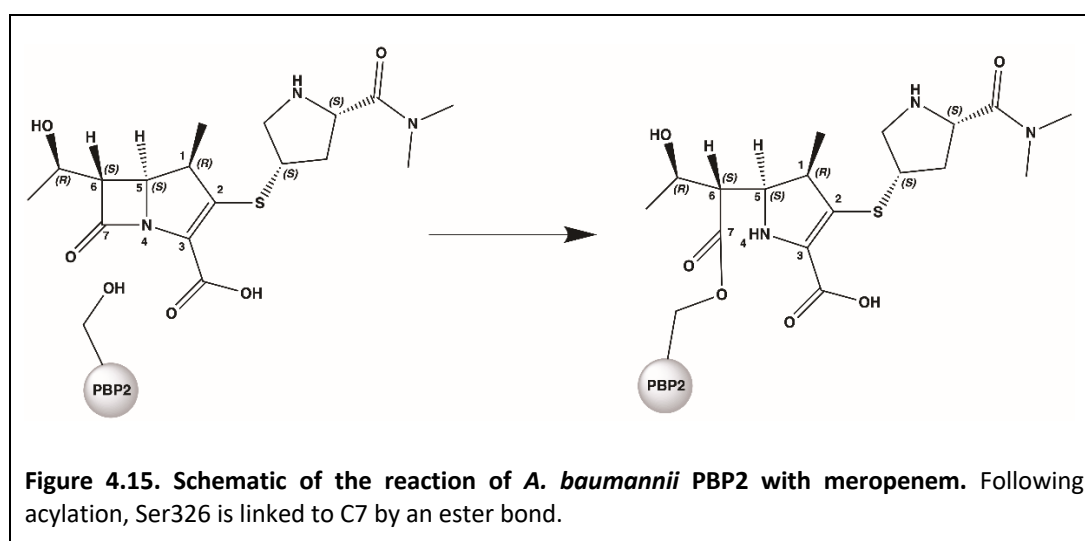
The meropenem acyl-linkage carbonyl oxygen is within hydrogen bonding distance to the amide nitrogens of Ser326 and Thr540. The hydroxyl of the 6 α -hydroxyethyl group forms hydrogen bonds with the carboxylate of Asp385. The β -lactam ring nitrogen is within hydrogen bonding distance of the Ser383-OH, and the β -lactam carboxylate forms typical interactions with the K-T/S-G-T motif (figure 4.17) (table 4.10). The R₁ side chain extends towards the exit of the active site pocket and is positioned between α 21 and the α 19- β 17 loop of PBP2 chain A and B. Electron density beyond the thioether sulphur atom is weak and discontinuous, suggesting that the R₁ side chain does not form strong interactions with PBP2 and is flexible. Interestingly, residues 524-526 from the α 19- β 17 loop are disordered in chain A, which may correlate with the poor electron density for the R₁ group of meropenem in this chain. In chain B, the electron density around the R₂ group is better defined, and residues 524-526 are ordered. Despite the poor quality of electron density, it can be discerned that the R₁ chain adopts a different orientation in the binding site of chain A compared to chain B. A reason for this could be to prevent a possible steric clash between the pyrrolidine ring and the symmetry related molecule packing against the active site of chain A. The flexibility of the R₁ chain is not a novelty, and

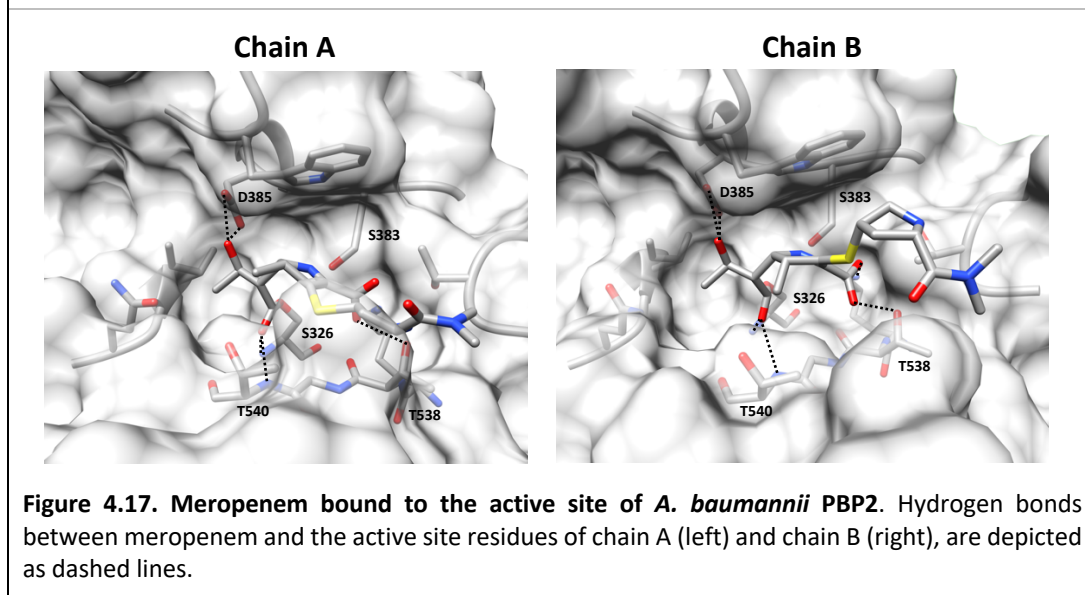
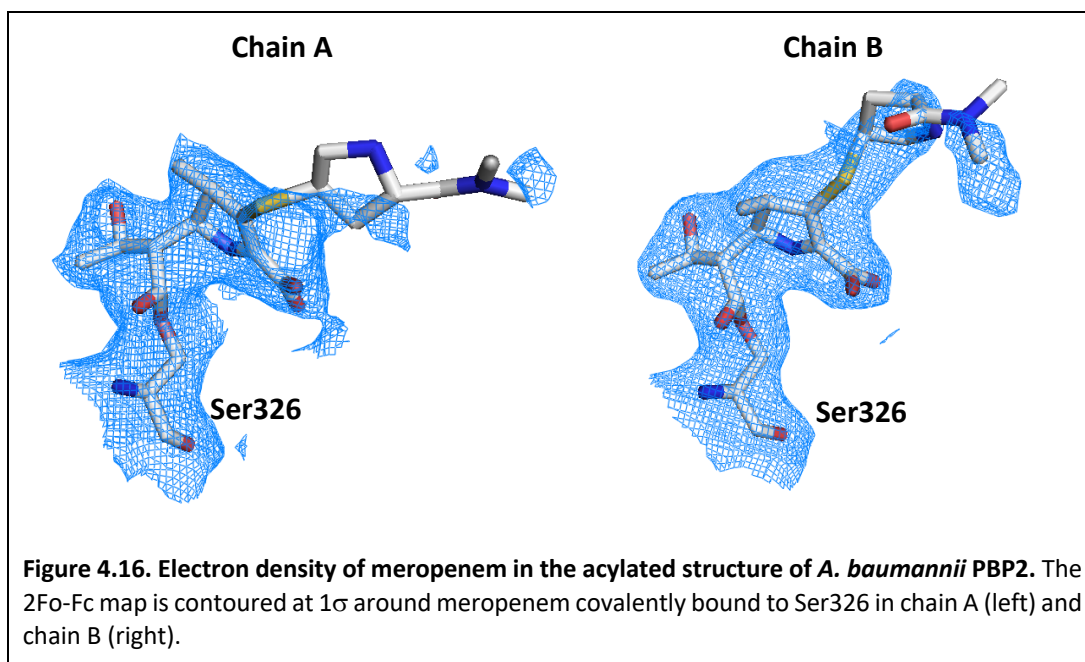
it is evident when comparing structures of PBPs, for instance *P. aeruginosa* PBP3 (3PBR.pdb), *E. coli* PBP5 (6NTZ.pdb) and *M. tuberculosis* DD-peptidase Rv3330 (4PPR.pdb), and β -lactamases, for instance BlaC (3DWZ.pdb), OXA-13 (1H8Y.pdb) and OXA-23 (4JF4.pdb), bound to meropenem (Han *et al.*, 2010, Caveney *et al.*, 2019, Prigozhin *et al.*, 2014, Hugonnet *et al.*, 2009, Pernot *et al.*, 2001, Smith *et al.*, 2013).

Interestingly, carbapenems can undergo pyrroline tautomerization from Δ^2 to Δ^1 following opening of the β -lactam ring, resulting in a double-bond shift from C2-C3 to C3-N4. As a consequence, C2 hybridisation changes from sp^2 (planar) to sp^3 (tetrahedral)(Jeon *et al.*, 2015). The PBP2: meropenem structure reveals that on acylation, the antibiotic maintains the Δ^2 tautomeric form in both polypeptides of the asu.

Chain A			Chain B		
Meropenem	PBP2	Distance (Å)	Meropenem	PBP2	Distance (Å)
O6	Ser326-N	2.8	O6	Ser326-N	2.7
	Thr540-N	3.1		Thr540-N	3.2
O8	Asp385-OD1	2.9	O8	Asp385-OD1	3.2
	Asp385-OD2	2.8		Asp385-OD2	2.8
N10	Ser383-OG	3.1	N10	Ser383-OG	2.9
O13	Thr538-OG1	2.7	O13	Thr538-OG1	2.9
				O12	Lys537-NZ

Table 4.10. List of polar interactions observed in the active site of *A. baumannii* PBP2 in complex with meropenem. Note the atom numbering refers to the meropenem molecule deposited in PDB with code MER.





Superimposition of the free- and meropenem bound structures of PBP2 reveals that, no major conformational rearrangements are associated with acylation by this antibiotic (figure 4.18). In chain A, the rmsd between the 533 C α atoms is 0.273 Å, whereas in chain B, the rmsd between the 524 C α atoms is 0.269 Å. Particularly, the rmsd of all atoms of residues surrounding the ligand (aa. 326, 329, 366, 383, 385, 449-451, 523-527, 537-540, 589, 590) is 0.698 Å in chain A and 0.800 Å in chain B.

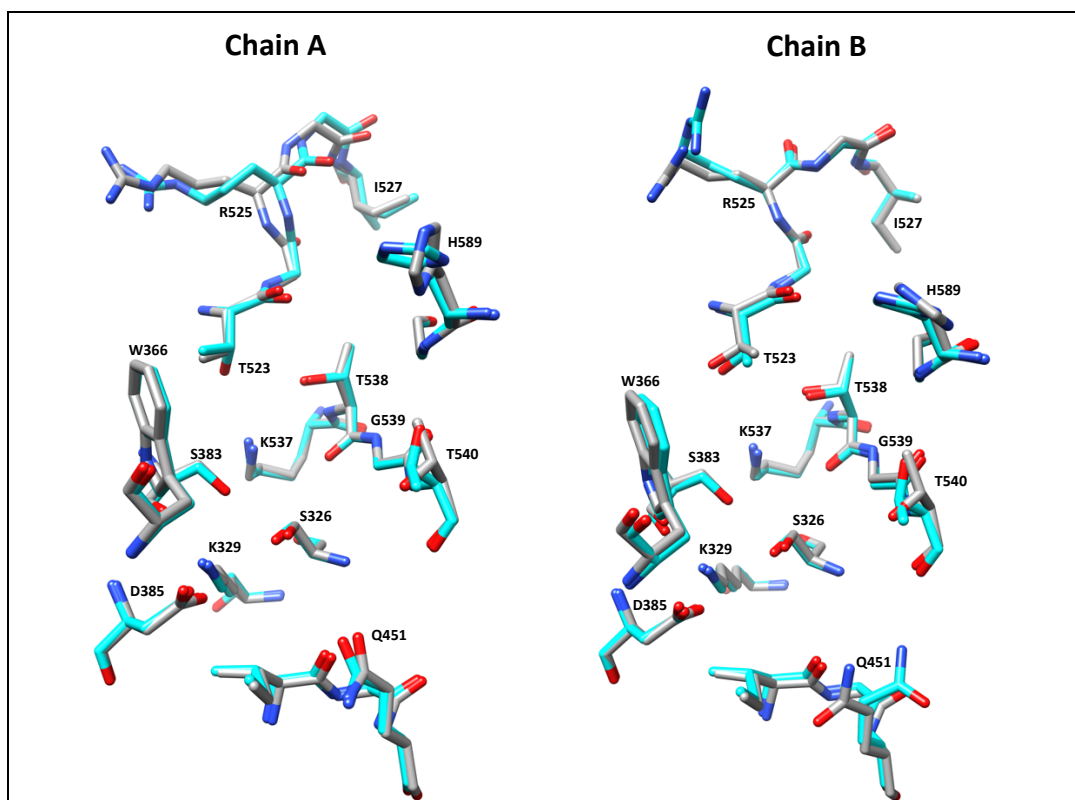


Figure 4.18. Active site of PBP2 unbound and in complex with meropenem. PBP2: meropenem structure (grey) superimposed to the PBP2 structure (cyan), in chain A (left) and chain B (right).

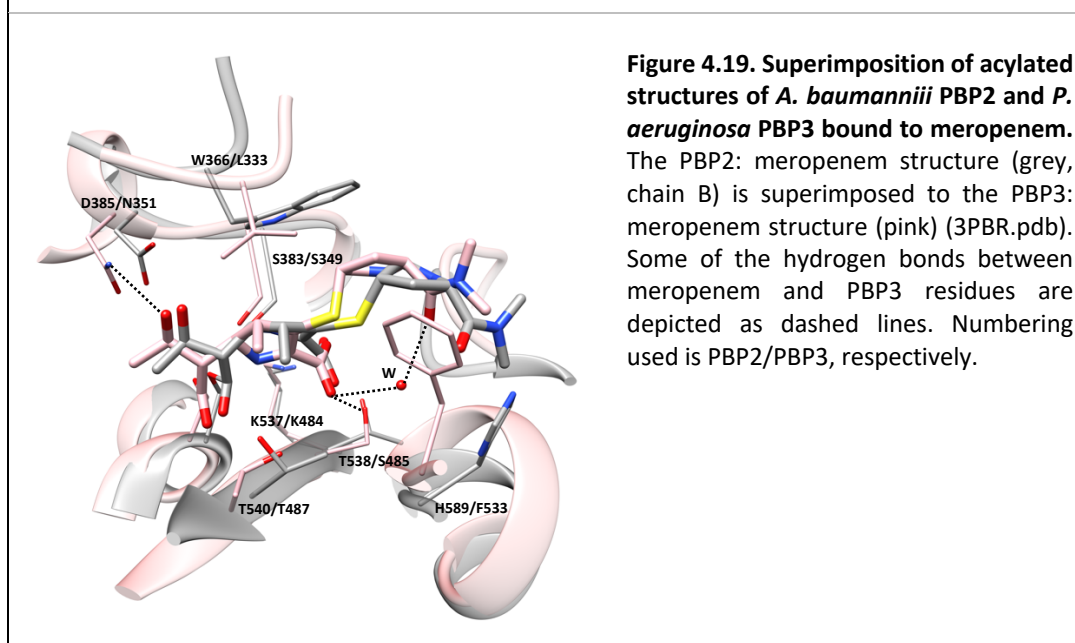


Figure 4.19. Superimposition of acylated structures of *A. baumannii* PBP2 and *P. aeruginosa* PBP3 bound to meropenem. The PBP2: meropenem structure (grey, chain B) is superimposed to the PBP3: meropenem structure (pink) (3PBR.pdb). Some of the hydrogen bonds between meropenem and PBP3 residues are depicted as dashed lines. Numbering used is PBP2/PBP3, respectively.

The binding mode of meropenem in complex with PBP2 (chain B) was compared to that of *P. aeruginosa* PBP3 (figure 4.19). Overall, the binding pose of meropenem in the two proteins is comparable, and the hydrogen bonds formed with the oxyanion hole main chain nitrogens and the K-T/S-G-T motif are conserved in PBP3. In contrast

to the PBP2: meropenem structure, in PBP3, meropenem hydrogen bonds to Asn351 (Asp385 in PBP2) and the R₁ chain is stabilised by indirect hydrogen bonds with the I347 and G535 backbone, involving bridging water molecules. Also, binding of meropenem to PBP3 is accompanied by significant conformational changes (Han 2010).

4.3 Interactions of *A. baumannii* PBP2 with DBOs

4.3.1 Interactions of *A. baumannii* PBP2 with avibactam

4.3.1.1 *In-vivo* and *in-vitro* activities of avibactam from the literature

Avibactam is the first non- β -lactam β -lactamase inhibitor of a new class of drugs containing a diazabicyclooctane scaffold (Bonney *et al.*, 2004; Ehmann *et al.*, 2012, Stachyra *et al.*, 2010) (figure 4.20). Research on DBOs as potential β -lactamase inhibitors began in the mid-1990s at Hoechst Marion Roussel, and was then pursued by pharma companies like Sanofi-Aventis and AstraZeneca, that resulted in the development of avibactam in the early 2000s (Coleman, 2011). Avibactam is a potent inhibitor of class A (e.g. TEM-1, CTX-M-15, SHV-1 and KPC-2) and class C (e.g. P99 and AmpC) serine β -lactamases, and moderately active toward class D OXA β -lactamases (OXA-10, -24 and -48) (Ehmann *et al.*, 2012; Lahiri *et al.*, 2014). However, avibactam does not inactivate class B metallo β -lactamases. Avibactam inactivates serine β -lactamases through acylation of the nucleophilic serine and formation of a stable carbamoyl-enzyme complex. Distinct from β -lactam-based β -lactamase inhibitors (i.e., clavulanic acid, tazobactam and sulbactam), deacylation does not involve hydrolysis, but proceeds through reversible recyclization of the DBO ring and consequent release of intact avibactam.

Avibactam has been approved in the USA and EU for clinical use, in combination with the third-generation cephalosporin ceftazidime, for the treatment of complicated urinary tract infections (cUTIs), including pyelonephritis; complicated intra-abdominal infections; hospital-acquired (HAP) and ventilator associated pneumonia (VAP), in patients with limited therapeutic options (Zhanel *et al.*, 2013; Shirley, 2018, EMA, 2018; Papp-Wallace and Bonomo, 2016). Additional combinations of

avibactam with ceftaroline and aztreonam are in clinical development (Castanheira *et al.*, 2012; Wang *et al.*, 2014).

Avibactam exhibits limited intrinsic antimicrobial activity (table 4.11), due to poor binding of PBPs. However, avibactam can acylate PBP2 to some extent in Gram-negative bacteria (table 4.12, figure 4.21) (Asli *et al.*, 2016; Bulitta *et al.*, 2018; Sutaria *et al.*, 2018), causing formation of spheroplasts (King *et al.*, 2016).

At the time this work was started, structural information on the binding of diazabicyclooctane scaffold containing molecules to PBP2 was not available. The DBO scaffold seems a promising alternative to the β -lactam ring in the generation of new PBP inhibitors, hence structural studies of *A. baumannii* PBP2 and avibactam were undertaken to elucidate the binding mode of this new chemotype.

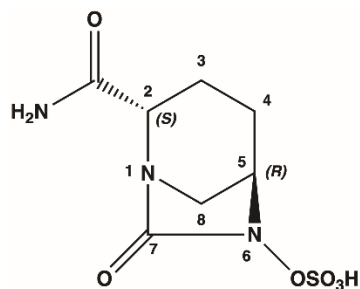


Figure 4.20. Chemical structure of avibactam.

Organism	MIC ($\mu\text{g/mL}$)
Gram-positive bacteria	
<i>S. pneumoniae</i> R6	256
<i>S. aureus</i> ATCC 29213	256
Gram-negative bacteria	
<i>E. coli</i> K-12	8
<i>P. aeruginosa</i> 1771	>128
<i>H. influenzae</i> Rd	64
<i>K. pneumoniae</i> ATCC 43816	16

Table 4.11. Antimicrobial activity of avibactam. MIC of avibactam against a panel of Gram-positive and Gram-negative bacteria, from the literature (Asli *et al.*, 2016; Sutaria *et al.*, 2018).

- avibactam



+ avibactam



Figure 4.21. Effect of avibactam *in-vivo*. Brightfield microscopy of *E. coli* untreated (left) and treated (right) with avibactam. Images from King *et al.* (2016).

PBP	IC ₅₀ ($\mu\text{g/mL}$)				
	<i>E. coli</i> K-12	<i>P. aeruginosa</i> 1771	<i>H. influenzae</i> Rd	<i>K. pneumoniae</i> ATCC 43816	<i>A. baumannii</i> ATCC 19606
1a	>13	>13	>32	>256	>256
1b	>13	>13	>32	>256	>256
2	0.92	1.1	3	2	2
3	>13	1.8	>32	>256	>256

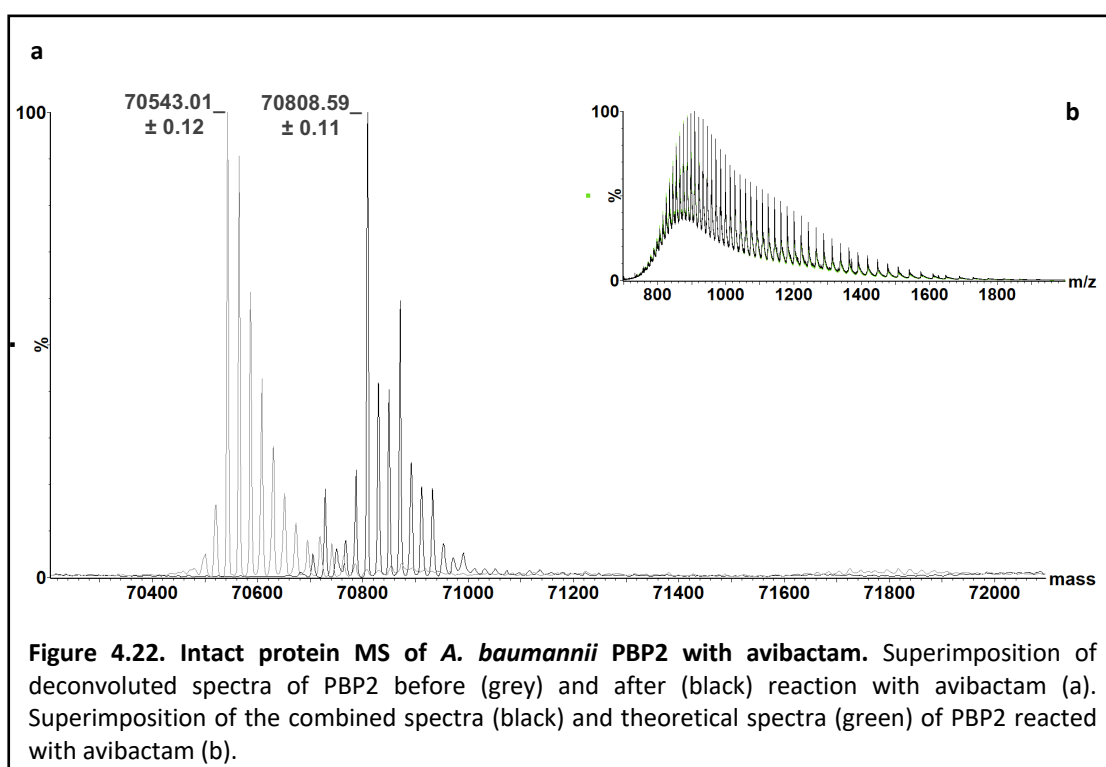
Table 4.12. PBP sensitivity to avibactam acylation in various Gram-negative pathogens. IC₅₀ are from gel based bocillin-FL competition assays using bacterial cell membranes published by Asli *et al.* (2016), Bulitta *et al.* (2018) and Sutaria *et al.* (2018). IC₅₀ defines the concentration of compound that reduces by 50% the binding of bocillin-FL to individual PBPs.

4.3.1.2 Mass spectrometry of *A. baumannii* PBP2 with avibactam

The binding of avibactam (exact mass 265.04 Da) to *A. baumannii* PBP2 was confirmed by intact protein mass spectrometry (2.6.2). PBP2 was reacted with avibactam as in 4.2.1.2, spectra were acquired and deconvoluted in the mass range 60000-80000 Da.

Protein	Compound	Calculated mass (Da) (\pm error)	Δ mass (Da)
PBP2 _{WT}	none	70543.01 (\pm 0.12)	reference
PBP2 _{WT}	avibactam	70808.61 (\pm 0.10)	+ 265.60

Table 4.13. MS of PBP2_{WT} before and after reaction with 10-fold molar excess of avibactam. Δ mass is the difference between the observed mass of the protein unbound (reference) and acylated by avibactam.



Following the reaction of PBP2 with avibactam, a peak at higher mass appeared in the mass spectra, consistent with the formation of a covalent complex with the drug. The observed mass accounted for the entirety of the molecule bound to PBP2, thus pointing to an acylation mechanism analogous to that seen in serine β -lactamases (Ehmann *et al.*, 2012) (figure 4.25, table 4.14).

4.3.1.3 Structure of *A. baumannii* PBP2 bound to avibactam

4.3.1.3.1 Crystallisation, data collection and structure determination

Crystals of *A. baumannii* PBP2 were produced as in 4.2.1.3.1. Diffracting PBP2 crystals grew in 2 % (w/v) PEG1000, 0.1 M sodium phosphate dibasic/citric acid pH 4.2, 20 % (v/v) ethanol and 2 mM zinc chloride. Crystals were soaked for 18 min in cryoprotectant solution (mother liquor + 25 % v/v glycerol) supplemented with avibactam at 10 mM final concentration. Crystals were harvested and flash vitrified in liquid nitrogen (figure 4.23)

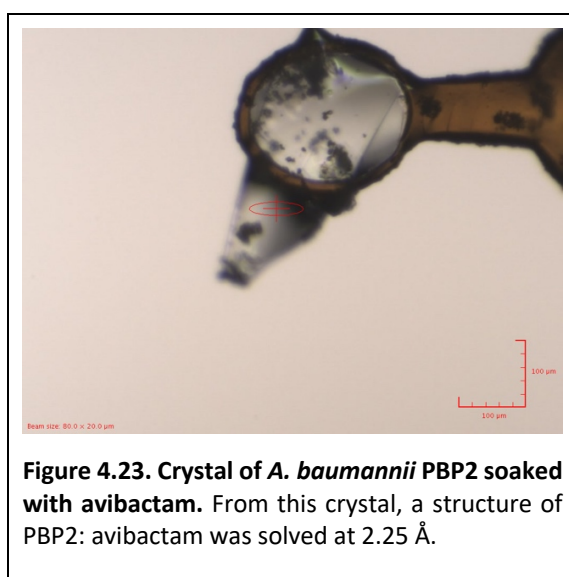
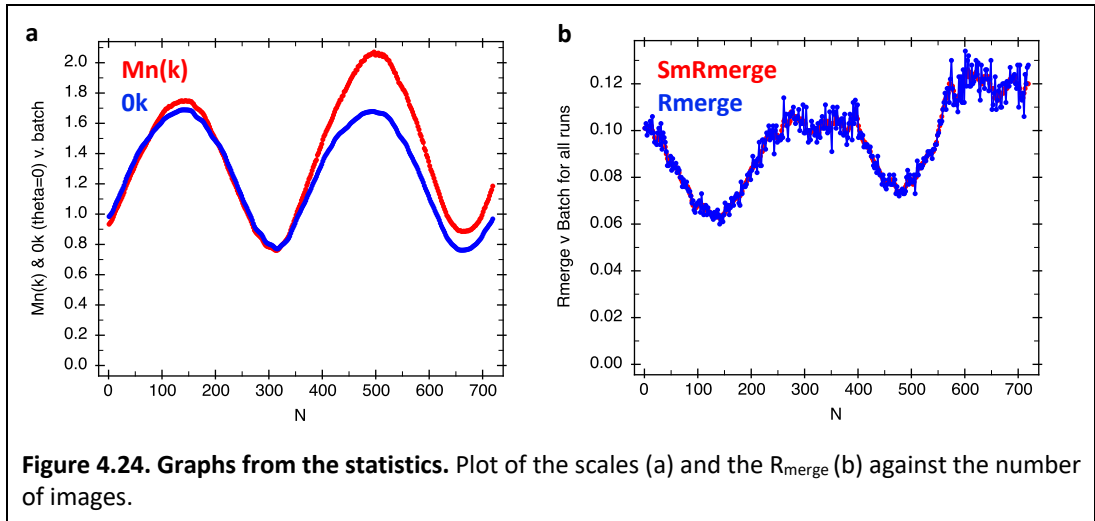


Figure 4.23. Crystal of *A. baumannii* PBP2 soaked with avibactam. From this crystal, a structure of PBP2: avibactam was solved at 2.25 Å.

Data collection was performed at the I03 beamline (DLS, Didcot, United Kingdom) in remote access, using a wavelength of 0.9762 Å and a Pilatus 6M-F detector. A complete dataset was obtained by collecting 720 images with an oscillation step of 0.5° and 0.075 s exposure time, at 2.5 Å resolution. Beam size was 80x20 µm and transmission was 50%.

The dataset was processed as in 4.2.1.3.1 (figure 4.24, table 4.14). There was clear electron density for avibactam in the difference density map, and for its covalent linkage to Ser326 in both molecules of the asu. Avibactam (entry NXL) was manually fitted into the electron density map, and the structure was refined with local NCS restraints (table 4.15). The co-structure has been refined with Refmac5 and is currently under a cyclic process of refinement and validation prior to deposition.



	Overall	Inner Shell	Outer Shell
Low resolution limit	41.74	41.74	2.30
High resolution limit	2.25	11.25	2.25
Rmerge (within I+/I-)	0.089	0.030	0.788
Rmerge (all I+ and I-)	0.093	0.032	0.835
Rmeas (within I+/I-)	0.097	0.033	0.892
Rmeas (all I+ & I-)	0.097	0.034	0.888
Rpim (within I+/I-)	0.039	0.013	0.408
Rpim (all I+ & I-)	0.028	0.010	0.293
Rmerge in top intensity bin	0.035	-	-
Total number of observations	896540	7778	38174
Total number unique	77350	689	4396
Mean($I/sd(I)$)	18.2	50.7	2.7
Mn(I) half-set correlation CC(1/2)	0.999	1.000	0.861
Completeness	99.8	98.3	96.7
Multiplicity	11.6	11.3	8.7
Mean (Chi^2)	1.00	0.71	0.96
Anomalous completeness	99.7	99.2	95.3
Anomalous multiplicity	5.9	6.6	4.4
DelAnom correlation between half-sets	-0.011	0.223	0.003
Mid-Slope of Anom Normal Probability	0.990	-	-

Table 4.14. Statistics of the PBP2: avibactam dataset. Output data from Aimless.

No. atoms		B-factors (Å ²)	
Protein	8356	Protein	58
Ligand	38	Ligand	77
Water	16	Water	51
R.m.s deviations		Ramachandran plot	
Bond lengths (Å)	0.0086	Favoured (%)	95.6
Bond angles (°)	1.5390	Allowed (%)	4.0
		Outliers (%)	0.4

Table 4.15. Statistics of the PBP2: avibactam dataset. Data refinement with Refmac5 and validation with Procheck and Rampage.

4.3.1.3.2 Structure of the PBP2- avibactam complex

The structure of *A. baumannii* PBP2 bound to avibactam was determined at 2.25 Å resolution, in space group I 2 2 2 and unit cell parameters of a= 120.98 Å b= 151.84 Å c= 177.42 Å and $\alpha = \beta = \gamma = 90^\circ$, and refined to R_{work} 0.2140 and R_{free} 0.2468 (statistics provided in table 4.14- 4.15).

Electron density for avibactam is strong and well resolved (figure 4.26), and the overall binding conformation of this ligand is analogous to the carbamyl-avibactam structures of serine β -lactamases, for instance CTX-M-15 (pdb 4S2I) and OXA-48 (pdb 4S2K) (King *et al.*, 2015), and the recently published *E. coli* PBP2 (pdb 6G9F) (Levy *et al.*, 2019).

Avibactam is covalently bound to Ser326 and is stabilised by a number of polar interactions in the active site of PBP2 (figure 4.25, 4.27). The carbamate carbonyl of avibactam occupies the canonical oxyanion hole, forming hydrogen bonds with the main chain amides of the catalytic Ser326, and Thr540 from the K-T/S-G-T motif. The carboxamide group of avibactam points away from the catalytic core and is directed towards the entrance of the binding cleft, where it makes an indirect hydrogen bond with the Asp385 side chain via the water molecule W1 (figure 4.27). The piperidine ring adopts a chair conformation and makes van der Waals interactions mainly with the Trp366 indole ring, that leans from the β -hairpin region and sits atop the catalytic core. The sulfamate moiety of avibactam substitutes the carboxylate group in penicillins and makes hydrogen bonds with the side chains of residues from the S-X-N/D and K-T/S-G-T motifs, and water molecules (table 4.16). Interestingly, the

sulfamate group adopts two different orientations in chain A and chain B, which affects the network of interactions with nearby residues (figure 4.27). Such flexibility has been already reported in various structures of avibactam: β -lactamase complexes.

Chain A			Chain B		
Avibactam	PBP2	Distance (Å)	Avibactam	PBP2	Distance (Å)
OAC	Ser326-N	2.9	OAC	Ser326-N	2.7
	Thr540-N	3.1		Thr540-N	3.2
	Wat2	3.3	NAA	Wat1	3
NAA	Wat2	3.1	OAD	Wat2	3.1
NAA	Wat1	2.8		Thr538-OG1	3.1
OAE	Wat3	2.3		Gly539-N	3.3
OAD	Thr538-OG1	2	OAE	Ser383-OG	3
OAG	Gly539-N	3.3		Lys537-NZ	3

Table 4.16. List of polar interactions observed in the binding site of *A. baumannii* PBP2 in complex with avibactam. Note the atom numbering refers to the avibactam molecule deposited in PDB with code NXL.

Comparison with the native PBP2 structure indicates that, the binding of avibactam does not cause major rearrangements in the TP site as well as the pedestal domain of the protein. In fact, PBP2 and PBP2: avibactam structures have a rmsd between their C α atoms of 0.362 Å in chain A and 0.272 Å in chain B. The rmsd between all the atoms of the catalytic site residues (537-542, 521-527, 324-330, 446-452, 379-388, 364-372 and 587-592) is 0.578 Å in chain A and 0.701 Å in chain B.

The most prominent movement observed in both chains is the shift of the peptide backbone of the K-T/S-G-T motif by approximately 0.5 Å, towards the N-terminal of the β 17-strand (figure 4.28). This backbone rearrangement is presumably required for the optimal interaction with the drug and to avoid steric hindrance with its sulfamate group. Accommodation of the sulfamate moiety in the binding pocket additionally causes retraction of Thr523 by approximately 0.2 Å in chain A and 0.5 Å in chain B, possibly to prevent steric clash. Additional movements include the rotation of the Ser326-O γ towards the C7 of avibactam following ester bond formation, and rotation of the Lys537 amine group towards the sulfamate oxygen to establish an interaction.

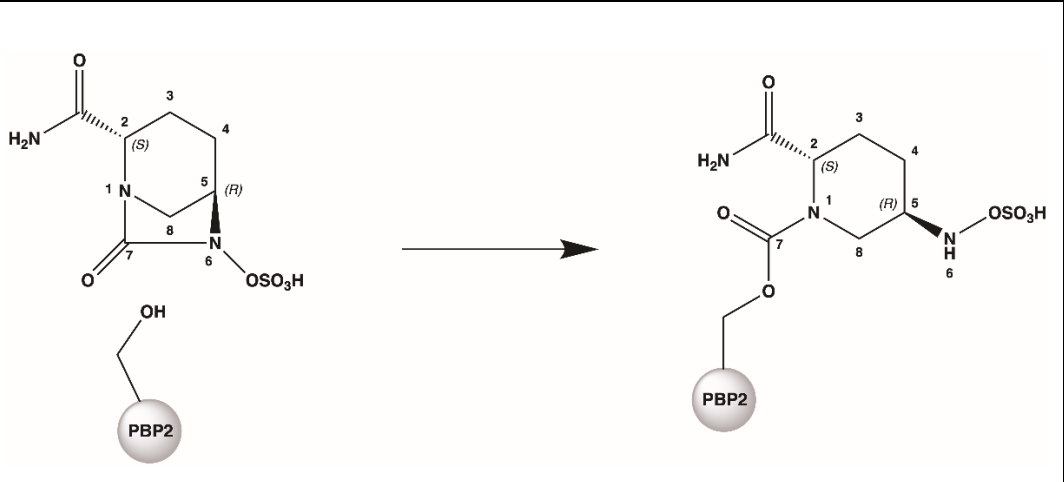


Figure 4.25. Schematic of the reaction of *A. baumannii* PBP2 with avibactam. Following acylation, Ser326 is linked to C7 via carbamoyl linkage.

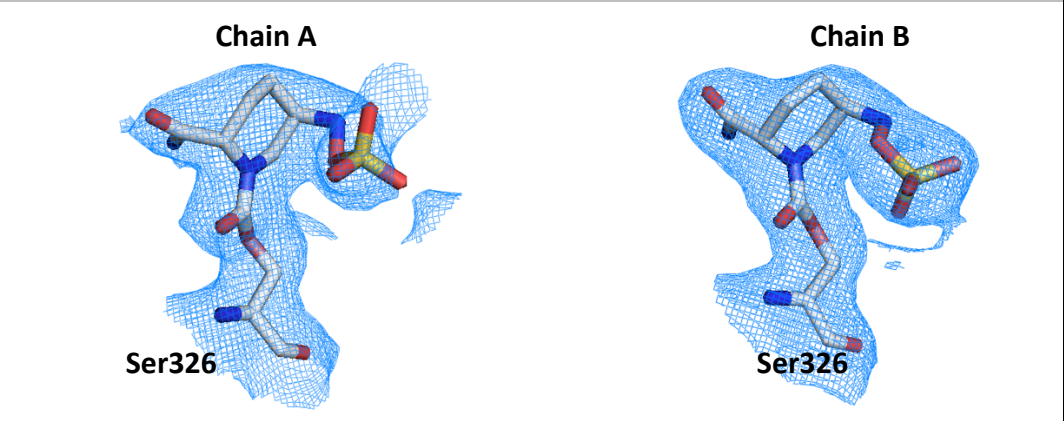


Figure 4.26. Electron density of avibactam in the acylated structure of *A. baumannii* PBP2. The 2Fo-Fc map is contoured at 1σ around avibactam, covalently bound to Ser326 in chain A (left) and chain B (right).

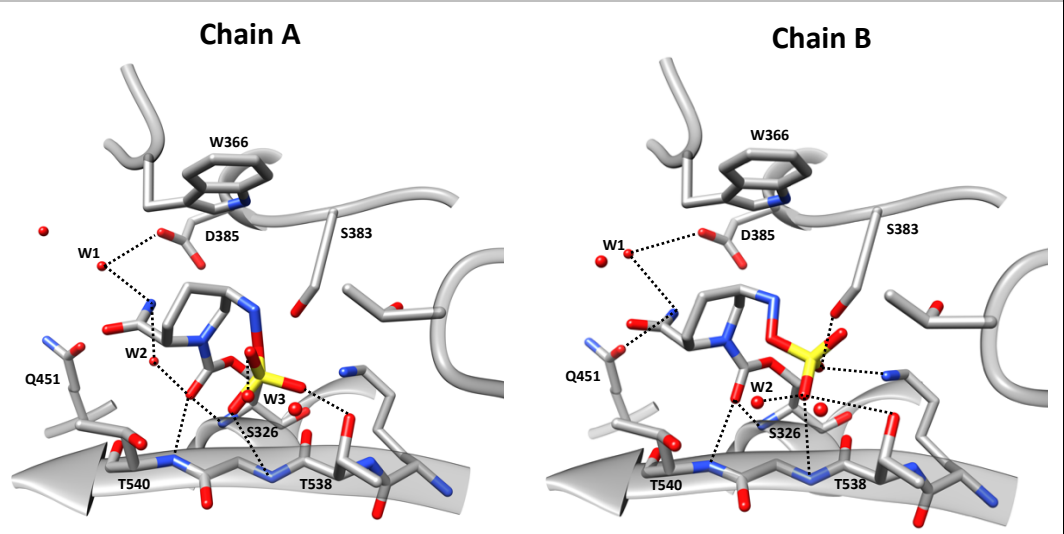


Figure 4.27. Avibactam bound to the active site of *A. baumannii* PBP2. Hydrogen bonds between avibactam and the active site residues of chain A (left) and chain B (right), are depicted as dashed lines.

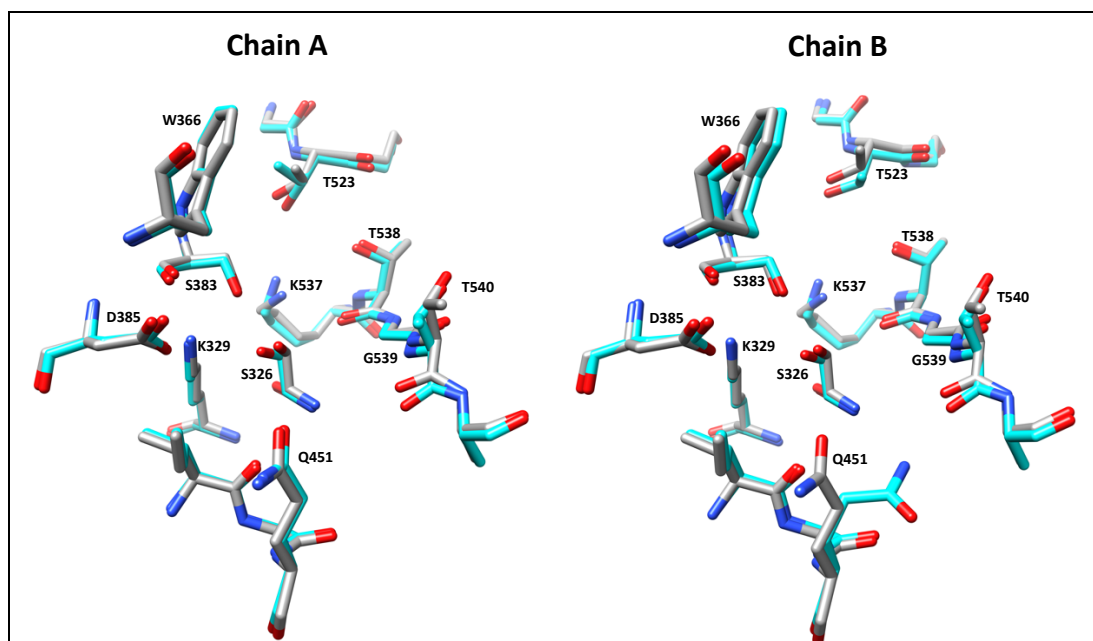


Figure 4.28. Comparison of avibactam bound-PBP2 with the native structure. Residues from the TP site of PBP2 and PBP2: avibactam structures are superimposed, and drawn in cyan and grey sticks, respectively, in chain A (left) and B (right). Avibactam is covalently attached to Ser326 in the liganded structure, and it has been omitted for clarity together with water molecules.

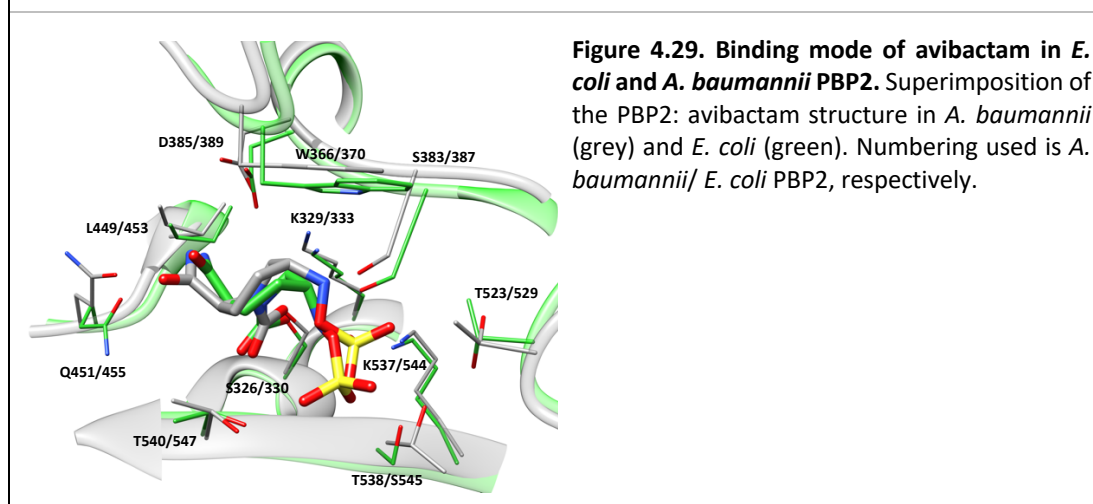


Figure 4.29. Binding mode of avibactam in *E. coli* and *A. baumannii* PBP2. Superimposition of the PBP2: avibactam structure in *A. baumannii* (grey) and *E. coli* (green). Numbering used is *A. baumannii*/*E. coli* PBP2, respectively.

In molecule B, the Gln451 side chain rotates in direction of the avibactam carboxamide moiety, though they are close but not within hydrogen bonding distance.

Overall, avibactam binds to *A. baumannii* PBP2 in a similar fashion to that when bound to *E. coli* PBP2 (Levy *et al.*, 2019)(figure 4.29). For structural comparison, only chain B of *A. baumannii* PBP2 is considered, due to the better electron density for the ligand. The carbonyl oxygen atom of avibactam is situated in the oxyanion hole

and interacts with equivalent residues in the two proteins. The 6-membered ring adopts a similar chair conformation and makes apolar contacts with a conserved Trp (Trp370- *E. coli* PBP2). The carboxamide group is oriented in a similar way, but in *E. coli* PBP2 is within hydrogen bonding distance to the conserved Asp (Asp389- *E. coli* PBP2). The sulfamate moiety is differently oriented in the two structures, and strongly hydrogen bonds to Thr547 and Ser545 (H-bond distance 2.2 Å) in *E. coli* PBP2.

4.3.2 Interactions of *A. baumannii* PBP2 with zidebactam

4.3.2.1 *In-vivo* and *in-vitro* activities of zidebactam from the literature

Zidebactam (also called WCK5107) is a compound from a new series of diazabicyclooctane derivatives, called bicyclo-acyl hydrazide (BCH), discovered at Wockhardt Research Centre (India)(Papp-Wallace *et al.*, 2018). Based on the observation that avibactam is a specific but weak PBP2 binder with no useful antibacterial activity (4.3.1.1 table 4.11), the generation of new DBO derivatives with improved PBP2 binding affinity, was pursued by Wockhardt. Extensive medicinal chemistry efforts have led to a new generation of potent PBP2 inhibitors, exhibiting comparable or even better PBP2 inhibition than mecillinam, and importantly, resistance to β -lactamase hydrolysis due to replacement of the β -lactam ring with a DBO scaffold (i.e. Zidebactam, WCK5153, WCK4234)(Papp-Wallace *et al.*, 2018). One such a molecule is zidebactam, a derivative of avibactam in which the carboxamide functionality at C2 has been linked to a side chain consisting in piperidine-3-carboxylic acid hydrazide (figure 4.30).

Zidebactam is a new type of antibacterial agent showing three modes of action. Firstly, zidebactam is an inhibitor of class A and C serine β -lactamases, exhibiting a reversible acylation mechanism like avibactam (Papp-Wallace *et al.*, 2018). Secondly, zidebactam is a specific and potent PBP2 inhibitor (table 4.17) in Enterobacteriaceae and nonfermenting Gram-negative bacilli (Papp-Wallace *et al.*, 2018, Moya *et al.*, 2017b), in actual fact working as a dual-action inhibitor of PBPs and β -lactamases (Moya *et al.*, 2017b, Moya *et al.*, 2017a, Moya *et al.*, 2019). Lastly, zidebactam is a β -lactam enhancer (Morinaka *et al.*, 2015). β -lactam enhancer activity refers to the

synergistic effect produced when, a PBP2-targeting agent like zidebactam is paired with a PBP3 targeting β -lactam antibiotic, thus effectively causing simultaneous inhibition of multiple PBPs. Enhanced bacterial killing induced by concurrent inactivation of PBP2 and PBP3 has also been described for dual β -lactam combinations, such as mecillinam and aztreonam in *E. coli* (Satta *et al.*, 1995). The advantage of such a DBO- β -lactam combination over the use of a dual- β -lactam combination or carbapenems targeting multiple PBPs (4.2.2.1), is the extra β -lactamase protection offered by the DBO partner. Although, zidebactam does not provide coverage against the class B and class D β -lactamases, the intrinsic stability of the drug to β -lactamase hydrolysis ensures PBP2 inhibition-mediated cell killing (Bhagwat *et al.*, 2019). It is for the same reason that the use of a DBO- β -lactam combination could be more beneficial compared to the recently approved ceftazidime-avibactam and meropenem-vaborbactam combinations, which do not offer therapeutic coverage for infections caused by metallo- β -lactamase and class-D β -lactamase producing clinical isolates.

WCK5222, a combination of zidebactam and cefepime, a PBP3-targeting cephalosporin, exhibits potent *in-vitro* activity against multidrug-resistant Gram-negative pathogens (i.e., *Enterobacteriales*, *P. aeruginosa* and *A. baumannii*)(Sader *et al.*, 2017, Papp-Wallace *et al.*, 2018, Thomson *et al.*, 2019), also *in-vivo* activity in neutropenic murine lung and thigh infection models (Bhagwat *et al.*, 2019), and is currently under clinical development (WHO, 2017). Zidebactam antibacterial activity is variable against Enterobacteriaceae, and low MIC values have been reported against *E. coli* and *Citrobacter* species (table 4.18). *A. baumannii* is relatively resistant to zidebactam alone (table 4.18), even though the compound causes PBP2 inhibition in living cells as suggested by spheroplast formation at sub-MIC concentrations (figure 4.31). This observation is consistent with the phenotype of the PBP2 deleted strain of *A. baumannii* ATCC 17978 reviewed in chapter 3 (3.6.2) (Geisinger *et al.*, 2018), that emphasises the non-essentiality of the PBP2 enzymatic activity for the viability of this pathogen.

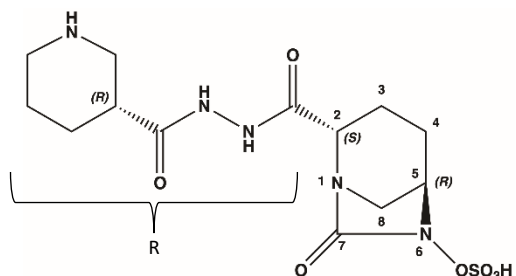


Figure 4.30. Chemical structure of zidebactam.

Organism (no. of isolates)	MIC ₅₀ /MIC ₉₀ (µg/mL)
<i>E. coli</i> (2,494)	0.12/ 0.12
<i>Klebsiella spp.</i> (1,517)	0.5/ >64
<i>P. mirabilis</i> (383)	>64/ >64
<i>Enterobacter spp.</i> (752)	0.12/ >64
<i>M. morgani</i> (117)	>64/ >64
<i>Citrobacter spp.</i> (259)	0.12/ 0.5
<i>S. marcescens</i> (282)	>64/ >64
<i>P. aeruginosa</i> (1,291)	4/ 8
<i>Acinetobacter spp.</i> (639)	>64/ >64
Organism	MIC (µg/mL)
<i>A. baumannii</i> ATCC 19606	≥ 1,024
<i>P. aeruginosa</i> PAO1	4
<i>K. pneumoniae</i> 4338 (VIM-1 producer)	> 256

Table 4.18. Antimicrobial activity of zidebactam. Susceptibility to zidebactam in Gram-negative bacteria, from the literature (Moya *et al.* (2017a; 2017b; 2019); Sader *et al.*, 2017).

PBP	IC ₅₀ (µg/mL)		
	<i>P. aeruginosa</i> PAO1	<i>A. baumannii</i> ATCC 19606	<i>K. pneumoniae</i> 52145
1a	>4	>2	>2
1b	>4	>2	>2
2	0.26 ± 0.06	0.01 ± 0.003	0.08 ± 0.02
3	>4	>2	>2

Table 4.17. PBP sensitivity to zidebactam acylation in various Gram-negative pathogens. IC₅₀ are from gel based bocillin-FL competition assays using bacterial cell membranes, published by Moya *et al.* (2017a; 2017b; 2019). IC₅₀ defines the concentration of compound that reduces by 50% the binding of bocillin-FL to individual PBPs.

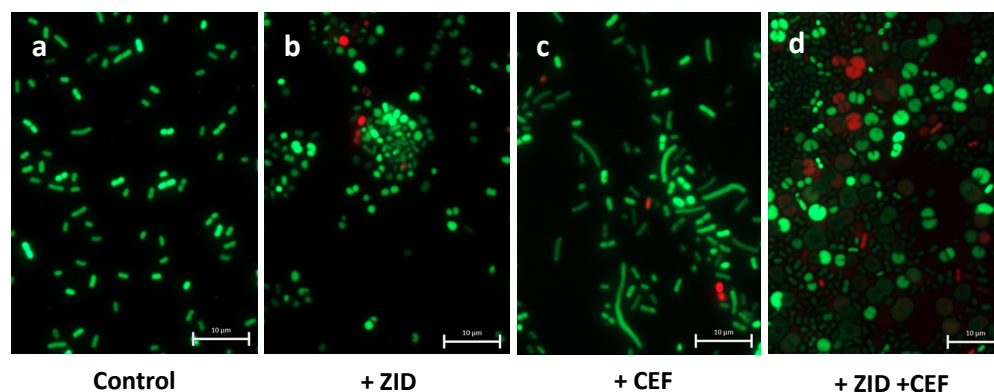


Figure 4.31. Microscopy-based live-dead staining of *A. baumannii* MDR ST2 expressing OXA-23. Bacteria were imaged before (a), and after 3 h exposure to 8 µg/mL zidebactam (b), 8 µg/mL cefepime (MIC= 64 µg/mL) (c), 8 µg/mL zidebactam plus 8 µg/mL cefepime (d). Live and dead cells are stained green and red, respectively. Images from Moya *et al.* (2017b).

On the other hand, when zidebactam is combined with cefepime, the two agents exhibit synergistic killing of MDR *A. baumannii* (OXA-23-producing ST2 international clone), and induce formation of enlarged spheroplasts, resulting from concurrent PBP2 and PBP3 inhibition (figure 4.31).

To help clarify the molecular basis of the excellent binding specificity of zidebactam towards PBP2, structural studies of *A. baumannii* PBP2 with this molecule have been performed, in this work.

4.3.2.2 Mass spectrometry of *A. baumannii* PBP2 with zidebactam

Zidebactam (exact mass 391.12 Da) covalently binds to *A. baumannii* PBP2 as confirmed by intact protein mass spectrometry (2.6.2).

Protein	Compound	Calculated mass (Da) (\pm error)	Δ mass (Da)
PBP2 _{WT}	none	70543.01 (\pm 0.12)	reference
PBP2 _{WT}	zidebactam	70934.63 (\pm 0.06)	+ 391.62

Table 4.19. MS of PBP2_{WT} before and after reaction with 10-fold molar excess of zidebactam. Δ mass is the difference in observed mass between the protein unbound (reference) and acylated by zidebactam.

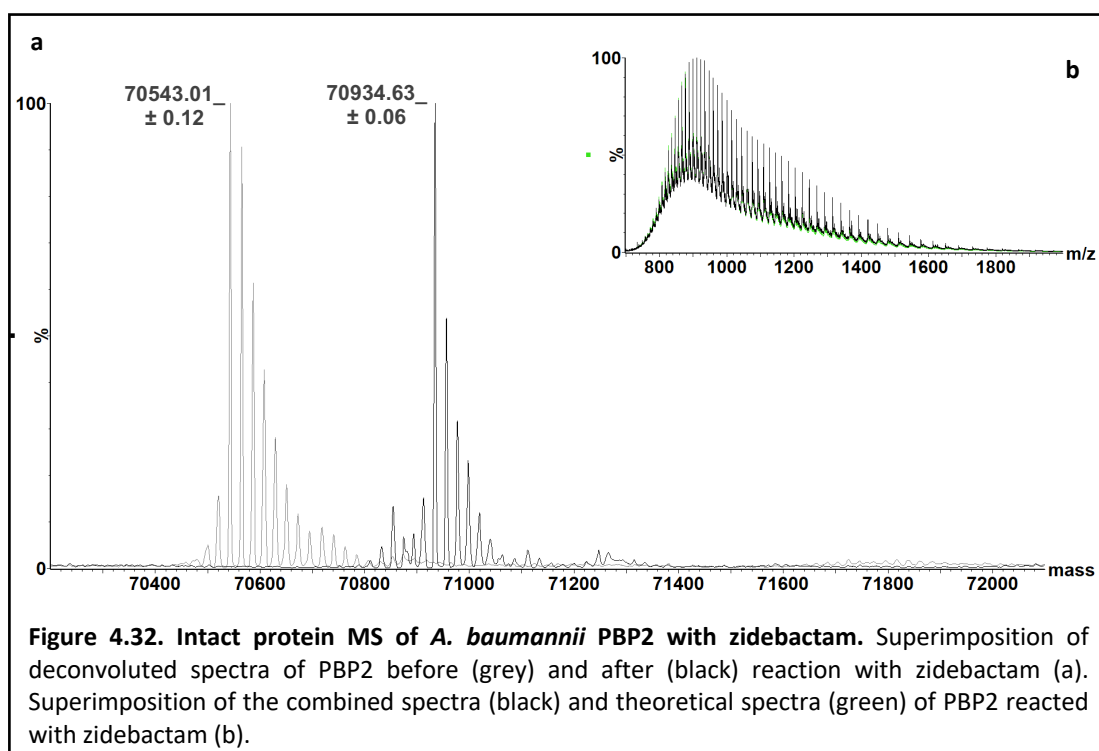


Figure 4.32. Intact protein MS of *A. baumannii* PBP2 with zidebactam. Superimposition of deconvoluted spectra of PBP2 before (grey) and after (black) reaction with zidebactam (a). Superimposition of the combined spectra (black) and theoretical spectra (green) of PBP2 reacted with zidebactam (b).

PBP2 was reacted with zidebactam as in 4.2.1.2, spectra were acquired and deconvoluted in the mass range 60000-80000 Da. The new peak at 70934.63 ± 0.05 Da accounts for the full molecule bound to PBP2, and similarly to avibactam, acylation occurs by the same mechanism.

4.3.2.3 Structure of *A. baumannii* PBP2 bound to zidebactam

4.3.2.3.1 Crystallisation, data collection and structure determination

Crystals of *A. baumannii* PBP2 were produced as in 4.2.1.3.1. Diffracting PBP2 crystals grew in 6 % (w/v) PEG1000, 100 mM sodium phosphate dibasic/citric acid pH 4.2, 20 % (v/v) ethanol and 2 mM zinc chloride. Crystals were soaked for 18 min in cryoprotectant solution (mother liquor + 25 % v/v glycerol) supplemented with zidebactam at 10 mM final concentration. Crystals were harvested and flash vitrified in liquid nitrogen (figure 4.33)

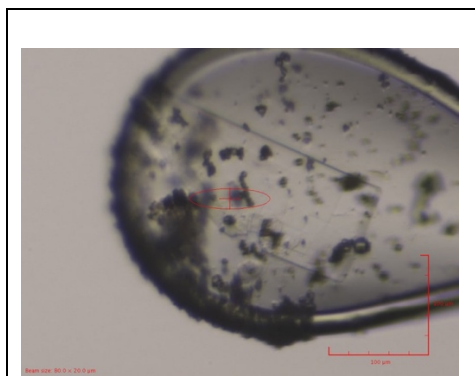


Figure 4.33. Crystal of *A. baumannii* PBP2 soaked with zidebactam. A structure of PBP2 in complex with zidebactam was solved at 2.3 Å.

Diffraction data were collected as in 4.3.1.3.1. The dataset was processed as in 4.2.1.3.1 (figure 4.34, table 4.20). The ligand was manually fitted into the electron density map in Coot and the structure refined (2.4.6.5) (table 4.21). The co-structure has been refined with Refmac5 and is currently under a cyclic process of refinement and validation prior to deposition.

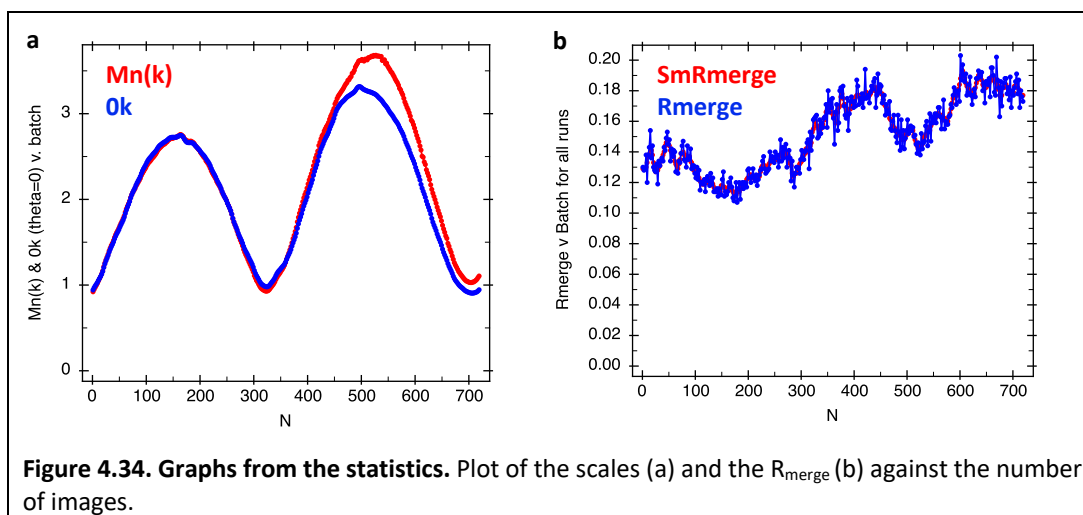


Figure 4.34. Graphs from the statistics. Plot of the scales (a) and the R_{merge} (b) against the number of images.

	Overall	Inner Shell	Outer Shell
Low resolution limit	46.63	46.63	2.35
High resolution limit	2.30	11.27	2.30
Rmerge (within I+/I-)	0.150	0.039	1.449
Rmerge (all I+ and I-)	0.156	0.040	1.523
Rmeas (within I+/I-)	0.164	0.042	1.603
Rmeas (all I+ & I-)	0.163	0.043	1.600
Rpim (within I+/I-)	0.065	0.017	0.679
Rpim (all I+ & I-)	0.047	0.013	0.485
Rmerge in top intensity bin	0.046	-	-
Total number of observations	883566	7782	48596
Total number unique	73740	698	4509
Mean($(I)/sd(I)$)	13.3	41.7	1.8
Mn(I) half-set correlation CC(1/2)	0.984	0.998	0.737
Completeness	100.0	98.6	100.0
Multiplicity	12.0	11.1	10.8
Mean (χ^2)	1.01	0.73	0.93
Anomalous completeness	100.0	99.4	100.0
Anomalous multiplicity	6.1	6.6	5.5
DelAnom correlation between half-sets	- 0.013	0.114	0.012
Mid-Slope of Anom Normal Probability	1.003	-	-

Table 4.20. Statistics of the PBP2: zidebactam dataset. Output data from Aimless.

No. atoms		B-factors (Å ²)	
Protein	8377	Protein	58
Ligand	54	Ligand	86
Water	9	Water	54
R.m.s deviations		Ramachandran plot	
Bond lengths (Å)	0.0080	Favoured (%)	95.2
Bond angles (°)	1.5243	Allowed (%)	4.5
		Outliers (%)	0.4

Table 4.21. Statistics of the PBP2: zidebactam dataset. Data refinement with Refmac5 and validation with Procheck and Rampage.

4.3.2.3.2 Structure of the PBP2- zidebactam complex

The structure of *A. baumannii* PBP2 in complex with zidebactam was solved at 2.3 Å resolution, in space group I 2 2 2 with unit cell parameters of a= 120.98 Å b= 151.84 Å c= 177.42 Å, $\alpha = \beta = \gamma = 90^\circ$ and refined to R_{work} 0.2178 and R_{free} 0.2597 (statistics provided in table 4.20- 4.21).

There is clear electron density corresponding to the ester-linkage between C7 and S326-O γ and for most of the ligand, with the exception of the piperidine ring partially visible (figure 4.35- 4.36). Zidebactam is present in both protomers of the asu, where it binds the catalytic site in a similar fashion. The carbonyl oxygen is located in the oxyanion hole formed by the backbone nitrogen of S326 and T540, the 6-membered ring adopts a chair conformation and the sulfamate moiety makes hydrogen bonds with residues of the K-T/S-G-T motif (table 4.22, figure 4.37). The R-chain projects away from the catalytic core towards the entrance of the binding site cleft, and it does not make direct contacts with the protein. Instead, a number of H-bonds mediated by water, are observed between the R-chain and the amino acid side chains of Q451, Q542 and the carbonyl backbone of T540 located at the base of the cleft (table 4.22, figure 4.37).

As observed with previously described liganded structures of *A. baumannii* PBP2, binding of zidebactam does not induce domain restructuring or important conformational changes in the TP active site of the protein (figure 4.38).

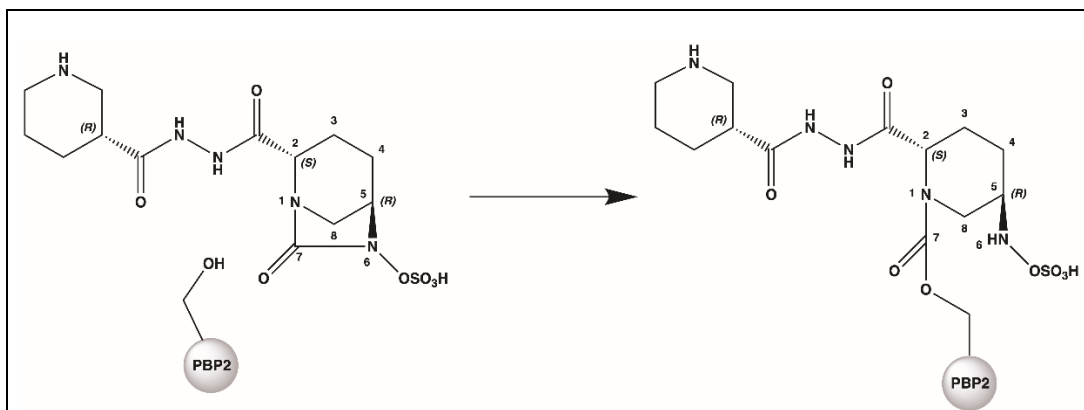


Figure 4.35. Schematic of the reaction of *A. baumannii* PBP2 with zidebactam. Following acylation, Ser326 is linked to C7 via an ester bond.

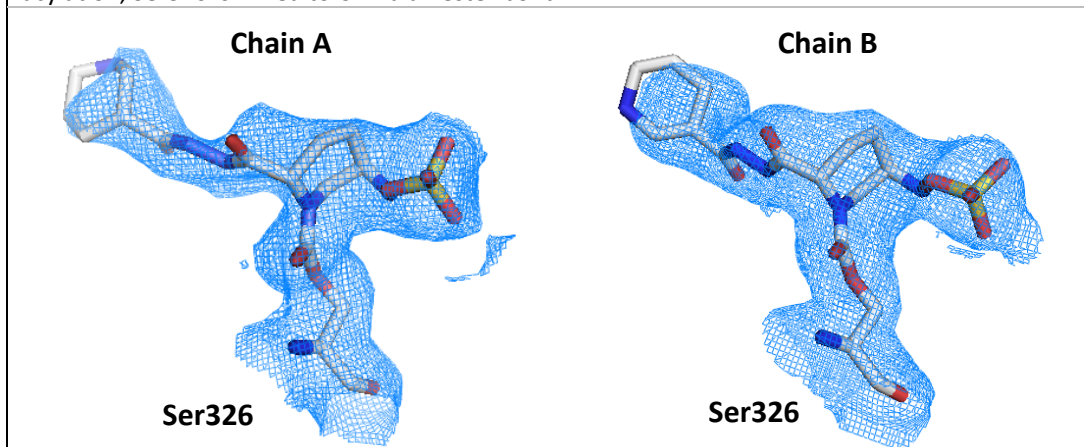


Figure 4.36. Electron density of zidebactam in the acylated structure of *A. baumannii* PBP2. The 2Fo-Fc map is contoured at 1σ around zidebactam covalently bound to Ser326 in chain A (left) and chain B (right).

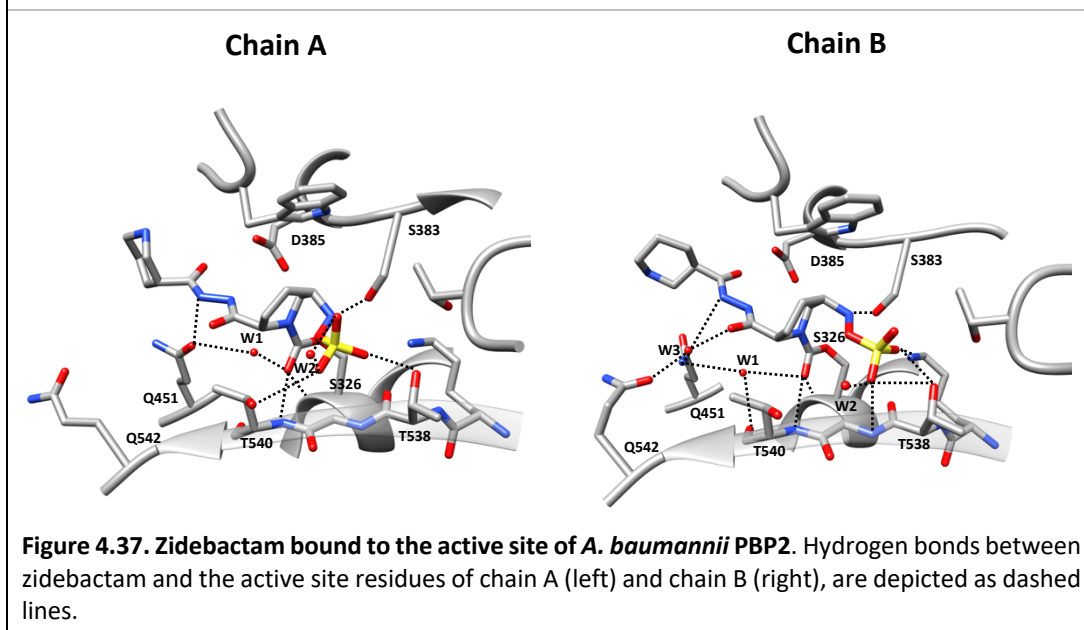


Figure 4.37. Zidebactam bound to the active site of *A. baumannii* PBP2. Hydrogen bonds between zidebactam and the active site residues of chain A (left) and chain B (right), are depicted as dashed lines.

Chain A			Chain B		
Zidebactam	PBP2	Distance (Å)	Zidebactam	PBP2	Distance (Å)
OAA	Ser326-N	2.9	OAA	Ser326-N	2.8
	Thr540-N	3.2		Thr540-N	3.3
	Wat1	3.0		Wat1	3.4
NAR	Ser383-OG	3.3	NAR	Ser383-OG	3.0
OAF	Wat2	3.1	OAE	Lys537-NZ	3.2
OAD	Wat2	2.5	OAE	Thr538-OG1	2.6
	Gly590-N	3.3	OAD	Thr538-OG1	3.1
	Thr540-OG1	3.4		Wat2	2.6
OAE	Thr538-OG1	2.5		Gly539-N	3.2
NAP	Gln451-OE1	3.2	O	Wat3	2.5
			NAP	Wat3	3.3

Table 4.22. List of polar interactions observed in the binding site of *A. baumannii* PBP2 in complex with zidebactam. Note the atom numbering refers to the zidebactam molecule deposited in PDB with code C8V.

The PBP2 and PBP2: zidebactam structures superimpose with a rmsd between C α atoms of 0.300 Å in chain A and 0.283 Å in chain B. The rmsd between all the atoms of the catalytic site residues of the liganded and unliganded structures (residues 537-542, 521-527, 324-330, 446-452, 379-388, 364-372 and 587-592) is 0.568 Å in chain A and 0.714 Å in chain B. The binding of zidebactam causes only minor conformational adjustments in the binding site cleft. Similarly to previously described *A. baumannii* PBP2 structures, these include a small movement of the β 17 peptide backbone for the stabilisation of the ligand carbonyl group in the oxyanion hole, rotamer change of K537 such that it can H-bond the sulfamate group of the drug, and rotation of Ser326-O γ towards the C7 of zidebactam following acylation. In chain B, Q451 and Q542 side chains change conformation, presumably to participate in the extensive water-mediated H-bond network formed with the R-chain of zidebactam (figure 4.37).

The structure of *A. baumannii* PBP2: avibactam allows direct comparison with the complex of the DBO derivative zidebactam bound to the same enzyme (figure 4.39). There is a striking resemblance in the binding pose of the DBO core in the two molecules, which results in the same type of interactions formed within the active site (figure 4.39). Zidebactam is ~300-fold more potent than avibactam in inhibiting PBP2 (IC₅₀ 0.025 and 7.546 μ M, respectively) (Bulitta *et al.*, 2018; Moya *et al.*, 2017a); since the two molecules differ only in the composition of the R-chain, this might play

an important role in the definition of the specificity and potency profile of zidebactam. The structural data would point to the additional H-bond interactions formed by the R-chain of zidebactam with the protein, as described earlier, as a possible explanation for the improved potency of the drug.

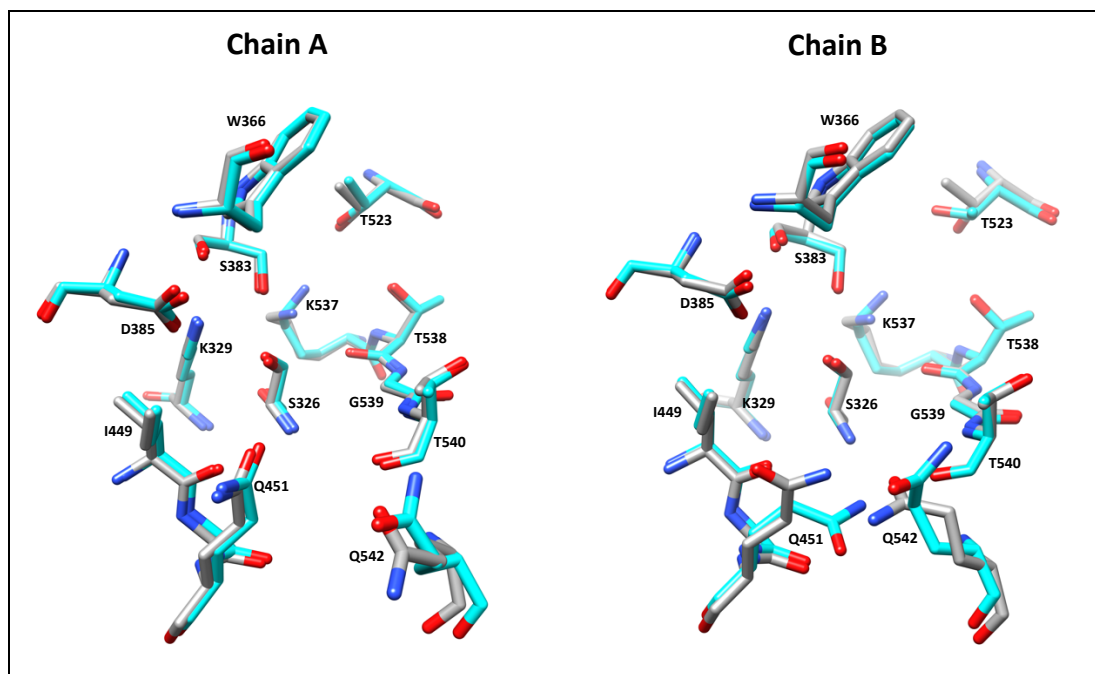


Figure 4.38. Comparison of zidebactam bound-PBP2 with the native structure. Residues from the TP site of PBP2 and PBP2: zidebactam are superimposed, and drawn in cyan and grey sticks, respectively, in chain A (left) and B (right). Zidebactam is covalently attached to Ser326 in the liganded structure, and it has been omitted for clarity together with water molecules.

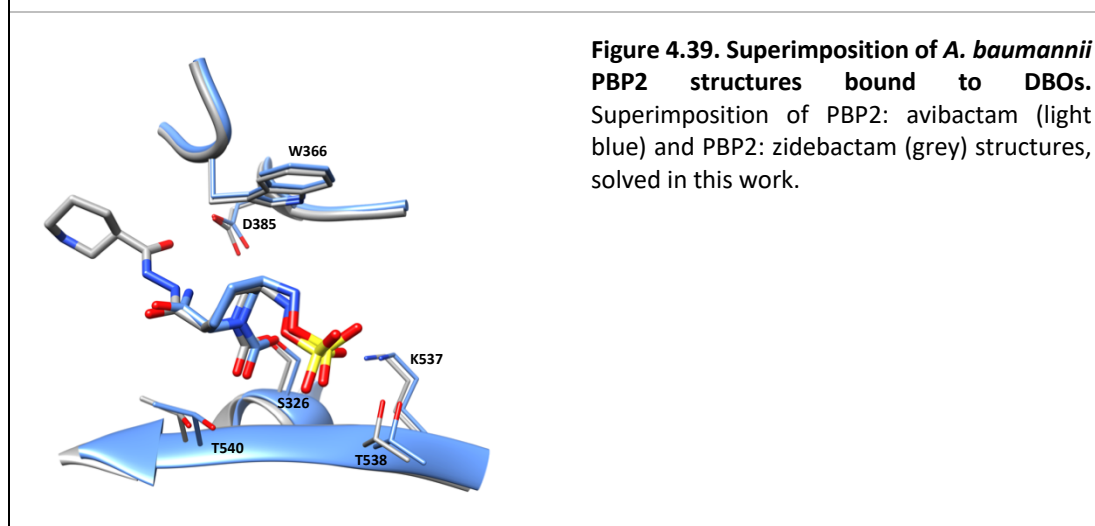
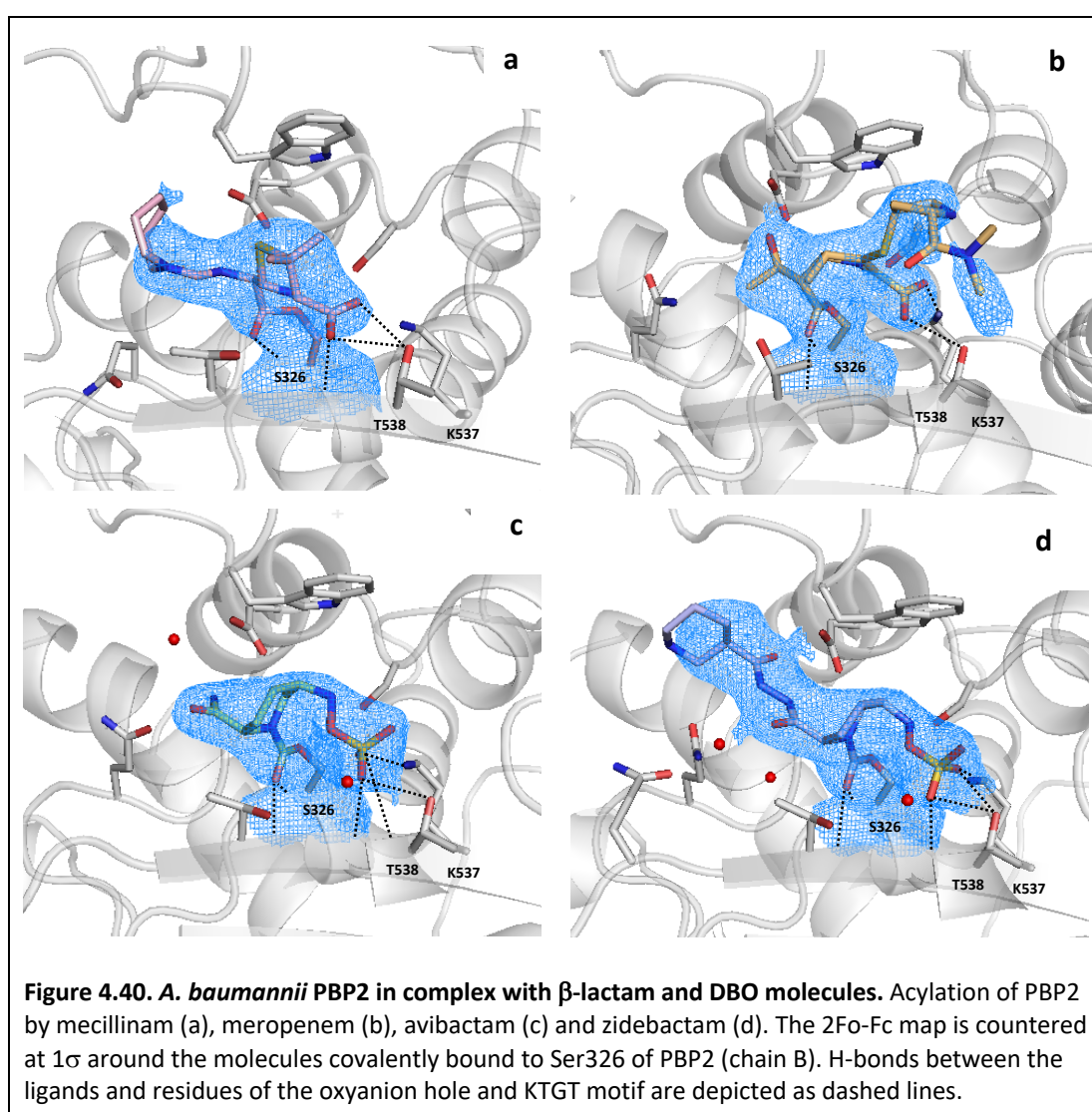


Figure 4.39. Superimposition of *A. baumannii* PBP2 structures bound to DBOs. Superimposition of PBP2: avibactam (light blue) and PBP2: zidebactam (grey) structures, solved in this work.

In this chapter, the binding mode of four clinically relevant molecules (i.e., mecillinam, meropenem, avibactam and zidebactam) was investigated, using crystallographic structures of *A. baumannii* PBP2 (figure 4.40). Despite the presence of distinct scaffolds (i.e., β -lactam and diazabicyclooctane), these molecules share a common mechanism of reaction with PBP2 that involves ring opening, and molecular rearrangement upon acylation of the catalytic serine (Ser326). It is noteworthy that when these two classes of molecules are covalently bound to the active site of PBP2, some conserved protein-ligand interactions can be observed, in spite of the different scaffolds used.



These include i) the H-bonding of the ligand carbonyl oxygen with the protein oxyanion hole, that play an important role in stabilising the transition state of the

reaction with PBPs (Hermann *et al.*, 2005); ii) the H-bonding of the carboxylate group in β -lactam antibiotics and sulfamate group of DBO molecules with the KTGT motif, that seems to be a key recognition element for binding to PBPs (Konaklieva, 2014), and a trigger for an acylation-competent state of the enzyme as reported in structures of *N. gonorrhoeae* PBP2 (Singh *et al.*, 2019)(figure 4.40).

4.4 Distinctive features in the active site of *A. baumannii* PBP2

4.4.1 Active site comparison with PBP1a and PBP3

The TP domain of PBPs, although sharing common motifs in the binding site that are important for the catalysis of transpeptidation or carboxypeptidation, display structural and physicochemical differences that could affect the dynamics of interaction with the PG substrate, and small ligands such as antibiotics. These differences may explain the different inhibitory potency shown by β -lactam and non β -lactam PBP targeting compounds. Therefore, critical evaluation of the binding site features would be important to rationalise protein-ligand interactions, and to guide the optimisation of existing molecules towards a better efficacy profile, against clinically relevant pathogens such as *A. baumannii*.

There are variations at the mouth of the binding site cleft, that result in differently shaped entrances to the active site (figure 4.41a-d). In *A. baumannii* PBP2, the entrance to the catalytic site is wide and shallow while in *A. baumannii* PBP1a it is narrow and deep (figure 4.41b-c). This is caused by the different length of the equivalent of the loop β 17- β 18 in PBP2, being shorter in PBP1a (aa 674-677) and much longer in PBP2 (aa 542-563) (figure 4.41a). Upon binding of β -lactams such as penicillin G (3UDI.pdb), PBP1a does not experience important rearrangements in this region, possibly due to the small size of the loop, which does not allow great conformational adjustments, thus resulting in access restriction. This loop is highly variable among PBPs, and it could be important for the binding of the PG substrate. Drug-resistant mutations mapping in this region would indicate that it does also play a role in the dynamics of antibiotic binding (Contreras-Martel *et al.*, 2009; Bellini *et al.*, 2019).

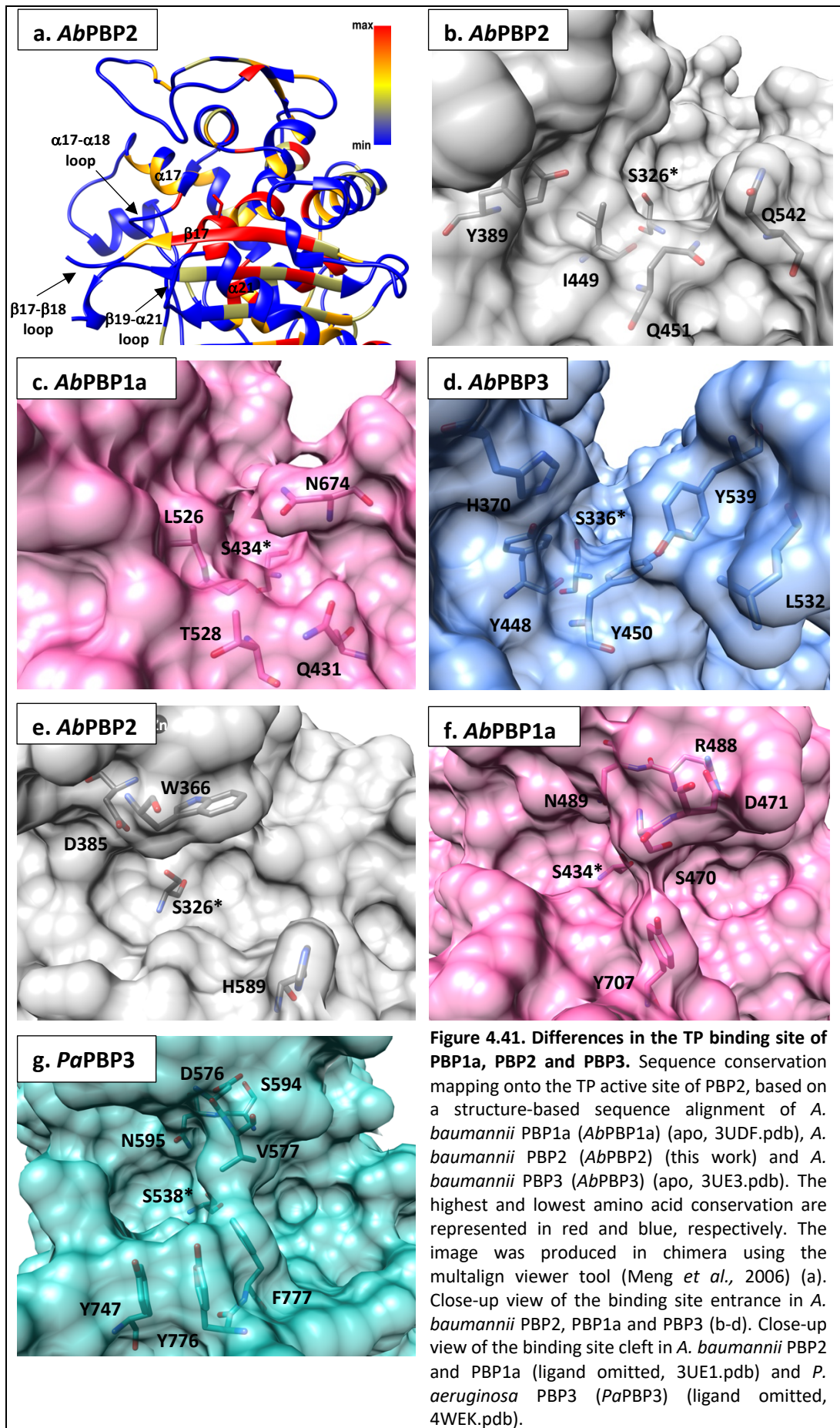
The different depth of the active site entrance is due to the different length of the equivalent of the loop $\alpha 17$ - $\alpha 18$ in PBP2, being two residues shorter in *A. baumannii* PBP1a (figure 4.41a). This results in the formation of a sub-pocket within which there is sufficient room to accommodate bulky side chains, for instance the aminothiazole-containing group of MC-1 and aztreonam (Han *et al.*, 2011). In the structure of *A. baumannii* PBP3, the equivalent of the loop $\beta 17$ - $\beta 18$ in PBP2 is modelled, and the active site entrance is restricted by the bulky side chains of Y448, Y450, Y539 and H370 (figure 4.41d). The three tyrosine residues and Leu532 definitely confer a hydrophobic character to the mouth of the active site of this PBP3. However, upon ligand binding to *A. baumannii* PBP3 a substantial reshaping of the region could occur, including the Tyr450 side chain flipping toward the solvent-exposed surface, as observed in liganded structures of *P. aeruginosa* PBP3 (Han *et al.*, 2010). The binding of molecules investigated in this chapter (i.e., mecillinam, meropenem, avibactam and zidebactam) to *A. baumannii* PBP2, occurs without significant rearrangement in this region. The $\beta 17$ - $\beta 18$ loop could not be modelled, regardless of the ligand bound, indicating that it does not form stabilising interactions neither with the ligand nor with the rest of the protein.

Striking differences exist between PBP1a, PBP2 and PBP3 around the catalytic serine of the TP domain, due to variation of the amino acids making the delimiting walls of the binding cleft, resulting in a different architecture of the active site. Some differences are located at the equivalent of the $\beta 19$ - $\alpha 21$ loop in PBP2 (figure 4.41a), where this loop is shorter in this protein (aa 585-589) compared to *A. baumannii* PBP1a (aa 696-707) and *A. baumannii* PBP3 (aa 567-574). Furthermore, this loop contains bulky residues in *A. baumannii* PBP1a (Y707) and *A. baumannii* PBP3 (Y573) which can be reoriented to protrude into the catalytic core and interact with residues from the opposite wall of the cleft, namely Ser470 and Thr375, respectively. This would result in the formation of a bridge that partially bury the catalytic Ser and the acylated molecule, thus conferring stability to the complex, as observed in structures of liganded *A. baumannii* PBP1a and *P. aeruginosa* PBP3 (figure 4.41f-g) (Han *et al.*, 2011; Han *et al.*, 2010).

Diversely, the β 19- α 21 loop is quite rigid upon ligand binding in *A. baumannii* PBP2, and none of the conformational rearrangements described above for Y707 and Y573 in *A. baumannii* PBP1a and PBP3, respectively, occur in PBP2 that displays a histidine (589) in place of tyrosine. Interestingly, even though the formation of a stabilising bridge across the binding cleft is not possible in PBP2, this protein possesses a tryptophan (366) in the same position as Ser470 (*A. baumannii* PBP1a) and Thr375 (*A. baumannii* PBP3), which could provide itself some stabilising effect on the formation of the acyl-complex (figure 4.41e). Trp366 may also provide further stabilisation by stacking interactions, to molecules bearing a ring attached to the active group, as observed in the structure of *E. coli* PBP2 bound to the DBO derivative CPD4 (Levy *et al.*, 2019)

Another remarkable difference in the active site of PBP1a/PBP2/PBP3 is represented by the conserved S-X-N/D motif, variable in the third position. Sequence alignments show that, the elongasome PBP2 distinctively carries Asp in third position (S-X-D) whereas, PBP1a/PBP1b/PBP3 display Asn (S-X-N) (figure S8). Aspartate and asparagine display different physicochemical properties, the Asp being an H-bond acceptor and negatively charged at physiological pH, the Asn being an H-bond donor and neutral at physiological pH. It is not hard to imagine that such amino acid substitution could impact the interaction of the protein with ligands. As a matter of fact, mecillinam bears a positively charged side chain group that interact with Asp385 in *A. baumannii* PBP2. Moreover, this molecule does not show activity against any other PBP other than PBP2, whereas, PBP2 is not generally well targeted by acyl-amino penicillins, such as penicillin G.

A. baumannii PBP2 remarkably shows a Zn-binding site sitting atop the catalytic core (3.5.3). This metal-coordination site is a distinctive attribute of PBP2 from the pathogen *A. baumannii* and is predicted to be present in other bacterial species as well (3.8). The binding of β -lactam and DBO compounds examined in this work, does not disturb either the coordination of the zinc atom nor the conformation of the loop containing the residues coordinating the metal (D350, D365 and H371), compared to the non-acylated structure of PBP2.



Notably, the Zn-binding site is replaced by a salt bridge (D471-R488) and a H-bond (D374-S391/D332-S350) in *A. baumannii* PBP1a and *A. baumannii* PBP3/*P. aeruginosa* PBP3, respectively. The binding of β -lactam antibiotics to these proteins does not disrupt the conserved interaction, although small shifts in the relative position of the loop are possible to accommodate different side chains.

The terminal side of the pocket, unlike the entrance and the core of the binding site cleft, does not undergo major conformational adjustments upon ligand binding in *A. baumannii* PBP1a and *P. aeruginosa* PBP3. This region is rich in Gly and other small size residues, and is contacted by the R₁ side chain of carbapenems, and the side chain of siderophore-conjugated monocarbams, although limited interactions are observed (Han *et al.*, 2011; Han *et al.*, 2010). Compared to the entrance of the binding site cleft, investigation of the cavity exit has been less successful in providing molecules with enhanced potency for specific PBPs, in SAR studies (Murphy-Benenato *et al.*, 2015).

4.4.2 Dissecting the role of Asp385

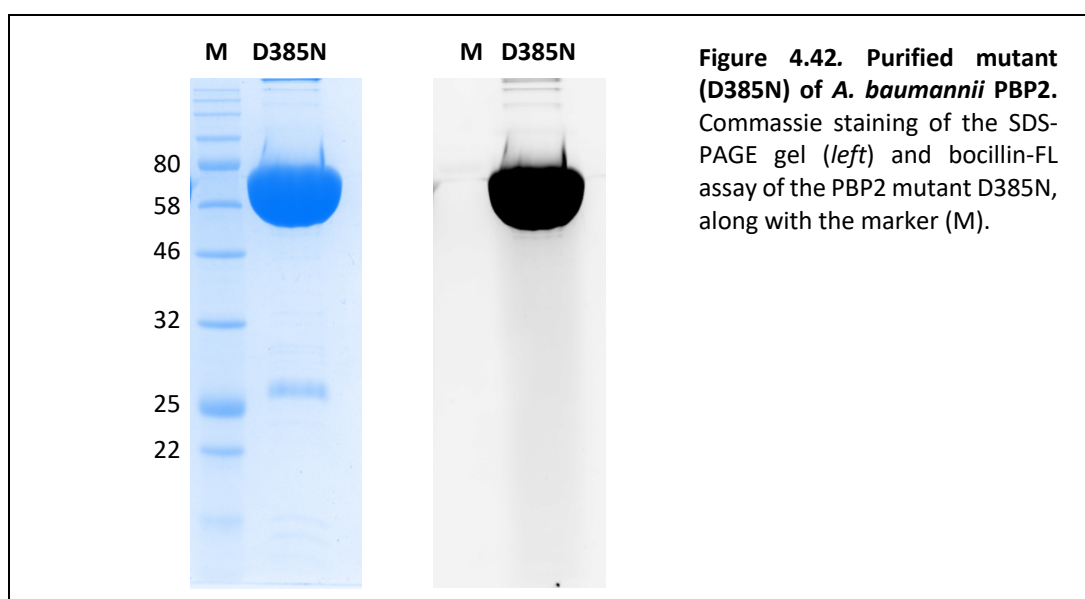
4.4.2.1 Generation of PBP2 D385N mutant

It is striking that PBP2 from all rod-shaped Gram-negative bacteria has an aspartate in place of asparagine in the conserved S-X-N/D motif. It is also remarkable that, a β -lactam such as mecillinam, bearing an amidino link in place of the classical acyl-amino link of penicillins, specifically targets PBP2 only. To shed light on this peculiar interaction, a structure of PBP2 bound to mecillinam was solved (4.2.1.3). The structure reveals typical interactions for the thiazolidine ring with the K-T/S-G-T motif, which are common to other HMW-PBPs bound to penicillins (Han *et al.*, 2011; Ren *et al.*, 2016; King *et al.*, 2017b). Thus, it is unlikely that the thiazolidine moiety of mecillinam confers preferential binding to PBP2. The hexamethyleneimine ring is disordered in the PBP2: mecillinam co-structure due to lack of interaction with protein residues, hence its sole presence might not be sufficient to explain the excellent PBP2 binding affinity of this drug, either. Conversely, the positively charged amidino group, unique to mecillinam, strongly interacts with the carboxylate of Asp385, and this interaction is more likely to explain the selective targeting.

There is corroborating evidence of the importance of this interaction for the binding of mecillinam, *in-vivo*. For instance, Thulin *et al.* (2015), isolated laboratory mutants of *E. coli* MG1655 resistant to mecillinam. Substitution of Asp389 to Gly in *E. coli* PBP2, equivalent to Asp385 in *A. baumannii* PBP2, caused more than 100-fold increase in the mecillinam MIC (= 16 $\mu\text{g}/\text{mL}$) when compared to the control (= 0.125 $\mu\text{g}/\text{mL}$). Notably, the mutation D389G did not cause an increase in MIC of non-selective PBP2 antibiotics like meropenem, cefotaxime and ampicillin, but for some of them, a slight improvement in MIC was even observed. Thus, a favourable interaction with the conserved aspartic acid in PBP2 would be critical for the antimicrobial activity exhibited by mecillinam. Another piece of evidence comes from Rosenkilde *et al.*, (2019), who showed how mutation of Asn135 to Asp (the third residue of the S-X-N/D motif) in the β -lactamase CTX-M-15, makes *E. coli* MG1655 resistant to mecillinam (50-fold increase in mecillinam MIC between CTX-M-15_{WT} and CTX-M-15_{N135D} expressing *E. coli* MG1655). In fact, mecillinam is

relatively stable to hydrolysis by the serine β -lactamase CTX-M-15_{WT}, and the mutation N135D is likely to introduce a favourable interaction with the drug, similarly to that observed in the complex of *A. baumannii* PBP2 (Asp385) with mecillinam. Hence, the increased affinity of mecillinam for CTX-M-15_{N135D}, would possibly cause an increased rate of hydrolysis, that would explain the increase in MIC. In essence, the Asn/Asp in the S-X-N/D motif, seems to affect the binding of mecillinam to PBPs and serine β -lactamases (at least in CTX-M-15), which account for the antimicrobial activity and antimicrobial resistance profile of mecillinam, respectively.

Replacement of the amidino group with an amide group likewise other penicillins, could help clarify the contribution of this moiety to the unusual PBP binding preference of mecillinam. Since such a molecule is not available yet, another way of trialling the importance of the interaction between the amidino group and the aspartate, is to mutate the aspartate of the S-X-N/D motif to asparagine, most frequently encountered in HMW- and LMW-PBPs, and serine β -lactamase. For this purpose, a mutant of *A. baumannii* PBP2 was generated where the Asp385 was substituted with asparagine.



The mutation was introduced by site-directed mutagenesis (2.2.8), using the plasmid pMIC10 as a template and resulting in pMIC11 (table S2). The mutation was confirmed by DNA sequencing. The mutant D385N was expressed and purified according to the protocol established for the wild-type PBP2 (figure 4.42) (3.2).

4.4.2.2 Mass spectrometry of D385N PBP2 with mecillinam

The mutant D385N of PBP2 was analysed by intact protein mass spectrometry (2.6) to both confirm the presence of the mutation and investigate whether the mutant retained its ability to bind mecillinam (exact mass: 325.15 Da). Protein was incubated with a 10-fold molar excess of mecillinam for 1 min, and reaction was stopped by the addition of 0.1 % (v/v) formic acid final concentration. Spectra were acquired and deconvoluted as in 4.2.1.2 (table 4.23, figure 4.43). PBP2 wild type was used as a control in this experiment (table 4.23, figure 4.44).

The calculated mass of D385N PBP2 is 1 Da lower compared to the mass of wild-type PBP2, as it would be expected from the substitution of Asp to Asn. Moreover, the mutation D385N does not prevent binding of mecillinam to PBP2, as suggested by the appearance of a peak consistent with the formation of such covalent adduct.

Protein	Compound	Calculated mass (Da) (\pm error)	Δ mass (Da)
PBP2 _{WT}	none	70542.71 (\pm 0.03)	reference
PBP2 _{WT}	mecillinam	70542.77 (\pm 0.05)	-
PBP2 _{WT}	mecillinam	70868.20 (\pm 0.13)	+ 325.49
PBP2 _{D385N}	none	70541.65 (\pm 0.07)	reference
PBP2 _{D385N}	mecillinam	70541.82 (\pm 0.08)	-
PBP2 _{D385N}	mecillinam	70867.13 (\pm 0.09)	+ 325.48

Table 4.23. MS of PBP2_{WT} before and after reaction with 10-fold molar excess of mecillinam. Δ mass is the difference in observed mass between the protein unbound (reference) and acylated by mecillinam.

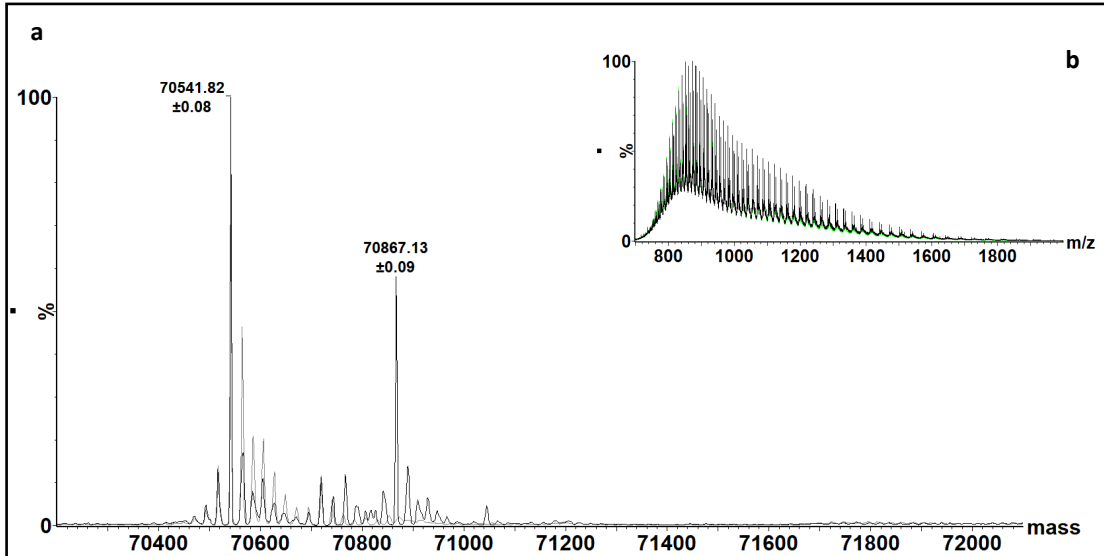


Figure 4.43. Intact protein MS of *A. baumannii* PBP2 D385N mutant with mecillinam. Superimposition of deconvoluted spectra of D385N PBP2 before (grey) and after (black) reaction with mecillinam (a). Superimposition of the combined spectra (black) and theoretical spectra (green) of D385N PBP2 reacted with mecillinam (b).

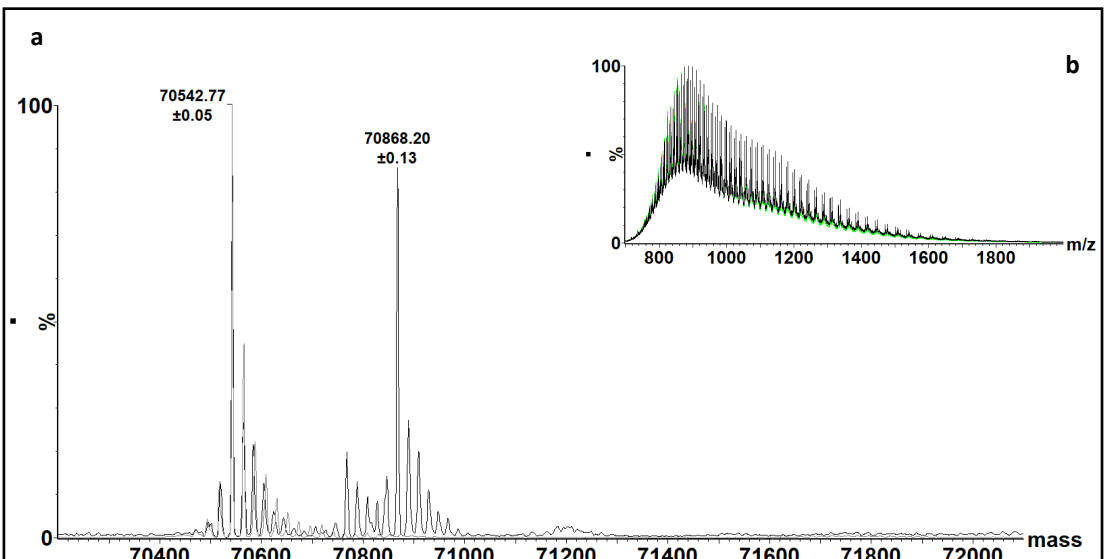


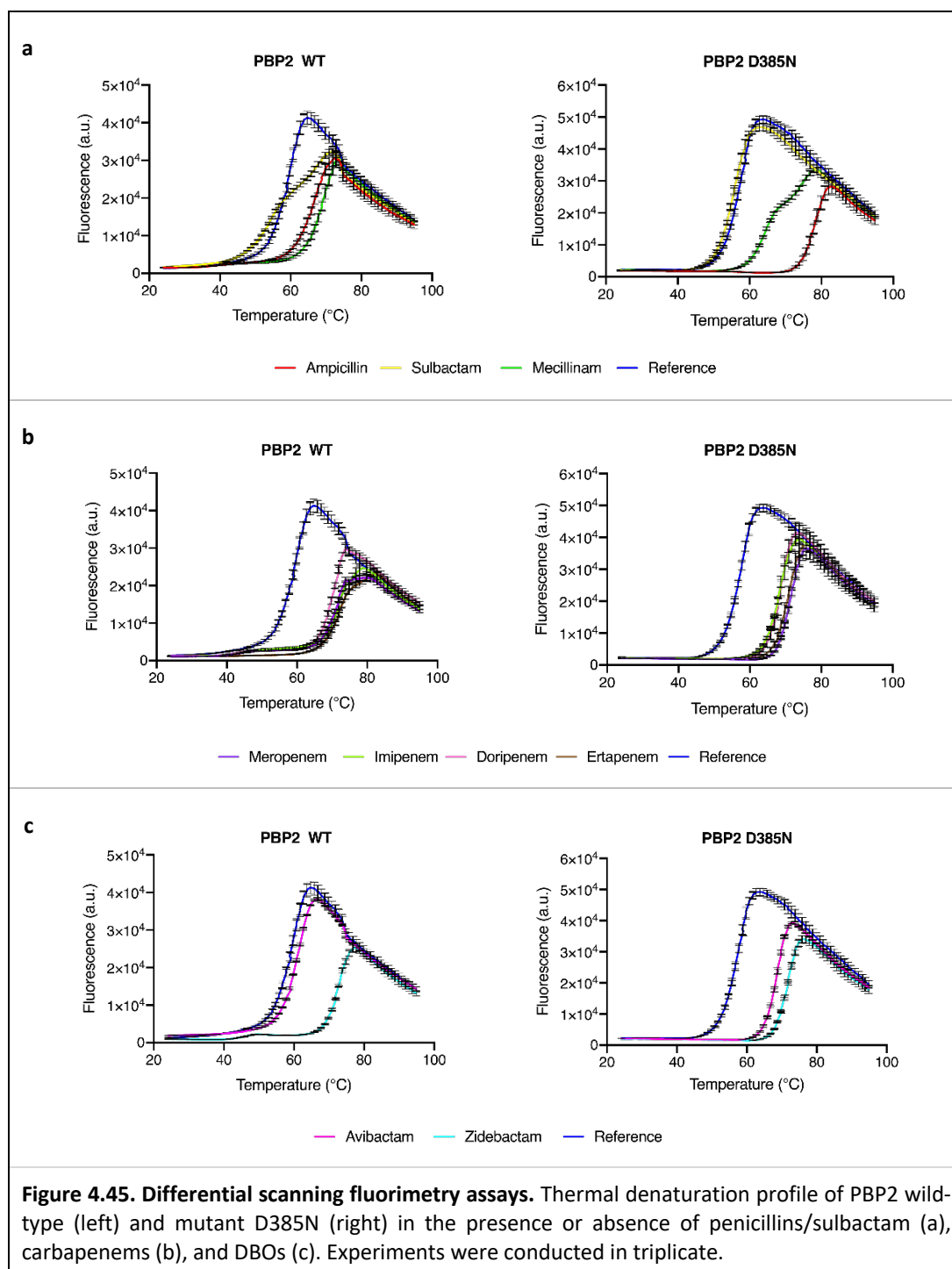
Figure 4.44. Intact protein MS of *A. baumannii* PBP2 wild-type with mecillinam. Superimposition of deconvoluted spectra of PBP2 WT before (grey) and after (black) reaction with mecillinam (a). Superimposition of the combined spectra (black) and theoretical spectra (green) of PBP2 WT reacted with mecillinam (b).

4.4.2.2 Differential scanning fluorimetry assays of PBP2 with β -lactams and DBOs

Differential scanning fluorimetry (DSF) was employed to investigate the impact on protein thermostability, of the interaction of a range of β -lactam and non β -lactam compounds with PBP2 (2.5.2). Both PBP2_{WT} and PBP2_{D385N} were analysed, to determine whether or not the substitution of Asp to Asn could have an effect on protein stability following molecule binding. DSF had been previously used to assess the interaction of various antibiotics with PBPs (Han *et al.*, 2011; Ren *et al.*, 2016; Filippova *et al.*, 2016) and L,D-transpeptidases (Libreros-Zúñiga *et al.*, 2018). The thermal shift assay was run as described in 2.5.2, and antibiotics were tested at 1 mM final concentration. The melting temperatures (T_m) of PBP2_{WT} and PBP2_{D385N} were measured and compared to the T_m of corresponding acyl-enzyme complexes (table 4.24, figure 4.45).

PBP2 _{WT}	ΔT_m (°C) \pm SD	PBP2 _{D385N}	ΔT_m (°C) \pm SD
+ Ampicillin	+ 7.03 \pm 0.11	+ Ampicillin	+ 21.10 \pm 0.18
+ Sulbactam	- 2.08 \pm 0.11	+ Sulbactam	- 1.56 \pm 0.18
+ Mecillinam	+ 10.09 \pm 0.13	+ Mecillinam	+ 9.57 \pm 0.19
+ Meropenem	+ 10.59 \pm 0.15	+ Meropenem	+ 14.34 \pm 0.17
+ Imipenem	+ 12.38 \pm 0.14	+ Imipenem	+ 11.10 \pm 0.13
+ Doripenem	+ 12.37 \pm 0.27	+ Doripenem	+ 11.52 \pm 0.25
+ Ertapenem	+ 12.11 \pm 0.13	+ Ertapenem	+ 13.64 \pm 0.37
+ Avibactam	+ 1.46 \pm 0.17	+ Avibactam	+ 11.48 \pm 0.17
+ Zidebactam	+ 12.83 \pm 0.12	+ Zidebactam	+ 14.54 \pm 0.13

Table 4.24. Differential scanning fluorimetry assays. Thermal shift caused by the interaction of β -lactam (ampicillin, sulbactam, mecillinam, meropenem, imipenem, doripenem and ertapenem) and non- β -lactam (avibactam and zidebactam) compounds with PBP2 wild-type and mutant D385N. ΔT_m is the difference between the T_m of the protein unreacted and the T_m of the protein reacted with antibiotics. Experiments were conducted in triplicate. Values are mean \pm standard deviation.



The DSF data show that both penicillins and DBOs shift the T_m of PBP2_{WT} and PBP2_{D385N} by more than 1°C in the positive direction. Particularly mecillinam, the carbapenems and zidebactam induce a significant positive T_m shift (> 9°C), indicating that binding of these compounds has a marked positive effect on protein stability. Conversely, sulbactam causes a negative T_m shift, indicating that this molecule induces unstable conformations of the protein. Interestingly, the DSF results are

consistent with the published inhibitory activities (IC_{50}) of the test molecules against *A. baumannii* PBP2_{WT}. In fact the nanomolar active molecules (for instance mecillinam, meropenem, imipenem, doripenem and zidebactam), tested in bocillin-FL competition assays, have all shown the greatest stabilising effect on PBP2, while the low micromolar inhibitors (for instance avibactam) have induced a moderate protein stabilisation (Bulitta *et al.*, 2018). Notably, sulbactam is not a PBP2 inhibitor (Moya *et al.*, 2017a; Penwell *et al.*, 2015) and causes the protein to be less stable.

The D385N substitution, surprisingly, has not resulted in any important change of the T_m shifts caused by the nanomolar inhibitors, including the PBP2-targeting molecules mecillinam and zidebactam, when compared to PBP2_{WT}. The binding of sulbactam has not been affected by this mutation, either. In contrast, the mutation has impacted the interaction of the protein with ampicillin and avibactam, showing a significantly increased stabilisation upon binding to these molecules ($\geq 10^\circ\text{C}$) compared to PBP2_{WT}. The increased protein stabilisation may arise from the formation of a new hydrogen bond between the side chain carbonyl group of ampicillin and avibactam, with the amide group of Asn385, similarly to the interaction of ampicillin with *E. coli* PBP1b (5HL9.pdb) and penicillin G with *A. baumannii* PBP1a (4.2.1.3.2), and avibactam with CTX-M-15 (4S2I.pdb) (King *et al.*, 2017b; Han *et al.*, 2011; King *et al.*, 2015).

Interestingly, the presence of Asp in position 385 only slightly increases the melting temperature of the protein itself (T_m of PBP2_{WT} is 59.6°C and PBP2_{D385N} is 56.9°C), implying that the absolute preference toward Asp rather than Asn may not be entirely explained by a particular thermostability requirement of the enzyme.

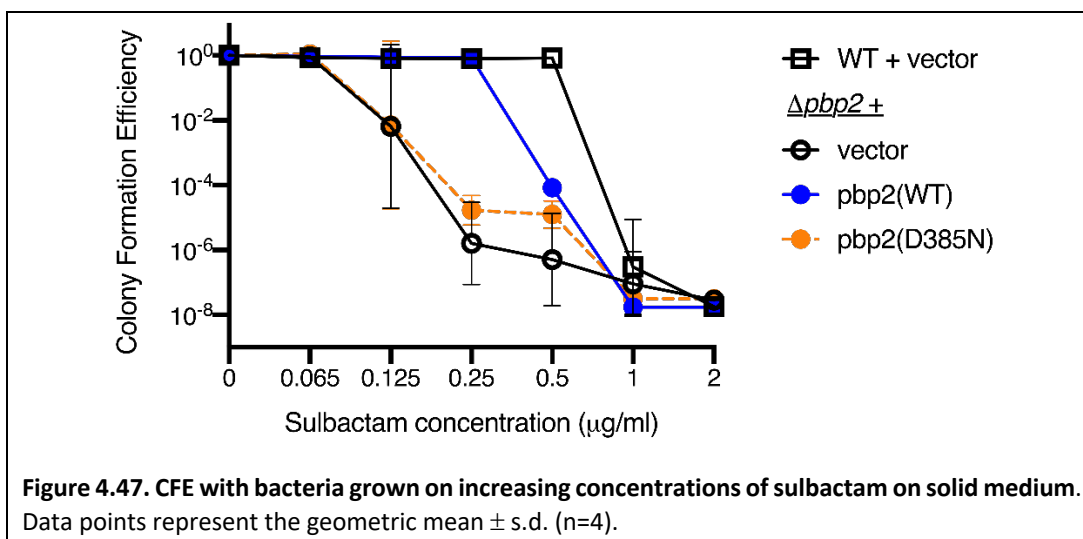
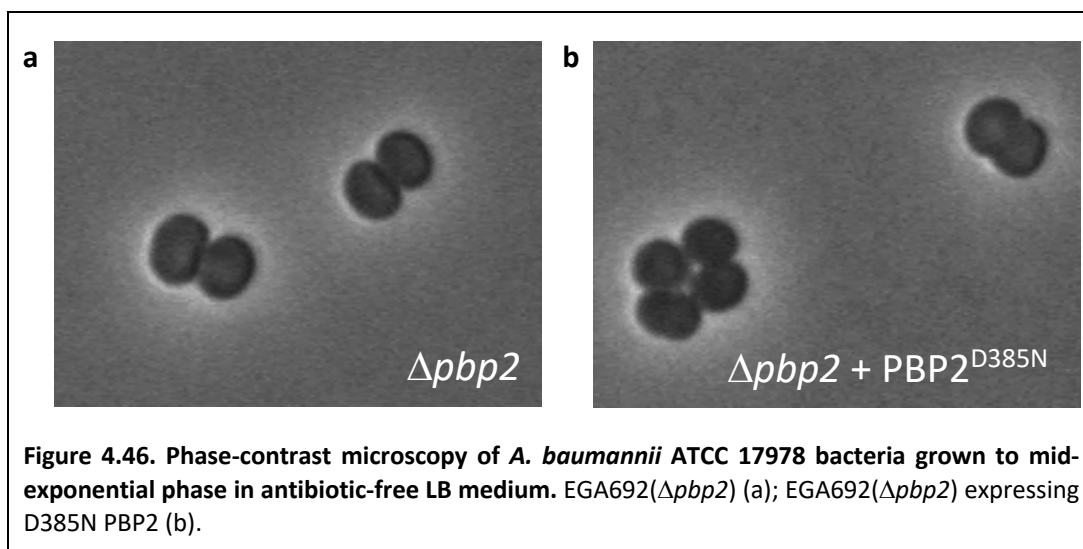
4.4.2.3 *In-vivo* studies of PBP2 D385N mutant

The elongasome-specific transpeptidase PBP2, distinctively carries aspartate rather than asparagine in the third position of the conserved S-X-N/D motif. Although the TP active site of PBP2 recognises the same substrate stem-peptide (L-ala- γ -D-Glu-meso-DAP-D-ala-D-ala) and catalyses the same type of reaction as PBPs carrying Asn

in place of Asp (S-X-N motif, i.e., PBP1a, PBP1b, and PBP3), the reason behind this remarkable amino acid substitution is unknown. Currently, studies aimed at addressing the biological significance of the conserved aspartate in the S-X-D motif of PBP2 from rod-shaped Gram-negative bacteria, are lacking.

To determine the impact of a D385N mutation on the transpeptidase activity of PBP2 *in-vivo*, a PBP2 deficient *A. baumannii* ATCC 17978 strain (EGA692(Δ *pbp2*)) was complemented with a PBP2 gene carrying the mutation D385N. The mutation D385N was introduced in pMIC01 by site-directed mutagenesis, using primers 0104-F and 0104-R (table S1), yielding the pUC19 derived plasmid pMIC12. The presence of the mutation was confirmed by DNA sequencing using the 0099-primer (table S1). The mutated insert was amplified by PCR using Eddie-F and Eddie-R primers, cut with EcoRI and PstI restriction enzymes and ligated into pEGE305, resulting in pEGE311.

Similarly to the zinc-binding site mutants discussed in 3.6.2, the effect of the D385N mutation on the enzymatic activity of PBP2 was studied by observing the cell morphology of EGA692(Δ *pbp2*) (Geisinger *et al.*, 2018) expressing the D385N PBP2, and assessing its susceptibility to sulbactam. Expression of D385N PBP2 *in-vivo* was confirmed by Western blot (figure 3.21 in 3.6.2). Surprisingly, it was found that the strain phenocopied the PBP2 deficient EGA692(Δ *pbp2*) strain, with formation of spheroplasts, indicative of a severely impaired PG elongation (figure 4.46). Moreover, the strain was hypersensitive to sulbactam, as was the PBP2 deficient EGA692(Δ *pbp2*) (figure 4.47), thus pointing to an important role played by Asp385 in the catalytic activity of PBP2, which somehow cannot be equally fulfilled by Asn.



4.5 Discussion and future work

This work sought to provide a detailed structural understanding of *A. baumannii* PBP2 inhibition by standard β -lactams and new-generation DBO agents, and to clarify the role of Asp385 in the targeting of PBP2 by selective antibiotics, and in transpeptidase activity.

To elucidate the molecular details of PBP2 transpeptidase inhibition, acyl-enzyme co-crystal structures of PBP2 in complex with mecillinam, meropenem, avibactam, and zidebactam have been solved at reasonable resolution (2.2-2.6 Å). All co-crystal structures have been generated by soaking experiments, since crystal packing contacts do not prevent ligand binding into the active site, as observed in the PBP2 structure. However, the binding site in chain A is found to be partially buried by a

neighbouring molecule, which might explain why the binding of any ligand in this chain usually requires longer soak times. Hence, description of the ligand binding mode in chain B has been considered more reliable. All co-crystal structures have been solved in the same space group as the PBP2 structure (I 2 2 2), and the small change in cell dimensions are likely to be caused by the presence of the ligand. The discovery of a zinc-binding site in the structure of *A. baumannii* PBP2, prompted the addition of zinc chloride in the original crystallisation condition to aid saturation of the metal-coordination site and promote crystal growth.

All crystal structures contain clear, unambiguous Fo-Fc ligand omit electron density for the acyl- linkage to the O γ of the catalytic Ser326, thus corroborating the formation of a covalent adduct seen by mass spectrometry of PBP2 with studied molecules, and confirming the anticipated acylation site. In all the PBP2 structures, electron density for the core group of the molecule is well resolved, corresponding to the penicillin and carbapenem moieties in mecillinam and meropenem, respectively, and the diazabicyclooctane ring in avibactam and zidebactam, which undergo ring opening following acylation of the catalytic Ser326. The carboxylate and sulphonamide groups attached to β -lactams and DBOs, respectively, project into close proximity to the K-T/S-G-T motif and the corresponding electron density is also well resolved. The various R- chains connected to the ligand core group orient away from the catalytic core toward the bulk solvent, and the corresponding electron density is more or less clear, depending on the molecule. Upon binding of the β -lactam and DBO compounds studied here, minimal changes occur in the TP active site as indicated by the low rmsd of the TP active site residues in the bound and unbound enzyme (rmsd of C α < 0.3 Å). Small protein rearrangements include rotamer shift of the catalytic Ser upon acylation, small shift of the β 17 peptide backbone, side chain rotamer changes of nearby residues and rearrangement of the hydrogen bonding network. The lack of large domain reorganisation or active site restructuring are indicative of an active site that is structurally predisposed for inhibitor binding.

One of the molecules investigated in this work is meropenem, a β -lactam antibiotic from the carbapenem class representing one of the still few available therapeutic

options for the treatment of infections caused by MDR *A. baumannii*. Meropenem targets multiples PBPs, primarily PBP2 and PBP3. The crystal structure of *A. baumannii* PBP2 with meropenem reveals that, beyond the thioether sulphur atom of the R₁ chain, the ligand is flexible and does not strongly interact with the protein, where the corresponding electron density is weak and discontinuous. In bocillin-FL competition assays, meropenem, imipenem, doripenem, and biapenem show comparable IC₅₀ values against *A. baumannii* PBP2 (Bulitta *et al.*, 2018), despite the variations of the group linked to the sulphur atom in the chain. Therefore, this part of the molecule may account little for the inhibitory potency against PBP2. Comparison of the structures of *A. baumannii* PBP2 and *P. aeruginosa* PBP3 in complex with meropenem would suggest that, stabilisation of the methyl pyrroline group by hydrophobic interactions could contribute to the inhibitory potency of the carbapenem class. This interaction would be provided by a conserved Trp366 in *A. baumannii* PBP2, whereas in *P. aeruginosa* PBP3, a hydrophobic bridge created by the vicinity of Val333 to Phe533 could serve the same function (Han *et al.*, 2010). The additional interaction of the pyrroline ring nitrogen with the hydroxyl of Ser383/Ser349 (*A. baumannii* PBP2/*P. aeruginosa* PBP3) may also provide additional stabilisation to the acyl-enzyme complex.

A new promising class of PBP inhibitors is represented by the DBOs, and in this work the first ever structure of zidebactam bound to its target enzyme PBP2, has been determined, along with the PBP2: avibactam structure for comparison. Chemically, the only difference between zidebactam and avibactam is the presence of a C2 chain extending from the carboxamide group of avibactam, to which the enhanced potency of zidebactam could be ascribed. Avibactam is a weak but specific PBP2 targeting inhibitor, and derivatisation of the DBO scaffold at various positions C2/C3/C4 has led to the development of novel compounds with enhanced PBP2 inhibitory activity, other than zidebactam. Examples include FPI1465, ETX2514 and CPD4 (King *et al.*, 2016; Durand-Réville *et al.*, 2017; Levy *et al.*, 2019).

According to the *in-vitro* activity data reported for avibactam (4.3.1.1), PBP2 would have a TP active site that facilitates the binding of a DBO scaffold, while PBP1a/PBP1b/PBP3 do not. Examination of the HMW-PBP apo-structures does not

offer a clear justification for the good/poor binding of avibactam to these proteins. Analysis of the structures of *A. baumannii* and *E. coli* PBP2 bound to avibactam does not reveal obvious protein attributes that could justify the exclusion of this molecule from binding other PBP active sites, since the main protein-ligand interactions involve the conserved motifs. A co-crystal structure of *E. coli* PBP1b with FPI1465, a modified version of avibactam where the C2 carboxamide has been linked to a pyrrolidine containing group, could offer a hint in this respect. FPI1465 is a slow binder of PBP1b, and it does not show useful activity against this protein (IC_{50} *E. coli* PBP1a/PBP1b/PBP3 > 2000 μ M, IC_{50} *E. coli* PBP2 14.8 ± 1.1 μ M) (King *et al.*, 2016). In *E. coli* PBP1b: avibactam structure, the 6-membered ring adopts a less stable “boat” conformation in comparison to the more stable “chair” observed in PBP2 and β -lactamase structures. As a result of this different ligand conformation, the N6 nitrogen is not within H-bonding distance to Ser572 (first residue of the S-X-N motif). Since Ser572 could participate in the transfer of a proton to the N1 nitrogen in β -lactams and N6 nitrogen in DBOs, during the formation of the acyl-enzyme complex, the authors suggest that the suboptimal positioning of this residue could be responsible for the poor inhibition of PBP1b by DBOs (King *et al.*, 2016). It is unknown if the same is true for PBP1a and PBP3, due to the lack of co-structures with DBOs, and it is unclear why DBOs would adopt a different conformation in the TP active site of PBP1b compared to PBP2. Also, the determinants for the selective binding of the DBO scaffold to PBP2, have not been elucidated yet.

There are several factors to keep in mind, when trying to rationalise the inhibitory activities of β -lactams and DBOs, by using the structural data generated on the acyl-PBP2 complexes.

Firstly, the X-ray structure represents an averaged model of a dynamic protein, that loses information about protein motions. To take into account the protein conformational dynamics in the study of the protein-ligand complexes, various experimental methods could be used including molecular dynamic simulations, that can provide insight into the local flexibility of functional residues, and structural flexibility of the overall binding site (Durrant and McCammon, 2011).

Secondly, the co-structure is a representation of the final reaction product (the protein-ligand covalent adduct), that does not report the state of the ligand and the protein in the pre-covalent Michaelis-Menten complex. Acylation by a PBP inhibitor critically depends on the efficiency of formation of the pre-covalent complex, which in turn depends on how well the molecule can complement the active site. Structures of the Michaelis-Menten complex of PBPs with covalent binders, could provide valuable information on the interactions that determine the rapid/slow acylation of a ligand, which could help rationalise the different inhibitory potency of β -lactams and DBOs against different PBPs.

Work from Beadle *et al.* (2002) is enlightening in this respect, as it shows the different binding modes that the β -lactam cephalothin adopt in the pre-covalent, acylated, and post-covalent complex during the hydrolysis reaction catalysed by AmpC. Therefore, it can be speculated that the slow acylation of DBOs by PBP1a/PBP1b/PBP3 could derive from some type of steric clash or unfavourable interactions within the active site, that prevents ligand binding when the DBO scaffold is still intact. Structures of *A. baumannii* PBP2 with inhibitors show that, the TP active site is conformationally quite static following acylation by β -lactams and DBOs, compared to other HMW-PBPs, that appear to be conformationally more flexible in reshaping the active site to accommodate the bound ligand. Therefore, it could be hypothesised that the selectivity of DBOs towards PBP2 may arise from a TP active site being pre-organised for the binding of this scaffold, that does not require energetically or sterically unfeasible conformational changes.

Thirdly, the inhibitory potency of a covalent ligand, that is dependent on the efficiency of formation of the Michaelis-Menten complex, relies not only on protein recognition events but also protein desolvation effects. Studies by Han *et al.* (2010; 2011) clearly describe the effect of solvent rearrangement on the binding of β -lactams to PBPs, and show a correlation between desolvation energies (calculated with WaterMap), protein thermal stabilities (measured with DSF) and second-order acylation rate constants (calculated with rapid quenched flow). A computational analysis of the hydration site energies in the active site of HMW-PBPs could possibly help rationalise the preferred binding of DBOs to PBP2 over PBP1a/PBP1b/PBP3.

Another molecule examined in the PBP2 structural studies is mecillinam. Mecillinam is a β -lactam antibiotic with excellent inhibitory activities against PBP2, that differs from other penicillins in the chemistry of the R-chain. The co-structure PBP2: mecillinam reveals a possible electrostatic interaction taking place between the amidino link and the Asp385 carboxylate group, that could contribute to the characteristic PBP binding profile of the molecule. *In-vivo* data performed in *E. coli* would also support the importance of this interaction in conferring PBP2-mediated antibacterial activity (Thulin *et al.*, 2015). In other HMW-PBPs, the Asp385 of the conserved motif S-X-D is replaced by Asn and this substitution could perhaps justify the poor binding of mecillinam to these proteins.

PBP2 structural data have been aligned with biophysical analyses to rationalise the activities of a range of β -lactams and DBOs against this enzyme. Remarkably, the thermal shift assay results are pretty much congruent with the potency of the molecules tested, in that nanomolar inhibitors (for instance mecillinam, meropenem, zidebactam) shift the protein T_m positively and stabilize PBP2 the most, whereas poor inhibitors (for instance sulbactam) cause a negative shift of the protein T_m , and hence destabilise PBP2. In this assay thermal denaturation is not reversible, thus it is not possible to measure the noncovalent interaction energies ($\Delta G_{\text{interaction}}$) associated with the covalent complex, from the T_m values (Beadle *et al.*, 2001). The measure of $\Delta G_{\text{interaction}}$ indicative of the fit of a ligand into the PBP2 active site following acylation, could provide additional information to help understand the targeting of PBP2 by selective and non-selective inhibitors. Therefore, the thermal shift assay could be used just as a quick and easy analysis, to gain some insight into the potency of PBP inhibitors.

The role of the conserved Asp in PBP2 from rod-shaped Gram-negative bacteria has not been explored so far, with regard to inhibitor binding affinities and catalysis of the transpeptidation reaction.

To address the impact of Asp on the binding of selective and non-selective ligands, the mutation D385N was introduced in *A. baumannii* PBP2, and studied in thermal shift assays. Although this mutation is not clinically relevant, it may help understand

the requirement of Asp in a position typically occupied by Asn in the S-X-D/N motif. The mutation D385N, does not greatly impact the thermal stability of the protein alone, but it largely increases the stabilisation of the protein when bound to submicromolar inhibitors (for instance ampicillin and avibactam), possibly due to the formation of a favourable interaction with Asn. Surprisingly, the magnitude of thermal stabilisation produced by the binding of mecillinam remains fairly unchanged, possibly suggesting that interaction with Asp may be important for ligand recognition but does not contribute much to the thermodynamic stabilisation of the complex, or as an alternative, a compensatory effect for the loss of interaction with Asp could be present. Because the thermal shift assay results are not conclusive regarding the role of Asp385 in ligand binding, additional *in-vitro* binding assays would be required. One such assay is the bocillin-FL competition assay (Papp-Wallace *et al.*, 2012) run with purified *A. baumannii* PBP2 wild-type and D385N mutant, against the same panel of PBP inhibitors. This would provide a measurement of the affinity of each protein for the inhibitors tested, hence the relevance of Asp in the interaction with selective PBP2-targeting inhibitors such as mecillinam.

To evaluate the importance of the conservation of Asp385 for the transpeptidase activity of the enzyme, the mutation D385N was studied in *in-vivo* experiments performed in *A. baumannii* 17978. Unexpectedly, the mutation has a deleterious effect on the functioning of the elongasome system, as evidenced by the formation of spheroplasts, possibly due to an aberrant PBP2 catalysed transpeptidation. Due to the lack of an *in-vitro* enzymatic assay to study the kinetics of the reactions catalysed by PBP2, it is not possible to know the severity of the disruption caused by the mutation D385N, and whether the mutation affects the transpeptidase activity only, or the carboxypeptidase activity only, or both. Hence, to rationalise the presence of Asp in the S-X-D/N motif of PBP2, a combined *in-vivo* and *in-vitro* approach would be necessary. Furthermore, it would be useful to know if the phenotypic response caused by the D385N substitution, is restricted to *A. baumannii* only, or it applies to other rod-shape Gram-negative bacteria such as *E. coli*.

CHAPTER 5

Exploring the interaction of ampicillin-derived molecules with PBPs in Gram-negative bacteria

5.1 Introduction to chapter 5

β -lactams are the most used class of antibiotics and are among the safest classes of antibiotics on the market. However, although being generally safe, β -lactam antibiotics are recognised as the most frequent cause of drug-induced immunological reactions (Owens, 2008; Blumenthal *et al.*, 2018). Hypersensitivity reactions to penicillins and cephalosporins include most commonly rash, pruritus, and urticaria, while anaphylaxis is a rare event (Owens, 2008). Self-reported β -lactam allergy is common (5-15 % of patients), however up to 95% of patients with a history of penicillin allergy, are not allergic when skin tested (Salkind *et al.*, 2001; Sacco *et al.*, 2017). Several risk factors have been associated with immediate hypersensitivity reactions, including the chemistry and metabolism of the drug. It is known that β -lactams can acylate lysine residue amino groups of proteins, resulting in the formation of covalent conjugates that show immunogenic properties (Bertucci *et al.*, 2001; Lafaye and Lapresle, 1988a). Once administered, β -lactams can also undergo degradation and these degradation products may also elicit an immune response (Mirakian *et al.*, 2015). β -lactam antibiotics, most notably penicillins and cephalosporins, when stored for a few days at room temperature can also form polymers (Grant *et al.*, 1962; Larsen and Bundgaard, 1978), which have been shown to display strong immunogenic properties in animal experiments (Dewdney *et al.*, 1971; Ahlstedt *et al.*, 1976). Ampicillin is one of such β -lactams that can undergo polymerisation by aminolysis. Interestingly, ampicillin polymers display an intact β -lactam ring at their C-terminal and their reactivities towards PBPs and β -lactamases have been poorly explored so far.

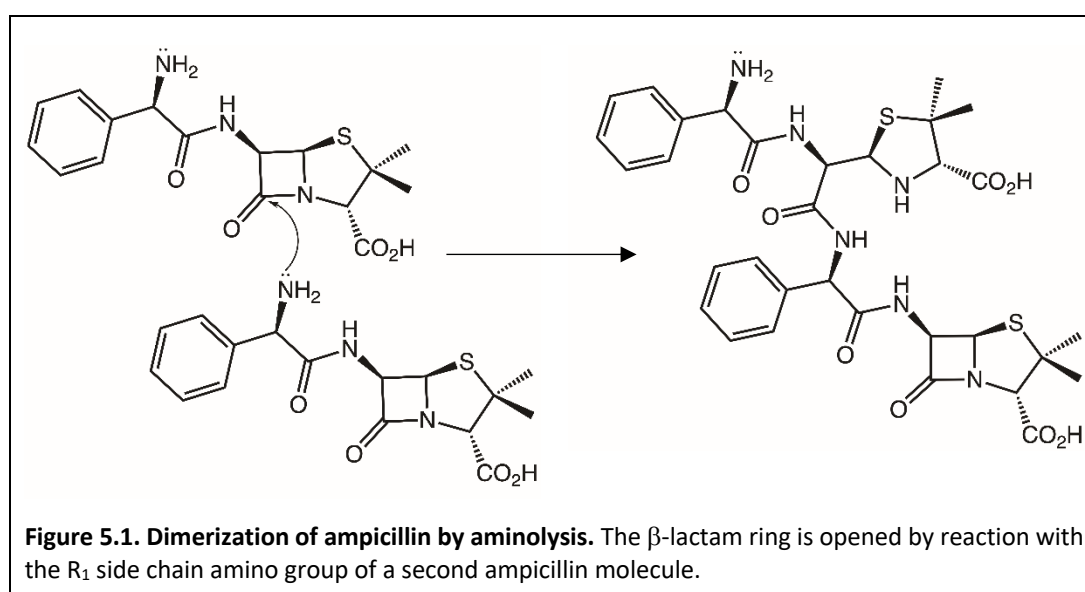
The work described in this chapter aims at elucidating the interactions of ampicillin-derived polymers with PBPs, from prominent ESKAPE pathogens. Moreover, susceptibility to β -lactamase hydrolysis has also been investigated, as well as antimicrobial potency against a panel of clinically relevant Gram-positive and Gram-negative bacteria.

The work presented in this chapter received support from Dr Adrian Lloyd (University of Warwick) who provided assistance and guidance in the execution of the MS experiments. Dr Avinash Punekar and Dr Dom Bellini (both previously of the University of Warwick) solved the X-ray crystallographic structures presented in this chapter, and Dr Chris Lohans (previously of Oxford University) helped in the execution of the NMR experiments. John Moat (AMR screening facility, University of Warwick) provided guidance in the execution of the MIC testing.

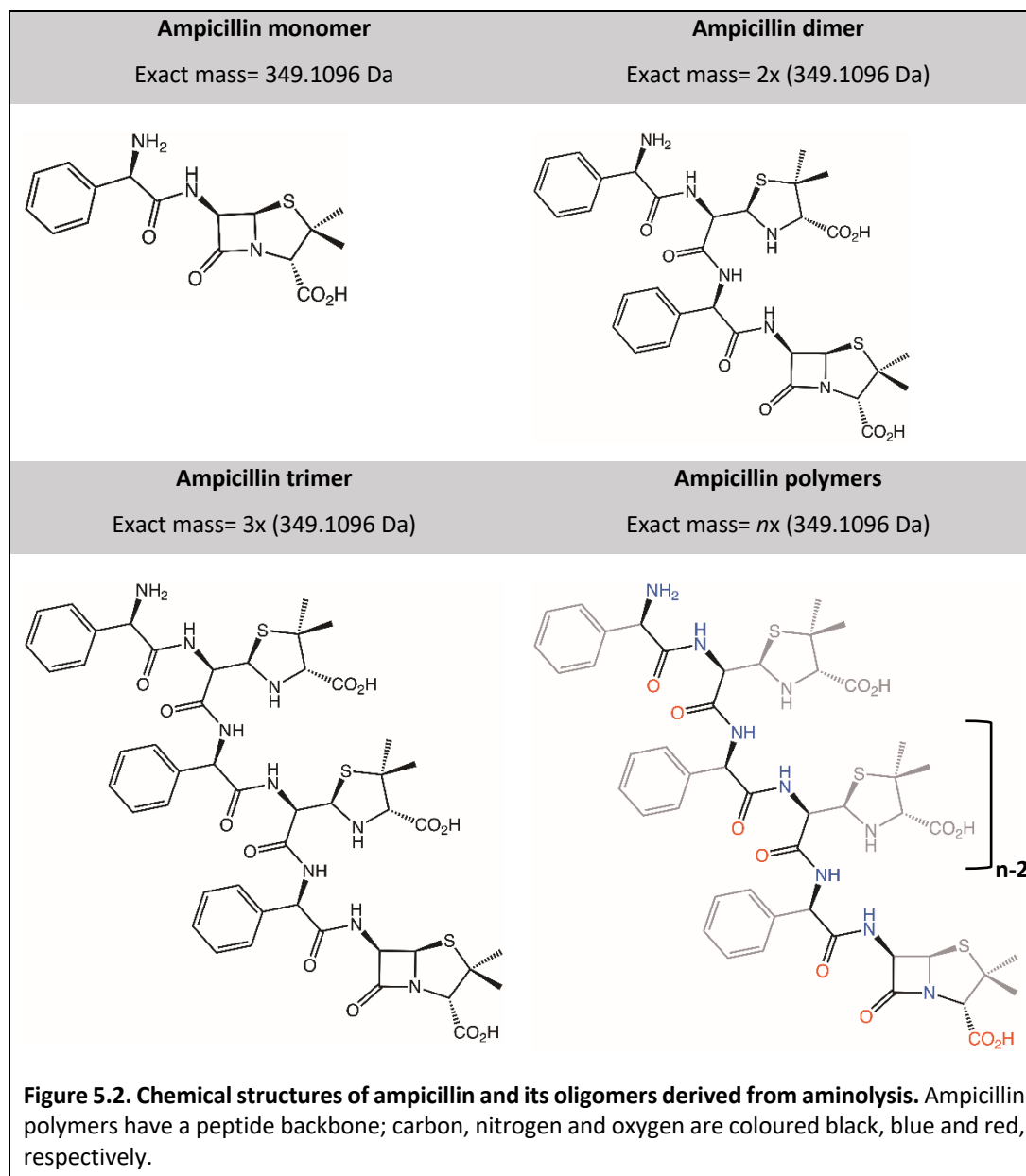
5.2 Formation of ampicillin oligomers: the reaction

The reaction leading to the polymerisation of aminopenicillins, for instance 6-APA, ampicillin and amoxicillin, was described as early as 1962 (Grant *et al.*, 1962). In this thesis work, only the ampicillin polymers have been investigated.

Ampicillin polymers are formed through the nucleophilic attack by the primary amino group of one ampicillin molecule, on the β -lactam carbonyl moiety of a second ampicillin molecule, resulting in amide bond formation (figure 5.1). This process (aminolysis) results in the generation of β -lactam polymers with n length (n = number of ampicillin units), and *mass* equal to $n \times$ mass of ampicillin monomer (349.11 Da) (figure 5.2). The C-terminal ampicillin unit contains an intact β -lactam ring, that is liable to attack by another ampicillin molecule, and the process can continue to form higher molecular weight polymers.



Interestingly, ampicillin polymers display a peptide backbone originating from the penicillin core and the presence of a primary amino group on the acyl- side chain (figure 5.2). Therefore, ampicillin polymers could potentially adopt secondary structure conformations and, due to the presence of a C-terminal intact β -lactam ring, retain binding activity towards PBPs.



5.3 Cloning, expression and purification of PBPs

The ability of ampicillin polymers to acylate HMW- and LMW- PBPs from the ESKAPE pathogens *P. aeruginosa* and *A. baumannii*, was explored by intact protein MS. Production of such proteins is described below.

5.3.1 *P. aeruginosa* PBP1a and its mutant S461A

The nucleotide sequence encoding for a truncated version of PBP1a devoid of the transmembrane helix (Δ 36-822, expected MW= 90006.66 Da) was amplified from the genomic DNA of *P. aeruginosa* PAO1, using 0097-F and 0097-R primers (table S1). The amplified sequence was cloned into a pET-47b vector using EcoRI and HindIII restriction enzymes, resulting in pMIC13 plasmid (table S2, figure S4).

pMIC13 was transformed in competent *E. coli* BL21 (DE3) cells, and protein expression was achieved by autoinduction (2.3.1).

The cell paste was resuspended in 10 volumes (w/v) of buffer A (25 mM Tris-HCl, 400 mM NaCl, pH 8) supplemented with 20 mM imidazole, 2.5 % (w/v) CHAPS and DNase I, prior to sonication (2.3.2). PBP1a was first purified by nickel affinity chromatography, and protein was eluted by applying a step gradient of 20-500 mM imidazole. The fractions containing protein were pooled and concentrated, and further purified by size exclusion chromatography in buffer A (2.3.3 and 2.3.5). The purity of PBP1a was assessed by SDS-PAGE and its ability to bind bocillin-FL was also verified. The final yield of purified *P. aeruginosa* PBP1a was approximately 17 mg per litre of culture.

The catalytically inactive mutant S461A (expected MW= 89990.66 Da) was generated by site-directed mutagenesis (2.2.8), using the pMIC13 plasmid as template and 0094-F and 0094-R primers, resulting in pMIC14 plasmid (table S1-S2). The presence of the mutation was confirmed by DNA sequencing using the 0093 primer (table S1). PBP1a S461A was expressed and purified according to the protocol established for the wild-type protein.

5.3.2 *A. baumannii* PBP1a

DNA encoding the periplasmic domain of PBP1a (Δ 51-764, expected MW= 82151.40 Da with Cys reduced) was amplified from the genomic DNA of *A. baumannii* ATCC 19606, using 0096-F and 0096-R primers (table S1). The nucleotide sequence was cloned into a pET-47b vector using BamHI and Sall restriction enzymes, resulting in pMIC15 plasmid (table S2, figure S1).

Competent *E. coli* BL21 (DE3) cells were transformed with pMIC15, and protein was produced in autoinduction medium (2.3.1).

Purification of *A. baumannii* PBP1a followed the protocol used for *P. aeruginosa* PBP1a (5.3.1). SDS-PAGE and bocillin-FL assays were used to confirm the purity of the protein, and the correct folding and reactivity of the TP domain by binding of, and acylation by the fluorescent penicillin, respectively. The final yield of purified *A. baumannii* PBP1a was approximately 8 mg per litre of culture.

5.3.3 *A. baumannii* PBP3

The nucleotide sequence encoding for a soluble form of PBP3 (Δ 64-610, expected MW= 62493.63 Da) was amplified from the genomic DNA of *A. baumannii* ATCC 19606, using 0095-F and 0095-R primers (table S1). The nucleotide sequence was cloned into a pET-47b vector using KpnI and EcoRI restriction enzymes, resulting in pMIC16 plasmid (table S2, figure S3).

Competent *E. coli* C41(DE3) cells were transformed with pMIC16 and the recombinant protein was overexpressed by autoinduction (2.3.1). PBP3 was purified as in 5.3.1. The purified protein was labelled by bocillin-FL and analysed by SDS-PAGE.

5.3.4 *E. coli* DacB

The nucleotide sequence encoding *E. coli* DacB (PBP4) (Δ 21-477, expected MW= 51780.04 Da with Cys reduced) was amplified from a pET21-based construct available in our laboratory, using 0092-F and 0092-R primers (table S1). The

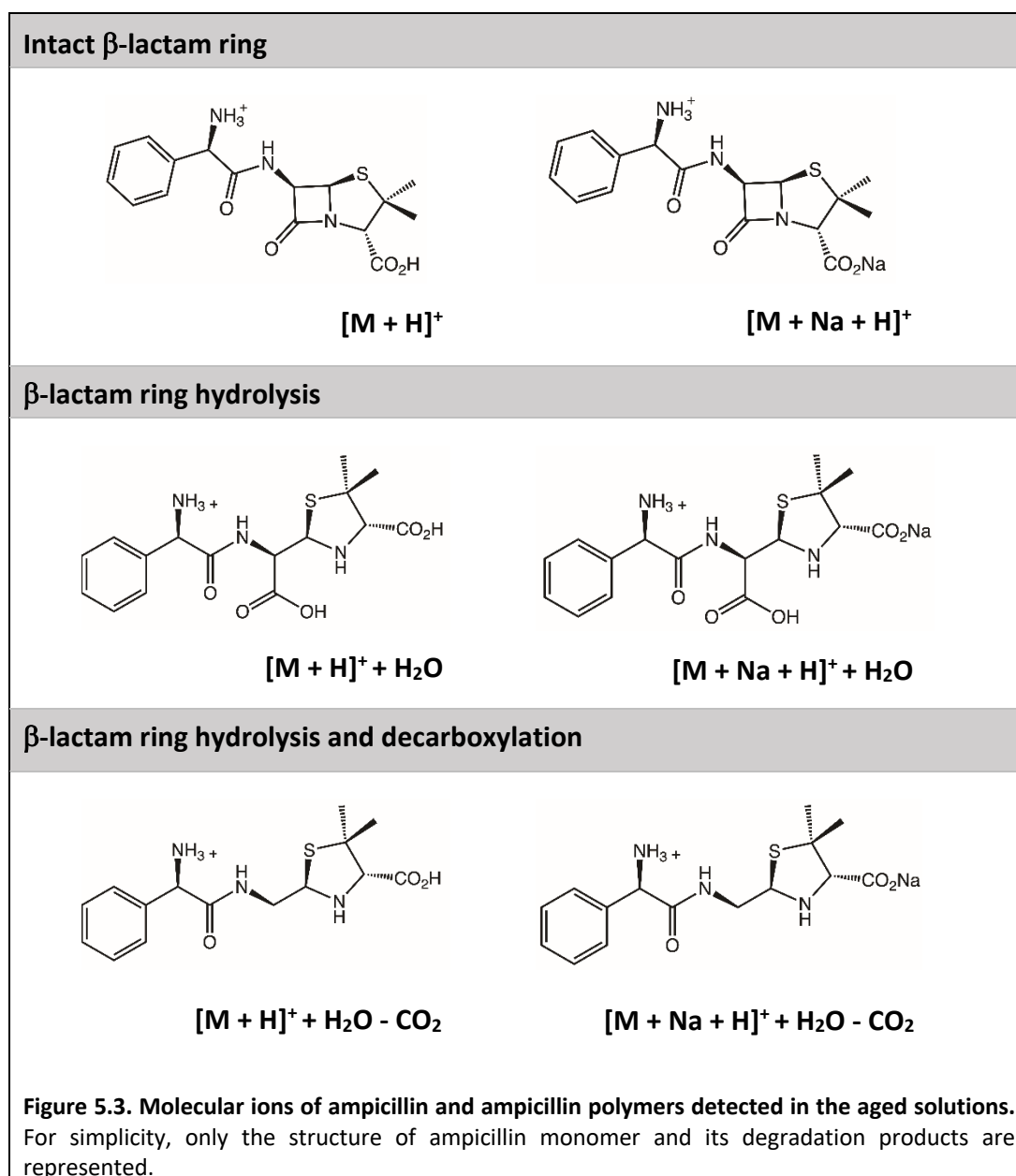
nucleotide sequence was cloned into a pET-28a vector using NdeI and BamHI restriction enzymes, resulting in pMIC17 plasmid (table S2, figure S6). Protein was expressed according to the protocol used for *P. aeruginosa* PBP1a (5.3.1).

5.4 Mass spectrometry of ampicillin in a time course experiment with PBPs

A 20 % (w/v) and 50 % (w/v) stock solutions of ampicillin sodium salt were prepared in LC/MS grade water. The stocks were stored at either room temperature in the dark or at -20°C, for two weeks, to probe the polymerisation reaction in these conditions (for simplicity, abbreviations ampS1, ampS2, and ampS3 will be used for the 20 % (w/v) ampicillin solution stored at room temperature, the 50 % (w/v) ampicillin solution stored at room temperature, and the 50 % (w/v) ampicillin solution stored at -20°C, respectively). Aliquots were withdrawn on the first, seventh and fourteenth day of storage, and analysed by ESI-MS (2.6.1), to observe the compositional changes of the ampicillin solution over the time course of the experiment. Also, at each time point ampS1, ampS2, and ampS3 were reacted with *P. aeruginosa* PBP1a, to assess the ability of ampicillin and ampicillin polymers to acylate this protein. The reaction with PBPs was carried out at 37°C for 30 min, at 10-fold molar excess of ampicillin (2.6.3).

The ESI-MS spectra of ampS1, ampS2, and ampS3 sampled at different time points, revealed a number of molecular species other than ampicillin monomer. Additional molecules included the ampicillin polymers (dimer/trimer/tetramer), and degradation products generated by hydrolysis of the β -lactam ring (penicilloic acid form) and further decarboxylation (penilloic acid form). For each molecule, the protonated molecular ion $[M+H]^+$ and its sodiated adduct $[M+Na+H]^+$ could be detected (figure 5.3) (table 5.1-5.3). Over the duration of storage at room temperature of ampS1 and ampS2, a decrease in the relative peak intensity of ampicillin monomer was concomitant with an increase in the relative peak intensity of ampicillin polymers and degradation products (table 5.1, 5.2) (figure S9a-c, S9d-f),

although these reactions seemed to occur more rapidly in ampS2. Conversely, ampS3 was much less affected by the side reactions during the time of storage at -20°C , as no significant changes in relative peak intensity were observed (table 5.3) (figure S9g-h), consistent with the good practice of storing ampicillin solutions at -20°C or keeping them on ice when used in research.



20 % (w/v) ampicillin stored at room temperature (ampS1)								
Molecule	Molecular ion	m/z (Da)	Day-1 (%)	Sum %	Day-7 (%)	Sum %	Day-14 (%)	Sum %
Ampicillin monomer	[M + H] ⁺	350.12	29.06	37.65	12.35	16.73	7.38	10.50
	[M + Na+ H] ⁺	372.10	8.59		4.38		3.11	
Degradation products								
Lactam hydration	[M + H] ⁺ + H ₂ O	368.13	5.35	10.90	3.84	12.99	4.88	16.48
	[M + Na+ H] ⁺ + H ₂ O	390.11	0.96		2.30		3.67	
Lactam hydration and decarboxylation	[M + H] ⁺ + H ₂ O - CO ₂	324.14	4.21		6.02		6.75	
	[M + Na+ H] ⁺ + H ₂ O - CO ₂	346.12	0.38		0.84		1.18	
Ampicillin dimer	[M + H] ⁺	699.23	31.00	40.17	23.23	41.59	19.51	37.47
	[M + Na+ H] ⁺	721.21	9.16		18.36		17.96	
Degradation products								
Lactam hydration	[M + H] ⁺ + H ₂ O	717.24	3.58	6.51	5.57	14.96	7.32	20.55
	[M + Na+ H] ⁺ + H ₂ O	739.22	1.90		4.39		7.69	
Lactam hydration and decarboxylation	[M + H] ⁺ + H ₂ O - CO ₂	673.25	0.89		4.22		4.70	
	[M + Na+ H] ⁺ + H ₂ O - CO ₂	695.23	0.14		0.78		0.83	
Ampicillin trimer	[M + H] ⁺	1048.34	2.17	2.52	5.78	8.20	4.95	7.53
	[M + Na+ H] ⁺	1070.32	0.35		2.42		2.59	
Degradation products								
Lactam hydration	[M + H] ⁺ + H ₂ O	1066.35	1.06	1.48	2.20	3.56	3.10	5.35
	[M + Na+ H] ⁺ + H ₂ O	1088.33	0.35		0.91		1.74	
Lactam hydration and decarboxylation	[M + H] ⁺ + H ₂ O - CO ₂	1022.36	0.05		0.34		0.37	
	[M + Na+ H] ⁺ + H ₂ O - CO ₂	1044.34	0.02		0.11		0.13	
Ampicillin tetramer	[M + H] ⁺	1397.45	0.13	0.25	0.64	1.02	0.61	1.04
	[M + Na+ H] ⁺	1419.43	0.11		0.38		0.42	
Degradation products								
Lactam hydration	[M + H] ⁺ + H ₂ O	1415.46	0.28	0.53	0.47	0.94	0.50	1.09
	[M + Na+ H] ⁺ + H ₂ O	1437.44	0.23		0.37		0.48	
Lactam hydration and decarboxylation	[M + H] ⁺ + H ₂ O - CO ₂	1371.47	0.01		0.05		0.06	
	[M + Na+ H] ⁺ + H ₂ O - CO ₂	1393.45	0.01		0.04		0.04	

Table 5.1. List of molecular ions identified in the ESI-MS spectra of a 20 % (w/v) ampicillin solution stored at room temperature for two weeks. Spectra were acquired at day -1, -7 and -14 of the time course experiment. For each molecular ion, the relative intensity of the peak is provided as percentage. All the calculated m/z values were consistent with the expected values.

50 % (w/v) ampicillin stored at room temperature (ampS2)								
Molecule	Molecular ion	m/z (Da)	Day-1 (%)	Sum %	Day-7 (%)	Sum %	Day-14 (%)	Sum %
Ampicillin monomer	[M + H] ⁺	350.12	24.04	32.47	6.89	9.33	2.98	5.13
	[M + Na+ H] ⁺	372.10	8.43		2.44		2.15	
Degradation products								
Lactam hydration	[M + H] ⁺ + H ₂ O	368.13	4.92	10.84	4.33	13.78	4.70	19.65
	[M + Na+ H] ⁺ + H ₂ O	390.11	1.12		2.50		4.23	
Lactam hydration and decarboxylation	[M + H] ⁺ + H ₂ O - CO ₂	324.14	4.34		6.12		8.98	
	[M + Na+ H] ⁺ + H ₂ O - CO ₂	346.12	0.46		0.84		1.73	
Ampicillin dimer	[M + H] ⁺	699.23	33.95	44.51	19.18	35.87	12.19	25.70
	[M + Na+ H] ⁺	721.21	10.55		16.69		13.51	
Degradation products								
Lactam hydration	[M + H] ⁺ + H ₂ O	717.24	3.38	7.08	7.47	22.14	8.31	34.12
	[M + Na+ H] ⁺ + H ₂ O	739.22	2.44		7.57		12.35	
Lactam hydration and decarboxylation	[M + H] ⁺ + H ₂ O - CO ₂	673.25	1.10		6.05		10.93	
	[M + Na+ H] ⁺ + H ₂ O - CO ₂	695.23	0.16		1.05		2.53	
Ampicillin trimer	[M + H] ⁺	1048.34	2.39	2.73	6.53	9.85	2.89	5.10
	[M + Na+ H] ⁺	1070.32	0.34		3.32		2.22	
Degradation products								
Lactam hydration	[M + H] ⁺ + H ₂ O	1066.35	1.08	1.51	3.27	6.24	3.24	8.14
	[M + Na+ H] ⁺ + H ₂ O	1088.33	0.37		2.18		3.39	
Lactam hydration and decarboxylation	[M + H] ⁺ + H ₂ O - CO ₂	1022.36	0.05		0.59		1.06	
	[M + Na+ H] ⁺ + H ₂ O - CO ₂	1044.34	0.01		0.20		0.45	
Ampicillin tetramer	[M + H] ⁺	1397.45	0.15	0.29	0.84	1.41	0.38	0.77
	[M + Na+ H] ⁺	1419.43	0.14		0.56		0.40	
Degradation products								
Lactam hydration	[M + H] ⁺ + H ₂ O	1415.46	0.30	0.58	0.67	1.39	0.52	1.39
	[M + Na+ H] ⁺ + H ₂ O	1437.44	0.26		0.57		0.63	
Lactam hydration and decarboxylation	[M + H] ⁺ + H ₂ O - CO ₂	1371.47	0.01		0.09		0.14	
	[M + Na+ H] ⁺ + H ₂ O - CO ₂	1393.45	0.01		0.06		0.10	

Table 5.2. List of molecular ions identified in the ESI-MS spectra of a 50 % (w/v) ampicillin solution stored at room temperature for two weeks. Spectra were acquired at day -1, -7 and -14 of the time course experiment. For each molecular ion, the relative intensity of the peak is provided as percentage. All the calculated m/z values were consistent with the expected values.

50 % (w/v) ampicillin stored at -20°C (ampS3)						
Molecule	Molecular ion	m/z (Da)	Day-1 (%)	Sum %	Day-14 (%)	Sum %
Ampicillin monomer	[M + H] ⁺	350.12	24.80	35.31	28.77	39.70
	[M + Na+ H] ⁺	372.10	10.51		10.92	
Degradation products						
Lactam hydration	[M + H] ⁺ + H ₂ O	368.13	4.70	10.32	5.05	10.55
	[M + Na+ H] ⁺ + H ₂ O	390.11	1.30		1.27	
Lactam hydration and decarboxylation	[M + H] ⁺ + H ₂ O - CO ₂	324.14	3.82		3.75	
	[M + Na+ H] ⁺ + H ₂ O - CO ₂	346.12	0.50		0.47	
Ampicillin dimer	[M + H] ⁺	699.23	31.53	43.26	27.04	38.97
	[M + Na+ H] ⁺	721.21	11.73		11.93	
Degradation products						
Lactam hydration	[M + H] ⁺ + H ₂ O	717.24	3.09	6.87	3.19	6.56
	[M + Na+ H] ⁺ + H ₂ O	739.22	2.74		2.49	
Lactam hydration and decarboxylation	[M + H] ⁺ + H ₂ O - CO ₂	673.25	0.88		0.76	
	[M + Na+ H] ⁺ + H ₂ O - CO ₂	695.23	0.16		0.12	
Ampicillin trimer	[M + H] ⁺	1048.34	1.95	2.27	2.10	2.41
	[M + Na+ H] ⁺	1070.32	0.32		0.31	
Degradation products						
Lactam hydration	[M + H] ⁺ + H ₂ O	1066.35	0.86	1.28	0.92	1.27
	[M + Na+ H] ⁺ + H ₂ O	1088.33	0.37		0.32	
Lactam hydration and decarboxylation	[M + H] ⁺ + H ₂ O - CO ₂	1022.36	0.04		0.03	
	[M + Na+ H] ⁺ + H ₂ O - CO ₂	1044.34	0.01		0.01	
Ampicillin tetramer	[M + H] ⁺	1397.45	0.10	0.22	0.09	0.17
	[M + Na+ H] ⁺	1419.43	0.12		0.08	
Degradation products						
Lactam hydration	[M + H] ⁺ + H ₂ O	1415.46	0.22	0.48	0.18	0.37
	[M + Na+ H] ⁺ + H ₂ O	1437.44	0.24		0.18	
Lactam hydration and decarboxylation	[M + H] ⁺ + H ₂ O - CO ₂	1371.47	0.01		0.01	
	[M + Na+ H] ⁺ + H ₂ O - CO ₂	1393.45	0.01		0.00	

Table 5.3. List of molecular ions identified in the ESI-MS spectra of a 50% (w/v) ampicillin solution stored at -20°C for two weeks. Spectra were acquired on the first day and after 14 days of storage. For each molecular ion, the relative intensity of the peak is provided as percentage. All the calculated m/z values were consistent with the expected values.

The ampicillin degradation products reported by the ESI-MS spectra lack an intact β -lactam ring, therefore were not expected to bind covalently to PBP1a. In contrast, ampicillin and ampicillin polymers that retain an intact β -lactam were predicted to react with the TP active site of the protein. This hypothesis was confirmed by ESI-MS analysis of PBP1a reacted with ampS1, ampS2, and ampS3 at different time points of the experiment (table 5.4) (figure 5.4, 5.5).

The spectra showed that PBP1a can be acylated by ampicillin and ampicillin polymers. The relative intensity of the peaks corresponding to the protein adducts formed with the polymers, increased over time reflecting the compositional changes observed in the stock solutions (table 5.1, 5.2) (figure 5.4, 5.5). When PBP1a was reacted with ampS2, adducts formed with higher molecular weight polymers (i.e ampicillin pentamer) could be clearly distinguished, as well as unreacted PBP1a, possibly due to the presence of substantial β -lactam degradation reactions, noticed in the stock solution (figure 5.5a-c). This was not true when PBP1a was reacted with ampS3 (figure 5.5d), whose reactivity for the ampicillin solution remained fairly unchanged after 14 days of storage.

To confirm the ability of ampicillin polymers to form covalent adducts with PBPs, *P. aeruginosa* PBP1a and *P. aeruginosa* PBP3 were reacted with pure ampicillin dimer and pure ampicillin trimer (Toronto Research Chemicals) (table 5.5 figure 5.6a-b). As expected, the proteins were acylated by the polymers. To definitely exclude the possibility that PBP1a could be acylated by multiple monomeric ampicillin molecules when reacted with the aged solutions, S461A PBP1a mutated in the catalytic Ser was tested (table 5.4, figure 5.6c) As expected, the mutant itself had a lower mass compared to the wild-type protein, consistent with the presence of the mutation. Reaction of S461A PBP1a with 14-days old ampS2, showed lack of any modification, thus confirming the binding of ampicillin polymers to PBP1a, and excluding the presence of secondary binding sites.

Further MS experiments were undertaken to check the reactivity of the ampicillin polymers against other HMW-PBPs (table 5.5). *A. baumannii* PBP1a, PBP2, and PBP3

were reacted with a 10 % (w/v) aged ampicillin solution kept at room temperature between 1-3 months. All the protein tested were acylated by ampicillin polymers of various length (figure 5.7a-c). The ability of ampicillin polymers to acylate LMW-PBPs such as *E. coli* DacB (LMW-PBP4) was also confirmed (table 5.5, figure 5.7d).

PaPBP1a +ampS1									
	Day-1			Day-7			Day-14		
Ampicillin	Calculated mass (± error) (Da)	Δmass (Da)	%	Calculated mass (± error) (Da)	Δmass (Da)	%	Calculated mass (± error) (Da)	Δmass (Da)	%
+ Monomer	90354.26 (± 0.09)	+ 349.10	93.1	90353.94 (± 0.26)	+ 348.78	56.8	90354.57 (± 0.13)	+ 349.41	42.9
+ Dimer	90701.88 (± 1.49)	+ 696.72	6.9	90703.23 (± 0.30)	+ 698.07	33.2	90703.82 (± 0.17)	+ 698.66	40.3
+ Trimer	-	-	-	91052.23 (± 0.67)	+ 1047.07	10.1	91053.15 (± 0.44)	+ 1047.99	12.3
+ Tetramer	-	-	-	-	-	-	91402.30 (± 1.14)	+ 1397.14	4.5

PaPBP1a +ampS2									
	Day-1			Day-7			Day-14		
Ampicillin	Calculated mass (± error) (Da)	Δmass (Da)	%	Calculated mass (± error) (Da)	Δmass (Da)	%	Calculated mass (± error) (Da)	Δmass (Da)	%
none	-	-	-	-	-	-	90005.19 (± 0.80)	-	21.1
+ Monomer	90353.65 (± 0.15)	+ 348.49	91.5	90354.38 (± 0.29)	+ 349.22	41.3	90354.21 (± 0.31)	+ 349.05	19.9
+ Dimer	90701.63 (± 2.12)	+ 696.47	8.5	90703.66 (± 0.18)	+ 698.50	37.4	90703.89 (± 0.22)	+ 698.73	37.9
+ Trimer	-	-	-	91053.03 (± 0.52)	+ 1047.87	14.6	91052.84 (± 0.78)	+ 1047.68	11.0
+ Tetramer	-	-	-	91401.56 (± 2.65)	+ 1396.40	6.7	91402.32 (± 1.03)	+ 1397.16	6.0
+ Pentamer	-	-	-	-	-	-	91751.34 (± 1.45)	+ 1746.18	4.1

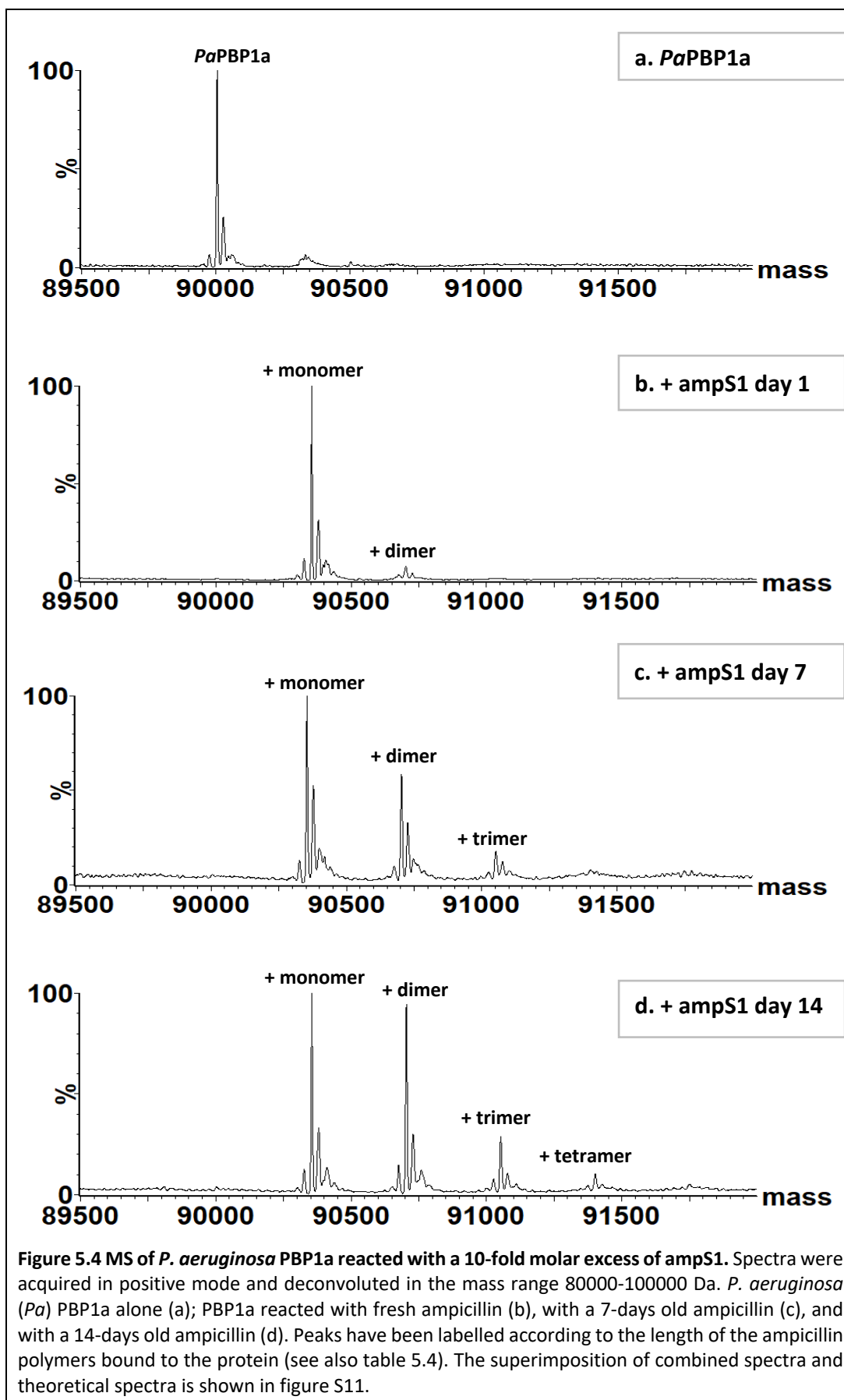
PaPBP1a +ampS3						S461A PaPBP1a +ampS2		
	Day-1			Day-14				Day-14
Ampicillin	Calculated mass (± error) (Da)	Δmass (Da)	%	Calculated mass (± error) (Da)	Δmass (Da)	%	Ampicillin	Calculated mass (± error) (Da)
+Monomer	90353.65 (± 0.15)	+ 348.49	93.1	90354.48 (± 0.20)	+ 349.32	88.9	none	89989.88 (± 0.12)
+Dimer	90701.63 (± 2.12)	+ 696.47	6.9	90702.11 (± 1.04)	+ 696.95	11.1	+ mon/polymer	-

Table 5.4. List of peaks identified in the ESI-MS spectra of *P. aeruginosa* PBP1a reacted with a 10-fold molar excess of an aged ampicillin solution. PBP1a (*Pa*= *P. aeruginosa*) was reacted with either ampS1, ampS2 or ampS3 (spectra shown in figure 5.4 and 5.5). Spectra were acquired at day -1, -7 and -14 of the aging solution. Mutant S461A PBP1a was used as a control to confirm the absence of acylation by ampicillin and its polymers (spectra shown in figure 5.6c). Δmass is the difference in observed mass between the protein reacted with the antibiotic and the untreated protein (*Pa*PBP1a WT: 90005.16 ± 0.37 Da, S461A: 89990.06 ± 0.21 Da). For each protein species, the relative intensity of the peak is provided as percentage.

	<i>Pa</i> PBP1a + ampicillin polymers		<i>Pa</i> PBP3 + ampicillin polymers	
	Calculated mass (± error) (Da)	Δmass (Da)	Calculated mass (± error) (Da)	Δmass (Da)
+ pure dimer	90703.45 (± 0.74)	+ 698.29	58653.45 (± 0.03)	+ 697.79
+ pure trimer	91053.74 (± 0.17)	+ 1048.58	59003.14 (± 0.02)	+ 1047.48

	<i>Ab</i> PBP1a + aged ampicillin		<i>Ab</i> PBP2 + aged ampicillin		<i>Ab</i> PBP3 + aged ampicillin		<i>Ec</i> DacB + aged ampicillin	
Ampicillin	Calculated mass (± error) (Da)	Δmass (Da)						
none	-	-	70543.48 (± 0.10)	-	62492.68 (± 0.83)	-	51774.75 (± 0.10)	-
+ Monomer	82497.22 (± 0.82)	+ 349.02	70892.79 (± 0.90)	+ 349.53	62841.33 (± 0.83)	+ 348.99	52123.51(± 0.77)	+ 348.96
+ Dimer	82846.72 (± 0.34)	+ 698.52	71242.33 (± 0.22)	+ 699.07	63190.95 (± 0.25)	+ 698.61	52473.41 (± 0.42)	+ 698.86
+ Trimer	83196.66 (± 0.91)	+1048.46	71591.01 (± 1.00)	+ 1047.75	63539.92 (± 0.91)	+ 1047.58	-	-
+ Tetramer	83545.63 (± 1.83)	+ 1397.43	71941.26 (± 0.69)	+ 1398.00	63889.50 (± 1.12)	+ 1397.16	-	-
+ Pentamer	83895.11 (± 1.15)	+ 1746.91	72288.91 (± 2.07)	+ 1745.65	64238.91 (± 1.90)	+ 1746.57	-	-
+ Hexamer	-	-	72639.88 (± 2.04)	+ 2096.62	-	-	-	-

Table 5.5. List of peaks identified in the ESI-MS spectra shown in figure 5.6a-b and 5.7. Δmass is the difference in observed mass between the protein reacted with the antibiotic and the untreated protein (*Pa*PBP1a: 90005.16 ± 0.37 Da; *Pa*PBP3: 57955.66 ± 0.04 Da; *Ab*PBP1a: 82148.20 ± 0.14 Da; *Ab*PBP2: 70543.26 ± 0.04 Da; *Ab*PBP3: 62492.34 ± 0.13 Da; *Ec*DacB: 51774.55 ± 0.05) (*Pa*= *P. aeruginosa*; *Ab*= *A. baumannii*; *Ec*= *E. coli*).



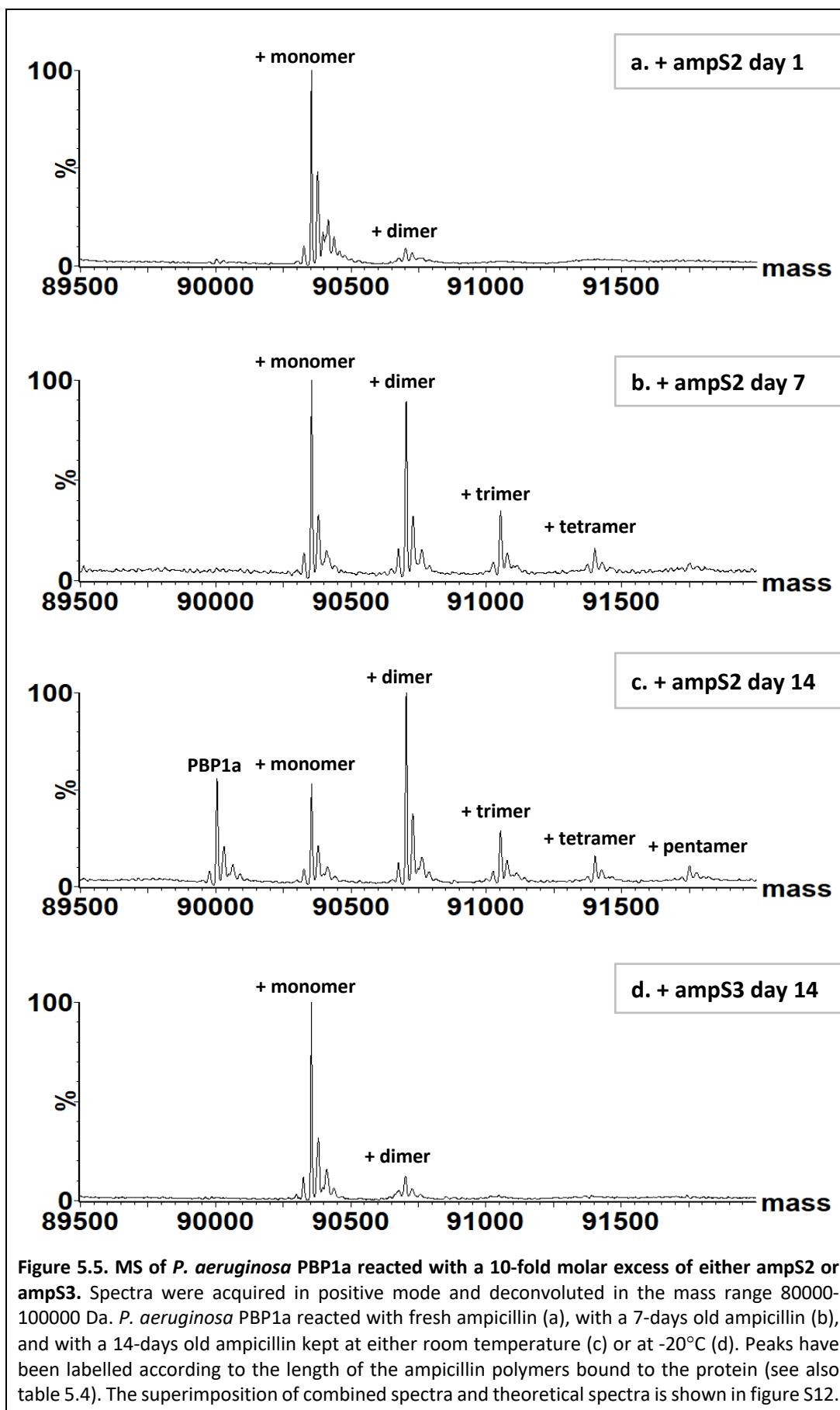
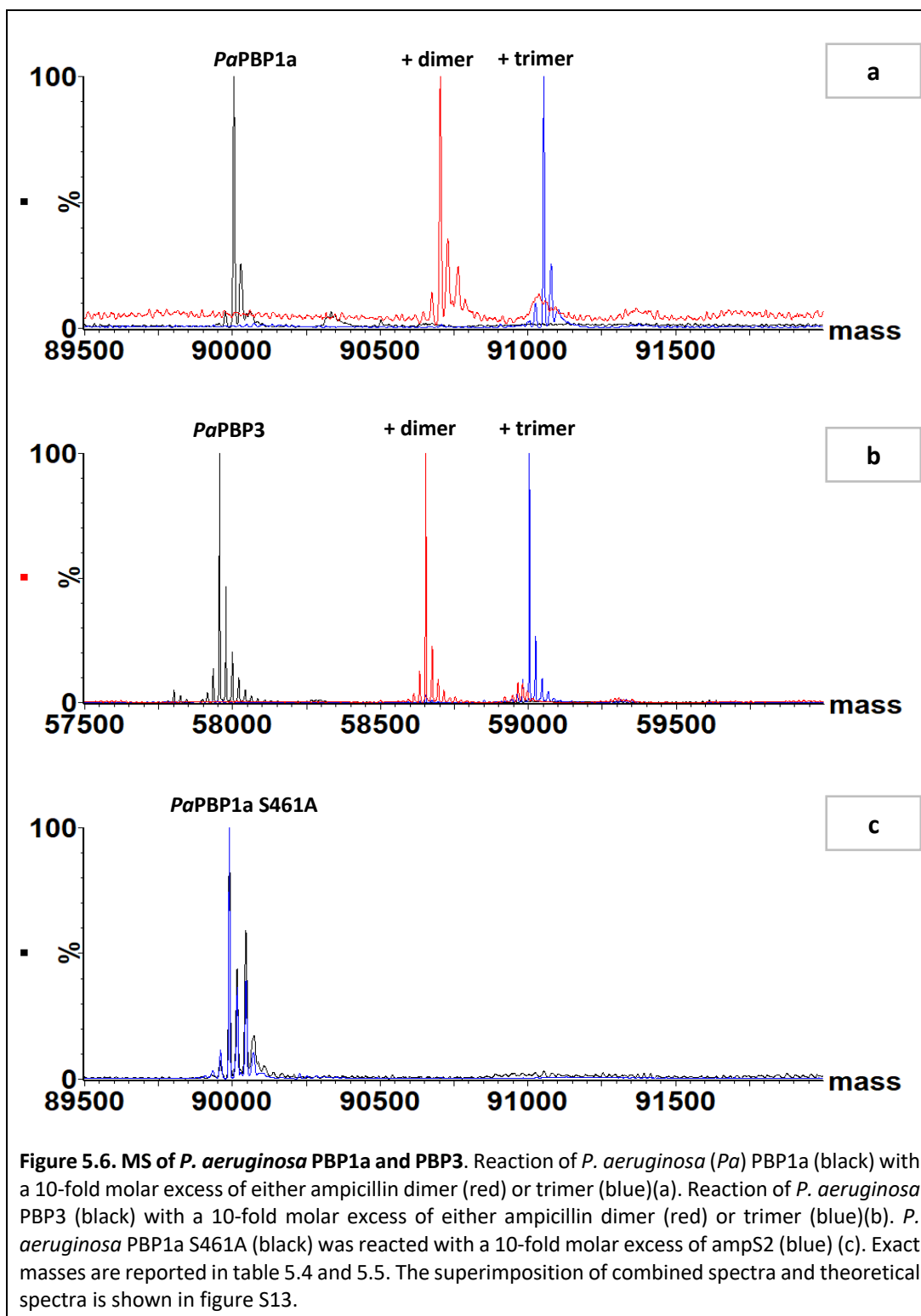
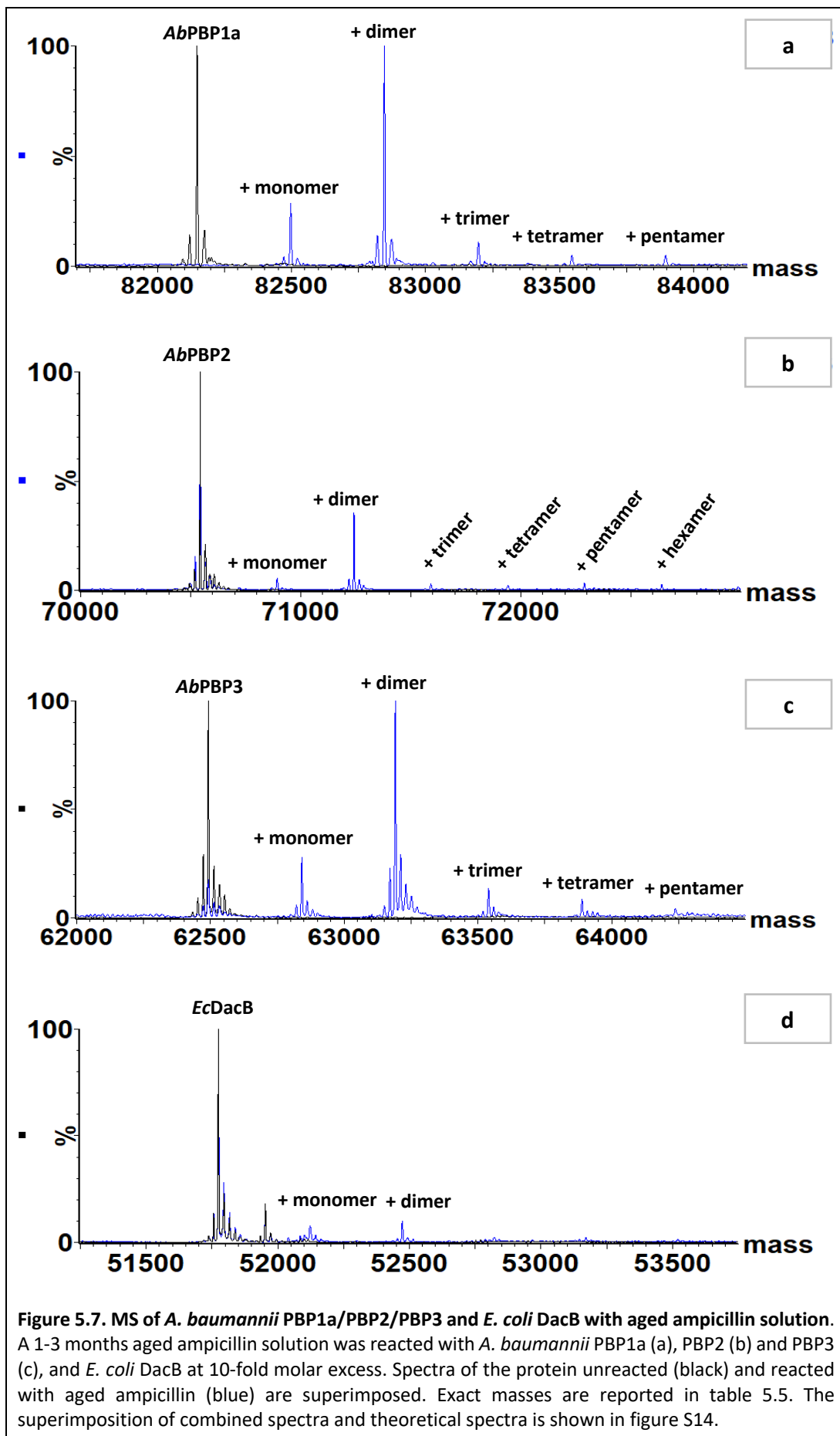


Figure 5.5. MS of *P. aeruginosa* PBP1a reacted with a 10-fold molar excess of either ampS2 or ampS3. Spectra were acquired in positive mode and deconvoluted in the mass range 80000-100000 Da. *P. aeruginosa* PBP1a reacted with fresh ampicillin (a), with a 7-days old ampicillin (b), and with a 14-days old ampicillin kept at either room temperature (c) or at -20°C (d). Peaks have been labelled according to the length of the ampicillin polymers bound to the protein (see also table 5.4). The superimposition of combined spectra and theoretical spectra is shown in figure S12.

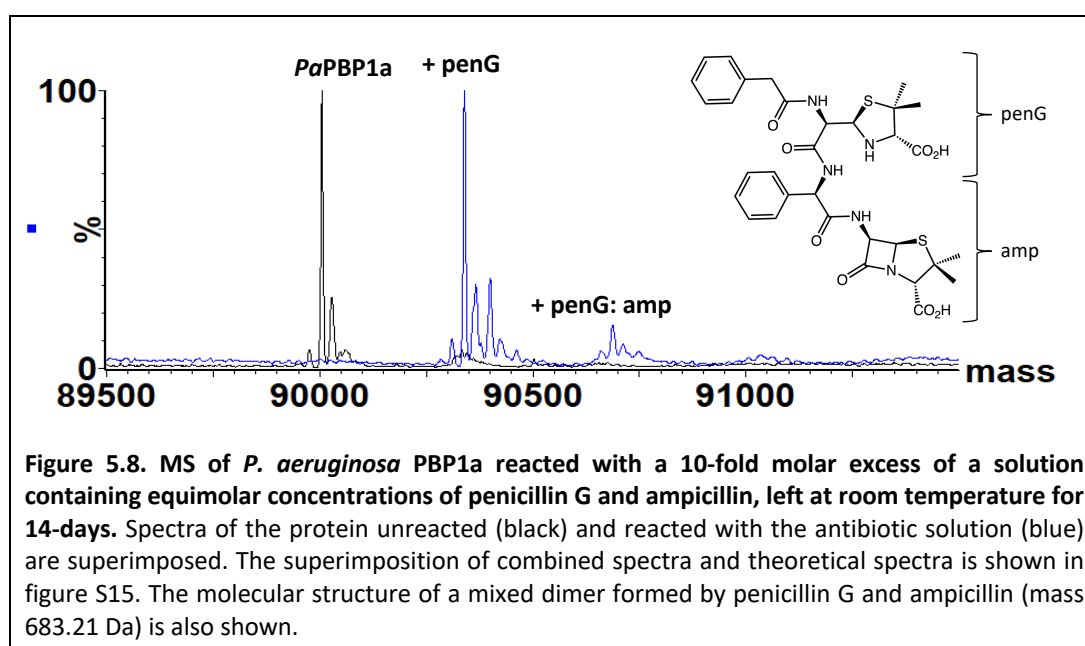




In another experiment, ampicillin was tested for its ability to form mixed polymers with a β -lactam antibiotic lacking a primary amine group, such as the analogue penicillin G. An equimolar solution of ampicillin (exact mass: 349.11 Da) and penicillin G (exact mass: 334.10 Da) was prepared in LC/MS grade water and left at room temperature for 14 days (figure S10). A dimer formed by condensation of penicillin G and ampicillin ($[M + H]^+$ $m/z= 684.22$ Da) and its sodiated version ($[M + Na+ H]^+$ $m/z= 706.20$ Da) were detected, as well as a trimer produced by polymerisation of two ampicillin units and one penicillin G molecule ($[M + H]^+$ 1033.33 Da) and its sodiated adduct ($[M + Na+ H]^+$ 1055.31 Da) (figure S10). Polymers made of ampicillin only, were also present in this solution as shown in previous experiments (table 5.1-5.2). The binding of *P. aeruginosa* PBP1a to the mixed polymers was confirmed (figure 5.8, table 5.6).

<i>Pa</i> PBP1a + mixed polymers		
	Calculated mass (\pm error) (Da)	Δ mass (Da)
+ penG	90339.57 (\pm 0.16)	+334.41
+ penG:amp	90687.80 (\pm 0.96)	+682.64

Table 5.6. List of peaks identified in the ESI-MS spectra of *P. aeruginosa* PBP1a shown in figure 5.8. Δ mass is the difference in observed mass between the protein reacted with the antibiotic and the unreacted protein (*Pa*PBP1a: 90005.16 \pm 0.37 Da).



5.5 Structural studies of *P. aeruginosa* PBP1a

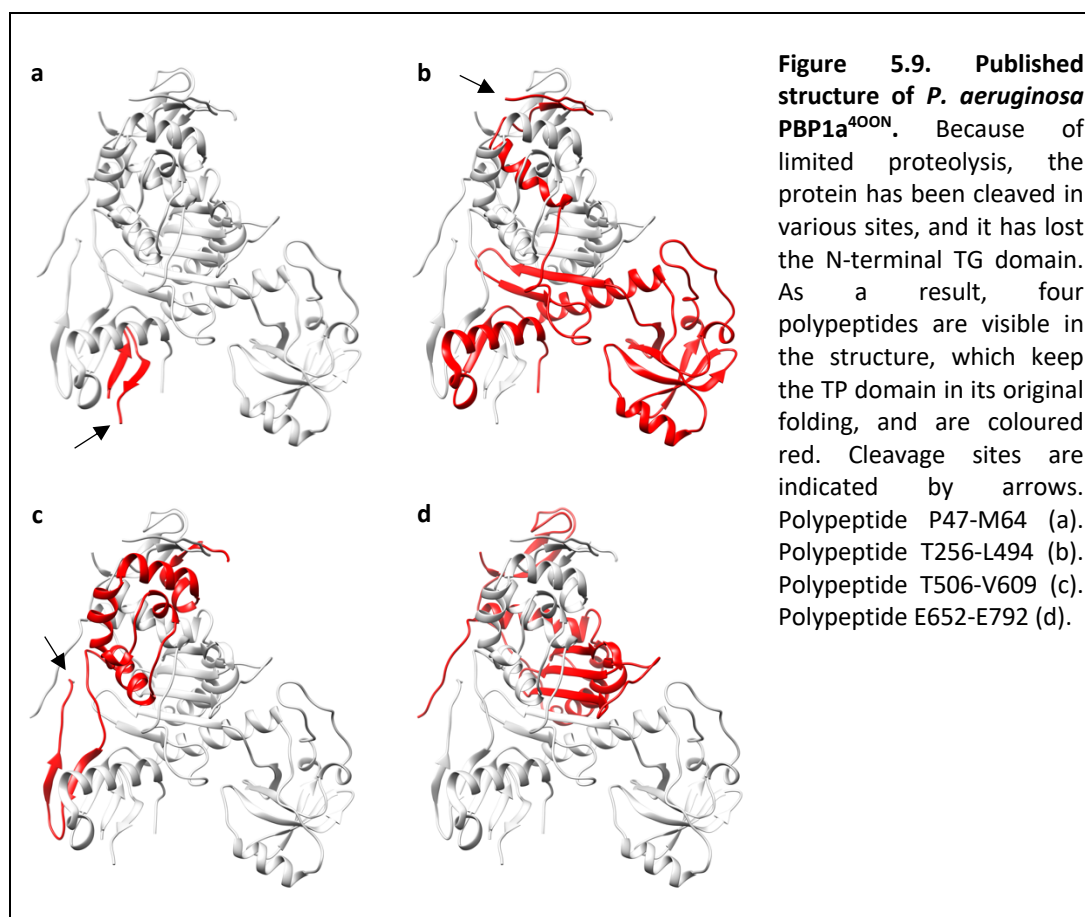
MS experiments have shown that ampicillin polymers can covalently bind to HMW- and LMW-PBPs. The mechanism of binding is likely to be equivalent to that of classical β -lactam antibiotics such as ampicillin monomer, since the mutant S461A of *P. aeruginosa* PBP1a could not form covalent adducts with the ampicillin polymers. Although the binding mode of ampicillin monomer within the TP active site of PBPs is known (see the complex with *E. coli* PBP1b- 5HL9.pdb, *E. coli* PBP4- 2EX6.pdb and *E. coli* PBP6- 3ITA.pdb) (King *et al.*, 2017b; Kishida *et al.*, 2006; Chen *et al.*, 2009), the molecular details of the interaction of ampicillin polymers with PBPs have not been determined yet. A crystallographic structure of an HMW-PBP with such polymers would be desirable, as it could reveal for instance unprecedented protein conformational changes upon ligand binding, previously unseen protein-ligand contacts, or secondary structure conformations adopted by the ampicillin polymers that could inform the design of new PBP inhibitors.

For these reasons, crystallisation of PBP1a from *P. aeruginosa* was attempted. This protein was chosen because it is an important bifunctional enzyme in the cell wall elongation machinery of rod-shaped bacteria, and *P. aeruginosa* is a prominent ESKAPE pathogen the clinical prevalence of which makes the discovery of new effective antibiotics a matter of utmost urgency. Moreover, *P. aeruginosa* PBP1a had been already crystallised in complex with a β -lactam inhibitor and its structure solved (Starr *et al.*, 2014), indicating that the protein is amenable to crystallisation and suitable for studying ligand interactions with the TP active site.

5.5.1 Controlled proteolysis of *P. aeruginosa* PBP1a

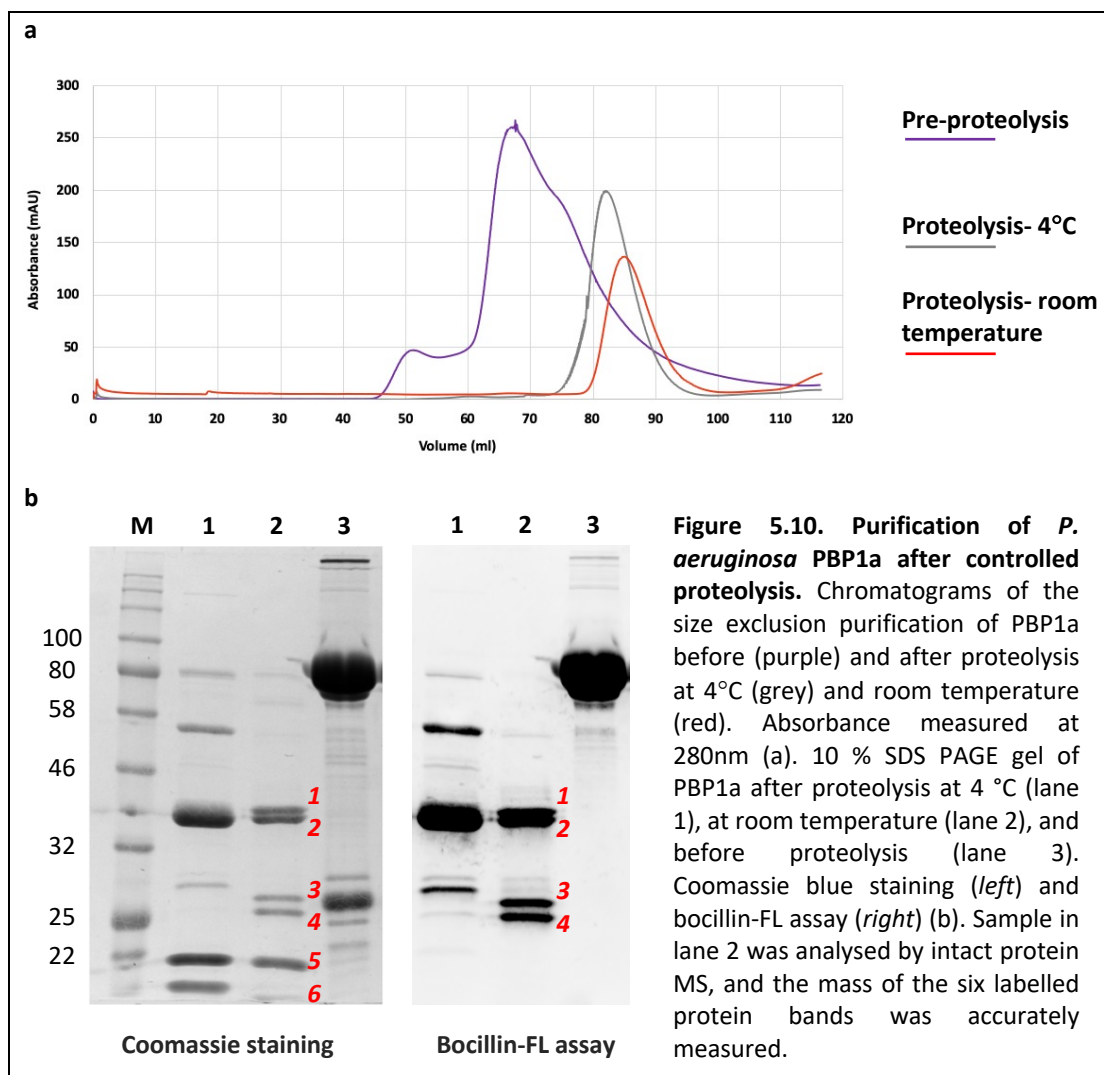
Starr *et al.* (2014) were able to crystallise a proteolyzed form of *P. aeruginosa* PBP1a (4OON.pdb) (for simplicity named PBP1a^{4OON} to differentiate it from the PBP1a structure solved in this work), that includes an almost intact transpeptidase domain and two additional domains. PBP1a^{4OON} was crystallised as an ensemble of four polypeptides, that despite proteolysis, maintained the original folding from the uncleaved protein (figure 5.9).

Limited proteolysis of purified PBP1a (5.3.1) was trialled at both 4°C and room temperature, for 2 h incubation. Controlled proteolysis by trypsin (sequencing grade modified trypsin, Promega) was performed in the ratio 1 µg trypsin: 136 µg protein. This compares with the treatment of PBP1a^{400N} which was proteolysed at 4°C for 2 h, in the ratio 1 µg trypsin: 204 µg protein (Starr *et al.*, 2014).



Following limited proteolysis, PBP1a was further purified by size exclusion chromatography as in 5.3.1, in order to purify the protein unit containing the TP domain from trypsin and any unwanted fragments produced by tryptic digestion (figure 5.10a). Purified protein was then labelled with bocillin-FL (2.5.1)(Zhao *et al.*, 1999), to check the ability of the cleaved protein to bind this β-lactam, so as to confirm the TP domain was correctly folded. The bocillin-stained protein was then analysed by SDS-PAGE (figure 5.10b) in order to assess the homogeneity of the protein samples intended to crystallise.

The elution volume of the trypsin cleaved proteins purified by size exclusion chromatography was higher than that of the intact PBP1a, indicative of protein species with decreased molecular weight (figure 5.10a). On SDS-PAGE analysis, multiple polypeptides of smaller size compared to the intact PBP1a were observed (figure 5.10b), consistent with proteolysis. However, the tryptic digestion was not perfect, since polypeptides of different sizes were stained by bocillin-FL, suggesting the presence of different molecular weight protein species bearing the TP domain, resulting from differences in the extent of proteolysis (figure 5.10b).



The temperature at which proteolysis was carried out also greatly affected the digestion profiles, with the 4 °C digested sample still populated by some uncleaved protein. Overall, 10 mg of protein underwent proteolysis at 4 °C and room temperature, where approximately 5 mg and 2.5 mg of digested protein was

recovered, respectively. The fractions containing protein of interest were pooled and concentrated for the set-up of crystallization plates.

5.5.2 MS of the room temperature tryptic cleaved PBP1a

PBP1a treated with trypsin at room temperature, was analysed by intact protein MS (2.6.2) in order to calculate the mass of the polypeptides observed in the SDS-PAGE gel, so as to predict the positions where trypsin had cleaved the protein.

The deconvoluted spectra of cleaved PBP1a showed six major peaks (figure 5.11), corresponding to the six bands of the SDS-PAGE gel, for convenience labelled from 1 to 6 in figure 5.10b and in table 5.7. The amino acid sequence corresponding to the six polypeptides was identified, knowing the exact mass of each polypeptide (determined by MS) and the potential cleavage sites for trypsin. Polypeptides 1-4 were stained by bocillin, indicating that these polypeptides covered the sequence including the catalytic Ser461, while polypeptides 5-6 were not labelled by bocillin, therefore corresponding to different sections of the protein sequence.

Polypeptide	1	2	3	4	5	6
Sequence	Q153-K501	Q153-K496	Y240-K501	Y240-K496	A647-F822	N502-K646
Calculated mass (Da) (\pm error) <i>reference</i>	39080.07 (\pm 0.14)	38413.23 (\pm 0.27)	29070.76 (\pm 0.32)	28404.72 (\pm 0.64)	19187.15 (\pm 0.11)	15759.07 (\pm 0.12)
Expected molecular weight (Da)	39081.29	38414.47	29071.62	28404.80	19187.66	15759.60

Table 5.7. Sequence and mass of the six polypeptides separated by SDS-PAGE and identified in the MS spectra of *P. aeruginosa* PBP1a digested at room temperature with trypsin. The MS spectra is shown in figure 5.11.

The ability of the cleaved PBP1a to react with additional molecules other than bocillin, was investigated by protein MS. Cleaved PBP1a was reacted with a solution of 20 % (w/v) aged ampicillin (stored at room temperature for 7 days to allow polymerisation) and fresh ceftazidime (table 5.8). Ceftazidime is a third-generation cephalosporin with good *in-vitro* activity against *Pseudomonas*, and high affinity for only PBP1a and PBP3 (Hayes and Orr, 1983). As expected, polypeptides 1-4 were able to covalently bind to ampicillin monomer (mass 349.11 Da), ampicillin dimer (mass 698.22 Da), and ceftazidime (mass 467.49 Da) (table 5.8) (figure 5.12 and 5.13), as

their sequence included the catalytic Ser. Binding of ceftazidime is known to occur concomitantly to the departure of the C3' leaving group (figure 5.14), upon acylation of the catalytic serine, and the observed increase in polypeptide mass reflected this (table 5.8, figure 5.13). The MS experiments indicated that the proteolysed PBP1a could bind to a different range of β -lactams, therefore, the protein preparation was suitable for structural studies of the protein in complex with these inhibitors.

Polypeptide	Proteolysed PBP1a + aged ampicillin		Proteolysed PBP1a + ceftazidime	
	Calculated mass (\pm error) (Da)	Δ mass (Da)	Calculated mass (\pm error) (Da)	Δ mass (Da)
1	39429.66 (\pm 0.17) 39778.41 (\pm 0.16)	+ 349.59 + 698.34	39547.46 (\pm 0.21)	+ 467.39
2	38763.08 (\pm 0.39)	+ 349.85	38880.67 (\pm 0.24)	+ 467.44
3	29420.29 (\pm 0.35) 29768.85 (\pm 0.83)	+ 349.53 + 698.09	29538.19 (\pm 0.29)	+ 467.43
4	28754.30 (\pm 0.82)	+ 349.58	28871.18 (\pm 0.71)	+ 466.46
5	19187.13 (\pm 0.09)	-	19187.13 (\pm 0.07)	-
6	15759.17 (\pm 0.11)	-	15759.37 (\pm 0.11)	-

Table 5.8. MS of tryptic digested *P. aeruginosa* PBP1a reacted with either aged ampicillin or fresh ceftazidime. MS spectra were acquired after reaction with either a 10-fold molar excess of aged ampicillin solution kept at room temperature (20 % w/v, 7-days old) or fresh ceftazidime, for 30 min at 37 °C. Δ mass is the difference in observed mass between the polypeptides reacted with the antibiotic and the unreacted polypeptides (reference masses in table 5.7). Spectra shown in figure 5.12 and 5.13.

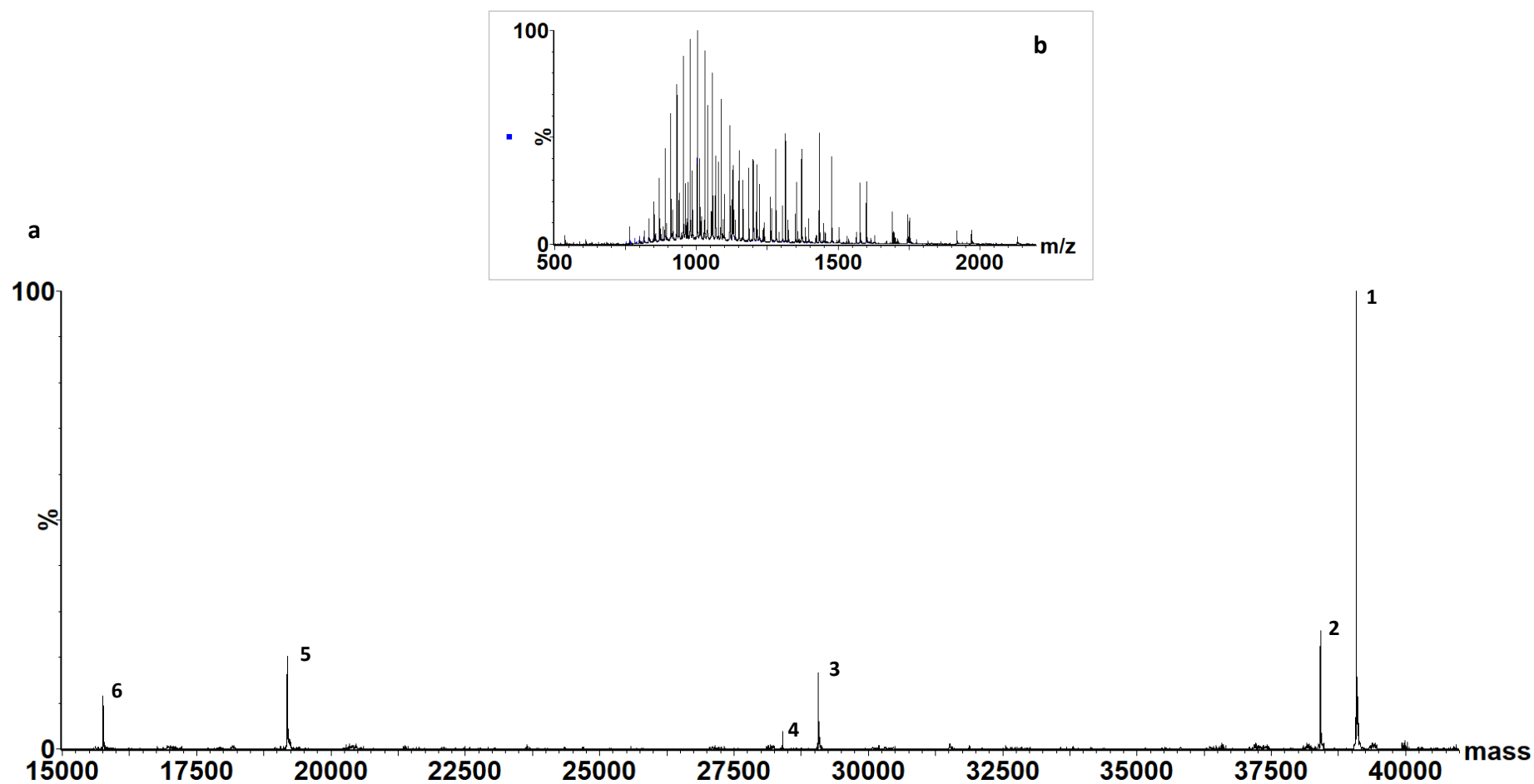


Figure 5.11. MS of *P. aeruginosa* PBP1a proteolyzed at room temperature. Spectra were acquired in positive mode and deconvoluted in the mass range 10000-100000 Da, where the 15000-40000 Da range is shown (a). Superimposition of the combined spectra (black) and theoretical spectra (blue) of PBP1a (b). Peaks are labelled as in table 5.7.

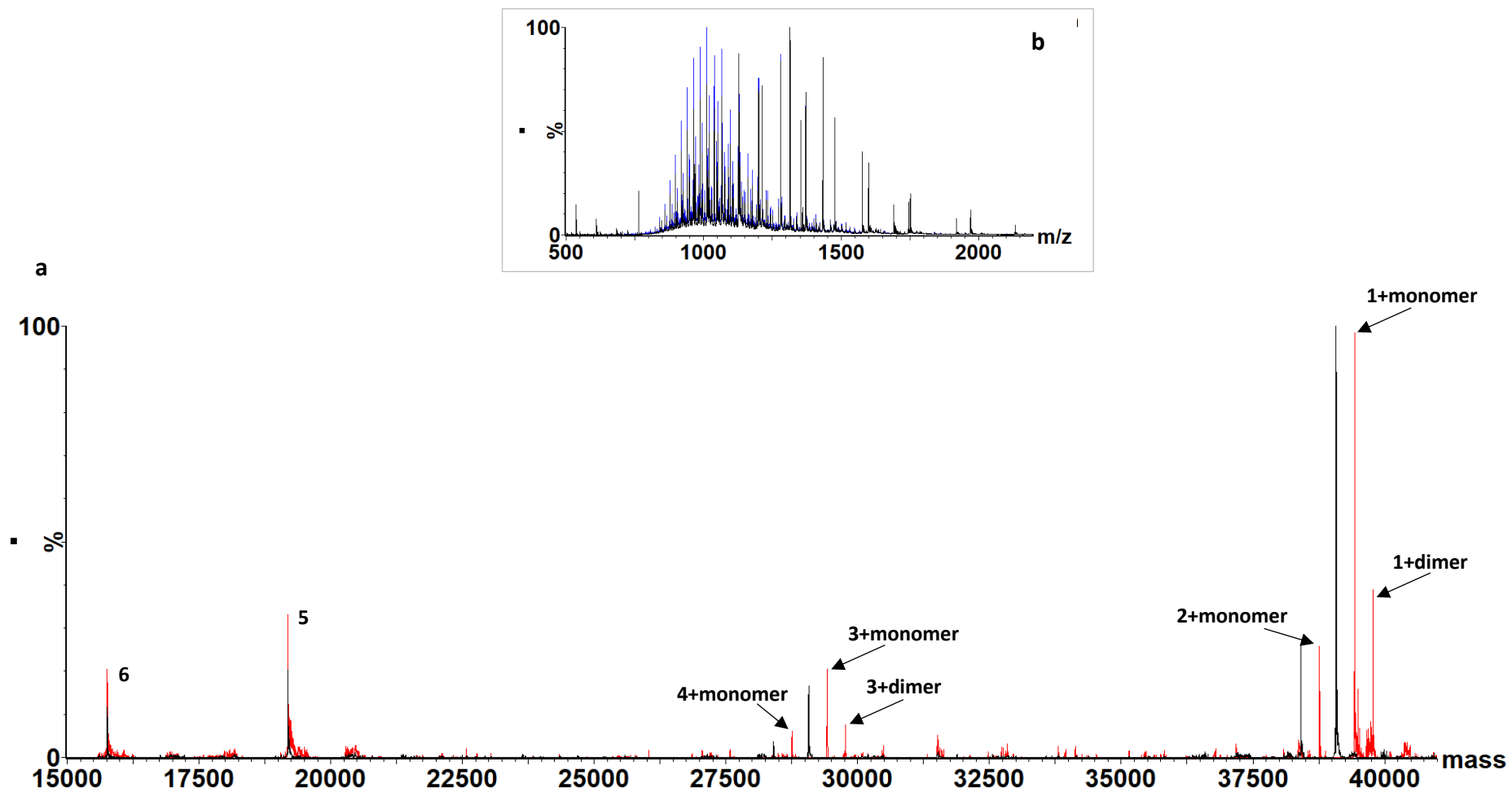


Figure 5.12. MS of *P. aeruginosa* PBP1a proteolyzed at room temperature and reacted with a 10-fold molar excess of a solution of aged ampicillin. Spectra were acquired in positive mode and deconvoluted in the mass range 10000-100000 Da, where the 15000-40000 Da range is shown. Superimposition of deconvoluted spectra of PBP1a before (black) and after reaction with aged ampicillin (red). The six polypeptides are labelled as in table 5.7 (a). Superimposition of the combined spectra (black) and theoretical spectra (blue) of PBP1a after reaction with aged ampicillin (b).

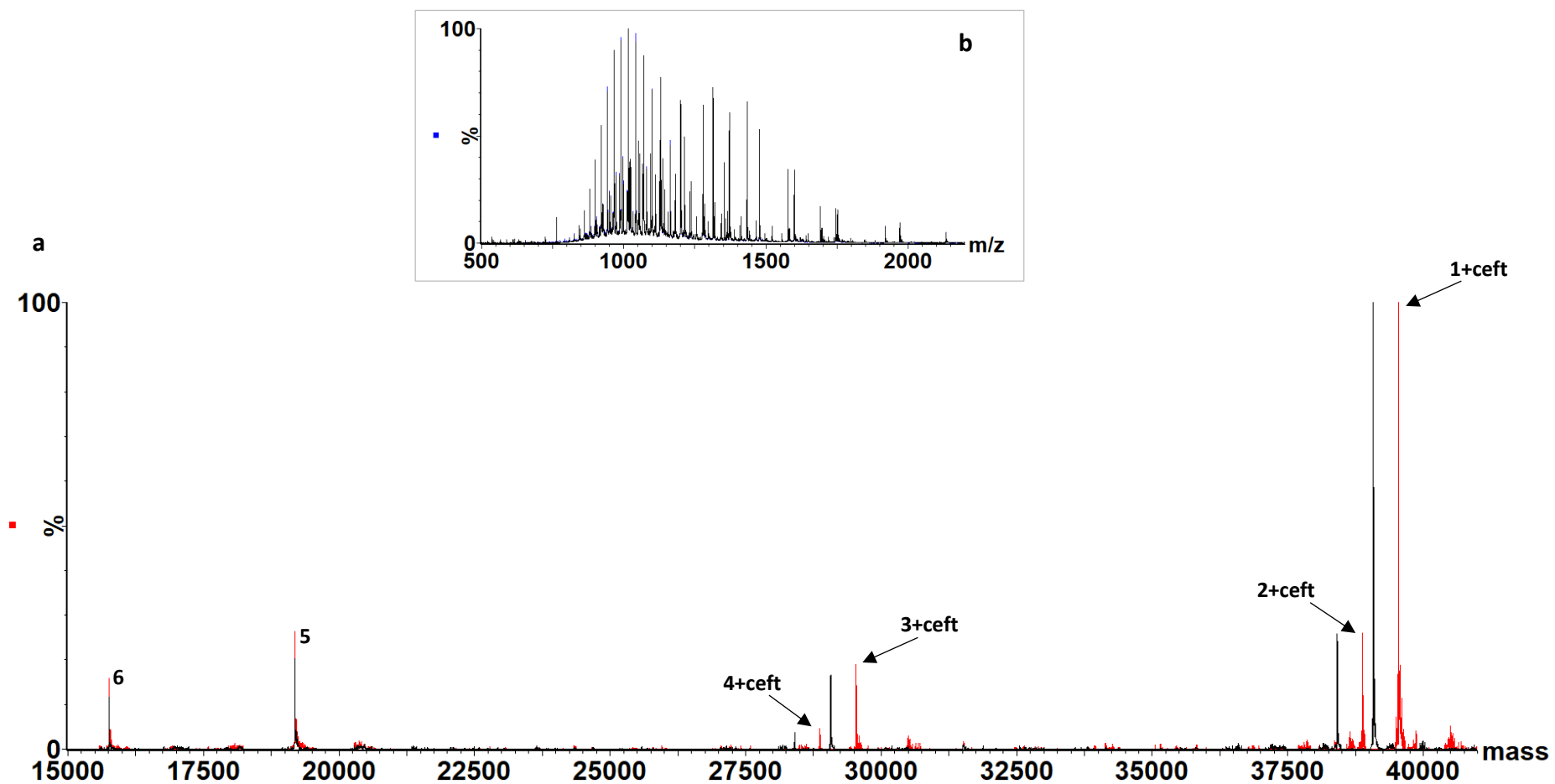
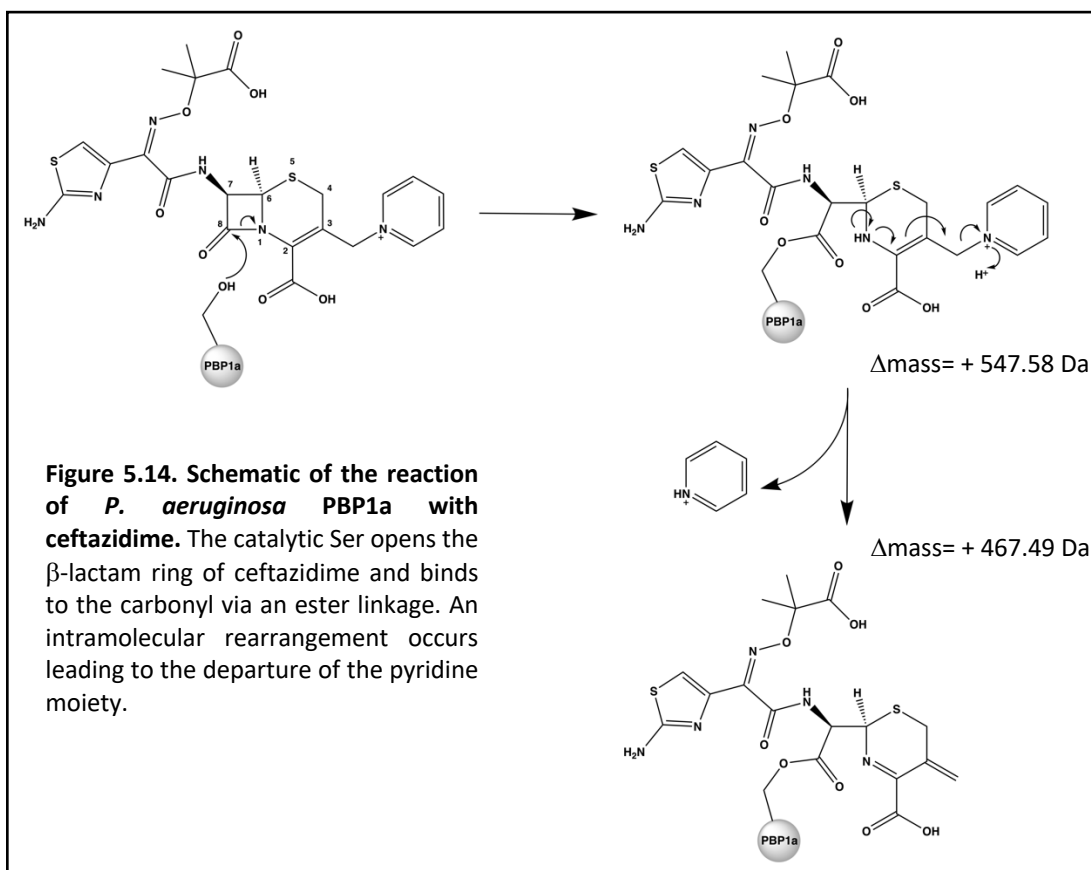


Figure 5.13. MS of *P. aeruginosa* PBP1a proteolyzed at room temperature and reacted with a 10-fold molar excess of fresh ceftazidime. Spectra were acquired in positive mode and deconvoluted in the mass range 10000-100000 Da, where the 15000-40000 Da range is shown. Superimposition of deconvoluted spectra of PBP1a before (black) and after reaction with ceftazidime (red). The six polypeptides are labelled as in table 5.7 (a). Superimposition of the combined spectra (black) and theoretical spectra (blue) of PBP1a after reaction with ceftazidime (b).



5.5.3 Crystallisation of *P. aeruginosa* PBP1a

The structure PBP1a^{400N} was determined from protein crystals grown in 0.1 M sodium citrate tribasic dihydrate pH 5.6 and 1 M ammonium phosphate monobasic (condition 11 in Crystal Screen HT - Hampton Research) (Starr *et al.*, 2014). According to the published protocol, protein crystallised at room temperature by sitting drop vapour diffusion in 2-3 weeks, where the protein was concentrated to 10 mg/mL and mixed with an equal volume of mother liquor (Starr *et al.*, 2014).

The published crystallisation protocol was trialled with PBP1a proteolyzed at either 4°C or room temperature, but no crystal growth was observed.

The 96 conditions of the Crystal Screen HT (Hampton Research) were then trialled by sitting drop vapour diffusion. The two proteolytic preparations of PBP1a (4°C and room temperature digestion) were both tested, and crystallisation was attempted at two different temperatures, i.e, 4°C and room temperature. Crystal hits were obtained from this screening (figure 5.15a-b), where the 4°C proteolytic preparation

of PBP1a produced a shower of small crystals in 4 weeks, with protein concentrated to 11 mg/mL. Crystals grew at 4°C in 0.1 M MES pH 6.5 and 12 % (w/v) PEG20000 (condition 70), in 200 nL drops (100 nL protein plus 100 nL reservoir solution) (figure 5.15a). The room temperature tryptic digested PBP1a preparation, also produced crystals in 17 days. Protein was concentrated to 15 mg/mL and crystals grew at room temperature in 0.1 M HEPES sodium pH 7.5, 10 % (v/v) 2-propanol and 20 % (w/v) PEG4000 (condition 41), in 200 nL drops (100 nL protein plus 100 nL reservoir solution) (figure 5.15b). However, these two crystal hits were not suitable for collection, thus requiring crystal growth optimisation.

Crystal optimisation was attempted by setting up a matrix of the coarse condition where each component of the crystallisation solution was systematically varied (for instance precipitant concentration, pH, type of buffer). Also, the use of additives was explored (Additive screen HT).

The 4°C proteolytic preparation of PBP1a produced bigger crystals in 0.1 M HEPES pH 7.5 and 14 % (w/v) PEG20000 (figure 5.15c) in 3-4 weeks. These crystals grew at 4°C in 400 nL drops (200 nL protein plus 200 nL reservoir solution), and protein was concentrated to 21 mg/mL. These crystals were collected and analysed at the I03 beam line (Diamond Light Source, UK). Despite being protein crystals, diffraction was poor.

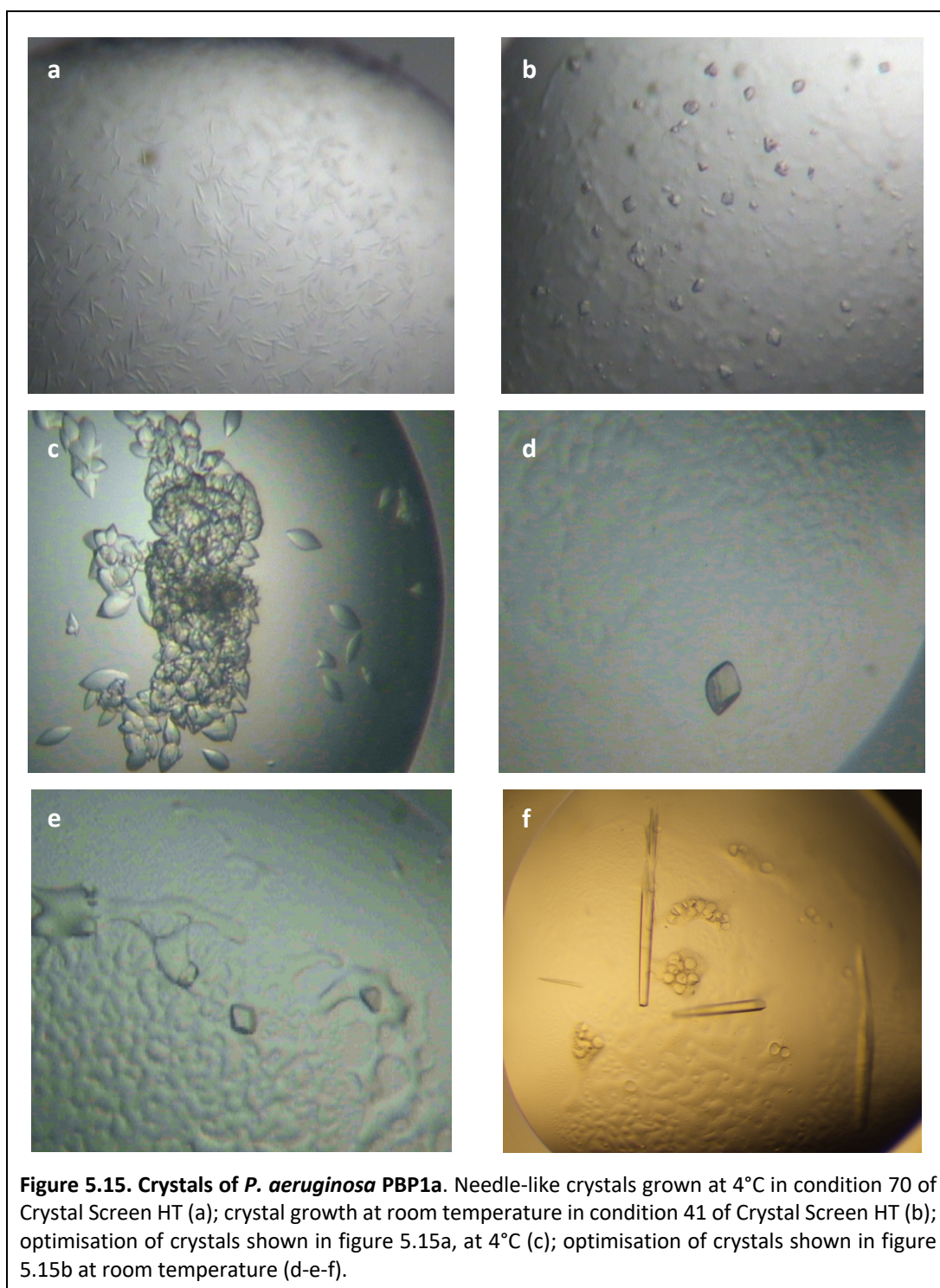
Optimisation of the room temperature crystallisation condition, for the room temperature tryptic digested PBP1a preparation, did however produce diffracting crystals that allowed to determine structures of PBP1a and its acyl- complex with ampicillin. Protein was concentrated to 20 mg/mL, and diffracting crystals grew at room temperature in 400 nL drops (200 nL protein plus 200 nL reservoir solution), in 4-8 weeks, in the following crystallisation solutions.

Condition 1: crystals grew in 0.1 M MES pH 6.5, 6 % (v/v) 2-propanol and 20 % (w/v) PEG4000 (figure 5.15d).

Condition 2: crystals grew in 0.1 M HEPES pH 7.5, 10 % (v/v) 2-propanol and 20 % (w/v) PEG4000 supplemented with 0.02 M taurine (figure 5.15e)

Condition 3: same as condition 2, but taurine was replaced with 0.06 M glycyl-glycyl-glycine.

With the aim of further improving the diffraction of crystals grown in condition 1-3, many optimisation screenings were performed. Although bigger crystals were observed in many of the conditions tested (figure 5.15f), they all diffracted poorly. Further attempts to reproduce the diffracting PBP1a crystals (figure 5.15d-e) also failed.



5.5.4 Structural studies of *P. aeruginosa* PBP1a

5.5.4.1 Crystal harvesting, data collection and structure determination

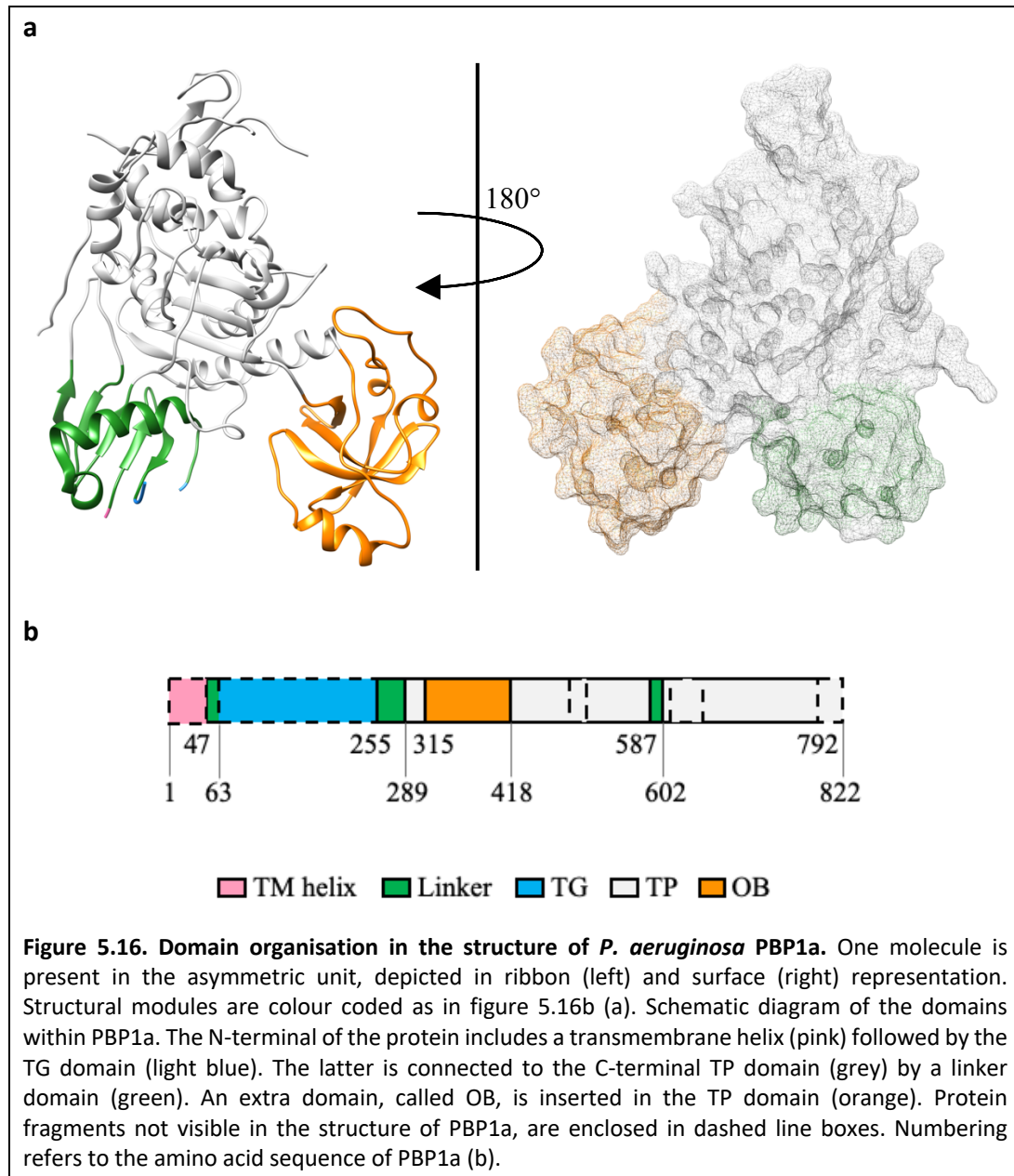
Crystals grown in condition 2 (5.5.3) were looped and flash-vitrified in liquid nitrogen. Crystals grown in condition 1 (5.5.3) were soaked in mother liquor containing 2 mM ampicillin, for 4 h and 30 min, prior to looping and flash-cooling in liquid nitrogen. The dataset for a crystal of PBP1a was collected at the I03 beamline (DLS, Didcot, United Kingdom) as follows: 1800 images were collected with an oscillation step of 0.1° and a 0.2 s exposure time, at 2.8 Å resolution, with a beam size of 80x20 µm and transmission of 50 %. The dataset for a crystal of PBP1a in complex with ampicillin was collected at the I03 beamline as follows: 3600 images were collected with an oscillation step of 0.1° and a 0.2 s exposure time, at 3 Å resolution, with a beam size of 80x20 µm and transmission of 50 %. *P. aeruginosa* PBP1a structures were solved by Dr Avinash Punekar by molecular replacement using PBP1a^{400N} as a search model. The PBP1a dataset was processed using xia2 3dii (Winter, 2010), while the PBP1a:ampicillin dataset was processed using autoPROC 1.0.5 (Vonrhein et al., 2011). Structures were phased with MoRDa (Vagin and Lebedev, 2015), model building and ligand fitting were performed with Coot (Emsley and Cowtan, 2004), and structures were refined with Buster (Blanc *et al.*, 2004).

5.5.4.2 Overall structure of PBP1a

The X-ray structure of *P. aeruginosa* PBP1a solved in this thesis work, is comparable to the structure of PBP1a^{400N} in terms of resolution (3.2 Å PBP1a^{400N} vs 3.06 Å this work), protein architecture and domain composition (figure 5.9, 5.16a) (table 5.9). Notably, the published tryptic digestion protocol and crystallisation condition are different from the ones used in this work. This would be reflected in the different space group (P4₁2₁2) and different unit cell parameters (a=b= 113.77 Å, c= 123.46 Å; $\alpha = \beta = \gamma = 90^\circ$) of PBP1a^{400N} compared to the PBP1a structure determined here (table 5.9). The structure of PBP1a superimposes well to PBP1a^{400N}, with a rmsd of 0.8 Å for 469 C α atoms.

Based on the amino acid conservation of the structural modules with other PBPs (see structures of *A. baumannii* PBP1a, *H. influenzae* PBP1a and *E. coli* PBP1b), the full-

length version of *P. aeruginosa* PBP1a would be expected to have an initial transmembrane α -helix, followed by the N-terminal transglycosylase domain (TG) which connects to the C-terminal transpeptidase domain (TP) via the linker and OB (oligonucleotide/oligosaccharide binding) domains (figure 5.16b).



The structure of PBP1a reveals four main polypeptides: I46-R65, Q255-P486, T506-E611 and F651-E792 (figure 5.17).

Due to the cleavage of the protein and the modest resolution of the crystallographic structure, it is likely that the crystallised polypeptides possess more residues at the

N-terminal and C-terminal ends, which may not be visible in the structure due to their weak or absent electron density caused by their flexibility. Comparing the sequence of the crystallised polypeptides with the sequence of the polypeptides detected in solution by MS (table 5.10, figure 5.18), a correspondence can be found. The crystallised polypeptide Q255-P486 could derive from one of four polypeptides observed in MS (1-4) that were also labelled by bocillin, whereas the crystallised polypeptides T506-E611 and F651-E792 are likely to derive from unique polypeptides (5 and 6 respectively) (table 5.10).

Data collection	PBP1a	PBP1a: ampicillin
Space group	P3 ₂ 21	P3 ₂ 21
Cell dimensions a, b, c (Å) α, β, γ (°)	115.92, 115.92, 81.63 90, 90, 120	117.53, 117.53, 82.32 90, 90, 120
Resolution (Å)	40.82-8.29 (3.11-3.06)	64.01-8.75 (3.28-3.23)
R_{meas}	0.084 (1.596)	0.171 (1.045)
$I/\sigma I$	22.7 (1.8)	14.9 (2.1)
CC (1/2)	1.0 (0.5)	1.0 (0.4)
Completeness (%)	100 (100)	99.7 (92.9)
Multiplicity	8.5 (8.9)	15.4 (5.5)
No. of reflections	5656 (5506)	9346 (2803)
No. of unique reflections	669 (616)	605 (514)
Refinement		
Resolution (Å)	37.94- 3.06	58.76- 3.23
No. reflections	12085	10112
R_{work}/ R_{free}	0.22/ 0.32	0.22/ 0.31
No. atoms Protein Water Other	3898 79 7	3824 57 25
B-factors (Å ²) Protein Water Other	76 36 103	56 27 58
R.m.s.deviation Bond lengths (Å) Bond angles (°)	0.01 1.25	0.01 1.19
Favored/allowed/disallowed (%)	89.4, 8.7, 1.8	91.7, 7.0, 1.2

Table 5.9. Data collection and refinement statistics for *P. aeruginosa* PBP1a structures. The highest resolution shell is shown in parenthesis.

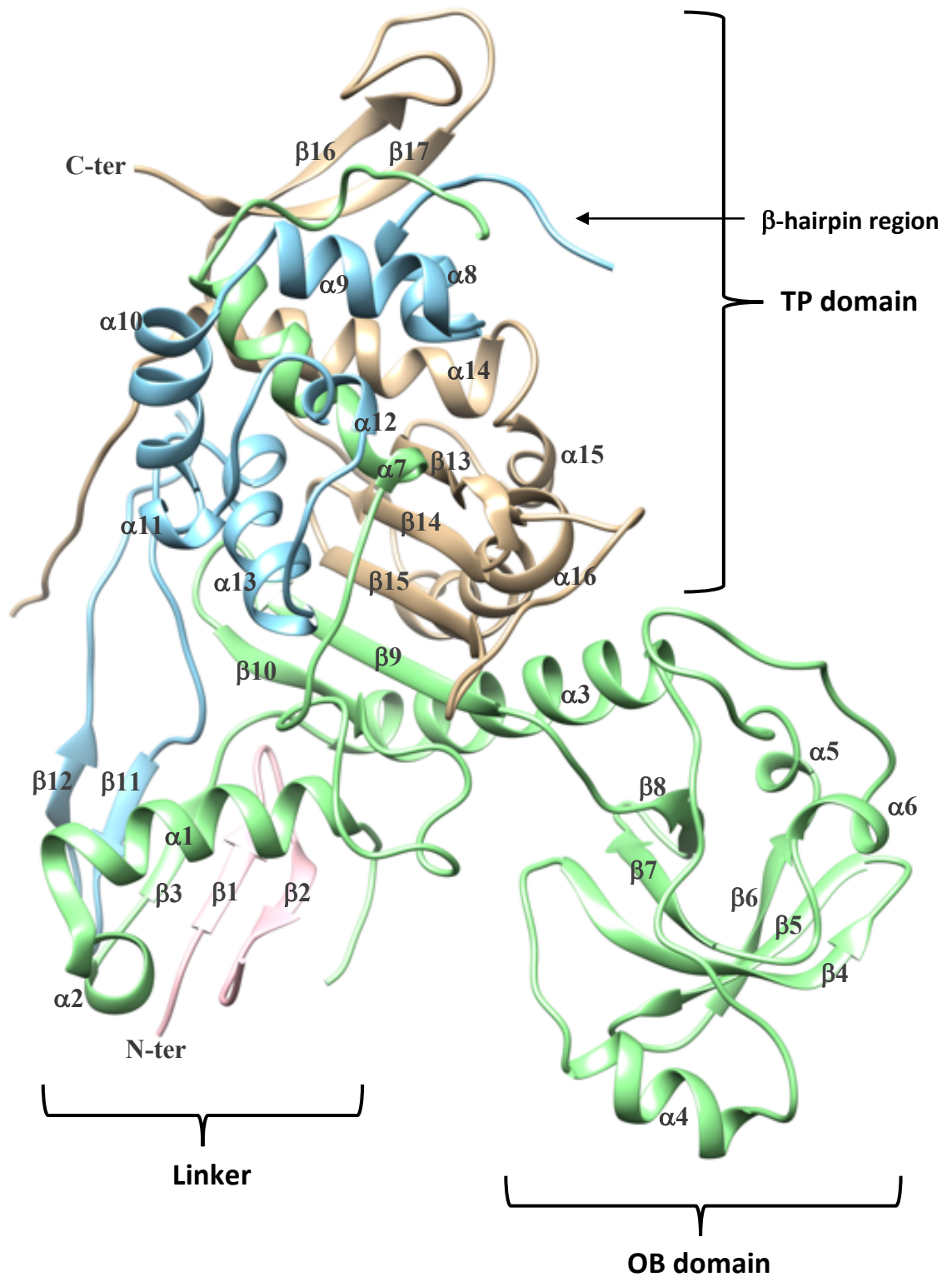
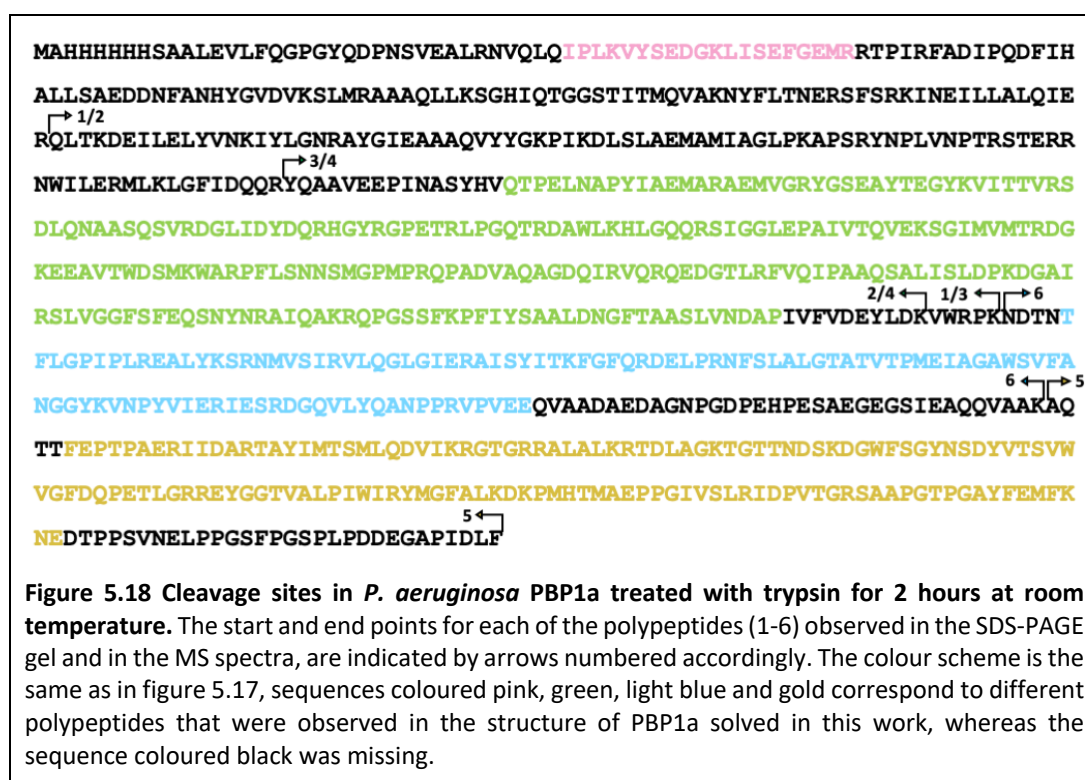


Figure 5.17. Structure of *P. aeruginosa* PBP1a solved in this work. Due to limited proteolysis, the TG domain is absent and some stretches of polypeptide are not observed. The four polypeptides that comprise the structure are: I46-R65 (pink), Q255-P486 (green), T506-E611(light blue) and F651-E792 (gold), and their sequence is shown in figure 5.18. Secondary structure elements are labelled.

Crystallised polypeptide	MS polypeptide
I46-R65	-
Q255-P486	Q153-K501 (1)
Q255-P486	Q153-K496 (2)
Q255-P486	Y240-K501 (3)
Q255-P486	Y240-K496 (4)
T506-E611	N502-K646 (6)
F651-E792	A647-F822 (5)

Table 5.10. Comparison between the polypeptides of the tryptic digested *P. aeruginosa* PBP1a protein observed in solution by MS, and in the X-ray structure. The MS polypeptides are numbered 1-6 as in table 5.7 and their sequence is provided in figure 5.18.



The short crystallised polypeptide I46-R65, could not be assigned to any polypeptide from the MS spectra, with confidence, as deconvolution in the range 3000-45000 Da (deconvolution not shown) produced multiple peaks at the low masses, and with very low intensity compared to the six major peaks reported in figure 5.11.

The polypeptides present in the PBP1a structure solved in this work are comparable to the ones visible in PBP1a^{400N} (P47-M64, T256-L494, T506-V609 and E652-E792). Despite the controlled proteolysis with trypsin, the PBP1a structure maintains a well-

preserved TP domain, probably due to the non-covalent interactions responsible for maintaining the tertiary structure of this region of the protein. There is missing electron density for most of the β -hairpin region situated atop the catalytic site between $\alpha 7$ and $\alpha 8$, due to trypsin cleavage and protein flexibility (figure 5.17). For the same reason, the loop connecting $\alpha 14$ to $\beta 12$ is only partially visible. The linker module, connecting the TP and TG domains, and the OB domain are complete and well resolved. On the other hand, the structure entirely lacks the TG domain as a result of proteolysis, as it may be more susceptible to cleavage (5.16b, 5.17).

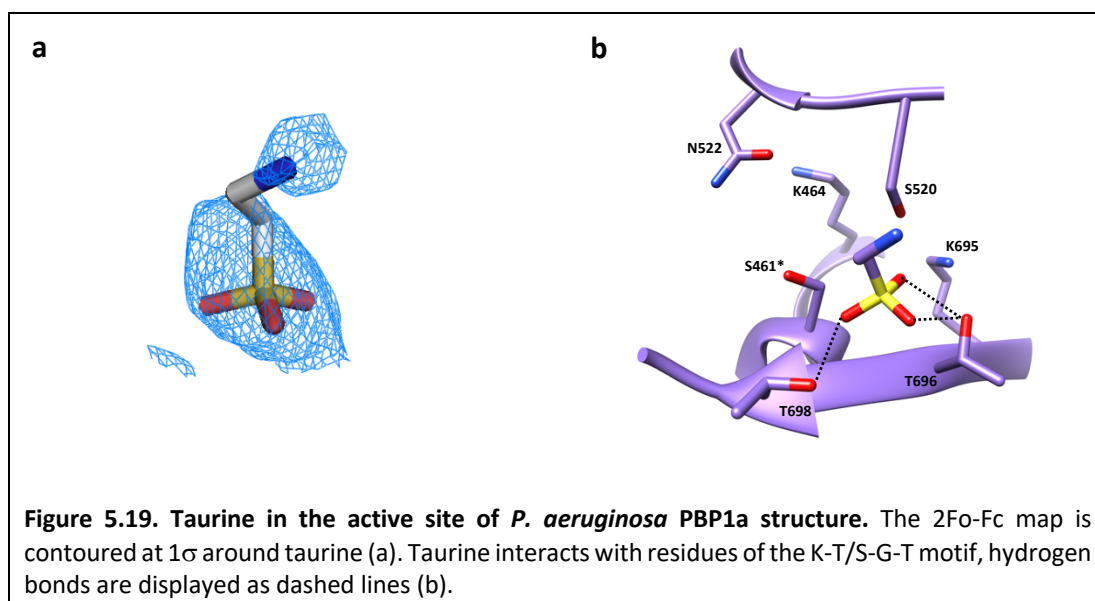
5.5.4.2.1 The transpeptidase domain

The transpeptidase domain (aa. 292-792) presents the typical fold of PBPs and serine- β lactamases. The catalytic serine (Ser461) is located deep at the centre of a groove which is formed by the pairing of two subdomains. The α -subdomain contains helices $\alpha 7$ - $\alpha 13$ and forms one side of the groove, whereas the α/β subdomain includes a five-antiparallel stranded β -sheet surrounded by helices $\alpha 3$, $\alpha 14$ - $\alpha 16$, and forms the opposite wall.

All the classical TP signature motifs are present: S-X-X-K (Ser461-Ser462-Phe463-Lys464), K-T/S-G-T (Lys695-Thr696-Gly697-Thr698) and S-X-N/D (Ser520-Arg521-Asn522). The middle residue of the S-X-N/D motif (i.e., Arg521) is expected to form a conserved hydrogen bond with Asp503, as shown in the structure of *A. baumannii* PBP1a (3UDF.pdb). However, the loop bearing Asp503 analogous to the β -hairpin region in the structure of *A. baumannii* PBP2 (3.5.3.2), is not visible. Strands $\beta 13$ and $\beta 14$ are connected by a loop that is much shorter in PBP1a (and class A HMW-PBPs), than class B HMW-PBPs, as already mentioned in 3.5.1.2. On the other hand, the C-terminal region of PBP1a could be mostly modelled, and this consists of a long loop running along the side of the TP domain, followed by two antiparallel strands $\beta 16$ and $\beta 17$, that resides atop $\alpha 14$ (figure 5.17).

The TP active site of the PBP1a structure showed an extra electron density consistent with a non-covalent binder, and was attributed to taurine, an additive present in the

crystallisation condition (figure 5.19a). Taurine occupies the carboxylate pocket of the active site, where its sulfonic moiety establishes interactions with the K-T/S-G-T motif, similar to the carboxylate group of penicillins (see PBP2: mecillinam in 4.2.1.3.2) or the sulfamate group in DBOs (see PBP2: avibactam and PBP2:zidebactam in 4.3.1.3.2 and 4.3.2.3.2) (figure 5.19b).



5.5.4.2.2 Additional domains

The structure of PBP1a possesses an interdomain linker composed of five antiparallel β -strands and two perpendicular α -helices. The linker domain superimposes well with its counterpart in homologue structures (see structures of *A. baumannii* PBP1a, *H. influenzae* PBP1a and *E. coli* PBP1b) (figure 5.17).

An additional domain is present in PBP1a and it is termed OB (oligonucleotide/oligosaccharide binding)-fold domain (figure 5.17). This domain, first reported in the structure of *A. baumannii* PBP1a (Han *et al.*, 2011), is a distinctive feature of subclass A1- PBPs. The OB domain is globular and consists of a five-stranded β -barrel core flanked by helices α 4- α 6, and it is inserted in the TP domain between α 3 and β 9. The OB domain interacts with the C-terminal domain of LpoA *in-vivo*, and this interaction is known to modulate the enzymatic activities of PBP1a (Typas *et al.*, 2010). In contrast, PBP1b displays a different domain called UB2H,

inserted between the linker and the TG domains (Sung *et al.*, 2009), which is recognised by the PBP1b regulator LpoB (Egan *et al.*, 2014).

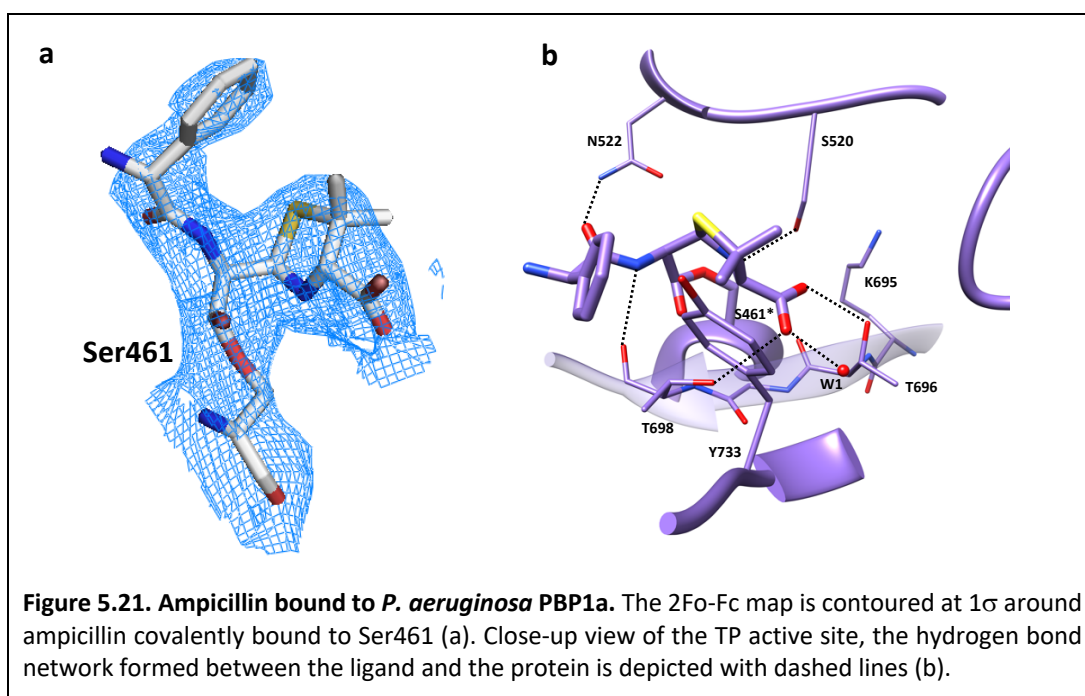
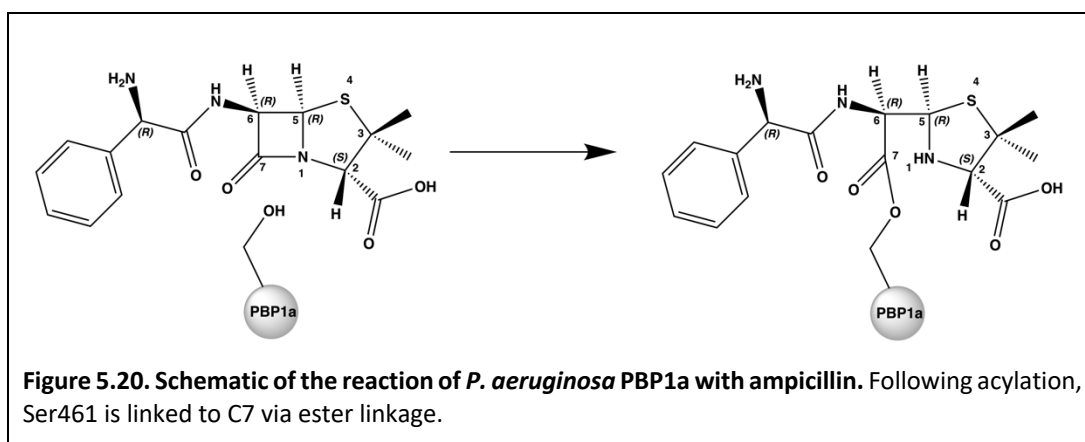
5.5.4.3 Structure of PBP1a bound to ampicillin

An X-ray structure of *P. aeruginosa* PBP1a in complex with ampicillin was determined in this work (table 5.9). There was clear electron density corresponding to ampicillin and its acyl-ester linkage to the catalytic Ser461 (figure 5.21a), consistent with the formation of a covalent adduct as observed in the MS experiments, occurring through the same acylation mechanism typical of β -lactam antibiotics (figure 5.20). The acyl-linkage carbonyl oxygen of ampicillin was directed into the oxyanion hole formed by the backbone nitrogen atoms of Ser461 and Thr698. The five-membered thiazolidine ring nitrogen atom of the drug was within hydrogen bonding distance of the Ser520 hydroxyl group, while its carboxylate moiety established typical hydrogen bonding interactions with the K-T/S-G-T motif. The ampicillin R chain extended towards the entrance of the pocket, where its amide group hydrogen bonded to the Asn522 side chain carboxamide and the Thr698 backbone carbonyl group. Tyr733 phenyl ring was engaged in van der Waals interactions with the ampicillin benzyl group and the thiazolidine *gem*-dimethyl group (figure 5.21b).

An X-ray structure of PBP1a in complex with ceftazidime was also determined at 3.3 Å resolution, from crystals grown in condition 3 (5.5.3) (data not shown). Electron density corresponding to the ligand was partial and visible only for the ester-linkage formed between Ser461-O γ and the C8 carbonyl, and the 6-membered dihydrothiazine ring of the cephalosporin (figure 5.14). Electron density for the bulky aminothiazole containing side chain at C7 position was absent, as well as for the pyridine leaving group.

The structure PBP1a^{400N} shows the binding mode of a sideromimic-conjugated lactivicin analogue bearing the ceftazidime side chain attached to the cycloserine ring (Starr *et al.*, 2014), where this side chain is modelled and interacts with residues at the entrance of the pocket. Therefore, it is possible that the reason why the

ceftazidime side chain at C7 could not be modelled here, is because of the poor quality of the PBP1a dataset collected in this work rather than ligand flexibility.



5.6 Structural studies of *P. aeruginosa* PBP3 with ampicillin polymers

5.6.1 X-ray structure of *P. aeruginosa* PBP3 bound to ampicillin dimer

Due to unsuccessful trials in generating structures of *P. aeruginosa* PBP1a in complex with ampicillin oligomers, structural studies of *P. aeruginosa* PBP3 were undertaken in order to elucidate the binding mode of these molecules. PBP3 was chosen because

it is an essential protein of the divisome complex in *P. aeruginosa*, it is easy to crystallise and the crystals can diffract at resolution $<2 \text{ \AA}$, thus allowing accurate modelling of the protein-ligand complex (Bellini *et al.*, 2019). The periplasmic domain of PBP3(Δ 50-579)(figure S5) was expressed, purified and crystallised in 25 % (w/v) PEG3350, 0.1 M Bis-Tris propane pH 7.8 and 1 % (w/v) protamine sulphate, at room temperature by Dr Dom Bellini (Bellini *et al.*, 2019). PBP3 crystals were soaked for 20 min in mother liquor supplemented with 20 % glycerol and either 13 mM ampicillin dimer or 9 mM ampicillin trimer, prior to flash-cooling in liquid nitrogen. Datasets were collected at the I03 beam line (Diamond Light Source, UK) and were processed with Dials (Winter *et al.*, 2018). Models were phased by molecular replacement using MrBump (Keegan and Winn, 2008). Manual building and ligand fitting were performed in Coot (Emsley and Cowtan, 2004), and the structures refined with Refmac5 (Murshudov *et al.*, 2011; Bellini *et al.*, 2019). The X-ray structures of *P. aeruginosa* PBP3 bound to ampicillin dimer (1.67 \AA resolution) (table 5.11) and ampicillin trimer (1.87 \AA resolution) were determined by Dr Dom Bellini, in this work.

PBP3 is a class B PBP, and its structure is reminiscent of that of *A. baumannii* PBP2 solved in this work. The overall structure is elongated and consists of a non-catalytic domain at the N-terminus and a transpeptidase domain at the C-terminus (figure 5.23a). The structures of *P. aeruginosa* PBP3 determined here reveal the presence of the ampicillin oligomer covalently attached to the catalytic Ser294. As expected, the catalytic residue is acylated by the carbonyl group of the intact β -lactam ring situated at the C-terminal of the polymer, indicative of a reaction that follows the same acylating mechanisms of ampicillin monomer (figure 5.22). In the structure of PBP3: ampicillin dimer, there is full electron density for both ampicillin units of the ligand, thus allowing complete modelling of the dimer (figure 5.23b). In the structure of PBP3: ampicillin trimer, there is electron density corresponding to the C-terminal acylating ampicillin and the middle-ampicillin units, whereas electron density is missing for the N-terminal ampicillin unit extending towards the bulk solvent. The structure of PBP3: trimer is virtually identical to that of PBP3: dimer, and does not provide additional information on the conformational state of the last ampicillin unit, possibly due to flexibility and lack of strong interactions with residues at the mouth

of the active site. For these reasons, only the PBP3: dimer structure will be discussed in this chapter.

<i>P. aeruginosa</i> PBP3: ampicillin dimer			
Data collection		Refinement	
Space group	P2 ₁ 2 ₁ 2 ₁	Resolution (Å)	60.56- 1.67
Cell dimensions		No. reflections	56372
a, b, c (Å)	68.39, 82.71, 88.91	<i>R</i> _{work} / <i>R</i> _{free}	0.21/ 0.25
α, β, γ (°)	90, 90, 90	No. atoms	
Resolution (Å)	60.60-4.53 (1.70-1.67)	Protein	3865
<i>R</i> _{meas}	0.028 (0.795)	Water	133
<i>I</i> / <i>σ</i> <i>I</i>	56.7 (1.8)	Other	48
CC (1/2)	1 (0.5)	B-factors (Å ²)	
Completeness (%)	100 (100)	Protein	40
Multiplicity	8.1 (5.5)	Water	33
No. of reflections	25843 (16023)	Other	34
No. of unique reflections	3204 (2933)	R.m.s. deviations	
		Bond lengths (Å)	0.01
		Bond angles (°)	1.75
		Favoured/ allowed/ disallowed (%)	97.6%/2.2%/ 0.2%

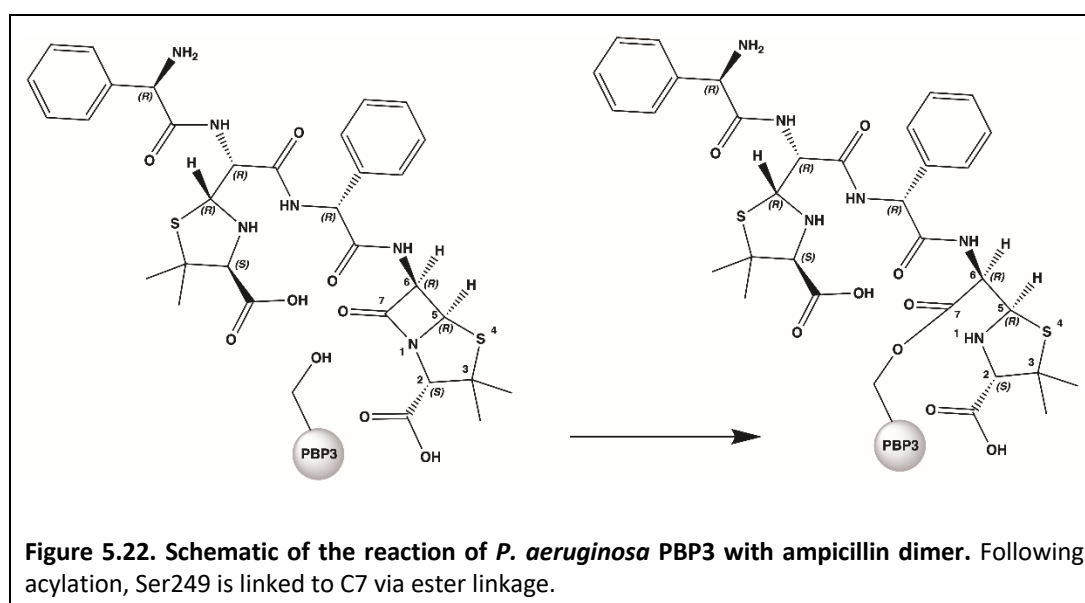
Table 5.11. Data collection and refinement statistics for *P. aeruginosa* PBP3 bound to ampicillin dimer. The highest resolution shell is shown in parenthesis.

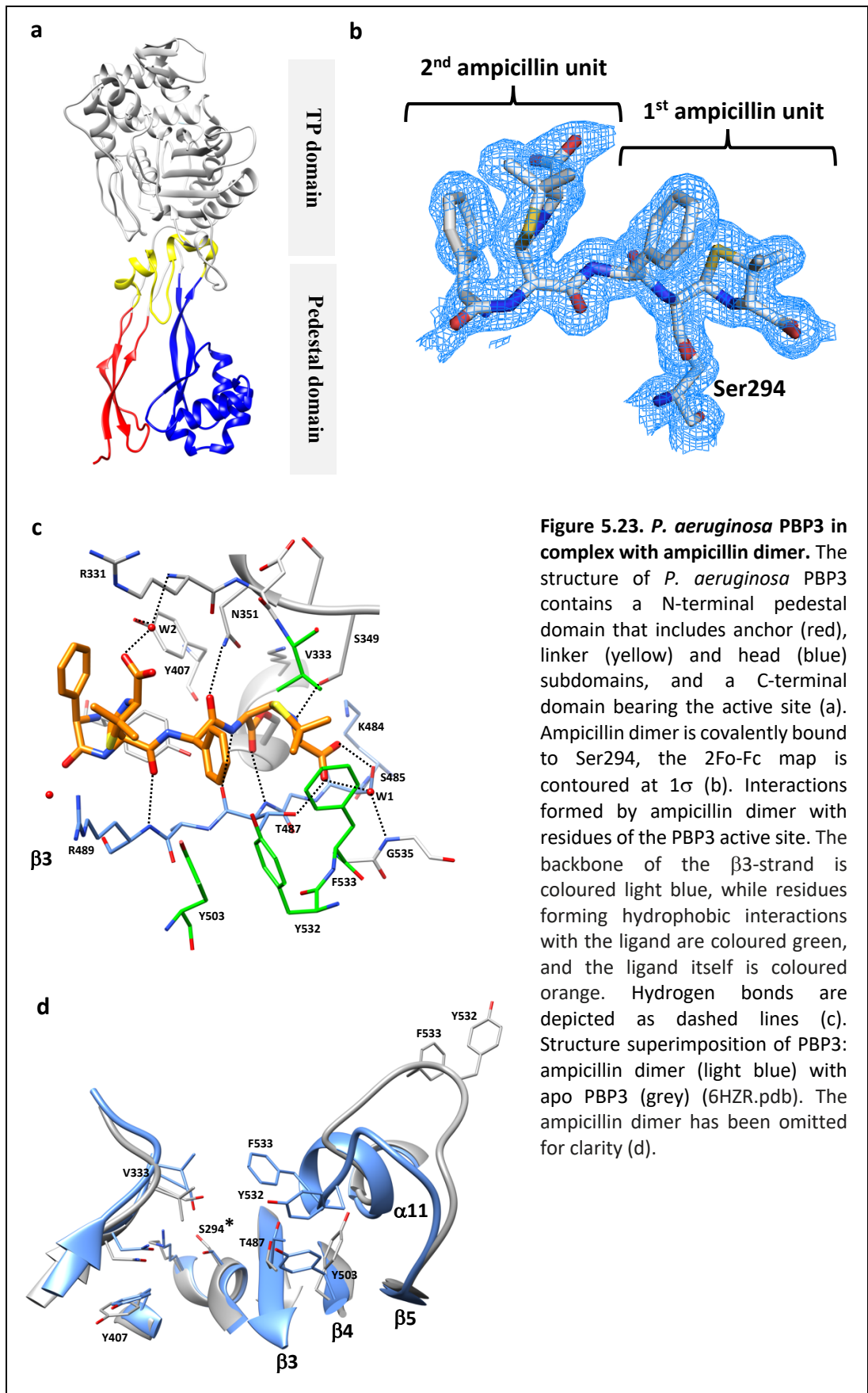
The binding mode of the acylating ampicillin unit of the dimer within the TP active site of PBP3, is analogous to that of ampicillin monomer liganded to PBP1a (figure 5.21b). For convenience, the atoms of the C-terminal and N-terminal ampicillin units will be marked with single and double quotation marks, respectively, to make the description easier. The carbonyl oxygen of the ester bond between Ser294-O γ and C7' of the C-terminal ampicillin is located into the oxyanion hole and forms typical hydrogen bonds with the main chain amide nitrogens of Ser294 and Thr487 (figure 5.23c). The thiazolidine N1' hydrogen bonds to Ser349 hydroxyl group, whereas the C2' carboxylate is anchored to the site by hydrogen bonds with Ser485 and Thr487 hydroxyl groups. The carboxylate moiety also hydrogen bonds with the Gly535 main chain amide nitrogen, through an intervening water molecule (W1, figure 5.23c). The amide bond at C6', is wedged between the Asn351 side chain and the Thr487 carbonyl backbone.

Condensation of the first ampicillin unit to the second one, extends the ligand towards the mouth of the active site where additional interactions are possible. The

C7'' carbonyl group hydrogen bonds to the Arg489 main chain amide nitrogen, in actual fact expanding the hydrogen bonding network between the KSGT peptide backbone and the ampicillin dimer peptide backbone, generating a short antiparallel β -sheet type of interaction. The amide nitrogen attached to C6'' is close to Arg489 main chain carbonyl but not within hydrogen bonding distance. Additional interactions involving the second ampicillin unit include water-mediated hydrogen bonds between the C2'' carboxylate with the Tyr407 hydroxyl group, and the Arg331 main chain amide nitrogen (W2, figure 5.23c).

Binding of the ampicillin dimer is accompanied by notable conformational adjustments in the PBP3 active site, analogous to the binding of other β -lactams to *P. aeruginosa* PBP3 (Han *et al.*, 2010; Murphy-Benenato *et al.*, 2015; Starr *et al.*, 2014). The conformational changes affect mostly the loop connecting β_5 to α_{11} , that is displaced from its position in the apo structure (outward conformation) towards the core of the catalytic pocket (inward conformation) (figure 5.23d). This structural rearrangement results in the formation of an aromatic wall, composed of Tyr532 and Phe533 from the β_5 - α_{11} loop together with Tyr503 from the adjacent β_4 strand, that accommodates the bulky *gem*-dimethyl group on C3' and the benzyl ring from the first ampicillin unit, thus providing stabilising van der Waals interactions (figure 5.23c).





A hydrophobic bridge is also formed by the approach of Phe533 to Val333, that further stabilises the *gem*-dimethyl group and the thiazolidine ring of the first ampicillin unit. The C-terminal end of the β 3-strand shifts by approximately 4 Å upward, presumably to facilitate the backbone-to-backbone interactions with the peptidic ligand and to reduce the steric hindrance at the active site entrance. Additional adjustments include the reorientation of the side chains of K297 and S349, and of S249 for the formation of the ester bond. The β 3- β 4 loop is not visible, possibly due to flexibility and lack of interactions with the ligand.

5.7 MIC testing of ampicillin oligomers

Mass spectrometry and X-ray crystallography showed that, like ampicillin monomer, ampicillin dimer and trimer were able to acylate essential and non-essential PBPs from various Gram-negative bacteria. The antibacterial activities of ampicillin and ampicillin oligomers were explored in MIC testing, using laboratory reference strains of clinically important Gram-positive and Gram-negative bacteria, including ESKAPE pathogens (table 5.12) (2.8). When testing the wild-type strains, the ampicillin oligomers were at least 16-fold less active than traditional ampicillin and had MIC values in the high sub-micromolar range.

A possible reason for the attenuated antimicrobial activity of the ampicillin polymers was the low permeability of the outer membrane in Gram-negative bacteria. To test this hypothesis, strains of *E. coli* and *P. aeruginosa* engineered to express a mutant of FhuA (a passive diffusion channel to allow transport of large hydrophilic molecules) (Braun *et al.*, 2002) and deleted for TolC (an outer membrane efflux protein important for drug detoxification) (Augustus *et al.*, 2004) were used. Both ampicillin dimer and trimer became at least 8-fold more active in the *E. coli* FhuA TolC- strain, while only the dimer gained significant activity in the *P. aeruginosa* FhuA TolC- strain. Moreover, some of the strains used were β -lactamase producers such as *K. pneumoniae* ATCC 700603 (ESBL- SHV-18), *E. cloacae* NCTC 13405 (AmpC) and *A. baumannii* NCTC 13420 (MDR clinical isolate carbapenem-resistant), which could also account for the observed resistant phenotypes against ampicillin and its

polymers. Another strain used was *S. typhimurium* ATCC 19585, this was susceptible to ampicillin but resistant to the polymers possibly because of reduced drug penetration.

The Gram-positive strains *S. aureus* ATCC 29213 and *E. faecalis* ATCC 29212 were also more susceptible to ampicillin than the polymers, possibly because the negative charge of the ampicillin polymers compared to the zwitterionic form of ampicillin could reduce the interaction with the Gram-positive cell surface, which is rich in anionic polymers (Silhavy *et al.*, 2010).

Organism	MIC ($\mu\text{g/mL}$)		
	ampicillin	dimer	trimer
Gram-positive			
<i>S. aureus</i> ATCC 29213	1	64	32
<i>E. faecalis</i> ATCC 29212	2	32	>256
Gram-negative			
<i>E. coli</i> ATCC 25922	4	128	>256
<i>E. coli</i> FhuA TolC-	4	2	32
<i>P. aeruginosa</i> PAO1	>256	256	>256
<i>P. aeruginosa</i> FhuA TolC-	128	16	256
<i>K. pneumoniae</i> ATCC 700603	>256	>256	>256
<i>A. baumannii</i> NCTC 13420	>256	>256	>256
<i>E. cloacae</i> NCTC 13405	>256	256	>256
<i>S. typhimurium</i> ATCC 19585	2	128	>256

Table 5.12. Antimicrobial activity of ampicillin and ampicillin polymers against a panel of Gram-positive and Gram-negative bacteria. MIC values are from either a single or a duplicate test.

5.8 NMR studies of ampicillin oligomers

β -lactamases (BLs) are an important mechanism of resistance developed by bacteria to rapidly inactivate β -lactam antibiotics, thus protecting them from cell death. To overcome β -lactamase-mediated resistance, labile β -lactam antibiotics are used with β -lactamase inhibitors (BLIs), although the rapid expansion and evolution of the β -lactamase family has represented a constant threat to the efficacy of these combinations, and BLIs covering all β -lactamase classes have been difficult to develop (Bush and Bradford, 2016). BLIs do not typically possess antimicrobial

activity, although a few exceptions exist where both PBP and BL inhibition is achieved (for instance sulbactam and the new DBO class reviewed in the introduction and chapter 4).

So far, little has been accomplished in the discovery of PBP- targeting molecules that are immune to the activity of β -lactamases, one of the reasons being the structural similarity of the active sites and the conservation of the reaction mechanisms. In the effort to identify such molecules, the ampicillin oligomers were investigated in NMR analysis in order to determine the resistance/susceptibility to hydrolytic attack by β -lactamases. Three representative and clinically important β -lactamase enzymes were tested, namely NDM-1 (class-B), AmpC (class-C), and OXA-23 (class-D), kindly provided by the Schofield group (Department of chemistry, University of Oxford). ^1H NMR spectra were collected (2.7) for the molecules, before and after addition of the β -lactamases to study the impact of the latter on the former. Spectra analysis was focused in the range 1.5-1 ppm to monitor the peaks corresponding to the *gem*-dimethyl group (figures 5.24 and 5.25). A shift in the position of these peaks after addition of the enzyme, was an indication of β -lactam hydrolysis. These experiments were performed in collaboration with Dr Chris Lohans (previously at University of Oxford).

Ampicillin monomer possesses two methyl groups at C3, which are detected as two peaks at approximately 1.4 and 1.35 ppm. Addition of either NDM-1 or AmpC caused the loss of these signals and appearance of two new peaks at lower ppm, consistent with hydrolysis of the molecule by β -lactamase activity (Lohans *et al.*, 2019)(figure 5.24a). Ampicillin dimer and trimer have two and three *gem*-dimethyl groups, which generated four and six peaks in the range 1.4-1.05 ppm, respectively (5.24b-c). These molecules were trialled with AmpC, NDM-1 and OXA-23, and in all cases β -lactam hydrolysis was detected (5.24a-c).

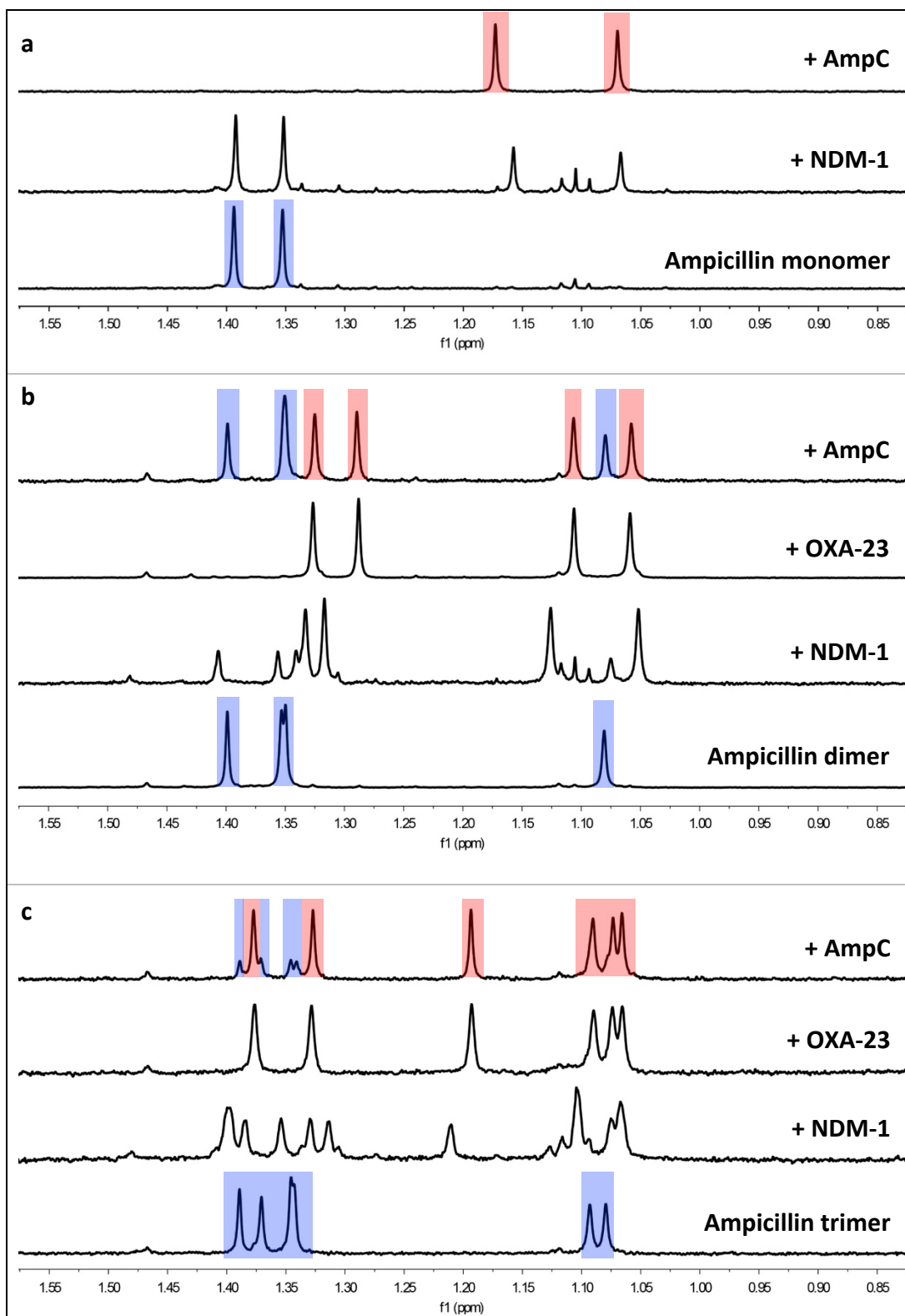
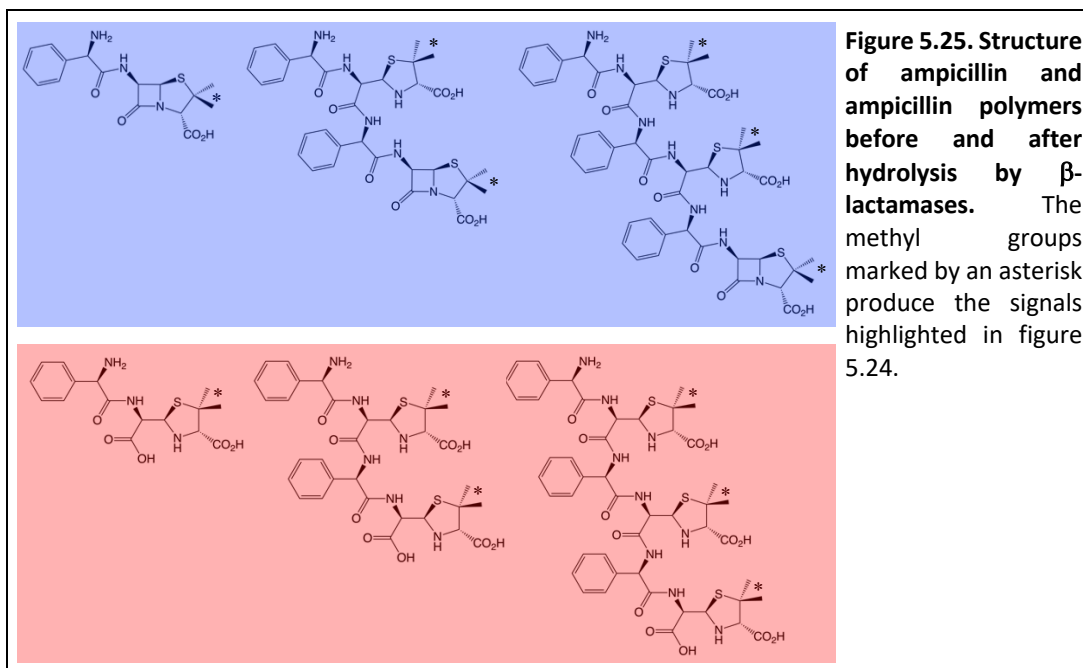
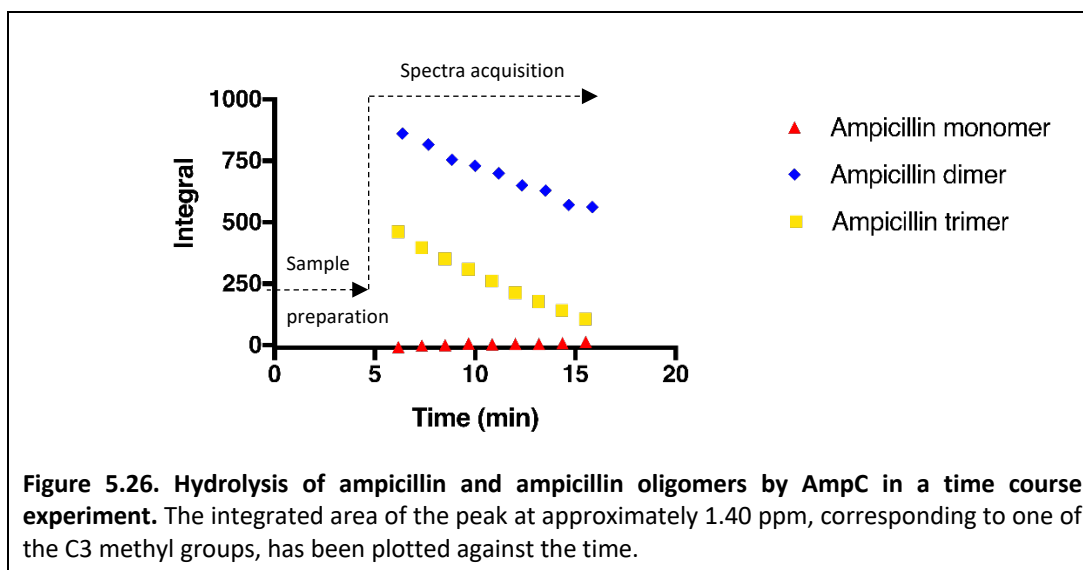


Figure 5.24. Reaction of ampicillin and its oligomers with β -lactamases. $^1\text{H-NMR}$ spectra showing the methyl group resonances of the molecules ampicillin (a), ampicillin dimer (b), and ampicillin trimer (c) before and after addition of the enzymes. Peaks corresponding to the methyl group in the unhydrolysed and hydrolysed molecules are highlighted in purple and red, respectively, in selected spectra (structure of these molecules are shown in figure 5.25). All enzymes were used at $5\ \mu\text{M}$ (2.7), except in the assay of ampicillin trimer with NDM-1 ($5\ \text{nM}$).



The results shown in the $^1\text{H-NMR}$ spectra provided qualitative information on the susceptibility of the test molecules to AmpC/NDM-1/OXA-23 hydrolysis, as they corresponded to different time points of the β -lactamase assays, thus comparative discussion of the relative activity of the β -lactamases towards ampicillin and ampicillin polymers would not be meaningful.

As ampicillin dimer and trimer were found not to be resistant to β -lactamase hydrolysis, the next question to address was whether or not the oligomers were hydrolysed at different rates compared to ampicillin monomer. To investigate this, the test molecules were analysed in a time course experiment with AmpC at the same experimental conditions (2.7) (figure S16-S18). $^1\text{H-NMR}$ spectra were collected at regular intervals, and the area of a selected methyl group peak was integrated and plotted against time (figure 5.26). Notably, at the start of the spectra acquisition (which was delayed by approximately 5 min due to sample preparation), ampicillin monomer was fully hydrolysed. Conversely, some unhydrolysed ampicillin dimer and trimer was still present, and the hydrolysis reaction with the dimer seemed to be the slowest one.



5.9 Discussion and future work

Penicillin degradation products have been the subject of intense studies in the past, beginning from the 1960s, with regard to elicitation of immune responses in patient treated with β -lactam antibiotics. The presence of anti-penicilloyl antibodies in penicillin treated patients has been reported in several studies (Lafaye and Lapresle, 1988a, Adkinson Jr, 1984), as well as the covalent binding of penicilloyl groups to albumin (Lafaye and Lapresle, 1988b; Bertucci *et al.*, 2001; DiPiro *et al.*, 1993; Yvon *et al.*, 1990). Polymerisation by aminolysis of aminopenicillins, such as ampicillin, reduces the concentration of active molecule in solution. Ampicillin polymers have been shown to possess strong antigenic properties in animals (Dewdney *et al.*, 1971; Smith *et al.*, 1971; Ahlstedt *et al.*, 1976), therefore, they could play a part in eliciting penicilloyl-specific allergic reactions in humans. It is therefore important to prevent the formation of polymers in clinically used ampicillin medications, a factor that needs to be taken into account during development and storage of the drug. For instance, it has been shown that β -cyclodextrin can inhibit polymerisation of ampicillin in aqueous solution, possibly via inclusion complexation (Aki *et al.*, 1990). The formation of ampicillin polymers occurs when ampicillin is dissolved in aqueous solution, and is ongoing upon storage at room temperature (Dewdney *et al.*, 1971; Larsen and Bundgaard, 1978). The rate of polymerisation has been reported to be

dependent upon pH and initial concentration of the ampicillin solution (Robinson-Fuentes *et al.*, 1997).

In this work, the polymerisation of ampicillin was investigated in different conditions of temperature and ampicillin concentration. In agreement with previous reports (Grant *et al.*, 1962; Larsen and Bundgaard, 1978), the formation of polymers was observed when storing highly concentrated ampicillin solutions at room temperature, and the rate of polymerisation increased when the concentration of ampicillin stock solution was increased (20 % w/v versus 50 % w/v). However, other molecular species were also detected and consistent with the formation of degradation products caused by hydrolysis of the β -lactam ring and subsequent decarboxylation (Robinson-Fuentes *et al.*, 1997). Temperature significantly affected the rate of ampicillin polymer formation, as storage at -20°C greatly suppressed the appearance of high-molecular weight polymers during the course of the experiment.

The ampicillin polymers were studied with respect to their ability to acylate Gram-negative PBPs from prominent ESKAPE pathogens, such as *P. aeruginosa*, *A. baumannii* and *E. coli*. Since the binding properties of ampicillin polymers have been poorly investigated so far, it was of great interest to elucidate the molecular details of the interaction with PBPs, and the potential secondary structure conformations adopted by the polymers, arising from the presence of a peptide backbone.

The covalent binding of ampicillin polymers (up to the hexamer) to the catalytic serine of various PBPs, was observed by mass spectrometry, and the existence of secondary binding sites for ampicillin was excluded. A similar observation was reported by Steiner *et al.* (2017) in which the binding of 6-APA dimer to Ldt_{Mt2} (L,D-transpeptidase from *M. tuberculosis*) was detected by MS, although the authors attributed the formation of the dimer to a possible transpeptidation reaction occurring in the active site between 6-APA molecules, without a mention of the potential formation of the dimerised 6-APA by aminolysis in solution. In this work, the formation of ampicillin polymers and mixed penicillin G/ampicillin polymers was shown to occur in solution.

After the binding of ampicillin polymers to PBPs was ascertained, a detailed analysis of the covalent adducts formed by ampicillin and ampicillin oligomers at the enzyme transpeptidase active site was pursued by X-ray crystallography. Attempts to replicate the published crystallisation conditions for structures of *P. aeruginosa* PBP1a were unsuccessful. However, new crystallisation conditions were screened, and *P. aeruginosa* PBP1a crystals diffracting in the resolution range 3-3.3 Å were generated. Crystals were flash-cooled in liquid nitrogen without addition of cryoprotectant, as only few crystals appeared in the crystallisation drops after more than a month, and this raised the suspicion of them being salt crystals. In case they were protein crystals, it was decided to prevent crystal damage caused by the use of an inappropriate cryoprotective agent, although radiation damage was unavoidable. Therefore, it is likely that better quality diffraction data could have been generated from the PBP1a crystals, had the selection of cryoprotectant been explored. Several attempts were made afterwards to optimise the crystallisation conditions or at least, reproduce the same diffracting crystals, but they were unsuccessful. This could be due to small variations in protein preparation, and the requirement for a critical trypsin digestion step that did not produce a homogeneous sample, as observed in SDS-PAGE and MS analysis, therefore complicating the crystallisation process. Furthermore, the PBP1a crystals were generated at room temperature over the summer, and seasonal fluctuations of the temperature in the storage room due to poor temperature control, could be another explanation for the low reproducibility of the crystals.

From the *P. aeruginosa* PBP1a crystals, structures of the protein covalently bound to ampicillin and without antibiotic were obtained. The R_{free} value of the models is considerably higher compared to the R_{work} (table 5.9), due to the low resolution of the datasets and the incomplete refinement of the structures, that was focused mainly in the active site region. Further refinement and validation work will be required prior to structure deposition. Consistent with the PBP1a structure already in PDB (4OON.pdb), PBP1a crystallised as an ensemble of four polypeptides that held together despite the tryptic cleavage, and maintained the domains (TP, OB and linker) in the correct folding. MS analysis allowed the localisation of the sites used by

trypsin in the cleavage of the protein and resulting in multiple peptides as seen in SDS-PAGE.

Unexpectedly, a taurine molecule was found in the active site of *P. aeruginosa* PBP1a, this molecule being present in the crystallisation solution. Taurine bound non-covalently to the carboxylate sub-pocket of the active site, highlighting the strong interaction that can occur between this side of the pocket and ligands bearing well positioned negatively charged groups. In the past, a few PBPs were accidentally co-crystallised with small non-covalent binders found in the TP active site, and these were present in the crystallisation condition. Examples include citrate in a structure of a beta-lactamase/D-alanine carboxypeptidase from *Yersinia pestis* (3RJU.pdb), tartrate in a structure of *Listeria monocytogenes* PBP4 (3ZG7.pdb), and CHES in a structure of PBP3 from *Legionella pneumophila* (4ZTK.pdb) (Jeong *et al.*, 2013). These molecules, together with taurine could represent a potential fragment-based starting point for the design of non-covalent PBP inhibitors, and it would be interesting to determine if taurine had an effect on PBP1a activity.

The structure of *P. aeruginosa* PBP1a in complex with ampicillin monomer, did not show particularly significant conformational rearrangements occurring upon ligand binding, and the ampicillin binding mode was consistent with that of other analogues, such as penicillin G crystallised in complex with *A. baumannii* PBP1a (3UDI.pdb).

Penicillin binding protein 3 is an essential protein for the viability of *P. aeruginosa*, hence an excellent target for the discovery of new antibiotics. Novel structures of *P. aeruginosa* PBP3 in complex with short ampicillin polymers (ampicillin dimer and trimer) were generated at high-resolution (<2 Å), elucidating for the first time the binding mode of these type of molecules. While a second ampicillin unit provided additional interactions with the protein, electron density was absent for the third unit in the trimer, suggesting that there were no strong interactions occurring with residues outside the catalytic pocket. The region around the entrance of the active site has been poorly targeted so far, possibly due to the fact that this is solvent

exposed and rich in loops, which makes it more difficult to exploit for the design of new ligands.

The ampicillin oligomers possess a peptide backbone, and β -sheet-like interactions occurred between this and the β 3-strand including the KSGT motif of PBP3. Although, secondary structure conformations were not observed for ampicillin dimer and trimer within the TP site, these cannot be excluded for longer polymers such as the pentamer and the hexamer found covalently bound to PBPs in MS experiments. X-ray structures of PBPs with the high-molecular weight ampicillin polymers ($n > 3$) would be useful in detecting possible ligand conformational arrangements and possible interactions outside the TP pocket, that could inform new strategies for the targeting of PBPs.

The antimicrobial activity of ampicillin and the dimer and trimer polymers was also explored in this work. The poor activity of the polymers compared to the ampicillin monomer could be ascribed to the physicochemical properties of these molecules. To start with, the ampicillin monomer has a net charge of zero whereas the ampicillin oligomers have a net negative charge at physiological pH, as during aminolysis the primary amine group of the attacking molecule is lost, resulting in ampicillin oligomers (with n units) having n carboxylic groups and only one primary amine. The outer- membrane of Gram-negative bacteria is notoriously negatively charged, due to the presence of molecules such as LPS (Silhavy *et al.*, 2010), which would hinder the passage of the ampicillin oligomers. The polymers displayed better activity against Gram-positive bacteria such as *S. aureus* and *E. faecalis*, possibly due to the lack of an outer- membrane.

Another reason for the poor antimicrobial activity of the polymers could be their high-molecular weight, that would likely exclude transport across the membranes by passive diffusion, and possibly other transport mechanisms. The gain in antimicrobial activity obtained in engineered *E. coli* and *P. aeruginosa* strains for improved membrane permeabilization, would be consistent with this hypothesis. Since the 1960s, only isolated and discordant antimicrobial activities of β -lactam polymers have been reported, although, due to the limitations of the chromatographic

separation techniques used to purify the polymers from the aged β -lactam solutions, it is likely that a mixture of molecules rather than singly purified polymers were tested (Batchelor *et al.*, 1962; Smith and Marshall, 1971).

The poor antibacterial activity of the polymers compared to ampicillin monomer, could also arise from a different PBP binding profile of the oligomers, for instance preferential binding to non-essential PBPs, and/or poor binding affinity to the essential PBPs. Although, the MS experiments have shown that the ampicillin polymers can acylate PBPs possibly leading to enzyme inhibition, which would be responsible for the observed *in-vivo* activities, data regarding the kinetics of binding are currently lacking. Importantly, it would be useful to know the inhibitory potency of the ampicillin polymers against PBPs, to understand whether or not the presence of extra ampicillin units in the molecule would offer an advantage compared to ampicillin monomer. It would be ideal to generate IC₅₀ data (the concentration that inhibits 50 % of the enzymatic activity) of ampicillin and its polymers in an enzymatic assay that can measure in real-time the transpeptidase and carboxypeptidase activity of HMW-PBPs, by using the natural substrate Lipid II, to resemble the *in-vivo* situation as closely as possible.

In this respect, such an assay has been developed at the University of Warwick by Dr Adrian Lloyd (Catherwood *et al.*, 2020) to study the enzymatic activities of *E. coli* PBP1b. The assay has shown applicability for the study of a range of HMW-PBPs from Gram-positive and Gram-negative bacteria (unpublished data), by using the appropriate Lipid II substrates. The assay could be optimised also for use with *P. aeruginosa* PBP1a and PBP3, to study the inhibitory activities of ampicillin and its polymers, that would complement the structural biology studies. In this regard some preliminary experiments on *P. aeruginosa* PBP1a were started during the PhD (data not shown), confirming the transpeptidase and carboxypeptidase activities of the enzyme following the protocol described by Catherwood *et al.* (2020), and work remains ongoing.

Another type of assay that could be used to compare the binding potency of ampicillin and ampicillin polymers, is the nitrocefin competition assay. This assay can be used with PBPs that present a relatively high β -lactamase activity towards the chromogenic β -lactam nitrocefin, allowing the spectrophotometric measurement of turnover rate. Nitrocefin could be used in a competition assay with ampicillin and ampicillin polymers to determine the IC_{50} (in this assay it indicates the concentration of test compound that reduces by 50 % the nitrocefin turnover rate), from which the binding potency of these molecules could be inferred.

The nitrocefin competition assay is cost-effective to run, however, it is considered a simplistic method to look at the potency of a test molecule, because it is not based on competition with the polymerised natural substrate lipid II. The same limitations apply to the bocillin-FL assay, a competition assay with the fluorescently labelled bocillin, widely used to generate IC_{50} values (in this assay it refers to the concentration of test compound that reduces by 50 % the binding of bocillin) for different PBP inhibitors. Therefore, caution should be taken when comparing data from β -lactam competition assays with others, including antimicrobial activity data.

Finally, the potential β -lactamase resistance of the ampicillin polymers was evaluated in NMR assays. The ampicillin dimer and trimer were susceptible to hydrolysis by different β -lactamases (i. e. AmpC, NDM-1 and OXA-23), although the polymers were hydrolysed at slower rate compared to ampicillin monomer, at least by AmpC. This result would suggest that, the addition of extra ampicillin units in the molecule could potentially interfere with the rapid binding of the enzyme to the polymers, possibly due to a hindrance effect caused by the high-molecular weight of these molecules. This might be relevant to the design of antibiotics that are more stable to β -lactamase activity and therefore more likely to be effective in inhibiting the proliferation of antibiotic resistant pathogens.

CHAPTER 6

Discussion

6.1 Discussion

Penicillin binding proteins are a class of enzymes exclusive to bacteria, that catalyse a variety of reactions in the synthesis and remodelling of peptidoglycan, among others, the transpeptidation reaction between nascent glycan chains and pre-existing PG chains of the bacterial cell wall (Sauvage *et al.*, 2008; Typas *et al.*, 2012). Due to the essential role played by this reaction in bacterial cell wall growth during elongation and division, transpeptidation is considered a prime target in the therapeutic treatment of bacterial infections. In this regard, the antimicrobial activity of β -lactam antibiotics is attributed to their ability to irreversibly block the synthesis of new PG, by targeting the transpeptidase active site of essential PBPs (Kong *et al.*, 2010). β -lactam antibiotics have a long track record as first choice drugs in the treatment of patients affected by different types of bacterial infections, owing to the excellent clinical efficacy and safety (Demain and Elander, 1999). However, the longstanding clinical use of these antimicrobial agents has been hindered by the emergence of mechanisms of antibiotic resistance, particularly drug inactivation by β -lactamases (Bush, 2018). This, in addition to the lack of success in developing new classes of antibiotics in the last 30 years, has increased the threat to human health posed by multi-drug resistance infections, for which less and less effective therapeutic treatments are left.

Since the introduction of penicillin and elucidation of its mode of action, research on the bacterial cell wall has been focused on two aspects. The first is the discovery of new antibiotics targeting PBPs, leading to the development of a range of β -lactam inhibitors (Bush and Bradford, 2016) and exploration of new scaffolds as potential new classes of PBP inhibitors, such as DBOs (Papp-Wallace *et al.*, 2018). Also, new therapeutic treatments have been designed to overcome specific mechanisms of antimicrobial resistance, including combinations of β -lactams with other antibiotics such as β -lactams, aminoglycosides, fluoroquinolones and macrolides (Rahme *et al.*, 2014; Vazquez *et al.*, 2005; Bliziotis *et al.*, 2005; Al-Hasan *et al.*, 2009), and with β -lactam adjuvants such as β -lactamase inhibitors (Bush and Bradford, 2016).

A second aspect in this perspective is the understanding of the PBP functions and regulations *in-vivo*, and the spatial and temporal coordination of these enzymatic activities with other proteins of the PG synthase machineries (Typas *et al.*, 2012) which may lead to novel intervention opportunities and strategies.

P. aeruginosa and *A. baumannii* are two pathogens with increasing resistance rates to last-line antibiotics such as carbapenems, and for which new and effective antibiotic treatments are urgently needed. In these bacteria, PBP1a, PBP2 and PBP3 were investigated by crystallographic and biophysical techniques to provide insight into the structures and interaction of these proteins with molecules containing β -lactam and DBO scaffolds, that could be useful to guide the rational design of new PBP-targeting molecules. Additionally, *in-vivo* experiments were performed to probe the importance of specific PBP2 structural elements for the bacterial cell wall elongation function in *A. baumannii*, that could help towards deconvoluting the precise role played by specific PBP2 structural features in the activity of the elongasome machinery.

X-ray crystallographic structures of *P. aeruginosa* PBP1a and PBP3, both previously reported (Bellini *et al.*, 2019; Starr *et al.*, 2014), were solved in complex with ampicillin and ampicillin polymers, respectively. These structures confirmed the mechanism of enzyme inactivation to be equivalent to that of other β -lactam compounds, that is acylation of the PBP catalytic serine by the intact β -lactam ring of ampicillin and ampicillin dimer and trimer. While the binding mode of ampicillin to *P. aeruginosa* PBP1a was comparable to that seen in other HMW-PBP structures, such as *E. coli* PBP1b (King *et al.*, 2017b), the molecular details of the interaction of ampicillin polymers with PBPs were unknown and were elucidated in structures of *P. aeruginosa* PBP3 bound to ampicillin dimer and trimer, in this work. Interestingly, the ampicillin dimer could form a short double-stranded antiparallel β -sheet with the protein backbone encompassing the KSGT motif, owing to the presence of a peptide backbone in the ampicillin polymers, whereas the extra ampicillin unit in the trimer

could not be modelled possibly indicating the lack of interactions with the protein, outside the active site.

Ampicillin polymers could be formed by aminolysis, and this reaction was accelerated when concentrated aqueous solutions of ampicillin were left at room temperature, compared to when stored at -20 °C. Moreover, mass spectrometry experiments showed that, binding of ampicillin polymers to PBPs was not exclusive to *P. aeruginosa* PBP3. In fact, different HMW-PBPs from different Gram-negative pathogens could be covalently modified by the ampicillin polymers, mostly likely through acylation of the catalytic serine as seen in structures of *P. aeruginosa* PBP3 in complex with ampicillin dimer and trimer.

Differently from ampicillin, ampicillin dimer and trimer showed poor antimicrobial activity against a panel of Gram-positive and Gram-negative bacteria. This suggested that, despite their ability to acylate PBPs *in-vitro*, the ampicillin polymers may not have the right physicochemical properties to permeate the cell envelope, and therefore inactivate PBPs *in-vivo*. Conversely, the ampicillin polymers seemed to be more resistant to hydrolysis by the β -lactamase AmpC, than ampicillin monomer in NMR experiments. This suggested that a bulky substituent linked to the intact β -lactam ring, such as the additional ampicillin units in the ampicillin polymers, could impair the binding of β -lactams to this enzyme.

Since the ampicillin polymers have a peptide backbone, it would be interesting to further investigate whether binding to PBPs is retained, once these polymers are hydrolysed by β -lactamases, as this structural information could also be used in the design of new non- β -lactam inhibitors of PBPs. Interestingly, a few hydrolysed β -lactam antibiotics have been crystallised in the active site of *P. aeruginosa* PBP3, suggesting that the targeting of PBPs by non-covalent inhibitors could be possible, thus circumventing the β -lactamase-mediated resistance (Ren *et al.*, 2016, van Berkel *et al.*, 2013).

The first three-dimensional structure of PBP2 from *A. baumannii* was generated in this work and revealed, besides the classical pedestal and transpeptidase domain organisation of bPBPs, the presence of an unexpected zinc-binding site located

nearby the TP active site. The metal coordination site appeared to fulfil a structural rather than catalytic role, by tethering the β -hairpin loop to the SCD motif of PBP2. Structural comparisons with other HMW-PBPs showed that this structural rearrangement was conserved across bacteria, and varied in the form of physical interaction taking place between residues of the β -hairpin region and the middle residue of the SXN/D motif (i.e., H-bonding, salt bridge and disulphide bond).

Disruption of the zinc coordination site, by either chemical treatment with EDTA or insertion of mutations that would hamper the tetrahedral coordination of the metal, greatly reduced the thermostability of the protein in DSF experiments. Moreover, the functionality of the elongasome machinery in *A. baumannii* ATCC17978 was compromised in *in-vivo* experiments, when alanine scanning mutagenesis of the PBP2 residues coordinating the zinc was performed (D350A, D365A, H371A and C384A), as indicated by the rod-to-sphere morphological change.

An equivalent zinc-binding site could also be present in other PBPs of Gram-positive and Gram-negative bacteria, based on sequence alignments. One of these candidates is *B. subtilis* SpoVD, and preliminary work was carried out on its wild-type and mutant C332D version, to test for the presence of a metal-coordination site.

Taken together, the *in-vitro* and *in-vivo* data pointed to a critical role played by the proper folding of the β -hairpin region in the TP domain of PBP2, for cell wall elongation in *A. baumannii*. The β -hairpin loop tethered to the SXN/D motif could play an active role in the conformational changes that support the processivity and catalytic activity of PBP2, due to its vicinity to the catalytic centre, or being a structural element required for the interaction with other proteins of the elongasome machinery. Moreover, this structural feature is conserved across HMW-PBPs of different bacteria, hence it could be a common requirement for the proper activity of the elongasome and divisome in various bacteria.

Based on the mere presence of a zinc-binding site in the TP domain of *A. baumannii* PBP2 that is essential for cell wall elongation, it could be speculated that a zinc-dependent regulation of the elongasome activity might exist in this bacteria. It is not

yet known, whether the PBP2 zinc-binding site is an absolute requirement for the activity of the elongasome in *A. baumannii*, and to address this question, surrogates of the zinc-binding site could be analysed in cell morphological and antibiotic susceptibility assays. For instance, the zinc-binding site could be replaced by a hydrogen bonding interaction (Asp-Ser) by mutating Cys384 to Ser, that in turn could form an H-bond with Asp365 (Asp365-Cys384Ser) as observed in the structure of *P. aeruginosa* PBP3. Also, the zinc-coordination could be replaced by a disulphide bond, as is the case for *M. tuberculosis* PBPA, by mutating His371 to Cys in order to allow a potential disulphide bond to form (His371Cys-Cys384). Irrespective of the mutations introduced, the loss of zinc-coordination would have to be confirmed by experimental analysis such as ICP-MS, as the zinc coordination could still be preserved, particularly in the His371Cys mutant where cysteine is a frequent residue in zinc-binding sites.

Another structural detail was noted in *A. baumannii* PBP2, that is the presence of aspartate in place of asparagine in the third position of the conserved S-X-N/D motif, within the transpeptidase active site. This amino acid substitution is common to PBP2 proteins of elongated Gram-negative bacteria, and as yet, it is not well understood the significance of such substitution. Surprisingly, *in-vivo* experiments performed in this work suggested that, an Asp to Asn mutation in the SCD motif of *A. baumannii* PBP2 (D385N) would not support proper cell wall elongation in this bacteria. Therefore, an aspartate would be critically required in the S-X-N/D motif of PBP2 for the correct functioning of the elongasome, in *A. baumannii* and possibly other Gram-negative bacteria where this aspartate is conserved. In light of these data, the variation of the third residue in the S-X-N/D motif of PBPs could be critical for the catalytic activity of these enzymes, a detail that may have been overlooked in the past years of research on PBPs, and that now certainly deserve further attention.

The new X-ray crystallographic structure of *A. baumannii* PBP2 determined in this work, made it possible to understand the molecular details of the PBP2 interactions with clinically relevant drugs from the β -lactam (mecillinam and meropenem) and

DBO (avibactam and zidebactam) classes. Two types of protein-ligand interactions were notable in particular, as they seemed to be a distinctive feature of PBP2, and therefore could be taken into account in the synthesis of new PBP2 selective compounds. One of these is the salt bridge between the mecillinam amidine linker and the Asp385, the other is the hydrophobic interaction between Trp366 and the thiazolidine and pyrroline rings of the β -lactams, and the piperidine ring of DBOs. The importance of such interactions for the potency of mecillinam, meropenem, avibactam and zidebactam towards PBP2, could be tested in complementary studies where wild-type and mutated PBP2 proteins (D385N and W366/F/V/A) could be used in competition *in-vitro* assays, such as the Bocillin-FL binding assay (Zhao *et al.*, 1999). Interestingly, when the wild-type PBP2 was analysed in DSF experiments with a range of β -lactam antibiotics and DBOs, a reasonable consistency could be found between the magnitude of thermal shifts and the potency of the compounds tested.

Non β -lactam molecules that selectively target PBP2, are currently being pursued as β -lactam enhancers, to be used in combination with β -lactam antibiotics that potently inhibit other HMW-PBPs, as part of a multitarget therapeutic strategy.

To aid the discovery of new PBP2-selective molecules with β -lactam enhancing activity, the structure of *A. baumannii* PBP2 determined in this work could be used in a range of crystallographic and computational approaches.

i) Crystals of *A. baumannii* PBP2 diffracted at good resolution and were amenable for soaking experiments, therefore could be used in the structural aided drug design (SADD) of new PBP2 inhibitors. In this respect, the structure of PBP2 could be aligned with structure-activity relationship (SAR) studies, where it could help rationalise the impact of different chemical modifications of the active scaffold, on the inhibitory activity of the molecule (Hughes *et al.*, 2011).

As an example, the recently published X-ray crystallographic structure of *E. coli* PBP2 was used with SAR studies of the DBO scaffold, to rationally design CPD4, a potent PBP2 inhibitor (IC_{50} = 0.01 μ M) and antimicrobial agent with an MIC of 0.016 μ g/mL and 2 μ g/mL against *E. coli* and *P. aeruginosa*,

respectively (Levy *et al.*, 2019). Moreover, structural studies of *P. aeruginosa* PBP3 allowed to get further insight into the SAR trends of triazolone-based siderophore-conjugated monocarbams, highly potent antipseudomonal agents but with suboptimal physicochemical properties for clinical use (Murphy-Benenato *et al.*, 2015).

- ii) The discovery of novel chemotypes targeting PBP2 could be aided by a fragment screening. This approach consists of screening low molecular weight molecules (< 250 Da) by using biophysical methods such as NMR, SPR and X-ray crystallography. This screening could provide fragment hits which could be further developed into larger molecules so as to increase ligand potency and target selectivity (Lamoree and Hubbard, 2018). Crystals of *A. baumannii* PBP2 could be used in the high-throughput screening of fragment collections (typically ranging from hundreds to a few thousands) by using X-ray crystallography as the primary screening method, with fragment libraries selective for covalent or non-covalent binders, or both (Hartshorn *et al.*, 2005). As an alternative, the structure of PBP2 could be used in the validation of the fragment hits identified by other methods, and in the process of fragment progression to lead compound.

Fragment-based approaches have been successfully applied in the discovery of novel inhibitors of bacterial proteins relevant in AMR, such as β -lactamases (Eidam *et al.*, 2012) DNA gyrase and the cell division protein FtsZ (Haydon *et al.*, 2008; Lamoree and Hubbard, 2018).

- iii) Potential novel hit compounds that bind to PBP2 could be found in structure-based high-throughput virtual screening programs, where compounds from large virtual chemical libraries (thousands to millions) could be docked into the active site of *A. baumannii* PBP2 (Cheng *et al.*, 2012). In this work it was found that, *A. baumannii* PBP2 did not undergo significant structural rearrangements upon binding of β -lactam (mecillinam and meropenem) and DBO (avibactam and zidebactam) compounds. From a drug-design perspective this is an advantage given that, virtual screening experiments would require only a single PBP2 structure rather than multiple structures of the same protein in different conformations, and the rational optimisation of

the molecule binding affinity would be straightforward. To increase screening efficiency and minimize the computational time required by the virtual screening, so as to accelerate the hit identification, the large size of compound libraries could be reduced by excluding *a priori* molecules displaying unwanted chemical groups, for example the β -lactam ring if chemical novelty is sought, and using a pharmacophore model (Yang, 2010). Since the co-structures of *A. baumannii* PBP2 in complex with β -lactams and DBOs revealed noteworthy interactions involving Asp385 and Trp366, a pharmacophore model inclusive of chemical functionalities that preserve the interactions with these residues would be reasonable.

A similar approach where ligand-based pharmacophore modelling and docking-based virtual screening were combined, led to the discovery of novel non-covalent chemical scaffolds (aminothiadiazole and *ortho*-phenoxydiphenylurea) targeting PBP2x from the resistant *S. pneumoniae* 5204 strain (Miguet *et al.*, 2009).

Whatever drug-discovery approach is embraced by scientists to find new PBP2-selective inhibitors, it is of critical importance that the physicochemical profile of antibacterial active compounds is taken into consideration, both in high-throughput screening projects and hit-to-lead optimisation phases, as poor drug penetration into bacteria is a common challenge in antimicrobial drug discovery (O'Shea and Moser, 2008; Richter *et al.*, 2017).

Bibliography

- ABRAHAM, E. P. & CHAIN, E. 1940. An enzyme from bacteria able to destroy penicillin. *Nature*, 146, 837.
- ADKINSON JR, N. F. 1984. Risk factors for drug allergy. *Journal of Allergy and Clinical Immunology*, 74, 567-572.
- AHLSTEDT, S., KRISTOFFERSSON, A., SVÄRD, P.-O., THOR, L. & ÖRTENGREN, B. 1976. Ampicillin polymers as elicitors of passive cutaneous anaphylaxis. *International Archives of Allergy and Immunology*, 51, 131-139.
- AKI, H., YAMAMOTO, K., SAWAI, N. & YAMAMOTO, M. 1990. Inhibitory effect of beta-cyclodextrin on ampicillin polymerization in aqueous solution. *Drug Design and Delivery*, 7, 59-63.
- AL-HASAN, M. N., WILSON, J. W., LAHR, B. D., THOMSEN, K. M., ECKEL-PASSOW, J. E., VETTER, E. A., TLEYJEH, I. M. & BADDOUR, L. M. 2009. Beta-lactam and fluoroquinolone combination antibiotic therapy for bacteremia caused by gram-negative *bacilli*. *Antimicrobial Agents and Chemotherapy*, 53, 1386-1394.
- ALEXEEVA, S., GADELLA JR, T. W., VERHEUL, J., VERHOEVEN, G. S. & DEN BLAAUWEN, T. 2010. Direct interactions of early and late assembling division proteins in *Escherichia coli* cells resolved by FRET. *Molecular Microbiology*, 77, 384-398.
- ALM, R. A., JOHNSTONE, M. R. & LAHIRI, S. D. 2015. Characterization of *Escherichia coli* NDM isolates with decreased susceptibility to aztreonam/avibactam: role of a novel insertion in PBP3. *Journal of Antimicrobial Chemotherapy*, 70, 1420-1428.
- AMBLER, R. P. 1980. The structure of β -lactamases. *Philosophical Transactions of the Royal Society of London. B, Biological Sciences*, 289, 321-331.
- APPELBAUM, P. C. 2012. 2012 and beyond: potential for the start of a second pre-antibiotic era? *Journal of Antimicrobial Chemotherapy*, 67, 2062-2068.
- ASLAM, B., WANG, W., ARSHAD, M. I., KHURSHID, M., MUZAMMIL, S., RASOOL, M. H., NISAR, M. A., ALVI, R. F., ASLAM, M. A., QAMAR, M. U., SALAMAT, M. K. F. & BALOCH, Z. 2018. Antibiotic resistance: a rundown of a global crisis. *Infectious Drug Resistance*, 11, 1645-1658.
- ASLI, A., BROUILLETTE, E., KRAUSE, K. M., NICHOLS, W. W. & MALOUIN, F. 2016. Distinctive binding of avibactam to penicillin-binding proteins of Gram-negative and Gram-positive bacteria. *Antimicrobial Agents and Chemotherapy*, 60, 752-756.
- AUGUSTUS, A. M., CELAYA, T., HUSAIN, F., HUMBAR, M. & MISRA, R. 2004. Antibiotic-sensitive TolC mutants and their suppressors. *Journal of Bacteriology*, 186, 1851-1860.
- AUTA, A., HADI, M. A., OGA, E., ADEWUYI, E. O., ABDU-AGUYE, S. N., ADELOYE, D., STRICKLAND-HODGE, B. & MORGAN, D. J. 2019. Global access to antibiotics without prescription in community pharmacies: A systematic review and meta-analysis. *Journal of Infection*, 78, 8-18.
- AVDIC, E. 2017. Mecillinam (Amdinocillin) and Pivmecillinam. *Kucers' The Use of Antibiotics: A Clinical Review of Antibacterial, Antifungal, Antiparasitic, and Antiviral Drugs, Volume 1*, CRC Press, 208.
- AZEVEDO, F., PEREIRA, H. & JOHANSSON, B. 2017. Colony PCR. *PCR*. Springer.

- BALTZER, B., LUND, F. & RASTRUP-ANDERSEN, N. 1979. Degradation of mecillinam in aqueous solution. *Journal of Pharmaceutical Sciences*, 68, 1207-1215.
- BANZHAF, M., VAN DEN BERG VAN SAPAROE, B., TERRAK, M., FRAIPONT, C., EGAN, A., PHILIPPE, J., ZAPUN, A., BREUKINK, E., NGUYEN-DISTÈCHE, M. & DEN BLAAUWEN, T. 2012. Cooperativity of peptidoglycan synthases active in bacterial cell elongation. *Molecular Microbiology*, 85, 179-194.
- BARON, S. 1996. *Mycoplasmas--Medical Microbiology*, University of Texas Medical Branch at Galveston.
- BARRETT, D., WANG, T.-S. A., YUAN, Y., ZHANG, Y., KAHNE, D. & WALKER, S. 2007. Analysis of glycan polymers produced by peptidoglycan glycosyltransferases. *Journal of Biological Chemistry*, 282, 31964-31971.
- BARRETEAU, H., KOVAČ, A., BONIFACE, A., SOVA, M., GOBEC, S. & BLANOT, D. 2008. Cytoplasmic steps of peptidoglycan biosynthesis. *FEMS Microbiology Reviews*, 32, 168-207.
- BARTLETT, J. G., GILBERT, D. N. & SPELLBERG, B. 2013. Seven ways to preserve the miracle of antibiotics. *Clinical Infectious Disease*, 56, 1445-50.
- BATCHELOR, F., COLE, M., GAZZARD, D. & ROLINSON, G. 1962. Penicillin-like substances in preparations of 6-aminopenicillanic acid. *Nature*, 195, 954.
- BATTYE, T. G. G., KONTOGIANNIS, L., JOHNSON, O., POWELL, H. R. & LESLIE, A. G. 2011. iMOSFLM: a new graphical interface for diffraction-image processing with MOSFLM. *Acta Crystallographica Section D: Biological Crystallography*, 67, 271-281.
- BEADLE, B. M., NICHOLAS, R. A. & SHOICHET, B. K. 2001. Interaction energies between β -lactam antibiotics and *E. coli* penicillin-binding protein 5 by reversible thermal denaturation. *Protein Science*, 10, 1254-1259.
- BEADLE, B. M., TREHAN, I., FOCIA, P. J. & SHOICHET, B. K. 2002. Structural milestones in the reaction pathway of an amide hydrolase: substrate, acyl, and product complexes of cephalothin with AmpC β -lactamase. *Structure*, 10, 413-424.
- BELLINI, D., KOEKEMOER, L., NEWMAN, H. & DOWSON, C. G. 2019. Novel and Improved Crystal Structures of *H. influenzae*, *E. coli* and *P. aeruginosa* Penicillin-Binding Protein 3 (PBP3) and *N. gonorrhoeae* PBP2: Toward a Better Understanding of β -Lactam Target-Mediated Resistance. *Journal of Molecular Biology*, 431, 3501-3519
- BERG, K. H., STRAUME, D. & HÅVARSTEIN, L. S. 2014. The function of the transmembrane and cytoplasmic domains of pneumococcal penicillin-binding proteins 2x and 2b extends beyond that of simple anchoring devices. *Microbiology*, 160, 1585-1598.
- BERN, M., CAVAL, T., KIL, Y. J., TANG, W., BECKER, C., CARLSON, E., KLETTER, D., SEN, K. I., GALY, N. & HAGEMANS, D. 2018. Parsimonious charge deconvolution for native mass spectrometry. *Journal of Proteome Research*, 17, 1216-1226.
- BERTUCCI, C., BARSOTTI, M. C., RAFFAELLI, A. & SALVADORI, P. 2001. Binding properties of human albumin modified by covalent binding of penicillin. *Biochimica et Biophysica Acta (BBA)-Protein Structure and Molecular Enzymology*, 1544, 386-392.
- BHAGWAT, S., PERIASAMY, H., TAKALKAR, S., PALWE, S., KHANDE, H. & PATEL, M. 2019. The Novel β -Lactam Enhancer Zidebactam Augments the In Vivo Pharmacodynamic Activity of Cefepime in a Neutropenic Mouse Lung

- Acinetobacter baumannii* Infection Model. *Antimicrobial Agents and Chemotherapy*, 63, e02146-18.
- BHAVNANI, D., PHATINAWIN, L., CHANTRA, S., OLSEN, S. J. & SIMMERMAN, J. M. 2007. The influence of rapid influenza diagnostic testing on antibiotic prescribing patterns in rural Thailand. *International Journal of Infectious Diseases*, 11, 355-359.
- BLANC, E., ROVERSI, P., VONRHEIN, C., FLENSBURG, C., LEA, S. & BRICOGNE, G. 2004. Refinement of severely incomplete structures with maximum likelihood in BUSTER–TNT. *Acta Crystallographica Section D: Biological Crystallography*, 60, 2210-2221.
- BLIZIOTIS, I. A., SAMONIS, G., VARDAKAS, K. Z., CHRYSANTHOPOULOU, S. & FALAGAS, M. E. 2005. Effect of Aminoglycoside and β -Lactam Combination Therapy versus β -Lactam Monotherapy on the Emergence of Antimicrobial Resistance: A Meta-analysis of Randomized, Controlled Trials. *Clinical Infectious Diseases*, 41, 149-158.
- BLUMENTHAL, K. G., PETER, J. G., TRUBIANO, J. A. & PHILLIPS, E. J. 2018. Antibiotic allergy. *The Lancet*.
- BOLLA, J. R., SAUER, J. B., WU, D., MEHMOOD, S., ALLISON, T. M. & ROBINSON, C. V. 2018. Direct observation of the influence of cardiolipin and antibiotics on lipid II binding to MurJ. *Nature Chemistry*, 10, 363.
- BONNEFOY, A., DUPUIS-HAMELIN, C., STEIER, V., DELACHAUME, C., SEYS, C., STACHYRA, T., FAIRLEY, M., GUITTON, M. & LAMPILAS, M. 2004. In vitro activity of AVE1330A, an innovative broad-spectrum non- β -lactam β -lactamase inhibitor. *Journal of Antimicrobial Chemotherapy*, 54, 410-417.
- BONOMO, R. A. 2017. β -Lactamases: A Focus on Current Challenges. *Cold Spring Harbor Perspectives in Medicine*, 7, a025239.
- BORCK HØG, B., KORSGAARD, H. B., WOLFF SÖNKSEN, U., BAGER, F., BORTOLAIA, V., ELLIS-IVERSEN, J., HENDRIKSEN, R. S., JENSEN L. B., VOROBIEVA, V. (2017). DANMAP 2016 - Use of antimicrobial agents and occurrence of antimicrobial resistance in bacteria from food animals, food and humans in Denmark. Statens Serum Institut, National Veterinary Institute, Technical University of Denmark National Food Institute, Technical University of Denmark. ISSN 1600-2032.
- BOUHSS, A., TRUNKFIELD, A. E., BUGG, T. D. & MENGIN-LECREULX, D. 2007. The biosynthesis of peptidoglycan lipid-linked intermediates. *FEMS Microbiology reviews*, 32, 208-233.
- BRAUN, M., KILLMANN, H., MAIER, E., BENZ, R. & BRAUN, V. 2002. Diffusion through channel derivatives of the *Escherichia coli* FhuA transport protein. *European Journal of Biochemistry*, 269, 4948-4959.
- BRÖTZ-OESTERHELT, H. & SASS, P. 2010. Postgenomic strategies in antibacterial drug discovery. *Future Microbiology*, 5, 1553-1579.
- BRUSSOW, H. 2017. Adjuncts and alternatives in the time of antibiotic resistance and in-feed antibiotic bans. *Microbial Biotechnology*, 10, 674-677.
- BUDD, A., BLANDIN, S., LEVASHINA, E. A. & GIBSON, T. J. 2004. Bacterial α 2-macroglobulins: colonization factors acquired by horizontal gene transfer from the metazoan genome? *Genome Biology*, 5, R38.

- BUKOWSKA-FANIBAND, E. & HEDERSTEDT, L. 2017. Transpeptidase activity of penicillin-binding protein S po VD in peptidoglycan synthesis conditionally depends on the disulfide reductase S to A. *Molecular Microbiology*, 105, 98-114.
- BULITTA, J., SHAN, J., MOYA, B., SUTARIA, D., BOYCE, J., BONOMO, R. A., LANDERSDORFER, C., VELKOV, T. 2018. First comprehensive penicillin-binding protein (PBP) occupancy patterns of beta-lactams in *Acinetobacter baumannii* (AB). Poster presented at: 28th ECCMID conference; 2018 April 21-24; Madrid, Spain.
- BULYCHEV, A. & MOBASHERY, S. 1999. Class C β -lactamases operate at the diffusion limit for turnover of their preferred cephalosporin substrates. *Antimicrobial Agents and Chemotherapy*, 43, 1743-1746.
- BUSH, K. 2013a. The ABCD's of β -lactamase nomenclature. *Journal of Infection and Chemotherapy*, 19, 549-559.
- BUSH, K. 2013b. Proliferation and significance of clinically relevant β -lactamases. *Annals of the New York Academy of Sciences*, 1277, 84-90.
- BUSH, K. 2018. Past and present perspectives on β -lactamases. *Antimicrobial Agents and Chemotherapy*, 62, e01076-18.
- BUSH, K. & BRADFORD, P. A. 2016. β -Lactams and β -lactamase inhibitors: an overview. *Cold Spring Harbor Perspectives in Medicine*, 6, a025247.
- CALIENDO, A. M., GILBERT, D. N., GINOCCHIO, C. C., HANSON, K. E., MAY, L., QUINN, T. C., TENOVER, F. C., ALLAND, D., BLASCHKE, A. J., BONOMO, R. A., CARROLL, K. C., FERRARO, M. J., HIRSCHHORN, L. R., JOSEPH, W. P., KARCHMER, T., MACINTYRE, A. T., RELLER, L. B., JACKSON, A. F. & INFECTIOUS DISEASES SOCIETY OF AMERICA. 2013. Better tests, better care: improved diagnostics for infectious diseases. *Clinical Infectious Diseases*, 57 Suppl 3, S139-70.
- CALVEZ, P., BREUKINK, E., ROPER, D. I., DIB, M., CONTRERAS-MARTEL, C. & ZAPUN, A. 2017. Substitutions in PBP2b from β -Lactam-resistant *Streptococcus pneumoniae* Have Different Effects on Enzymatic Activity and Drug Reactivity. *Journal of Biological Chemistry*, 292, 2854-2865.
- CARAPITO, R., CHESNEL, L., VERNET, T. & ZAPUN, A. 2006. Pneumococcal β -lactam resistance due to a conformational change in penicillin-binding protein 2x. *Journal of Biological Chemistry*, 281, 1771-1777.
- CASTANHEIRA, M., SADER, H. S., FARRELL, D. J., MENDES, R. E. & JONES, R. N. 2012. Activity of ceftaroline-avibactam tested against Gram-negative organism populations, including strains expressing one or more β -lactamases and methicillin-resistant *Staphylococcus aureus* carrying various staphylococcal cassette chromosome mec types. *Antimicrobial Agents and Chemotherapy*, 56, 4779-4785.
- CASTANON, J. 2007. History of the use of antibiotic as growth promoters in European poultry feeds. *Poultry Science*, 86, 2466-2471.
- CATHERWOOD, A. C., LLOYD, A. J., TOD, J. A., CHAUHAN, S., SLADE, S. E., WALKOWIAK, G. P., GALLEY, N. F., PUNEKAR, A. S., SMART, K., REA, D., ROPER, D. I. & DOWSON, C. G. 2020. Substrate and Stereochemical Control of Peptidoglycan Cross-Linking by Transpeptidation by *Escherichia coli* PBP1B. *Journal of the American Chemical Society*, 142, 5034-5048.

- CAVENEY, N. A., CABALLERO, G., VOEDTS, H., NICIFOROVIC, A., WORRALL, L. J., VUCKOVIC, M., FONVIELLE, M., HUGONNET, J.-E., ARTHUR, M. & STRYNADKA, N. C. J. 2019. Structural insight into YcbB-mediated beta-lactam resistance in *Escherichia coli*. *Nature Communications*, 10, 1849.
- CHEN, Y., ZHANG, W., SHI, Q., HESEK, D., LEE, M., MOBASHERY, S. & SHOICHET, B. K. 2009. Crystal structures of penicillin-binding protein 6 from *Escherichia coli*. *Journal of the American Chemical Society*, 131, 14345-14354.
- CHENG, T., LI, Q., ZHOU, Z., WANG, Y. & BRYANT, S. H. 2012. Structure-based virtual screening for drug discovery: a problem-centric review. *The AAPS Journal*, 14, 133-141.
- CHO, H., UEHARA, T. & BERNHARDT, T. G. 2014. Beta-lactam antibiotics induce a lethal malfunctioning of the bacterial cell wall synthesis machinery. *Cell*, 159, 1300-1311.
- CHO, H., WIVAGG, C. N., KAPOOR, M., BARRY, Z., ROHS, P. D., SUH, H., MARTO, J. A., GARNER, E. C. & BERNHARDT, T. G. 2016. Bacterial cell wall biogenesis is mediated by SEDS and PBP polymerase families functioning semi-autonomously. *Nature Microbiology*, 1, 16172.
- CHOW, C., XU, H. & BLANCHARD, J. S. 2013. Kinetic characterization of hydrolysis of nitrocefin, cefoxitin, and Meropenem by β -lactamase from *Mycobacterium tuberculosis*. *Biochemistry*, 52, 4097-4104.
- CLARK, S. T., SINHA, U., ZHANG, Y., WANG, P. W., DONALDSON, S. L., COBURN, B., WATERS, V. J., YAU, Y. C., TULLIS, D. E. & GUTTMAN, D. S. 2019. Penicillin-binding protein 3 is a common adaptive target among *Pseudomonas aeruginosa* isolates from adult cystic fibrosis patients treated with β -lactams. *International Journal of Antimicrobial Agents*, 53, 620-628.
- COICO, R. 2005. Gram staining. *Current Protocols in Microbiology*, A. 3C. 1-A. 3C. 2.
- COLEMAN, K. 2011. Diazabicyclooctanes (DBOs): a potent new class of non- β -lactam β -lactamase inhibitors. *Current Opinion in Microbiology*, 14, 550-555.
- CONTRERAS-MARTEL, C., AMOROSO, A., WOON, E. C., ZERVOSEN, A., INGLIS, S., MARTINS, A., VERLAINE, O., RYDZIK, A. M., JOB, V. & LUXEN, A. 2011. Structure-guided design of cell wall biosynthesis inhibitors that overcome β -lactam resistance in *Staphylococcus aureus* (MRSA). *ACS Chemical Biology*, 6, 943-951.
- CONTRERAS-MARTEL, C., DAHOUT-GONZALEZ, C., MARTINS, A. D. S., KOTNIK, M. & DESSEN, A. 2009. PBP active site flexibility as the key mechanism for β -lactam resistance in pneumococci. *Journal of Molecular Biology*, 387, 899-909.
- CONTRERAS-MARTEL, C., MARTINS, A., ECOBICHON, C., TRINDADE, D. M., MATTEÍ, P.-J., HICHAM, S., HARDOUIN, P., GHACHI, M. E., BONECA, I. G. & DESSEN, A. 2017. Molecular architecture of the PBP2–MreC core bacterial cell wall synthesis complex. *Nature Communications*, 8, 776.
- CORPORATION, P., DOYLE, K. & MILES, J. 1996. *Protocols and applications guide*, Promega Corporation.
- COSGROVE, S. E. 2006. The relationship between antimicrobial resistance and patient outcomes: mortality, length of hospital stay, and health care costs. *Clinical Infectious Diseases*, 42, S82-S89.

- COWTAN, K. 2006. The Buccaneer software for automated model building. 1. Tracing protein chains. *Acta Crystallographica Section D: Biological Crystallography*, 62, 1002-1011.
- COWTAN, K. 2010. Recent developments in classical density modification. *Acta Crystallographica Section D: Biological Crystallography*, 66, 470-478.
- CURTIS, N., ORR, D., ROSS, G. & BOULTON, M. 1979. Competition of beta-lactam antibiotics for the penicillin-binding proteins of *Pseudomonas aeruginosa*, *Enterobacter cloacae*, *Klebsiella aerogenes*, *Proteus rettgeri*, and *Escherichia coli*: comparison with antibacterial activity and effects upon bacterial morphology. *Antimicrobial Agents and Chemotherapy*, 16, 325-328.
- DABERNAT, H., DELMAS, C., SEGUY, M., PELISSIER, R., FAUCON, G., BENNAMANI, S. & PASQUIER, C. 2002. Diversity of β -lactam resistance-conferring amino acid substitutions in penicillin-binding protein 3 of *Haemophilus influenzae*. *Antimicrobial Agents and Chemotherapy*, 46, 2208-2218.
- DASGUPTA, A., DATTA, P., KUNDU, M. & BASU, J. 2006. The serine/threonine kinase PknB of *Mycobacterium tuberculosis* phosphorylates PBPA, a penicillin-binding protein required for cell division. *Microbiology*, 152, 493-504.
- DAVE, K., PALZKILL, T. & PRATT, R. F. 2013. Neutral β -Lactams Inactivate High Molecular Mass Penicillin-Binding Proteins of Class B1, Including PBP2a of MRSA. *ACS Medicinal Chemistry Letters*, 5, 154-157.
- DAVIES, J. & DAVIES, D. 2010. Origins and evolution of antibiotic resistance. *Microbiology and Molecular Biology Reviews*, 74, 417-433.
- DAVIES, T. A., SHANG, W., BUSH, K. & FLAMM, R. K. 2008. Affinity of doripenem and comparators to penicillin-binding proteins in *Escherichia coli* and *Pseudomonas aeruginosa*. *Antimicrobial Agents and Chemotherapy*, 52, 1510-1512.
- DEMAIN, A. L. & ELANDER, R. P. 1999. The β -lactam antibiotics: past, present, and future. *Antonie Van Leeuwenhoek*, 75, 5-19.
- DENOME, S. A., ELF, P. K., HENDERSON, T. A., NELSON, D. E. & YOUNG, K. D. 1999. *Escherichia coli* mutants lacking all possible combinations of eight penicillin binding proteins: viability, characteristics, and implications for peptidoglycan synthesis. *Journal of Bacteriology*, 181, 3981-3993.
- DESSEN, A., MOUZ, N., GORDON, E., HOPKINS, J. & DIDEBERG, O. 2001. Crystal structure of PBP2x from a highly penicillin-resistant *Streptococcus pneumoniae* clinical isolate a mosaic framework containing 83 mutations. *Journal of Biological Chemistry*, 276, 45106-45112.
- DEWAR, S., REED, L. C. & KOERNER, R. J. 2013. Emerging clinical role of pivmecillinam in the treatment of urinary tract infection in the context of multidrug-resistant bacteria. *Journal of Antimicrobial Chemotherapy*, 69, 303-308.
- DEWDNEY, J. M., SMITH, H. & WHEELER, A. W. 1971. The formation of antigenic polymers in aqueous solutions of β -lactam antibodies. *Immunology*, 21, 517.
- DHILLON, S. 2018. Meropenem/vaborbactam: a review in complicated urinary tract infections. *Drugs*, 78, 1259-1270.
- DI LALLO, G., FAGIOLI, M., BARIONOVI, D., GHELARDINI, P. & PAOLOZZI, L. 2003. Use of a two-hybrid assay to study the assembly of a complex multicomponent protein machinery: bacterial septosome differentiation. *Microbiology*, 149, 3353-3359.

- DIPIRO, J. T., ADKINSON, N. F. & HAMILTON, R. G. 1993. Facilitation of penicillin haptentation to serum proteins. *Antimicrobial Agents and Chemotherapy*, 37, 1463-1467.
- DRAMSI, S., MAGNET, S., DAVISON, S. & ARTHUR, M. 2008. Covalent attachment of proteins to peptidoglycan. *FEMS Microbiology Reviews*, 32, 307-320.
- DRAWZ, S. M. & BONOMO, R. A. 2010. Three decades of β -lactamase inhibitors. *Clinical Microbiology Reviews*, 23, 160-201.
- DU, D., WANG-KAN, X., NEUBERGER, A., VAN VEEN, H. W., POS, K. M., PIDDOCK, L. J. V. & LUISI, B. F. 2018. Multidrug efflux pumps: structure, function and regulation. *Nature Reviews Microbiology*, 16, 523-539.
- DURAND-RÉVILLE, T. F., GULER, S., COMITA-PREVOIR, J., CHEN, B., BIFULCO, N., HUYNH, H., LAHIRI, S., SHAPIRO, A. B., MCLEOD, S. M. & CARTER, N. M. 2017. ETX2514 is a broad-spectrum β -lactamase inhibitor for the treatment of drug-resistant Gram-negative bacteria including *Acinetobacter baumannii*. *Nature microbiology*, 2, 17104.
- DURRANT, J. D. & MCCAMMON, J. A. 2011. Molecular dynamics simulations and drug discovery. *BMC Biology*, 9, 71.
- DYE, N. A., PINCUS, Z., THERIOT, J. A., SHAPIRO, L. & GITAI, Z. 2005. Two independent spiral structures control cell shape in *Caulobacter*. *Proceedings of the National Academy of Sciences*, 102, 18608-13.
- ECDC, 2016. Strategies and action plans on antimicrobial resistance. *European Centre for Disease Prevention and Control*. Accessed September 2019. <https://ecdc.europa.eu/en/publications-data/directory-guidance-prevention-and-control/antimicrobial-resistance-strategies>
- EDGAR, T., BOYD, S. D. & PALAMÉ, M. J. 2008. Sustainability for behaviour change in the fight against antibiotic resistance: a social marketing framework. *Journal of Antimicrobial Chemotherapy*, 63, 230-237.
- EDOO, Z., ARTHUR, M. & HUGONNET, J.-E. 2017. Reversible inactivation of a peptidoglycan transpeptidase by a β -lactam antibiotic mediated by β -lactam ring recyclization in the enzyme active site. *Scientific Reports*, 7, 9136.
- EDWARDS, J., TURNER, P., WANNOP, C., WITHNELL, E., GRINDEY, A. & NAIRN, K. 1989. In vitro antibacterial activity of SM-7338, a carbapenem antibiotic with stability to dehydropeptidase I. *Antimicrobial Agents and Chemotherapy*, 33, 215-222.
- EGAN, A. J., BIBOY, J., VAN'T VEER, I., BREUKINK, E. & VOLLMER, W. 2015. Activities and regulation of peptidoglycan synthases. *Philosophical Transactions of the Royal Society B: Biological Sciences*, 370, 20150031.
- EGAN, A. J., CLEVERLEY, R. M., PETERS, K., LEWIS, R. J. & VOLLMER, W. 2017. Regulation of bacterial cell wall growth. *The FEBS journal*, 284, 851-867.
- EGAN, A. J., JEAN, N. L., KOUMOUTSI, A., BOUGAULT, C. M., BIBOY, J., SASSINE, J., SOLOVYOVA, A. S., BREUKINK, E., TYPAS, A. & VOLLMER, W. 2014. Outer-membrane lipoprotein LpoB spans the periplasm to stimulate the peptidoglycan synthase PBP1B. *Proceedings of the National Academy of Sciences*, 111, 8197-8202.
- EHMANN, D. E., JAHIĆ, H., ROSS, P. L., GU, R.-F., HU, J., KERN, G., WALKUP, G. K. & FISHER, S. L. 2012. Avibactam is a covalent, reversible, non- β -lactam β -

- lactamase inhibitor. *Proceedings of the National Academy of Sciences*, 109, 11663-11668.
- EIDAM, O., ROMAGNOLI, C., DALMASSO, G., BARELIER, S., CASELLI, E., BONNET, R., SHOICHET, B. K. & PRATI, F. 2012. Fragment-guided design of subnanomolar β -lactamase inhibitors active in vivo. *Proceedings of the National Academy of Sciences*, 109, 17448-17453.
- EL GHACHI, M., MATTEI, P. J., ECOBICHON, C., MARTINS, A., HOOS, S., SCHMITT, C., COLLAND, F., EBEL, C., PREVOST, M. C., GABEL, F., ENGLAND, P., DESSEN, A. & BONECA, I. G. 2011. Characterization of the elongasome core PBP2 : MreC complex of *Helicobacter pylori*. *Molecular microbiology*, 82, 68-86.
- EMA. 2018. Zavicefta: summary of product characteristics. *European Medicines Agency*. Accessed Mar 2018. Available at: https://www.ema.europa.eu/en/documents/product-information/zavicefta-epar-product-information_en.pdf
- EMAMI, K., GUYET, A., KAWAI, Y., DEVI, J., WU, L. J., ALLENBY, N., DANIEL, R. A. & ERRINGTON, J. 2017. RodA as the missing glycosyltransferase in *Bacillus subtilis* and antibiotic discovery for the peptidoglycan polymerase pathway. *Nature Microbiology*, 2, 16253.
- EMSLEY, P. & COWTAN, K. 2004. Coot: model-building tools for molecular graphics. *Acta Crystallographica Section D: Biological Crystallography*, 60, 2126-2132.
- EMSLEY, P., LOHKAMP, B., SCOTT, W. G. & COWTAN, K. 2010. Features and development of Coot. *Acta Crystallographica Section D: Biological Crystallography*, 66, 486-501.
- ERRINGTON, J. 2013. L-form bacteria, cell walls and the origins of life. *Open Biology*, 3, 120143.
- ERRINGTON, J., DANIEL, R. A. & SCHEFFERS, D.-J. 2003. Cytokinesis in bacteria. *Microbiol. Mol. Biol. Rev.*, 67, 52-65.
- ERRINGTON, J., DANIEL, R. A. & SCHEFFERS, D.-J. 2003. Cytokinesis in bacteria. *Microbiol. Mol. Biol. Rev.*, 67, 52-65.
- EVANS, P. 2006. Scaling and assessment of data quality. *Acta Crystallographica Section D: Biological Crystallography*, 62, 72-82.
- EVANS, P. R. & MURSHUDOV, G. N. 2013. How good are my data and what is the resolution? *Acta Crystallographica Section D: Biological Crystallography*, 69, 1204-1214.
- FASS, R. J. 1980. Activity of mecillinam alone and in combination with other beta-lactam antibiotics. *Antimicrob Agents Chemother*, 18, 906-12.
- FAY, A., MEYER, P. & DWORKIN, J. 2010. Interactions between late-acting proteins required for peptidoglycan synthesis during sporulation. *Journal of Molecular Biology*, 399, 547-561.
- FEDAROVICH, A., COOK, E., TOMBERG, J., NICHOLAS, R. A. & DAVIES, C. 2014. Structural effect of the Asp345a insertion in penicillin-binding protein 2 from penicillin-resistant strains of *Neisseria gonorrhoeae*. *Biochemistry*, 53, 7596-603.
- FEDAROVICH, A., NICHOLAS, R. A. & DAVIES, C. 2010. Unusual conformation of the SxN motif in the crystal structure of penicillin-binding protein A from *Mycobacterium tuberculosis*. *Journal of Molecular Biology*, 398, 54-65.

- FEDAROVICH, A., NICHOLAS, R. A. & DAVIES, C. 2012. The role of the beta5-alpha11 loop in the active-site dynamics of acylated penicillin-binding protein A from *Mycobacterium tuberculosis*. *Journal of Molecular Biology*, 418, 316-30.
- FENTON, A. K., MANUSE, S., FLORES-KIM, J., GARCIA, P. S., MERCY, C., GRANGEASSE, C., BERNHARDT, T. G. & RUDNER, D. Z. 2018. Phosphorylation-dependent activation of the cell wall synthase PBP2a in *Streptococcus pneumoniae* by MacP. *Proceedings of the National Academy of Sciences*, 115, 2812-2817.
- FILIPPOVA, E. V., KIESER, K. J., LUAN, C. H., WAWRZAK, Z., KIRYUKHINA, O., RUBIN, E. J. & ANDERSON, W. F. 2016. Crystal structures of the transpeptidase domain of the *Mycobacterium tuberculosis* penicillin-binding protein PonA1 reveal potential mechanisms of antibiotic resistance. *The FEBS Journal*, 283, 2206-2218.
- FOUNOU, L. L., FOUNOU, R. C. & ESSACK, S. Y. 2016. Antibiotic Resistance in the Food Chain: A Developing Country-Perspective. *Frontiers in Microbiology*, 7, 1881.
- FRAIPONT, C., ALEXEEVA, S., WOLF, B., VAN DER PLOEG, R., SCHLOESSER, M., DEN BLAAUWEN, T. & NGUYEN-DISTECHE, M. 2011. The integral membrane FtsW protein and peptidoglycan synthase PBP3 form a subcomplex in *Escherichia coli*. *Microbiology*, 157, 251-259.
- FRENCH, S. & WILSON, K. 1978. On the treatment of negative intensity observations. *Acta Crystallographica Section A: Crystal Physics, Diffraction, Theoretical and General Crystallography*, 34, 517-525.
- FRIEDRICH, A. W. 2019. Control of hospital acquired infections and antimicrobial resistance in Europe: the way to go. *Wien Med Wochenschr*, 169, 25-30.
- GEISINGER, E. & ISBERG, R. R. 2015. Antibiotic modulation of capsular exopolysaccharide and virulence in *Acinetobacter baumannii*. *PLoS Pathogens*, 11, e1004691.
- GEISINGER, E., MORTMAN, N. J., VARGAS-CUEBAS, G., TAI, A. K. & ISBERG, R. R. 2018. A global regulatory system links virulence and antibiotic resistance to envelope homeostasis in *Acinetobacter baumannii*. *PLoS Pathogens*, 14, e1007030.
- GELBAND, H., MILLER-PETRIE, M., PANT, S., GANDRA, S., LEVINSON, J., BARTER, D., WHITE, A. & LAXMINARAYAN, R. 2015. State of the world's antibiotics, 2015. Washington, DC: Center for Disease Dynamics. *Economics & Policy*.
- GOFFIN, C. & GHUYSEN, J.-M. 1998. Multimodular penicillin-binding proteins: an enigmatic family of orthologs and paralogs. *Microbiology and Molecular Biology Reviews*, 62, 1079-1093.
- GONZALEZ-BELLO, C. 2017. Antibiotic adjuvants—A strategy to unlock bacterial resistance to antibiotics. *Bioorganic & Medicinal Chemistry Letters*, 27, 4221-4228.
- GRANINGER, W. 2003. Pivmecillinam—therapy of choice for lower urinary tract infection. *International journal of antimicrobial agents*, 22, 73-78.
- GRANT, N. H., CLARK, D. E. & ALBURN, H. E. 1962. Poly-6-aminopenicillanic acid. *Journal of the American Chemical Society*, 84, 876-877.
- GRANT, S. G., JESSEE, J., BLOOM, F. R. & HANAHAN, D. 1990. Differential plasmid rescue from transgenic mouse DNAs into *Escherichia coli* methylation-restriction mutants. *Proceedings of the National Academy of Sciences*, 87, 4645-4649.

- GREBE, T. & HAKENBECK, R. 1996. Penicillin-binding proteins 2b and 2x of *Streptococcus pneumoniae* are primary resistance determinants for different classes of beta-lactam antibiotics. *Antimicrobial Agents and Chemotherapy*, 40, 829-34.
- GREENE, N. G., FUMEAUX, C. & BERNHARDT, T. G. 2018. Conserved mechanism of cell-wall synthase regulation revealed by the identification of a new PBP activator in *Pseudomonas aeruginosa*. *Proceedings of the National Academy of Sciences*, 115, 3150-3155.
- GRIGORYAN, L., HAAIJER-RUSKAMP, F. M., BURGERHOF, J. G., MECHTLER, R., DESCHEPPER, R., TAMBIC-ANDRASEVIC, A., ANDRAJATI, R., MONNET, D. L., CUNNEY, R., DI MATTEO, A., EDELSEIN, H., VALINTELIENE, R., ALKERWI, A., SCICLUNA, E., GRZESIOWSKI, P., BARA, A. C., TESAR, T., CIZMAN, M., CAMPOS, J., LUNDBORG, C. S. & BIRKIN, J. 2006. Self-medication with antimicrobial drugs in Europe. *Emerging Infectious Disease*, 12, 452-9.
- GUPTA, K., HOOTON, T. M., NABER, K. G., WULLT, B., COLGAN, R., MILLER, L. G., MORAN, G. J., NICOLLE, L. E., RAZ, R. & SCHAEFFER, A. J. 2011. International clinical practice guidelines for the treatment of acute uncomplicated cystitis and pyelonephritis in women: a 2010 update by the Infectious Diseases Society of America and the European Society for Microbiology and Infectious Diseases. *Clinical Infectious Diseases*, 52, e103-e120.
- HAN, S., CASPERS, N., ZANIEWSKI, R. P., LACEY, B. M., TOMARAS, A. P., FENG, X., GEOGHEGAN, K. F. & SHANMUGASUNDARAM, V. 2011. Distinctive attributes of β -lactam target proteins in *Acinetobacter baumannii* relevant to development of new antibiotics. *Journal of the American Chemical Society*, 133, 20536-20545.
- HAN, S., ZANIEWSKI, R. P., MARR, E. S., LACEY, B. M., TOMARAS, A. P., EVDOKIMOV, A., MILLER, J. R. & SHANMUGASUNDARAM, V. 2010. Structural basis for effectiveness of siderophore-conjugated monocarbams against clinically relevant strains of *Pseudomonas aeruginosa*. *Proceedings of the National Academy of Sciences*, 107, 22002-22007.
- HARTSHORN, M. J., MURRAY, C. W., CLEASBY, A., FREDERICKSON, M., TICKLE, I. J. & JHOTI, H. 2005. Fragment-based lead discovery using X-ray crystallography. *Journal of Medicinal Chemistry*, 48, 403-413.
- HAYDON, D. J., STOKES, N. R., URE, R., GALBRAITH, G., BENNETT, J. M., BROWN, D. R., BAKER, P. J., BARYNIN, V. V., RICE, D. W., SEDELNIKOVA, S. E., HEAL, J. R., SHERIDAN, J. M., AIWALE, S. T., CHAUHAN, P. K., SRIVASTAVA, A., TANEJA, A., COLLINS, I., ERRINGTON, J. & CZAPLEWSKI, L. G. 2008. An inhibitor of FtsZ with potent and selective anti-staphylococcal activity. *Science*, 321, 1673-5.
- HAYES, M. V. & ORR, D. C. 1983. Mode of action of ceftazidime: affinity for the penicillin-binding proteins of *Escherichia coli* K12, *Pseudomonas aeruginosa* and *Staphylococcus aureus*. *Journal of Antimicrobial Chemotherapy*, 12, 119-126.
- HAYHURST, E. J., KAILAS, L., HOBBS, J. K. & FOSTER, S. J. 2008. Cell wall peptidoglycan architecture in *Bacillus subtilis*. *Proceedings of the National Academy of Sciences*, 105, 14603-8.
- HERMANN, J. C., HENSEN, C., RIDDER, L., MULHOLLAND, A. J. & HÖLTJE, H.-D. 2005. Mechanisms of antibiotic resistance: QM/MM modeling of the acylation

- reaction of a class A β -lactamase with benzylpenicillin. *Journal of the American Chemical Society*, 127, 4454-4465.
- HICKMAN, R. A., HUGHES, D., CARS, T., MALMBERG, C. & CARS, O. 2014. Cell-wall-inhibiting antibiotic combinations with activity against multidrug-resistant *Klebsiella pneumoniae* and *Escherichia coli*. *Clinical Microbiology and Infection*, 20, O267-O273.
- HOELZER, K., WONG, N., THOMAS, J., TALKINGTON, K., JUNGMAN, E. & COUKELL, A. 2017. Antimicrobial drug use in food-producing animals and associated human health risks: what, and how strong, is the evidence? *BMC Veterinary Research*, 13, 211.
- HOLMES, A. H., MOORE, L. S., SUNDSFJORD, A., STEINBAKK, M., REGMI, S., KARKEY, A., GUERIN, P. J. & PIDDOCK, L. J. 2016. Understanding the mechanisms and drivers of antimicrobial resistance. *Lancet*, 387, 176-87.
- HOOTON, T. M. 2000. Pathogenesis of urinary tract infections: an update. *Journal of Antimicrobial Chemotherapy*, 46, 1-7.
- HSUEH, P.-R., CHEN, W.-H. & LUH, K.-T. 2005. Relationships between antimicrobial use and antimicrobial resistance in Gram-negative bacteria causing nosocomial infections from 1991–2003 at a university hospital in Taiwan. *International Journal of Antimicrobial Agents*, 26, 463-472.
- HUGHES, J. P., REES, S., KALINDJIAN, S. B. & PHILPOTT, K. L. 2011. Principles of early drug discovery. *British Journal of Pharmacology*, 162, 1239-49.
- HUGONNET, J. E., MENGIN-LECREULX, D., MONTON, A., DEN BLAAUWEN, T., CARBONNELLE, E., VECKERLE, C., BRUN, Y. V., VAN NIEUWENHZE, M., BOUCHIER, C., TU, K., RICE, L. B. & ARTHUR, M. 2016. Factors essential for L,D-transpeptidase-mediated peptidoglycan cross-linking and beta-lactam resistance in *Escherichia coli*. *Elife*, 5, e19469.
- HUGONNET, J.-E., TREMBLAY, L. W., BOSHOF, H. I., BARRY, C. E. & BLANCHARD, J. S. 2009. Meropenem-clavulanate is effective against extensively drug-resistant *Mycobacterium tuberculosis*. *Science*, 323, 1215-1218.
- HUYNH, K. & PARTCH, C. L. 2015. Analysis of protein stability and ligand interactions by thermal shift assay. *Current Protocols in Protein Science*, 79, 28.9. 1-28.9. 14.
- INOUE, A., MURATA, Y., TAKAHASHI, H., TSUJI, N., FUJISAKI, S. & KATO, J.-I. 2008. Involvement of an essential gene, *mviN*, in murein synthesis in *Escherichia coli*. *Journal of Bacteriology*, 190, 7298-7301.
- JAFFE, A., CHABBERT, Y. A. & SEMONIN, O. 1982. Role of porin proteins OmpF and OmpC in the permeation of beta-lactams. *Antimicrobial Agents and Chemotherapy*, 22, 942-948.
- JANARDHANAN, J., BOULEY, R., MARTÍNEZ-CABALLERO, S., PENG, Z., BATUECAS-MORDILLO, M., MEISEL, J. E., DING, D., SCHROEDER, V. A., WOLTER, W. R. & MAHASANAN, K. V. 2019. The Quinazolinone Allosteric Inhibitor of PBP 2a Synergizes with Piperacillin and Tazobactam against Methicillin-Resistant *Staphylococcus aureus*. *Antimicrobial Agents and Chemotherapy*, 63, e02637-18.
- JEON, J., LEE, J., LEE, J., PARK, K., KARIM, A., LEE, C.-R., JEONG, B. & LEE, S. 2015. Structural basis for carbapenem-hydrolyzing mechanisms of

- carbapenemases conferring antibiotic resistance. *International Journal of Molecular Sciences*, 16, 9654-9692.
- JEONG, J.-H., KIM, Y.-S., ROJVIRIYA, C., HA, S.-C., KANG, B. S. & KIM, Y.-G. 2013. Crystal structures of bifunctional penicillin-binding protein 4 from *Listeria monocytogenes*. *Antimicrobial Agents and Chemotherapy*, 57, 3507-3512.
- KANTARDJIEFF, K. A. & RUPP, B. 2003. Matthews coefficient probabilities: improved estimates for unit cell contents of proteins, DNA, and protein–nucleic acid complex crystals. *Protein Science*, 12, 1865-1871.
- KEEGAN, R. M. & WINN, M. D. 2008. MrBUMP: an automated pipeline for molecular replacement. *Acta Crystallographica Section D: Biological Crystallography*, 64, 119-124.
- KIESER, K. J., BOUTTE, C. C., KESTER, J. C., BAER, C. E., BARCZAK, A. K., MENICHE, X., CHAO, M. C., REGO, E. H., SASSETTI, C. M. & FORTUNE, S. M. 2015. Phosphorylation of the peptidoglycan synthase PonA1 governs the rate of polar elongation in mycobacteria. *PLoS Pathogens*, 11, e1005010.
- KING, A. M., KING, D. T., FRENCH, S., BROUILLETTE, E., ASLI, A., ALEXANDER, J. A. N., VUCKOVIC, M., MAITI, S. N., PARR JR, T. R. & BROWN, E. D. 2016. Structural and kinetic characterization of diazabicyclooctanes as dual inhibitors of both serine- β -lactamases and penicillin-binding proteins. *ACS Chemical Biology*, 11, 864-868.
- KING, D. T., SOBHANIFAR, S. & STRYNADKA, N. C. 2016. One ring to rule them all: Current trends in combating bacterial resistance to the β -lactams. *Protein Science*, 25, 787-803.
- KING, D. T., SOBHANIFAR, S. & STRYNADKA, N. C. 2017a. The mechanisms of resistance to β -lactam antibiotics. *Handbook of Antimicrobial Resistance*, 177-201.
- KING, D. T., WASNEY, G. A., NOSELLA, M., FONG, A. & STRYNADKA, N. C. 2017b. Structural insights into inhibition of *Escherichia coli* penicillin-binding protein 1B. *Journal of Biological Chemistry*, 292, 979-993.
- KIRCHHELLE, C. 2018. Pharming animals: a global history of antibiotics in food production (1935–2017). *Palgrave Communications*, 4, 96.
- KISHIDA, H., UNZAI, S., ROPER, D. I., LLOYD, A., PARK, S.-Y. & TAME, J. R. 2006. Crystal structure of penicillin binding protein 4 (dacB) from *Escherichia coli*, both in the native form and covalently linked to various antibiotics. *Biochemistry*, 45, 783-792.
- KOCAOGLU, O. & CARLSON, E. E. 2015. Profiling of beta-lactam selectivity for penicillin-binding proteins in *Escherichia coli* strain DC2. *Antimicrobial Agents and Chemotherapy*, 59, 2785-90.
- KOHANSKI, M. A., DWYER, D. J. & COLLINS, J. J. 2010. How antibiotics kill bacteria: from targets to networks. *Nature Reviews Microbiology*, 8, 423-435.
- KONAKLIEVA, M. I. 2014. Molecular Targets of beta-Lactam-Based Antimicrobials: Beyond the Usual Suspects. *Antibiotics (Basel)*, 3, 128-42.
- KONG, K. F., SCHNEPER, L. & MATHEE, K. 2010. Beta-lactam antibiotics: from antibiosis to resistance and bacteriology. *Apmis*, 118, 1-36.
- KRĘŻEL, A., LEŚNIAK, W., JEŻOWSKA-BOJCZUK, M., MŁYNARZ, P., BRASUŃ, J., KOZŁOWSKI, H. & BAL, W. 2001. Coordination of heavy metals by

- dithiothreitol, a commonly used thiol group protectant. *Journal of Inorganic Biochemistry*, 84, 77-88.
- KRISTIANSSON, E., FICK, J., JANZON, A., GRABIC, R., RUTGERSSON, C., WEIJDEGARD, B., SODERSTROM, H. & LARSSON, D. G. 2011. Pyrosequencing of antibiotic-contaminated river sediments reveals high levels of resistance and gene transfer elements. *PLoS One*, 6, e17038.
- KRUSE, T., BORK-JENSEN, J. & GERDES, K. 2005. The morphogenetic MreBCD proteins of *Escherichia coli* form an essential membrane-bound complex. *Molecular Microbiology*, 55, 78-89.
- LAFAYE, P. & LAPRESLE, C. 1988a. Fixation of penicilloyl groups to albumin and appearance of anti-penicilloyl antibodies in penicillin-treated patients. *The Journal of Clinical Investigation*, 82, 7-12.
- LAFAYE, P. & LAPRESLE, C. 1988b. Identification of two fixation sites for penicilloyl groups on the albumin molecule from penicillin-treated patients. *FEBS Letters*, 234, 305-308.
- LAHIRI, S. D., MANGANI, S., JAHIC, H., BENVENUTI, M., DURAND-REVILLE, T. F., DE LUCA, F., EHMANN, D. E., ROSSOLINI, G. M., ALM, R. A. & DOCQUIER, J.-D. 2014. Molecular basis of selective inhibition and slow reversibility of avibactam against class D carbapenemases: a structure-guided study of OXA-24 and OXA-48. *ACS Chemical Biology*, 10, 591-600.
- LAITAOJA, M., VALJAKKA, J. & JÄNIS, J. 2013. Zinc coordination spheres in protein structures. *Inorganic Chemistry*, 52, 10983-10991.
- LAKEMEYER, M., ZHAO, W., MANDL, F. A., HAMMANN, P. & SIEBER, S. A. 2018. Thinking Outside the Box—Novel Antibacterials To Tackle the Resistance Crisis. *Angewandte Chemie International Edition*, 57, 14440-14475.
- LAMOREE, B. & HUBBARD, R. E. 2018. Using Fragment-Based Approaches to Discover New Antibiotics. *SLAS DISCOVERY: Advancing Life Sciences R&D*, 23, 495-510.
- LARSEN, C. & BUNDGAARD, H. 1978. Polymerization of Penicillins: V. Separation, identification and quantitative determination of Antigenic Polymerization products in Ampicillin Sodium preparations by high-performance liquid chromatography. *Journal of Chromatography A*, 147, 143-150.
- LASKOWSKI, R. A., MACARTHUR, M. W., MOSS, D. S. & THORNTON, J. M. 1993. PROCHECK: a program to check the stereochemical quality of protein structures. *Journal of applied crystallography*, 26, 283-291.
- LAVOLLAY, M., ARTHUR, M., FOURGEAUD, M., DUBOST, L., MARIE, A., VEZIRIS, N., BLANOT, D., GUTMANN, L. & MAINARDI, J.-L. 2008. The peptidoglycan of stationary-phase Mycobacterium tuberculosis predominantly contains cross-links generated by L, D-transpeptidation. *Journal of Bacteriology*, 190, 4360-4366.
- LEAVER, M. & ERRINGTON, J. 2005. Roles for MreC and MreD proteins in helical growth of the cylindrical cell wall in *Bacillus subtilis*. *Molecular Microbiology*, 57, 1196-209.
- LEBEDEV, A. A., YOUNG, P., ISUPOV, M. N., MOROZ, O. V., VAGIN, A. A. & MURSHUDOV, G. N. 2012. JLigand: a graphical tool for the CCP4 template-restraint library. *Acta Crystallographica Section D: Biological Crystallography*, 68, 431-440.

- LEE, B. 1971. Conformation of penicillin as a transition-state analog of the substrate of peptidoglycan transpeptidase. *Journal of Molecular Biology*, 61, 463-469.
- LEE, W., MCDONOUGH, M. A., KOTRA, L., LI, Z. H., SILVAGGI, N. R., TAKEDA, Y., KELLY, J. A. & MOBASHERY, S. 2001. A 1.2-Å snapshot of the final step of bacterial cell wall biosynthesis. *Proceedings of the National Academy of Sciences of the United States of America*, 98, 1427-31.
- LEGAREE, B. A. & CLARKE, A. J. 2008. Interaction of penicillin-binding protein 2 with soluble lytic transglycosylase B1 in *Pseudomonas aeruginosa*. *Journal of Bacteriology*, 190, 6922-6926.
- LEGAREE, B. A., DANIELS, K., WEADGE, J. T., COCKBURN, D. & CLARKE, A. J. 2007. Function of penicillin-binding protein 2 in viability and morphology of *Pseudomonas aeruginosa*. *Journal of Antimicrobial Chemotherapy*, 59, 411-424.
- LEO PHARMA INC. 2018. SELEXID (pivmecillinam hydrochloride) Product Monograph, Version 2.0. *LEO Pharma Incorporated*, 1-42.
- LEVY, N., BRUNEAU, J. M., LE ROUZIC, E., BONNARD, D., LE STRAT, F., CARAVANO, A., CHEVREUIL, F., BARBION, J., CHASSET, S., LEDOUSSAL, B., MOREAU, F. & RUFF, M. 2019. Structural Basis for *E. coli* Penicillin Binding Protein (PBP) 2 Inhibition, a Platform for Drug Design. *Journal of Medicinal Chemistry*, 62, 4742-4754.
- LIBREROS-ZÚÑIGA, G. A., DOS SANTOS SILVA, C., SALGADO FERREIRA, R. & DIAS, M. V. B. 2018. Structural Basis for the Interaction and Processing of β -Lactam Antibiotics by I, d-Transpeptidase 3 (LdtMt3) from *Mycobacterium tuberculosis*. *ACS Infectious Diseases*, 5, 260-271.
- LIM, L. M., LY, N., ANDERSON, D., YANG, J. C., MACANDER, L., JARKOWSKI III, A., FORREST, A., BULITTA, J. B. & TSUJI, B. T. 2010. Resurgence of colistin: a review of resistance, toxicity, pharmacodynamics, and dosing. *Pharmacotherapy: The Journal of Human Pharmacology and Drug Therapy*, 30, 1279-1291.
- LIU, X., MEIRESONNE, N. Y., BOUHSS, A. & DEN BLAAUWEN, T. 2018. FtsW activity and lipid II synthesis are required for recruitment of MurJ to midcell during cell division in *Escherichia coli*. *Molecular Microbiology*, 109, 855-884.
- LIU, Y., MÖLLER, M. C., PETERSEN, L., SÖDERBERG, C. A. & HEDERSTEDT, L. 2010. Penicillin-binding protein SpoVD disulphide is a target for StoA in *Bacillus subtilis* forespores. *Molecular microbiology*, 75, 46-60.
- LIVERMORE, D. M., SEFTON, A. M. & SCOTT, G. M. 2003. Properties and potential of ertapenem. *Journal of Antimicrobial Chemotherapy*, 52, 331-344.
- LOHANS, C. T., CHAN, H. H., MALLA, T. R., KUMAR, K., KAMPS, J. J., MCARDLE, D. J., VAN GROESEN, E., DE MUNNIK, M., TOOKE, C. L. & SPENCER, J. 2019. Non-Hydrolytic β -Lactam Antibiotic Fragmentation by I, d-Transpeptidases and Serine β -Lactamase Cysteine Variants. *Angewandte Chemie*, 131, 2012-2016.
- LONERGAN, Z. R., NAIRN, B. L., WANG, J., HSU, Y. P., HESSE, L. E., BEAVERS, W. N., CHAZIN, W. J., TRINIDAD, J. C., VANNIEUWENHZE, M. S., GIEDROC, D. P. & SKAAR, E. P. 2019. An *Acinetobacter baumannii*, Zinc-Regulated Peptidase Maintains Cell Wall Integrity during Immune-Mediated Nutrient Sequestration. *Cell Reports*, 26, 2009-2018 e6.

- LONG, F., VAGIN, A. A., YOUNG, P. & MURSHUDOV, G. N. 2008. BALBES: a molecular-replacement pipeline. *Acta Crystallographica Section D: Biological Crystallography*, 64, 125-132.
- LOVELL, S. C., DAVIS, I. W., ARENDALL III, W. B., DE BAKKER, P. I., WORD, J. M., PRISANT, M. G., RICHARDSON, J. S. & RICHARDSON, D. C. 2003. Structure validation by C α geometry: ϕ , ψ and C β deviation. *Proteins: Structure, Function, and Bioinformatics*, 50, 437-450.
- LOVERING, A. L., DE CASTRO, L. H., LIM, D. & STRYNADKA, N. C. 2007. Structural insight into the transglycosylation step of bacterial cell-wall biosynthesis. *Science*, 315, 1402-1405.
- LOVERING, A. L., SAFADI, S. S. & STRYNADKA, N. C. 2012. Structural perspective of peptidoglycan biosynthesis and assembly. *Annual Review of Biochemistry*, 81, 451-478.
- LUND, F. & TYBRING, L. 1972. 6 β -amidinopenicillanic acids—a new group of antibiotics. *Nature New Biology*, 236, 135-137.
- MACHEBOEUF, P., FISCHER, D. S., BROWN, T., JR., ZERVOSEN, A., LUXEN, A., JORIS, B., DESSEN, A. & SCHOFIELD, C. J. 2007. Structural and mechanistic basis of penicillin-binding protein inhibition by lactivicins. *Nature Chemical Biology*, 3, 565-9.
- MACHEBOEUF, P., LEMAIRE, D., MARTINS, A. D. S., DIDEBERG, O., JAMIN, M. & DESSEN, A. 2008. Trapping of an acyl-enzyme intermediate in a penicillin-binding protein (PBP)-catalyzed reaction. *Journal of Molecular Biology*, 376, 405-413.
- MACKENZIE, F. M., BRUCE, J., STRUELENS, M., GOOSSENS, H., MOLLISON, J., GOULD, I. M. & GROUP, A. S. 2007. Antimicrobial drug use and infection control practices associated with the prevalence of methicillin-resistant *Staphylococcus aureus* in European hospitals. *Clinical Microbiology and Infection*, 13, 269-276.
- MAGIORAKOS, A. P., SRINIVASAN, A., CAREY, R., CARMELI, Y., FALAGAS, M., GISKE, C., HARBARTH, S., HINDLER, J., KAHLMETER, G. & OLSSON-LILJEQUIST, B. 2012. Multidrug-resistant, extensively drug-resistant and pandrug-resistant bacteria: an international expert proposal for interim standard definitions for acquired resistance. *Clinical Microbiology and Infection*, 18, 268-281.
- MAITI, S. N., NGUYEN, D., KHAN, J. & LING, R. 2014. Bicyclic compounds and their use as antibacterial agents and β -lactamase inhibitors. Google Patents.
- MANYI-LOH, C., MAMPHWELI, S., MEYER, E. & OKOH, A. 2018. Antibiotic use in agriculture and its consequential resistance in environmental sources: potential public health implications. *Molecules*, 23, 795.
- MARKOVSKI, M., BOHRHUNTER, J. L., LUPOLI, T. J., UEHARA, T., WALKER, S., KAHNE, D. E. & BERNHARDT, T. G. 2016. Cofactor bypass variants reveal a conformational control mechanism governing cell wall polymerase activity. *Proceedings of the National Academy of Sciences*, 113, 4788-4793.
- MASSOVA, I. & MOBASHERY, S. 1998. Kinship and diversification of bacterial penicillin-binding proteins and β -lactamases. *Antimicrobial Agents and Chemotherapy*, 42, 1-17.

- MATSUHASHI, S., KAMIRYO, T., BLUMBERG, P. M., LINNETT, P., WILLOUGHBY, E. & STROMINGER, J. L. 1974. Mechanism of action and development of resistance to a new amidino penicillin. *Journal of Bacteriology*, 117, 578-587.
- MAULDIN, P. D., SALGADO, C. D., HANSEN, I. S., DURUP, D. T. & BOSSO, J. A. 2010. Attributable hospital cost and length of stay associated with health care-associated infections caused by antibiotic-resistant gram-negative bacteria. *Antimicrobial Agents and Chemotherapy*, 54, 109-115.
- MCCALL, K. A., HUANG, C.-C. & FIERKE, C. A. 2000. Function and mechanism of zinc metalloenzymes. *The Journal of nutrition*, 130, 1437S-1446S.
- MCCOY, A. J., GROSSE-KUNSTLEVE, R. W., ADAMS, P. D., WINN, M. D., STORONI, L. C. & READ, R. J. 2007. Phaser crystallographic software. *Journal of Applied Crystallography*, 40, 658-674.
- MCDONOUGH, M. A., ANDERSON, J. W., SILVAGGI, N. R., PRATT, R., KNOX, J. R. & KELLY, J. A. 2002. Structures of two kinetic intermediates reveal species specificity of penicillin-binding proteins. *Journal of Molecular Biology*, 322, 111-122.
- MCGANN, P., SNESRUD, E., MAYBANK, R., COREY, B., ONG, A. C., CLIFFORD, R., HINKLE, M., WHITMAN, T., LESH, E. & SCHAECHER, K. E. 2016. *Escherichia coli* harboring mcr-1 and blaCTX-M on a novel IncF plasmid: first report of mcr-1 in the United States. *Antimicrobial Agents and Chemotherapy*, 60, 4420-4421.
- MEESKE, A. J., RILEY, E. P., ROBINS, W. P., UEHARA, T., MEKALANOS, J. J., KAHNE, D., WALKER, S., KRUSE, A. C., BERNHARDT, T. G. & RUDNER, D. Z. 2016. SEDS proteins are a widespread family of bacterial cell wall polymerases. *Nature*, 537, 634.
- MENG, E. C., PETERSEN, E. F., COUCH, G. S., HUANG, C. C. & FERRIN, T. E. 2006. Tools for integrated sequence-structure analysis with UCSF Chimera. *BMC Bioinformatics*, 7, 339.
- MEYER, E., SCHWAB, F., SCHROEREN-BOERSCH, B. & GASTMEIER, P. 2010. Dramatic increase of third-generation cephalosporin-resistant *E. coli* in German intensive care units: secular trends in antibiotic drug use and bacterial resistance, 2001 to 2008. *Critical Care*, 14, R113.
- MICHAEL, C. A., DOMINEY-HOWES, D. & LABBATE, M. 2014. The antimicrobial resistance crisis: causes, consequences, and management. *Frontiers in Public Health*, 2, 145.
- MIGUET, L., ZERVOSEN, A., GERARDS, T., PASHA, F. A., LUXEN, A., DISTECHE-NGUYEN, M. & THOMAS, A. 2009. Discovery of new inhibitors of resistant *Streptococcus pneumoniae* penicillin binding protein (PBP) 2x by structure-based virtual screening. *Journal of Medicinal Chemistry*, 52, 5926-36.
- MIRAKIAN, R., LEECH, S., KRISHNA, M., RICHTER, A., HUBER, P., FAROOQUE, S., KHAN, N., PIRMOHAMED, M., CLARK, A. & NASSER, S. 2015. Management of allergy to penicillins and other beta-lactams. *Clinical & Experimental Allergy*, 45, 300-327.
- MIROUX, B. & WALKER, J. E. 1996. Over-production of proteins in *Escherichia coli*: mutant hosts that allow synthesis of some membrane proteins and globular proteins at high levels. *Journal of Molecular Biology*, 260, 289-298.

- MOELLERING JR, R. C., ELIOPOULOS, G. M. & SENTOCHNIK, D. E. 1989. The carbapenems: new broad spectrum β -lactam antibiotics. *Journal of Antimicrobial Chemotherapy*, 24, 1-7.
- MOHAMMADI, T., SIJBRANDI, R., LUTTERS, M., VERHEUL, J., MARTIN, N. I., DEN BLAAUWEN, T., DE KRUIJFF, B. & BREUKINK, E. 2014. Specificity of the transport of lipid II by FtsW in *Escherichia coli*. *Journal of Biological Chemistry*, 289, 14707-18.
- MOHAMMADI, T., VAN DAM, V., SIJBRANDI, R., VERNET, T., ZAPUN, A., BOUHSS, A., DIEPEVEEN-DE BRUIN, M., NGUYEN-DISTÈCHE, M., DE KRUIJFF, B. & BREUKINK, E. 2011. Identification of FtsW as a transporter of lipid-linked cell wall precursors across the membrane. *The EMBO Journal*, 30, 1425-1432.
- MOHR, J. F., 3RD 2008. Update on the efficacy and tolerability of meropenem in the treatment of serious bacterial infections. *Clinical Infectious Diseases*, 47 Suppl 1, S41-51.
- MOJICA, M., A BONOMO, R. & FAST, W. 2016. B1-Metallo- β -lactamases: where do we stand? *Current Drug Targets*, 17, 1029-1050.
- MÖLLMANN, U., HEINISCH, L., BAUERNFEIND, A., KÖHLER, T. & ANKEL-FUCHS, D. 2009. Siderophores as drug delivery agents: application of the "Trojan Horse" strategy. *Biometals*, 22, 615-624.
- MONAHAN, L. G., TURNBULL, L., OSVATH, S. R., BIRCH, D., CHARLES, I. G. & WHITCHURCH, C. B. 2014. Rapid conversion of *Pseudomonas aeruginosa* to a spherical cell morphotype facilitates tolerance to carbapenems and penicillins but increases susceptibility to antimicrobial peptides. *Antimicrobial Agents and Chemotherapy*, 58, 1956-1962.
- MONSERRAT-MARTINEZ, A., GAMBIN, Y. & SIERECKI, E. 2019. Thinking outside the bug: Molecular targets and strategies to overcome antibiotic resistance. *International Journal of Molecular Sciences*, 20, 1255.
- MORGAN, D. J., OKEKE, I. N., LAXMINARAYAN, R., PERENCEVICH, E. N. & WEISENBERG, S. 2011. Non-prescription antimicrobial use worldwide: a systematic review. *The Lancet Infectious Diseases*, 11, 692-701.
- MORINAKA, A., TSUTSUMI, Y., YAMADA, M., SUZUKI, K., WATANABE, T., ABE, T., FURUUCHI, T., INAMURA, S., SAKAMAKI, Y. & MITSUHASHI, N. 2015. OP0595, a new diazabicyclooctane: mode of action as a serine β -lactamase inhibitor, antibiotic and β -lactam 'enhancer'. *Journal of Antimicrobial Chemotherapy*, 70, 2779-2786.
- MOYA, B., BARCELO, I. M., BHAGWAT, S., PATEL, M., BOU, G., PAPP-WALLACE, K. M., BONOMO, R. A. & OLIVER, A. 2017a. Potent beta-Lactam Enhancer Activity of Zidebactam and WCK 5153 against *Acinetobacter baumannii*, Including Carbapenemase-Producing Clinical Isolates. *Antimicrobial Agents and Chemotherapy*, 61.
- MOYA, B., BARCELO, I. M., BHAGWAT, S., PATEL, M., BOU, G., PAPP-WALLACE, K. M., BONOMO, R. A. & OLIVER, A. 2017b. WCK 5107 (Zidebactam) & WCK 5153: Novel inhibitors of PBP2 showing potent " β -lactam enhancer" activity against *Pseudomonas aeruginosa*, including multidrug-resistant metallo- β -lactamase-producing high-risk clones. *Antimicrobial Agents and Chemotherapy*, AAC. 02529-16.

- MOYA, B., BARCELO, I. M., CABOT, G., TORRENS, G., PALWE, S., JOSHI, P., UMARKAR, K., TAKALKAR, S., PERIASAMY, H. & BHAGWAT, S. 2019. In Vitro and In Vivo Activities of β -Lactams in Combination with the Novel β -Lactam Enhancers Zidebactam and WCK 5153 against Multidrug-Resistant Metallo- β -Lactamase-Producing *Klebsiella pneumoniae*. *Antimicrobial Agents and Chemotherapy*, 63, e00128-19.
- MULLARD, A. 2018. FDA approves first drug under new antibacterial and antifungal drug programme. *Nature Reviews Drug Discovery*, 17, 777.
- MÜNCH, D. & SAHL, H.-G. 2015. Structural variations of the cell wall precursor lipid II in Gram-positive bacteria—Impact on binding and efficacy of antimicrobial peptides. *Biochimica et Biophysica Acta (BBA)-Biomembranes*, 1848, 3062-3071.
- MUNITA, J. M. & ARIAS, C. A. 2016. Mechanisms of antibiotic resistance. *Microbiology Spectrum*, 4.
- MURPHY-BENENATO, K. E., DANGEL, B., DAVIS, H. E., DURAND-RÉVILLE, T. F., FERGUSON, A. D., GAO, N., JAHIĆ, H., MUELLER, J. P., MANYAK, E. L. & QUIROGA, O. 2015. SAR and structural analysis of siderophore-conjugated monocarbam inhibitors of *Pseudomonas aeruginosa* PBP3. *ACS Medicinal Chemistry Letters*, 6, 537-542.
- MURSHUDOV, G. N., SKUBÁK, P., LEBEDEV, A. A., PANNU, N. S., STEINER, R. A., NICHOLLS, R. A., WINN, M. D., LONG, F. & VAGIN, A. A. 2011. REFMAC5 for the refinement of macromolecular crystal structures. *Acta Crystallographica Section D: Biological Crystallography*, 67, 355-367.
- NEILANDS, J. 1995. Siderophores: structure and function of microbial iron transport compounds. *Journal of Biological Chemistry*, 270, 26723-26726.
- NEVES, D., ESTROZI, L. F., JOB, V., GABEL, F., SCHOEHN, G. & DESSEN, A. 2012. Conformational states of a bacterial α 2-macroglobulin resemble those of human complement C3. *PLoS One*, 7, e35384.
- NICHOLAS, R. A., KRINGS, S., TOMBERG, J., NICOLA, G. & DAVIES, C. 2003. Crystal structure of wild-type penicillin-binding protein 5 from *Escherichia coli* implications for deacylation of the acyl-enzyme complex. *Journal of Biological Chemistry*, 278, 52826-52833.
- NICOLA, G., FEDAROVICH, A., NICHOLAS, R. A. & DAVIES, C. 2005a. A large displacement of the SXN motif of Cys115-modified penicillin-binding protein 5 from *Escherichia coli*. *Biochemical Journal*, 392, 55-63.
- NICOLA, G., PEDDI, S., STEFANOVA, M., NICHOLAS, R. A., GUTHEIL, W. G. & DAVIES, C. 2005b. Crystal structure of *Escherichia coli* penicillin-binding protein 5 bound to a tripeptide boronic acid inhibitor: a role for Ser-110 in deacylation. *Biochemistry*, 44, 8207-8217.
- NICOLA, G., TOMBERG, J., PRATT, R., NICHOLAS, R. A. & DAVIES, C. 2010. Crystal structures of covalent complexes of β -lactam antibiotics with *Escherichia coli* penicillin-binding protein 5: toward an understanding of antibiotic specificity. *Biochemistry*, 49, 8094-8104.
- NICOLLE, L. E. 2000. Pivmecillinam in the treatment of urinary tract infections. *Journal of antimicrobial chemotherapy*, 46, 35-39.
- NICOLLE, L. B. 2001. EPIDEMIOLOGY-Epidemiology of Urinary Tract Infection. *Infections in Medicine*, 18, 153-162.

- NIKAIDO, H. 2003. Molecular basis of bacterial outer membrane permeability revisited. *Microbiology and Molecular Biology Reviews*, 67, 593-656.
- NIKAIDO, H. & VAARA, M. 1985. Molecular basis of bacterial outer membrane permeability. *Microbiological Reviews*, 49, 1.
- NIKOLAIDIS, I., IZORÉ, T., JOB, V., THIELENS, N., BREUKINK, E. & DESSEN, A. 2012. Calcium-dependent complex formation between PBP2 and lytic transglycosylase SltB1 of *Pseudomonas aeruginosa*. *Microbial Drug Resistance*, 18, 298-305.
- NORM/NORM-VET 2016. Usage of antimicrobial agents and occurrence of antimicrobial resistance in Norway. *Tromsø / Oslo 2017*, ISSN:1502-2307 (print) / 1890-9965 (electronic).
- NOZAKI, Y., KATAYAMA, N., ONO, H., TSUBOTANI, S., HARADA, S., OKAZAKI, H. & NAKAO, Y. 1987. Binding of a non- β -lactam antibiotic to penicillin-binding proteins. *Nature*, 325, 179.
- O'CALLAGHAN, C. H., MORRIS, A., KIRBY, S. M. & SHINGLER, A. 1972. Novel method for detection of β -lactamases by using a chromogenic cephalosporin substrate. *Antimicrobial Agents and Chemotherapy*, 1, 283-288.
- OCAN, M., OBUKU, E. A., BWANGA, F., AKENA, D., RICHARD, S., OGWAL-OKENG, J. & OBUA, C. 2015. Household antimicrobial self-medication: a systematic review and meta-analysis of the burden, risk factors and outcomes in developing countries. *BMC Public Health*, 15, 742.
- O'NEIL, J. 2014. Review on Antimicrobial Resistance. Antimicrobial Resistance: Tackling a Crisis for the Health and Wealth of Nations 2014.
- O'SHEA, R. & MOSER, H. E. 2008. Physicochemical properties of antibacterial compounds: implications for drug discovery. *Journal of Medicinal Chemistry*, 51, 2871-8.
- OWENS, R. C. 2008. An overview of harms associated with β -lactam antimicrobials: where do the carbapenems fit in? *Critical Care*, 12, S3.
- PAGE, M. I. 1984. The mechanisms of reactions of β -lactam antibiotics. *Accounts of Chemical Research*, 17, 144-151.
- PAGE, M. G., DANTIER, C. & DESARBRE, E. 2010. In vitro properties of BAL30072, a novel siderophore sulfactam with activity against multiresistant gram-negative bacilli. *Antimicrobial Agents and Chemotherapy*, 54, 2291-2302.
- PAPP-WALLACE, K. M. & BONOMO, R. A. 2016. New β -lactamase inhibitors in the clinic. *Infectious Disease Clinics*, 30, 441-464.
- PAPP-WALLACE, K. M., ENDIMIANI, A., TARACILA, M. A. & BONOMO, R. A. 2011. Carbapenems: past, present, and future. *Antimicrobial Agents and Chemotherapy*, 55, 4943-4960.
- PAPP-WALLACE, K. M., NGUYEN, N. Q., JACOBS, M. R., BETHEL, C. R., BARNES, M. D., KUMAR, V., BAJAKSOUZIAN, S., RUDIN, S. D., RATHER, P. N. & BHAVSAR, S. 2018. Strategic Approaches to Overcome Resistance against Gram-Negative Pathogens Using β -Lactamase Inhibitors and β -Lactam Enhancers: Activity of Three Novel Diazabicyclooctanes WCK 5153, Zidebactam (WCK 5107), and WCK 4234. *Journal of Medicinal Chemistry*, 61, 4067-4086.
- PAPP-WALLACE, K. M., SENKFOR, B., GATTA, J., CHAI, W., TARACILA, M. A., SHANMUGASUNDARAM, V., HAN, S., ZANIEWSKI, R. P., LACEY, B. M. & TOMARAS, A. P. 2012. Early Insights into the Interactions of Different β -

- Lactam Antibiotics and β -Lactamase Inhibitors against Soluble Forms of *Acinetobacter baumannii* PBP1a and PBP3. *Antimicrobial Agents and Chemotherapy*, AAC. 01027-12.
- PARADIS-BLEAU, C., MARKOVSKI, M., UEHARA, T., LUPOLI, T. J., WALKER, S., KAHNE, D. E. & BERNHARDT, T. G. 2010. Lipoprotein cofactors located in the outer membrane activate bacterial cell wall polymerases. *Cell*, 143, 1110-1120.
- PAYNE, D. J., MILLER, L. F., FINDLAY, D., ANDERSON, J. & MARKS, L. 2015. Time for a change: addressing R&D and commercialization challenges for antibacterials. *Philosophical Transactions of the Royal Society B: Biological Sciences*, 370, 20140086.
- PENWELL, W. F., SHAPIRO, A. B., GIACOBBE, R. A., GU, R.-F., GAO, N., THRESHER, J., MCLAUGHLIN, R. E., HUBAND, M. D., DEJONGE, B. L. & EHMANN, D. E. 2015. Molecular mechanisms of sulbactam antibacterial activity and resistance determinants in *Acinetobacter baumannii*. *Antimicrobial Agents and Chemotherapy*, 59, 1680-1689.
- PEREZ, F., HUJER, A. M., HUJER, K. M., DECKER, B. K., RATHER, P. N. & BONOMO, R. A. 2007. Global challenge of multidrug-resistant *Acinetobacter baumannii*. *Antimicrobial Agents and Chemotherapy*, 51, 3471-84.
- PERNOT, L., FRÉNOIS, F., RYBKINE, T., L'HERMITE, G., PETRELLA, S., DELETTRE, J., JARLIER, V., COLLATZ, E. & SOUGAKOFF, W. 2001. Crystal structures of the class D β -lactamase OXA-13 in the native form and in complex with meropenem. *Journal of Molecular Biology*, 310, 859-874.
- PISABARRO, A. G., DE PEDRO, M. A. & VÁZQUEZ, D. 1985. Structural modifications in the peptidoglycan of *Escherichia coli* associated with changes in the state of growth of the culture. *Journal of Bacteriology*, 161, 238-242.
- PETTERSEN, E. F., GODDARD, T. D., HUANG, C. C., COUCH, G. S., GREENBLATT, D. M., MENG, E. C. & FERRIN, T. E. 2004. UCSF Chimera—a visualization system for exploratory research and analysis. *Journal of Computational Chemistry*, 25, 1605-1612.
- POOLE, K. 2001. Multidrug efflux pumps and antimicrobial resistance in *Pseudomonas aeruginosa* and related organisms. *Journal of Molecular Microbiology and Biotechnology*, 3, 255-264.
- POOLE, K. 2004a. Efflux-mediated multi-resistance in Gram-negative bacteria. *Clinical Microbiology and Infection*, 10, 12-26.
- POOLE, K. 2004b. Resistance to β -lactam antibiotics. *Cellular and Molecular Life Sciences CMLS*, 61, 2200-2223.
- POWELL, A. J., TOMBERG, J., DEACON, A. M., NICHOLAS, R. A. & DAVIES, C. 2009. Crystal structures of penicillin-binding protein 2 from penicillin-susceptible and resistant strains of *Neisseria gonorrhoeae* reveal an unexpectedly subtle mechanism for antibiotic resistance. *Journal of Biological Chemistry*, 284, 1202-12.
- PRESTINACI, F., PEZZOTTI, P. & PANTOSTI, A. 2015. Antimicrobial resistance: a global multifaceted phenomenon. *Pathogens and Global Health*, 109, 309-318.
- PRIGOZHIN, D. M., KRIEGER, I. V., HUIZAR, J. P., MAVRICI, D., WALDO, G. S., HUNG, L.-W., SACCHETTINI, J. C., TERWILLIGER, T. C. & ALBER, T. 2014. Subfamily-specific adaptations in the structures of two penicillin-binding proteins from *Mycobacterium tuberculosis*. *PloS one*, 9, e116249.

- QIAO, Y., SRISUKNIMIT, V., RUBINO, F., SCHAEFER, K., RUIZ, N., WALKER, S. & KAHNE, D. 2017. Lipid II overproduction allows direct assay of transpeptidase inhibition by β -lactams. *Nature Chemical Biology*, 13, 793.
- RAHME, C., BUTTERFIELD, J. M., NICASIO, A. M. & LODISE, T. P. 2014. Dual beta-lactam therapy for serious Gram-negative infections: is it time to revisit? *Diagnostic Microbiology and Infectious Disease*, 80, 239-259.
- REN, J., NETTLESHIP, J. E., MALES, A., STUART, D. I. & OWENS, R. J. 2016. Crystal structures of penicillin-binding protein 3 in complexes with azlocillin and cefoperazone in both acylated and deacylated forms. *FEBS Letters*, 590, 288-297.
- RICHTER, M. F., DROWN, B. S., RILEY, A. P., GARCIA, A., SHIRAI, T., SVEC, R. L. & HERGENROTHER, P. J. 2017. Predictive compound accumulation rules yield a broad-spectrum antibiotic. *Nature*, 545, 299.
- ROBINSON-FUENTES, V., JEFFERIES, T. & BRANCH, S. 1997. Degradation pathways of ampicillin in alkaline solutions. *Journal of Pharmacy and Pharmacology*, 49, 843-851.
- ROHS, P. D. A., BUSS, J., SIM, S. I., SQUYRES, G. R., SRISUKNIMIT, V., SMITH, M., CHO, H., SJODT, M., KRUSE, A. C., GARNER, E. C., WALKER, S., KAHNE, D. E. & BERNHARDT, T. G. 2018. A central role for PBP2 in the activation of peptidoglycan polymerization by the bacterial cell elongation machinery. *PLOS Genetics*, 14, e1007726.
- ROYCHOUDHURY, S., KAISER, R. E., BREMS, D. N. & YEH, W.-K. 1996. Specific interaction between beta-lactams and soluble penicillin-binding protein 2a from methicillin-resistant *Staphylococcus aureus*: development of a chromogenic assay. *Antimicrobial Agents and Chemotherapy*, 40, 2075-2079.
- RUBINO, F. A., KUMAR, S., RUIZ, N., WALKER, S. & KAHNE, D. E. 2018. Membrane potential is required for MurJ function. *Journal of the American Chemical Society*, 140, 4481-4484.
- RUIZ, N. 2008. Bioinformatics identification of MurJ (MviN) as the peptidoglycan lipid II flippase in *Escherichia coli*. *Proceedings of the National Academy of Sciences*, 105, 15553-15557.
- RUIZ, N. 2015. Lipid flippases for bacterial peptidoglycan biosynthesis. *Lipid insights*, 8, 21.
- SACCO, K., BATES, A., BRIGHAM, T., IMAM, J. & BURTON, M. 2017. Clinical outcomes following inpatient penicillin allergy testing: A systematic review and meta-analysis. *Allergy*, 72, 1288-1296.
- SADER, H. S., CASTANHEIRA, M., HUBAND, M., JONES, R. N. & FLAMM, R. K. 2017. WCK 5222 (cefepime-zidebactam) antimicrobial activity against clinical isolates of Gram-negative bacteria collected worldwide in 2015. *Antimicrobial Agents and Chemotherapy*, 61, e00072-17.
- SALKIND, A. R., CUDDY, P. G. & FOXWORTH, J. W. 2001. Is This Patient Allergic to Penicillin? An Evidence-Based Analysis of the Likelihood of Penicillin Allergy. *JAMA*, 285, 2498-2505.
- SATTA, G., CORNAGLIA, G., MAZZARIOL, A., GOLINI, G., VALISENA, S. & FONTANA, R. 1995. Target for bacteriostatic and bactericidal activities of beta-lactam antibiotics against *Escherichia coli* resides in different penicillin-binding proteins. *Antimicrobial Agents and Chemotherapy*, 39, 812-818.

- SAUVAGE, E., DEROUAUX, A., FRAIPONT, C., JORIS, M., HERMAN, R., ROCABOY, M., SCHLOESSER, M., DUMAS, J., KERFF, F. & NGUYEN-DISTECHE, M. 2014. Crystal structure of penicillin-binding protein 3 (PBP3) from *Escherichia coli*. *PLoS One*, 9, e98042.
- SAUVAGE, E., DUEZ, C., HERMAN, R., KERFF, F., PETRELLA, S., ANDERSON, J. W., ADEDIRAN, S. A., PRATT, R. F., FRÈRE, J.-M. & CHARLIER, P. 2007. Crystal structure of the *Bacillus subtilis* penicillin-binding protein 4a, and its complex with a peptidoglycan mimetic peptide. *Journal of Molecular Biology*, 371, 528-539.
- SAUVAGE, E., KERFF, F., TERRAK, M., AYALA, J. A. & CHARLIER, P. 2008. The penicillin-binding proteins: structure and role in peptidoglycan biosynthesis. *FEMS Microbiology Reviews*, 32, 234-258.
- SAUVAGE, E. & TERRAK, M. 2016. Glycosyltransferases and transpeptidases/penicillin-binding proteins: valuable targets for new antibacterials. *Antibiotics*, 5, 12.
- SCHIFFER, G. & HÖLTJE, J.-V. 1999. Cloning and characterization of PBP 1C, a third member of the multimodular class A penicillin-binding proteins of *Escherichia coli*. *Journal of Biological Chemistry*, 274, 32031-32039.
- SHAM, L.-T., BUTLER, E. K., LEBAR, M. D., KAHNE, D., BERNHARDT, T. G. & RUIZ, N. 2014. MurJ is the flippase of lipid-linked precursors for peptidoglycan biogenesis. *Science*, 345, 220-222.
- SHAPIRO, A. B., COMITA-PREVOIR, J. & SYLVESTER, M. 2019. 5-Carboxytetramethylrhodamine-Ampicillin Fluorescence Anisotropy-Based Assay of *Escherichia coli* Penicillin-Binding Protein 2 Transpeptidase Inhibition. *ACS Infectious Diseases*, 5, 56863-872.
- SHAPIRO, A. B., GAO, N., GU, R.-F. & THRESHER, J. 2014. Fluorescence anisotropy-based measurement of *Pseudomonas aeruginosa* penicillin-binding protein 2 transpeptidase inhibitor acylation rate constants. *Analytical Biochemistry*, 463, 15-22.
- SHAPIRO, A. B., GU, R. F., GAO, N., LIVCHAK, S. & THRESHER, J. 2013. Continuous fluorescence anisotropy-based assay of BOCILLIN FL penicillin reaction with penicillin binding protein 3. *Analytical Biochemistry*, 439, 37-43.
- SHARIFZADEH, S., BOERSMA, M. J., KOCAOGLU, O., SHOKRI, A., BROWN, C. L., SHIRLEY, J. D., WINKLER, M. E. & CARLSON, E. E. 2017. Novel electrophilic scaffold for imaging of essential penicillin-binding proteins in *Streptococcus pneumoniae*. *ACS Chemical Biology*, 12, 2849-2857.
- SHARMA, P. & TOWSE, A. 2010. New drugs to tackle antimicrobial resistance: analysis of EU policy options. Available at SSRN 2640028.
- SHI, Q., MEROUEH, S. O., FISHER, J. F. & MOBASHERY, S. 2011. A computational evaluation of the mechanism of penicillin-binding protein-catalyzed cross-linking of the bacterial cell wall. *Journal of the American Chemical Society*, 133, 5274-5283.
- SHIRLEY, M. 2018. Ceftazidime-Avibactam: A Review in the Treatment of Serious Gram-Negative Bacterial Infections. *Drugs*, 78, 675-692.
- SHORE, A. C. & COLEMAN, D. C. 2013. Staphylococcal cassette chromosome mec: recent advances and new insights. *International Journal of Medical Microbiology*, 303, 350-359.

- SIEVERS, F., WILM, A., DINEEN, D., GIBSON, T. J., KARPLUS, K., LI, W., LOPEZ, R., MCWILLIAM, H., REMMERT, M., SÖDING, J., THOMPSON, J. D. & HIGGINS, D. G. 2011. Fast, scalable generation of high-quality protein multiple sequence alignments using Clustal Omega. *Molecular Systems Biology*, 7, 539-539.
- SILHAVY, T. J., KAHNE, D. & WALKER, S. 2010. The bacterial cell envelope. *Cold Spring Harbor Perspectives in Biology*, 2, a000414.
- SILVAGGI, N. R., ANDERSON, J. W., BRINSMADÉ, S. R., PRATT, R. & KELLY, J. A. 2003. The crystal structure of phosphonate-inhibited D-Ala-D-Ala peptidase reveals an analogue of a tetrahedral transition state. *Biochemistry*, 42, 1199-1208.
- SILVAGGI, N. R., JOSEPHINE, H. R., KUZIN, A. P., NAGARAJAN, R., PRATT, R. & KELLY, J. A. 2005. Crystal structures of complexes between the R61 DD-peptidase and peptidoglycan-mimetic β -lactams: a non-covalent complex with a "perfect penicillin". *Journal of Molecular Biology*, 345, 521-533.
- SILVER, L. L. 2011. Challenges of antibacterial discovery. *Clin Microbiol Rev*, 24, 71-109.
- SINGER, A. C., SHAW, H., RHODES, V. & HART, A. 2016. Review of Antimicrobial Resistance in the Environment and Its Relevance to Environmental Regulators. *Frontiers in Microbiology*, 7, 1728.
- SINGH, A., TOMBERG, J., NICHOLAS, R. A. & DAVIES, C. 2019. Recognition of the β -lactam carboxylate triggers acylation of *Neisseria gonorrhoeae* penicillin-binding protein 2. *Journal of Biological Chemistry*, 294, 14020-14032.
- SINGH, S. B. 2014. Confronting the challenges of discovery of novel antibacterial agents. *Bioorganic & Medicinal Chemistry Letters*, 24, 3683-9.
- SJODT, M., BROCK, K., DOBIHAL, G., ROHS, P. D. A., GREEN, A. G., HOPF, T. A., MEESKE, A. J., SRISUKNIMIT, V., KAHNE, D., WALKER, S., MARKS, D. S., BERNHARDT, T. G., RUDNER, D. Z. & KRUSE, A. C. 2018. Structure of the peptidoglycan polymerase RodA resolved by evolutionary coupling analysis. *Nature*, 556, 118.
- SKARP, K.-P., SHAMS, A., MONTELIN, H., LAGERBÄCK, P. & TÄNGDÉN, T. 2019. Synergistic and bactericidal activities of mecillinam, amoxicillin and clavulanic acid combinations against extended-spectrum β -lactamase (ESBL)-producing *Escherichia coli* in 24-h time–kill experiments. *International Journal of Antimicrobial Agents*, 53, 74-79.
- SMART, O. S., HORSKÝ, V., GORE, S., SVOBODOVÁ VAŘEKOVÁ, R., BENDO VÁ, V., KLEYWEGT, G. J. & VELANKAR, S. 2018. Worldwide Protein Data Bank validation information: usage and trends. *Acta Crystallographica Section D: Structural Biology*, 74, 237-244.
- SMITH, C. A., ANTUNES, N. T., STEWART, N. K., TOTH, M., KUMARASIRI, M., CHANG, M., MOBASHERY, S. & VAKULENKO, S. B. 2013. Structural basis for carbapenemase activity of the OXA-23 β -lactamase from *Acinetobacter baumannii*. *Chemistry & Biology*, 20, 1107-1115.
- SMITH, H., DEWDNEY, J. M. & WHEELER, A. 1971. A comparison of the amounts and the antigenicity of polymeric materials formed in aqueous solution by some β -lactam antibiotics. *Immunology*, 21, 527.
- SMITH, H. & MARSHALL, A. C. 1971. Biological Sciences: Polymers Formed by some β -Lactam Antibiotics. *Nature*, 232, 45-46.

- SOUGAKOFF, W. & JARLIER, V. 2000. Comparative potency of mecillinam and other β -lactam antibiotics against *Escherichia coli* strains producing different β -lactamases. *Journal of Antimicrobial Chemotherapy*, 46, 9-14.
- SPELLBERG, B., BRASS, E. P., BRADLEY, J. S., LEWIS, R. J., SHLAES, D., AMBROSE, P. G., DAS, A., BOUCHER, H. W., DOI, Y., BARTLETT, J. G., BONOMO, R. A., LAROSA, S. P., TALBOT, G. H., BENJAMIN, D., GUIDOS, R. J., JEZEK, A. & GILBERT, D. N. 2012. White Paper: Recommendations on the Conduct of Superiority and Organism-Specific Clinical Trials of Antibacterial Agents for the Treatment of Infections Caused by Drug-Resistant Bacterial Pathogens. *Clinical Infectious Diseases*, 55, 1031-1046.
- SPRATT, B. G. 1975. Distinct penicillin binding proteins involved in the division, elongation, and shape of *Escherichia coli* K12. *Proceedings of the National Academy of Sciences*, 72, 2999-3003.
- SPRATT, B. G. 1977. The mechanism of action of mecillinam. *Journal of Antimicrobial Chemotherapy*, 3, 13-19.
- STACHYRA, T., PECHEREAU, M. C., BRUNEAU, J. M., CLAUDON, M., FRERE, J. M., MIOSSEC, C., COLEMAN, K. & BLACK, M. T. 2010. Mechanistic studies of the inactivation of TEM-1 and P99 by NXL104, a novel non-beta-lactam beta-lactamase inhibitor. *Antimicrobial Agents and Chemotherapy*, 54, 5132-8.
- STARR, J., BROWN, M. F., ASCHENBRENNER, L., CASPERS, N., CHE, Y., GERSTENBERGER, B. S., HUBAND, M., KNAFELS, J. D., LEMMON, M. M. & LI, C. 2014. Siderophore receptor-mediated uptake of lactivicin analogues in gram-negative bacteria. *Journal of Medicinal Chemistry*, 57, 3845-3855.
- STEFANOVA, M. E., TOMBERG, J., OLESKY, M., HÖLTJE, J.-V., GUTHEIL, W. G. & NICHOLAS, R. A. 2003. *Neisseria gonorrhoeae* penicillin-binding protein 3 exhibits exceptionally high carboxypeptidase and β -lactam binding activities. *Biochemistry*, 42, 14614-14625.
- STUDIER, F. W. 2005. Protein production by auto-induction in high-density shaking cultures. *Protein Expression and Purification*, 41, 207-234.
- STUDIER, F. W. & MOFFATT, B. A. 1986. Use of bacteriophage T7 RNA polymerase to direct selective high-level expression of cloned genes. *Journal of Molecular Biology*, 189, 113-130.
- SUNAGAWA, M., MATSUMURA, H., INOUE, T., FUKASAWA, M. & KATO, M. 1990. A novel carbapenem antibiotic, SM-7338 structure-activity relationships. *The Journal of Antibiotics*, 43, 519-532.
- SUNG, M. T., LAI, Y. T., HUANG, C. Y., CHOU, L. Y., SHIH, H. W., CHENG, W. C., WONG, C. H. & MA, C. 2009. Crystal structure of the membrane-bound bifunctional transglycosylase PBP1b from *Escherichia coli*. *Proceedings of the National Academy of Sciences of the United States of America*, 106, 8824-9.
- SUTARIA, D. S., MOYA, B., GREEN, K. B., KIM, T. H., TAO, X., JIAO, Y., LOUIE, A., DRUSANO, G. L. & BULITTA, J. B. 2018. First penicillin-binding protein occupancy patterns of β -lactams and β -lactamase inhibitors in *Klebsiella pneumoniae*. *Antimicrobial Agents and Chemotherapy*, 62, e00282-18.
- TACCONELLI, E., CARRARA, E., SAVOLDI, A., HARBARTH, S., MENDELSON, M., MONNET, D. L., PULCINI, C., KAHLMETER, G., KLUYTMANS, J., CARMELI, Y., OUELLETTE, M., OUTTERSON, K., PATEL, J., CAVALERI, M., COX, E. M., HOUCHEMS, C. R., GRAYSON, M. L., HANSEN, P., SINGH, N.,

- THEURETZBACHER, U., MAGRINI, N. & GROUP, W. H. O. P. P. L. W. 2018. Discovery, research, and development of new antibiotics: the WHO priority list of antibiotic-resistant bacteria and tuberculosis. *Lancet Infectious Diseases*, 18, 318-327.
- TAGUCHI, A., WELSH, M. A., MARMONT, L. S., LEE, W., SJODT, M., KRUSE, A. C., KAHNE, D., BERNHARDT, T. G. & WALKER, S. 2019. FtsW is a peptidoglycan polymerase that is functional only in complex with its cognate penicillin-binding protein. *Nature Microbiology*, 4, 587-594.
- TAKAHATA, S., SENJU, N., OSAKI, Y., YOSHIDA, T. & IDA, T. 2006. Amino acid substitutions in mosaic penicillin-binding protein 2 associated with reduced susceptibility to cefixime in clinical isolates of *Neisseria gonorrhoeae*. *Antimicrobial Agents and Chemotherapy*, 50, 3638-45.
- TANG, K. L., CAFFREY, N. P., NÓBREGA, D. B., CORK, S. C., RONKSLEY, P. E., BARKEMA, H. W., POLACHEK, A. J., GANSHORN, H., SHARMA, N., KELLNER, J. D. & GHALI, W. A. 2017. Restricting the use of antibiotics in food-producing animals and its associations with antibiotic resistance in food-producing animals and human beings: a systematic review and meta-analysis. *The Lancet. Planetary Health*, 1, e316-e327.
- TÄRNBERG, M., ÖSTHOLM-BALKHED, Å., MONSTEIN, H.-J., HÄLLGREN, A., HANBERGER, H. & NILSSON, L. E. 2011. In vitro activity of beta-lactam antibiotics against CTX-M-producing *Escherichia coli*. *European Journal of Clinical Microbiology & Infectious Diseases*, 30, 981-987.
- THOMSON, K. S., ABDELGHANI, S., SNYDER, J. W. & THOMSON, G. K. 2019. Activity of Cefepime-Zidebactam against Multidrug-Resistant (MDR) Gram-Negative Pathogens. *Antibiotics*, 8, 32.
- THULIN, E., SUNDQVIST, M. & ANDERSSON, D. I. 2015. Amdinocillin (mecillinam) resistance mutations in clinical isolates and laboratory-selected mutants of *Escherichia coli*. *Antimicrobial agents and chemotherapy*, 59, 1718-1727.
- TIPPER, D. J. & STROMINGER, J. L. 1965. Mechanism of action of penicillins: a proposal based on their structural similarity to acyl-D-alanyl-D-alanine. *Proceedings of the National Academy of Sciences of the United States of America*, 54, 1133.
- TITELMAN, E., IVERSEN, A., KAHLMETER, G. & GISKE, C. G. 2011. Antimicrobial susceptibility to parenteral and oral agents in a largely polyclonal collection of CTX-M-14 and CTX-M-15-producing *Escherichia coli* and *Klebsiella pneumoniae*. *APMIS*, 119, 853-863.
- TOMBERG, J., TEMPLE, B., FEDAROVICH, A., DAVIES, C. & NICHOLAS, R. A. 2012. A highly conserved interaction involving the middle residue of the SXN active-site motif is crucial for function of class B penicillin-binding proteins: mutational and computational analysis of PBP 2 from *N. gonorrhoeae*. *Biochemistry*, 51, 2775-2784.
- TRIP, E. N. & SCHEFFERS, D.-J. 2015. A 1 MDa protein complex containing critical components of the *Escherichia coli* divisome. *Scientific reports*, 5, 18190.
- TYPAS, A., BANZHAF, M., GROSS, C. A. & VOLLMER, W. 2012. From the regulation of peptidoglycan synthesis to bacterial growth and morphology. *Nature Reviews Microbiology*, 10, 123-136.

- TYPAS, A., BANZHAF, M., VAN SAPAROEAE, B. V. D. B., VERHEUL, J., BIBOY, J., NICHOLS, R. J., ZIETEK, M., BEILHARZ, K., KANNENBERG, K. & VON RECHENBERG, M. 2010. Regulation of peptidoglycan synthesis by outer-membrane proteins. *Cell*, 143, 1097-1109.
- UK GOV. 2019. Tackling antimicrobial resistance 2019-2024 — the UK's five-year national action plan. *UK Government*. Accessed June 2019. Available at: https://assets.publishing.service.gov.uk/government/uploads/system/uploads/attachment_data/file/773130/uk-amr-5-year-national-action-plan.pdf
- US FDA. 2018. Limited Population Pathway for Antibacterial and Antifungal Drugs Guidance for Industry. *US Food and Drug Administration*. Accessed June 2019. Available at: <https://www.fda.gov/drugs/development-resources/limited-population-pathway-antibacterial-and-antifungal-drugs-lpad-pathway>
- VAGIN, A. & LEBEDEV, A. 2015. MoRDa, an automatic molecular replacement pipeline. *Acta Crystallogr. A*, 71, s19.
- VALASATAVA, Y., ROSATO, A., CAVALLARO, G. & ANDREINI, C. 2014. MetaS 3, a database-mining tool for the identification of structurally similar metal sites. *JBIC Journal of Biological Inorganic Chemistry*, 19, 937-945.
- VAN BERKEL, S. S., NETTLESHIP, J. E., LEUNG, I. K., BREM, J. R., CHOI, H., STUART, D. I., CLARIDGE, T. D., MCDONOUGH, M. A., OWENS, R. J. & REN, J. 2013. Binding of (5 S)-Penicilloic Acid to Penicillin Binding Protein 3. *ACS Chemical Biology*, 8, 2112-2116.
- VAN DER BIJ, A. K. & PITOUT, J. D. 2012. The role of international travel in the worldwide spread of multiresistant Enterobacteriaceae. *Journal of Antimicrobial Chemotherapy*, 67, 2090-100.
- VATS, P., SHIH, Y. L. & ROTHFIELD, L. 2009. Assembly of the MreB-associated cytoskeletal ring of *Escherichia coli*. *Molecular Microbiology*, 72, 170-82.
- VAZQUEZ, E. G., MENSA, J., MARTINEZ, J., MARCOS, M., PUIG, J., ORTEGA, M. & TORRES, A. 2005. Lower mortality among patients with community-acquired pneumonia treated with a macrolide plus a beta-lactam agent versus a beta-lactam agent alone. *European Journal of Clinical Microbiology and Infectious Diseases*, 24, 190-195.
- VENTOLA, C. L. 2015. The antibiotic resistance crisis: part 1: causes and threats. *Pharmacy and Therapeutics*, 40, 277.
- VILA, J., MARTÍ, S. & SANCHEZ-CÉSPEDES, J. 2007. Porins, efflux pumps and multidrug resistance in *Acinetobacter baumannii*. *Journal of Antimicrobial Chemotherapy*, 59, 1210-1215.
- VINELLA, D., D'ARI, R., JAFFE, A. & BOULOC, P. 1992. Penicillin binding protein 2 is dispensable in *Escherichia coli* when ppGpp synthesis is induced. *The EMBO Journal*, 11, 1493-1501.
- VINELLA, D., JOSELEAU-PETIT, D., THÉVENET, D., BOULOC, P. & D'ARI, R. 1993. Penicillin-binding protein 2 inactivation in *Escherichia coli* results in cell division inhibition, which is relieved by FtsZ overexpression. *Journal of Bacteriology*, 175, 6704-6710.
- VOLLMER, W. 2008. Structural variation in the glycan strands of bacterial peptidoglycan. *FEMS Microbiology Reviews*, 32, 287-306.

- VOLLMER, W., BLANOT, D. & DE PEDRO, M. A. 2008. Peptidoglycan structure and architecture. *FEMS Microbiology Reviews*, 32, 149-167.
- VOLLMER, W. & HÖLTJE, J.-V. 2004. The architecture of the murein (peptidoglycan) in gram-negative bacteria: vertical scaffold or horizontal layer (s)? *Journal of Bacteriology*, 186, 5978-5987.
- VOLLMER, W. & SELIGMAN, S. J. 2010. Architecture of peptidoglycan: more data and more models. *Trends in Microbiology*, 18, 59-66.
- VONRHEIN, C., FLENSBURG, C., KELLER, P., SHARFF, A., SMART, O., PACIOREK, W., WOMACK, T. & BRICOGNE, G. 2011. Data processing and analysis with the autoPROC toolbox. *Acta Crystallographica Section D: Biological Crystallography*, 67, 293-302.
- WACHI, M., DOI, M., TAMAKI, S., PARK, W., NAKAJIMA-IIJIMA, S. & MATSUHASHI, M. 1987. Mutant isolation and molecular cloning of mre genes, which determine cell shape, sensitivity to mecillinam, and amount of penicillin-binding proteins in *Escherichia coli*. *Journal of Bacteriology*, 169, 4935-4940.
- WALSH, C. 2003. Antibiotics: actions, origins, resistance, *American Society for Microbiology*, 13, 3059–3060.
- WANG, X., ZHANG, F., ZHAO, C., WANG, Z., NICHOLS, W. W., TESTA, R., LI, H., CHEN, H., HE, W. & WANG, Q. 2014. In vitro activities of ceftazidime-avibactam and aztreonam-avibactam against 372 Gram-negative bacilli collected in 2011 and 2012 from 11 teaching hospitals in China. *Antimicrobial Agents and Chemotherapy*, 58, 1774-1778.
- WHO. 2014. Antimicrobial resistance: global report on surveillance, *World Health Organization*. Accessed June 2019. Available at: <https://www.who.int/drugresistance/documents/surveillancereport/en/>
- WHO. 2016. Health care-associated infections fact sheet. *World Health Organization*. Accessed June 2019. Available at: https://www.who.int/qpsc/country_work/qpsc_ccisc_fact_sheet_en.pdf
- WHO. 2017. Antibacterial agents in clinical development: an analysis of the antibacterial clinical development pipeline, including tuberculosis. *World Health Organization*. Accessed June 2019. Available at: https://www.who.int/medicines/areas/rational_use/antibacterial_agents_clinical_development/en/
- WHO. 2018. Global antimicrobial resistance surveillance system (GLASS) report: early implementation 2017-2018. *World Health Organization*. Available at: <https://www.who.int/glass/resources/publications/early-implementation-report-2017-2018/en/>
- WINN, M. D., BALLARD, C. C., COWTAN, K. D., DODSON, E. J., EMSLEY, P., EVANS, P. R., KEEGAN, R. M., KRISSINEL, E. B., LESLIE, A. G. & MCCOY, A. 2011. Overview of the CCP4 suite and current developments. *Acta Crystallographica Section D: Biological Crystallography*, 67, 235-242.
- WINTER, G. 2010. xia2: an expert system for macromolecular crystallography data reduction. *Journal of Applied Crystallography*, 43, 186-190.
- WINTER, G., WATERMAN, D. G., PARKHURST, J. M., BREWSTER, A. S., GILDEA, R. J., GERSTEL, M., FUENTES-MONTERO, L., VOLLMAR, M., MICHELS-CLARK, T. & YOUNG, I. D. 2018. DIALS: implementation and evaluation of a new integration package. *Acta Crystallographica Section D*, 74, 85-97.

- WOON, E. C. Y., ZERVOSEN, A., SAUVAGE, E., SIMMONS, K. J., ZIVEC, M., INGLIS, S. R., FISHWICK, C. W. G., GOBEC, S., CHARLIER, P., LUXEN, A. & SCHOFIELD, C. J. 2011. Structure guided development of potent reversibly binding penicillin binding protein inhibitors. *ACS Medicinal Chemistry Letters*, 2, 219-223.
- WUIJTS, S., VAN DEN BERG, H. H., MILLER, J., ABEBE, L., SOBSEY, M., ANDREMONT, A., MEDLICOTT, K. O., VAN PASSEL, M. W. & DE RODA HUSMAN, A. M. 2017. Towards a research agenda for water, sanitation and antimicrobial resistance. *Journal of Water and Health*, 15, 175-184.
- YANG, S. Y. 2010. Pharmacophore modeling and applications in drug discovery: challenges and recent advances. *Drug Discovery Today*, 15, 444-50.
- YOSHIMURA, F. & NIKAIDO, H. 1985. Diffusion of beta-lactam antibiotics through the porin channels of *Escherichia coli* K-12. *Antimicrobial Agents and Chemotherapy*, 27, 84-92.
- YOUSIF, S. Y., BROOME-SMITH, J. K. & SPRATT, B. G. 1985. Lysis of *Escherichia coli* by β -Lactam Antibiotics: Deletion Analysis of the Role of Penicillin-binding Proteins 1A and 1B. *Microbiology*, 131, 2839-2845.
- YVON, M., ANGLADE, P. & WAL, J.-M. 1990. Identification of the binding sites of benzyl penicilloyl, the allergenic metabolite of penicillin, on the serum albumin molecule. *FEBS letters*, 263, 237-240.
- ZERVOSEN, A., BOUILLEZ, A., HERMAN, A., AMOROSO, A., JORIS, B., SAUVAGE, E., CHARLIER, P. & LUXEN, A. 2012a. Synthesis and evaluation of boronic acids as inhibitors of penicillin binding proteins of classes A, B and C. *Bioorganic & Medicinal Chemistry*, 20, 3915-3924.
- ZERVOSEN, A., SAUVAGE, E., FRÈRE, J.-M., CHARLIER, P. & LUXEN, A. 2012b. Development of new drugs for an old target—the penicillin binding proteins. *Molecules*, 17, 12478-12505.
- ZHANEL, G. G., LAWSON, C. D., ADAM, H., SCHWEIZER, F., ZELENITSKY, S., LAGACÉ-WIENS, P. R., DENISUIK, A., RUBINSTEIN, E., GIN, A. S. & HOBAN, D. J. 2013. Ceftazidime-avibactam: a novel cephalosporin/ β -lactamase inhibitor combination. *Drugs*, 73, 159-177.
- ZHAO, G., MEIER, T. I., KAHL, S. D., GEE, K. R. & BLASZCZAK, L. C. 1999. BOCILLIN FL, a sensitive and commercially available reagent for detection of penicillin-binding proteins. *Antimicrobial Agents and Chemotherapy*, 43, 1124-1128.

Appendices

Name	Sequence	Restriction site/mutation
T7-F	5' TAATACGACTCACTATAGGG 3'	sequencing
T7-R	5' GCTAGTTATTGCTCAGCGG 3'	sequencing
M13-F	5' TGTA AACGACGGCCAGT 3'	sequencing
M13-R	5' CAGGAAACAGCTATGAC 3'	sequencing
pEGE305-F	5' CCTGGCGTTACCCAACCTTAATCG 3'	sequencing
pEGE305-R	5' CTACGATACGGGAGGGCTTAC 3'	sequencing
Eddie-F	5' CATTATGAATTCCATTTTCCCTAATCGTATGGTG 3'	EcoRI
Eddie-R	5' ATAATCTGCAGTTGATTTTTCATTATTCATCGACCTC 3'	PstI
0092-F	5' TTTGTGCATATGGCAAATGTTGATGAGTACATTACTC 3'	NdeI
0092-R	5' TTTGTGGGATCCTTAATTGTTCTGATAAATATCTTTATACAAAC- GGC 3'	BamHI
0093	5' GATCGACACCATGTTACGTG 3'	sequencing
0094-F	5' CCAACCGGGcCCTCTTTAAACCG 3'	S461A
0094-R	5' CGTTTTGCCTGGATGGCA 3'	S461A
0095-F	5' GTTTAAGGTACCAGGCCAATATTTTGCCTACTGAACGTA 3'	KpnI
0095-R	5' GGACGTGAATTCTTACCTGCGAATAGGATTTTCTGGAG 3'	EcoRI
0096-F	5' TTTGCGGGATCCGTTAAAACCATGCAAGTCTATACAGCCG 3'	BamHI
0096-R	5' TTTGCGGTCGACTTACTGAGCATCTTTTCTAAACGAACCC 3'	Sall
0097-F	5' GCGTTTGAATTCTGTTGAAGCGCTGCGTAAC 3'	EcoRI
0097-R	5' GCGATTAAGCTTTCAGAACAGGTCAATCGG 3'	HindIII
0098-F	5' ATAATGGTACCAGGCATCGGATAAAAACCGTATTCG 3'	KpnI
0098-R	5' GCTATAGAATTCTTATTCATCGACCTCGTTTGTAGCAGG 3'	EcoRI
0099	5' GATTTACTTCATGGAACACC 3'	sequencing
0100-F	5' TGCCATTTCCgccCCTGTTATT 3'	D350A
0100-R	5' GTAGCCCAATCAACAATTCC 3'	D350A
0101-F	5' CAAATTCCGTgccTGGAAAAAACCGG 3'	D365A
0101-R	5' TGCGAGTCGCCGGTAAA 3'	D365A
0102-F	5' AAAAACCGGTgctGGTATCGTGAAC 3'	H371A
0102-R	5' TTCCAGTCACGGAATTTG 3'	H371A
0103-F	5' TATCATGTCTgctGATACCTATTTTTATATTTTGGC 3'	C384A
0103-R	5' ATGGCTTTGTGCATGTTTC 3'	C384A
0104-F	5' CATGTCTTGaatACCTATTTTTATATTTTGGCTAA 3'	D385N
0104-R	5' ATAATGGCTTTGTGCATGTTCACAAT 3'	D385N
0105-F	5' TATCATGTCTgctGATACCTATTTTTATATTTTGGC 3'	C384A
0105-R	5' ATGGCTTTGTGCATGTTCACAATG 3'	C384A

Table S1. List of oligonucleotides used in this thesis. Mutations are shown in lower case letters.

Plasmid	Protein encoded
pET47b-based (kanamycin^R)	
pMIC06	Mutant D350A of PBP2 (aa 53-672) from <i>A. baumanniii</i> ATCC 17978
pMIC07	Mutant D365A of PBP2 (aa 53-672) from <i>A. baumanniii</i> ATCC 17978
pMIC08	Mutant H371A of PBP2 (aa 53-672) from <i>A. baumanniii</i> ATCC 17978
pMIC09	Mutant C384A of PBP2 (aa 53-672) from <i>A. baumanniii</i> ATCC 19606
pMIC10	Wild-type PBP2 (aa 53-672) from <i>A. baumanniii</i> ATCC 19606
pMIC11	Mutant D385N of PBP2 (aa 53-672) from <i>A. baumanniii</i> ATCC 19606
pMIC13	Wild-type PBP1a (aa 36-822) from <i>P. aeruginosa</i> PAO1
pMIC14	Mutant S461A of PBP1a (aa 36-822) from <i>P. aeruginosa</i> PAO1
pMIC15	Wild-type PBP1a (aa 51-764) from <i>A. baumannii</i> ATCC 19606
pMIC16	Wild-type PBP3 (aa 64-610) from <i>A. baumannii</i> ATCC 19606
pET28a-based (kanamycin^R)	
pMIC17	Wild-type DacB (aa 21-477) from <i>E. coli</i> K12
pUC19-based (ampicillin^R)	
pMIC01	Wild-type full length PBP2 from <i>A. baumanniii</i> ATCC 17978
pMIC02	Mutant D350A of full length PBP2 from <i>A. baumanniii</i> ATCC 17978
pMIC03	Mutant D365A of full length PBP2 from <i>A. baumanniii</i> ATCC 17978
pMIC04	Mutant H371A of full length PBP2 from <i>A. baumanniii</i> ATCC 17978
pMIC05	Mutant C384A of full length PBP2 from <i>A. baumanniii</i> ATCC 17978
pMIC12	Mutant D385N of full length PBP2 from <i>A. baumanniii</i> ATCC 17978
pEGE305-based (tetracycline^R)	
pEGE306	Wild-type full length PBP2 from <i>A. baumanniii</i> ATCC 17978
pEGE307	Mutant D350A of full length PBP2 from <i>A. baumanniii</i> ATCC 17978
pEGE308	Mutant D365A of full length PBP2 from <i>A. baumanniii</i> ATCC 17978
pEGE309	Mutant H371A of full length PBP2 from <i>A. baumanniii</i> ATCC 17978
pEGE310	Mutant C384A of full length PBP2 from <i>A. baumanniii</i> ATCC 17978
pEGE311	Mutant D385N of full length PBP2 from <i>A. baumanniii</i> ATCC 17978

Table S2. List of plasmids generated in this thesis.

		56	66	76	86
MAHHHHHSA	ALEVLFGQPG	YQDPLKPLQV	YTADNQLIAE	YGGKLSIPVE	YKQIPPNFIH
96	106	116	126	136	146
AFLAAEDSSF	FEHSGISFKG	LGRALSESVT	GSDVQTGGST	ITMQVAKNYY	LSPERTLKRK
156	166	176	186	196	206
LTEIFLARKI	EQNLKEDIL	SLYVKNKIFLG	KNAYGIAAAA	KIYYNKSINE	LSIAQMAMIA
216	226	236	246	256	266
GLPKAPSKYN	PVVNPERALE	RRNWILGRML	QLGYISQAEY	QKAVAEPINL	NMPNRDLNNI
276	286	296	306	316	326
HPYAGEMVRS	ELVKHFGEQA	IDSGYKVYTT	INAKRQAIIE	KAVQDGLIAY	DRRHGWRGAE
336	346	356	366	376	386
AHDKPLSEFR	AYANTYPAQV	TKVNSSSFEA	LMQDGSSTVTV	QWSGMSWARP	YRNANSVGAA
396	406	416	426	436	446
PSRASQIVKV	KDIVRLRPNE	AKTAWSLVQV	PKVQGQLIAI	NPNDGSIEAI	VGGINFYQSK
456	466	476	486	496	506
FNRALQGWRQ	PGSTIKPFLY	ALALERGMTP	YSMVNDSPIT	IGKWTPKNSD	GRYLGMIPLR
516	526	536	546	556	566
RALYLSRNTV	SVRLQLTVGI	ERTRQLFMDF	GLQEDQIPRN	YTIALGTPQV	LPIQMATGYA
576	586	596	606	616	626
TFANGGYRVQ	PHFIQRIEDA	YGKVIYEAKP	EYACIPCINA	PETDDAQVT	TPDDQVIEVT
636	646	656	666	676	686
NKELEQKEKT	TKQLNLKQTD	KNNSQYRQAQ	RILKSSSAYD	MANILRDVIE	HGTGRAALKI
696	706	716	726	736	746
GRSDLGGKTG	TTNDAKDAWF	AGFNGKLVTV	TWVGFDQPTT	LGRREYGGIA	ALPIWINFMG
756					
QALQGTAAAW	VRLEKDAQ				

Figure S1. Amino acid sequence of *A. baumannii* PBP1a Δ51-764 encoded by pMIC15. Extra amino acids are present at the N-terminal and derive from the pET47b vector (grey). Numbering refers to the UniProt entry G1C775.

		60	70	80	90
MAHHHHHSA	ALEVLFGQPG	YQASDKNRIR	LQPLPPARGY	IYDRNGVLLA	DNYPVFTATL
100	110	120	130	140	150
SKADVENVD	VIEQLQPILE	LTQEDVDREK	SRIKTARKTE	RVAIKLNLTE	TNIAKFSEVK
160	170	180	190	200	210
YKFPGVRIET	QMTRYYPHGD	LFAHVIGYVG	RINDKELKSI	DKDLYAGTNL	IGKIGVEKSY
220	230	240	250	260	270
EDLLHGTPGY	ESVEADAHSN	ILRHLGRKDP	TRGNDLYLSL	DYGLQVVASQ	QLAGRRGAIV
280	290	300	310	320	330
AIDPRTGEIL	ALVSSPSFNP	NLFVTGINHK	DYSSLRDNID	QPLYNRAVQG	VYPPGSTIKP
340	350	360	370	380	390
MEAMGGLHYG	IVDWATAISD	PGYFHLPGDS	HKFRDWKKTG	HGIVNMHKAI	IMSCDTYFYI
400	410	420	430	440	450
LANQMGIDQM	NQWMRQFGFG	QKTGVDLPSE	SEGLYPNPEW	KMRTRKSKWM	KGETISVSIG
460	470	480	490	500	510
QGAFTATPLQ	LAMATAITAN	HGSHVVPHVL	RATHGAKPFT	VRNAPDGKIN	FNGTDEDWVK
520	530	540	550	560	570
MREAMIDVIQ	SGTGRGIRTP	LYQIAGKTGT	AQVKSIAQ GK	RYNEAALSER	QLDHGLFVGF
580	590	600	610	620	630
APADKPEIAI	AVIWENGRHG	GSAAQLAKPV	FDYWLLTRKK	NPIRPAHQV	NGGLMTAGIK
640	650	660	670		
PGELPSGNES	ASSTPATSAP	TSAAASTPQA	TPTRPATNEV	DE	

Figure S2. Amino acid sequence of *A. baumannii* PBP2 Δ 53-672 encoded by pMIC10. Extra amino acids are present at the N-terminal and derive from the pET47b vector (grey). Asp350, Asp365, His371 and Cys384 (numbering refers to the UniProt entry G1C6X4) were mutated to alanine in plasmids pMIC06/07/08/09, respectively. Asp385 (UniProt entry G1C6X4) was mutated to asparagine in pMIC11. Mutated residues are underlined.

		71	81	91	101
MAHHHHHSA	ALEVLFGQPG	YQANILRTER	IEAMRGVISD	RHGVPLAISS	PIMKIVIDPR
111	121	131	141	151	161
DYFETKHLVD	QITAEKQDP	NNRKLKRQLP	DKNLNLDELA	DVVGVDRADL	KKQMNARPRS
171	181	191	201	211	221
RYLVLKKEVP	PQQADLIMKG	NFQGVYAEKT	YKRYYPQPQP	NAQIIGLTNS	EGQGIEGLEM
231	241	251	261	271	281
QLNKQLSGVD	GEQKIIRDKR	GNRLKVSEVI	REGEPGENIT	LSIDSRLQYI	MYRELTAAGV
291	301	311	321	331	341
ANNARSATAI	AVDVKTGEIL	AMTSWPSYNP	NDKNGLSNKD	AMRNRGAIDM	FEPGSTMKPF
351	361	371	381	391	401
TISAALETGQ	YTPNTIVNTS	PGSMRLGWHT	IRDTHNYGAL	TVSGVVIKSS	NVGSAKIALS
411	421	431	441	451	461
LPKETLPSFF	NRVGFGRSA	VRFPGESSGL	VLPVNKLNSS	QIGTMAYGYG	LNATILQLAQ
471	481	491	501	511	521
GYAMLANHGV	KMPLSLHKLD	QPPKGEQVLN	PKIADQVLLM	LEQVTMPGGT	AKQANIPGYR
531	541	551	561	571	581
VGGKTGTAHK	LRADGKGYSN	NEYRALFAGV	APISDPRLAV	IVVVENPQGR	YGGGLVAAPV
591	601				
FARIMQESLR	LMNVPLDKPL	NTPENPIRR			

Figure S3. Amino acid sequence of *A. baumannii* PBP3 Δ64-610 encoded by pMIC16. Extra amino acids are present at the N-terminal and derive from the pET47b vector (grey). Numbering refers to the UniProt entry G1C6Z8.

			39	49	59	69
MAHHHHHSA	ALEVLFGQPG	YQDPNSVEAL	RNVQLQIPLK	VYSEDGKLIS	EFGEMRRTPI	
79	89	99	109	119	129	
RFADIPQDFI	HALLSAEDDN	FANHYGVDVK	SLMRAAAQLL	KSGHIQTGGS	TITMQVAKNY	
139	149	159	169	179	189	
FLTNERSFSR	KINEILLALQ	IERQLTKDEI	LELYVNKIYL	GNRAYGIEAA	AQVYYGKPIK	
199	209	219	229	239	249	
DLSLAEMAMI	AGLPKAPSRY	NPLVNPTRST	ERRNWILERM	LKLGFDQQR	YQAAVEEPIN	
259	269	279	289	299	309	
ASYHVQTPPEL	NAPYIAEMAR	AEMVGRYGSE	AYTEGYKVIT	TVRSDLQNAA	SQSVRDGLID	
319	329	339	349	359	369	
YDQRHGGRGP	ETRLPGQTRD	AWLKHLGQQR	SIGGLEPAIV	TQVEKSGIMV	MTRDGKEEAV	
379	389	399	409	419	429	
TWDSMKWARP	FLSNNSMGPM	PRQPADVAQA	GDQIRVQRQE	DGTLRFVQIP	AAQSALISLD	
439	449	459	469	479	489	
PKDGAIRSLV	GGFSFEQSNY	NRAIQAKRQP	GSSF ^u KPFIYS	AALDNGFTAA	SLVNDAPIVF	
499	509	519	529	539	549	
VDEYLDKVWR	PKNDTNTFLG	PIPLREALYK	SRNMVSIRVL	QGLGIERAIS	YITKFGFQRD	
559	569	579	589	599	609	
ELPRNFSLAL	GTATVTPMEI	AGAWSVFANG	GYKVNPYVIE	RIESRDGQVL	YQANPPRPV	
619	629	639	649	659	669	
EEQVAADAED	AGNPGDPEHP	ESAEEGESIE	AQQVAAKAQT	TFEPTPAERI	IDARTAYIMT	
679	689	699	709	719	729	
SMLQDVIKRG	TGRRALALKR	TDLAGKTGTT	NDSKDGWFSG	YNSDYVTSVW	VGFDQPETLG	
739	749	759	769	779	789	
RREYGGTVAL	PIWIRYMGFA	LKDKPMHTMA	EPPGIVSLRI	DPVTGRSAAP	GTPGAYFEMF	
799	809	819				
KNEDTPPSVN	ELPPGSFPGS	PLPDDEGAPI	DLF			

Figure S4. Amino acid sequence of *P. aeruginosa* PBP1a Δ 36-822 encoded by pMIC13. Ser461 (numbering refers to the UniProt entry Q07806) was mutated to alanine in pMIC14. Extra amino acids are present at the N-terminal and derive from the pET47b vector (grey). Mutated residues are underlined.

52	62	72	82	92	102
GPQYQDPARS	VRHIAIPAHR	GLITDRNGEP	LAVSTPVTTL	WANPKELMTA	KERWPQLAAA
112	122	132	142	152	162
LGQDTKLFAD	RIEQNAEREF	IYLVRLTPE	QGEVIALKV	PGVYSIEEFR	RFYPAGEVVA
172	182	192	202	212	222
HAVGFTDVDD	RGREGIELAF	DEWLAGVPGK	RQVLKDRRGR	VIKDVQVTKN	AKPGKTLALS
232	242	252	262	272	282
IDLRLQYLAH	RELRNALLEN	GAKAGSLVIM	DVKTGEILAM	TNQPTYNPNN	RRNLQPAAMR
292	302	312	322	332	342
NRAMIDVFEP	GSTVKPFSMS	AALASGRWKP	SDIVDVYPGT	LQIGRYTIRD	VSRNSRQLDL
352	362	372	382	392	402
TGILIKSSNV	GISKIAFDIG	AESIYSVMQQ	VGLGQDTGLG	FPGERVGNLP	NHRKWPKAET
412	422	432	442	452	462
ATLAYGYGLS	VTAIQLAHAY	AALANDGKSV	PLSMTRVDRV	PDGVQVISPE	VASTVQGMLQ
472	482	492	502	512	522
QVVEAQGGVF	RAQVPGYHAA	GKSGTARKVS	VGTKGYRENA	YRSLFAGFAP	ATDPRIAMVV
532	542	552	562	572	
VIDEPSKAGY	FGGLVSAPVF	SKVMAGALRL	MNVPPDNLPT	ATEQQQVNAA	PAKGGRG

Figure S5. Amino acid sequence of *P. aeruginosa* PBP3 Δ 50-579 encoded by pDB1. Extra amino acids are present at the N-terminal and derive from the pET47b vector (grey). The plasmid was a kind gift of Dr Dom Bellini (previously of University of Warwick) (Bellini *et al.*, 2019). Numbering refers to the UniProt entry G3XD46.

		29		39		49		59
MGSSHHHHHH	SSGLVPRGSH	MANVDEYITQ	LPAGANLALM	VQKVGASAPA	IDYHSQQMAL			
69	79	89	99	109	119			
PASTQKVITA	LAALIQLGPD	FRFTTTLETK	GNVENGVLKG	DLVARFGADP	TLKRQDIRNM			
129	139	149	159	169	179			
VATLKKSGVN	QIDGNVLIDT	SIFASHDKAP	GWPWNMTQC	FSAPPAAAIIV	DRNCFVSLSY			
189	199	209	219	229	239			
SAPKPGDMAF	IRVASIYPVT	MFSQVRTLPR	GSAEAQYCEL	DVVPGLNRF	TLTGCLPQRS			
249	259	269	279	289	299			
EPLPLAFVQ	DGASYAGAIL	KYELKQAGIT	WSGTLRQTQ	VNEPGTVVAS	KQSAPLHDL			
309	319	329	339	349	359			
KIMLKKSDNM	IADTVFERMIG	HARENVPGTW	RAGSDAVRQI	LRQQAGVDIG	NTIADGSGL			
369	379	389	399	409	419			
SRHNLIAPAT	MMQVLQYIAQ	HDNELNFISM	LPLAGYDGSL	QYRAGLHQAG	VDGKVSAGTG			
429	439	449	459	469				
SLQGVYNLAG	FITTASGQRM	AFVQYLSGYA	VEPADQRNRR	IPLVRFESRL	YKDIYQNN			

Figure S6. Amino acid sequence of *E. coli* DacB Δ 21-477 encoded by pMIC17. Extra amino acids are present at the N-terminal and derive from the pET28a vector (grey). Numbering refers to the UniProt entry P24228.

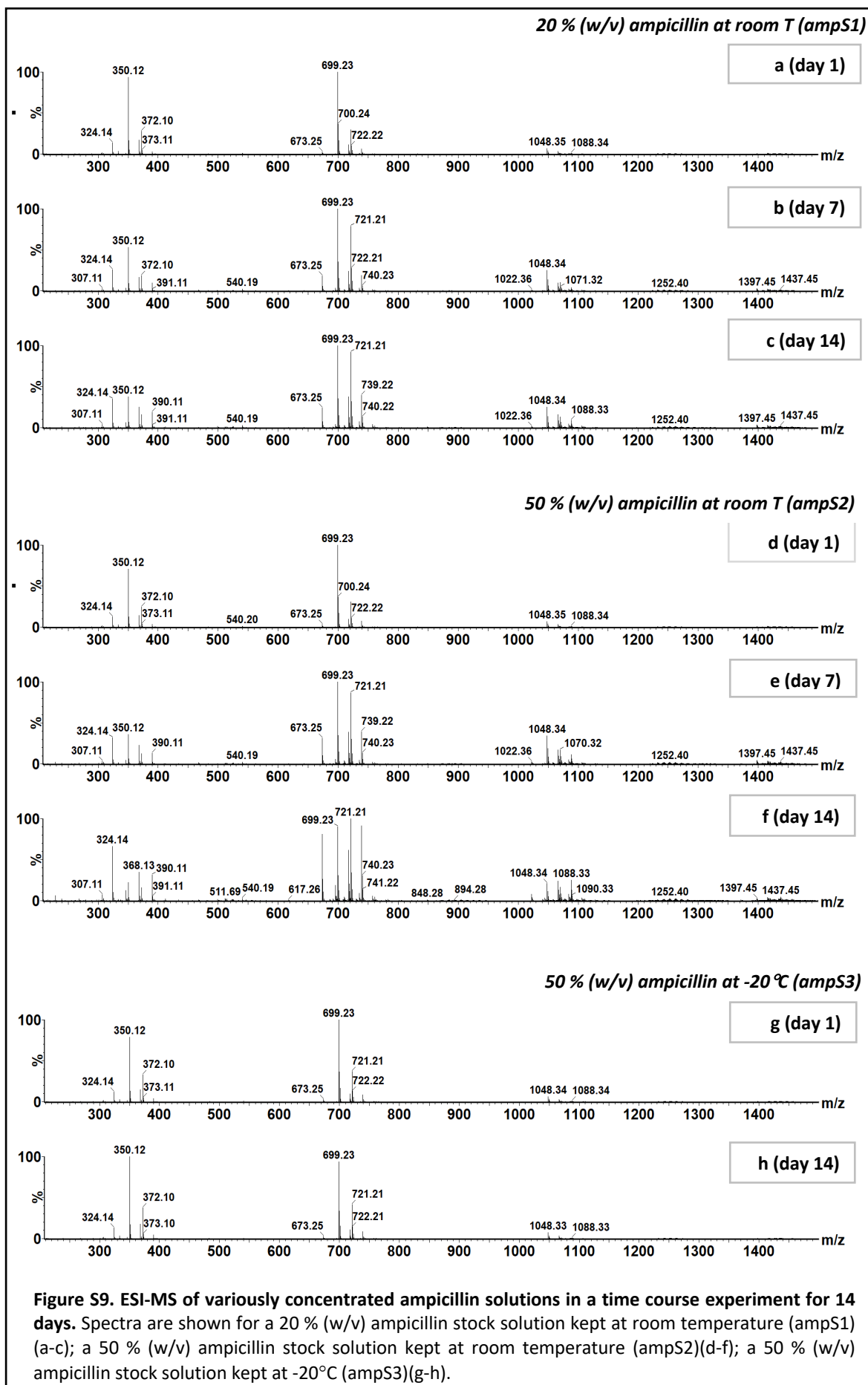
<i>Ec</i> PBP1a	-----MKFVKYFLILA-VCCILLGAGSIYGLYRYIEPQLPDVATLKDVRLE-----QIPMQ-----	49
<i>Kp</i> PBP1a	-----MKFVKYLLILA-VCCVLLGAGSIFGLYKYIEPQLPDVATLKDVRLE-----QIPMQ-----	49
<i>Ab</i> PBP1a	-----MKKLSSLGfVRPIFLII-IIILVSLPMGFYGMVLYIAPTLEPMSLKKAPL-----LKPLQ-----	55
<i>Pa</i> PBP1a	-----MRLKFLWWTWC-VTLICGVLLSfSGAYLYLSPSLPSVEALRNVQL-----QIPLK-----	49
<i>Ec</i> PBP1b	MAGNDREP IGRKGPTRPVKQKVSRRRYEDDDDDYDDY--DDYEDEEPMPRKGGK-KGKGRKPRGKRWLWLLKLAIVFAVLA IYGVYLDQKIR----SRIDGKVV----QLPAAVYGR	109
<i>Kp</i> PBP1b	MAGDDREP IGRKGRPSRPTKQKVTRRRVREEDYDDEYDDDDYDEDEKVPVPRKA--KGKGGKPRKRKRWLWLLVKLGIVFAVLA IYGVYLDQKIR----SRIDGKVV----ELPAAVYGR	109
<i>Ab</i> PBP1b	-----MKFERGIGFFALIFSIILVIGAFIALSIYLRDLNIIIR----EKFEQGQRW----DIPAKVFAR	54
<i>Pa</i> PBP1b	-----MTRPRSPRSRNSKARPAPGLNKWLSWALKLGLVGLVLLAGFAIYLDVAVVQ----EKFSGRRW----TIPAKVYAR	67
<i>Ec</i> PBP2	-----MKLQN---SFRD-YTAESALFVRRALVAFGLIILLTGVLIANLYNLQIVRFTDYQTRSNNENRIKLVPIAPS----	67
<i>Kp</i> PBP2	-----MKLQN---SFRD-YTAESALFVRRALVAFGLIILLTGVLIANLYNVQIVRFDDYQTRSNNENRIKLVPIPPS----	67
<i>Ab</i> PBP2	-----MKQHF---PLKD-IQEKRIYGRIFFAVGLVILICLLVSLASRYAYLQIFHYDEFSTASDKNRIQLPLPPA----	67
<i>Pa</i> PBP2	-----MPQPI---HLKD-HEKDARLVRRRVIVGAVAVVLLTTLVLRVARYHLQVTQYEHSTLSENNRVHVQPIPT----	67
<i>Ab</i> PBP3	-----MVDKRTKQTRKKQQSIS-EKPSLAFDMWRFYLLWAVVLLCFVVLIIARAFYVQVINKDFLQNKANANILRTERIEAM----	75
<i>Pa</i> PBP3	-----MKL-NYFQGALYPWRFCVIVGLLLAMVGAIVWRIVDLHVIDHDFLKGQGDARSVRHIAIPAH----	61
<i>Ec</i> PBP3	-----MKAAAKTQKPKR-QEEHANFISWRFALLCGCILLALAFLLGRVAVLQVISPDMLVKEGDMRSLRVQVSTST----	70
<i>Kp</i> PBP3	-----MKAAPKTPKAKR-QEEQANFISWRFALLCGCILLALAFLLGRVAVLQVISPDMLVQRQGDMSLRVQEVSTA----	70
<i>Ec</i> PBP1a	-----IYSADGELI---AQYGE-KR	65
<i>Kp</i> PBP1a	-----VYSADGELI---AQYGE-KR	65
<i>Ab</i> PBP1a	-----VYTADNQLI---AEYGG-KL	71
<i>Pa</i> PBP1a	-----VYSEDGKLI---SEFGE-MR	65
<i>Ec</i> PBP1b	MVNLEPDMTISKNEVMKLEATQYRQVSKMTRPGEFTVQANSIEM---IRRPFDFFPDSKEGQVRA-----RLTFDGDHLATIVNMENNRQFGFFRLDPRLITMISSPNG-EQ	212
<i>Kp</i> PBP1b	MVNLEPDMQISKNEVRLLNATQYRQVSAMTRPGEYTVQANSIEM---IRRPFDFFPDSKEGQVRA-----RLTFDGDHLETIENMDNNRQFGFFRLDPRLITMLQSPNG-EQ	212
<i>Ab</i> PBP1b	PLEIYNNAPI TQANFTQELKLLGYKTSNNDKSGTYVAQGSNMVY---HTRGFYDGDSEIEPEQVL-----ELSFANDQVVEVRS-TKPSSTGVARLEPLLIIGGIYPQHN-ED	156
<i>Pa</i> PBP1b	PLELFLNGLKLRSREDFLRELDALGYRREPSVSGPGTVSVAASAVEL---NTRGFQFYEGAEPARQV-----RVRFNNGNYVSGLSQ-ANGKELAVARLEPLLIIGGLYPAHH-ED	169
<i>Ec</i> PBP2	-----RGI IYDRNGIPLALNRTIYQIEMMPEKVDNVQQTLD-----ALRSVVDLTDDD---IAAFRKE----RARSHR-FT	130
<i>Kp</i> PBP2	-----RGI IYDRNGTPLALNRTIYQLEMMPEKVDNVQQTLD-----ALRDVVDLTDDD---IAGFKKE----RARSHR-FT	130
<i>Ab</i> PBP2	-----RGY IYDRNGVLLADNYPVFTATLSKADVENVDTVIE-----QLQPILELTQED---VDRFKSR----IKTARK-TE	130
<i>Pa</i> PBP2	-----RGI IFDRNGVI IADNRPSFSLTITRERTEDLQKTLD-----TLVEILGLTEDD---RAIFEKR----MKQGRRPF	131
<i>Ab</i> PBP3	-----RGV ISDRHGVPLAISSPIMKIVI DPRDYFETKHLYDQITAEELKQDPNNRKLKRLQLPDKNLNLDELADVGVGD---RADLKKQ----MNA RPR-SR	162
<i>Pa</i> PBP3	-----RGL I TDRNGEPLAVSTPVTTLWANPKELMT---A-----KERWQPLAAALGQD---TKLFADR----IEQNAE-RE	121
<i>Ec</i> PBP3	-----RGM I TDRSGRPLAVSVPVKA IWADPKVHDAGGISV-----GDRWKALANALNIP---LDQLSAR----INANPK-GR	135
<i>Kp</i> PBP3	-----RGM I TDRSGRPLAVSVPVKA IWADPKELHDAGGVTL-----DTRWKALADALNMP---LDQLATR----INTNPR-MR	135
<i>Ec</i> PBP1a	RIPVTLQDQIPPEMVK-----AFIATEDSRFYEHHGVDVPGIFRAASVALFSGHASQGASTITQQLARNFFLSPERTLMRKIKEVFLAIRIEQLLTKDEILELYLNKIYLYGR--	172
<i>Kp</i> PBP1a	RIPVTLQDQIPPELVK-----AFIATEDSRFYEHHGVDVPGIFRAASVAMFSGHASQGASTITQQLARNFFLSPERTLMRKIKEAFLAIRIEQLLNKDEILELYLNKIYLYGR--	172
<i>Ab</i> PBP1a	SIPVEYKQIPPNFIH-----AFILAAEDSFFFEHSGISFKGLGRALSESVTGSDVQTGGSTITMVAKNYFLSPERTLKRKLTIEIFLARKIEQNLSKEDILSLYVNNKIFLGKN--	178
<i>Pa</i> PBP1a	RTPIRFADIPQDFIH-----ALLSAEDDNFANHYGVVKSMLRAAAQLKSGHIQTGGSTITMVAKNYFLTNSERSFSRKINEILLALQIERQLTKDEILELYVNNKIYLGNR--	172
<i>Ec</i> PBP1b	RLFVPRSGFPDLLVD-----TLLATEDRHFYEHGDIGSISYIGRAVLANLTAGRTVQGASTLTQQLVKNLFLSSERSYWRKANEAYMALIMDARYSKDRILELYMNEVYLGQSGD	321
<i>Kp</i> PBP1b	RLFVPRSGFPDLLVD-----TLLATEDRHFYEHGDIGSISYIGRAVLANLTAGRTVQGASTLTQQLVKNLFLSSERSYWRKANEAYMALIVDARYSKDRILELYMNEVYLGQSGD	321
<i>Ab</i> PBP1b	RVLIKLNSVPKPLIE-----ALISTEDRNFYHHGHSISIRGTARALVSNV-TGGRRQGGSTLTQQLVKNFYLTPERTLKRKVNREALMALLIELHYSKDEILEAYLNEVNLGQNGN	264
<i>Pa</i> PBP1b	RILVKLDQVPTYLID-----TLVAVEDRDFWNHGHVSLKSVARAVWNTTAGQLRQGGSTLTQQLVKNFYLSRKNINEAMAVLLELHYDKRDILESYLEVNLVFLGQDQ	278
<i>Ec</i> PBP2	SIPVKTN-LTEVQVARFAVNQYRFPGEVVEKGYKRRYYPYGSALTHVIGYV-----SK-----INDKDVRLNNDGKLANYAATHDIGKLGIERYYEDVLHGQTY	224
<i>Kp</i> PBP2	SIPVKVN-LSEVQVARFAVNQYRFPGEVVEKGYKRRYYPYNSALTHVIGYV-----SK-----INDKDVDRLDKREGKLANYASTHDIGKLGIERYYEDVLHGQTY	224

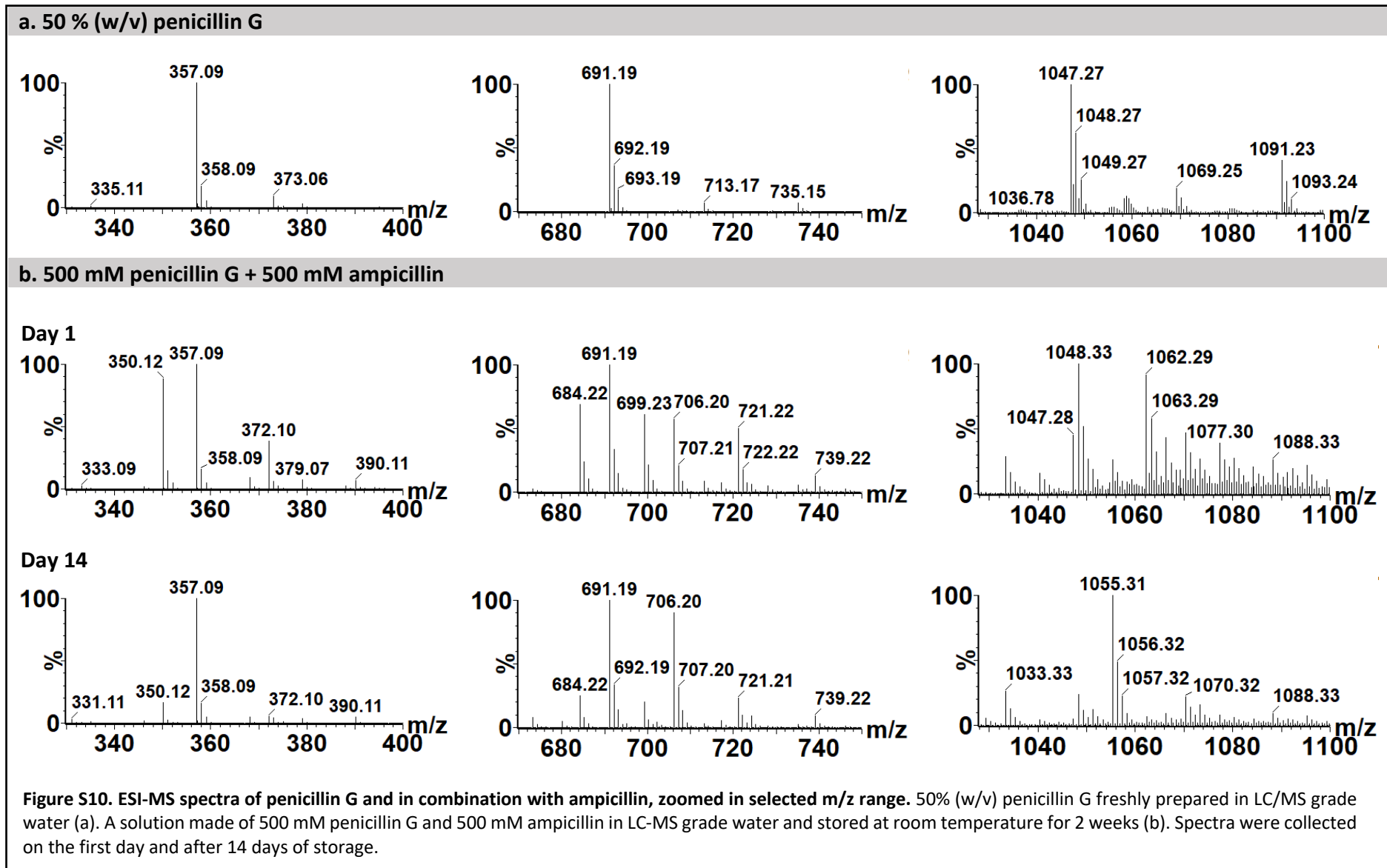
Ab_PBP2	RVAIKLN-LTETNIAKFSEVKYKFPGVRIETQMTRYYPHGDLFAHVIGYV-----GR-----INDKELKSIDK----DLYAGTNLIGKIGVEKSYEDLLHGTPGY	220
Pa_PBP2	PVPIMFE-LNEEQIARIAVNQFRLPGVDVATQFVRHYPLKEHFAHSVGYV-----GR-----INEQELKNLDP----INYSGTHHIGKTGIERFYESELHGTVGY	221
Ab_PBP3	YLVLKKE-VPPQQAD--LIMKGNFQGVYAECTYKRYYPQPQPNQAQIIGLT-----N-----SEGQIGIEGLEMLQNLKQLSGVDGE	233
Pa_PBP3	FIYLVRG-LTPEQGE--GVIALKVPGVYSIEEFRFYPAGEVVAHAVGFT-----D-----VDDRGREGIELAFDEWLAGVPGK	192
Ec_PBP3	FIYLARQ-VNPDMD--YIKKLLKPGIHLREESRRYYPSEVTAHLIGFT-----N-----VDSQIGIEGVEKSFDKWLTGQPGE	206
Kp_PBP3	FIYLARQ-VNPDMD--YIKKLLKPGIHLREESRRYYPSEVTAHLIGFT-----N-----VDSQIGIEGVEKSFDKWLTGQPGE	206
	: . : . *	
Ec_PBP1a	--AYGVGAAAQVYFGKTVDQTLTNEMAVIAGLPKAPSTFNPLYSMRAVARRNVVLSRMLDEGYITQQQFDQTRTEAINANYHAPETAFSAPYLSEMVRQEMVNRYESAY-EDGYRIYT	289
Kp_PBP1a	--AYGVGAAAQVYFGKPIDQTLTSEMVIAGLPKAPSTFNPLYSMRAVARRNVVLSRMLSEGYITQAQYDEARSEPIDASYHAPKIAFSAPYLSEMVRQEMVNRYESAY-EDGYRVYT	289
Ab_PBP1a	--AYGIAAAAKIYYNKSINELSAQMAMIAGLPKAPSKYNPVVNERALERRNWIIGRMLQLGYISQAEYQKAVAEPINLNMPNRDLNNIHPYAGEMVRSELVKHFGQAI-DSGYKVYT	295
Pa_PBP1a	--AYGIEAAAQVYFGKPIKDLSLAEMAMIAGLPKAPSRYNPLVNPTSTERRNWIILERMLKLGFIIDQQRQAQAVEEPINASYHVQTPELNAPYIAEMARAEMVGRYGEAY-TEGYKVIT	289
Ec_PBP1b	NEIRGFPLASLYYFGRPVEELSLDQQALLVGMVKGASVYNPWRNPKLALERRNLVLRLLQQQVIDQELYDML SARPLGVQPRGGVI-SPQPAFMQLVRQELQAKLGDVKDLSGVKIFT	440
Kp_PBP1b	NEIRGFPLASLYYFGRPVEELSLDQQALLVGMVKGASVYNPWRNPKLALERRNLVLRLLQQQVIDQELYDML SARPLGVQPRGGAI-SPQPAFMQMVQRQELQAKLGDVKDLSGVKIFT	440
Ab_PBP1b	YSINGYGLASQFYFGLPLRELNVAAQAYLVGLVQGPSLYNPWKNPEGAKNRRDVLNMMRVMGYLTQAEYETEIARPLNVLSKPSLGPAPKFPDFLDIVRRQLRTEYQESDLTNQGLRIFT	384
Pa_PBP1b	RAIHGFGLASQYFFSQPLAELKLDQVALLVGMVKGPSYFNPRYPDRALARRNLVLDVLAEQGVATQQEVDAAKLRPLGVTRQGSMDSSYPAFLDLVKRQLRQDYRDEDLTHEEGLRIFT	398
Ec_PBP2	-----EEVEVNNRG-----RVIRQLKEVP-PQAGHDIYL	252
Kp_PBP2	-----EEVEVNNRG-----RVIRQLKEVP-PQAGRDIYL	252
Ab_PBP2	-----ESVEADAHS-----NILRHLGRKD-PTRGNDLYL	248
Pa_PBP2	-----EEVETNARG-----RVLRLVLRKTD-PIPGKDIVL	249
Ab_PBP3	-----QKIIRDKRG-----NRLKVSEVIREGEPGENITL	262
Pa_PBP3	-----RQVLKDRRG-----RVIKDVQVTKNAKPGKTLAL	221
Ec_PBP3	-----RIVRKDRYG-----RVIEDISSTD-SQAAHNLAL	234
Kp_PBP3	-----RIVRKDRYG-----RVIEDISSTD-SQAAHNLAL	234
	. : . :	
Ec_PBP1a	TITRKNVQAAQQAVRNNVLDYDMRHGVRGYPANVLWVKGESAWDNKIKITDCLKALPTYGFLLPAAVTSANPQQATAMLADGSTVALSMEGVRWARPYRSDTQQGFTPRKVTVDVLQGTGQQIW	409
Kp_PBP1a	TITRKNVQAAQQAVRNNVLDYDMRHGVRGYPASVWLVKVGETPWETKIVDSLKRQSGYGLFPVAVVTSANAQEAVALLANGDSVSLTMEGVRWARRFISDTQQGATPRKVNDDVQAGQQIW	409
Ab_PBP1a	TINAKRQATAEKAVQDGLAAYDRRHGWRGAEAH-----KPLSEFRAYANTYPAQVTKVNSSSFEALMQDGSTVTVQVSGMSWARPYRNANSVGAAPSRASQIVKVKDIVR	401
Pa_PBP1a	TVRSDDLQNAASQSVRDGLIDYDQRHGVRGYPETRLPGQTRDAWL-----KHLGQQRSIGGLEPAIVTQVEKSGIMVMTRDGKEEAVTWDSMKWARPFLSNNMGMPPRQPADVAQAGDQIR	404
Ec_PBP1b	TFDSVAQDAAEKAAVEGIPALKKQ-----	464
Kp_PBP1b	TFDSVAQDAAEKAASEGIPVLKQ-----	464
Ab_PBP1b	TLDPPIAQTQVQNAFKASVERLANSN-----P-----	410
Pa_PBP1b	SFDPILQEKAETSUNETLKRLSGR-----	422
Ec_PBP2	TLDLKLQQYIETLLA-----GS-----	269
Kp_PBP2	TLDLKLQQYIETLLA-----GS-----	269
Ab_PBP2	SLDYGLQVVASQQLA-----GR-----	265
Pa_PBP2	SIDSRLQEAENALA-----GR-----	266
Ab_PBP3	SIDSRLQYIMYRELTAAGVANNAR-----	286
Pa_PBP3	SIDRLQYLAHRELRNALLENGAK-----	245
Ec_PBP3	SIDERLQALVYRELNNAVAFNKAE-----	258
Kp_PBP3	SIDERLQALVYRELNNAVAFNKAE-----	258
	: . *	
Ec_PBP1a	VRQVG--DAWFLAQVPEVNSALVSNPQNGAVMALVGGFDF-----NQSKFNRAQALRQVGSNIKPFPLYTAAMDK--GLTLASMLNDVPI SRWDASAGSDWQP	504
Kp_PBP1a	VRKVG--DSWFLSQLPDVNSALVSNPQNGAIALVGGFDF-----NQSKFNRAQALRQVGSNIKPFPLYTAAMDK--GLTLASMLNDVPI SRWDAGAGSDWRP	504

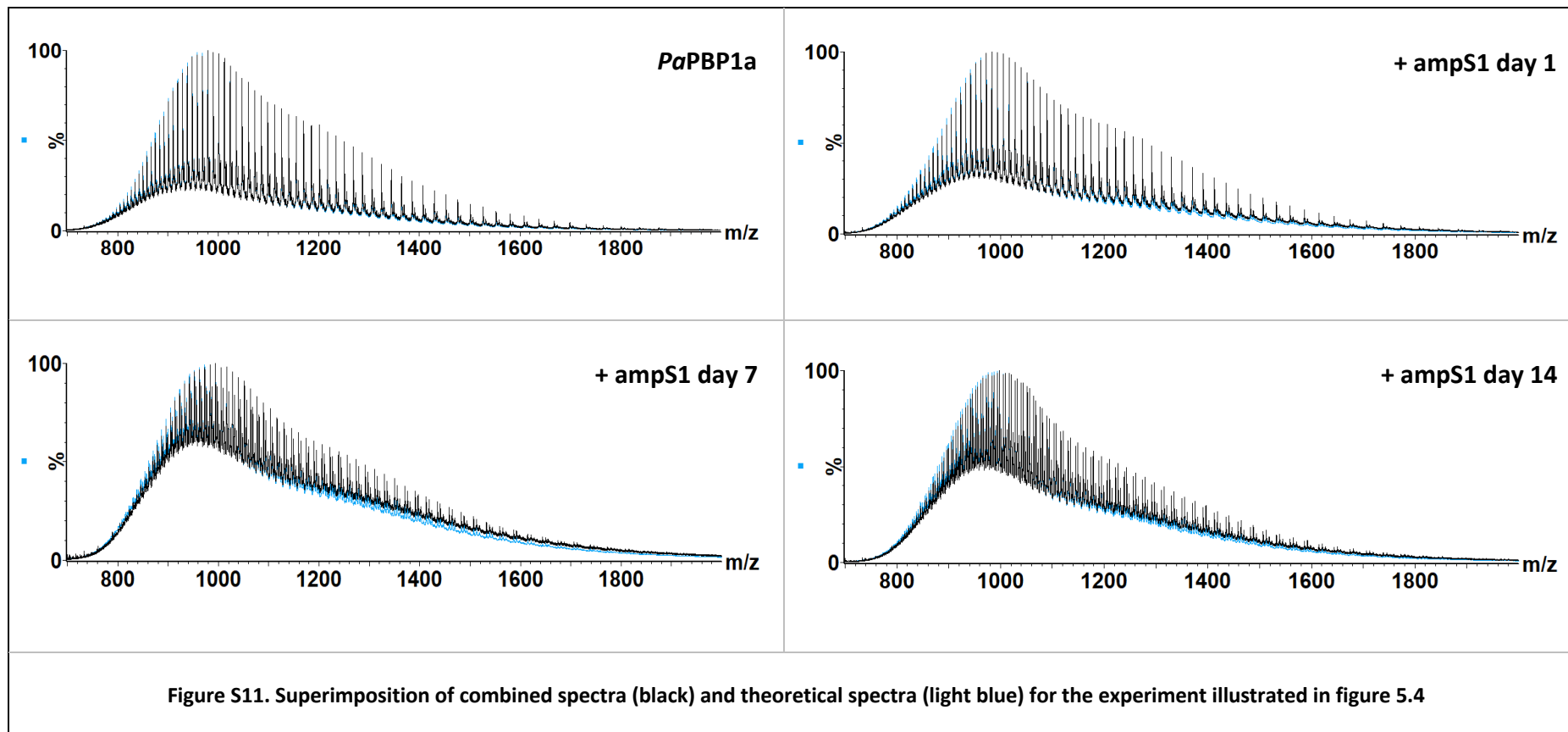
Ab_PBP1a	LRPNEAKTAWSLVQVPKVGQQLIAINPNDSIEAIVGGYNF-----YQSKFNALQGWQPGSTIKPFLYALALER--GMTFYSMVNDSPITI-----GKWTP	492
Pa_PBP1a	VQRQED-GTLRFVQIPAAQSALISLDPKDGAIKSLVGGFSF-----EQSNYNRAIQAKRQPGSSFKPFIYSAALDN--GFTAASLVNDAPIVFVDEYLDKVVWRP	500
Ec_PBP1b	-----RKLSDLETAVVVDRFSGEVRAMVGGSEP-----QFAGYNRAMQARRSIGSLAKPATYLTALSQPKIYRLNTWIADAPIAL-RQPNGQVWSP	550
Kp_PBP1b	-----RKLADLETAMVVDRFTGEVRAMVGGAEF-----QFAGYNRAMQARRSIGSLAKPATYLTALSQPNQYRLNTWIADAPVTI-RLSNGQTWSP	550
Ab_PBP1b	-----ARLKNLQGAVALIAHPENGELIAAVGST-Q-----DFTGFNRALDAKRVQVGSLLKPVIIYLSAIES--GRYNWASQIEDAPISV-PVDGKSWTP	494
Pa_PBP1b	-----KGVDDQVEAMVVTNPETGEIQALIGSRDP-----RFAGFNALDAVRPIGSLIKPAVYLTALERSPKYTLTTWVQDEPFAV-KGQDQGVWRP	508
Ec_PBP2	-----RAAVVVTDPRTGGVLAALVSTPSYDPLNFVDGISSKDYALLNDPNTPLVNRATQGVYPPASTVKPYVAVSALSA-GVITRNTSLFD-PGWW---QLPGSEKR	366
Kp_PBP2	-----RAAVVVTDPRTGAILALVSTPSYDPLNFVDGISSKDYALLNDPNTPLVNRATQGVYPPASTVKPYVAVSALSA-GVITRNTSLFD-PGWW---QLPGSEKR	366
Ab_PBP2	-----RGAIVAIDPRTGEILALVSSPSFNPNLFTVGINHKDYSSLRDNIDQPLYNRAVQGVYPPGSTIKPMEAMGGLHY-GIVDWATAISD-PGYF---HLPDGSBK	362
Pa_PBP2	-----RGAIVAIQPSTGDVLAAMVQPSYDPLNFVTGISFKAYAELRSDIDRPLYNRVLRLGLYPPGSTVTKPAVALAGLDA-GVVTPTSRVFD-PGYF---QLPNYDHK	363
Ab_PBP3	-----SATAIAVDVKTGEILAMTSWPSYNPNNDKN-GLSN-----KDAMRNRAIDMFEPGSTMKPFTISAALET-GQYTPNTIVNTSPGSM---RLG--WHT	371
Pa_PBP3	-----AGSLVIMDVKTGEILAMTNQPTYNPNRR-NLQ-----PAAMRNRAMIDVFEPGSTVTKPFMSAALAS-GRWKPSDIVDVPGLT---QIG--RYT	329
Ec_PBP3	-----SGSAVLVDVNTGEVLAMANSPSYNPNLS-GTP-----KEAMRNRTITDVFEPGSTVTKPMVMVMTALQR-GVVRENSVLNTIPYR---IN--GHE	340
Kp_PBP3	-----SGSAVLVDVNTGEVLAMANSPSYNPNNA-GTA-----KDTMRNRAITDVFEPGSTVTKPMVMVMTALQR-GIVNENTVLNTVPYR----IN--GHE	340
	: . * : : . ** . * ** . : : *	
Ec_PBP1a	KNSPPQY--AGPIRLRQLGQSKNVVMVRAMRAMGVDYAAEYLQRFGFPQNI VH-----TESLALGSASFTPMQVARGYAVMANGGFLVDPWFIS	593
Kp_PBP1a	KNSPPQY--AGPIRLRQLGQSKNVVMVRAMRAMGVDYAAEYLQRFGFPQNI VH-----TESLALGSASFTPLQVARGYSVMANGGFLVNPFFIS	593
Ab_PBP1a	KNSDGRY--LGMIPLRALYLSRNTVSVRLQLQTVGIERTRQLFMDFLQEDQIPR-----NYTIALGTPOVLP IQMATGYATFANGGYRVQPHFIQ	581
Pa_PBP1a	KNDTNTF--LGIPLREALYKSRNMVSVRLVQLGLGIERAISYITKFGFQRDELPR-----NFSLALGTATVTPMEIAGAWSVFANGGYKVNPNVIE	589
Ec_PBP1b	QNDDRRYSSEGRVMLVDALTRSMNVPTVNLGMALGLPAVTETWIKLVKPKDQLHP-----VPAMLLGALNLTPIEVAQAFQTIASGGNRAPLSALR	641
Kp_PBP1b	QNDDRRFS--GQVMLVDALTRSMNVPTVNLGMALGLPAVVDTWTKLGAPKNQLNA-----VPSMLLALNLTPIEVAQAFQTIASGGNRAPLSALR	639
Ab_PBP1b	KNYSGGG--HGIVLSEALANSYNLSAVRLGQEFGLSTFTNNLRKFGVEST-IPA-----YPSIFLGAVNMSPMEVLGIYENFATGGFKYPTRAIR	582
Pa_PBP1b	QNYDRRS--HGTIFLYQLGLANSYNLSTAKLGLDVGVPNVLQTVARLGINRD-WPA-----YPSMLLGAAGLSLMEVATMYQTIASGGNTPLRGIR	596
Ec_PBP2	YRDWKKW--GHGRLNVTRSLAESADTFYQVAYDMGIDRLSEWMSKFGYGHYTGIDLAEERSGNMPTREWKQRKFKKWPYQGDITIPVIGIGQGYWTATPIQMSKALMILINDGIVKVPHLML	485
Kp_PBP2	YRDWKKW--GHGHLNVTKALEESADTFYQVAYDMGIDRLSEWMSKFGYGHYTGIDLSEERSGNMPTREWKLRKFKKWPYQGDITIPVIGIGQGYWTATPIQMNKALMILINDGIVKVPHLML	485
Ab_PBP2	FRDWKKT--GHGIVNMHKAIIMSCDITYFYILANQMGIDQMNQWMRQFGFGQKTVGDLPSSEGLYPNPEWKMRTRKSKWMKGETISVSIQGAFTATPLQLAMATAITANHGSHVPHVLR	481
Pa_PBP2	YRNWNRY--GDGWVSLSAIYRSNDTYFYDLAHLKGLIDRLHAFMSRFQFGQKVALDMFGEADGLMPSREWKRKTRRQVWYPGETLILGIGQGYMQATPIQLAQM TALLANKGHWIRPHLAK	482
Ab_PBP3	IRDTHNY--GALTVSGVIKSSNVGSAKIALSLPKETLPSFFNRVGFGRKSAVRFPGESSGLVLPV-----NKLNSSQIGTMAYGYGL-NATILQLAQGYAMLANHGVMKPLSLH-	478
Pa_PBP3	IRDVSRN--SRQLDLTGILIKSSNVGISKIAFDIGAESIYSVMQVGLGQDTGLGFPGERVGNLPH-----RKWPKAETATLAYGYGL-SVTATQLAHAYAALANDGKSVPLSMT-	437
Ec_PBP3	IKDVARY--SELTLTGVLQKSSNVGSKLALAMPSSALVDITYSRFGLGKATNLGLVGERSGLYPQK-----QRWSDIERATFSFGYGL-MVTPQLARVYATIGSYGIYRPLSIT-	447
Kp_PBP3	IKDVARY--SELTLTGVLQKSSNVGSKLALAMPSSALVDITYSRFGLGKATNLGLVGERSGLYPQK-----QRWSDIERATFSFGYGL-MVTPQLARVYATIGSYGIYRPLSIT-	447
	. : : * : . *	
Ec_PBP1a	KIENDQGGVI FEAKPKVACPECDIPVIYGDTQKSNVLENNDVEDVAISREQQNVSV-PMPQLEQANQALVAKTGAQEYAPHVINTPL--AFLIKSALNTNIFGEPGWGQTGWGRAGR-D-LQ	709
Kp_PBP1a	KIENDQGGVLFEEERPKIACPCQCDLPIYGDTPKSNVLENKDVEDVTTSAEPQNGVNPQPQLEQANQSLVAQSGAQEYAPHVINTPL--AFLIKSALNSNIFGEPGMGTGWGRAGR-D-LQ	710
Ab_PBP1a	RIEDAYGKVIYEAKPEYACIPCINAPETDDAQTTPDDQVIEVTNKELEQKEK-TTKQLNLKQTDKNS-----QYRQAQRILKSSS--AYDMANILRDVI-----EHGTG-RAALK-IG	687
Pa_PBP1a	RIESRDGQVLYQANPRPVVEEQVAADAEDAGNPGDPEHPESAEGEGSIE-----AQQVAAKAQTF-----EPTPAERIIDART--AYIMTSMQLQDVI-----KRGTG-RRALA-LK	688
Ec_PBP1b	SVIAEDGKVLVYQSFP-----QAERAVPAQA--AYLTLWMTQQVV-----QRGTGRQLGAK-YP	691
Kp_PBP1b	SVIAEDGTVLYQSYP-----QAERAVPAQA--AYMTLWMTQQVV-----QRGTGRQLGAK-YP	689
Ab_PBP1b	SVVDANGRLLDYGL-----NVQQTIDPSV--GYIMNYGLQQVM-----SSGTGRAAYNSLSP	633
Pa_PBP1b	SVLTADGQPLKRYPF-----QVEQRFDSGA--VYLVQNAMQRVM-----REGTGRSVYSQLPS	647
Ec_PBP2	STAEDGKQVPVW-QP-----HEP-----PVGD----IHSGYWEIAKDGMYGVA-----NRPNGTAHKYFASA	537
Kp_PBP2	STVEDGKQVPVW-QP-----HEP-----PVGD----IHSGYWEIAKDGMYGVA-----NRNGTAHKYFASA	537
Ab_PBP2	ATHGAKPF-----TV-----RNA-----PDGKINFNGTDEDWVKMREAMDVI-----QSGTGRG--IRT	530
Pa_PBP2	TIDGQPPV-----DP-----DPM-----PDIVL--RDPANWDRVDYGMQQVV-----HGARGTARKVGTAS	531

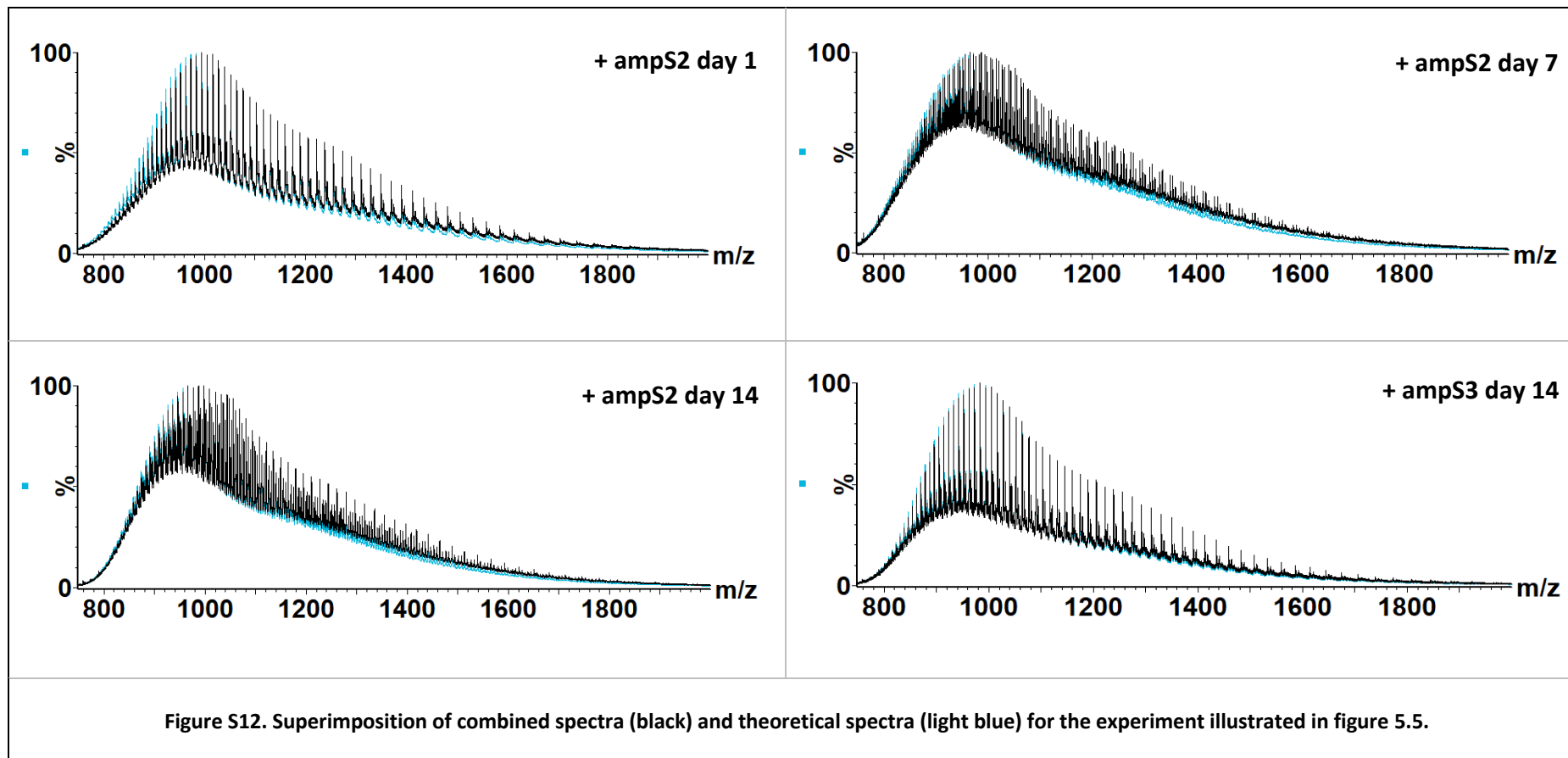
Ab_PBP3	-----KL-----DQP-----	-----PKGEQVLNP---KIADQVLLMLEQV-----	-----TMPGGTAK-QANIP	518		
Pa_PBP3	-----RV-----DRV-----	-----PDGVQVISP---EVASTVQGMLOQV-----	-----VEAQGGVF-RAQVP	477		
Ec_PBP3	-----KV-----DPP-----	-----VPERVFPE---SIVRTVVHMMESV-----	-----ALPGGGGV-KAAIK	487		
Kp_PBP3	-----KV-----DPP-----	-----VPERVFPE---SLVRTVVHMMESV-----	-----ALPGGGGV-KAAIK	487		
			:			
			*			
Ec_PBP1a	RRDIGGKTGTTNSS-----	-----KDAWFSGYGPGVVTSVWIGFDDHRRNLGHTTASGAIKDQISGYEGGAKSAQPAWDAYMKAVLEGVPEQPLTPPPGIV---	-----TVNIDRST	808		
Kp_PBP1a	RHDIGGKTGTTNSS-----	-----KDAWFSGYGPGVVTSVWIGFDDHRRDLGRTTASGAIKDQISGYEGGAKSAQPAWDSFMKSVLEGVPEEPLTPPPGIV---	-----TVNIDRST	809		
Ab_PBP1a	RSDLGGKTGTTNDA-----	-----KDAWFAGFNGKLVTVTWVGFQPT-TLGR-----	-----REYGGIAALPIWINFMGQALQGTAAWVRLEKDAQAPISRDKQEV	775		
Pa_PBP1a	RTDLAGKTGTTNDS-----	-----KDGWFSGYNSDYVTSVWVGFQPE-TLGR-----	-----REYGGTVALPIWIRYMGFALKDKPMHTMAEPPGI---	773		
Ec_PBP1b	NLHLAGKTGTTNNN-----	-----VDTWFAGIDGSTVTTITWVGRDNNQPT-----	-----KLYGASGAMSIYQRYLANQTPTPL--NLVPPEDIA---	772		
Kp_PBP1b	GLHLAGKTGTTNNN-----	-----VDTWFAGIDGSQVTITWVGRDNNQPT-----	-----KLYGASGAMSIYQRYLANQTPTPL--VLTVPEDVV---	770		
Ab_PBP1b	ALKLAGKSGTTNDT-----	-----RDSWFAGYSGNHVAVVWGLDDNKVT-----	-----GLTGSSGALPWWINVMKQLRQTPV--NLRQPDVSQ---	714		
Pa_PBP1b	SLTLAGKTGTSNDS-----	-----RDSWFSGFGGDLQAVVWLGRRDNGKT-----	-----PLTGATGALQVWASFMKKAHPQSL--EMPMPENVV---	728		
Ec_PBP2	PYKIAAKSGTAQVFGLKANETYNAHKIAERLRDHKLMTAFAPYNN-----	-----PQVA-----	-----VAMILENGGAGPAV-GTLMRQILDHIMLGDNNTDLPAENPAVAAAE-----	631		
Kp_PBP2	PYKIAAKSGTAQVFGLKANETYNAHRIERLRDHKLMTAFAPYNN-----	-----PQVA-----	-----VAMILENGGAGPAV-GTIMRQILDHIMLGDNNTLTPSENPAVTAGE-----	631		
Ab_PBP2	LYQIAGKTGTAQVKSIAQGKRYNEAALSERQLDHGLFVGFAPADK-----	-----PEIA-----	-----IAVIWENGRHGG-SAAQLAKPVFDYWLLTRKKNPIRPAHQVNGGLM--TAGIKPGE	633		
Pa_PBP2	AYLLIAGKSGTAQVVAIKQNERYDRSKLLERHRDHALFVGFAPANN-----	-----PQIA-----	-----VAVMVENGESGSGVAAPVVKQVMDAWLLDEHGKKAEYAEPV-----	622		
Ab_PBP3	GYRVGGKTGTAHKLADGKGYSNNE-----	-----YRALFAGVAPISD-----	-----PRLA-----	610		
Pa_PBP3	GYHAAGKSGTARKVSVGTGKYRENA-----	-----YRSLFAGFAPATD-----	-----PRIA-----	573		
Ec_PBP3	GYRIAIAKTGTAKKV--GPDGRYINK-----	-----YIAYTAGVAPASQ-----	-----PRFA-----	582		
Kp_PBP3	GYRIAIAKTGTAKKV--GPDGRYINK-----	-----YIAYTAGVAPASH-----	-----PRFA-----	582		
	. * : * * : .					
Ec_PBP1a	GQLAN-----	GGNSREEYFIEGTQPTQQAV--HEV-----	-----GTTIIDNGE-----	-----A-----	-----QELF-----	850
Kp_PBP1a	GQLAN-----	GGNSRAEYFIEGTQPTQQAV--REV-----	-----GTTLDGGG-----	-----ET-----	-----HELFL-----	852
Ab_PBP1a	TEVGDKKTYRAAPPLARPLYRPAPPQPKTTNNDFDDLPGEIIVPSKTPPPAMKPSQGA-----			-----APK-----	-----REKDELENLINQIE-----	851
Pa_PBP1a	---GR-SAAPGTPGAYFEMFKNEDTPPSV-----	-----NE-----	-----LPPGSFPGSPLPDDEG-----	-----AP-----	-----IDLF-----	822
Ec_PBP1b	---N---FVCSGGMRI LPVW--	-----TSDPQSLCQQSEMQ-----	-----QQPS-----	-----GNPFDQSSQPQQPQQQ---	-----PAQQEQKSDGVAGWIKDMFGSN-----	844
Kp_PBP1b	---N---FVCSGGMRLPVW--	-----TTQPDALCRQEMMQQQQLQQEA---	-----KNPFNQSGQQQQQQQQQQQPQKQEQKSDGVAGWIKDMFGSN-----			851
Ab_PBP1b	GDLA---QACDGAVYI PMLA--	-----HTVPHR-----	-----ATPC-----	-----GAPYYQ--VDPTYTPQSDNTIPEPQDDNTDSYIRESENQMEQDLSNNTRI ISSGSYNN		798
Pa_PBP1b	GQGSAA--ADCPNAVQMPYIR--	-----GSEPAQ-----	-----GPGC---	-----GSQNPAGEVM---	-----DWVRGWLN---	774
Ec_PBP2	-----	-----DH-----				633
Kp_PBP2	-----	-----DQ-----				633
Ab_PBP2	-----	-----LPSGNESASSTPATSAPTSAASSTPQ-----	-----ATPTRPATNEVDE-----			672
Pa_PBP2	-----	-----APLAAAVAKPE-----	-----PTAAEPEAPALEQ-----			646
Ab_PBP3	-----	-----AKGGRG-----				610
Pa_PBP3	-----	-----GTGGRS-----				579
Ec_PBP3	-----	-----GTGGRS-----				588
Kp_PBP3	-----	-----GTGGRS-----				588

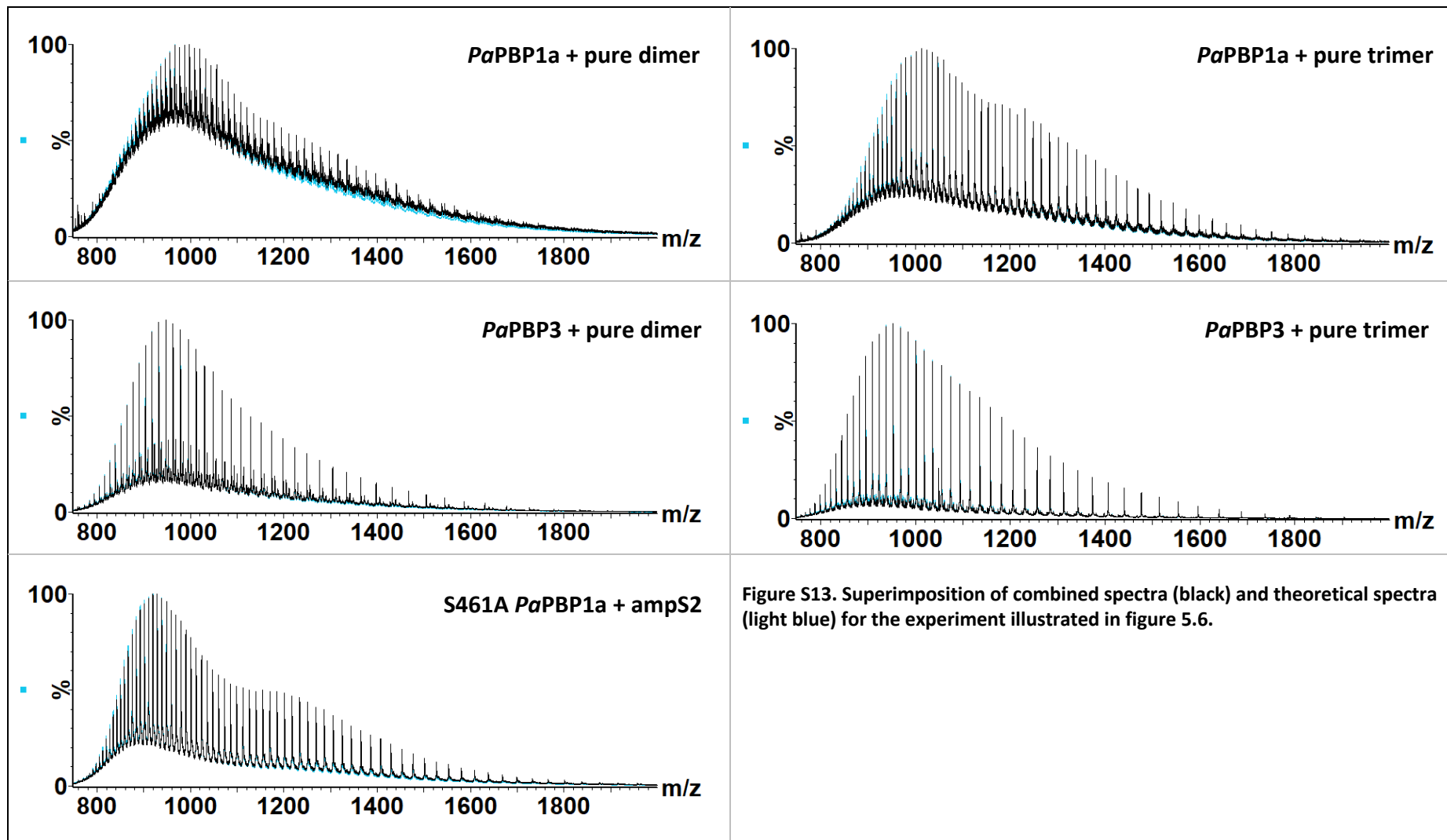
Figure S8. Sequence alignment of HMW-PBPs from selected ESKAPE pathogens. *E. coli* K12 (*Ec*), *K. pneumoniae* ATCC 13883 (*Kp*), *P. aeruginosa* PAO1 (*Pa*) and *A. baumannii* ATCC 19606 (*Ab*). The conserved motifs in the transglycosylase domain of the bifunctional PBPs are highlighted in black, while the motifs conserved in the transpeptidase domain of monofunctional and bifunctional PBPs are highlighted in grey. Multiple sequence alignment produced with Clustal Omega (Sievers *et al.*, 2011).

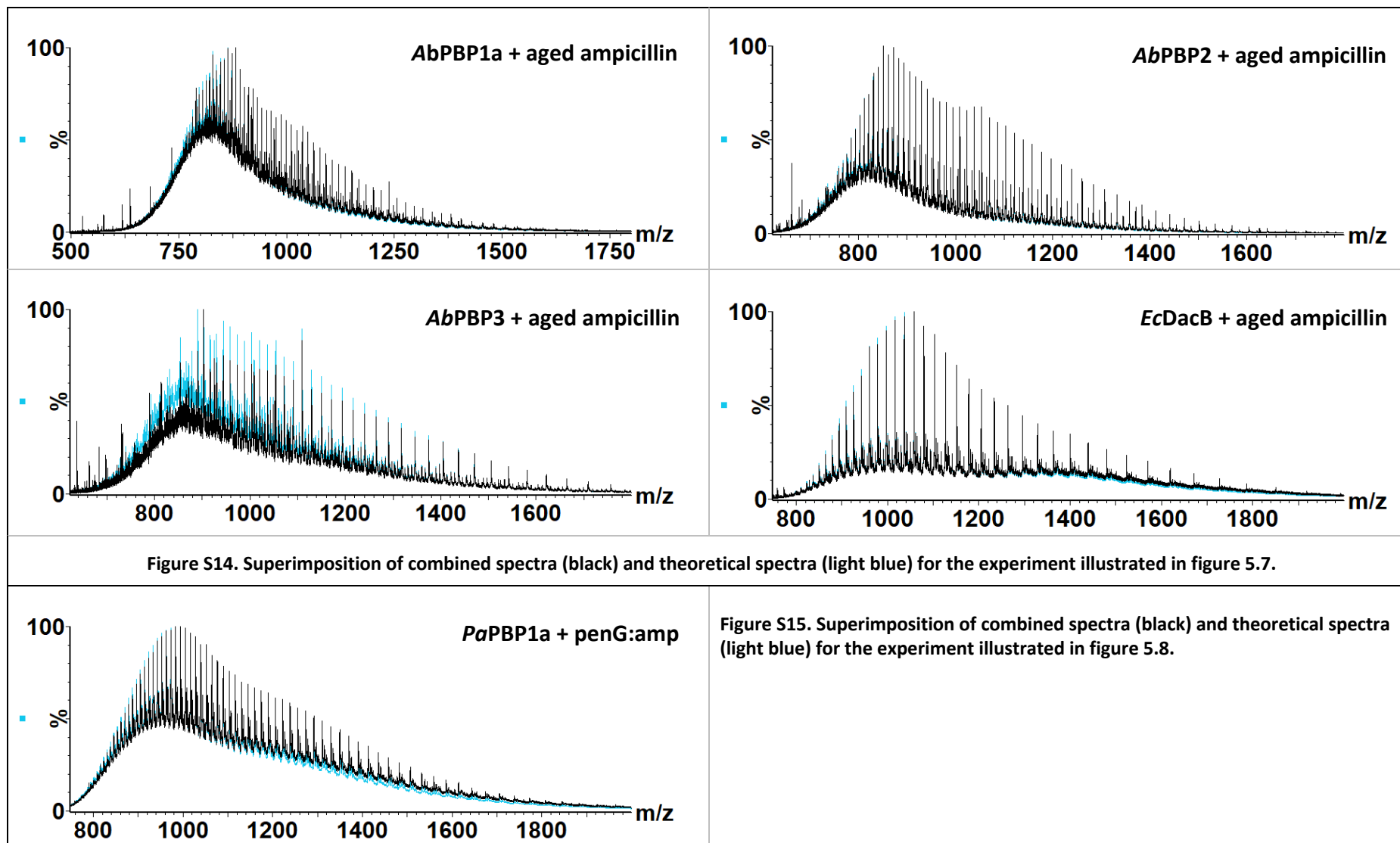


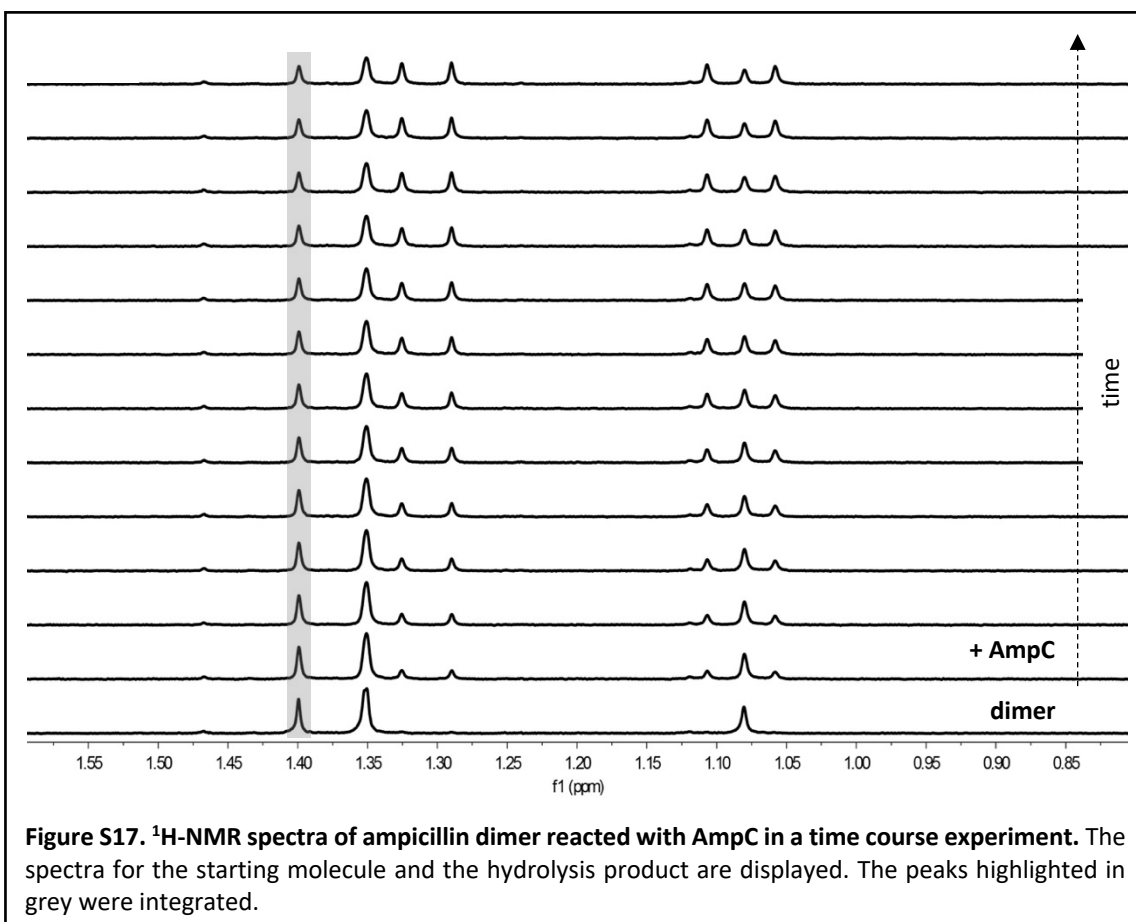
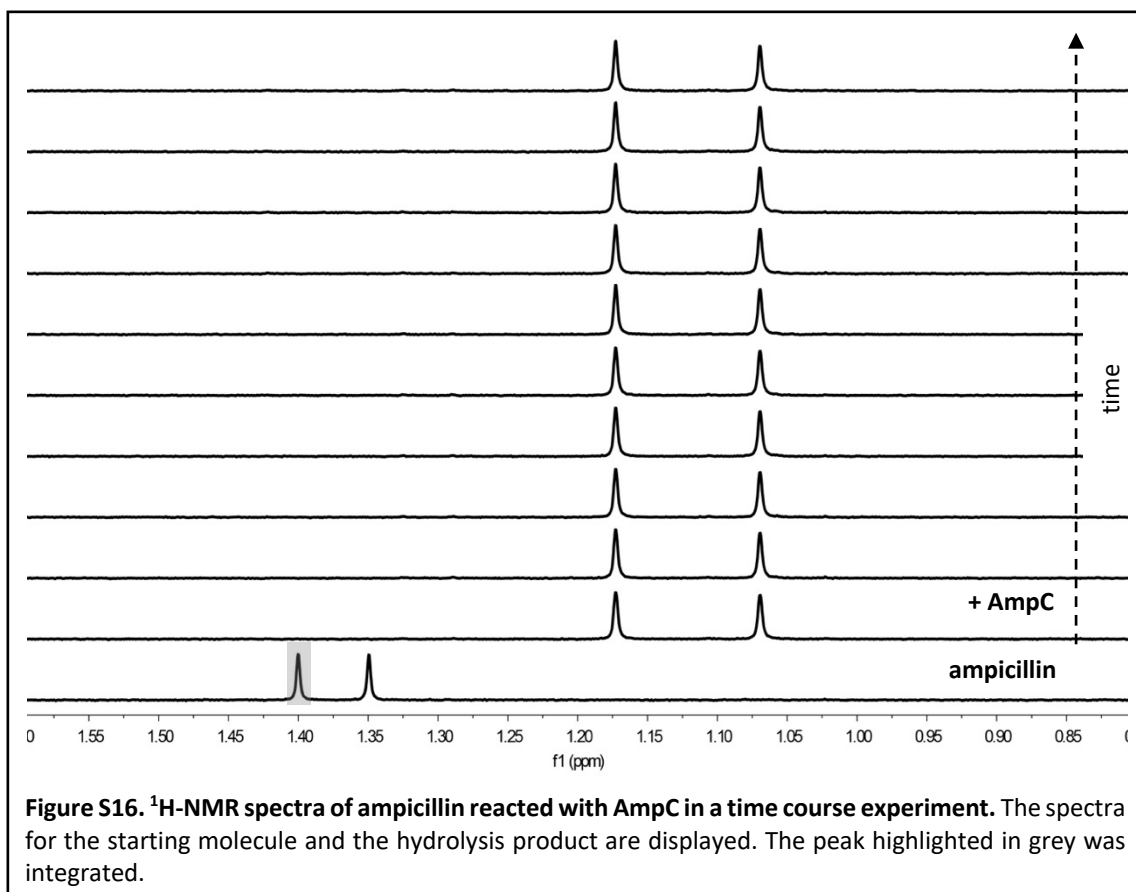












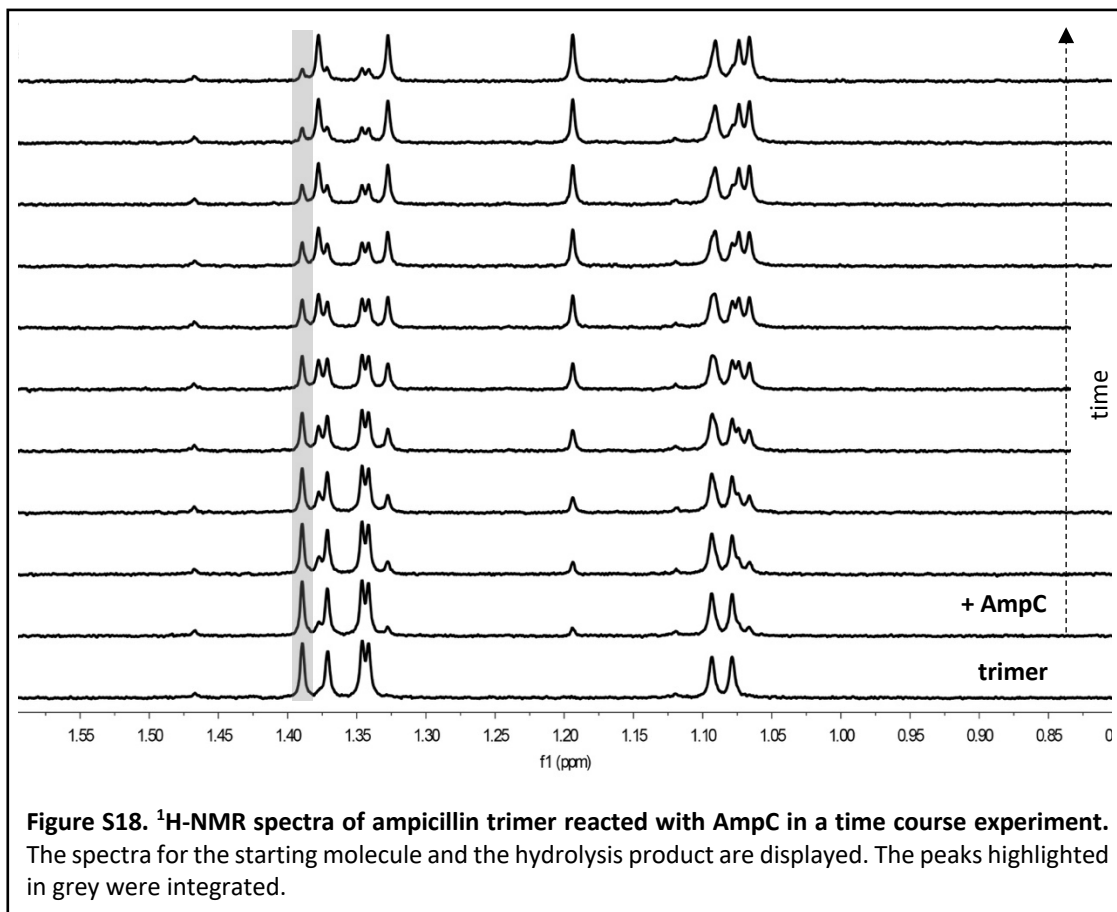


Figure S18. ¹H-NMR spectra of ampicillin trimer reacted with AmpC in a time course experiment. The spectra for the starting molecule and the hydrolysis product are displayed. The peaks highlighted in grey were integrated.